

Iñaki Adánez Rubio

# Combustión de carbón con captura de CO<sub>2</sub> utilizando transportadores sólidos de oxígeno basados en óxido de cobre

Departamento  
Ingeniería Química y Tecnologías del Medio Ambiente

Director/es  
Abad Secades, Alberto  
Gayán Sanz, Pilar

<http://zaguan.unizar.es/collection/Tesis>



**Universidad**  
Zaragoza

Tesis Doctoral

COMBUSTIÓN DE CARBÓN CON CAPTURA DE  
CO<sub>2</sub> UTILIZANDO TRANSPORTADORES SÓLIDOS  
DE OXÍGENO BASADOS EN ÓXIDO DE COBRE

Autor

Iñaki Adánez Rubio

Director/es

Abad Secades, Alberto  
Gayán Sanz, Pilar

**UNIVERSIDAD DE ZARAGOZA**

Ingeniería Química y Tecnologías del Medio Ambiente



**CONSEJO SUPERIOR DE INVESTIGACIONES CIENTÍFICAS**

**(C.S.I.C.)**

**INSTITUTO DE CARBOQUÍMICA**



**COMBUSTIÓN DE CARBÓN CON CAPTURA DE CO<sub>2</sub>  
UTILIZANDO TRANSPORTADORES SÓLIDOS DE  
OXÍGENO BASADOS EN ÓXIDO DE COBRE**

**TESIS DOCTORAL**

**Iñaki Adánez Rubio**



**CONSEJO SUPERIOR DE INVESTIGACIONES CIENTÍFICAS**

**(C.S.I.C.)**

**INSTITUTO DE CARBOQUÍMICA**



**COMBUSTIÓN DE CARBÓN CON CAPTURA DE CO<sub>2</sub>  
UTILIZANDO TRANSPORTADORES SÓLIDOS DE  
OXÍGENO BASADOS EN ÓXIDO DE COBRE**

Memoria presentada en el Departamento de  
Ingeniería Química y Tecnologías del Medio Ambiente de la Universidad de Zaragoza  
para optar al grado de Doctor por:

Iñaki Adánez Rubio

Diciembre 2014

Directores:

Alberto Abad Secades

Pilar Gayán Sanz



**Alberto Abad Secades**, Científico Titular del CSIC, y

**Pilar Gayán Sanz**, Científico Titular del CSIC,

**CERTIFICAN:**

que la presente memoria, titulada:

**“Combustión de carbón con captura de CO<sub>2</sub> utilizando transportadores sólidos de oxígeno basados en óxido de cobre”**

ha sido realizada bajo nuestra dirección en el Instituto de Carboquímica (ICB-CSIC) de Zaragoza por D. Iñaki Adánez Rubio, se corresponde con el proyecto de tesis aprobado el 11 de septiembre de 2014 por la Comisión de Doctorado de la Universidad de Zaragoza y autorizamos su presentación como compendio de publicaciones.

Y para que así conste, firmamos el presente certificado en Zaragoza a 11 de Diciembre de 2014.

Fdo.: Dr. Alberto Abad Secades

Fdo.: Dra. Pilar Gayán Sanz





## Agradecimientos

El desarrollo de esta Tesis se realizó durante 2009-2014 en el Instituto de Carboquímica (ICB-CSIC), que pertenece al Consejo Superior de Investigaciones Científicas. Se llevó a cabo parte de la investigación y trabajo experimental durante una estancia de tres meses en la Universidad Tecnológica de Chalmers en Gotemburgo (Suecia).

Este trabajo está parcialmente financiado por la Comisión Europea, mediante el programa RFCS bajo los proyectos ECLAIR (contrato RFCP-CT-2008-0008) y ACCLAIM (contrato RFCP-CT-2012-00006), por la compañía ALSTOM Power Boilers y por el Ministerio de Ciencia e Innovación (PN ENE2010-19550 y ENE2011-26354). El objetivo de estos proyectos era estudiar la captura de CO<sub>2</sub> en el proceso *Chemical Looping Combustion* para combustibles sólidos. Agradezco a estas instituciones su apoyo económico y al CSIC por la beca predoctoral JAE Pre. recibida.

Me gustaría expresar mi gratitud al Dr. Juan Adánez, la Dr. María Jesús Lázaro y al Dr. Luís de Diego como directores del Instituto de Carboquímica. Quiero mostrar mi agradecimiento particular a mis directores de esta tesis el Dr. Alberto Abad y la Dr. Pilar Gayán por su paciencia, su consejo y su guía fundamental en el desarrollo de esta tesis. Por su puesto, mil gracias al resto de los investigadores del grupo: Luis, Paco y Juan.

También agradecer al Dr. Anders Lyngfelt, Dr. Tobias Mattisson y al Dr. Henrik Leion y al resto del Departamento de Energía y Medio Ambiente de Chalmers por la oportunidad de trabajar en un su grupo y utilizar sus instalaciones. Gracias a mi compañero Mehdi por su ayuda en los laboratorios de Chalmers durante todas las horas de experimentación.

Gracias a mis compañeros y personal del ICB, por haberme acogido en el Instituto y haberme hecho uno más del centro. Y en especial a los compañeros del despacho y de la nave tanto a los que estuvieron como a los que están: MA, Ana, José, Saúl, Diego, Tere, Arancha, Marga, Cristina, María, Carmen Rosa, Javi, Anabel, Kike, Margarita y

Cristina. Por todos esos buenos momentos pasados, risas, charlas y reflexiones juntos. Se os echa de menos a los que ahora no estáis. Como olvidarme de la hora del café de todos los días, las risas y buenos ratos que nos sirven para despejarnos todas las mañanas: Arturo, Mei e Imanol.

No puedo dejar de mencionar la gratitud que siento para los amigos de siempre, los que empezamos a ir juntos en el instituto y a los que más tarde nos conocimos en la Universidad, a todos ellos por los buenos ratos, las risas, las confianzas, sin los cuales pasar meses en la biblioteca estudiando hubieran sido un horror. Por todo lo que hemos vivido juntos y todo lo que nos queda por vivir, gracias. Raúl, Nuria, Rubén, Jorge, Lorena, Silvia, Guille, Fernando y David. Por otro lado, mis amigos del grupo de wargames, a mis chichimecas, con los cuales se nos pasan las tardes volando, recreando Waterloo, conquistando Roma a lomos de un elefante junto a Aníbal, rompiendo el cerco a Bastogne con Patton o atacando naves en llamas más allá de Orión. Ignacio, Borja, Miguel y Carlos, sin vosotros esto no hubiera sido lo mismo.

Gracias a mi familia, en especial a mis hermanos Imanol e Iosu, y a mis padres Amalia y Juan. Por vuestro apoyo incondicional, por los valores que me habéis inculcado y por despertar en mi el deseo de aprender y la curiosidad infinita. Ser lo que soy es gracias a vosotros.

Y a ti Silvia, gracias. Por ser la luz que ilumina mi camino, por lo maravillosa que eres.

## INDICE

<b>1</b>	<b>Introducción.....</b>	<b>1</b>
1.1	Efecto invernadero y cambio climático.....	3
1.2	Captura y Almacenamiento de CO <sub>2</sub> (CAC).....	8
1.2.1	Tecnologías de Captura de CO <sub>2</sub> .....	10
1.2.2	Transporte de CO <sub>2</sub> .....	13
1.2.3	Almacenamiento de CO <sub>2</sub> .....	15
1.3	Impacto de la implementación de los procesos CAC en la generación de energía .....	17
1.4	Combustión con transportadores sólidos de oxígeno: <i>Chemical Looping Combustion</i> (CLC) .....	21
1.4.1	Transportadores sólidos de oxígeno.....	22
1.4.2	CLC con combustibles sólidos.....	25
1.5	<i>Chemical Looping with Oxygen Uncoupling</i> (CLOU).....	28
1.6	Objetivo y plan de trabajo .....	34
1.7	Publicaciones Científicas y Congresos.....	37
<b>2</b>	<b>Sección experimental.....</b>	<b>41</b>
2.1	Preparación de transportadores de oxígeno.....	43
2.1.1	Impregnación húmeda incipiente.....	43
2.1.2	Extrusión .....	44
2.1.3	Compresión .....	44
2.1.4	<i>Spray Drying</i> .....	44
2.2	Combustibles sólidos.....	47
2.3	Técnicas de caracterización empleadas .....	48
2.4	Instalaciones Experimentales .....	49
2.4.1	Termobalanza.....	49
2.4.2	Reactor de Lecho Fluidizado Discontinuo I (ciclos N <sub>2</sub> -aire).....	52
2.4.3	Reactor de Lecho Fluidizado Discontinuo II (ciclos CH <sub>4</sub> -aire).....	54
2.4.4	Reactor de Lecho Fluidizado Discontinuo III (ciclos carbón-aire) .....	56
2.4.5	Unidad CLOU en continuo para combustibles sólidos (1.5 kW <sub>t</sub> ).....	60

<b>3</b>	<b>Resultados y discusión.....</b>	<b>69</b>
3.1	Desarrollo de transportadores de oxígeno .....	71
3.1.1	Transportadores de oxígeno preparados por impregnación incipiente ...	73
3.1.2	Transportadores de oxígeno preparados por mezcla másica y extrusión	74
3.1.3	Transportadores de oxígeno preparados por mezcla másica y compresión .....	76
3.1.4	Evaluación de transportadores de oxígeno preparados por <i>spray drying</i>	86
3.1.5	Estudio de otros materiales preparados por <i>spray drying</i> .....	92
3.1.6	Selección de un transportador de oxígeno .....	97
3.2	Análisis de la transferencia de oxígeno en la combustión de carbón .....	99
3.2.1	Efecto de la relación entre el transportador de oxígeno y el carbón.....	101
3.2.2	Regiones de combustión .....	105
3.2.3	Determinación de la velocidad máxima de generación de oxígeno durante la combustión de char .....	109
3.3	Demostración del proceso en una planta en continuo de 1.5 kW <sub>t</sub> con diferentes combustibles sólidos.....	112
3.3.1	Evaluación preliminar de la capacidad para transferir oxígeno del transportador de oxígeno en continuo.....	112
3.3.2	Demostración del proceso en una planta en continuo de 1.5 kW <sub>t</sub> con carbón.....	115
3.3.3	Evaluación del proceso en la combustión de carbones de diferente rango .....	124
3.3.4	Combustión de biomasa.....	127
3.4	Estudio del efecto del azufre del combustible .....	131
3.5	Caracterización del transportador de oxígeno .....	139
3.6	Comparación entre los procesos CLOU y <i>iG-CLC</i> .....	143
<b>4</b>	<b>Modelado del proceso CLOU .....</b>	<b>147</b>
4.1	Introducción al diseño de un proceso CLOU .....	149
4.2	Cinética de las reacciones de reducción y oxidación del transportador de oxígeno Cu <sub>60</sub> MgAl <sub>1</sub> SD .....	151
4.2.1	Reducción del CuO a Cu <sub>2</sub> O .....	152
4.2.2	Oxidación del Cu <sub>2</sub> O a CuO.....	159
4.3	Modelado simplificado del proceso CLOU.....	163

4.3.1	Circulación de sólidos e inventarios mínimos de transportador de oxígeno.....	163
4.3.2	Eficacia de captura de CO <sub>2</sub> para diferentes combustibles .....	167
<b>5</b>	<b>Conclusiones.....</b>	<b>177</b>
<b>6</b>	<b>Acrónimos, notaciones y símbolos .....</b>	<b>187</b>
<b>7</b>	<b>Bibliografía.....</b>	<b>195</b>
	<b>Apéndice - Artículos.....</b>	<b>203</b>



# **1 Introducción**





## 1.1 Efecto invernadero y cambio climático.

Se ha demostrado científicamente que la actividad humana está potenciando el efecto invernadero de la atmósfera terrestre [1]. El efecto invernadero se debe a que parte de la radiación emitida por la superficie de la Tierra es absorbida por el CO<sub>2</sub>, H<sub>2</sub>O y otros gases existentes en la atmósfera. Los principales gases responsables del efecto invernadero son H<sub>2</sub>O, CO<sub>2</sub>, CH<sub>4</sub>, CFCs, N<sub>2</sub>O y SF<sub>6</sub>. El efecto invernadero es el responsable de que las temperaturas medias de la Tierra sean de 15°C frente a los -15°C que habría sin la existencia del mismo [1]. En las últimas décadas este efecto está siendo potenciado debido al aumento de las concentraciones de los gases que lo producen. Esta potenciación del efecto invernadero está produciendo un calentamiento del planeta, lo que puede llegar a producir un cambio del sistema climático global [2]. Si se continúa con la tendencia actual en las emisiones de gases de efecto invernadero, se prevén importantes consecuencias medioambientales, para la biodiversidad del planeta, así como en aspectos sociales y económicos [3]. En la Tabla 1.1 se muestra el potencial de efecto invernadero de estos gases y su evolución con el tiempo.

**Tabla 1.1.** Potencial de calentamiento global para varios gases antropogénicos [2].

Gas	Potencial de calentamiento global para varios horizontes temporales		
	20 años	100 años	500 años
CO <sub>2</sub>	1	1	1
CH <sub>4</sub>	56	21	6.5
N <sub>2</sub> O	280	310	170
HFC-23	9100	11700	9800
HFC-32	2100	650	200
SF <sub>6</sub>	16300	23900	34900

Aunque el CO<sub>2</sub> es el gas con menor potencial de efecto invernadero de forma individual, sí que es el gas con mayor contribución al calentamiento global debido al gran volumen que es emitido a la atmósfera anualmente, como se puede ver en la Figura 1.1. Así en el año 2010 [1], cerca del 80% de la emisiones correspondientes a gases de efecto invernadero eran de CO<sub>2</sub>.

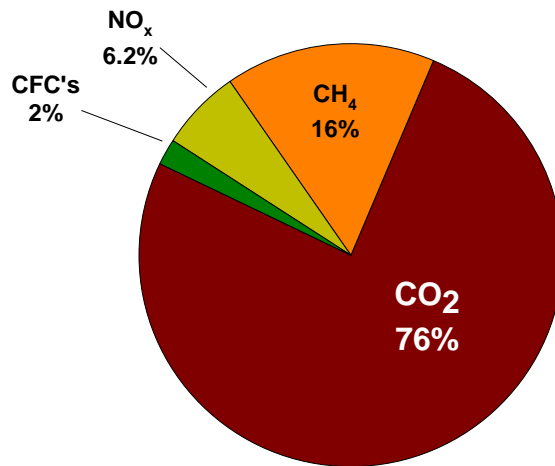


**Figura 1.1.** Emisiones de gases de efecto invernadero en el año 2010 a nivel mundial, adaptado de [1] .

Esta preponderancia del CO<sub>2</sub> es debida principalmente al uso de combustibles fósiles en la generación de energía. En la Figura 1.2 se muestra el consumo de energía primaria mundial en el año 2011 según la Agencia Internacional de la Energía (IEA). Como se puede observar, más del 80% procede de combustibles fósiles, es decir petróleo, carbón y gas natural. El resto está diversificada entre nuclear y renovables tales como hidráulica, eólica, solar o biomasa [4].

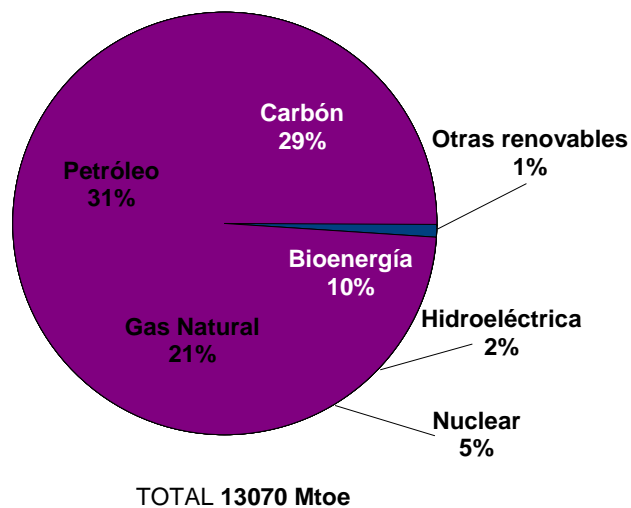


**Figura 1.2.** Distribución de la generación de energía primaria mundial en el año 2011, adaptado de [4].

Este mix energético resultante a nivel global, con predominio de los combustibles fósiles, será el predominante durante al menos la primera mitad del siglo XXI. La Figura 1.3 muestra las previsiones para la evolución del consumo de energía primaria hasta el año 2035 realizado por la IEA [4]. Como se puede observar, los combustibles

con mayor expectativa de crecimiento son el gas natural y las nuevas energías renovables, seguidos de la energía nuclear y la biomasa. No obstante, aunque el crecimiento en el uso de petróleo y carbón es comparativamente menor, estas dos fuentes de energía seguirán siendo las más utilizadas.

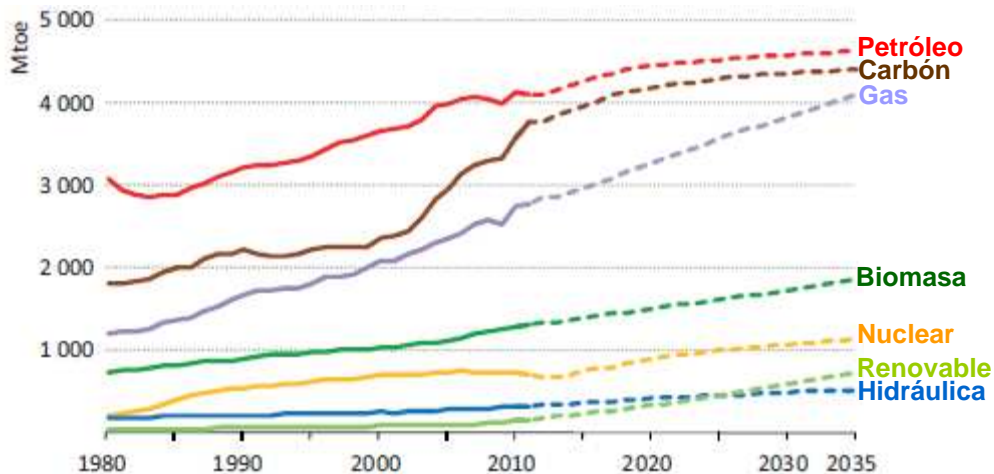


**Figura 1.3.** Evolución de consumo de energía primaria mundial hasta el año 2035 [4]

Este aumento en el consumo de combustibles fósiles viene dado principalmente por el crecimiento económico de países en vías en desarrollo, que conlleva un aumento en las necesidades energéticas de dichos países. Está previsto un crecimiento de la demanda energética muy alto por parte de China (31%), India (18%), Oriente medio (10%) y Brasil (5%) [4]. Respecto a las reservas de dichos combustibles, en la Figura 1.4 se muestran las reservas estimadas mundiales en función de la producción a finales de 2011 para el carbón, y del 2012 para gas y petróleo. Como se puede observar, las reservas probadas para gas y petróleo son de 61 y 54 años, respectivamente. Estas reservas aumentan día a día, pero siendo cada vez mayor la complicación técnica para su extracción. Estas reservas podrían aumentarse aplicando nuevas tecnologías de extracción como el “*fracking*” o la extracción de petróleo de arenas bituminosas, con el uso intensivo de técnicas de extracción mejorada de petróleo (EOR), la extracción de gas y petróleo “*off-shore*” y las reservas presentes en el Ártico. Todo ello daría como resultado un aumento significativo de la reservas a 233 y 178 años, para gas y petróleo respectivamente [4]. No obstante, el uso de alguna de estas opciones conlleva una gran confrontación social.

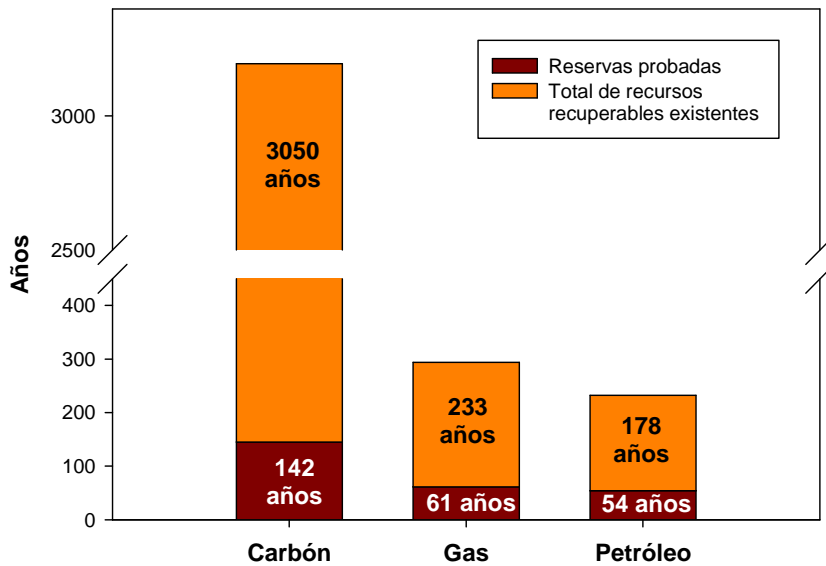


**Figura 1.4.** Reservas mundiales probadas y estimadas de combustibles fósiles en función de la producción a finales de 2011 (carbón) y del 2012 (gas y petróleo), adaptado de [4].

Respecto al carbón, las reservas probadas ascienden a 142 años con el nivel de producción de finales de 2011. La cantidad de carbón recuperable según las últimas estimaciones de la IEA asciende a 20 veces la cantidad de reservas probadas, aunque cada vez son de más difícil acceso [4].

Existen varias propuestas para poner freno al crecimiento de las emisiones de CO<sub>2</sub> a nivel mundial, siendo la más importante la conocida como Protocolo de Kyoto. Éste fue firmado en el año 1997 y su entrada en funcionamiento se produjo en el año 2005 al adherirse Rusia a dicho protocolo. De esta forma se cumplía el requisito de la firma de 55 Partes (países, regiones, etc.) que al menos representasen al 55% de las emisiones mundiales. Ahora bien, los objetivos del mismo son bastante modestos, ya que se proponía únicamente para el año 2012 una reducción de las emisiones de CO<sub>2</sub> del 5.5% con respecto a las de 1990, lo cual no se cumplió. Más recientemente se propuso durante la reunión COP15 [5] en el año 2009 que el aumento máximo de la temperatura media del planeta durante el siglo XXI debía ser de 2 °C y por lo tanto la concentración de CO<sub>2</sub> a finales de siglo no debe exceder los 450 ppm. En Doha en el 2012 se celebró la reunión COP18 [6], donde se llegó al acuerdo de prorrogar el protocolo de Kyoto a 2020, pero únicamente se contó con el apoyo de los países que emiten un 15% del CO<sub>2</sub> total. Se quedaron fuera los grandes emisores de CO<sub>2</sub> como EEUU, Canadá, Japón y Rusia. Además, países emergentes como Brasil, India y sobretodo China no se les

aplican las reducciones de emisiones contempladas en Kyoto. A día de hoy, China es el mayor emisor de CO<sub>2</sub> a nivel mundial.

Estas propuestas cobran día a día más importancia, ya que las emisiones de CO<sub>2</sub> siguen creciendo y por tanto aumentando la concentración de CO<sub>2</sub> en la atmósfera. La Figura 1.5 muestra la evolución de la concentración de CO<sub>2</sub> medida desde el observatorio Mauna Loa, Hawai (EE.UU.), perteneciente al Instituto Oceanográfico de San Diego (California, EE.UU.) [7]. Como se puede observar, el aumento es muy pronunciado en los últimos 60 años, y lo que es más preocupante, sigue con la misma tendencia de aumentar. De este modo, durante el mes de Abril de 2014, la concentración de CO<sub>2</sub> ha superado los 400 ppm, lo que hace más urgente todavía emprender medidas para frenar este aumento.

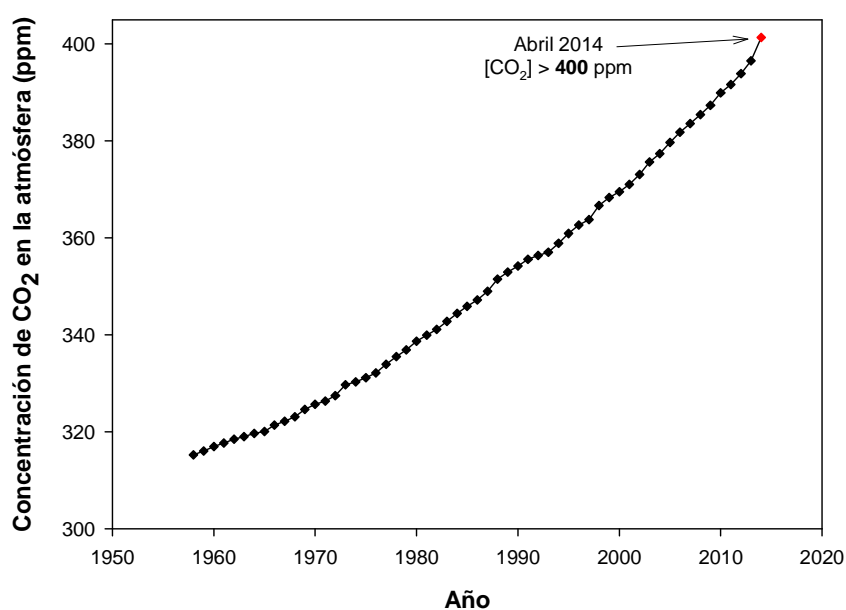


**Figura 1.5.** Evolución de la concentración de CO<sub>2</sub> en la atmósfera, (CO2Now.org, [7]).

Para conseguir estabilizar la concentración de CO<sub>2</sub> en la atmósfera en el año 2050 al doble del valor preindustrial, es necesario realizar conjuntamente numerosas actuaciones cuya entidad dependerá del escenario económico existente en el planeta, ya que el crecimiento económico y la generación de energía están directamente relacionados. En la Figura 1.6 se muestran las reducciones de CO<sub>2</sub> que hay que realizar por distintas vías en un escenario intermedio (550 ppm de CO<sub>2</sub> en la atmósfera en el año 2050), que ha sido realizado por el IEA para conseguir este objetivo [8]. Como se puede observar, la contribución de las distintas opciones tecnológicas para disminuir las

emisiones de CO<sub>2</sub> varía en función de la tecnología y su estado de desarrollo. El incremento de la eficacia energética de las tecnologías ya existentes, tanto a la hora de producir la energía como durante su consumo, supondría el 42% de la disminución de las emisiones de CO<sub>2</sub> a nivel global. Por otro lado, el aumento en el empleo de energías renovables, biocombustibles y energía nuclear supondrían una profunda reducción del 31% en las emisiones de CO<sub>2</sub>. Sin embargo, la incertidumbre sobre el periodo de tiempo que llevaría tener disponibles estas alternativas tecnológicas así como que actualmente el 81% del consumo de energía a nivel global proviene de fuentes fósiles, hace que sea necesaria una etapa de transición donde la obtención de energía por medio de combustibles fósiles siga predominando y a la vez se reduzcan las emisiones de CO<sub>2</sub>. Esto puede lograrse usando tecnologías de Captura y Almacenamiento de CO<sub>2</sub> (CAC). Así con este escenario propuesto, las tecnologías de CAC deberían contribuir con un 14% a la disminución total de emisiones [8].

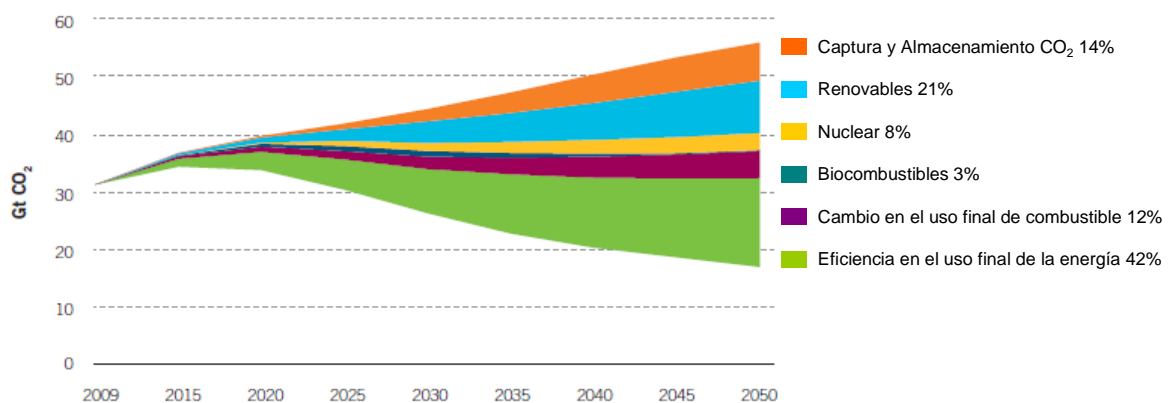


**Figura 1.6.** Estrategias para la disminución de emisiones de CO<sub>2</sub> [8].

Por lo tanto, para cumplir los objetivos de reducción de emisiones en la generación de energía, es necesario desarrollar e implantar la captura y el almacenamiento de CO<sub>2</sub> (CAC) a corto plazo.

## 1.2 Captura y Almacenamiento de CO<sub>2</sub> (CAC)

La captura y el almacenamiento de CO<sub>2</sub> consisten en los siguientes procesos consecutivos: (1) separación del CO<sub>2</sub> emitido por la industria y fuentes relacionadas con la generación de energía del resto de gases que lo acompañan; (2) el transporte de CO<sub>2</sub> a un lugar de almacenamiento; y (3) su aislamiento de la atmósfera a largo plazo (de

siglos a milenios). La aplicación más directa de esta vía de reducción de emisiones de CO<sub>2</sub> puede realizarse en las centrales de producción de energía eléctrica, ya que son fuentes de emisión de CO<sub>2</sub> focalizadas y además representan el 42% de las emisiones totales de CO<sub>2</sub> antropogénicas mundiales [4] como se puede ver en la Figura 1.7.

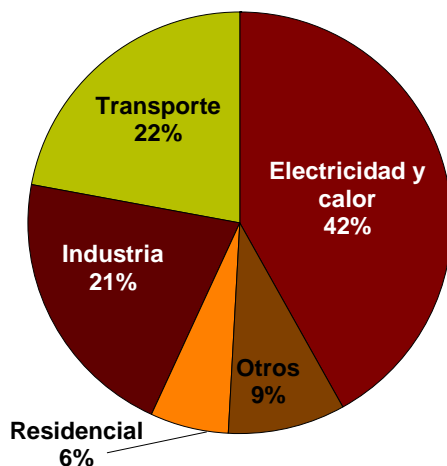


**Figura 1.7.** Emisiones de CO<sub>2</sub> mundiales por sectores año 2011, adaptado de [4].

En las centrales de producción de energía, el combustible más importante a nivel global es el carbón, a la vez que es el combustible que más emisiones de CO<sub>2</sub> genera por MW<sub>e</sub>. El uso de este combustible a la hora de producir energía depende tanto de la disponibilidad de otros combustibles como del desarrollo del país en cuestión. Como se puede apreciar en la Figura 1.8 los dos grandes países en vías de desarrollo, China e India, muestran una alta dependencia del carbón a la hora de producir energía eléctrica en grandes instalaciones de combustión. Por otro lado, en los países más desarrollados (EEUU, EU, Japón y Rusia) la contribución del carbón a la generación de energía es menor debido a que cuentan con un mix energético más distribuido, principalmente con el uso de gas natural, petróleo y energía nuclear, junto a la implementación de energías renovables. Finalmente cabe destacar Brasil como un caso diferente, donde la producción de electricidad es principalmente por medio de plantas hidroeléctricas [4].

La aplicación de sistemas CAC conlleva una modificación en los actuales sistemas de generación de energía eléctrica que pueden llegar a tener importantes penalizaciones tanto energéticas como económicas. Existen pocas vías de captura del CO<sub>2</sub> disponibles comercialmente para su uso, tanto en los dispositivos ya existentes como en nuevos sistemas de generación de energía. Las vías de captura de CO<sub>2</sub> existentes proceden de



tecnologías de producción de hidrógeno y purificación de CO<sub>2</sub>. Estas instalaciones tienen una menor escala que una gran instalación de combustión. En instalaciones de combustión solo se han probado a nivel demostración, del orden de 30 MW<sub>t</sub> [9]. Por ello, existe en los últimos años una importante actividad científica y tecnológica para desarrollar métodos eficientes de captura de CO<sub>2</sub>. Por otra parte, a la hora de almacenar el CO<sub>2</sub> se necesitan buscar almacenes seguros y baratos, así como sistemas de transporte con la menor penalización energética posible.

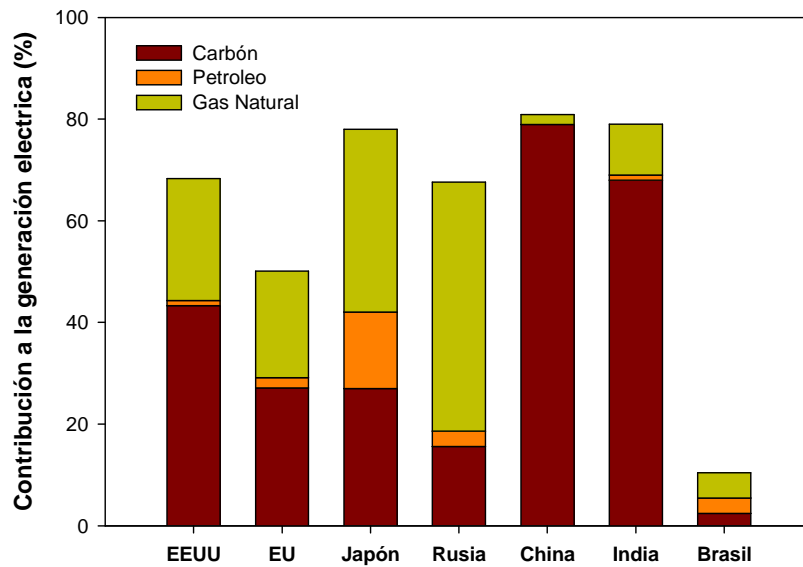


**Figura 1.8.** Contribución de los combustibles fósiles a la generación eléctrica por países en el año 2011, adaptado de [4].

### 1.2.1 Tecnologías de Captura de CO<sub>2</sub>

La corriente de gas generada en la combustión de combustibles fósiles contiene entre el 4 y el 14% de CO<sub>2</sub>, dependiendo del combustible utilizado, siendo el resto principalmente N<sub>2</sub>. Si se quisiera almacenar directamente esa corriente los costes de transporte serían prohibitivos, debido a la dificultad de mover un caudal tan alto y a las dificultades técnicas de comprimir una corriente diluida de CO<sub>2</sub>. Asimismo, se disminuiría el tiempo de utilización de los depósitos de CO<sub>2</sub>. Por ello es necesaria la utilización de tecnologías que permitan la separación del CO<sub>2</sub> del resto de gases de la combustión. Existen tres posibles vías de captura de CO<sub>2</sub> en los sistemas de producción de energía:

### *Captura posterior a la combustión*

En estos sistemas de captura de  $\text{CO}_2$  se separa el  $\text{CO}_2$  de los gases de combustión producidos en la combustión del combustible primario con aire, como se muestra en la Figura 1.9. Para llevar a cabo la separación existen diferentes métodos: absorción física o química, membranas, métodos criogénicos, adsorción, etc. De estos procesos de captura los más desarrollados a día de hoy son los métodos químicos de absorción con aminas. El proceso de captura de  $\text{CO}_2$  se lleva a cabo en torres de absorción, donde la amina se rocía a contracorriente de los gases de salida de la combustión, absorbiéndose en el proceso gran parte del  $\text{CO}_2$  presente. A continuación, la amina se regenera en una torre de regeneración por arrastre con vapor y se produce una corriente concentrada de  $\text{CO}_2$  para su posterior almacenamiento.

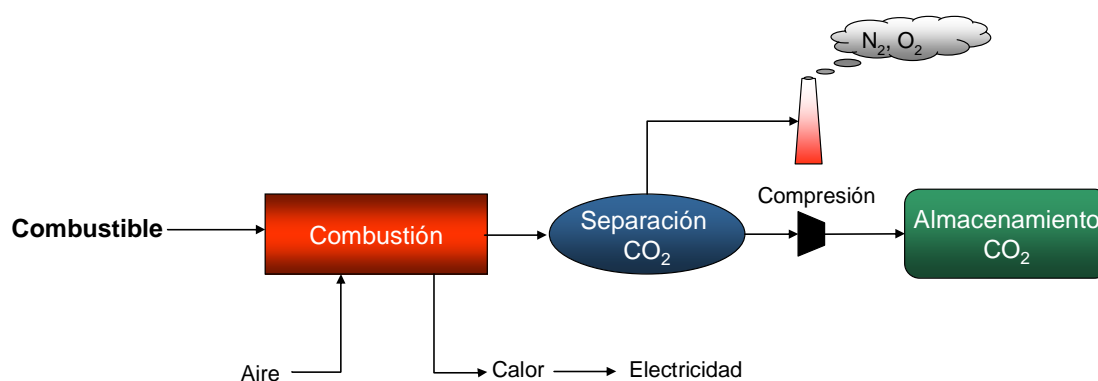


**Figura 1.9.** Captura de  $\text{CO}_2$  posterior a la combustión.

Estos procesos tienen una penalización energética elevada debido a la necesaria regeneración del absorbente para su reutilización. Además, la separación de  $\text{CO}_2$  ha de realizarse en una corriente diluida (concentración de  $\text{CO}_2$  entre el 4-15%) y a presión atmosférica, lo que aumenta los costes de operación y de inversión. Se estima una pérdida global de rendimiento energético usando estas tecnologías entre 8% y 16% en centrales de carbón y entre un 5% y un 10% en centrales de ciclo combinado de gas natural [10].

### *Captura previa a la combustión*

En la Figura 1.10 se muestra el esquema general de los sistemas de captura de  $\text{CO}_2$  previa a la combustión. En este proceso se lleva a cabo la gasificación o reformado de combustibles fósiles que da lugar a una corriente rica en  $\text{CO}$  y  $\text{H}_2$ . Este gas de síntesis se lleva a un reactor *Water Gas Shift* (WGS) donde se transforma el  $\text{CO}$  en  $\text{CO}_2$  produciendo en el proceso  $\text{H}_2$ . Finalmente se separa el  $\text{CO}_2$  de la corriente gaseosa, por

un proceso semejante al utilizado en la captura de CO<sub>2</sub> posterior a la combustión, obteniéndose una corriente de H<sub>2</sub> prácticamente pura. La mayor ventaja de este proceso es que genera H<sub>2</sub> como producto, que puede ser aprovechado de diferentes formas, tanto en la combustión en turbinas de gas para la producción de energía eléctrica, como para su uso en el transporte por medio de celdas de combustible y/o motores de combustión interna.

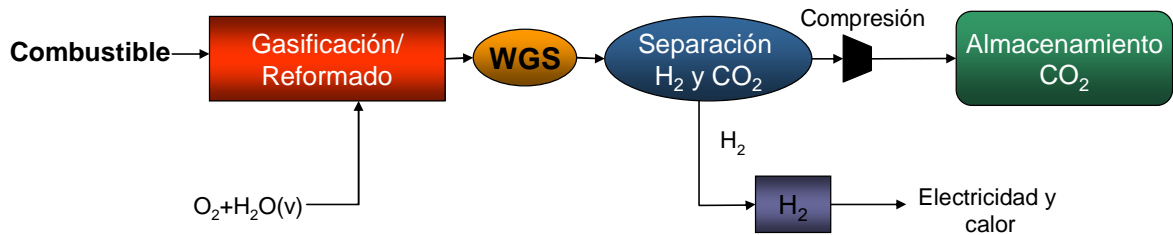


**Figura 1.10.** Captura de CO<sub>2</sub> previa a la combustión.

Estos procesos tienen menores penalizaciones energéticas, ya que la separación CO<sub>2</sub>-H<sub>2</sub> se realiza a presiones medias (20-40 atm), y concentraciones de CO<sub>2</sub> altas (~40%) por lo que la penalización energética del proceso de separación es menor que en el caso de la separación posterior a la combustión. Sin embargo, hay que señalar que para el proceso de gasificación se usa O<sub>2</sub>, el cual hay que separar del aire por métodos criogénicos. Se estima una penalización energética en una planta de reformado de gas natural entre el 4% y el 11% y en la gasificación de carbón entre el 7% y el 13% [10].

#### *Combustión sin N<sub>2</sub> u oxicombustión*

Los sistemas de combustión sin nitrógeno (oxicombustión) utilizan oxígeno en lugar de aire para la combustión del combustible con objeto de producir un gas de combustión compuesto únicamente por vapor de agua y CO<sub>2</sub>. Esto da origen a una corriente con alta concentración de CO<sub>2</sub> y fácilmente separable del vapor de agua por condensación. Un esquema de este proceso se puede observar en la Figura 1.11.

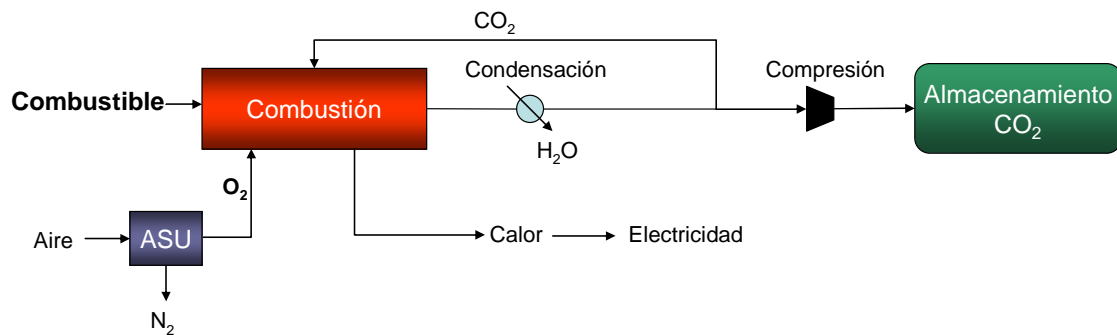


**Figura 1.11.** Captura de CO<sub>2</sub> por oxidación.

Además, al llevarse a cabo la combustión con O<sub>2</sub> se produciría un incremento muy elevado de la temperatura en la cámara de combustión. Para evitarlo se debe recircular CO<sub>2</sub> para rebajar la temperatura de combustión. El inconveniente de esta tecnología es el empleo de O<sub>2</sub> puro cuya producción tiene una importante penalización energética debida al proceso de separación del O<sub>2</sub> del aire. Se estima una pérdida de rendimiento alrededor del 6-9% para planta de carbón y entre 5 y 12% para plantas de gas natural [10].

### 1.2.2 Transporte de CO<sub>2</sub>

Antes del almacenamiento del CO<sub>2</sub> secuestrado, este debe pasar por una serie de etapas para su compresión y posterior transporte al punto de inyección. El CO<sub>2</sub> transportado variará en sus propiedades en función del tipo de proceso y del combustible usado. Estas propiedades incidirán directamente en los efectos sobre el material del ceoducto, principalmente las impurezas presentes, junto a la presión y temperatura del CO<sub>2</sub>. Por lo tanto, para determinar los materiales necesarios para el ceoducto es necesario conocer y establecer límites a los siguientes parámetros:

- Composición e impurezas.
- Presión.
- Temperatura.
- Viabilidad industrial de los materiales.
- Integración de las infraestructuras de transporte con las instalaciones de captura y las de almacenamiento.

Respecto a la composición e impurezas, ambos parámetros van a depender tanto de la tecnología de combustión como del combustible empleado. Por ejemplo, la concentración de oxígeno en dicha corriente variaría desde trazas si se utiliza tecnologías de pre-combustión hasta un 2% usando un proceso de oxicomcombustión [11]. A día de hoy, en la EU no existe ninguna especificación de la calidad mínima exigida para el transporte de CO<sub>2</sub>. No obstante el proyecto DYNAMIS ha realizado un estudio para especificar la calidad de una corriente de CO<sub>2</sub> para realizar un transporte y almacenamiento seguros. La composición de la corriente de CO<sub>2</sub> para cumplir estos requisitos se muestran en la Tabla 1.2 [12].

**Tabla 1.2.** Composición del CO<sub>2</sub> para cumplir con un transporte y almacenamientos seguro según el estudio DYNAMIS [12].

Compuesto	Concentración
H <sub>2</sub> O	500 ppm
H <sub>2</sub> S	200 ppm
CO	2000 ppm
O <sub>2</sub>	< 4%
CH <sub>4</sub>	< 4%
N <sub>2</sub>	< 4%
Ar	< 4%
H <sub>2</sub>	< 4%
SO <sub>x</sub>	100 ppm
NO <sub>x</sub>	100 ppm
CO <sub>2</sub>	> 95.5%

Una vez determinada la composición del CO<sub>2</sub> a transportar, se necesita conocer en qué condiciones de presión y temperatura debe ser transportado. Ambos parámetros van a depender del tipo de transporte elegido. Así, si se transporta el CO<sub>2</sub> por tubería, este deberá ser comprimido a presiones entre 100 y 200 bar, donde el CO<sub>2</sub> está en fase densa y se comporta como un líquido [11]. Por otro lado, en el transporte por barco el CO<sub>2</sub> debe ser licuado a -30°C y entre 15-20 bares de presión. Actualmente ya existen barcos para el transporte de CO<sub>2</sub> a pequeña escala para aplicaciones industriales y alimentarias [11], y por la tanto ya existe una reglamentación internacional para su transporte marítimo.

Respecto a los costes de ambos tipos de transporte, este va a depender de la distancia y de la escala del proyecto. A escala comercial, la cantidad de CO<sub>2</sub> a transportar variaría entre los 10 y 20 Mt por año en función de si la corriente procede de una gran central

térmica o del agrupamiento de varias fuentes de emisión. La Tabla 1.3 muestra los costes de transporte estimados para cada tecnología en función de la distancia.

**Tabla 1.3.** Estimación de costes (€/ton CO<sub>2</sub>) para redes a escala comercial en el transporte de 20 Mtpa de CO<sub>2</sub>, adaptada de [11].

Distancia (km)	180	500	750	1500
Tubería en tierra	1.5	3.7	5.3	-
Tubería en mar	3.4	6.0	8.2	16.3
Barco (incluida licuefacción)	11.1	12.2	13.2	13.1

Se puede observar que los costes de transporte por tubería son proporcionales a la distancia, a diferencia del transporte por barco donde estos costes son prácticamente fijos. Otra diferencia a tener en cuenta es que los principales costes asociados al transporte por tubería son debidos a costes de inversión (~90%) frente a los costes del transporte marítimo, donde principalmente los costes son operativos (>50%) [11]. Por lo tanto, para grandes distancias es recomendable el uso de transporte marítimo por barco usando una tecnología ya establecida y probada.

Respecto al transporte terrestre de CO<sub>2</sub> (*onshore*), existe una larga experiencia relacionada con la tecnología de Recuperación Mejorada de Petróleo (EOR). EEUU cuenta con la mayor red de transporte de CO<sub>2</sub>, transportando 45 Mt/año de CO<sub>2</sub> a lo largo de un entramado de unos 6300 km de ceoductos [11]. La región principal donde está instalada esta red de ceoductos se encuentra al oeste de Texas y Nuevo México, denominada Región *Permian Basin*. La línea de transporte más antigua data del año 1972, de 225 km de longitud (línea *Canyon Reef Carriers*, Texas), mientras que el ceoducto de mayor extensión es la línea Cortez con un total de 808 km [11].

### 1.2.3 Almacenamiento de CO<sub>2</sub>.

Finalmente, el último paso es el almacenamiento del CO<sub>2</sub> capturado. Hay diversas formas de almacenamiento, pero todas deben cumplir con unos criterios comunes. Estos criterios son:

- Seguridad: estabilidad en el almacenamiento, sin fugas. Duración del almacenamiento de siglos a milenios.

- Minimizar costes, incluido el transporte.
- Minimizar riesgos medioambientales y el impacto ambiental.
- Cumplir con la legislación vigente.

Para el almacenamiento de CO<sub>2</sub> se están estudiando principalmente dos opciones: almacenamiento geológico y el almacenamiento oceánico [2].

La capacidad global de almacenamiento de CO<sub>2</sub> depende del lugar elegido. Como se puede ver en la Tabla 1.4, la mayor capacidad de almacenamiento es el oceánico, seguido de los acuíferos salinos y los yacimientos de gas y petróleo usado. El principal problema del almacenamiento oceánico es el impacto ambiental que podría generar en las zonas donde se deposite, ya que al formarse carbonatos y bicarbonatos produce una bajada del pH de la zona. Debido a ello, este tipo de almacenamiento ha pasado a un segundo plano. Será necesario un mayor esfuerzo investigador en el tema para minimizar los posibles efectos que causaría este tipo de almacenamiento.

**Tabla 1.4.** Capacidad de almacenamiento de CO<sub>2</sub> de diferentes emplazamientos. Emisiones actuales ~ 27 Gt CO<sub>2</sub>/año

Opción	Capacidad (Gt CO <sub>2</sub> )
Océano	18000 – 7*10 <sup>7</sup>
Acuíferos salinos	1700 - 3700
Pozos agotados (gas y petróleo)	675 - 900
Pozos de carbón inexplorables	3 - 200

Actualmente la opción más viable de almacenamiento se considera que es en acuíferos salinos saturados a gran profundidad (800-900 m). El conocimiento de la tecnología necesaria para este tipo de almacenamiento proviene de la experiencia en su uso en el proceso “Enhanced Oil Recovery” (EOR) para la extracción mejorada de petróleo. Existen varios proyectos para su aplicación en el almacenamiento de CO<sub>2</sub>. La plataforma de Sleipner ha sido el primer proyecto a escala comercial dedicado al almacenamiento en un acuífero salino profundo de CO<sub>2</sub> (a 800m de profundidad). La plataforma de Sleipner está situada a 250 km al norte de la costa noruega en el Mar del Norte. De ella se extrae gas natural con alta concentración de CO<sub>2</sub> (alrededor del 9%). Desde 1996 se está inyectando en una formación salina de la propia plataforma del orden de 1 Mt de CO<sub>2</sub> al año, y en la cual se espera introducir alrededor de 20 Mt de

CO<sub>2</sub> durante su vida útil [13]. Por otro lado, el proyecto In Salah en Argelia, puesto en marcha en el año 2004, también almacenaba el CO<sub>2</sub> procedente de la extracción de gas natural. Se inyectaba, en un acuífero salino, hasta 4000 toneladas de CO<sub>2</sub> al día [14]. En la actualidad, el proceso de inyección ha concluido. Además existen dos proyectos de investigación donde se ha inyectado una cantidad pequeña de CO<sub>2</sub> en formaciones profundas: Frio en Texas, EE.UU. [15], y Minami-Nagaoka en Japón [16]. La Tabla 1.5 muestra un resumen de los proyectos de almacenamiento de CO<sub>2</sub> en acuíferos salinos, así como su estado actual y la capacidad de almacenamiento. Como se puede observar, a parte de Sleipner, se han iniciado otros proyectos a escala comercial en los últimos años como son los de Gorgon (Australia) y Snohvit (Noruega), así como ensayos piloto o demostración.

**Tabla 1.5.** Proyectos de almacenamiento de CO<sub>2</sub> en acuíferos salinos profundos [17].

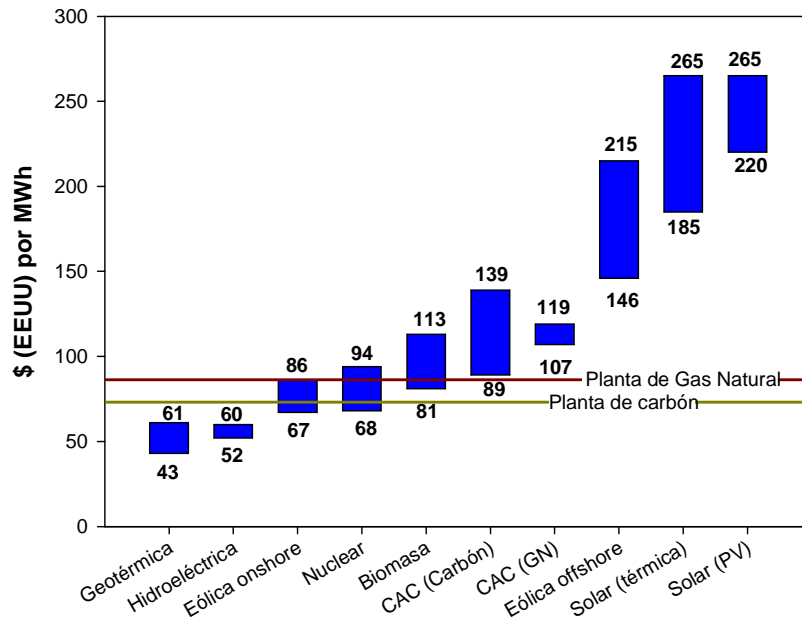
Proyecto	País	Escala	Estado	Fecha de inicio y conclusión	Capacidad total (Mt de CO <sub>2</sub> )
Sleipner	Noruega	Comercial	Existente	1996	20
In Salah	Argelia	Comercial	Finalizado	2004-2012	17
Ketzin	Alemania	Demostración	Existente	2007	0.06
Snohvit	Noruega	Comercial	Existente	2007-8	---
Minami-Nagaoka	Japón	Demostración	Finalizado	2002	0.01
Frio	EE.UU.	Piloto	Finalizado	2004-6	3·10 <sup>-6</sup>
Teapot Dome	EE.UU.	Demostración	Existente	2006	0.01
Gorgon	Australia	Comercial	Existente	2009-11	---
Otway	Australia	Piloto	Existente	2007	0.1

### 1.3 Impacto de la implementación de los procesos CAC en la generación de energía

En el apartado 1.2.1 se han mostrado las diferentes vías de captura de CO<sub>2</sub>. Sin embargo todas ellas presentan una importante disminución en la eficacia energética, así como un aumento significativo de los costes de generación de energía. Además, la captura del CO<sub>2</sub> supone el coste principal de la CAC, ya que el coste del transporte (entre 5 y 11 €/ton CO<sub>2</sub>) y el almacenamiento (1 a 15 €/ton CO<sub>2</sub>) son una parte relativamente pequeña del coste total [18]. La introducción de las tecnologías de CAC en la generación de electricidad obviamente tiene un coste económico adicional. Sin embargo, se considera que una vez superadas las fases de desarrollo y demostración de los procesos CAC, estos serán competitivos con otras tecnología de bajo contenido en carbono [19]. La

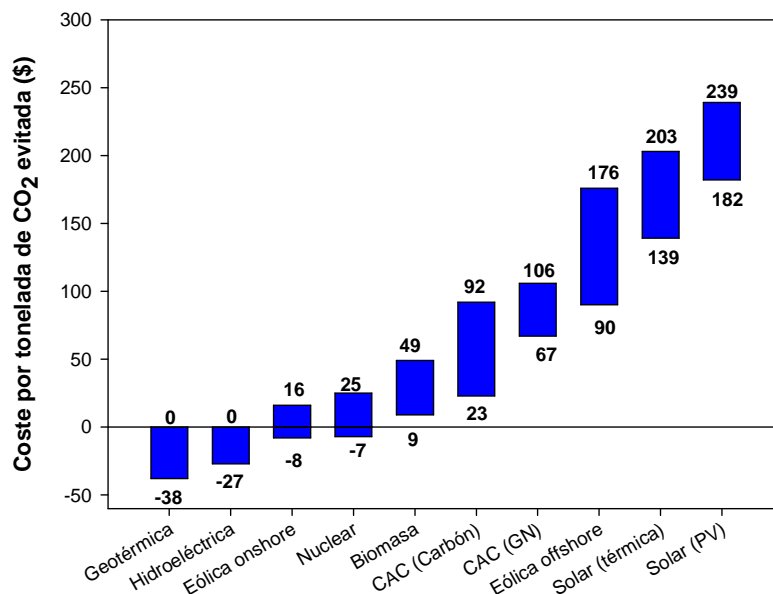


Figura 1.12 muestra los costes por MWh para las diferentes tecnologías bajas en carbono.



**Figura 1.12.** Costes de generación de electricidad por MWh para diferentes tecnologías bajas en carbono [19]. Líneas continuas: planta de gas natural y de carbón sin tecnologías CAC.

Aunque estos costes pueden variar de un país a otro, se puede observar que las tecnologías de producción de energía con sistemas CAC pueden generar energía a un coste competitivo comparado con otras tecnologías de producción de energía con bajo contenido en carbono como son la eólica *offshore* o energía solar tanto térmica como fotovoltaica.



**Figura 1.13.** Costes de CO<sub>2</sub> evitado. En todos los casos, excepto en el de CAC (GN), la cantidad de CO<sub>2</sub> evitado es relativo a las emisiones de una planta de carbón pulverizado supercrítica. Para CAC (GN), la planta de referencia es planta de ciclo combinado [19].

La Figura 1.13 compara los costes del CO<sub>2</sub> evitado usando distintas tecnologías para la obtención de energía con bajas emisiones en carbono en comparación con plantas de generación de energía con combustibles fósiles integradas junto a un sistema CAC [19]. Se puede observar que las tecnologías de CAC podrían tener unos costes aceptables en función del precio del combustible. El precio del combustible es fundamental para saber cuál será el futuro coste por tonelada de CO<sub>2</sub> evitada. Por ejemplo para una planta de carbón pulverizado supercrítico mejorada con sistemas CAC, dicho coste varía entre 23 y 92 \$ por tonelada de CO<sub>2</sub> evitada. En el caso de una planta de gas natural con ciclo combinado con sistemas CAC, los costes varían entre 67 y 106 \$ por tonelada de CO<sub>2</sub> evitada. Se puede observar que los costes por tonelada de CO<sub>2</sub> evitada son inferiores usando carbón como combustible en comparación con el gas natural y a la vez, ambos son inferiores a los costes de usar energía solar (tanto térmica como fotovoltaica) o energía eólica *offshore*.

Como se ha visto en la Figura 1.4 el carbón es el combustible fósil con mayores reservas probadas y estimadas, además de ser un combustible principalmente usado para la generación de electricidad (ver Figura 1.8). Por lo tanto, es una fuente concentrada de generación de CO<sub>2</sub>, donde los sistemas CAC son más factibles de implementar. La captura de CO<sub>2</sub> en plantas térmicas de carbón se puede llevar a cabo con las tres tecnologías presentadas en el apartado 1.2.1: post-combustión, pre-combustión y oxicombustión. La Figura 1.14 muestra los costes por tonelada de CO<sub>2</sub> evitada usando los tres sistemas CAC para una planta térmica de carbón (antracita), usando para los cálculos un precio medio del carbón de 2.4 €/GJ [20]. Como se puede observar, no existen a priori datos para descartar o favorecer ninguna de las tecnologías. Por lo tanto, se está desarrollando la demostración a escala industrial de las tres tecnologías de captura de CO<sub>2</sub>. Se puede observar que el coste de usar tecnologías de pre-combustión es mayor que en el caso de la post-combustión. Esto es debido a que la obtención de electricidad a partir de la tecnología de pre-combustión está menos desarrollada y, por tanto, los cálculos de costes son más conservadores. De todas formas, hay una necesidad evidente de realizar un esfuerzo para reducir costes en la tecnología de oxicombustión, principalmente en el proceso de separación de aire [20].

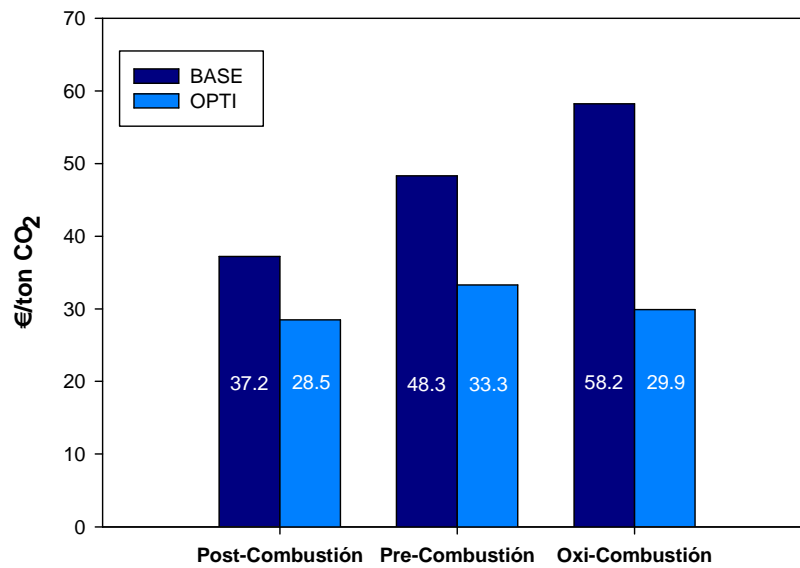


**Figura 1.14.** Costes de CO<sub>2</sub> evitado para una planta de carbón (antracita) con diferentes sistemas de captura de CO<sub>2</sub> [20]. BASE: planta de energía con tecnologías actuales de CAC; OPTI: planta de energía optimizada para usar tecnologías CAC.

Respecto a las tecnologías de oxidcombustión, aunque muestran un coste por tonelada de CO<sub>2</sub> evitada muy similar a los obtenidos con tecnologías post-combustión (caso OPTI), se estima que el coste eléctrico es ligeramente inferior para una planta de generación de energía optimizada para el uso de tecnologías CAC (63 €/MWh frente a los 67.2 €/MWh de la post-combustión) [20]. Por lo tanto, es la tecnología que potencialmente representa la opción más económica de las tres. Sin embargo, al ser la tecnología más joven, necesita de un gran esfuerzo investigador y económico para ponerla a punto y reducir los actuales costes. Por estos motivos se están investigando nuevos procesos de captura de CO<sub>2</sub> para reducir la penalización energética y los costes de captura de CO<sub>2</sub>.

Dentro de los sistemas de combustión sin nitrógeno (oxidcombustión), se ha propuesto el proceso de combustión indirecta o *Chemical Looping Combustion* (CLC) [21, 22] como una alternativa viable a la producción de energía con captura de CO<sub>2</sub>. Este es el proceso en el cual se centra esta Tesis Doctoral. Este proceso tiene menor coste de captura que cualquier otro proceso evaluado, ya sea post-, pre- u oxidcombustión. De hecho, se estima que para el proceso CLC, el coste por tonelada de CO<sub>2</sub> evitada es de 6-13 €, frente a los 28-37 € para una central de ciclo combinado con gasificación integrada, o 29-58 € para el proceso de oxidcombustión [23].

## 1.4 Combustión con transportadores sólidos de oxígeno: *Chemical Looping Combustion (CLC)*

El proceso CLC se basa en realizar la transferencia de oxígeno del aire al combustible por medio de un transportador de oxígeno en forma de óxido metálico ( $Me_xO_y$ ), sin poner en ningún momento en contacto el combustible con el aire. Para ello, se utilizan dos reactores de lecho fluidizado interconectados, como se muestra en la Figura 1.15 [24], con el transportador de oxígeno circulando continuamente entre ellos. Esta configuración, que es similar a la existente en una caldera de lecho fluidizado circulante (CFB), permite un buen contacto sólido-gas y una circulación adecuada del transportador sólido de oxígeno entre ambos reactores.

En el caso de usar el sistema CuO/Cu como transportador de oxígeno y  $CH_4$  como combustible, el proceso que tiene lugar es el siguiente. En el reactor de reducción, Ecuación 1.1, el óxido metálico (CuO) se reduce a metal (Cu) por reacción con el combustible. Al oxidarse el combustible se genera únicamente  $CO_2$  y vapor de agua, fácilmente separables por condensación, quedando una corriente gaseosa de  $CO_2$  lista para su transporte y almacenamiento. En el reactor de oxidación, Ecuación 1.2, el transportador de oxígeno reducido (Cu) se regenera oxidándose a CuO con el oxígeno del aire y obteniéndose a la salida una corriente de  $N_2$ , junto con  $O_2$  si se ha introducido aire en exceso.

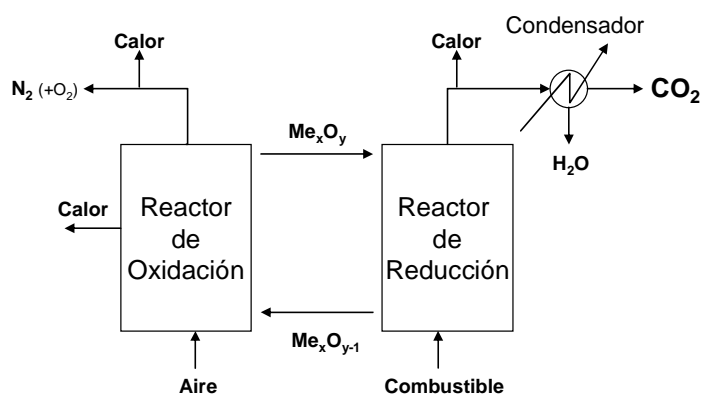
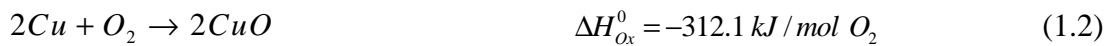


Figura 1.15. Esquema conceptual del proceso CLC

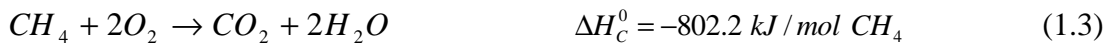
### Reacción de Reducción



### Reacción de Oxidación



### Combustión directa



La energía generada en la combustión es equivalente a la obtenida en la combustión convencional, ya que la suma estequiométrica de las entalpías de reacción de las dos reacciones (1.1 y 1.2) es la correspondiente a la de la combustión directa (1.3). Este sistema tiene una baja penalización energética debido a que no existe la separación de CO<sub>2</sub> de ningún otro gas (excepto el H<sub>2</sub>O). Esta es la principal ventaja del sistema CLC frente a cualquier otro sistema de captura de CO<sub>2</sub> (absorción química, física, sistemas de adsorción, etc.).

Se han realizado diferentes estudios que avalan la viabilidad de este proceso con distintos prototipos en plantas de CLC tanto con combustibles gaseosos (CH<sub>4</sub>, gas de síntesis, etc.) en un intervalo de potencia entre 10 y 140 kW<sub>t</sub>, como con combustibles sólidos (carbón y biomasa) en plantas de entre 10 kW<sub>t</sub> y 3 MW<sub>t</sub>, usando óxidos de diferentes metales como transportadores de oxígeno (Ni, Cu, Fe, Co o Mn) [23].

#### 1.4.1 Transportadores sólidos de oxígeno

El concepto de combustión con transportadores sólidos de oxígeno se fundamenta en el uso de la tecnología existente de lechos fluidizados circulantes (CFB). Sin embargo, existe un factor clave para el desarrollo del proceso: el transportador sólido de oxígeno. Las partículas del transportador sólido de oxígeno tienen que cumplir unos requisitos sin los cuales no es operativo. Estos son los siguientes:

- Posibilidad de lograr un elevado grado de combustión a CO<sub>2</sub> y H<sub>2</sub>O (idealmente combustión completa) por consideraciones termodinámicas.
- Reactividad elevada y mantenida a través de los ciclos, tanto en la reacción de reducción como en la de oxidación, para reducir la cantidad de sólido necesario en los reactores y la renovación del material.

- Elevada capacidad de transporte de oxígeno, para reducir la cantidad de sólido circulante.
- Resistencia a la atrición para evitar la pérdida de sólido por elutriación y la renovación del material.
- Baja o nula tendencia a la deposición de carbono.
- Ser resistente a la desactivación por compuestos de azufre.
- No presentar problemas de defluidización o aglomeración durante la reacción.
- Ser seguro medioambientalmente.
- Fácil de preparar si es sintético y abundante si es natural o un residuo, para reducir costes.
- Tamaño de partícula adecuado para su uso en lechos fluidizados.

Las dos primeras características van a depender intrínsecamente del sistema redox utilizado. Los compuestos activos propuestos para el proceso CLC son los óxidos de hierro, cobre, cobalto, níquel y manganeso, junto al sulfato de calcio [23]. El análisis termodinámico de los diferentes sistemas redox propuestos muestra la relación de productos que se puede obtener. Así, con los sistemas CuO/Cu, Mn<sub>3</sub>O<sub>4</sub>/MnO, Fe<sub>2</sub>O<sub>3</sub>/Fe<sub>3</sub>O<sub>4</sub> y Co<sub>3</sub>O<sub>4</sub>/CoO se puede obtener combustión completa a CO<sub>2</sub> y H<sub>2</sub>O en las condiciones de operación del proceso CLC. Para transportadores basados en el NiO se obtendrán como máximo conversiones del gas del 99-99.5% con pequeñas cantidades de CO y H<sub>2</sub> que no se pueden convertir [23].

Cuando se utiliza un óxido metálico puro, en muchos casos la reactividad disminuye rápidamente con el número de ciclos. Por esta razón se utilizan mezclados con un material inerte [25]. Además, de esta forma se aumenta la resistencia mecánica de los materiales y su superficie de reacción. Incluso en algunos materiales mejora la conductividad iónica del oxígeno. La capacidad de transporte de un óxido metálico se define como:

$$R_o = \frac{m_{ox} - m_{red}}{m_{ox}} \quad (1.4)$$

donde  $m_{ox}$  es la masa del material totalmente oxidado y  $m_{red}$  es la masa en su forma reducida. Cuando se añade un material inerte al transportador de oxígeno, su capacidad de transporte disminuye, ya que para la misma cantidad de transportador de oxígeno es

menor la cantidad de oxígeno disponible para el proceso. Por lo tanto, la capacidad de transporte de oxígeno efectiva ( $R_{TO}$ ) es la siguiente:

$$R_{TO} = R_O * x_{MeO} \quad (1.5)$$

donde  $x_{MeO}$  es la fracción de óxido metálico activo en el transportador de oxígeno. Los materiales generalmente usados como inertes son:  $Al_2O_3$ ,  $MgAl_2O_4$ ,  $ZrO_2$ ,  $TiO_2$ ,  $NiAl_2O_4$ ,  $SiO_2$  y sepiolita. Adánez y col. [23] realizaron una exhaustiva recopilación de los transportadores de oxígeno usados en el proceso de CLC.

El coste y las características medioambientales dependen también del óxido metálico utilizado. Respecto a la toxicidad de los diferentes materiales, tanto el níquel como el cobalto son considerados como los más problemáticos. Por otro lado, son los materiales con un mayor coste económico. Por otra parte, los compuestos de hierro son considerados no tóxicos para aplicaciones del proceso CLC [23]. El cobre y el manganeso únicamente presentan problemas en disolución. Respecto al cobre, García-Labiano y col. [26] realizaron un estudio sobre el tratamiento de residuos de transportadores de oxígeno basados en óxido de cobre procedentes de una planta de CLC. En este estudio se llegó a la conclusión de que el residuo final tras el proceso de recuperación puede ser calificado como residuo estable y no reactivo y aceptable para depositar en vertederos para residuos no peligrosos.

Respecto al resto de propiedades, estas deben de ser caracterizadas experimentalmente para cada material usado. La velocidad de atrición es uno de los parámetros más importantes, ya que está directamente relacionada con el tiempo de vida medio de las partículas en el sistema CLC. Se considera atrición a la formación de finos debido al estrés físico-químico al que se ven sometidas las partículas en un lecho fluidizado circulante como el CLC utilizado en el proceso. Estas partículas son elutriadas fuera del sistema debido a que por su pequeño tamaño no son recogidas por los ciclones [27]. Finalmente, la aglomeración de las partículas de un transportador de oxígeno debe ser evitada en un sistema de dos lechos fluidizados interconectados, ya que ésta perturba la circulación de sólidos entre los reactores y además puede generar canales de paso preferente del gas, empeorando el contacto entre el gas reactante y el transportador de oxígeno.

### 1.4.2 CLC con combustibles sólidos

El sistema CLC fue desarrollado inicialmente para la utilización de combustibles gaseosos, principalmente gas natural [23, 28]. Sin embargo, el uso de combustibles sólidos es muy conveniente ya que estos combustibles, como se ha visto en la Figura 1.4, son más abundantes en la naturaleza y, por lo tanto, más baratos. Además, este tipo de combustibles son los que más contribuyen a las emisiones de  $\text{CO}_2$ . Por lo tanto, se hace muy interesante el desarrollo de una tecnología CLC que permita el uso de carbón como combustible.

Para poder utilizar este tipo de combustibles en un sistema CLC hace falta su gasificación previa, ya que es necesario que el combustible esté en forma gaseosa para su oxidación por reacción con el transportador de oxígeno. Existen dos opciones para realizar esta operación integrada al proceso CLC: gasificación previa o in situ.

En el caso de la gasificación previa, es necesaria la utilización de un reactor externo al sistema CLC que gasifique el combustible para que este pueda ser empleado en el proceso. El agente gasificante debería ser una mezcla de  $\text{O}_2$ /vapor de agua, por lo que es necesaria una unidad de separación de aire, lo cual encarece el proceso de captura de  $\text{CO}_2$ . Como se puede ver en la Figura 1.16 el gas de síntesis producido se alimenta al reactor de reducción donde se quema por el transportador de oxígeno en una reacción directa gas-sólido para generar una corriente de salida de vapor de agua y  $\text{CO}_2$ .

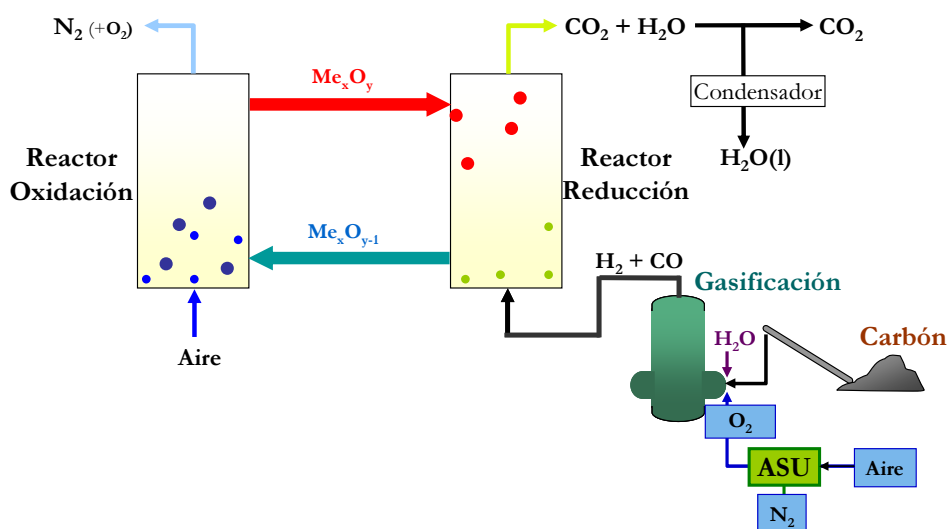
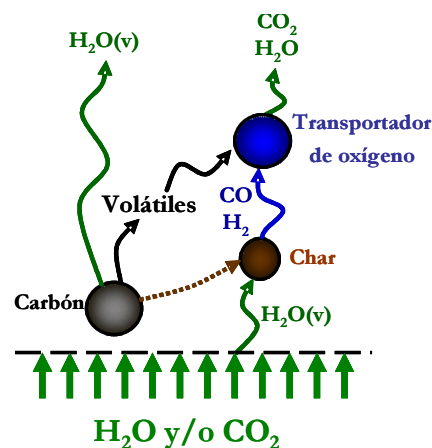


Figura 1.16. Proceso de combustión en un sistema CLC con gasificación previa del combustible sólido.



La otra opción corresponde al proceso CLC con gasificación *in-situ* (*iG-CLC*) donde se realizan ambos procesos en el mismo reactor [29, 30]. La característica principal del proceso *iG-CLC* es la gasificación del combustible sólido en el reactor de reducción. En este proceso, se alimenta el combustible sólido directamente al reactor de reducción junto al agente gasificante necesario. En este caso se puede utilizar  $H_2O$  o mezclas  $H_2O/CO_2$  recirculado para la fluidización, que además actuaran como agentes gasificantes. Como se puede ver en la Figura 1.17, al alimentar el combustible al reactor de reducción, éste se desvolatiliza produciendo una corriente de volátiles y un residuo carbonoso o char. Los volátiles producidos reaccionan directamente con el transportador de oxígeno en una reacción convencional gas-sólido; sin embargo, la reacción sólido-sólido entre el char y el transportador de oxígeno es lenta y por lo tanto hay que gasificarlo para que la reacción se lleve a cabo en un intervalo de tiempo razonable. Para ello, se puede utilizar una mezcla de  $CO_2/H_2O$  que gasifica el char. Los productos gaseosos de la gasificación ( $CO + H_2$ ) se queman al igual que los volátiles con el transportador de oxígeno. La principal ventaja de este proceso frente al de CLC con gasificación separada, es que no se requiere el uso de  $O_2$  puro ya que la energía necesaria para la gasificación o se genera *in-situ* por la oxidación del  $CO$  y del  $H_2$  con el transportador de oxígeno, o la transfiere el transportador de oxígeno como calor sensible desde el reactor de oxidación.



**Figura 1.17.** Proceso de combustión en el reactor de reducción en un proceso *iG-CLC* con gasificación del combustible *in-situ*.

El principal inconveniente de este proceso es la lenta gasificación del combustible en el del reactor de reducción, que provoca que parte del char sin reaccionar sea transferido al reactor de oxidación, donde se quema en contacto con el aire, generando  $CO_2$  en la

corriente de salida de este reactor. De este modo se pierde eficacia a la hora de capturar  $\text{CO}_2$  por parte del sistema. Para solucionarlo, es necesario el aumento del tiempo de residencia en el reactor de reducción, lo que supone una mayor cantidad de transportador de oxígeno en el sistema y, por lo tanto, más coste de material y mayor tamaño de las instalaciones necesarias. Otra posible solución es la instalación de un sistema de separación de carbono entre el reactor de reducción y el reactor de oxidación, que permita separar selectivamente el char no gasificado del transportador de oxígeno reducido. Este char separado es recirculado al reactor de reducción, aumentando su tiempo de residencia y permitiendo su gasificación. El uso de un *carbon stripper*, propuesto por Cao y Pan en 2006 [29], como sistema de separación de carbono ha demostrado ser muy efectivo para aumentar la eficacia de captura de  $\text{CO}_2$  del sistema [31].

Por otro lado, las unidades *iG-CLC* operadas hasta la fecha han demostrado la presencia de gases inquemados a la salida del reactor de reducción [32]. Estos productos inquemados pueden causar problemas a la hora del transporte y almacenamiento del  $\text{CO}_2$  [33]. Existen diferentes soluciones sugeridas para eliminar los gases inquemados de la corriente de salida: instalar un segundo reactor de reducción, recircular los gases de salida de nuevo dentro del reactor de reducción o instalar un reactor de *oxygen polishing* [32]. Esta última opción consiste en instalar un reactor corriente abajo del reactor de reducción para quemar por completo los inquemados con una corriente pura de  $\text{O}_2$ .

Finalmente, debido a la presencia de cenizas mezcladas con el transportador de oxígeno, se prefiere el uso de materiales de precios reducidos, ya sean minerales (ilmenita, hematita) o residuos de otros procesos industriales (residuo de bauxita) [34] más baratos que los materiales sintéticos, debido a que es necesaria una extracción continua de las cenizas que van acompañadas del transportador de oxígeno. No obstante, estos materiales suelen ser menos reactivos que los sintéticos.

## 1.5 Chemical Looping with Oxygen Uncoupling (CLOU)

El proceso *iG-CLC* conlleva sustanciales ventajas frente al proceso CLC con gasificación previa. No obstante, tiene dos inconvenientes: la baja velocidad de conversión del char durante la gasificación y la dificultad para obtener combustión completa. Para aumentar la velocidad de conversión del char en el reactor de reducción y la eficacia de combustión se propuso el proceso *Chemical Looping with Oxygen Uncoupling* (CLOU) [35], que trata de aprovechar la capacidad de algunos óxidos metálicos de generar  $O_2$  gaseoso a alta temperatura de forma reversible. En la Figura 1.18 se puede observar el proceso de combustión que se lleva a cabo en el reactor de reducción en el proceso CLOU. En este proceso se alimenta directamente el combustible sólido en el reactor de reducción y al mismo tiempo el transportador de oxígeno libera  $O_2$  en las condiciones de operación de ese reactor.

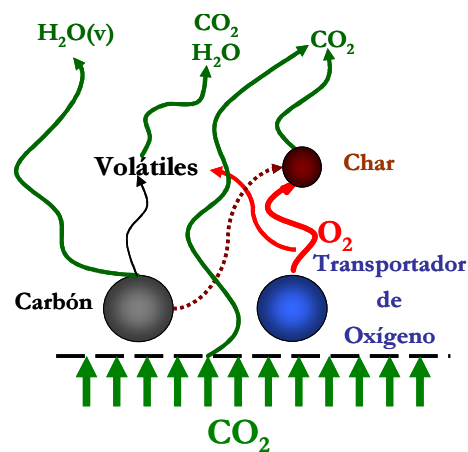


**Figura 1.18.** Proceso de combustión en el reactor de reducción en un proceso CLOU.

En el proceso CLOU la oxidación del combustible sólido ocurre en dos pasos. Primero el transportador de oxígeno se descompone y libera oxígeno gaseoso según la Ecuación (1.6):



A continuación, el combustible reacciona con el oxígeno, como en una combustión convencional, para producir  $CO_2$  y  $H_2O$ , según la Ecuación (1.7):



El transportador reducido en el reactor de reducción es transportado al reactor de oxidación, donde reacciona con el oxígeno del aire, Ecuación (1.8):



El proceso CLOU tiene las mismas ventajas que el proceso CLC. De este modo, la entalpía total desprendida en los reactores de reducción y oxidación es la misma que en una combustión convencional. También el CO<sub>2</sub> y el H<sub>2</sub>O están separados inherentemente del N<sub>2</sub> del aire, por lo que no hay gasto energético de separación.

Los transportadores de oxígeno para el proceso CLOU deben tener unas características especiales necesarias para reaccionar de forma reversible con el oxígeno a alta temperatura, de forma que sean capaces de liberar oxígeno en el reactor de reducción y recuperarlo en el reactor de oxidación. El proceso se basa en el uso del equilibrio redox de descomposición de algunos óxidos metálicos ( $Me_xO_y \leftrightarrow Me_xO_{y-1} + \frac{1}{2}O_2$ ) para generar O<sub>2</sub> a alta temperatura, entre 800 y 1200 °C, y posteriormente regenerarse con aire. Se han identificado tres sistemas de óxidos metálicos que presentan estas características: CuO/Cu<sub>2</sub>O, Mn<sub>2</sub>O<sub>3</sub>/Mn<sub>3</sub>O<sub>4</sub>, y Co<sub>3</sub>O<sub>4</sub>/CoO [35].

En la Figura 1.19 se muestran la concentración de oxígeno en equilibrio en función de la temperatura para los tres sistemas redox considerados para el proceso CLOU.

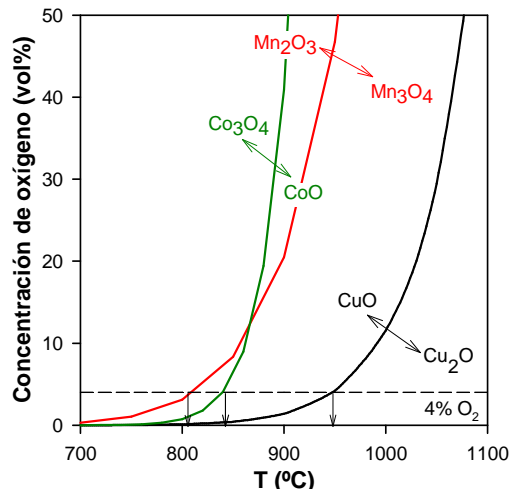


**Figura 1.19.** Concentración de O<sub>2</sub> en el equilibrio para los sistemas CuO/Cu<sub>2</sub>O, Mn<sub>2</sub>O<sub>3</sub>/Mn<sub>3</sub>O<sub>4</sub>, y Co<sub>3</sub>O<sub>4</sub>/CoO en función de la temperatura [37].

Un punto clave del proceso es la temperatura de operación del reactor de oxidación para poder conseguir un máximo aprovechamiento del aire utilizado. En principio, podemos suponer que se use un 20% de exceso de aire, de forma similar a las calderas convencionales de combustión de carbón, lo que supone que la concentración de O<sub>2</sub> a la salida del reactor de oxidación es del 4%. La temperatura necesaria para obtener esta

concentración a la salida del reactor de oxidación varía en función del sistema de óxido metálico utilizado.

En el caso del sistema CuO/Cu<sub>2</sub>O esta concentración se obtiene sobre los 950 °C. Sin embargo, para el sistema Mn<sub>2</sub>O<sub>3</sub>/Mn<sub>3</sub>O<sub>4</sub> habría que descender hasta los 815 °C y a los 840 °C en el sistema Co<sub>3</sub>O<sub>4</sub>/CoO, para obtener la misma concentración a la salida del reactor de oxidación. Por otro lado, la temperatura de operación en el reactor de reducción debe de ser suficientemente alta para obtener una alta velocidad de descomposición, ya que esta depende tanto de la constante de reacción como de la concentración de oxígeno en equilibrio, siendo esta más elevada cuanto más alta sea la temperatura. La Tabla 1.6 muestra la ventana de operación en un sistema CLOU con los diferentes transportadores de oxígeno propuestos. Como se puede observar la diferencia de temperaturas entre ambos reactores es mayor en el sistema Mn<sub>2</sub>O<sub>3</sub>/Mn<sub>3</sub>O<sub>4</sub> y Co<sub>3</sub>O<sub>4</sub>/CoO que en el CuO/Cu<sub>2</sub>O. Aunque estas diferencias de temperaturas son asumibles en un sistema CLOU [35], dificulta la integración energética entre ambos reactores. Es más conveniente trabajar con el sistema CuO/Cu<sub>2</sub>O, cuya integración energética es más sencilla debido a la menor diferencia de temperatura entre reactores.

**Tabla 1.6.** Ventana de operación en cada reactor para los diferentes transportadores de oxígeno propuestos para el proceso CLOU.

Transportador de oxígeno	Temperatura RR (°C)	Temperatura RO (°C)
CuO/Cu <sub>2</sub> O	900-950	900-950
Mn <sub>2</sub> O <sub>3</sub> /Mn <sub>3</sub> O <sub>4</sub>	850-900	800-825
Co <sub>3</sub> O <sub>4</sub> /CoO	850-900	825-840

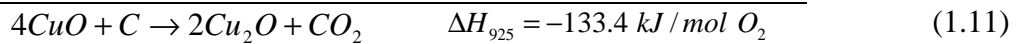
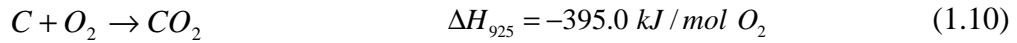
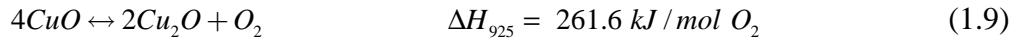
Respecto a la capacidad de transporte de oxígeno de los diferentes sistemas de óxidos metálicos, la capacidad de transporte de oxígeno es muy distinta para los tres sistemas redox considerados; ver Tabla 1.7. La capacidad de transporte de oxígeno del sistema Mn<sub>2</sub>O<sub>3</sub>/Mn<sub>3</sub>O<sub>4</sub> y del sistema Co<sub>3</sub>O<sub>4</sub>/CoO son un 33% y 66%, respectivamente, respecto a la capacidad del sistema CuO/Cu<sub>2</sub>O. Por lo tanto este último sistema redox es más atractivo para el proceso CLOU, ya que es necesaria menos cantidad de material para transportar la misma cantidad de oxígeno.

**Tabla 1.7.** Capacidad de transporte de oxígeno para los distintos pares redox en el proceso CLOU.

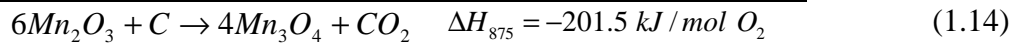
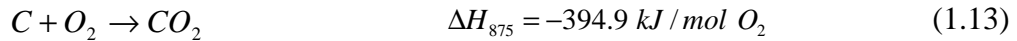
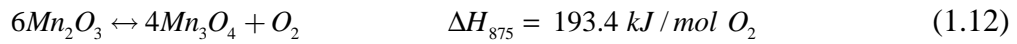
Transportador de oxígeno	g O <sub>2</sub> /100 g material
CuO/Cu <sub>2</sub> O	10
Mn <sub>2</sub> O <sub>3</sub> /Mn <sub>3</sub> O <sub>4</sub>	3.3
Co <sub>3</sub> O <sub>4</sub> /CoO	6.6

Finalmente, las siguientes reacciones muestran la entalpía de reacción de los tres sistemas redox propuestos. Se muestran tanto las reacciones de descomposición, como la reacción global de combustión en el reactor de reducción para la combustión de carbono en la ventana de operación propuesta anteriormente.

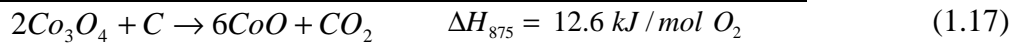
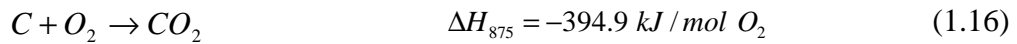
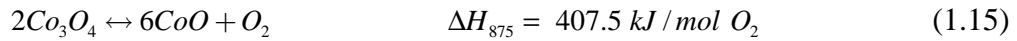
**CuO/Cu<sub>2</sub>O**



**Mn<sub>2</sub>O<sub>3</sub>/Mn<sub>3</sub>O<sub>4</sub>**



**Co<sub>3</sub>O<sub>4</sub>/CoO**



Con los tres metales, las reacción de liberación de oxígeno es endotérmica (R.1.9, R.1.12 y R.1.15). No obstante, al añadir la reacción de combustión, la reacción global en el reactor de reducción es exotérmica en los sistemas CuO/Cu<sub>2</sub>O y Mn<sub>2</sub>O<sub>3</sub>/Mn<sub>3</sub>O<sub>4</sub> (R.1.11 y R.1.14), pero es endotérmica para el sistema Co<sub>3</sub>O<sub>4</sub>/CoO (R. 1.17). La integración energética en el sistema CLOU determinará las temperaturas a la que deben operar ambos reactores para que el sistema sea estable y depende de si la reacción en el reactor de reducción es exotérmica o endotérmica. Si la reacción que tiene lugar en el reactor de reducción es exotérmica, es posible aumentar la temperatura de operación del reactor de reducción y elevar así la concentración de O<sub>2</sub> en el equilibrio, aumentando la velocidad de conversión del combustible. La integración energética obliga a extraer calor del reactor de oxidación y de esta forma se puede elegir una temperatura de operación inferior en el reactor de oxidación, lo que maximiza el aprovechamiento del aire introducido para la regeneración del transportador de oxígeno. Por lo tanto el

sistema deberá operar a diferentes temperaturas en el reactor de reducción y en el reactor de oxidación, para aprovechar las propiedades del equilibrio de descomposición-regeneración, como se ha visto con la Figura 1.19.

El desarrollo del proceso CLOU comenzó en el año 2009 con los trabajos de Mattisson y col. [35, 36] y se ha realizado de forma paralela a esta Tesis Doctoral. Ese año se publicaron los primeros trabajos sobre transportadores de oxígeno con propiedades CLOU, basados tanto en el óxido de cobre como en óxidos de manganeso [35, 36, 38-40]. Mattisson y col. estudiaron el proceso CLOU con transportadores de oxígeno de cobre soportados sobre  $ZrO_2$  o  $Al_2O_3$  en un reactor de lecho fluidizado discontinuo usando como combustible  $CH_4$  y coque de petróleo. En estos trabajos se obtuvo que la conversión de char en el proceso CLOU puede llegar a ser 2 órdenes de magnitud más rápida que en el proceso *i*G-CLC [35, 36]. Por otro lado, también se llevó a cabo el estudio de transportadores de oxígeno basados en óxidos de manganeso [39], y de una espinela de calcio-manganeso,  $CaMnO_3$  [40]. Ambos se analizaron en un reactor de lecho fluidizado discontinuo con  $CH_4$  y coque de petróleo, obteniéndose peores resultados que con los transportadores de óxido de cobre.

Debido a su mayor facilidad de integración energética entre reactores y su alta capacidad de transporte de oxígeno, se ha seleccionado el sistema  $CuO/Cu_2O$  en esta Tesis Doctoral como el más adecuado para su uso en el proceso CLOU.

Los prometedores resultados iniciales en el proceso CLOU han promovido el interés de varios equipos de investigación en el desarrollo de nuevos materiales con propiedades adecuadas para su uso como transportadores de oxígeno en el proceso CLOU. A día de hoy, hay unas 40 publicaciones focalizadas en el desarrollo y evaluación de transportadores de oxígeno para CLOU. Los estudios se centran en el análisis de la reactividad de los materiales tanto en TGA como en reactores de lecho fluidizado discontinuo, usando combustibles gaseosos ( $CH_4$ , gas de síntesis) o combustibles sólidos (diferentes tipos de carbones, char, coque o biomasa). La Tabla 1.8 muestra un resumen de los transportadores de oxígeno basados en óxido de cobre, existentes en la literatura para el proceso CLOU, clasificados por el contenido en  $CuO$ , el material utilizado como soporte y el método de producción.

**Tabla 1.8.** Transportadores de oxígeno basados en CuO para el proceso CLOU de la literatura hasta 2014.

CuO (%)	Otro Metal (%)	Material de soporte	Método prep. <sup>a</sup>	Combustible <sup>b</sup>	Instalación laboratorio <sup>c</sup>	Año, Ref.
5-87			Mineral	---	TGA, LFD	2012, [41]
21			Mineral	A	LFD	2014, [42]
100			n.d.	n.d.	TGA	2011, [43]
60	Fe <sub>2</sub> O <sub>3</sub>		SD	CH <sub>4</sub> , GS	LFD	2013-14, [44, 45]
40	Fe <sub>2</sub> O <sub>3</sub> (41)+Mn <sub>2</sub> O <sub>4</sub> (19)		SD	CH <sub>4</sub> , GS	LFD	2013-14, [44, 45]
31	Mn <sub>2</sub> O <sub>3</sub>		E	CH <sub>4</sub>	LFD	2013, [46]
5-61	Mn <sub>2</sub> O <sub>3</sub>		FG	CB	LFD	2013, [47]
70-90		Al <sub>2</sub> O <sub>3</sub>	CP	---	TGA	2014, [48]
60		Al <sub>2</sub> O <sub>3</sub>	FG	CH <sub>4</sub> , CP	LFD	2009, [36]
60		Al <sub>2</sub> O <sub>3</sub> ,	I, E	---	TGA	2011-12, [49]
40		Al <sub>2</sub> O <sub>3</sub>	SD	CH <sub>4</sub>	LFD	2011, [50]
30-53		Al <sub>2</sub> O <sub>3</sub>	CP	CO	LFD	2013, [51]
36	Fe <sub>2</sub> O <sub>3</sub> (40)	Al <sub>2</sub> O <sub>3</sub>	SD	CH <sub>4</sub> , GS	LFD	2013-14, [44, 45]
60		CeO <sub>2</sub>	E	CH <sub>4</sub> , GS		2012, [52]
40		CeO <sub>2</sub>	SD	CH <sub>4</sub> , GS, GN	LFD	2013-14, [44, 45]
40		CeO <sub>2</sub> +La <sub>2</sub> O <sub>3</sub>	SD	CH <sub>4</sub> , GS	LFD	2013-14, [44, 45]
n.d.		CeO <sub>2</sub>	CP	CH <sub>4</sub>	TGA, LFD	2012, [53]
60		Ce <sub>0.9</sub> Gd <sub>0.1</sub> O <sub>1.9</sub>	E	CH <sub>4</sub> , GS		2012, [52]
25-45		Cemento	MM	L	LFD	2013, [54]
n.d.		CuAl <sub>2</sub> O <sub>4</sub>	SG	A, B, CC, L	LFD	2013, [55]-[56]
70-90		MgAl <sub>2</sub> O <sub>4</sub>	CP	---	TGA	2014, [48]
60		MgAl <sub>2</sub> O <sub>4</sub> ,	I, P	---	TGA, LFD	2011-12, [49, 57]
60		MgAl <sub>2</sub> O <sub>4</sub>	SD	A, B, Bm, L	TGA, LFD	2012-14, [58-63]
40		MgAl <sub>2</sub> O <sub>4</sub>	SD	CH <sub>4</sub> , CB	LFD	2011-12, [50, 64]
40		MgAl <sub>2</sub> O <sub>4</sub>	SD	CH <sub>4</sub>	LFD	2013, [65]
40		MgAl <sub>2</sub> O <sub>4</sub>	SD	CH <sub>4</sub> , GS	LFD	2013, [44]
40		MgAl <sub>2</sub> O <sub>4</sub>	FG	---	Horno	2014, [66]
n.d.		MgAl <sub>2</sub> O <sub>4</sub>	CP	CH <sub>4</sub>	TGA, LFD	2012, [53]
40		MgAl+La <sub>2</sub> O <sub>3</sub>	SD	CH <sub>4</sub> , GS	LFD	2013-14, [44, 45]
40		MgAl+SiO <sub>2</sub>	SD	CH <sub>4</sub>	LFD	2013, [65]
40		MgAl+TiO <sub>2</sub>	SD	CH <sub>4</sub>	LFD	2013, [65]
60		MgO	P	---	TGA, LFD	2011-12, [49, 57]
40	Fe <sub>2</sub> O <sub>3</sub> (48)	MgO	SD	CH <sub>4</sub> , GS	LFD	2013-14, [44, 45]
n.d.		Mn <sub>2</sub> O <sub>3</sub>	CP	CH <sub>4</sub>	TGA, LFD	2012, [53]
60		Sepiolita	E, P	---	TGA, LFD	2013-14, [49, 57]
19-61		β-SiC	I, ER	---	TGA	2013, [67]
60		SiO <sub>2</sub>	E, P	---	TGA, LFD	2011-12, [49, 57]
60		SiO <sub>2</sub>	I	---	TGA	2013, [68]
40		SiO <sub>2</sub>	SD	CH <sub>4</sub>	LFD	2013, [65]
20		SiO <sub>2</sub>	I	---	TGA, LFD, LF	2012, [69]
n.d.		SiO <sub>2</sub>	n.d.	n.d.	TGA, LFD	2010, [38]
40		SiO <sub>2</sub> +TiO <sub>2</sub>	SD	CH <sub>4</sub>	LFD	2013, [65]
60		TiO <sub>2</sub>	E	---	TGA, LFD	2011-12, [49, 57]
60		TiO <sub>2</sub>	I	---	TGA	2013, [68]
50		TiO <sub>2</sub>	MM	---	TGA, LFD, LF	2012-14, [69-71]
40		TiO <sub>2</sub>	SD	CH <sub>4</sub>	LFD	2013, [65]
60		ZrO <sub>2</sub> ,	E, P	n.d.	TGA, LFD	2011-12, [49, 57]
55		ZrO <sub>2</sub>	n.d.	FG	TGA, LFD, LF	2012-14, [69-71]
40		ZrO <sub>2</sub>	FG	CP	LFD	2009, [35]
40		ZrO <sub>2</sub>	SD	CH <sub>4</sub> , GS, GN	LFD	2013-14, [44, 45]
40		ZrO <sub>2</sub> +CaO	FG	CH <sub>4</sub>	LFD	2013, [72]
40		ZrO <sub>2</sub> +CeO <sub>2</sub>	FG	CH <sub>4</sub>	LFD	2013, [72]
40		ZrO <sub>2</sub> +La <sub>2</sub> O <sub>3</sub>	SD	CH <sub>4</sub> , GS	LFD	2013-14, [44, 45]
40		ZrO <sub>2</sub> +MgO <sub>2</sub>	FG	CH <sub>4</sub>	LFD	2013, [72]
40		ZrO <sub>2</sub> -Y	SD	CH <sub>4</sub> , GS, GN	LFD	2013-14, [44, 45]

<sup>a</sup>Método de preparación:  
CP = Co-precipitación  
E = Extrusión  
ER = Evaporación rotativa  
FG = *Freeze granulation*  
I = Impregnación  
MM = Mezcla másica  
P = Presión  
SD = *Spray drying*

<sup>b</sup>Combustible:  
A = Antracita  
B = Carbón Bituminoso  
Bm = Biomasa  
CB= Char de Biomasa  
CC = Char de Carbón  
CP = Coque de Petróleo  
GS = Gas de Síntesis  
L = Lignito

<sup>c</sup>Instalación de laboratorio:  
LFD = Lecho fluidizado discontinuo  
LF = Lecho fijo  
TGA = Termobalanza  
  
n.d. = no disponible



Como puede observarse, existen más de 55 materiales diferentes que se han ido evaluando de forma paralela al desarrollo de esta Tesis Doctoral. Sin embargo, son muy pocos los materiales evaluados en sistemas CLOU en continuo, donde se puede evaluar realmente la idoneidad de un transportador de oxígeno para un sistema industrial y su comportamiento sobre las eficiencias de combustión y captura de CO<sub>2</sub>. La Tabla 1.9 muestra los diferentes materiales evaluados en experimentos en planta en continuo, utilizando combustibles sólidos, líquidos o gaseosos, para el proceso CLOU. Cabe destacar que los únicos trabajos en los que se demuestra el concepto CLOU con combustibles sólidos forman parte de esta Tesis Doctoral.

**Tabla 1.9.** Transportadores de oxígeno para el proceso CLOU evaluados en plantas en continuo de la literatura hasta 2014.

Cu (%)	Material de soporte	Método de preparación <sup>a</sup>	Combustible <sup>b</sup>		Potencia (W)	Tiempo Operación (h)	Año, Ref.
			Gas/Líquido	Sólido			
40	CeO <sub>2</sub>	SD	CH <sub>4</sub> , GS, GN		300	5	2013-14, [44, 45]
<b>60</b>	<b>MgAl<sub>2</sub>O<sub>4</sub></b>	<b>SD</b>		<b>A, B, Bm, L</b>	<b>1500</b>	<b>135</b>	<b>2012-14, Esta Tesis</b>
40	ZrO <sub>2</sub>	SD	CH <sub>4</sub> , GS, GN		300	7	2013-14, [44, 45]
20	ZrO <sub>2</sub>	SD	Q		300	17	2012, [73]
40	ZrO <sub>2</sub> -Y	SD	CH <sub>4</sub> , GS, GN		300	11	2013-14, [44, 45]
<sup>a</sup> Método de preparación: SD = <i>Spray drying</i>				<sup>b</sup> Combustible: A = Antracita B = Carbón Bituminoso Bm = Biomasa GN = Gas natural GS = Gas de Síntesis L = Lignito Q = Queroseno			

## 1.6 Objetivo y plan de trabajo

El objetivo de esta Tesis Doctoral ha sido demostrar la viabilidad de la combustión de diferentes combustibles sólidos (carbones de diferente rango y biomasa) con captura de CO<sub>2</sub> según el proceso denominado CLOU (*Chemical Looping with Oxygen Uncoupling*) en un sistema en continuo. En este caso se pretende utilizar la propiedad del CuO en un transportador de oxígeno para generar O<sub>2</sub> gaseoso.

El plan de trabajo llevado a cabo para cumplir el objetivo comenzó con el desarrollo y caracterización de diferentes transportadores de oxígeno basados en CuO adecuados para la combustión de combustibles sólidos (carbón o biomasa) mediante el proceso

CLOU. Se prepararon distintos materiales con diferentes contenidos en CuO, distintos soportes y utilizando varios métodos de preparación. Estos materiales se caracterizaron química y físicamente por diferentes técnicas: SEM-EDX, XRD, porosimetría de mercurio, adsorción de N<sub>2</sub> (BET), picnometría de He y determinación de la resistencia mecánica. Además, se determinó la reactividad de cada material tanto para el proceso de generación de oxígeno como para su regeneración.

En el Instituto de Carboquímica se realizó inicialmente una caracterización de transportadores de CuO por medio de la medida de sus reactividades redox en N<sub>2</sub> y aire en TGA y su resistencia mecánica, para los transportadores de oxígeno preparados por impregnación húmeda incipiente, extrusión, compresión y *spray drying*. También se determinó su capacidad de desprender oxígeno gaseoso a diferentes temperaturas, junto a la velocidad de atrición y la tendencia a la aglomeración durante un alto número de ciclos redox N<sub>2</sub>-aire en un reactor de lecho fluidizado discontinuo (Artículo I). Una vez seleccionados los mejores candidatos se llevó a cabo una segunda caracterización de transportadores de oxígeno basados en cobre preparados por un método industrial como es el *spray drying*. Uno de los materiales seleccionados contiene un 60% de CuO y se utilizó MgAl<sub>2</sub>O<sub>4</sub> como material inerte. Este material se caracterizó tanto física como químicamente (Artículo II). El resto de materiales seleccionados contenían un 40% de CuO y como inertes se emplearon MgAl<sub>2</sub>O<sub>4</sub>, SiO<sub>2</sub> y TiO<sub>2</sub>, tanto puros como mezclas de ellos en diferentes proporciones (Artículo III). Este trabajo se desarrolló durante una estancia en la Universidad Tecnológica de Chalmers (Gotemburgo, Suecia). Los transportadores preparados también se caracterizaron química y físicamente por diferentes técnicas y se determinó su reactividad y su capacidad de desprender oxígeno gaseoso a diferentes temperaturas. También se evaluó la velocidad de atrición y la tendencia a la aglomeración durante un alto número de ciclos redox en un reactor de lecho fluidizado discontinuo. De todo este proceso se seleccionó un transportador de oxígeno que cumplía todas las condiciones para ser usado como transportador de oxígeno en el proceso CLOU: alta reactividad, baja velocidad de atrición y sin tendencia a la aglomeración. Posteriormente, se analizó la capacidad del transportador de oxígeno para convertir un combustible sólido (carbón y char) en un reactor de lecho fluidizado discontinuo (Artículo IV). Adicionalmente, se analizó su máxima velocidad de generación oxígeno en función de la temperatura de reacción. Se encontró que el transportador de oxígeno era capaz de producir oxígeno en condiciones de equilibrio en

todas las condiciones operacionales analizadas, incluso cuando las conversiones del transportador de oxígeno eran altas.

Este transportador de oxígeno se utilizó en una planta en continuo consistente en dos reactores de lecho fluidizado interconectados con una potencia de 1.5 kW<sub>t</sub>, donde se demostró por primera vez durante más de 45 horas el proceso CLOU quemando un carbón bituminoso (Artículo V). Se determinaron las eficacias de combustión y captura de CO<sub>2</sub>, así como el efecto de las principales variables de operación.

Una vez demostrado el proceso, se estudió en la planta en continuo la capacidad del proceso CLOU para procesar distintos tipos de combustible sólido (Artículo VI). Se usaron carbones de reactividades muy diferentes: un lignito, dos carbones bituminosos y una antracita. Con los datos obtenidos se realizó un estudio de los inventarios de sólido mínimos necesarios para tener una alta eficacia de captura de CO<sub>2</sub> con diferentes combustibles. También se llevó a cabo la demostración del proceso CLOU cuando se utiliza un combustible renovable como es la biomasa, obteniéndose unos resultados muy prometedores respecto a la eficacia de captura de CO<sub>2</sub> y del inventario necesario (Artículo VII).

Continuando con el desarrollo del proceso CLOU, se llevó a cabo un estudio del efecto del azufre presente en el combustible (Artículo VIII). Para ello se utilizó en la planta en continuo un lignito con alto contenido en azufre (5.2% en peso) y se analizaron las emisiones de contaminantes, así como su posible efecto en el transportador de oxígeno.

Finalmente, se realizó una comparativa de los resultados obtenidos entre los procesos *i*G-CLC y CLOU en la planta en continuo con diferentes combustibles sólidos (Artículo IX). Se analizaron las diferencias en las eficacias de combustión y captura de CO<sub>2</sub> para tres carbones de diferente rango en ambos procesos. Además, se analizaron las diferencias en las velocidades de conversión de char por ambos procesos para relacionarlas con las diferencias encontradas en las eficiencias.

Para el diseño básico de los reactores de reducción y oxidación de un proceso CLOU es necesario conocer la cantidad de sólidos necesaria en los reactores de oxidación y reducción, así como la velocidad de circulación del transportador de oxígeno entre

ambos reactores. Para calcular los inventarios mínimos de sólidos necesarios se estudió la cinética de las reacciones de reducción y oxidación del transportador desarrollado (Artículo X) en la TGA. Con los datos cinéticos obtenidos, se realizó una optimización del inventario necesario tanto en el reactor de reducción como en el de oxidación para alcanzar elevados valores de captura de CO<sub>2</sub> usando diferentes combustibles sólidos.

## 1.7 Publicaciones Científicas y Congresos

Las publicaciones científicas realizadas en el desarrollo de esta Tesis Doctoral son las siguientes (numeradas con números romanos):

- I. P. Gayán, I. Adánez-Rubio, A. Abad, L. F. de Diego, F. García-Labiano, J. Adánez. *Development of Cu-based oxygen carriers for Chemical-Looping with Oxygen Uncoupling (CLOU) process*. Fuel 2012, 96, 226-238.
- II. I. Adánez-Rubio, P. Gayán, A. Abad, L.F. de Diego, F. García-Labiano, J. Adánez. *Evaluation of a spray-dried CuO/MgAl<sub>2</sub>O<sub>4</sub> oxygen carrier for the chemical-looping with oxygen uncoupling process*. Energy & Fuels 2012, 26, 3069-3081.
- III. I. Adánez-Rubio, M. Arjmand, H. Leion, P. Gayán, A. Abad, T. Mattisson, A. Lyngfelt. *Investigation of combined supports for Cu-based oxygen carriers for chemical-looping with oxygen uncoupling (CLOU)*. Energy & Fuels 2013, 27, 3918-3927.
- IV. I. Adánez-Rubio, A. Abad, P. Gayán, L. F. de Diego, F. García-Labiano, J. Adánez. *Identification of operational regions in the Chemical-Looping with Oxygen Uncoupling (CLOU) process with a Cu-based oxygen carrier*. Fuel 2012, 102, 634-645.
- V. A. Abad, I. Adánez-Rubio, P. Gayán, F. García-Labiano, L. F. de Diego, J. Adánez. *Demonstration of chemical-looping with oxygen uncoupling (CLOU) process in a 1.5 kW<sub>th</sub> continuously operating unit using a Cu-based oxygen-carrier*. Int. Journal of Greenhouse Gas Control 2012, 6, 189-200.
- VI. I. Adánez-Rubio, A. Abad, P. Gayán, L. F. de Diego, F. García-Labiano, J. Adánez. *Performance of CLOU process in the combustion of different types of coal with CO<sub>2</sub> capture*. International Journal of Greenhouse Gas Control 2013, 12, 430-440.

- VII. I. Adánez-Rubio, A. Abad, P. Gayán, L. F. de Diego, F. García-Labiano, J. Adánez. *Biomass combustion with CO<sub>2</sub> capture by Chemical Looping with Oxygen Uncoupling (CLOU)*. Fuel Processing Technology, 2014, vol. 124, no. 0, p. 104-114.
- VIII. I. Adánez-Rubio, A. Abad, P. Gayán, F. García-Labiano, L. F. de Diego, J. Adánez. *The fate of sulphur in the Cu-based Chemical Looping with Oxygen Uncoupling (CLOU) process*. Applied Energy 2014, 113,1855-1862.
- IX. J. Adánez, P. Gayán, I. Adánez-Rubio, A. Cuadrat, T. Mendiara, A. Abad, F. García-Labiano, L.F. de Diego. *Use of Chemical-Looping processes for coal combustion with CO<sub>2</sub> capture*. Energy Procedia 2013, 37, 540-549.
- X. I. Adánez-Rubio, P. Gayán, A. Abad, F. García-Labiano, L. F. de Diego, J. Adánez. *Kinetic analysis of a Cu-based oxygen carrier: Relevance of temperature and oxygen partial pressure on reduction and oxidation reactions rates in Chemical Looping with Oxygen Uncoupling (CLOU)*. Chemical Engineering Journal, 2014, vol. 256, no. 0, p. 69-84.

### **Informe de contribución**

I: Co-autor, responsable de parte del trabajo experimental, evaluación de datos y escritura.

II, III, IV, V, VI, VII, VIII: Autor principal, responsable del trabajo experimental, evaluación de datos y escritura.

IX: Co-autor, responsable del trabajo experimental y evaluación de datos.

X: Autor, desarrollo del modelo, evaluación de datos y escritura.

### **Contribuciones a congresos**

Del mismo modo se muestra a continuación la relación de congresos nacionales e internacionales en los que he participado durante el desarrollo de esta Tesis Doctoral y relacionado con ella.

1. I. Adánez-Rubio, A. Abad, P. Gayán. *Desarrollo de transportadores sólidos de oxígeno de CuO para la combustión de sólidos con captura de CO<sub>2</sub> en un proceso CLOU*. X Reunión del Grupo Español del Carbón, Girona (España), 10-12 Mayo del 2010.
2. I. Adánez-Rubio, P. Gayán, F. García-Labiano, L.F. de Diego, J. Adánez, A. Abad. *Development of CuO based oxygen-carrier materials suitable for Chemical-Looping with Oxygen Uncoupling (CLOU) process*. 10th International Conference on Greenhouse Gas Control Technologies (GHGT10), Amsterdam (Holanda), 19-23 Septiembre 2010.

3. I. Adánez-Rubio, P. Gayán, F. García-Labiano, L. F. de Diego, J. Adánez, A. Abad. ***Desarrollo de transportadores sólidos de oxígeno basados en CuO para el proceso CLOU.*** 4º Jornada de Jóvenes Investigadores (Química y Física) de Aragón, Zaragoza (España), 18 de Noviembre del 2010.
4. I. Adánez-Rubio, P. Gayán, A. Abad, F. García-Labiano, L. F. de Diego, J. Adánez. ***CO<sub>2</sub> Capture in Coal Combustion by Chemical-Looping with Oxygen Uncoupling (CLOU) with a Cu-based Oxygen-Carrier.*** 5º International Conference on Clean Coal Technologies (CCT2011), Zaragoza (España), 8-12 Mayo 2011.
5. E. Dvininov, H. Stephenson, P. Gayán, A. Abad, I. Adánez-Rubio, F. García-Labiano, L.F. de Diego, and J. Adánez. ***Cu-based Material for Chemical Looping Combustion Applications.*** EUROPACAT X Congress. 28 de Agosto - 2 de Septiembre del 2011. Glasgow (Escocia).
6. I. Adánez-Rubio, A. Abad, P. Gayán. ***Combustión de carbón con captura inherente de CO<sub>2</sub> mediante un proceso CLOU en una planta en continuo.*** XI Reunión del Grupo Español del Carbón (GEC). 23-26 octubre 2011. Badajoz (España).
7. I. Adánez-Rubio, A. Abad, P. Gayán, L. F. de Diego, F. García-Labiano, J. Adánez. ***Identification of Operational Regions in the Chemical-Looping with Oxygen Uncoupling (CLOU) Process with a Cu-based Oxygen-Carrier.*** International Conference on Coal Science and Technology (ICCS&T 2011) 9-13 Octubre del 2011. Oviedo (España).
8. I. Adánez-Rubio, P. Gayán, A. Abad, L. F. de Diego, F. García-Labiano, J. Adánez. ***Performance of CLOU process in the combustion of different types of coal with CO<sub>2</sub> capture.*** 21st International Conference on Fluidized bed Combustion. 3-6 de Junio del 2012. Napoles (Italia).
9. I. Adánez-Rubio, A. Abad, P. Gayán, F. García-Labiano, L. F. de Diego, J. Adánez. ***The fate of sulphur in the CLOU process using a Cu-based oxygen-carrier.*** 2<sup>nd</sup> International Conference on Chemical Looping. 26-28 de Septiembre del 2012. Darmstadt (Alemania).
10. J. Adánez, P. Gayán, I. Adánez-Rubio, A. Cuadrat, T. Mendiara, A. Abad, F. García-Labiano, L.F. de Diego. ***Use of Chemical-Looping processes for coal combustion with CO<sub>2</sub> capture.*** 11th International Conference on Greenhouse Gas Control Technologies (GHGT11). 18-22 de Noviembre del 2012. Kyoto (Japón).
11. I. Adánez-Rubio, A. Abad, P. Gayán. ***Combustión de biomasa con captura de CO<sub>2</sub> mediante un proceso CLOU.*** XII Reunión del Grupo Español del Carbón (GEC). 20-23 de Octubre del 2013. Madrid (España).
12. I. Adánez-Rubio, T. Mendiara, A. Abad, P. Gayán, F. García-Labiano, L. F. de Diego, J. Adánez. ***Pollutant emissions during coal combustion in iG-CLC and CLOU processes.*** 3<sup>rd</sup> International Conference on Chemical Looping. 9-11 de Septiembre del 2014. Gotemburgo (Suecia).



## **2 Sección experimental**





## 2.1 Preparación de transportadores de oxígeno

Los transportadores de oxígeno utilizados en esta Tesis Doctoral están compuestos por óxido de cobre II (CuO) como fuente de oxígeno para el proceso de combustión, y un inerte como aglutinante para aumentar la resistencia mecánica y la estabilidad del transportador de oxígeno. Durante la selección de transportadores de oxígeno, éstos se prepararon por métodos diferentes: impregnación húmeda incipiente, mezcla másica seguida de extrusión, mezcla másica y compresión y por *spay drying* utilizando como inertes  $\text{Al}_2\text{O}_3$ ,  $\text{MgAl}_2\text{O}_4$ , sepiolita,  $\text{SiO}_2$ ,  $\text{TiO}_2$ ,  $\text{ZrO}_2$  o  $\text{MgO}$ . Posteriormente se realizaron diferentes etapas de sinterización y tamizado para obtener partículas con resistencia mecánica y tamaño adecuado para su uso en el lecho fluidizado.

### 2.1.1 Impregnación húmeda incipiente

Se utilizaron los siguientes materiales como soporte poroso:  $\gamma\text{-Al}_2\text{O}_3$  comercial (Puralox Nwa-155, Sasol Germany GMBH),  $\alpha\text{-Al}_2\text{O}_3$  (obtenida por calcinación de  $\gamma\text{-Al}_2\text{O}_3$  a 1150 °C durante 2 horas), y  $\text{MgAl}_2\text{O}_4$  (preparado en el ICB-CSIC por impregnación de  $\gamma\text{-Al}_2\text{O}_3$  con nitrato de magnesio). Las partículas de  $\gamma\text{-Al}_2\text{O}_3$ ,  $\alpha\text{-Al}_2\text{O}_3$  y  $\text{MgAl}_2\text{O}_4$  tienen un tamaño de +0.1-0.3 mm con densidades de 1.3, 2.0 y 1.8 g/cm<sup>3</sup> y porosidades de 55.4 %, 47.3 % y 50.0 %, respectivamente. Para la preparación de los transportadores de oxígeno se preparó una disolución saturada de nitrato de cobre. A continuación se añadía sobre las partículas de soporte un volumen de esta disolución saturada correspondiente al volumen total de poros de las partículas. La disolución se añadió lentamente a las partículas del soporte, en condiciones de agitación completa y a temperatura ambiente. La cantidad de fase activa deseada se consigue aplicando sucesivas impregnaciones seguidas de calcinaciones a 550 °C, en atmósfera de aire durante 30 minutos, para descomponer el nitrato en el óxido metálico. Finalmente los transportadores se sinterizaban durante 1 hora a 850 °C. Se prepararon transportadores con contenidos en óxido de cobre del 15 al 33%.

### 2.1.2 Extrusión

Estos transportadores de oxígeno se prepararon usando óxido de cobre puro comercial (Panreac, pureza > 99.5%), con un tamaño de partícula <10  $\mu\text{m}$ . Como inertes se utilizaron:  $\text{Al}_2\text{O}_3$ , sepiolita (Absorbente General QP, Panreac, de composición  $\text{Mg}_4\text{Si}_6\text{O}_{15}(\text{OH})_2 \cdot 6\text{H}_2\text{O}$ ),  $\text{SiO}_2$  (99% pureza; Sigma Aldrich),  $\text{TiO}_2$  (99% pureza; Sigma Aldrich) y  $\text{ZrO}_2$  (99% pureza; Sigma Aldrich). El polvo mezclado, incluyendo el óxido metálico y el inerte en las condiciones deseadas, y un 10% de grafito (Sigma Aldrich;  $d_p$ : 1-2  $\mu\text{m}$ ), se convirtió, por adición de agua, en una pasta de viscosidad adecuada para ser extruida en una jeringuilla. Se obtuvieron extruidos cilíndricos con unos 2 mm de diámetro. Estos extruidos fueron suavemente secados a 80 °C durante una noche, cortados a la longitud deseada (sobre 4 mm) y sinterizados a diferentes temperaturas entre 950 y 1300 °C durante 6 horas en una mufla. Finalmente, los extruidos fueron molidos y tamizados a un tamaño adecuado para la experimentación (+0.1-0.3 mm).

### 2.1.3 Compresión

Los transportadores de oxígeno por compresión se prepararon usando óxido de cobre (II) puro comercial con tamaño de partícula <10  $\mu\text{m}$  (Panreac, pureza > 99.5%). Como inertes se utilizaron los siguientes óxidos comerciales:  $\text{MgAl}_2\text{O}_4$  (Baikowski, S30CR),  $\text{ZrO}_2$  (99% pureza; Sigma Aldrich), sepiolita (Absorbente General QP, Panreac) y  $\text{MgO}$  (99% pureza, Panreac). En la preparación se añade grafito a la mezcla como aditivo para la formación de porosidad durante la calcinación. La mezcla del óxido metálico activo y el sólido inerte en las proporciones deseadas, junto con 0.5-10% de grafito, se mezclaba en un molino de bolas durante 2 horas y posteriormente se pelletizaba por compresión en una prensa hidráulica a 160 bar, obteniéndose pellets cilíndricos de 10 mm de diámetro y 20 mm de longitud. Estos pellets fueron calcinados entre 950 y 1300 °C, durante 6-24 horas. Finalmente los pellets fueron molidos y tamizados para obtener el tamaño de partícula deseado (+0.1-0.3 mm).

### 2.1.4 *Spray Drying*

El *spray drying* es un método industrial de preparación de partículas que puede ser utilizado para la preparación de transportadores de oxígeno a gran escala. Las partículas de transportador de oxígeno fueron preparadas por la empresa VITO (Flemish Institute

for Technological Research, Belgium) usando CuO (Panreac, PRS) y distintos materiales como soportes: espinela de  $MgAl_2O_4$  (Baikowski, S30CR),  $TiO_2$  (Alfa Aesar),  $SiO_2$  (SilverBond M800, Sibelco) y  $ZrO_2$  (99% pureza; Sigma Aldrich).

Se prepararon transportadores de oxígeno con un contenido de CuO entre un 40% y un 60% y se utilizaron tanto un único inerte como mezclas de éstos en diferentes proporciones. Las partículas preparadas con un 40% de CuO fueron calcinadas durante 4 h a temperaturas que variaron entre los 950 y los 1030°C. Las partículas de transportador fueron tamizadas para obtener el tamaño de partícula deseado (+0.125-0.18 mm).



**Figura 2.1.** Transportador de oxígeno Cu60MgAl\_SD

Por otro lado, el transportador de oxígeno preparado por *spray drying* con un 60% de CuO y como soporte espinela de  $MgAl_2O_4$  fue calcinado a 1100 °C durante 12 h. No obstante, tras la recepción del material las partículas fueron calcinadas una segunda vez para incrementar su dureza. El tiempo total de calcinación de las partículas fue de 24 h a 1100 °C. Finalmente, las partículas de transportador fueron tamizadas para obtener el tamaño de partícula deseado (+0.1-0.3 mm). La designación de este transportador de oxígeno en la presente Tesis Doctoral es Cu60MgAl\_SD. La Figura 2.1 muestra una foto de estas partículas.

En la Tabla 2.1 se muestran todos los transportadores preparados. La nomenclatura utilizada en la tabla señala tanto el contenido en CuO, como el soporte, el método de preparación y la temperatura de calcinación.

**Tabla 2.1.** Condiciones de preparación de los diferentes transportadores de oxígeno desarrollados.

Transportador de oxígeno	CuO (%)	Soporte (%)	T <sup>a</sup> calcinación (°C)	Tiempo calcinación (h)	Grafito (%)
<b>Impregnación húmeda incipiente</b>					
Cu15 $\gamma$ -Al_I850	15	$\gamma$ -Al <sub>2</sub> O <sub>3</sub> (85)	850	6	---
Cu33 $\gamma$ -Al_I850	33	$\gamma$ -Al <sub>2</sub> O <sub>3</sub> (67)	850	6	---
Cu15 $\alpha$ -Al_I850	15	$\alpha$ -Al <sub>2</sub> O <sub>3</sub> (85)	850	6	---
Cu15MgAl_I850	15	MgAl <sub>2</sub> O <sub>4</sub> (85)	850	6	---
Cu21MgAl_I850	21	MgAl <sub>2</sub> O <sub>4</sub> (79)	850	6	---
<b>Mezcla másica y extrusión</b>					
Cu80Al_E1100	80	Al <sub>2</sub> O <sub>3</sub> (20)	1100	6	---
Cu60Al_E1100	60	Al <sub>2</sub> O <sub>3</sub> (40)	1100	6	---
Cu80Sep_E950	80	Sepiolita (20)	950	6	---
Cu60Si_E950	60	SiO <sub>2</sub> (40)	950	6	---
Cu80Si_E950	80	SiO <sub>2</sub> (20)	950	6	---
Cu40Ti_E950	40	TiO <sub>2</sub> (40)	950	6	---
Cu80Ti_E950	80	TiO <sub>2</sub> (20)	950	6	---
Cu60Ti_E950	60	TiO <sub>2</sub> (40)	950	6	---
Cu80Zr_E950	80	ZrO <sub>2</sub> (20)	950	6	---
Cu60Zr_E950	60	ZrO <sub>2</sub> (40)	950	6	---
<b>Mezcla másica y compresión</b>					
Cu60MgAl_P950	60	MgAl <sub>2</sub> O <sub>4</sub> (40)	950	6	10
Cu60MgAl_P1100	60	MgAl <sub>2</sub> O <sub>4</sub> (40)	1100	6	10
Cu60MgAl_P1300	60	MgAl <sub>2</sub> O <sub>4</sub> (40)	1300	6	10
Cu60MgAl_P1100a	60	MgAl <sub>2</sub> O <sub>4</sub> (40)	1100	6	0.5
Cu60MgAl_P1100b	60	MgAl <sub>2</sub> O <sub>4</sub> (40)	1100	12	0.5
Cu60Zr_P950a	60	ZrO <sub>2</sub> (40)	950	6	0.5
Cu40Zr_P1100a	40	ZrO <sub>2</sub> (40)	1100	6	0.5
Cu60Zr_P1100a	60	ZrO <sub>2</sub> (40)	1100	6	0.5
Cu60Mg_P1100a	60	MgO (40)	1100	6	0.5
Cu60Sep_P1100	60	Sepiolita (40)	1100	6	10
Cu60Si_P950	60	SiO <sub>2</sub> (40)	950	6	0.5
Cu60Si_P950	60	SiO <sub>2</sub> (40)	950	6	0.5
<b>Spray drying</b>					
Cu60MgAl_SD	60	MgAl <sub>2</sub> O <sub>4</sub> (40%)	1100	24	---
Cu40Zr_SD	40	ZrO <sub>2</sub> (60%)	1100	24	---
C4T6_950	40	TiO <sub>2</sub> (60)	950	4	---
C4T6_970	40	TiO <sub>2</sub> (60)	970	4	---
C4MA6_1000	40	MgAl <sub>2</sub> O <sub>4</sub> (60)	1000	4	---
C4MA6_1030	40	MgAl <sub>2</sub> O <sub>4</sub> (60)	1030	4	---
C4S6_1000	40	SiO <sub>2</sub> (60)	1000	4	---
C4S6_1030	40	SiO <sub>2</sub> (60)	1030	4	---
C4MA4T2_970	40	MgAl <sub>2</sub> O <sub>4</sub> (40) TiO <sub>2</sub> (20)	970	4	---
C4MA4T2_1000	40	MgAl <sub>2</sub> O <sub>4</sub> (40) TiO <sub>2</sub> (20)	1000	4	---
C4MA2T4_970	40	MgAl <sub>2</sub> O <sub>4</sub> (20) TiO <sub>2</sub> (40)	970	4	---
C4MA2T4_1000	40	MgAl <sub>2</sub> O <sub>4</sub> (20) TiO <sub>2</sub> (40)	1000	4	---
C4MA4S2_1000	40	MgAl <sub>2</sub> O <sub>4</sub> (40) SiO <sub>2</sub> (20)	1000	4	---
C4MA4S2_1030	40	MgAl <sub>2</sub> O <sub>4</sub> (40) SiO <sub>2</sub> (20)	1030	4	---
C4T4S2_950	40	TiO <sub>2</sub> (40) SiO <sub>2</sub> (20)	950	4	---
C4T4S2_970	40	TiO <sub>2</sub> (40) SiO <sub>2</sub> (20)	970	4	---
C4T2S4_1000	40	TiO <sub>2</sub> (20) SiO <sub>2</sub> (40)	1000	4	---
C4T2S4_1030	40	TiO <sub>2</sub> (20) SiO <sub>2</sub> (40)	1030	4	---

\*a = 0.5% grafito, b = 0.5% grafito + 12h de tiempo de calcinación.

## 2.2 Combustibles sólidos

Se han usado diversos combustibles sólidos durante la realización de esta Tesis Doctoral. Principalmente, se han usado carbones de diferente rango: una antracita española del Bierzo, tres carbones bituminosos procedentes de Colombia, Sudáfrica y República Checa, junto a un lignito de Teruel. Según la caracterización ASTM, el carbón de República Checa es un carbón bituminoso bajo en volátiles (BV), el sudafricano es un carbón bituminoso medio en volátiles (MV) y el de Colombia es un carbón bituminoso alto en volátiles (AV). Además se investigó el uso de biomasa de pino en el proceso CLOU, procedente de Ansó (Huesca), cuya principal característica es su elevado contenido en volátiles (82%), muy superior al de los carbones. El análisis inmediato y elemental junto al poder calorífico inferior (PCI) de los diferentes combustibles puede verse en la Tabla 2.2. Hay que resaltar el alto contenido en ceniza del lignito (25.2 %) y de la antracita (31.6 %). El tamaño de partícula usado para los carbones fue de +0.2-0.3 mm y para la biomasa de +0.5-2 mm.

Por otra parte, el carbón colombiano mostraba una alta tendencia a hincharse, obstruyendo la alimentación de carbón al reactor de reducción. Para evitar el hinchamiento se procedió a pre-tratar térmicamente el carbón. Para ello, el carbón se calentó a 180 °C en atmósfera de aire durante 28 horas [74]. El análisis del carbón pre-tratado se muestra también en la Tabla 2.2. Como principal característica cabe destacar que la pre-oxidación ha incrementado el contenido de oxígeno en el carbón del 7 al 17.6%, pero se eliminaba la tendencia al hinchamiento y a la aglomeración.

**Tabla 2.2.** Propiedades de los combustibles sólidos usados.

	Antracita	Bitum. BV	Bitum. MV	Bitum. AV Fresco	Bitum. AV Pre-tratado	Bitum. AV Char	Lignito	Biomasa
<b>Análisis Inmediato (%)</b>								
Humedad	1.0	2.0	4.2	7.5	2.3	6.4	12.6	4.2
Volátiles	7.5	17.1	25.5	34.0	33.0	3.0	28.6	81.0
Carbono Fijo	59.9	68.8	55.9	49.9	55.9	80.2	33.6	14.4
Ceniza	31.6	12.1	14.4	8.6	8.8	10.4	25.2	0.4
<b>Análisis Elemental (%)</b>								
C	60.7	75.8	69.3	70.8	65.8	79.8	45.4	51.4
H	2.1	3.7	3.9	3.9	3.3	0.7	2.5	6.5
N	0.9	1.9	1.9	1.7	1.6	1.3	0.6	0.3
S	1.3	0.4	0.9	0.5	0.6	0.6	5.2	0.0
O <sup>(1)</sup>	2.4	4.1	5.4	7.0	17.6	0.8	8.5	37.2
PCI (kJ/kg)	21900	28950	25500	25900	21900		16250	19200

<sup>(1)</sup>Oxígeno por balance

Finalmente, durante las investigaciones realizadas en esta Tesis Doctoral también se empleó como combustible char procedente del carbón colombiano “El Cerrejón”. Para producirlo, se llevó a cabo la desvolatilización del carbón bituminoso con alto contenido en volátiles pre-tratado. Para ello, partículas de carbón se desvolatilizaron en un reactor de lecho fluidizado discontinuo, usando N<sub>2</sub> como gas de fluidización. El reactor se calentó desde temperatura ambiente hasta 900 °C, con una rampa de calentamiento de 20 °C/min. Posteriormente se enfrió el reactor manteniendo el lecho fluidizado. El análisis elemental e inmediato del char producido se muestra en la Tabla 2.2. El tamaño de partícula del char estaba en el rango +0.2-0.3 mm y las partículas tenían una densidad de alrededor 1000 kg/m<sup>3</sup>.

### **2.3 Técnicas de caracterización empleadas**

Se caracterizaron muestras de partículas, tanto frescas como usadas, de los transportadores de oxígeno estudiados durante la realización de esta Tesis Doctoral por medio de diferentes técnicas.

Se determinó el área superficial de las partículas de transportadores de oxígeno por el método Brunauer-Emmett-Teller (BET) usando el equipo Micromeritics ASAP-2020, mientras que el volumen de poro se determinó por intrusión de Hg en un Quantachrome PoreMaster 33. Para la identificación de las fases cristalinas se usó un difractómetro de polvo policristalino Bruker AXS con un monocromador de grafito. Para determinar la densidad específica de las partículas de los transportadores de oxígeno se usó un picnómetro de Helio AccuPyc II 1340 de Micromeritics. Además, se analizaron las partículas de transportador de oxígeno por microscopía electrónica de barrido SEM EDX Hitachi S-3400 N de presión variable hasta 270 Pa con un analizador EDX Röntec XFlash de Si(Li). Se determinó la resistencia mecánica por medio del equipo Shimpo FGN-5X, que mide la fuerza ejercida sobre las partículas hasta su fractura. Para obtener el valor promedio de resistencia mecánica de los diferentes transportadores de oxígeno se realizaron 20 medidas de resistencia con cada uno.

## 2.4 Instalaciones Experimentales

### 2.4.1 Termobalanza

Se llevaron a cabo análisis de reactividad de los transportadores de oxígeno en sucesivos ciclos reducción-oxidación en un analizador termo-gravimétrico (TGA), modelo MQ2-M5 de CI electronics [75]. La Figura 2.2 muestra la instalación experimental utilizada.

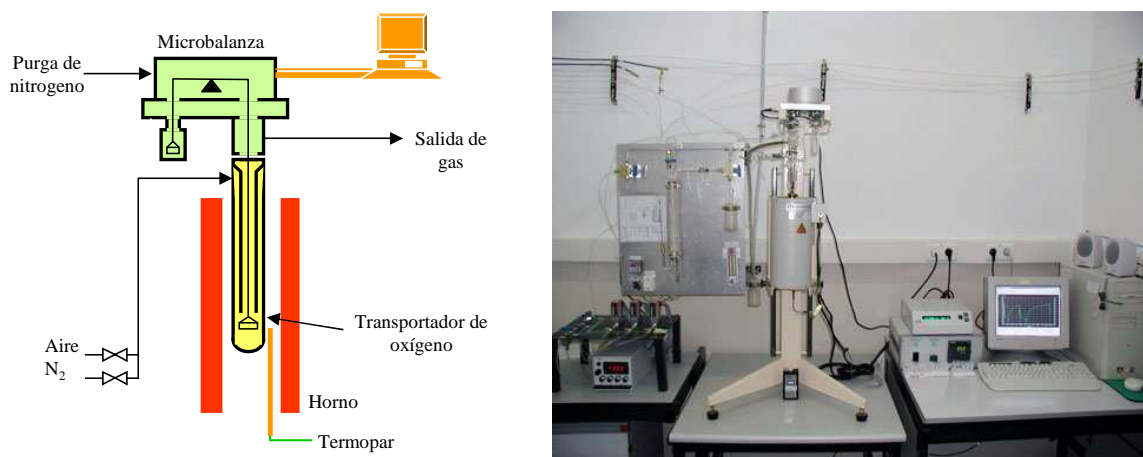


**Figura 2.2.** Esquema y fotografía del analizador termogravimétrico usado para la medida de la reactividad.

El reactor consiste en dos tubos concéntricos de cuarzo (de 24 mm y 10 mm d.i. respectivamente) emplazados en el interior de un horno que puede trabajar a temperaturas de hasta 1200 °C. La cantidad de muestra deseada se coloca en una cestilla de malla de platino (14 mm de diámetro y 8 mm de altura) para reducir la resistencia a la transferencia de masa alrededor de la muestra. La cestilla con la muestra queda suspendida de uno de los brazos de la balanza y se introduce en la zona de reacción. La temperatura y el peso de la muestra son registrados en un ordenador. El caudal de gases reactivos (25 NL/h) se controla mediante una serie de controladores de flujo másico, que son introducidos por la parte superior del reactor. El flujo de gases se calienta a la temperatura deseada al fluir hacia abajo por el anillo exterior del reactor, antes de entrar en contacto con la muestra, localizada en la parte inferior del reactor. El gas sale del reactor a través de un tubo de cuarzo interno. Un flujo continuo de N<sub>2</sub> (9 NL/h) fluye a través de la cabeza de la balanza para mantener la electrónica libre de gases reactivos.



Este flujo de gas no pasa por la zona de reacción, y se mezcla con el gas reactivo a la salida del sistema.

### *Procedimiento*

En primer lugar, el reactor se calentaba hasta la temperatura deseada (entre 900 y 1000 °C) en atmósfera de aire. Posteriormente se realiza el experimento sometiendo al transportador de oxígeno a condiciones alternas de reducción-oxidación.

En los ciclos de reducción y de oxidación de la muestra se utiliza como gas reactivo mezclas N<sub>2</sub>/aire. Durante la descomposición del CuO en Cu<sub>2</sub>O es necesario que la concentración de oxígeno en el gas reactivo sea inferior a la concentración de equilibrio a cada temperatura. Por otro lado, durante la oxidación ocurre lo contrario y la concentración de oxígeno en el gas reactivo debe ser superior a la concentración de equilibrio a cada temperatura.

### *Evaluación de datos*

De los experimentos de reactividad en TGA se obtienen datos de variación de masa en función del tiempo durante los ciclos de reducción y oxidación. Con estos datos se calcula la conversión del transportador de oxígeno de la siguiente forma:

$$\text{En la reducción:} \quad X_{red} = \frac{m_{ox} - m}{m_{ox} - m_{red}} \quad (2.1)$$

$$\text{En la oxidación:} \quad X_{ox} = 1 - \frac{m_{ox} - m}{m_{ox} - m_{red}} \quad (2.2)$$

donde  $m$  es la masa de la muestra en cualquier momento,  $m_{ox}$  es la masa de la muestra totalmente oxidada y  $m_{red}$  la masa de la muestra totalmente reducida. La velocidad de generación de oxígeno,  $r_{O_2,red}$ , se calcula con la siguiente expresión:

$$r_{O_2,red} = R_{TO} \cdot \frac{dX_{red}}{dt} \quad (2.3)$$

siendo  $R_{TO}$  la capacidad de transporte de oxígeno de las partículas.

Inicialmente, para establecer si la resistencia a la transferencia externa de masa y/o la resistencia a la difusión inter-partícula afectaban a la velocidad de reacción, se variaron la velocidad del flujo de gas, entre 10 y 40 NL/h, y la masa de muestra, entre 40 y 100 mg. La Figura 2.3 y la Figura 2.4 muestran las curvas conversión vs. tiempo obtenidas

durante la reducción y la oxidación con diferentes masas de muestra o flujos de gas en la TGA para el transportador de oxígeno Cu60MgAl\_P1100b. Se puede ver que con masas de muestra inferiores a 70 mg o flujos de gas mayores a 10 NL/h, las condiciones experimentales no afectaban a la evolución de la conversión obtenida. Tras este análisis se seleccionó el uso de 25 mg de muestra y un flujo de gas de 25 LN/h para evitar el efecto difusional en la determinación de las velocidades de reacción en la TGA.

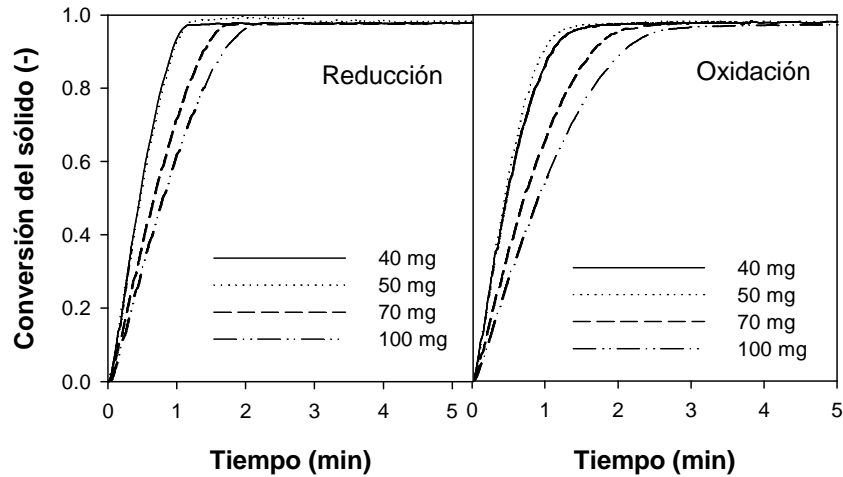


**Figura 2.3.** Efecto del peso de muestra usado en la TGA en las curvas conversión vs. tiempo durante los periodos de reducción y oxidación con el transportador de oxígeno Cu60MgAl\_P1100b. T = 1000 °C. Reducción: 100 vol. % N<sub>2</sub>. Oxidación: aire. Caudal gas: 25 NL/h.

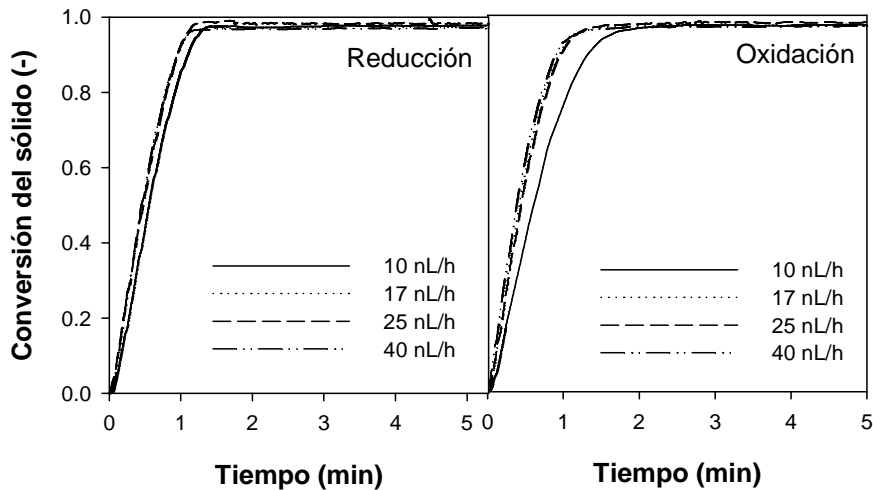


**Figura 2.4.** Efecto del flujo de gas alimentado a la TGA en las curvas conversión vs. tiempo tanto de reducción como en la oxidación usando como transportador de oxígeno Cu60MgAl\_P1100b. T = 1000°C. Reducción: 100 vol. % N<sub>2</sub>. Oxidación: aire. Masa: 50 mg.

## 2.4.2 Reactor de Lecho Fluidizado Discontinuo I (ciclos N<sub>2</sub>-aire)

Para observar el comportamiento de los diferentes transportadores de oxígeno, en condiciones similares a las existentes en el proceso CLOU, se llevaron a cabo multi-ciclos de reducción-oxidación en un reactor de lecho fluidizado discontinuo. En estos experimentos también se evaluó el comportamiento frente a la aglomeración y a la atrición que sufre el material.

En la Figura 2.5 se puede observar un esquema de la instalación experimental empleada. Esta consta de un sistema de alimentación de gas reactivo, un reactor de lecho fluidizado discontinuo, un sistema de recuperación del sólido elutriado y un sistema de análisis de gases. El reactor de lecho fluidizado discontinuo es un reactor de acero refractario de 54 mm de diametro interno y 500 mm de altura, con una zona de precalentamiento justo antes de la placa distribuidora. Todo el sistema (reactor de lecho fluidizado discontinuo y precalentador) se encuentra dentro de un horno eléctrico. El reactor tiene dos tomas de presión para la medida de la presión diferencial en el lecho. Los problemas de aglomeración, causantes de la pérdida de fluidización del lecho, se pueden detectar por una pérdida brusca de la presión diferencial del lecho durante la operación. Dos filtros calientes que operan alternativamente recogen el sólido elutriado del lecho durante los sucesivos ciclos de reducción-oxidación. Un analizador paramagnético de gases (SIEMENS OxyMat 5) mide la concentración de O<sub>2</sub> en continuo a la salida del reactor.

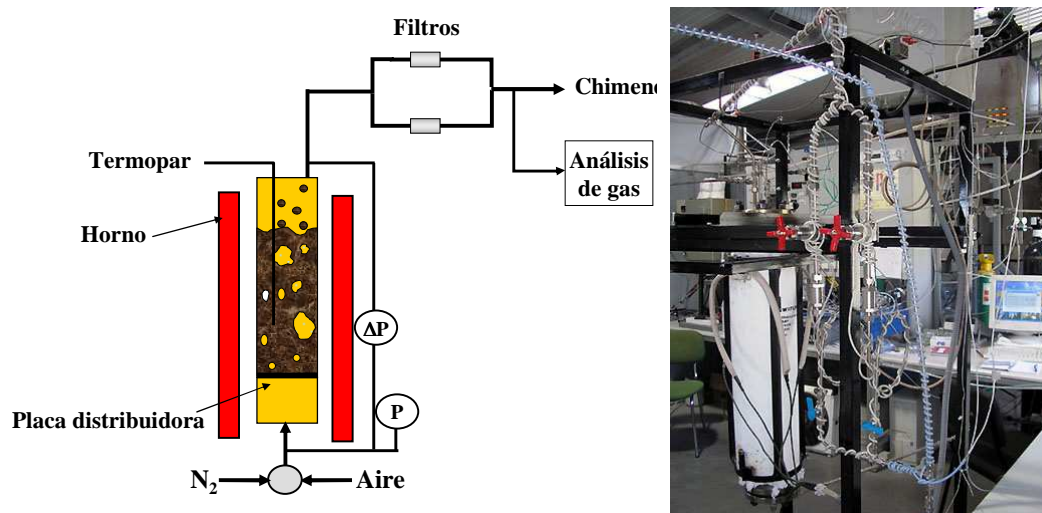


Figura 2.5. Instalación experimental de lecho fluidizado discontinuo I.

### *Procedimiento*

Para la realización de múltiples ciclos de reducción-oxidación y observar el comportamiento de los transportadores frente a la liberación de oxígeno, se cargan entre 200-400 g (en función de su densidad) de transportador de oxígeno para asegurar una altura del lecho superior a 50 mm en el interior del reactor de lecho fluidizado discontinuo. Los experimentos se llevan a cabo a temperaturas de 900, 950 y 1000 °C. La velocidad superficial del gas reactivo a la entrada del reactor se fijó entre 0.15-0.2 m/s, que representan 3.5-4 veces la velocidad de mínima fluidización del transportador de oxígeno. Durante las reducciones, la composición del gas es 100 % N<sub>2</sub> o CO<sub>2</sub> y durante la oxidación se utilizan diferentes concentraciones de O<sub>2</sub>, en un intervalo comprendido entre el 4 y el 21 % en N<sub>2</sub>. Los periodos de reducción se variaron entre 300 y 1800 segundos, dependiendo del material y de las condiciones de operación. Los periodos de oxidación se prolongaron hasta obtener la oxidación completa del transportador de oxígeno. La velocidad de oxidación se encontraba limitada por el aporte de oxígeno al sistema, por lo que los periodos de oxidación fueron largos, y fluctuaron entre los 120 y los 1800 segundos dependiendo de la concentración de O<sub>2</sub> utilizada.

Los sólidos elutriados, retenidos en los filtros, se recogen durante un número determinado de ciclos, se tamizan para obtener la fracción con  $d_p < 40 \mu\text{m}$  y se pesan para obtener datos de atrición del material. La velocidad de atrición se ha calculado por medio de la siguiente ecuación:

$$v_{\text{atrición}} = \frac{\frac{m}{m_{TO}} * 100 * 3600}{t} [\% / h] \quad (2.4)$$

donde  $v_{\text{atrición}}$  es la velocidad de atrición (%/h),  $m$  la masa de transportador de oxígeno elutriado con  $d_p < 40 \mu\text{m}$ ,  $m_{TO}$  la masa total de sólido en el lecho y  $t$  el tiempo de operación durante el que se recoge la muestra.

### *Evaluación de datos*

La conversión en función del tiempo de los transportadores de oxígeno durante los periodos de reducción y oxidación se calculó con las siguientes ecuaciones:

Reducción: 
$$X_{red} = \int_{t_0}^t \frac{F_{out}}{N_{O_2}} (y_{O_2,out}) dt \quad (2.5)$$

Oxidación: 
$$X_{ox} = \int_{t_0}^t \frac{1}{N_{O_2}} (F_{in} \cdot y_{O_2,in} - F_{out} \cdot y_{O_2,out}) dt \quad (2.6)$$

donde  $X$  es la conversión del transportador de oxígeno,  $F_{out}$  es el flujo molar del gas a la salida del reactor,  $y_{O_2,in}$  es la fracción molar de  $O_2$  a la entrada del reactor,  $y_{O_2,out}$  es la fracción molar de  $O_2$  a la salida del reactor,  $N_{O_2}$  son los moles de oxígeno que puede liberar el transportador de oxígeno desde el estado completamente oxidado, y  $t$  es el tiempo.

### 2.4.3 Reactor de Lecho Fluidizado Discontinuo II (ciclos $CH_4$ -aire)

Durante el desarrollo de esta Tesis Doctoral, también se llevó a cabo una caracterización de diferentes materiales para el proceso CLOU en la Universidad Tecnológica de Chalmers (Gotemburgo, Suecia). En concreto se analizó la reactividad de diferentes transportadores de oxígeno en un reactor de lecho fluidizado discontinuo. El reactor está fabricado en cuarzo, tiene una altura de 870 mm y 22 mm de diámetro interno. La Figura 2.6 muestra el esquema del dispositivo experimental. Contiene una placa distribuidora a una altura de 370 mm respecto a la parte inferior del reactor y una zona de precalentamiento del gas entre la entrada y la placa distribuidora. La temperatura se mide con 2 termopares, uno situado 5 mm por debajo de la placa distribuidora y otro 25 mm por encima y dentro el lecho. El reactor tiene dos tomas de presión para la medida de la presión diferencial en el lecho. La pérdida de presión se mide con transductores de presión (Honeywell) en una frecuencia de 20 Hz.

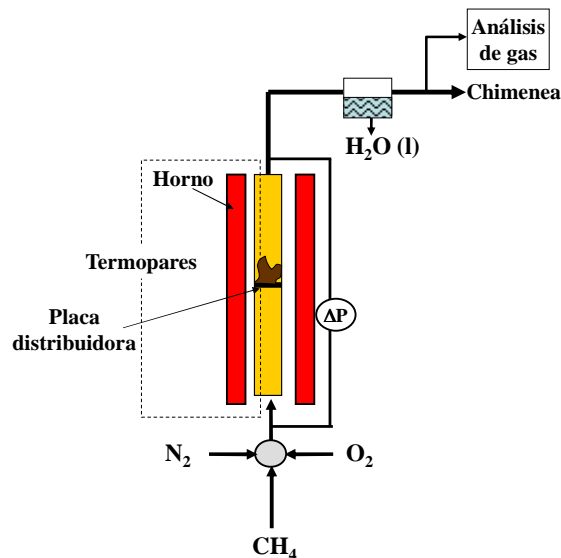


**Figura 2.6.** Instalación experimental de lecho fluidizado discontinuo II.

Los problemas de aglomeración, causantes de la pérdida de fluidización del lecho, se pueden detectar por una pérdida brusca de la presión diferencial del lecho durante la operación. El flujo de gas a la salida del reactor pasa a través de un condensador para eliminar el agua producida durante la oxidación del combustible. La composición del gas seco se mide con un analizador Rosemount NGA-2000 que mide la concentración de oxígeno a través de un canal paramagnético, el  $\text{H}_2$  a través de un canal de conductividad térmica y el  $\text{CO}_2$ ,  $\text{CO}$  y  $\text{CH}_4$  por canales infrarrojos con corrección para otros gases medidos.

### *Procedimiento*

Se introducen 15 g de transportador de oxígeno sobre la placa distribuidora y se calienta el reactor a  $900\text{ }^\circ\text{C}$  pasando una mezcla del 11% de  $\text{O}_2$  en  $\text{N}_2$  para mantener completamente oxidado el transportador de oxígeno antes de empezar los experimentos. Se realizaron ciclos redox donde la muestra de transportador de oxígeno se reduce con un gas inerte ( $\text{N}_2$ ) o con un combustible gaseoso ( $\text{CH}_4$ ), seguido de su oxidación con una mezcla del 11% de  $\text{O}_2$  en  $\text{N}_2$ . Se usaron caudales de gas de 27, 36 y 54 NL/min durante la reducción con  $\text{CH}_4$ , descomposición en  $\text{N}_2$  y oxidación, respectivamente. En primer lugar se llevaron a cabo 3 ciclos de reducción con  $\text{N}_2$  a 900, 925 y 950  $^\circ\text{C}$  durante 360 s con el objetivo de estudiar la generación de oxígeno. A continuación, se realizaron ciclos redox, en los que la reducción se realizó con un 100% de  $\text{CH}_4$  durante 20 s a las mismas tres temperaturas. En este caso, se usa  $\text{N}_2$  durante un periodo de purga

del reactor de 60 s entre la reducción con metano y la oxidación. Para la evaluación de cada transportador de oxígeno se realizaron 18 ciclos redox.

#### *Evaluación de datos*

La reactividad de un transportador de oxígeno se cuantifica en términos de rendimientos del gas o eficacia de conversión,  $\gamma_{CO_2}$ , y se define como la fracción de carbono en el combustible que se oxida a  $CO_2$  dividido por el carbono presente en los gases de salida del reactor, en este caso  $CO_2$ ,  $CO$  y  $CH_4$ .

$$\gamma_{CO_2} = \frac{y_{CO_2}}{y_{CO_2} + y_{CH_4} + y_{CO}} \quad (2.7)$$

donde  $y_i$  es la fracción molar de cada gas a la salida del reactor. Para facilitar la comparación entre los diferentes transportadores de oxígeno variando la temperatura, se usa el parámetro,  $\gamma_{CO_2,ave}$ , que se define como la conversión de gas promedio para todo el periodo de reducción. La conversión másica del transportador de oxígeno,  $\omega$ , se define como:

$$\omega = \frac{m}{m_{TO}} \quad (2.8)$$

donde  $m$  es la masa del transportador de oxígeno durante el experimento. La Ecuación (2.9) se emplea para calcular  $\omega$  en función del tiempo durante el periodo de reducción usando los valores medidos de concentración de varias especies gaseosas:

$$\omega_i = 1 - \int_{t_0}^t \frac{F_{out} M_O}{m_{TO}} (4y_{CO_2} + 3y_{CO} + 2y_{O_2} - y_{H_2}) dt \quad (2.9)$$

donde  $\omega_i$  es la conversión del sólido instantánea para cada tiempo  $t$ ,  $F_{out}$  es el flujo molar de gas seco a la salida del reactor medido por el analizador,  $M_O$  es la masa molar del oxígeno y  $t_0$  el tiempo inicial de la medición.

#### **2.4.4 Reactor de Lecho Fluidizado Discontinuo III (ciclos carbón-aire)**

Para evaluar la capacidad de los transportadores de oxígeno para convertir combustibles sólidos se realizaron experimentos en una instalación de lecho fluidizado discontinuo con un sistema de alimentación de gases y otro para alimentar el combustible sólido, así como un sistema para el análisis de los gases a la salida. La Figura 2.7 muestra un esquema de la instalación del laboratorio. El reactor tiene 54 mm de diámetro interno y

una altura de 700 mm. Está calentado por un horno eléctrico y tiene una zona para precalentar el gas entrante debajo de la placa distribuidora.

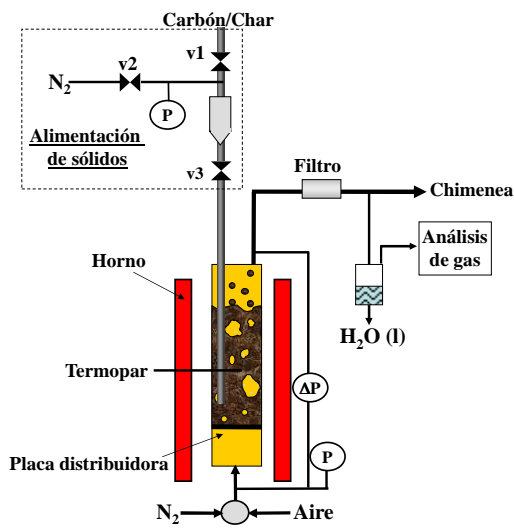


**Figura 2.7.** Instalación experimental de lecho fluidizado discontinuo III.

La temperatura en el interior del lecho se mide por medio de un termopar situado dentro del lecho de transportador de oxígeno. De esta forma, se puede controlar la temperatura de reacción. El reactor tiene dos tomas de presión para la medida de la presión diferencial en el lecho. Los problemas de aglomeración, causantes de la pérdida de fluidización del lecho, se pueden detectar por una pérdida brusca de la presión diferencial del lecho durante la operación. Las tomas de presión también son útiles para detectar el posible bloqueo de las tuberías corriente abajo del reactor debido a taponos por partículas elutriadas del lecho o condensación de alquitranes en puntos fríos.

### *Procedimiento*

El reactor se cargaba con alrededor de 240g de transportador de oxígeno sobre la placa distribuidora, asegurando una altura del lecho de al menos 50 mm en condiciones estáticas para que el termopar quedara dentro del lecho. En algunos experimentos, se diluyó el transportador de oxígeno con partículas de alúmina pura (+0.2-0.4 mm) para mantener la masa total de sólidos en el lecho, pero disminuyendo la cantidad de transportador de oxígeno en el reactor.

El sistema de alimentación de gases tenía conectados diferentes controladores de flujo másico, con lo que es posible alimentar alternativamente aire o nitrógeno. El flujo total



de gas era de 200 NL/h, que se corresponde con una velocidad del gas de 0.1 m/s a 900 °C. Se miden de forma continua la composición de los gases que salen del reactor, después de condensar el vapor de agua, usando diferentes analizadores de gases. Las concentraciones en base seca de CO, CO<sub>2</sub> y CH<sub>4</sub> se determinaron usando un analizador de infrarrojos no dispersivo (NDIR, en sus siglas en ingles). La concentración de H<sub>2</sub> se determinó por medio de un analizador de conductividad térmica del gas. Por otro lado, la concentración de O<sub>2</sub> se determinaba con un analizador paramagnético.

El sistema de alimentación de sólidos consistía en un tubo de 5 mm introducido por la parte superior del reactor que acaba a 20 mm de la placa distribuidora y entre 50-60 mm por debajo del nivel máximo del lecho fluidizado discontinuo. De este modo las partículas de combustible se alimentaban directamente en el interior del lecho fluidizado. La parte superior del tubo tiene un sistema de válvulas con un depósito donde el combustible se cargaba por la válvula v1 antes de empezar el experimento; ver Figura 2.7. Una vez introducido el sólido, el depósito se presuriza con 1 bar de sobrepresión con N<sub>2</sub> a través de la válvula v2. Una vez presurizado, se cerraba la válvula v2 y se abría y cerraba rápidamente v3. Al abrir la válvula v3 se despresuriza el depósito y se alimenta el combustible al lecho del reactor. De esta forma, se aseguraba de que las partículas de combustible entraban en el lecho evitando a la vez que saliese gas del reactor a través del depósito de combustible.

Durante la experimentación se expusieron las partículas de transportador de oxígeno secuencialmente a condiciones de reducción y oxidación. En los periodos de reducción se alimentaba al reactor cargas de carbón o char mientras el lecho se fluidizaba con N<sub>2</sub>. Se mantenía el lecho fluidizado con N<sub>2</sub> hasta que se quemaba por completo la carga de carbón o hasta que se agotaba el O<sub>2</sub> del transportador, lo que generalmente ocurría en menos de 120 segundos. Después de cada periodo de reducción, se oxidaban por completo las partículas de transportador con aire para comenzar un nuevo ciclo.

#### *Evaluación de resultados*

La velocidad instantánea de generación de oxígeno por masa de transportador,  $r_{O_2,red}(t)$ , se calcula con un balance a los átomos de oxígeno en el reactor:

$$r_{O_2,red}(t) = \frac{M_{O_2}}{m_{TO}} \left[ F_{O_2} + F_{CO_2} + 0.5(F_{CO} + F_{H_2O}) - 0.5F_{O,coal} \right] \quad (2.10)$$

El mayor valor para  $r_{O_2,red}$  se obtuvo cuando el carbón era introducido en el lecho y disminuía con la conversión de char, al existir menor demanda de oxígeno por parte del combustible. En el análisis de la presente Tesis Doctoral el valor inicial  $r_{O_2,red}(t=0)$  es el que se utiliza. El flujo molar de cada componente que sale del reactor,  $F_i$ , se calcula como:

$$F_i = F_{out} \cdot y_i \quad (2.11)$$

siendo  $F_{out}$  el flujo total de gas en base seca a la salida del reactor calculado usando el flujo de  $N_2$  en el reactor,  $F_{N_2}$ .

$$F_{out} = \frac{F_{N_2}}{(1 - \sum_i y_i)} \quad (2.12)$$

donde  $y_i$  es la fracción molar de cada componente del gas producto analizado. Los posibles gases  $i$  son  $O_2$ ,  $CO_2$ ,  $CO$ ,  $H_2$ ,  $H_2O$  y  $CH_4$ . Sin embargo, metano e hidrógeno no se detectaron en ninguno de los experimentos realizados. La concentración de agua no fue medida. Sin embargo, para considerar el oxígeno que sale en forma de  $H_2O$  por la oxidación del hidrógeno del combustible, se supone que la evolución del hidrógeno era uniforme en los periodos de desvolatilización y combustión del char, considerando el contenido de hidrógeno en el carbón y en el char producido.

Antes del periodo de reducción, las partículas de transportador de oxígeno estaban completamente oxidadas. Por lo tanto, la conversión inicial del transportador era  $X_{ox}=1$ . Como las partículas de transportador de oxígeno reaccionan durante el periodo de reducción, el grado de oxidación disminuye. Por lo tanto, la conversión del transportador de oxígeno se calcula con la integración de  $r_{O_2,red}$  en función del tiempo:

$$X_{ox}(t) = 1 - \frac{1}{N_{O_2}} \int_{t_0}^t r_{O_2,red}(t) dt \quad (2.13)$$

siendo  $N_{O_2}$  la cantidad molar de oxígeno en el transportador de oxígeno activo para el proceso CLOU, es decir el oxígeno disponible por la reducción de  $CuO$  a  $Cu_2O$  expresado como moles de  $O_2$ :

$$N_{O_2} = \frac{m_{TO} R_{TO}}{M_{O_2}} \quad (2.14)$$

En consecuencia, la conversión final de las partículas,  $X_f$ , se calcula integrando la Ecuación (2.13) para todo el tiempo en condiciones reductoras.

De la misma forma, se realiza el balance de oxígeno para calcular la velocidad de oxidación con aire –Ecuación (2.15)- y la evolución con el tiempo de la conversión del transportador de oxígeno,  $X_{ox}$  –Ecuación (2.16)–. En algunos casos, el char no se convertía completamente durante el periodo de reducción debido a que las partículas de transportador se quedaban sin oxígeno disponible. Por lo tanto, podía aparecer  $CO_2$  y  $CO$  durante el periodo de oxidación por la combustión del char remanente en el reactor, siendo el oxígeno consumido por el char tenido en cuenta en la Ecuación (2.15).

$$\left(-r_{O_2,ox}(t)\right) = \frac{M_{O_2}}{m_{TO}} \left[ 0.21F_{air} - F_{O_2} - (F_{CO_2} + 0.5F_{CO}) \right] \quad (2.15)$$

$$X_{ox}(t) = X_f + \frac{1}{N_{O_2}} \int_{t_0}^t \left(-r_{O_2,ox}(t)\right) dt \quad (2.16)$$

Cuando se utilizaba char como combustible, la velocidad de conversión de char por masa de char reaccionando en el reactor, se calcula como la velocidad de la combustión de carbono para dar  $CO_2$  o  $CO$ :

$$\left(-r_{char}(t)\right) = \frac{F_{CO_2} + F_{CO}}{\frac{m_{char} \cdot f_{C,fix}}{M_C} - \int_{t_0}^t (F_{CO_2} + F_{CO}) dt} \quad (2.17)$$

siendo  $m_{char}$  la masa de char en la carga de combustible y  $f_{c,fix}$  el contenido de carbono en el char.

Finalmente, se define el rendimiento a  $CO_2$  como la fracción de carbono que aparece como  $CO_2$  en los gases a la salida del reactor, que se calcula como:

$$\gamma_{CO_2} = \frac{F_{CO_2}}{F_{CO_2} + F_{CO}} \quad (2.18)$$

#### 2.4.5 Unidad CLOU en continuo para combustibles sólidos (1.5 kW<sub>t</sub>)

Para evaluar el proceso CLOU de forma similar a un proceso industrial es necesario la utilización de una planta piloto que pueda operar de forma continua respecto a la

alimentación de combustible y la circulación del transportador de oxígeno entre los diferentes reactores de reducción y oxidación. La Figuras 2.8 y 2.9 muestran un esquema y varias fotografías de la instalación ICB-CSIC-s1 para la combustión de combustibles sólidos por el proceso CLOU.

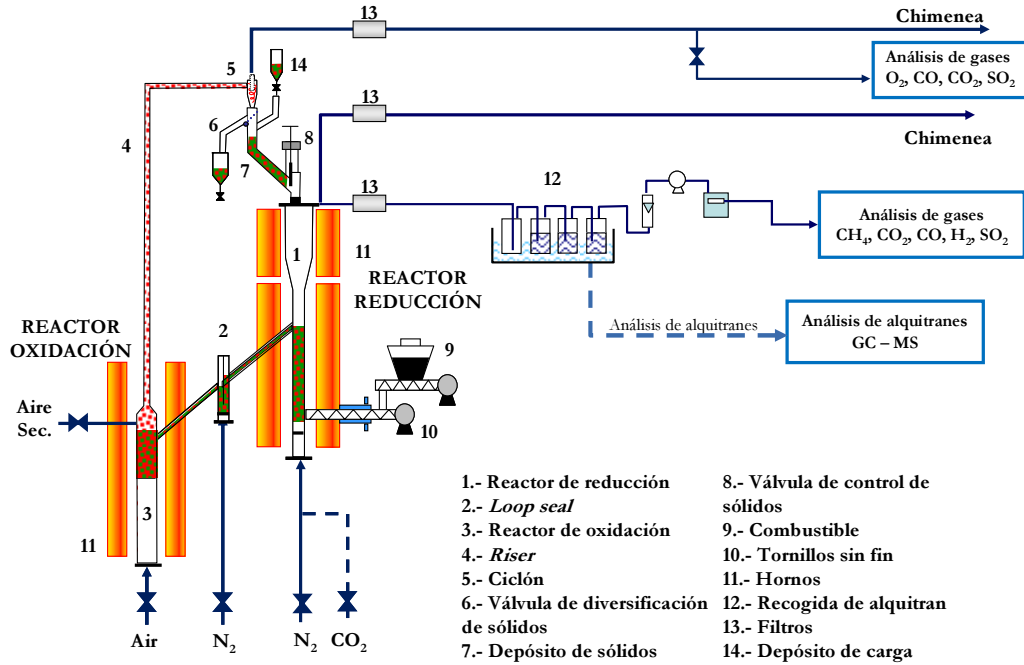


Figura 2.8. Esquema de la planta piloto CLOU de 1.5 kW<sub>t</sub> para la combustión de combustibles sólidos.



Figura 2.9. Unidad CLOU de 1.5 kW<sub>t</sub> en continuo para combustibles sólidos.

Esta instalación está básicamente compuesta por reactores de lecho fluidizado interconectados –el reactor de reducción (1) y el de oxidación (3)- unidos por un reactor

de cierre (2) por la parte inferior y un riser (4) para transportar los sólidos del reactor de oxidación al de reducción. Un ciclón (5) recupera los sólidos arrastrados del reactor de oxidación y una válvula de sólidos (8) controla el flujo de circulación de los sólidos en el sistema. Los reactores operan con una ligera sobrepresión respecto a la presión atmosférica, teniendo en cuenta las pérdidas de presión en los lechos y en las tuberías hacia la chimenea.

El combustible se alimenta por medio de un tornillo sinfín (9) directamente sobre la placa distribuidora del reactor de reducción para maximizar el tiempo de contacto del combustible y de los volátiles con el transportador de oxígeno. El tornillo sinfín consta de 2 secciones: la primera tiene la velocidad regulable para controlar el flujo de alimentación del combustible; la segunda, refrigerada por agua, gira a alta velocidad para minimizar la pirolisis del combustible en el propio tornillo antes de ser alimentado al sistema. Un pequeño flujo de N<sub>2</sub> (24 NL/h) se introduce al principio del tornillo sinfín para prevenir el flujo a contracorriente de volátiles.

El reactor de reducción consiste en un reactor de lecho fluidizado burbujeante con 50 mm de diámetro interno y 200 mm de altura del lecho. Como gas de fluidización se usa N<sub>2</sub> o CO<sub>2</sub>. El flujo de gas era de 250 NL/h, correspondiente a una velocidad del gas de 0.15 m/s a 900 °C. El transportador de oxígeno se descompone en el reactor de reducción, liberando oxígeno gaseoso en el lecho. El oxígeno liberado quema los volátiles y el char procedentes de la pirolisis del combustible en el reactor de reducción; ver Figura 1.18. Las partículas de transportador de oxígeno reducidas se transfieren al reactor de oxidación a través de un reactor de cierre (*loop seal*) de lecho fluidizado con forma de U, que tiene un diámetro interno de 30 mm. El reactor de cierre se fluidiza con un flujo de N<sub>2</sub> de 60 NL/h. Se realizaron experimentos preliminares para observar la distribución del gas alimentado al reactor de cierre, con los que se determinó que en las condiciones de operación el gas se distribuía aproximadamente al 50% en cada reactor (oxidación y reducción).

La oxidación del transportador tiene lugar en el reactor de oxidación. Junto al transportador de oxígeno puede transferirse char sin quemar. Este char se quema en el reactor de oxidación produciendo una disminución de la eficacia de captura de CO<sub>2</sub> del sistema. El reactor de oxidación es un reactor de lecho fluidizado burbujeante con un

diámetro interno de 80 mm y una altura de lecho de 100 mm, seguido por un *riser* de 30 mm de diámetro interno. El flujo de aire en el reactor de oxidación era de 1740 NL/h que corresponde a una velocidad del gas de 0.4 cm/s. Además, para ayudar en el arrastre de las partículas a través del *riser* se introduce un flujo de aire secundario de 240 NL/h en la parte superior del lecho burbujeante, hasta alcanzar una velocidad del gas en el *riser* de 3 m/s. Los gases de salida del reactor de oxidación pasan a través de un ciclón de alta eficiencia y por un filtro (13) antes de alcanzar la chimenea. El transportador de oxígeno regenerado y recuperado por el ciclón se envía a un depósito de sólidos (7) encima del reactor de reducción, listo para comenzar un nuevo ciclo. Este sólido vuelve al reactor de reducción por gravedad a través de la válvula de control de sólidos (8), que controla el caudal de sólidos que entran en el reactor de reducción. Justo debajo del ciclón hay una válvula de distribución (6) que permite la medición del caudal de sólidos en cualquier momento. Por lo tanto, el diseño del sistema permite el control y la medida de la circulación de sólidos entre ambos reactores. Las partículas de cenizas provenientes de la combustión del char no se recogen en el ciclón y son recuperadas posteriormente en el filtro. De esta forma, las partículas de cenizas no se acumulan en el sistema.

Debido a la pérdida de calor, el sistema no era auto-térmico, y para controlar individualmente la temperatura de los diferentes reactores se usaron varios hornos eléctricos situados en los reactores de oxidación y reducción, y en el *freeboard* por encima del lecho del reactor de reducción. Durante la operación del sistema, se monitorizaron las temperaturas de los reactores de oxidación, reducción, *freeboard* y del *riser*. Además se medía la variación de presión en importantes localizaciones del sistema, como en los reactores de oxidación, reducción y cierre.

Finalmente, cabe destacar que se impide la mezcla de gases entre el reactor de reducción y el de oxidación por medio de la existencia del reactor de cierre (2) y del depósito de sólidos (7). Por lo tanto, la presencia de oxígeno en los gases de salida del reactor de reducción es únicamente el resultado de la generación de oxígeno por parte del transportador de oxígeno.

### *Procedimiento*

La carga de los sólidos se realizaba a través del depósito de carga (14), por lo que primero se llenaba el reactor de reducción (1). A medida que se añadía más sólido se iban llenando el resto de reactores. El inventario óptimo de transportador de oxígeno en el sistema era entre 2 y 3 kg, de los cuales 0.7 a 0.8 kg de transportador se encontraban en el reactor de reducción. La cantidad de sólidos en el reactor de reducción se calculó a partir de la pérdida de carga medida en el reactor para cada experimento.

La temperatura en el reactor de reducción se varió entre 860 hasta 960°C, manteniéndose la temperatura del *freeboard* en 900 °C. Igualmente, la temperatura del reactor de oxidación se varió entre 900 y 950°C. El flujo de combustible alimentado al sistema dependió del combustible usado y se varió entre 0.08 y 0.26 kg/h.

Se analizaban de manera continua CO<sub>2</sub>, CO, H<sub>2</sub>, CH<sub>4</sub>, SO<sub>2</sub> y O<sub>2</sub> provenientes del reactor de reducción, mientras que de los gases del reactor de oxidación se analizaron CO<sub>2</sub>, CO, SO<sub>2</sub> y O<sub>2</sub>. Las concentraciones en base seca de CO, CO<sub>2</sub> y CH<sub>4</sub> se determinaron usando un analizador de infrarrojos no dispersivo (NDIR, en sus siglas en inglés) Maihak S710/UNOR, el H<sub>2</sub> por medio de un analizador de conductividad térmica del gas Maihak S710/THERMOR y el SO<sub>2</sub> por un analizador de infrarrojos Siemens Ultramat. Por otro lado, la concentración de O<sub>2</sub> se determina con un analizador paramagnético Maihak S710/OXOR-P. Los posibles alquitrans presentes en el gas de salida del reactor de reducción se determinaron siguiendo un protocolo de medida de alquitrans [76]. Siguiendo este protocolo se condensaba el agua en dos frascos lavadores refrigerados a 0 °C y posteriormente se recogían los alquitrans por absorción en isopropanol en 6 frascos lavadores refrigerados a -18 °C. En este sistema se recuperaba la mayoría del H<sub>2</sub>O (0 °C) y los componentes aromáticos de los alquitrans (-18 °C). Los alquitrans recogidos en isopropanol se analizaron por cromatografía Agilent 7890A y espectrometría de masas Agilent 5975C. Por otro lado, también se tomaron muestras puntuales del gas a la salida del reactor de reducción que se analizaron por cromatografía de gases HP5890 Series II para detectar la posible presencia de hidrocarburos ligeros (C<sub>2</sub>, C<sub>3</sub> y C<sub>4</sub>).

#### *Evaluación de los resultados*

En función del combustible alimentado a la planta y del flujo de transportador de oxígeno entre el reactor de oxidación y el de reducción se calcula el ratio transportador

de oxígeno/combustible,  $\phi$ . Este ratio se define como el cociente entre el oxígeno transportado por el transportador de oxígeno y el oxígeno demandado por el combustible para su completa combustión. Un valor de  $\phi = 1$  corresponde al flujo estequiométrico de CuO necesario para convertir totalmente el combustible a CO<sub>2</sub> y H<sub>2</sub>O, siendo el CuO reducido a Cu<sub>2</sub>O. Por lo tanto,  $\phi$  se calcula con la siguiente ecuación:

$$\phi = \frac{R_{TO} \dot{m}_{TO}}{\Omega_{SF} \dot{m}_{SF}} \quad (2.19)$$

donde  $\dot{m}_{TO}$  es el flujo de circulación de los sólidos y  $\dot{m}_{SF}$  es el flujo másico de combustible alimentado al reactor de reducción.  $\Omega_{SF}$  es la masa de oxígeno estequiométrica necesaria para convertir 1 kg de combustible a CO<sub>2</sub> y H<sub>2</sub>O. Este valor se calcula con los datos del análisis elemental e inmediato de cada combustible usando la siguiente ecuación:

$$\Omega_{SF} = \left( \frac{f_C}{M_C} + 0.25 \frac{f_H}{M_H} + \frac{f_S}{M_S} - \frac{f_O}{M_{O_2}} \right) \cdot M_{O_2} \quad (2.20)$$

donde  $f_i$  es la fracción másica del elemento  $i$  en el combustible. El flujo de aire en el reactor de oxidación se mantuvo constante durante los experimentos y siempre excedía el oxígeno estequiométrico demandado por el combustible. El ratio de exceso de aire,  $\lambda$ , se define en la Ecuación (2.21), y siempre se mantuvo por encima de 1.

$$\lambda = \frac{\text{Flujo de Oxígeno}}{\text{Demanda de Oxígeno}} = \frac{0.21 F_{\text{air}} M_{O_2}}{\Omega_{SF} \dot{m}_{SF}} \quad (2.21)$$

Para analizar la fiabilidad de los resultados, se realizan balances de materia al oxígeno, al carbono y al azufre usando las medidas de concentración de los diferentes compuestos en las corrientes de salida de los reactores de reducción y oxidación. El flujo de gas a la salida en base seca del reactor de reducción,  $F_{\text{outRR}}$ , se calcula como:

$$F_{\text{outRR}} = \frac{F_{\text{inRR}}}{1 - (y_{\text{CO}_2, \text{outRR}} + y_{\text{CO}, \text{outRR}} + y_{\text{H}_2, \text{outRR}} + y_{\text{CH}_4, \text{outRR}} + y_{\text{O}_2, \text{outRR}} + y_{\text{SO}_2, \text{outRR}})} \quad (2.22)$$

donde  $F_{\text{inRR}}$  es el flujo de gas entrante al reactor de reducción, es decir, incluye el N<sub>2</sub> introducido para fluidizar, N<sub>2</sub> del reactor de cierre y el N<sub>2</sub> introducido por el tornillo sinfín;  $y_{i, \text{outRR}}$  es la concentración del gas  $i$  en la corriente gaseosa a la salida del reactor de reducción en base seca.

El flujo de salida del reactor de oxidación,  $F_{\text{outRO}}$ , se calcula por medio de un balance al N<sub>2</sub>:



$$F_{\text{outRO}} = \frac{F_{\text{N}_2,\text{inRO}}}{1 - (y_{\text{O}_2,\text{outRO}} + y_{\text{CO}_2,\text{outRO}} + y_{\text{SO}_2,\text{outRO}})} \quad (2.23)$$

Así, los flujos de salida de cada gas  $i$  desde los reactores de reducción y oxidación se pueden calcular fácilmente usando su concentración:

$$F_{i,\text{out}} = y_{i,\text{out}} F_{\text{out}} \quad (2.24)$$

Como apunte indicar que se usa  $\text{N}_2$  como agente de fluidización en el reactor de reducción durante los experimentos, y por lo tanto el  $\text{CO}_2$  se produce únicamente en la combustión del combustible.

Con los flujos de gas, los balances de materia para el carbono, oxígeno y azufre se pueden calcular como:

$$\frac{f_C}{M_C} \dot{m}_{\text{SF}} = (F_{\text{CO}_2,\text{outRR}} + F_{\text{CO},\text{outRR}} + F_{\text{CH}_4,\text{outRR}}) + F_{\text{CO}_2,\text{outRO}} + F_{C,\text{elut}} \quad (2.25)$$

$$\begin{aligned} (F_{\text{CO}_2,\text{outRR}} + F_{\text{O}_2,\text{outRR}} + 0.5F_{\text{CO},\text{outRR}} + 0.5F_{\text{H}_2\text{O},\text{outRR}}) - \left( \frac{f_{\text{H}_2\text{O}}}{2M_{\text{H}_2\text{O}}} + \frac{f_{\text{O}}}{M_{\text{O}_2}} \right) \dot{m}_{\text{SF}} = \\ = F_{\text{O}_2,\text{inRO}} - (F_{\text{O}_2,\text{outRO}} + F_{\text{CO}_2,\text{outRO}}) \end{aligned} \quad (2.26)$$

$$f_S \cdot \dot{m}_{\text{SF}} = M_S (F_{\text{SO}_2,\text{outRR}} + F_{\text{SO}_2,\text{outRO}}) + S_{\text{ash}} \quad (2.27)$$

donde  $F_{C,\text{elut}}$  es el flujo de carbono elutriado desde el reactor de reducción como char inquemado. La concentración de agua no se medía. Sin embargo, para considerar el oxígeno que sale en forma de  $\text{H}_2\text{O}$  por la oxidación del hidrógeno del combustible, se supone que el agua procede tanto de la humedad como del hidrógeno contenido en el combustible:

$$F_{\text{H}_2\text{O},\text{outRR}} = \left( 0.5 \frac{f_H}{M_H} + \frac{f_{\text{H}_2\text{O}}}{M_{\text{H}_2\text{O}}} \right) \dot{m}_{\text{SF}} - F_{\text{H}_2,\text{outRR}} - 2F_{\text{CH}_4,\text{outRR}} \quad (2.28)$$

La evaluación del rendimiento del proceso CLOU con combustibles sólidos se realiza por medio del estudio del efecto de las variables de operación en la eficacia de captura de  $\text{CO}_2$ , la conversión del char y la eficacia de la combustión en el reactor de reducción.

La eficacia de captura de  $\text{CO}_2$ ,  $\eta_{\text{CC}}$ , se define como la fracción de carbono del combustible presente en los gases de salida del reactor de reducción. Este es el

verdadero CO<sub>2</sub> capturado en el sistema CLOU. El carbono no capturado saldrá como CO<sub>2</sub> junto al nitrógeno y el oxígeno sobrante a la salida del reactor de oxidación:

$$\eta_{CC} = 1 - \frac{F_{CO_2, outRO}}{\frac{f_C}{M_C} \cdot \dot{m}_{SF}} \quad (2.29)$$

La eficacia de captura de CO<sub>2</sub> depende de la conversión del char en el reactor de reducción,  $X_{char}$ . Este valor se calcula teniendo en cuenta que el carbono en los gases a la salida del reactor de reducción proviene del carbono contenido en los volátiles y en el char convertido. Así, el carbono en el char reactante procede del carbono alimentado en el sistema menos el flujo de carbono en los volátiles,  $F_{C, vol}$ , y las partículas de char elutriado,  $F_{C, elut}$ .

$$X_{char} = \frac{F_{CO_2, outRR} + F_{CO, outRR} + F_{CH_4, outRR} - F_{C, vol}}{\frac{f_C}{M_C} \dot{m}_{SF} - F_{C, vol} - F_{C, elut}} \quad (2.30)$$

El flujo molar de carbono contenido en los volátiles se calcula como:

$$F_{C, vol} = \frac{(f_C - f_{C, fix}) \dot{m}_{SF}}{M_C} \quad (2.31)$$

$f_{C, fix}$  es el carbono fijo calculado en el análisis del combustible; ver Tabla 2.2. La Ecuación (2.31) considera que la cantidad de volátiles generados en el reactor de reducción es la misma que muestra el análisis inmediato del combustible.

La conversión de char en el reactor de reducción está relacionada con la temperatura y el tiempo medio de residencia de los sólidos en el reactor de reducción,  $\tau_{RR}$ , calculado con la siguiente ecuación:

$$\tau_{RR} = \frac{m_{TO, RR}}{\dot{m}_{TO}} \quad (2.32)$$

$m_{TO, RR}$  es la masa de sólidos en el reactor de reducción y  $\dot{m}_{TO}$  el flujo de circulación de los sólidos entre los reactores de reducción y oxidación.

La velocidad de conversión del char en el reactor de reducción,  $(-r_{char})$ , se calcula con los valores de conversión del char en el reactor de reducción y el tiempo medio de residencia de las partículas de char en dicho reactor,  $\tau_{char}$ . La velocidad de conversión del char se calcula como:

$$(-r_{\text{char}}) = \frac{X_{\text{char}}}{\tau_{\text{char}}} \quad (2.33)$$

$\tau_{\text{char}}$  está relacionado con el tiempo medio de residencia de los sólidos en el reactor de reducción usando la siguiente expresión:

$$\tau_{\text{char}} = \tau_{\text{RR}} \cdot (1 - X_{\text{char}}) \quad (2.34)$$

Finalmente, la eficacia de combustión en el reactor de reducción,  $\eta_{\text{comb,RR}}$ , evalúa el grado de combustión respecto de la fracción de combustible convertido en el reactor de reducción. La eficacia de combustión en el reactor de reducción se calcula a través del cociente entre el oxígeno necesario para quemar los gases inquemados a la salida del reactor de reducción ( $\text{CH}_4$ ,  $\text{CO}$ ,  $\text{H}_2$ ) y el oxígeno necesario para la completa combustión del combustible convertido en el reactor de reducción. Así, la eficacia de combustión en el reactor de reducción se calcula como:

$$\eta_{\text{comb,RR}} = 1 - \frac{2F_{\text{CH}_4,\text{outRR}} + 0.5(F_{\text{CO},\text{outRR}} + F_{\text{H}_2,\text{outRR}})}{\frac{2\Omega_{\text{SF}}\dot{m}_{\text{SF}}}{M_{\text{O}_2}} - F_{\text{CO}_2,\text{outRO}} - F_{\text{C},\text{elut}}} \quad (2.35)$$

### **3 Resultados y discusión**



### 3.1 Desarrollo de transportadores de oxígeno

El objetivo de esta sección es desarrollar un transportador de oxígeno para el proceso CLOU basado en el óxido de cobre (CuO) que sea altamente reactivo y a la vez resistente a la atrición y a la aglomeración. Para ello se prepararon en primera instancia transportadores de oxígeno por tres métodos diferentes: impregnación húmeda incipiente, pelletización por extrusión y pelletización por compresión, ver Tabla 3.1. Estos transportadores se caracterizaron en TGA ya que permite analizar la reactividad de los transportadores de oxígeno en condiciones bien definidas y controladas, y en ausencia de complejos factores de fluidización, derivados de los procesos de transferencia de materia en la interfase burbuja-emulsión en un lecho fluidizado.

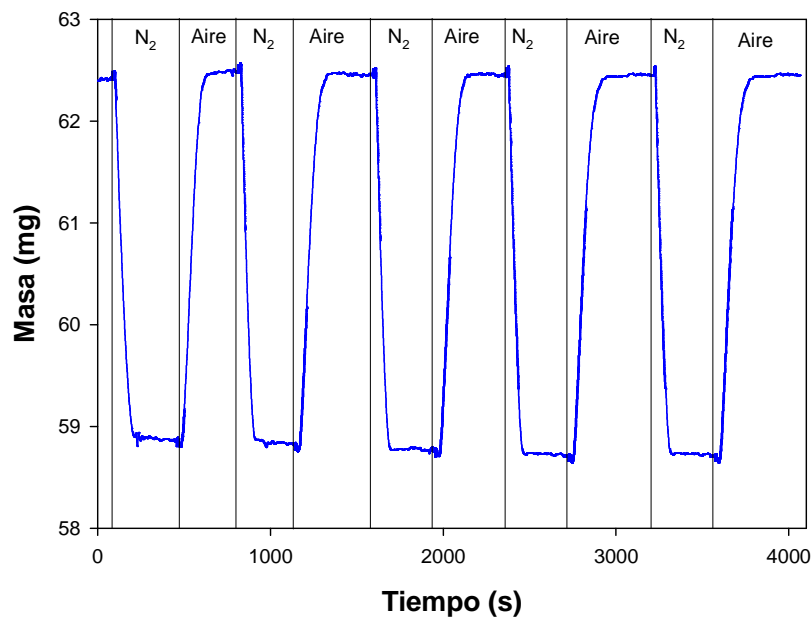


**Figura 3.1.** Termograma obtenido al realizar múltiples ciclos redox al transportador de oxígeno Cu60Zr\_P1100a. Temperatura 1000 °C

Para la caracterización de los transportadores de oxígeno, se realizaron 5 ciclos de reducción-oxidación para cada material analizado. En la Figura 3.1 se muestra un termograma típico de múltiples ciclos redox alternando atmósferas de  $N_2$  y aire para el transportador Cu60Zr\_P1100a a 1000 °C. En ausencia de oxígeno, es decir, en atmósfera de  $N_2$ , el transportador se descompone y libera  $O_2$ , observándose una disminución de la masa de muestra. Por el contrario, al poner en contacto el transportador de oxígeno con el oxígeno del aire, este se oxida, encontrando un aumento

de la masa de la muestra. Generalmente, tras el primer o segundo ciclo, el transportador de oxígeno se estabiliza alcanzándose velocidades de reacción constantes en los ciclos sucesivos. Para realizar las correspondientes comparaciones de reactividad se utilizó el 3º ciclo. A partir de los datos aportados por los termogramas de cada transportador de oxígeno, se calculan la conversión de reducción y oxidación de cada material, según las Ecuaciones (2.1) y (2.2). Con las curvas conversión tiempo se analizó el comportamiento de los transportadores de oxígeno preparados por diferentes métodos.

**Tabla 3.1.** Propiedades físicas de los transportadores de oxígeno preparados por impregnación o mezcla másica.

Transportador de oxígeno	Densidad de partícula (kg/m <sup>3</sup> )	Resistencia mecánica (N)	R <sub>TO</sub> (%)	(r <sub>O2</sub> )x10 <sup>3</sup> ( $\frac{kgO_2}{s \cdot kgOC}$ )
<b>Impregnación húmeda incipiente</b>				
Cu15γ-Al_I850	1600	2.5±0.5	1.5	0.64
Cu33γ-Al_I850	1900	3.0±0.4	3.3	1.03
Cu15α-Al_I850	2200	4.6±0.5	1.5	0.52
Cu15MgAl_I850	1900	2.1±0.3	1.5	1.32
Cu21MgAl_I850	2000	0.8±0.2	2.1	1.25
<b>Mezcla másica y extrusión</b>				
Cu60Al_E1100	3000	<0.5	6	1.67
Cu80Al_E1100	3900	2.6±0.5	8	0.99
Cu80Sep_E950	2300	0.8±0.3	8	1.76
Cu60Si_E950	2000	1.1±0.2	6	1.43
Cu80Si_E950	2900	0.9±0.2	8	1.75
Cu40Ti_E950	3400	2.3±0.4	4	1.19
Cu60Ti_E950	4000	2.2±0.2	6	---
Cu80Ti_E950	5200	2.2±0.4	8	0.64
Cu60Zr_E950	3000	<0.5	6	1.10
Cu80Zr_E950	3800	0.7±0.2	8	1.64
<b>Mezcla másica y compresión</b>				
Cu60MgAl_P950	3900	<0.5	6	---
Cu60MgAl_P1100	3800	1.2±0.3	6	1.47
Cu60MgAl_P1300	---	Melt	6	---
Cu60MgAl_P1100a	3700	1.7±0.3	6	1.50
Cu60MgAl_P1100b	3700	2.2±0.3	6	1.57
Cu60Zr_P950a	5400	<0.5	6	---
Cu40Zr_P1100a	4900	4.0±0.4	4	1.01
Cu60Zr_P1100a	5400	3.0±0.5	6	1.40
Cu60Mg_P1100a	4100	2.2±0.4	6	0.89
Cu60Sep_P1100	3900	2.2±0.5	6	1.45
Cu60Si_P950	2000	<0.5	6	---
Cu60Si_P950	---	Funde	6	---

Además, se determinó la resistencia mecánica de los diferentes materiales preparados. De todos los transportadores de oxígeno preparados, se seleccionaron aquellos que tenían una elevada reactividad y resistencia mecánica para su uso en un reactor de lecho

fluidizado discontinuo, donde se analizó su resistencia a la aglomeración y su velocidad de atrición.

Los transportadores de oxígeno más prometedores se prepararon por *spray drying* (método industrial de gran capacidad de producción), llevando a cabo los mismos análisis que para los transportadores de oxígeno anteriormente preparados. Viendo los buenos resultados obtenidos con los materiales preparados por *spray drying*, se evaluaron nuevos materiales preparados por este método en la Universidad Tecnológica de Chalmers (Gotemburgo, Suecia). Los resultados obtenidos forman parte de los Artículos I, II y III.

### **3.1.1 Transportadores de oxígeno preparados por impregnación incipiente**

En la Tabla 3.1 se muestran los transportadores de oxígeno obtenidos por impregnación incipiente, los cuales se prepararon usando como soporte  $\gamma\text{-Al}_2\text{O}_3$ ,  $\alpha\text{-Al}_2\text{O}_3$  y  $\text{MgAl}_2\text{O}_4$ , y cuyo contenido de CuO varió entre el 15 y el 33%.

En la Figura 3.2 se muestran las curvas de conversión de estos transportadores de oxígeno a 1000 °C para la reducción (descomposición) en 100% de  $\text{N}_2$  y la oxidación en aire obtenidos en el análisis termogravimétrico. Los transportadores de oxígeno preparados con  $\gamma\text{-Al}_2\text{O}_3$  como inerte presentan baja reactividad en las reacciones de reducción, además de una disminución significativa de la conversión máxima (relacionado con el  $R_{70}$  efectivo) con el aumento del número de ciclos. Esto se atribuye a la aparición de aluminato de cobre, ya que la oxidación del  $\text{CuAlO}_2$  formado durante la reducción es extremadamente lenta, como puede verse en la Figura 3.2(b). En esta figura se puede observar que la conversión del sólido en la oxidación es muy baja y por lo tanto en el siguiente ciclo de reducción hay menos oxígeno disponible y por tanto se reduce menos. Este comportamiento se observó para los materiales preparados con diferentes cantidades de CuO (15 y 33%), indicando que el contenido en Cu no mejora la reactividad de las muestras impregnadas. Resultados similares se obtuvieron con los transportadores de oxígeno impregnados sobre  $\alpha\text{-Al}_2\text{O}_3$ . En cambio, los transportadores de oxígeno preparados por impregnación utilizando como soporte  $\text{MgAl}_2\text{O}_4$ , muestran



una mayor reactividad en las reacciones de reducción y no presentan problemas de pérdida de reactividad ni de capacidad de transporte de oxígeno con los ciclos.

No obstante, la conversión máxima era de 0.6, lo que indica que su capacidad de transporte efectiva era menor que la teórica por su contenido en CuO. Por ejemplo, la capacidad de transporte para el Cu21MgAl era de  $R_{TO} = 1.26\%$ , lo cual es baja para su uso en el proceso CLOU. Además, estos transportadores de oxígeno presentan la característica de que al aumentar la cantidad de CuO se reduce su resistencia mecánica, llegando a valores inferiores a 1 N con un 21% de CuO (Cu21MgAl).

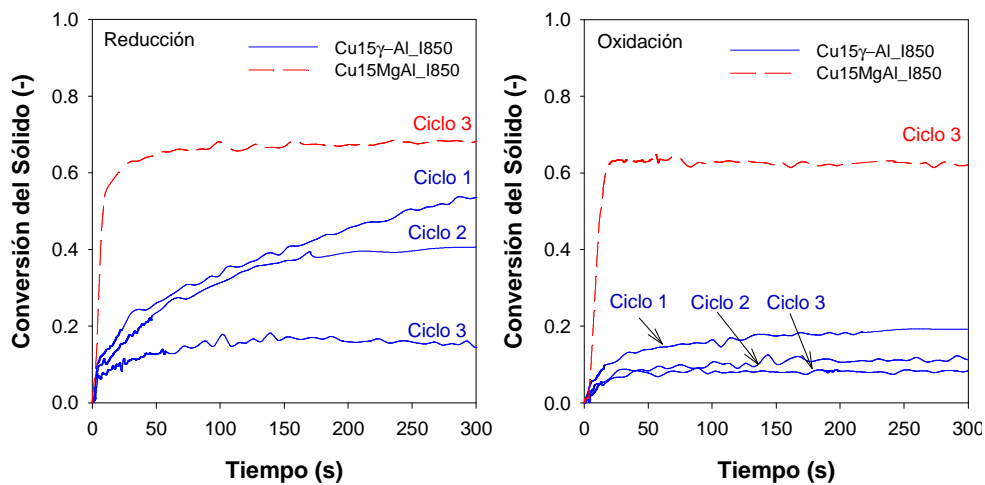


**Figura 3.2.** Variación de la conversión de reducción y oxidación con el tiempo de diferentes transportadores de oxígeno preparados por impregnación incipiente. Temperatura 1000°C; Reducción: N<sub>2</sub>. Oxidación: aire.

Por todo ello, los transportadores de oxígeno preparados por impregnación no se consideran adecuados para el proceso CLOU.

### 3.1.2 Transportadores de oxígeno preparados por mezcla másica y extrusión

También se prepararon transportadores de oxígeno mediante mezcla másica y extrusión, a partir de una mezcla física de los componentes deseados. Como se mostró en las Tablas 2.1 y 3.1 se utilizaron distintos materiales inertes y mayores contenidos en CuO (40-80%) que en los materiales preparados por impregnación.

En la Figura 3.3 se muestra la conversión durante la reducción a 1000°C y en la oxidación con un 21% de O<sub>2</sub> a 1000°C de los transportadores de oxígeno con un contenido del 80% en CuO. Como se puede ver, la reactividad de los diferentes transportadores de oxígeno depende del soporte utilizado. Los transportadores de oxígeno preparados con ZrO<sub>2</sub>, sepiolita, o SiO<sub>2</sub> como soporte muestran elevadas conversiones y altas velocidades de reacción, tanto en reducción como en oxidación. Además, mostraron una gran estabilidad con los ciclos. Los transportadores de oxígeno preparados con TiO<sub>2</sub> y Al<sub>2</sub>O<sub>3</sub> como soportes presentaban bajas conversiones máximas, tanto en la reducción como en la oxidación.

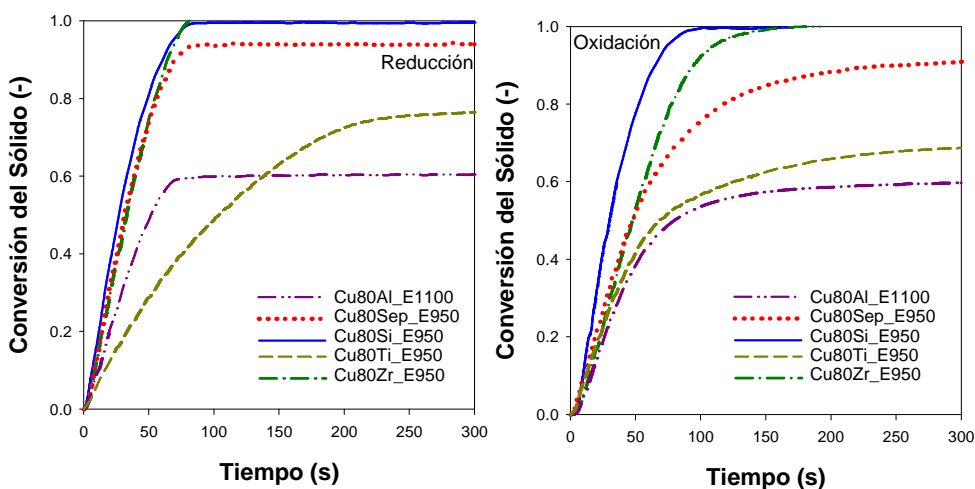


**Figura 3.3.** Conversión de reducción y oxidación frente al tiempo de diferentes transportadores de oxígeno preparados por mezcla másica y extrusión. Temperatura 1000°C; Tercer ciclo de la reducción en N<sub>2</sub> y la oxidación en aire.

Algunas de las muestras extraídas tras los experimentos llevados a cabo en TGA mostraban signos de aglomeración. Así, los transportadores de oxígeno preparados con Al<sub>2</sub>O<sub>3</sub>, ZrO<sub>2</sub> y TiO<sub>2</sub> como inertes con un contenido alto en CuO (80%) mostraban signos de aglomeración. Este hecho supone un riesgo importante para el uso de estas partículas en un lecho fluidizado y debe evitarse. Por ello, se prepararon y probaron transportadores de oxígeno con contenidos en CuO inferiores (60 y 40% respectivamente). La Tabla 3.2 muestra los resultados referentes a la aglomeración encontrada en los experimentos en TGA. Se puede ver que presentan aglomeración todos los transportadores de oxígeno preparados con TiO<sub>2</sub> como inerte. Sin embargo, los transportadores de oxígeno con un 60% de contenido en CuO y Al<sub>2</sub>O<sub>3</sub> o ZrO<sub>2</sub> no presentaban problemas de aglomeración.

Los transportadores de oxígeno que no aglomeraron y tenían alta reactividad presentaban menores valores de resistencia mecánica, tal y como se ha mostrado en la Tabla 3.2. Las partículas con valores de resistencia mecánica <1 N pueden generar problemas en su uso en lecho fluidizado debido a una alta atrición [77]. Debido a ello los transportadores de oxígeno preparados por mezcla másica y extrusión no se consideraron adecuados para su uso en el proceso CLOU.

**Tabla 3.2.** Propiedades de los transportadores de oxígeno preparados por mezcla másica y extrusión tras su uso en TGA.

Transportador	Soporte	% CuO	Aglomeración	Resistencia Mecánica	Reactividad Relativa
Cu80Al_E1100	Al <sub>2</sub> O <sub>3</sub>	80	Si	2.6	Baja
Cu60Al_E1100		60	No	<0.5	Baja
Cu80Sep_E950	Sepiolita	80	No	0.8	Alta
Cu80Si_E950	SiO <sub>2</sub>	80	No	0.9	Alta
Cu80Ti_E950	TiO <sub>2</sub>	80	Si	2.2	Baja
Cu60Ti_E950		60	Si	2.2	Baja
Cu40Ti_E950		40	Si	2.3	Baja
Cu80Zr_E950	ZrO <sub>2</sub>	80	Si	0.7	Alta
Cu600Zr_E950		60	No	<0.5	Alta

### 3.1.3 Transportadores de oxígeno preparados por mezcla másica y compresión

Vistos los resultados obtenidos para los transportadores de oxígeno preparados por impregnación incipiente con MgAl<sub>2</sub>O<sub>4</sub> como soporte y por mezcla másica y extrusión con sepiolita, ZrO<sub>2</sub> y SiO<sub>2</sub> como materiales inertes, se prepararon transportadores de oxígeno por este nuevo método con contenidos en CuO del 60%, utilizando estos materiales como inertes, es decir, MgAl<sub>2</sub>O<sub>4</sub>, ZrO<sub>2</sub>, sepiolita y SiO<sub>2</sub>. Además, se introdujo el MgO como un nuevo material para su utilización como soporte. Con este método se pretendía aumentar la resistencia mecánica de las partículas conservando su alta reactividad. Al preparar los transportadores de oxígeno con SiO<sub>2</sub> como inerte se obtenían unas partículas con una resistencia mecánica muy baja (<0.5N) o directamente se fundían al calcinarlas. Por lo tanto se decidió eliminar este material para los posteriores análisis en TGA.

### 3.1.3.1 Reactividad de los transportadores en TGA

En la Figura 3.4 se muestran las conversiones de reducción y oxidación de los transportadores de oxígeno preparados por pelletización por compresión usando diferentes soportes. Tanto en la reducción como en la oxidación, se puede observar que todos los transportadores presentan una alta velocidad de reacción. Además, todos estos materiales mantenían una reactividad constante en los sucesivos ciclos de reacción. Exceptuando el caso del transportador de oxígeno preparado con MgO como inerte, el resto de transportadores de oxígeno preparados por este método presentan una conversión máxima cercana a la unidad.

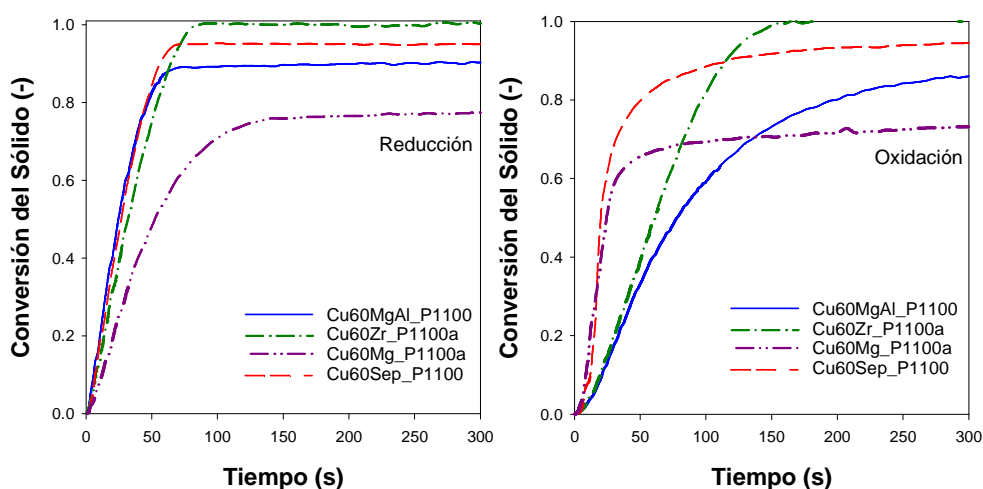


**Figura 3.4.** Conversión de reducción y oxidación con el tiempo de diferentes transportadores de oxígeno preparados por mezcla másica y compresión. Temperatura 1000°C; Tercer ciclo de la reducción con N<sub>2</sub> y de la oxidación con aire.

### 3.1.3.2 Caracterización en lecho fluidizado discontinuo I (ciclos N<sub>2</sub>-aire)

En vista de la alta reactividad y estabilidad con los ciclos obtenida en TGA, se prepararon lotes de 500 g de los transportadores de oxígeno preparados por mezcla másica y compresión con un contenido en CuO del 60% y usando como inertes MgAl<sub>2</sub>O<sub>4</sub>, ZrO<sub>2</sub>, sepiolita o MgO para ser analizados durante experimentos multi-ciclo en un reactor de lecho fluidizado discontinuo. A partir de estos experimentos se evaluaron las características de las reacciones de reducción-oxidación, así como se determinaron la velocidad de atrición y la tendencia a la aglomeración del material.

### Descomposición y regeneración de los transportadores de oxígeno

Se llevaron a cabo múltiples ciclos de reducción-oxidación con los transportadores de oxígeno preparados por mezcla másica y compresión en un reactor de lecho fluidizado discontinuo para determinar la capacidad de generación de oxígeno en una atmósfera de  $N_2$  en función de las condiciones de operación.

En la Figura 3.5 se puede observar que al comienzo del periodo de reducción se comienza a liberar oxígeno hasta alcanzar la concentración de oxígeno en equilibrio a la temperatura del lecho. A los 10 minutos, la concentración de oxígeno a la salida disminuye hasta valores muy por debajo de la concentración de equilibrio, lo que indica una disminución de la velocidad de liberación de oxígeno. Después de 22 minutos comienza la oxidación. La mayor parte de la reacción de oxidación se produce con una concentración de oxígeno a la salida cercana a la de equilibrio a dicha temperatura. Esto indica que las reacciones no están limitadas por la velocidad de reacción, sino por el equilibrio termodinámico.

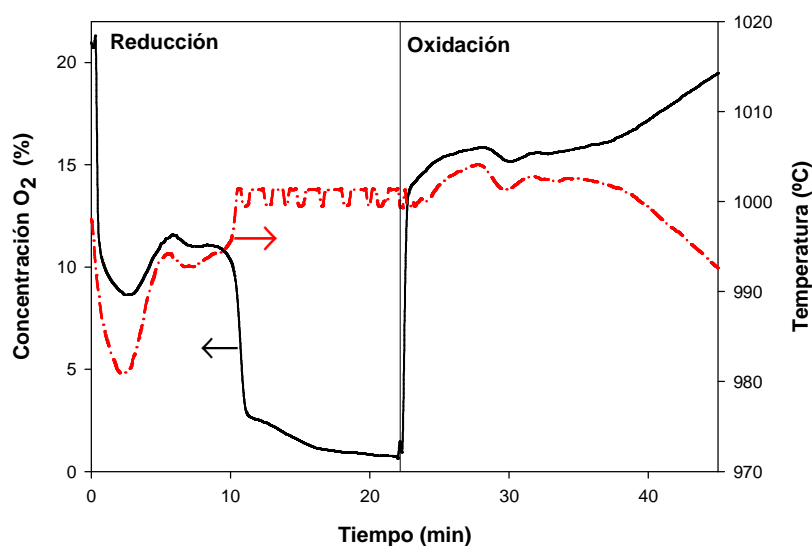


**Figura 3.5.** Evolución de la concentración de oxígeno y la temperatura en el lecho durante un ciclo de reducción-oxidación. Transportador de oxígeno: Cu60MgAl\_P1100. Temperatura 1000°C. Reducción:  $N_2$ . Oxidación: aire.

En la Figura 3.5 además se puede observar que hay variaciones relevantes en la temperatura medida en el lecho. Estas variaciones pueden explicarse según la entalpía de la reacción de reducción o de oxidación. Se produce una disminución de la temperatura del lecho al comienzo de la liberación de oxígeno y descomposición del CuO debido a la endotermicidad de esta reacción. Cuando comienza la oxidación se

produce un incremento de la temperatura debido a que dicha reacción es fuertemente exotérmica.

En el proceso CLOU, el gas introducido en el reactor de reducción es  $\text{CO}_2$  recirculado de la corriente de salida. Para realizar un estudio del posible efecto del gas de fluidización se llevaron a cabo experimentos usando como agentes de fluidización  $\text{N}_2$  puro o  $\text{CO}_2$  puro. En la Figura 3.6 se muestra la conversión del sólido y el perfil de concentración de oxígeno a la salida del reactor, durante el periodo de reducción a  $1000^\circ\text{C}$  con el transportador de oxígeno  $\text{Cu60MgAl\_P1100}$ , y usando diferentes gases de fluidización: 100 vol. %  $\text{N}_2$  o 100 vol. %  $\text{CO}_2$ .

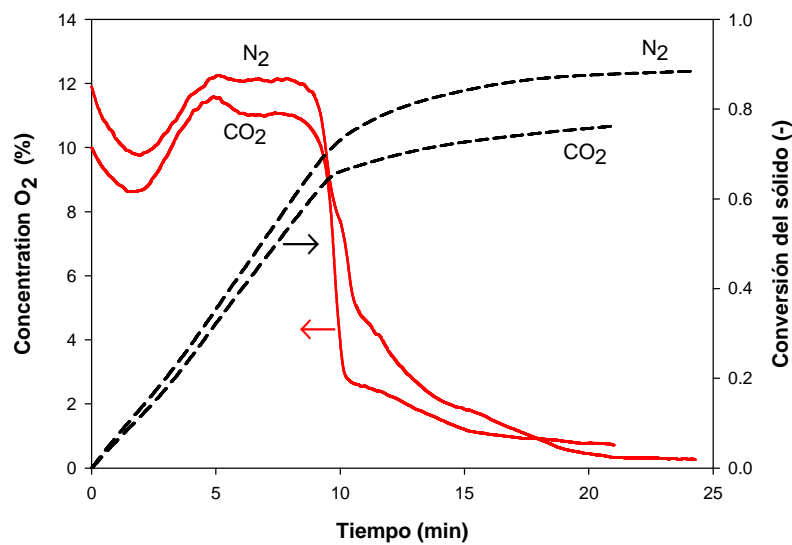


**Figura 3.6.** Evaluación de la concentración de  $\text{O}_2$  y de la conversión durante el periodo de reducción del transportador de oxígeno  $\text{Cu60MgAl\_P1100}$ , usando diferentes gases de fluidización ( $\text{N}_2$  o  $\text{CO}_2$ ) a  $1000^\circ\text{C}$ .

Como se puede observar, se obtuvieron resultados similares independientemente del gas utilizado. Las pequeñas diferencias se consideraron debidas a las diferencias en la capacidad calorífica de ambos gases, lo que provocaba pequeñas diferencias en la temperatura del reactor. También se puede observar que las conversiones del sólido obtenidas fueron muy similares independientemente del gas usado y la diferencia observada fue únicamente debida a las pequeñas variaciones en la temperatura de reacción en cada caso, la cual afecta a la cantidad de oxígeno liberada. De aquí en adelante se mostrarán los resultados utilizando como agente de fluidización  $\text{N}_2$  puro.

El efecto de la temperatura de reacción se analizó en el lecho fluidizado discontinuo usando temperaturas de  $900$ ,  $950$  y  $1000^\circ\text{C}$  durante los ciclos. Se observaron dos

comportamientos diferentes, según se lograsen obtener o no condiciones de equilibrio. En la Figura 3.7(a) se pueden observar los perfiles de concentración de  $O_2$  a la salida del reactor y la conversión del sólido  $Cu60Zr\_P1100a$  durante el periodo de reducción usando diferentes temperaturas de lecho. Con dicho sólido se alcanzaban concentraciones de oxígeno muy por debajo a la concentración de equilibrio, además de bajas conversiones del sólido. La baja concentración de  $O_2$  observado con  $Cu60Zr\_P1100a$  fue debida a la mala fluidización del sólido por problemas de aglomeración, como se comprobó posteriormente al extraer el sólido del reactor. Del mismo modo se comportaron los transportadores de oxígeno  $Cu60Sep\_P1100$  y  $Cu60Mg\_P1100$ .

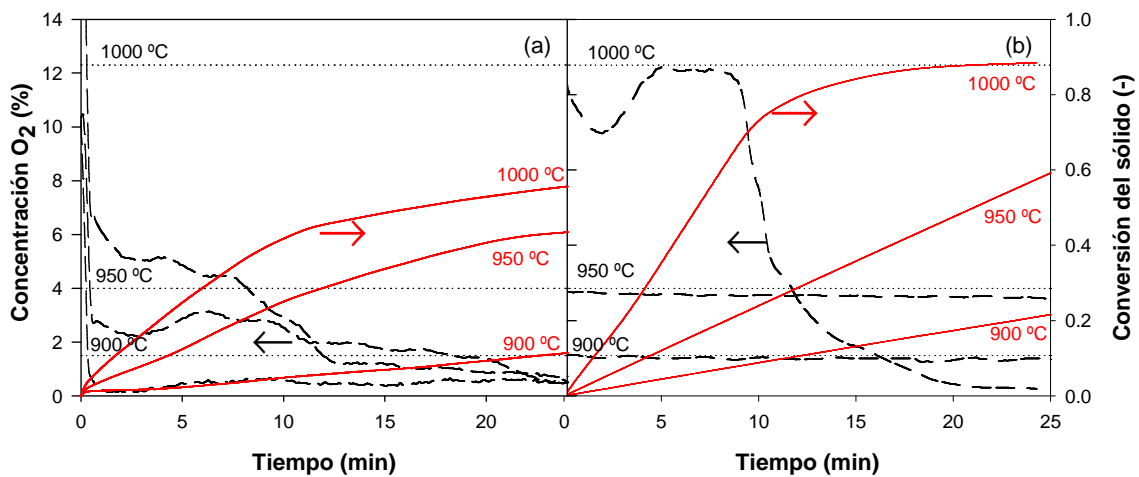


**Figura 3.7.** Evolución de la concentración de  $O_2$  y conversión del sólido durante el periodo de reducción, para diferentes temperaturas de lecho. Transportadores de oxígeno: (a)  $Cu60Zr\_P1100a$ ; (b)  $Cu60MgAl\_P1100$ . (···) Concentración de  $O_2$  en el equilibrio a cada temperatura. Gas de fluidización:  $N_2$ .

Por otro lado, la Figura 3.7(b) muestra los perfiles de concentración de  $O_2$  a la salida del reactor y la conversión del sólido  $Cu60MgAl\_P1100$  durante el periodo de reducción usando diferentes temperaturas de lecho. También se muestra la concentración de  $O_2$  en el equilibrio para cada temperatura. Como se puede observar la velocidad de liberación de oxígeno es constante y limitada por el equilibrio termodinámico del oxígeno. A  $1000^\circ C$ , el sólido alcanza prácticamente conversión completa en menos de 15 minutos. A  $900^\circ C$  la descomposición del sólido está limitada debido a la baja concentración de oxígeno liberada en el equilibrio.

### *Comportamiento de los transportadores de oxígeno frente a la aglomeración*

Uno de los parámetros más importantes para la selección de un transportador de oxígeno para el proceso CLOU es la resistencia a la aglomeración durante la fluidización. La aglomeración es un fenómeno por el cual las partículas del lecho se unen de forma más a menos fuerte, dejando de fluidizar e impidiendo que la reacción se lleve a cabo. Este efecto se detecta durante la operación en el lecho fluidizado discontinuo debido a que cae bruscamente la pérdida de carga en el lecho. Además, una vez el lecho ha dejado de fluidizar, la temperatura no es uniforme y difícil de controlar. Se han distinguido tres tipos de aglomeración:

- **Suave:** se elimina la aglomeración de las partículas variando las condiciones de fluidización.
- **Moderada:** es necesario realizar una parada de la operación para deshacer los aglomerados formados. Posteriormente se puede volver a operar con el mismo lote de partículas.
- **Fuerte:** es necesario detener la experimentación y no se puede volver a operar con el mismo lote de partículas debido a la elevada resistencia de los aglomerados.

En la Tabla 3.3 se muestra el comportamiento frente a la aglomeración de los transportadores de oxígeno preparados por mezcla másica y compresión que fueron analizados en el reactor de lecho fluidizado discontinuo.

**Tabla 3.3.** Comportamiento frente a la aglomeración de los transportadores de oxígeno probados en lecho fluidizado discontinuo.

Transportador	Soporte	Aglomeración en lecho fluidizado discontinuo
Cu60MgAl_P1100	MgAl <sub>2</sub> O <sub>4</sub>	No presenta
Cu60Zr_P1100a	ZrO <sub>2</sub> (60% CuO)	Moderada
Cu40Zr_P1100a	ZrO <sub>2</sub> (40% CuO)	Suave T>950°C
Cu60Sep_P1100	Sepiolita	Fuerte
Cu60Mg_P1100a	MgO	Fuerte

De producirse aglomeración, ésta siempre aparecerá en los primeros minutos de la descomposición del transportador de oxígeno de CuO a Cu<sub>2</sub>O. En un principio todos los transportadores preparados tenían un 60% de CuO. En las primeras pruebas en el reactor de lecho fluidizado discontinuo fueron descartados los transportadores de oxígeno



preparados con sepiolita y MgO como inertes, ya que presentaban una fuerte aglomeración a temperaturas bajas (900°C). Por otro lado, los transportadores de oxígeno con ZrO<sub>2</sub> como inerte presentan problemas de aglomeración moderados, que provocan que se alcancen bajas conversiones de descomposición (ver Figura 3.7(a)).

Para intentar solucionar el problema de la aglomeración moderada en el caso de usar ZrO<sub>2</sub> como inerte se decidió bajar la cantidad de fase activa del 60 al 40% de CuO en este transportador de oxígeno. De esta forma se consiguió que sólo se presentara aglomeración suave a temperaturas superiores a 950°C. Los transportadores preparados con MgAl<sub>2</sub>O<sub>4</sub> como inerte no presentaron problemas de aglomeración en ningún caso.

En la Figura 3.8 se pueden observar diferentes fotografías de los aglomerados y de partículas sueltas extraídas del con diferentes materiales. En las Figuras 3.8(a) y (b) se muestran partículas sueltas y sin aglomerar de los transportadores de oxígeno Cu60MgAl\_P1100 y Cu40Zr\_P1100a, que mostraron un buen comportamiento respecto a la generación de oxígeno en el lecho fluidizado. En la Figura 3.8(c) se muestra un aglomerado de tipo moderado correspondiente al transportador de oxígeno Cu60Zr\_P1100a. Por otra parte, en la Figura 3.8(d) se muestran los aglomerados de tipo fuerte correspondiente al transportador de oxígeno Cu60Mg\_P1100a.

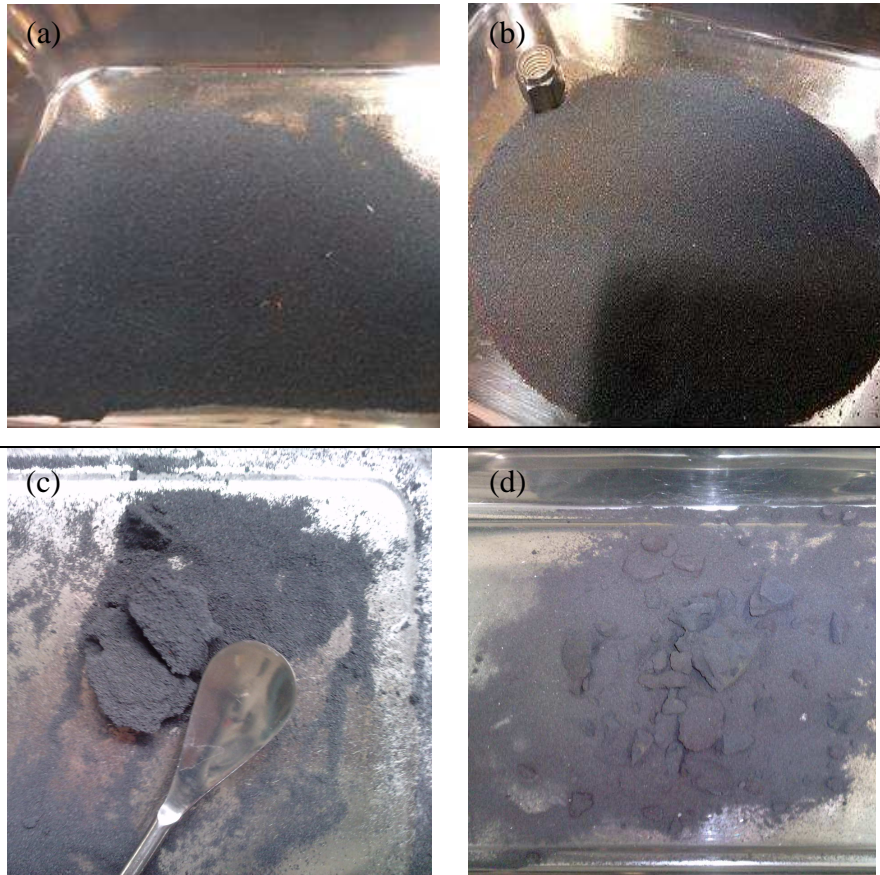


**Figura 3.8.** Fotografías de diferentes partículas extraídas del lecho fluidizado discontinuo. Partículas sin aglomerar: (a) Cu60MgAl\_P1100, (b) Cu40Zr\_P1100a; partículas aglomeradas (c) Cu60Zr\_P1100a, y (d) Cu60Mg\_P1100a.

#### *Comportamiento de los transportadores de oxígeno frente a la atrición*

Otro parámetro importante a la hora de seleccionar los materiales para el proceso CLOU es el comportamiento frente a la atrición. La atrición es el fenómeno por el cual las partículas de transportador de oxígeno se erosionan y/o desgastan al estar sometidas a condiciones de fluidización y son arrastradas por el gas de fluidización fuera del lecho. Se evalúa como atrición la masa de sólido elutriado durante los ciclos de operación en el reactor de lecho fluidizado discontinuo que tenga un tamaño de partícula inferior a 40  $\mu\text{m}$ . Se asume que las partículas más pequeñas de 40  $\mu\text{m}$  no serían recogidas en el sistema de ciclones en una planta industrial de CLOU.

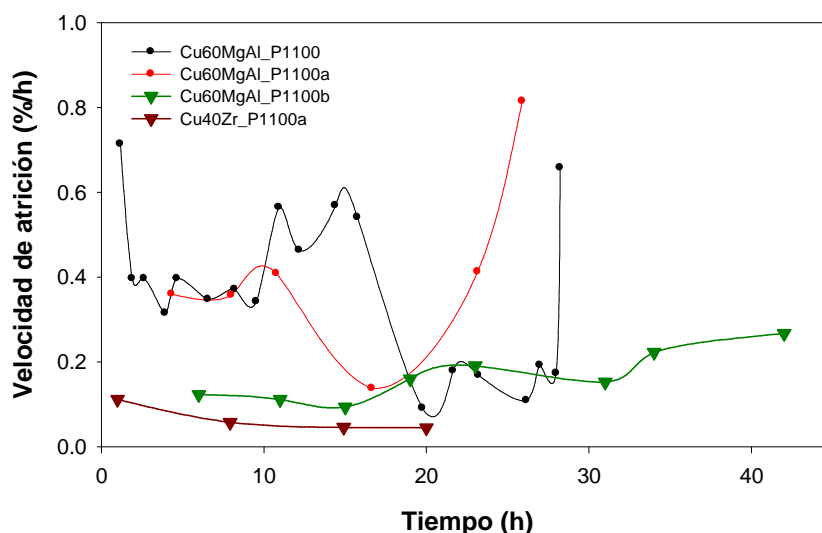


**Figura 3.9.** Velocidad de atrición para los transportadores de oxígeno Cu60MgAl\_P1100, Cu60MgAl\_P1100a, Cu60MgAl\_P1100b, y Cu40Zr\_P1100a en función de las horas de operación en el reactor de lecho fluidizado discontinuo.

En la Figura 3.9 se muestran las velocidades de atrición medidas con diferentes transportadores de oxígeno preparados por mezcla másica y compresión en función de las horas de operación en el lecho fluidizado discontinuo. Como se puede observar, la velocidad de atrición para el Cu40Zr\_P1100a es baja y estable. Por otro lado la velocidad de atrición para el Cu60MgAl\_P1100 es más elevada, y a partir de 20 horas de operación se produce la rotura de las partículas.

Para intentar disminuir esta velocidad de atrición, se prepararon dos transportadores de oxígeno con mayor resistencia mecánica. Primero, para la preparación del Cu60MgAl\_P1100a se disminuyó la porosidad de las partículas disminuyendo la cantidad de grafito utilizado en la preparación del 10% al 0.5%. Con ello se logró aumentar la resistencia mecánica de las partículas sin que se viese afectada la reactividad (ver Tablas 2.1 y 3.1). Como se puede observar, el transportador de oxígeno con un menor contenido en grafito presentaba un comportamiento similar al del transportador de oxígeno Cu60MgAl\_P1100. Finalmente, se aumentó el tiempo de calcinación durante la preparación del transportador, Cu60MgAl\_P1100b a 12 horas, aumentando de nuevo la resistencia mecánica a 2.2 N (ver Tablas 2.1 y 3.1). Con esto se logró disminuir significativamente la velocidad de atrición sin afectar a su reactividad. En la Figura 3.9 se observa que la velocidad de atrición oscilaba entre 0.1 y 0.2 %/h, lo cual se consideraba adecuado para su utilización en la planta experimental.

### 3.1.3.3 Propiedades físico-químicas de los transportadores de oxígeno preparados por mezcla másica y compresión

En la Tabla 3.4 se muestran los resultados obtenidos para los análisis de porosimetría, área BET, XRD y resistencia mecánica para los transportadores de oxígeno preparados por mezcla másica y compresión, utilizados en el reactor de lecho fluidizado discontinuo.

La porosidad de todos los transportadores de oxígeno es baja. No obstante, a pesar de la baja porosidad todas las partículas son muy reactivas. Sin embargo, la porosidad de las partículas aumentó tras los ciclos redox. De este modo, para la familia de transportadores de oxígeno de Cu60MgAl, con más de 30 horas de operación en el lecho fluidizado discontinuo, se duplica la porosidad de las partículas. Sin embargo, los transportadores de oxígeno Cu60Zr\_P1100a y Cu40Zr\_P1100a, con los cuales se realizaron 15 a 20 horas de operación, presentan un ligero aumento de esta propiedad.

**Tabla 3.4.** Propiedades físicas y químicas de los transportadores de oxígeno frescos y usados en lecho fluidizado discontinuo.

Transportador de oxígeno	Tiempo de Operación (h)	Porosidad (%)		Área BET (m <sup>2</sup> /g)		Resistencia mecánica (N)		XRD	
		Fresco	Usado	Fresco	Usado	Fresco	Usado	Fresco	Usado
Cu60MgAl_P1100	28	13.0	26.4	0.3	0.40	1.2	0.9	CuO,Cu <sub>2</sub> O, MgAl <sub>2</sub> O <sub>4</sub>	CuO, MgAl <sub>2</sub> O <sub>4</sub>
Cu60MgAl_P1100a	25	11.2	22.5	0.2	0.3	1.9	1.0	CuO,Cu <sub>2</sub> O, MgAl <sub>2</sub> O <sub>4</sub>	CuO, MgAl <sub>2</sub> O <sub>4</sub>
Cu60MgAl_P1100b	42	10.5	30.0	0.2	0.3	2.2	1.5	CuO,Cu <sub>2</sub> O, MgAl <sub>2</sub> O <sub>4</sub>	CuO, MgAl <sub>2</sub> O <sub>4</sub>
Cu60Zr_P1100a	10	7	9.1	0.1	0.1	4.8	4.6	CuO,Cu <sub>2</sub> O, ZrO <sub>2</sub>	CuO, ZrO <sub>2</sub>
Cu40Zr_P1100a	15	9	12.1	0.1	0.1	2.8	2.6	CuO,Cu <sub>2</sub> O, ZrO <sub>2</sub>	CuO, ZrO <sub>2</sub>
Cu60Sep_P1100	3	10.5	---	0.4	---	2.2	---	CuO,Cu <sub>2</sub> O, Sepiolita*	---
Cu60Mg_P1100a	5	9.7	---	0.3	---	2.2	---	CuO,Cu <sub>2</sub> O, MgO	---

\*Sepiolita: Aluminio-silicato que contiene calcio y potasio

Nota: Cu60Sep\_P1100 y Cu60Mg\_P1100a no se caracterizaron usados debido a que sólo se utilizaron 3 y 5 horas, respectivamente, en el lecho fluidizado discontinuo debido a la aglomeración que presentan.

Todos los transportadores de oxígeno preparados por mezcla másica y compresión tienen una resistencia mecánica superior a 1 N, que se ha considerado adecuada para trabajar bajo condiciones de fluidización [77]. Con los transportadores de oxígeno Cu60MgAl\_P1100 y Cu60MgAl\_P1100a la resistencia mecánica disminuye por debajo de 1 N tras los experimentos realizados en el reactor de lecho fluidizado discontinuo, lo que explicaría los altos valores de atrición observados en la Figura 3.9. Por otro lado,

los transportadores de oxígeno Cu60MgAl\_P1100b y Cu40Zr\_P1100a presentan una disminución menor de su resistencia mecánica tras la operación en el reactor de lecho fluidizado discontinuo, lo que está relacionado con su baja velocidad de atrición mostrada en la Figura 3.9.

En la Tabla 3.4 se muestran las fases cristalinas que se observan en los difractogramas obtenidos por XRD. En el caso de los transportadores de oxígeno frescos, aparece  $\text{Cu}_2\text{O}$ , debido a que a la temperatura de calcinación se dan las condiciones necesarias para que el  $\text{CuO}$  se descomponga a  $\text{Cu}_2\text{O}$  (a  $1100^\circ\text{C}$  la concentración de  $\text{O}_2$  en el equilibrio es superior al 21%; ver Figura 1.19). Además, también aparece  $\text{CuO}$  debido a una oxidación parcial durante el enfriamiento de las muestras en aire. Tras los experimentos en el lecho fluidizado discontinuo, solamente aparece la fase  $\text{CuO}$  debido a la completa oxidación en aire en el lecho. También se puede observar que no se produjo interacción entre el  $\text{CuO}$  y los diferentes materiales inertes usados, lo que justifica las elevadas conversiones obtenidas en la TGA; ver Figura 3.4.

Los resultados indican que los transportadores de oxígeno preparados con un 60% de  $\text{CuO}$  con  $\text{MgAl}_2\text{O}_4$  como inerte, y un 40% de  $\text{CuO}$  con  $\text{ZrO}_2$  tienen resultados satisfactorios respecto a su reactividad y su comportamiento en la fluidización.

#### **3.1.4 Evaluación de transportadores de oxígeno preparados por *spray drying***

La experiencia obtenida durante la evaluación de las partículas obtenidas en el laboratorio mediante el método de mezcla másica y compresión se ha utilizado para elegir las condiciones de preparación de las partículas de transportador de oxígeno mediante un método industrial. Un transportador de oxígeno con un 60% de  $\text{CuO}$  y 40% de  $\text{MgAl}_2\text{O}_4$  como material inerte, y con 40% de  $\text{CuO}$  y 60% de  $\text{ZrO}_2$  son adecuados para su uso en el proceso CLOU con adecuada reactividad y resistencia a la atrición. Para escalar la producción de transportadores de oxígeno de nivel de laboratorio a nivel industrial es necesaria la producción por un método a gran escala. Por lo tanto se prepararon estos transportadores de oxígeno por *spray drying*.

El transportador de oxígeno con 40% de CuO y ZrO<sub>2</sub> como inerte preparado por *spray drying* presentó una alta tendencia a la aglomeración a todas la temperaturas en el reactor de lecho fluidizado discontinuo y por tanto no se seleccionó para su posterior evaluación. Por el contrario, Así pues en esta sección se evaluó y caracterizó el transportador de oxígeno con un 60% de CuO y un 40% de MgAl<sub>2</sub>O<sub>4</sub> (Cu60MgAl\_SD) preparado por *spray drying* mostró un buen comportamiento, y por tanto se evaluó y en caracterizó tanto en TGA como en el reactor de lecho fluidizado discontinuo.

#### **3.1.4.1 Análisis de la reactividad en TGA**

El transportador de oxígeno Cu60MgAl\_SD se caracterizó en TGA para analizar las velocidades de generación de oxígeno y regeneración en función del número de ciclos, temperatura y concentración de oxígeno. Se encontró que tanto para la reducción como para la oxidación la velocidad de reacción era estable con los ciclos.

La Figura 3.10 muestra la conversión del transportador de oxígeno en función del tiempo a 1000 °C, tanto para la reducción (a) como para la oxidación (b). El transportador de oxígeno muestra altas velocidades de generación de oxígeno, alcanzando conversión completa del sólido en menos de 1 minuto. Estos resultados son muy similares a los obtenidos en la TGA para los transportadores de oxígeno preparados por pelletización por compresión, con velocidades de generación de oxígeno de  $1.66 \cdot 10^{-3}$  (kg O<sub>2</sub>/s·kg TO) frente a  $1.57 \cdot 10^{-3}$  (kg O<sub>2</sub>/s·kg TO) obtenidos para el transportador de oxígeno Cu60MgAl\_P1100b. Respecto a la oxidación, se puede observar también una alta velocidad de regeneración del transportador de oxígeno, la cual también es muy similar a la obtenida para el transportador de oxígeno preparado por mezcla másica y compresión (ver Figura 3.4).

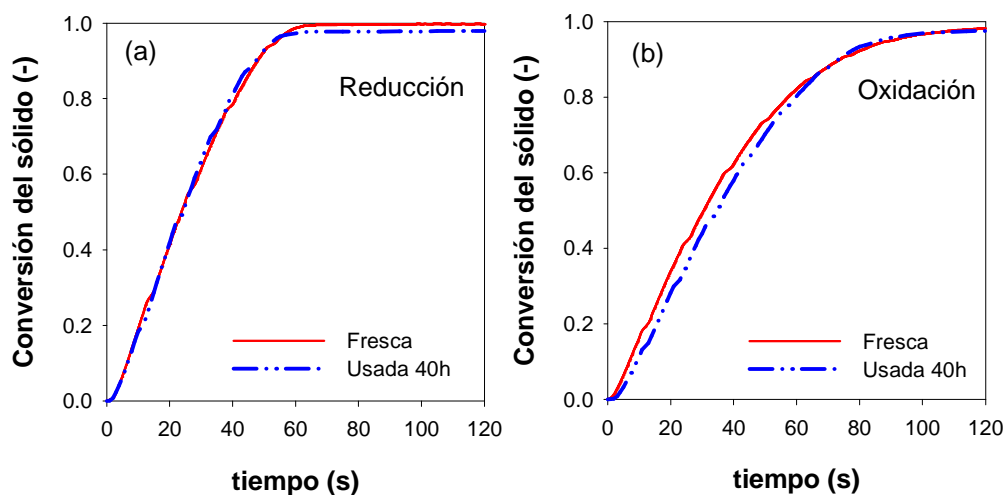


**Figura 3.10.** Curvas-conversión tiempo para las reacciones de descomposición y oxidación de muestras frescas y usadas en el reactor de lecho fluidizado discontinuo. Reducción en  $N_2$  y oxidación en aire a  $1000\text{ }^\circ\text{C}$  en la TGA.

### 3.1.4.2 Comportamiento del transportador de oxígeno Cu60MgAl\_SD en el reactor de lecho fluidizado discontinuo I (ciclos $N_2$ -Aire)

Se llevaron a cabo múltiples ciclos redox en el reactor de lecho fluidizado discontinuo para analizar la generación de oxígeno del material, así como su comportamiento frente a la aglomeración y la velocidad de atrición durante la fluidización. Se realizaron un total de 40h de fluidización a  $950\text{ }^\circ\text{C}$  durante 22 ciclos redox consecutivos.

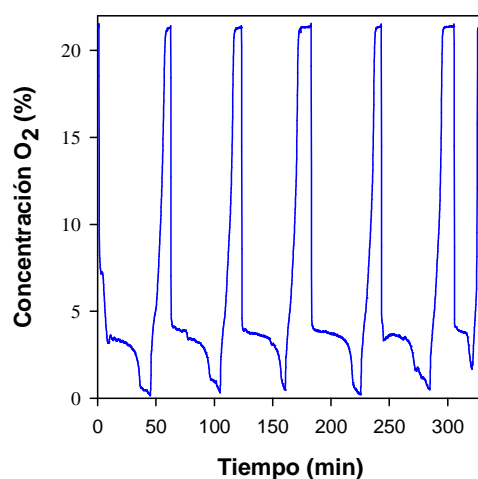


**Figura 3.11.** Concentración de oxígeno en función del tiempo para 6 ciclos redox consecutivos en el reactor de lecho fluidizado discontinuo para el transportador de oxígeno Cu60MgAl\_SD a  $950\text{ }^\circ\text{C}$ . Reducción:  $100\% N_2$ . Oxidación: Aire.

Como ejemplo, la Figura 3.11 muestra la concentración de oxígeno a la salida del reactor para 6 ciclos redox consecutivos para el transportador de oxígeno

Cu60MgAl\_SD. Se puede observar que el comportamiento del material fue estable durante todas las etapas de reducción-oxidación.

La Figura 3.12 muestra la conversión del transportador de oxígeno y el perfil de O<sub>2</sub> durante el periodo de reducción y oxidación durante un ciclo típico. También se muestra la concentración de O<sub>2</sub> en el equilibrio a 950°C. La concentración de O<sub>2</sub> está muy próxima al equilibrio durante la mayor parte del ciclo de reducción. El transportador de oxígeno muestra una velocidad de generación de oxígeno constante mientras la conversión de oxidación (X<sub>ox</sub>) del transportador de oxígeno se va reduciendo hasta un valor de X<sub>ox</sub> = 0.35.

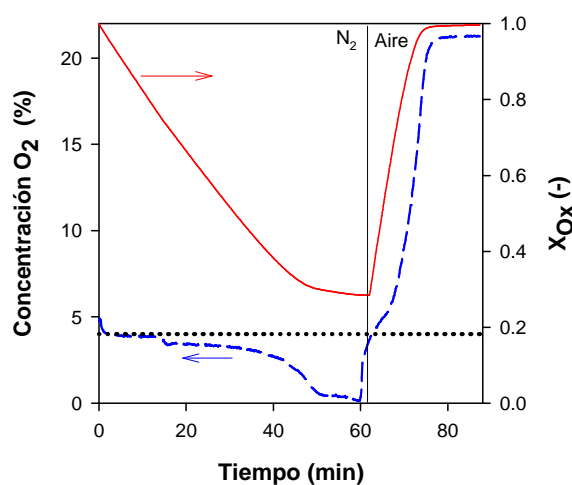


**Figura 3.12.** Evaluación de la concentración de O<sub>2</sub> (---) y de la conversión del transportador de oxígeno (—) durante un ciclo redox en el reactor lecho fluidizado discontinuo usando como transportador de oxígeno Cu60MgAl\_SD a 950 °C. Reducción: 100% N<sub>2</sub>. Oxidación: aire. (···) Concentración de equilibrio del oxígeno.

Los experimentos realizados en el reactor lecho fluidizado discontinuo son también útiles para determinar el comportamiento del transportador de oxígeno con respecto a la atrición y la aglomeración. La Figura 3.13 muestra la velocidad de atrición para el transportador Cu60MgAl\_SD en función del tiempo de operación. Se puede observar que la velocidad de atrición es estable y con un valor muy bajo (0.004 %/h), lo que corresponde a un tiempo de vida de las partículas de 25000 horas. Esta velocidad de atrición es mucho menor a la obtenida con el mejor de los materiales preparados por mezcla másica y compresión usando MgAl<sub>2</sub>O<sub>4</sub> como material inerte; ver Figura 3.9. Además, a pesar del alto contenido en CuO del material y de la alta temperatura usada en la fluidización, el transportador de oxígeno preparado por *spray drying* no presentó ninguna tendencia a la aglomeración durante los experimentos.



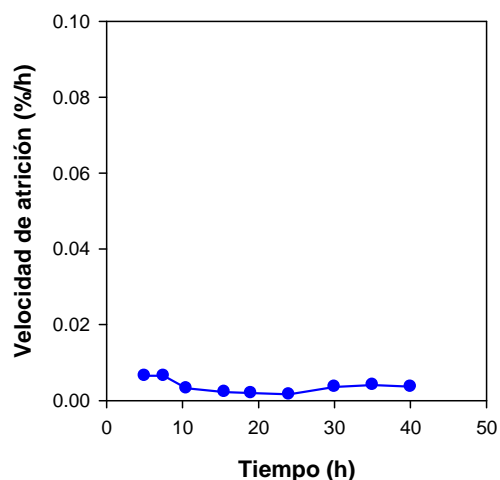


**Figure 3.13.** Velocidad de atrición para el Cu60MgAl\_SD durante los ciclos redox en función del tiempo de operación en el reactor lecho fluidizado discontinuo.

### 3.1.4.3 Caracterización del transportador de oxígeno Cu60MgAl\_SD

Se han caracterizado por diferentes técnicas las partículas del transportador de oxígeno Cu60MgAl\_SD, tanto frescas como tras 40h de fluidización en el reactor de lecho fluidizado. La Tabla 3.5 muestra las propiedades más relevantes para las partículas usadas en comparación con las frescas. El análisis XRD tanto de las muestras frescas como usadas revela la presencia de CuO y MgAl<sub>2</sub>O<sub>4</sub> como componentes principales. Por lo tanto, no se observan cambios en la estructura química del material.

**Tabla 3.5.** Propiedades de las partículas de transportador de oxígeno Cu60MgAl\_SD tanto frescas como usadas en el reactor de lecho fluidizado discontinuo.

	<i>Frescas</i>	<i>Usadas<sup>a</sup></i>
Contenido en CuO (%)	60	60
Capacidad de transporte de oxígeno, $R_{OC}$ (%)	6	6
Resistencia mecánica (N)	2.4	1.6
Densidad del sólido (kg/m <sup>3</sup> )	3860	3955
Porosidad (%)	16.1	24.0
Área superficial específica, BET (m <sup>2</sup> /g)	< 0.5	0.54
Fases principales, XRD	CuO, MgAl <sub>2</sub> O <sub>4</sub>	CuO, MgAl <sub>2</sub> O <sub>4</sub>

a: 40 h en el reactor de lecho fluidizado discontinuo

El contenido de cobre de todas las muestras se determinó por reducción completa usando un 15% de H<sub>2</sub> en N<sub>2</sub> a 850°C en la TGA. En todos los casos, tanto para partículas frescas como usadas, el contenido de CuO era del 60%. Además, se determinó que la reactividad de las partículas usadas era igual que la de las partículas frescas, tanto para la reducción en N<sub>2</sub> como para la oxidación en aire; ver Figura 3.10.

Tanto para las muestras frescas como para las usadas se encontraron valores muy bajos para el área específica BET de alrededor de  $0.5 \text{ m}^2/\text{g}$ . Sin embargo, las partículas frescas tenían una porosidad de 16.1% que aumentaba hasta 24% tras 40 horas de operación en el lecho fluidizado discontinuo. Además, se observa una disminución de la resistencia mecánica de las partículas desde 2.4 N a 1.6 N para las partículas usadas. Esta disminución de la resistencia mecánica está relacionada con el incremento de la porosidad, pero aún se mantiene por encima del mínimo acordado de 1 N [77].

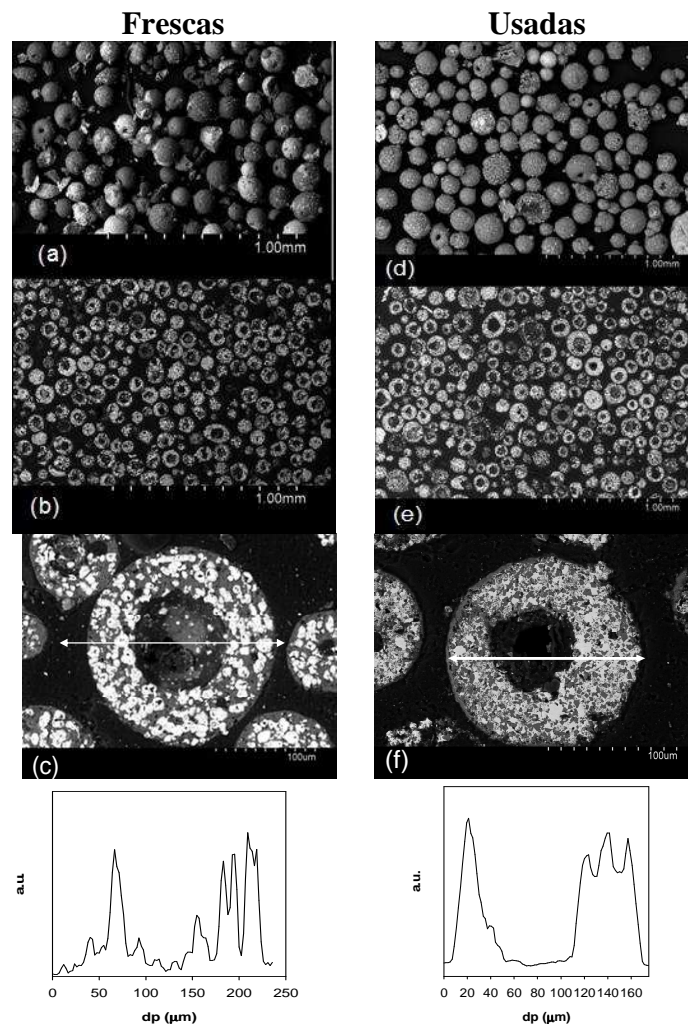


**Figure 3.14.** Imágenes SEM de partículas frescas (izquierda) y usadas (derecha) después de 40h en el reactor de lecho fluidizado discontinuo: (a, d) imágenes de las partículas enteras; (b, e) imágenes de la sección transversal de las partículas; (c, f) imagen y perfil EDX del Cu en la sección transversal de una partícula.

Finalmente, la Figura 3.14 muestra las imágenes SEM y el perfil EDX de las partículas frescas (izquierda) y usadas tras 40h en el reactor de lecho fluidizado discontinuo (derecha). Se puede observar que las partículas tienen una forma esférica muy regular

con una cavidad en el núcleo de las partículas, la cual es característica de las partículas preparadas por *spray drying*. En el perfil EDX de las partículas tanto frescas, Figura 3.14 (c), como usadas, Figura 3.14 (f), se puede observar que la distribución del CuO es uniforme en el interior de las partículas y que no ha cambiado tras 40h de operación.

### **3.1.5 Estudio de otros materiales preparados por *spray drying***

A la vista de los buenos resultados obtenidos con el material Cu60MgAl\_SD preparado por *spray drying*, se optó por incrementar la exploración de materiales para CLOU preparados por este mismo método industrial. Durante la estancia de investigación en la Universidad Tecnológica de Chalmers se investigó la reactividad y las características de diferentes transportadores de oxígeno basados en óxido de cobre preparados por *spray drying*. Como inertes se usaron MgAl<sub>2</sub>O<sub>4</sub>, TiO<sub>2</sub> y SiO<sub>2</sub>; materiales que habían dado buenos resultados en los test de reactividad, como se mostró en las Figuras 3.3 y 3.4. También se prepararon partículas con mezclas de estos inertes en diferente proporción, como se pueden ver en la Tabla 2.1. Estos transportadores de oxígeno se prepararon con un 40% de CuO para minimizar la tendencia a aglomeración (razón por la cual los materiales preparados con TiO<sub>2</sub> y SiO<sub>2</sub> habían sido desechados anteriormente), mientras que se mantiene una capacidad de transporte de oxígeno suficientemente alta para el proceso CLOU ( $R_{TO}=4\%$ ).

#### **3.1.5.1 Comportamiento de los transportadores de oxígeno en ciclos N<sub>2</sub>-aire**

Se realizaron múltiples ciclos redox en el reactor lecho fluidizado discontinuo II para investigar el comportamiento de los transportadores de oxígeno frente a la liberación de oxígeno y la resistencia a la aglomeración. Los transportadores con un 60% de TiO<sub>2</sub> (C4T6) y con una combinación del 20% de TiO<sub>2</sub> y un 40% de SiO<sub>2</sub> (C4T2S4) como soportes, aglomeraron durante el primer ciclo de reducción con N<sub>2</sub>, y por lo tanto no se continuaron estudiando.

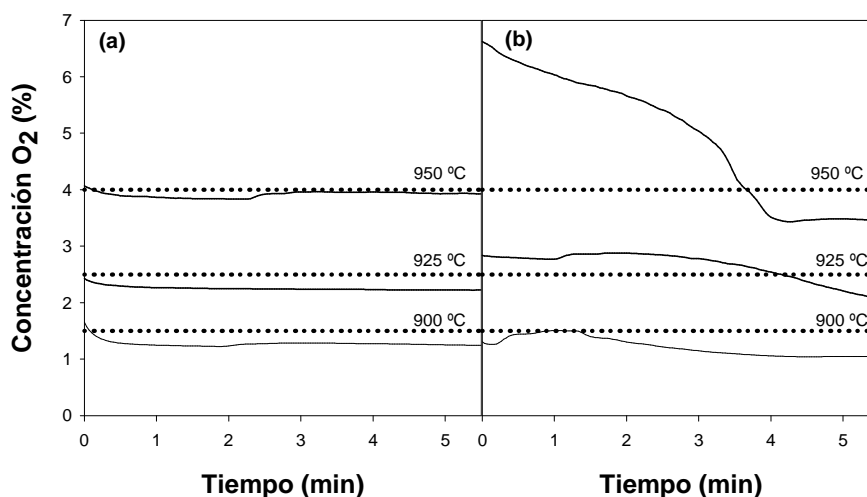


**Figura 3.15.** Concentración de oxígeno (—) medida a la salida del reactor de lecho fluidizado discontinuo II durante la reducción con N<sub>2</sub> a diferentes temperaturas del lecho. Transportador de oxígeno: (a) C4S6\_1000; (b) C4MA4T2\_970. Concentración de O<sub>2</sub> en el equilibrio para cada temperatura (···).

Como ejemplo, la Figura 3.15 muestra la concentración de oxígeno a la salida de reactor lecho fluidizado discontinuo para los transportadores de oxígeno C4S6\_1000 y C4MA4T2\_970 junto con la concentración de oxígeno en equilibrio, para tres temperaturas diferentes. Durante la reducción con N<sub>2</sub>, excepto materiales con un 40% MgAl<sub>2</sub>O<sub>4</sub> y 20% SiO<sub>2</sub> (C4MA4S2), todos los transportadores de oxígeno estudiados liberaban oxígeno con concentraciones cercanas a la correspondiente al equilibrio para cada temperatura estudiada.

### 3.1.5.2 Reactividad con metano

También se realizó la medida de la reactividad de estos materiales. En este caso, no se realizaron estudios en TGA, y el análisis de la reactividad se realizó utilizando CH<sub>4</sub> en el reactor de lecho fluidizado discontinuo II como gas reaccionante, ver sección 2.4.3. Se distinguen dos casos tipos, diferenciándose los materiales con los que se logra combustión completa de CH<sub>4</sub>, de los que no son capaces de convertir todo el CH<sub>4</sub> alimentado. La Figura 3.16 muestra los perfiles de temperatura y concentración de gas durante los experimentos de reactividad con metano a 925°C para los transportadores de oxígeno C4MA6\_1030 y C4MA4S2\_1030. Puede verse en la Figura 3.16(a) que para el transportador de oxígeno C4MA6\_1030 se obtiene conversión completa del combustible a CO<sub>2</sub> y H<sub>2</sub>O. Esto se debe a la rápida velocidad de generación de oxígeno por parte del transportador de oxígeno. Además, el transportador de oxígeno sigue

siendo capaz de liberar oxígeno con una concentración cercana a la de equilibrio. Hay que notar que durante la reducción, la temperatura en el lecho se incrementa alrededor de 25°C y por tanto el transportador de oxígeno libera mayor cantidad de oxígeno. Por otro lado, con el transportador C4MA4S2\_1030, Figura 3.16(b), no se obtuvo una conversión completa de CH<sub>4</sub>, apareciendo inquemados como CO y el propio CH<sub>4</sub> en la corriente de salida del reactor de lecho fluidizado discontinuo. Además, durante la reducción, descendió la concentración de O<sub>2</sub> existente junto con los productos de combustión. Estos efectos se atribuyen a que la velocidad de generación de oxígeno de C4MA4S2\_1030 es mucho más baja que la del C4MA6\_1030.

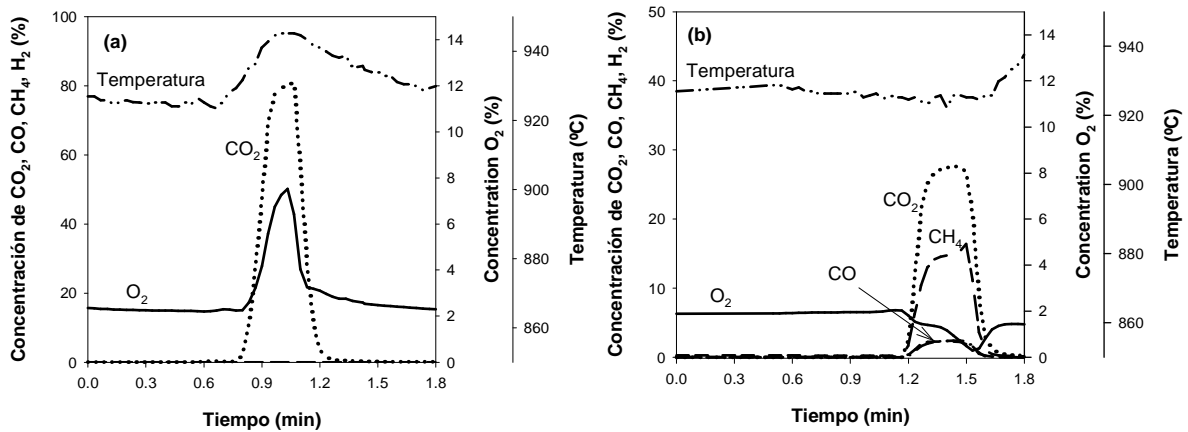


**Figura 3.16.** Evolución de la concentración y temperatura durante la reducción con CH<sub>4</sub> a 925°C para los transportadores de oxígeno: (a) C4MA6\_1030; (b) C4MA4S2\_1030.

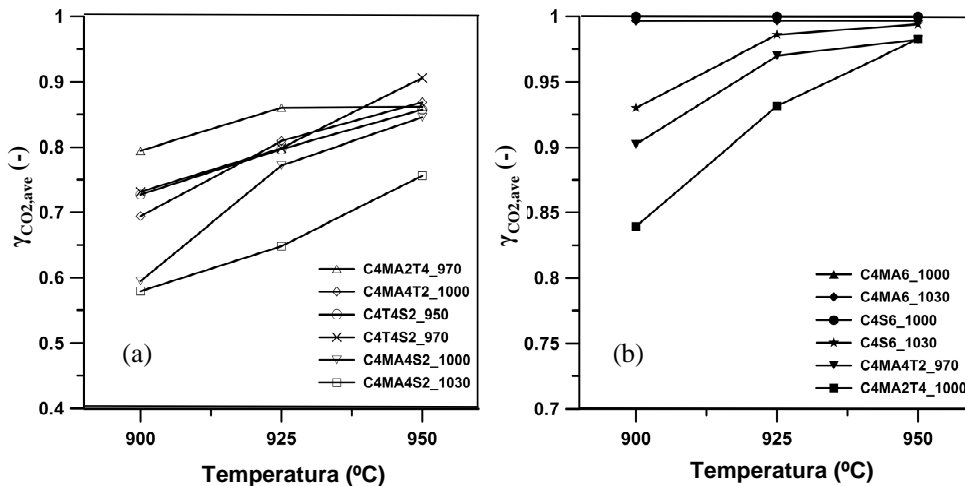


**Figura 3.17.** Rendimiento a gas promedio,  $\gamma_{CO_2,ave}$ , en función de la temperatura. Resistencia mecánica: (a) superior a 1; (b) 1 o inferior.

La Figura 3.17 muestra los valores del rendimiento a gas promedio,  $\gamma_{CO_2,ave}$ , durante el tercer ciclo de reducción en función de la temperatura para cada transportador de oxígeno estudiado usando metano como combustible. Se puede observar que para la mayoría de los transportadores, el rendimiento a gas promedio para el metano aumenta con la temperatura, debido a que al aumentar la temperatura aumenta la velocidad de la reacción.

Cabe destacar que existen tres transportadores de oxígeno que destacan por encima del resto. Estos son los dos preparados con  $MgAl_2O_4$  (C4MA6) y uno con  $SiO_2$  (C4S6) como inertes, los cuales muestran rendimiento a gas promedio de 1 para todas las temperaturas y además durante los ciclos de reducción con  $N_2$  liberan  $O_2$  a la concentración de equilibrio. Sin embargo, cuando se probaron mezclas de ambos inertes (C4MA4S2), la reactividad de los transportadores de oxígeno disminuyó sustancialmente. Por otro lado, en los transportadores de oxígeno donde se usaron mezclas  $MgAl_2O_4/TiO_2$  (C4MA2T4\_970 y C4MA4T2\_1000) y  $TiO_2/SiO_2$  (C4T4S2) como soporte, las resistencias mecánicas eran superiores a 1 N y presentaban razonables valores de conversión de combustible  $\gamma_{CO_2}$  superiores a 0.9.

Hay que resaltar que la dureza no tiene una correlación lineal con los valores de atrición y fragmentación que sufren las partículas en un sistema CLC real. No se observó formación de polvo o fragmentación de las partículas en ninguno de los transportadores de oxígeno probados durante los experimentos de reactividad. Sin embargo, debido al número total de ciclos realizados, así como la velocidad de gas usada es necesario realizar experimentos de larga duración para confirmar la estabilidad mecánica de los transportadores. Para obtener un índice de atrición que sirva para comparar la resistencia de las partículas en un lecho fluidizado se realizaron medidas de atrición en un equipo desarrollado en la Universidad Tecnológica de Chalmers [78] para pequeñas muestras de los transportadores de oxígeno. Para relacionar la atrición de las partículas con su reactividad, la Figura 3.18 muestra el rendimiento a gas promedio,  $\gamma_{CO_2,ave}$ , a  $925^\circ C$  para cada transportador de oxígeno estudiado en función de su velocidad de atrición,  $A_i$ . Se puede observar que los transportadores de oxígeno menos reactivos son los más resistentes a la atrición. Por lo tanto se tendrá que llegar a un compromiso entre la reactividad del transportador de oxígeno y su resistencia a la atrición.

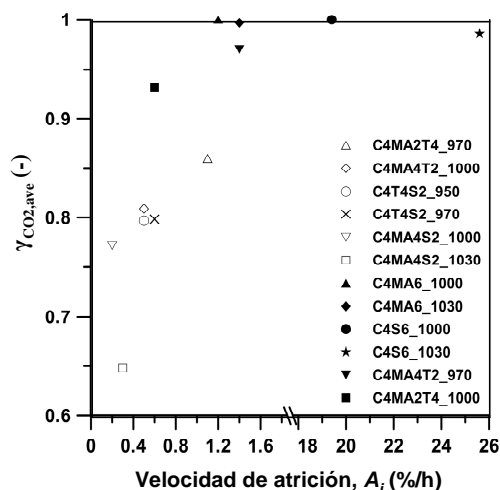


**Figura 3.18.** Rendimiento a gas promedio,  $\gamma_{CO_2,ave}$ , a 925°C en función de la velocidad de atrición,  $A_i$ , para los transportadores de oxígeno preparados por *spray drying*.

### 3.1.5.3 Propiedades físico-químicas de los transportadores de oxígeno preparados por *spray drying*

La Tabla 3.6 resume el estudio de las partículas de los transportadores de oxígeno respecto a los cambios físico-químicos sufridos durante los procesos redox a los que fueron sometidas.

**Tabla 3.6.** Propiedades físico-químicas de los transportadores de oxígeno preparados por *spray drying*.

Transportador de oxígeno	Densidad [g/cm <sup>3</sup> ]		Área BET [m <sup>2</sup> /g]		Fases Cristalinas detectadas, XRD
	Frescas	Usadas	Frescas	Usadas	
C4MA6_1000	0.97	0.80	8.81	7.99	CuO, MgAl <sub>2</sub> O <sub>4</sub>
C4MA6_1030	1.03	0.79	7.05	7.09	
C4S6_1000	0.93	0.91	1.10	1.58	CuO, SiO <sub>2</sub> (cuarzo), SiO <sub>2</sub> (cristobalita)
C4S6_1030	0.96	0.88	0.71	0.71	
C4MA4T2_970	1.54	1.34	0.21	0.67	MgAl <sub>2</sub> O <sub>4</sub> , MgTi <sub>2</sub> O <sub>5</sub> , CuO
C4MA4T2_1000	1.71	1.30	0.04	0.67	
C4MA2T4_970	1.55	1.30	0.25	0.74	MgAl <sub>2</sub> O <sub>4</sub> , TiO <sub>2</sub> , CuO, MgTi <sub>2</sub> O <sub>5</sub>
C4MA2T4_1000	1.54	1.18	0.04	0.58	
C4MA4S2_1000	1.67	1.10	0.25	0.68	CuMgSi <sub>2</sub> O <sub>6</sub> , CuO, MgAl <sub>2</sub> O <sub>4</sub>
C4MA4S2_1030	1.66	1.15	0.16	0.77	
C4T4S2_950	1.81	1.46	0.38	0.35	CuO, TiO <sub>2</sub> , SiO <sub>2</sub> (tridimita), SiO <sub>2</sub> (cuarzo)
C4T4S2_970	1.93	1.44	0.04	0.22	

Para la mayoría de las muestras se produjo una disminución de la densidad y un incremento del área BET de las partículas. Sin embargo, los transportadores de oxígeno no sufrieron cambios en sus respectivas fases cristalinas obtenidos en los análisis por XRD. Cabe destacar que en los transportadores de oxígeno que contenían MgAl<sub>2</sub>O<sub>4</sub> y

SiO<sub>2</sub> (C4MA4S2), el CuO había reaccionado con ambos inertes y se había formado un compuesto mixto CuMgSi<sub>2</sub>O<sub>6</sub>, muy probablemente un compuesto no reactivo, lo que explicaría la baja reactividad de estos transportadores de oxígeno tanto para la generación de oxígeno como para la combustión de CH<sub>4</sub>.

### 3.1.6 Selección de un transportador de oxígeno

La Tabla 3.7 resume la funcionalidad global de los transportadores de oxígeno preparados por *spray drying* con un 40% de CuO durante los ciclos de redox con N<sub>2</sub> y CH<sub>4</sub>.

**Tabla 3.7.** Funcionalidad global de los transportadores de oxígeno preparados por *spray drying*.

Transportador de oxígeno	Aglomeración	Concentración de O <sub>2</sub>	Reactividad	Resistencia Mecánica (N)	Velocidad de atrición, A <sub>i</sub> (%/h)
C4T6_950	Si	---	---	---	---
C4T6_970	Si	---	---	---	---
C4MA6_1000	No	Equilibrio	Muy Alta	0.6	1.2
C4MA6_1030	No	Equilibrio	Muy Alta	0.8	1.4
C4S6_1000	No	Equilibrio	Muy Alta	0.7	19.4
C4S6_1030	No	Equilibrio	Muy Alta	0.5	25.6
C4MA4T2_970	No	Ligeramente inferior al equilibrio	Alta	1.0	1.4
C4MA4T2_1000	No	Ligeramente inferior al equilibrio	Alta	1.5	0.5
C4MA2T4_970	No	Ligeramente inferior al equilibrio	Alta	1.3	1.1
C4MA2T4_1000	No	Ligeramente inferior al equilibrio	Alta	1.0	0.6
C4MA4S2_1000	No	Inferior al Equilibrio	Media	1.4	0.2
C4MA4S2_1030	No	Inferior al Equilibrio	Media	1.7	0.3
C4T4S2_950	No	Ligeramente inferior al equilibrio	Alta	1.7	0.5
C4T4S2_970	No	Ligeramente inferior al equilibrio	Alta	1.8	0.6
C4T2S4_1000	Si	---	---	---	---
C4T2S4_1030	Si	---	---	---	---
<b>Cu60MgAl_SD</b>	<b>No</b>	<b>Equilibrio</b>	<b>Muy alta</b>	<b>2.4</b>	<b>0.004</b>

\*Resistencia mecánica: Baja (<1 N); Media (+1-2 N); alta (>2 N)

En el estudio realizado con los materiales preparados por *spray drying* con un 40% de CuO se ha observado que la reactividad de los materiales se encuentra relacionada de algún modo con la resistencia mecánica. Algunos de los transportadores de oxígeno estudiados presentaban razonables valores de estabilidad mecánica, como indicaban los valores de resistencia mecánica en la Tabla 3.7. No obstante, se puede observar que los transportadores con mayor resistencia mecánica, ver Tabla 3.7, presentaban menor



conversión de  $\text{CH}_4$ , representado por el parámetro  $\gamma_{\text{CO}_2}$ . Esto se debía a una menor velocidad de generación de oxígeno, Figura 3.17(a), comparados con los transportadores de oxígeno con menor resistencia mecánica, como muestra la Figura 3.17(b). Así, la mayoría de los transportadores con una resistencia mecánica de 1 N o inferior mostraron conversiones del combustible cercanas al 100%. De este modo, aunque las partículas del transportador de oxígeno Cu4MA6 son las más reactivas, presentan bajas resistencias mecánicas (<1 N).

Por otro lado, el transportador de oxígeno Cu60MgAl\_SD mostró alta reactividad en TGA y en reactor de lecho fluidizado discontinuo. Por lo tanto, igual que en los transportadores de oxígeno preparados por mezcla másica y compresión, los transportadores de oxígeno con un 60% de óxido de cobre y usando como inerte  $\text{MgAl}_2\text{O}_4$  muestran altos valores de reactividad y de generación de oxígeno, así como unos valores de velocidad de atrición que los hacen buenos candidatos para el proceso CLOU. Por lo tanto se decidió seleccionar como el transportador de oxígeno más prometedor para el proceso CLOU el material Cu60MgAl\_SD y realizar su estudio pormenorizado durante la combustión de carbón tanto en un lecho fluidizado discontinuo como en una planta piloto en continuo.

### 3.2 Análisis de la transferencia de oxígeno en la combustión de carbón

Después del estudio de diferentes materiales como transportadores de oxígeno, mostrado en la sección 3.1, se seleccionó el transportador Cu60MgAl\_SD como el mejor candidato para el proceso CLOU. Para determinar su comportamiento frente a la generación de oxígeno en unas condiciones de operación similares a las que se tendrían en el proceso CLOU, se realizaron experimentos de múltiples ciclos redox en un reactor de lecho fluidizado discontinuo para combustibles sólidos (reactor de lecho fluidizado discontinuo III, Artículo IV).

Los experimentos se realizaron con una masa de lecho de 240 g. Durante el periodo de reducción se utilizaron pequeñas cargas de carbón bituminoso alto en volátiles o carbón colombiano “El Cerrejón” pre-tratado, con tamaños de partícula +0.1-0.3 mm. El cociente másico entre el transportador de oxígeno y el carbón se varió entre 12 y 1200. Se realizaron 34 ciclos redox con el transportador de oxígeno lo que resulta en un total de 31 horas de operación entre 900 y 950 °C. Durante este tiempo el transportador de oxígeno no mostró problemas de aglomeración, incluso cuando el transportador de oxígeno llegó a estar altamente reducido a Cu<sub>2</sub>O durante el periodo de reducción.

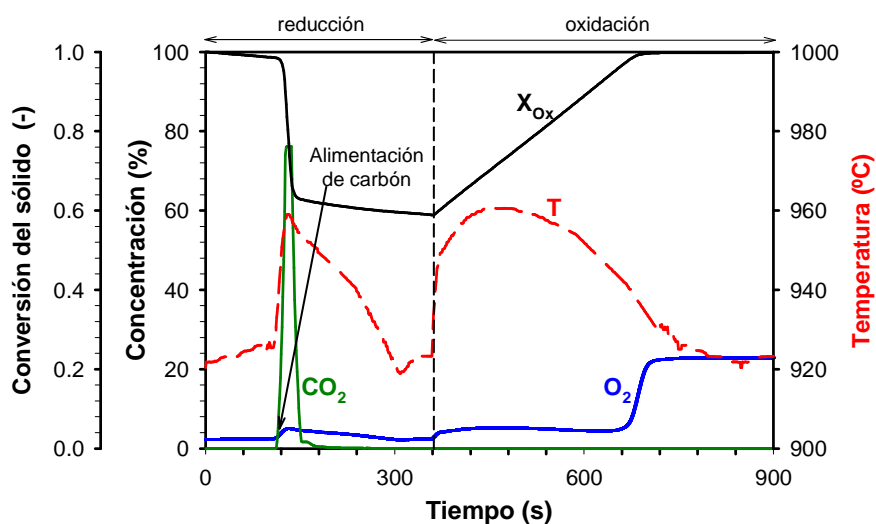


**Figura 3.19.** Concentraciones de O<sub>2</sub>, CO<sub>2</sub>, CO, H<sub>2</sub> y CH<sub>4</sub> durante un típico ciclo redox con Cu60MgAl\_SD. También se muestran la variación de conversión del transportador de oxígeno, X<sub>Ox</sub>, y la temperatura durante los periodos de reducción y oxidación. T<sub>0</sub> = 925°C; reducción con N<sub>2</sub> y oxidación con aire; fracción másica de transportador de oxígeno: 100%. Carga de carbón: 2g. Cociente TO/carbón = 120

A modo de ejemplo, la Figura 3.19 muestra las concentraciones de  $O_2$ ,  $CO_2$ ,  $CO$ ,  $CH_4$  y  $H_2$  medidas a la salida del reactor y la temperatura del lecho durante un ciclo redox típico a  $925^\circ C$  con un inventario de transportador de oxígeno de 240 g. Durante la reducción se utilizó como gas de fluidización  $N_2$ , y aire durante la oxidación. El tiempo  $t = 0$  corresponde al inicio del periodo de reducción, es decir cuando se reemplaza el aire de la oxidación por  $N_2$ .

Al comienzo, el transportador de oxígeno libera  $O_2$  hasta alcanzar la concentración de equilibrio a la temperatura del lecho. En este periodo de tiempo, la velocidad de conversión del transportador de oxígeno se encuentra limitada por la velocidad del gas, el cual arrastra el  $O_2$  producido en condiciones de equilibrio. Después de un corto periodo en atmósfera inerte se alimenta al reactor una carga de 2 g de partículas de carbón, tras la cual se observa  $CO_2$  y  $O_2$  en los gases de salida del reactor. No aparece ningún otro componente, como podría ser  $H_2$ ,  $CO$  o  $CH_4$ , lo que indica combustión completa de los volátiles y del char. La concentración de  $CO_2$  fue del 76% y se mantuvo constante durante alrededor de 8 segundos. Posteriormente se redujo a 0 cuando se alcanzó la combustión completa de la carga de carbón alimentada. Este resultado sugiere una rápida combustión del carbón y de generación de oxígeno. En estas condiciones, el flujo de gas de salida del reactor se incrementó por un factor de 5 con respecto a la corriente de  $N_2$  entrante debido a la gran cantidad de  $CO_2$  y  $H_2O$  generados durante la combustión del carbón. Además, la velocidad de generación de oxígeno fue tan alta como para suministrar oxígeno gaseoso ( $O_2$ ) en exceso junto a los gases de combustión. Durante la combustión la temperatura del lecho se incrementó unos  $30^\circ C$  debido a la exotermicidad de la reacción del  $CuO$  con el carbón, ver Ecuación 1.11. La concentración de oxígeno aumentó en el lecho junto a la temperatura, manteniéndose cerca del valor de la concentración en equilibrio cuando la temperatura variaba. Este hecho indica que el transportador de oxígeno es capaz de transferir el oxígeno demandado por el carbón para su combustión junto al  $O_2$  gaseoso necesario.

En la Figura 3.19 también se muestra la variación de la conversión del transportador de oxígeno,  $X_{O_x}$ , con el tiempo de reacción. Se puede observar que el transportador de oxígeno se convierte lentamente durante el periodo inicial previo a la alimentación de carbón debido a que la velocidad de generación de  $O_2$  estaba limitada por el hecho de que se alcanzaba la concentración de equilibrio en ausencia de combustible. Cuando se

alimenta carbón al lecho se produce una brusca variación de la conversión del transportador de oxígeno debido a la rápida transferencia de oxígeno del transportador de oxígeno al combustible. Después de que se quemara por completo el carbón, el transportador de oxígeno continuo generado  $O_2$ , debido a que no se redujo por completo durante la etapa de combustión, alcanzándose de nuevo la concentración de equilibrio. La variación de la conversión del sólido durante el periodo de reducción fue del 41%. El periodo de oxidación comenzó en  $t = 360$  s y se produjo un rápido incremento de la temperatura del lecho debido a lo altamente exotérmica que es la oxidación del  $Cu_2O$  a  $CuO$ . De forma similar a lo ocurrido en el periodo de reducción, la concentración de  $O_2$  se mantuvo próxima a la del equilibrio hasta que se oxidó por completo el transportador de oxígeno, lo cual concuerda con la alta reactividad del material observado en la TGA en el apartado 3.1.3.1.

Estas mismas series experimentales se realizaron a diferentes temperaturas iniciales,  $T_0$ , de 900, 925 y 950 °C. En estos casos, cuando se alimentaba el carbón al lecho la temperatura se incrementaba durante la combustión de carbón hasta 930, 955 y 980 °C, respectivamente. Dicha temperatura máxima se consideró la temperatura de reacción.

### **3.2.1 Efecto de la relación entre el transportador de oxígeno y el carbón**

Para analizar la combustión del carbón en CLOU debe de tenerse en cuenta que en el reactor de reducción se suceden dos procesos en serie: la generación de  $O_2$  y la combustión del carbón con el  $O_2$  generado. Si el flujo de oxígeno generado por el transportador de oxígeno es mayor que la velocidad de combustión del carbón, se alcanza la concentración de oxígeno en equilibrio, y por lo tanto la velocidad de combustión del carbón dependerá de la propia reactividad del carbón. Por el contrario, si no se alcanzase la concentración de  $O_2$  en equilibrio, la velocidad de combustión del carbón se vería limitada por la velocidad de generación de oxígeno. En las condiciones de operación seleccionadas para la Figura 3.19 la conversión del carbón estaba limitada por su propia reactividad, es decir por la velocidad de combustión del carbón a la concentración de  $O_2$  existente en el lecho y no por la velocidad a la que el transportador de oxígeno transfiere oxígeno al combustible, ya que había  $O_2$  libre en el reactor. El transportador de oxígeno, todavía era capaz de donar oxígeno a una mayor velocidad si

hubiera habido una mayor cantidad de carbón. Por ello se variaron las relaciones de transportador de oxígeno/combustible entre 12 y 1200.

Se observó que con cocientes inferiores a 35 el transportador de oxígeno se reducía por completo después de la alimentación del carbón quedando char sin quemar en el lecho. Por lo tanto, algo de char inquemado se quemaba en el periodo de oxidación posterior, lo cual era evidenciado por la presencia de  $\text{CO}_2$  en los gases a la salida del reactor. El valor de 35 para el cociente entre el transportador de oxígeno y el carbón estaba cerca del valor de oxígeno estequiométrico disponible en el lecho para convertir este carbón en  $\text{CO}_2$  y  $\text{H}_2\text{O}$ , que era de 30. El ratio observado era ligeramente superior al teórico debido a que parte del oxígeno en las partículas era liberado antes de la alimentación del carbón al lecho. No obstante, hay que destacar que lo que se pretende determinar es la velocidad de generación de oxígeno durante su reducción, siendo para ello irrelevante el hecho de que quedase char sin quemar al final de la etapa de reducción.

Para determinar la velocidad máxima de combustión de carbón y de transferencia de oxígeno por parte del transportador de oxígeno se realizaron experimentos variando la relación másica transportador de oxígeno a combustible. En primer lugar se llevaron a cabo experimentos variando la carga de carbón desde 0.2 a 2 g, lo que corresponde a ratios transportador de oxígeno carbón entre 1200 y 120. Como se esperaba, la concentración de  $\text{CO}_2$  a la salida del reactor se incrementó con la cantidad de carbón añadida ya que se quemaba más carbón, por lo que el transportador de oxígeno transfería más oxígeno. No se detectaron en ningún caso ni  $\text{CH}_4$ ,  $\text{CO}$  ni  $\text{H}_2$ , indicando combustión completa de los volátiles en el lecho, así como el carbono del char. De la evolución del  $\text{CO}_2$  y  $\text{O}_2$  en la fase gaseosa, es posible calcular la velocidad instantánea de transferencia de oxígeno,  $r_{\text{O}_2,red}$ , con la Ecuación (2.10). La Figura 3.20 muestra la velocidad instantánea de transferencia de oxígeno durante el periodo de combustión,  $r_{\text{O}_2,red}$ , en función del cociente másico entre transportador de oxígeno y el carbón alimentado. El efecto del cociente entre el transportador de oxígeno y el carbón es evidente en la velocidad de transferencia de oxígeno. En este caso se observó que  $r_{\text{O}_2,red}$  es inversamente proporcional al cociente entre el transportador de oxígeno y el carbón.

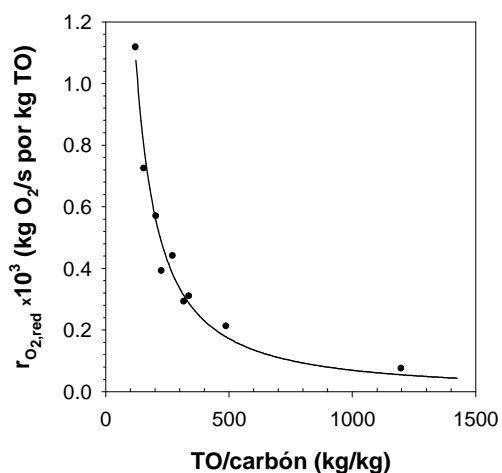


**Figure 3.20.** Velocidad instantánea de transferencia de oxígeno,  $r_{O_2,red}$ , para el Cu60MgAl\_SD en función del cociente másico entre el transportador de oxígeno y el carbón alimentado.  $T_{max} = 955^\circ\text{C}$ . Fracción másica de transportador de oxígeno en el reactor: 100 %.

El creciente requerimiento de oxígeno cuando la carga de carbón aumenta (es decir, cuando el cociente disminuye) es completamente satisfecho por el transportador de oxígeno. Por lo tanto, en las condiciones CLOU usadas en estos experimentos, el oxígeno generado por el transportador de oxígeno no está limitado por la reactividad del mismo, sino por la demanda de oxígeno por parte del carbón. Es decir, cuanto más oxígeno es demandado, más oxígeno es suministrado. Este hecho sugiere que una disminución del cociente entre el transportador de oxígeno y carbón podría permitir incrementar la velocidad de generación de oxígeno proporcionada por el transportador de oxígeno Cu60MgAl\_SD. Se observó que un descenso en dicho cociente por debajo de un valor de 50 causaba la aparición de CO junto a CO<sub>2</sub> en los gases de salida durante el periodo de reducción, así como una concentración de O<sub>2</sub> inferior a la de equilibrio. Sin embargo, no se encontraron en ningún caso ni CH<sub>4</sub> ni H<sub>2</sub>. Este hecho sugiere que la presencia de CO con los gases de combustión no es debido a la limitación del transportador de oxígeno para suministrar el oxígeno requerido por el combustible, sino más bien a la ineficiente combustión del char o de los volátiles a bajas concentraciones de O<sub>2</sub>. Además, se observó una concentración de oxígeno significativamente menor que la de equilibrio, lo que indicaba que la velocidad de transferencia de oxígeno está alcanzando el valor máximo dado por la reactividad del transportador de oxígeno.

Por lo tanto, la velocidad instantánea máxima de transferencia de oxígeno por el material no se pudo determinar durante esta serie experimental, siendo necesario

trabajar con mayores valores del cociente entre el transportador de oxígeno y carbón. Con el objetivo de disminuir el cociente entre el transportador de oxígeno y el carbón pero a la vez manteniendo la confianza en los resultados obtenidos, se realizó una serie experimental diluyendo el transportador de oxígeno con partículas de alúmina, pero manteniendo la masa total de sólidos en el reactor de 240 g. En esta segunda tanda de experimentos se utilizaron cargas de carbón en el rango 0.4-1.2 g a 925 °C usando una fracción másica de transportador de oxígeno del 10% en alúmina. Por lo tanto, el ratio transportador de oxígeno/carbón estaba en el rango 60-20. Finalmente, para determinar la velocidad máxima de transferencia de oxígeno se realizó una tercera serie experimental, donde la fracción másica de Cu60MgAl\_SD en el lecho fue de 2.5%, y las cargas de carbón eran entre 0.03 y 0.5 g, lo que corresponde a ratio transportador de oxígeno carbón entre 200 y 12.

La Figura 3.21 muestra la velocidad instantánea de transferencia de oxígeno en función del cociente másico entre el transportador de oxígeno y el carbón en escala doble logarítmica. Para observar la tendencia global de la velocidad de transferencia de oxígeno, se incluyen en la gráfica los resultados obtenidos con las diferentes diluciones del transportador de oxígeno en alúmina, es decir con fracciones másicas del 100%, del 10% y el 2.5%. Se puede observar una tendencia similar entre los datos obtenidos con las diferentes diluciones del transportador de oxígeno para similares cocientes másicos. Cuando disminuye el cociente transportador de oxígeno/carbón desde valores altos hasta valores de 25, la velocidad de transferencia de oxígeno aumenta. Sin embargo, se puede observar que a menores valores del cociente transportador de oxígeno/carbón la velocidad de transferencia de oxígeno alcanza un máximo, y no se obtienen mayores incrementos en la velocidad de transferencia de oxígeno aunque se disminuya el cociente transportador de oxígeno carbón. Por lo tanto, para cocientes inferiores a 25, donde se ha alcanzado la velocidad máxima de transferencia de oxígeno, la conversión del carbón está limitada por la velocidad de transferencia de oxígeno del transportador de oxígeno. El valor para la máxima velocidad de transferencia de oxígeno calculado fue de  $2.6 \cdot 10^{-3}$  kg O<sub>2</sub>/s por kg de transportador de oxígeno cuando la temperatura durante el periodo de reducción fue de 955 °C.

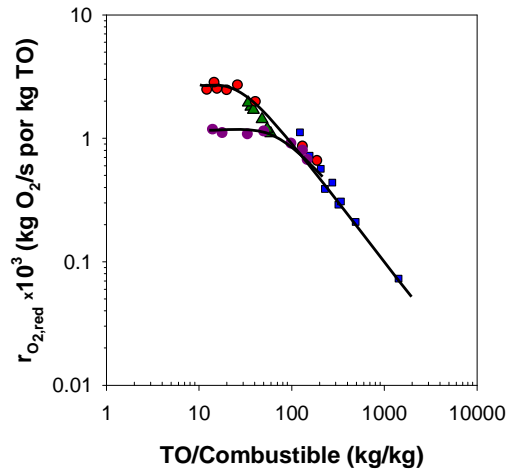


**Figura 3.21.** Velocidad instantánea de transferencia de oxígeno,  $r_{O_2,red}$ , para el transportador de oxígeno Cu60MgA\_SD en función del cociente másico entre el transportador de oxígeno y el combustible.  $T_{max}=955$  °C. Fracción másica del transportador de oxígeno en el reactor: (■) 100%; (▲) 10%; (●) 2.5% con carbón; (●) 2.5% de transportador de oxígeno con char.

A las otras temperaturas analizadas ( $T_0 = 900$  °C y  $T_0 = 950$  °C) se encontraron tendencias similares para las velocidades de generación de oxígeno en función del cociente transportador de oxígeno/carbón. No obstante, la velocidad máxima de generación de oxígeno aumentaba al aumentar la temperatura de reacción como puede verse en la Tabla 3.8.

**Tabla 3.8.** Valor máximo de la velocidad de generación de oxígeno,  $r_{O_2,max}$ , para el transportador de oxígeno Cu60MgAl\_SD y el inventario necesario calculado de transportador de oxígeno en el reactor de reducción para la combustión de carbón,  $m_{FR}$ , en función de la temperatura.

$T_{max}$ (°C)	$r_{O_2,max} \cdot 10^3$ (kgO <sub>2</sub> /s per kg TO)	$m_{FR}$ (kg TO/MW <sub>i</sub> )
930	2.1	39
955	2.6	32
980	2.8	29

### 3.2.2 Regiones de combustión

Analizando los productos de combustión al variar el cociente transportador de oxígeno/carbón se pueden delimitar diferentes regiones de combustión para el proceso CLOU. La Figura 3.22(a) muestra el rendimiento a CO<sub>2</sub>,  $\gamma_{CO_2}$ , mientras que en la Figura 3.22(b) se muestra el cociente entre la concentración de O<sub>2</sub> a la salida del reactor y la concentración de O<sub>2</sub> en equilibrio,  $O_2/O_{2,eq}$ . Según estos resultados se pueden



diferenciar tres regiones. Se define la **Región I** como la región donde no hay CO en los gases de salida del reactor, correspondiendo a cocientes transportador de oxígeno/carbón superiores a 50. La velocidad de transferencia de oxígeno para la frontera entre regiones era alrededor de  $1.4 \cdot 10^{-3}$  kg O<sub>2</sub>/s por kg de transportador de oxígeno.

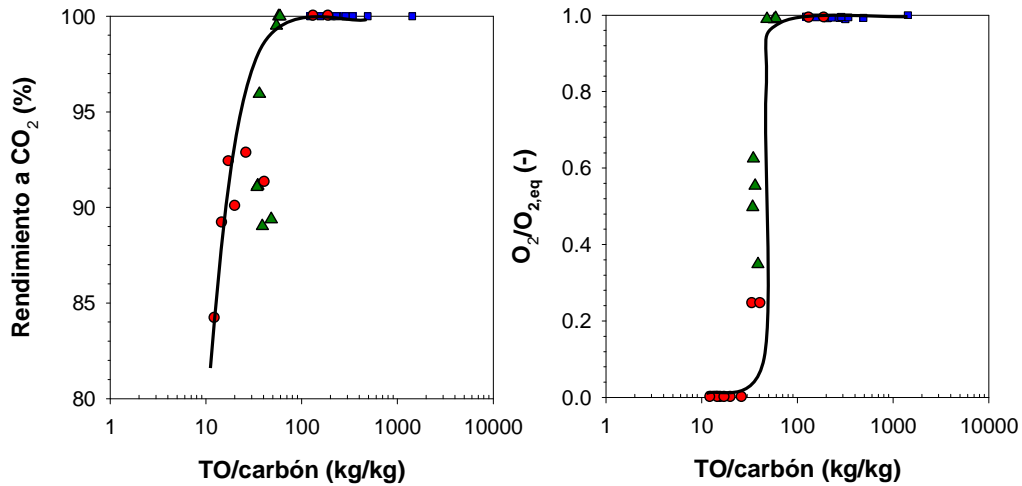


**Figura 3.22.** (a) Rendimiento a CO<sub>2</sub> y (b) cociente entre la concentración de O<sub>2</sub> a la salida del reactor y la concentración de O<sub>2</sub> en equilibrio, O<sub>2</sub>/O<sub>2,eq</sub>, en función del cociente másico entre el transportador de oxígeno y el carbón.  $T_{max} = 925$  °C. Fracción másica del transportador de oxígeno Cu60MgAl\_SD en el reactor: (■) 100 %; (▲) 10 %; (●) 2.5 %.

En la Figura 3.22 se puede observar que tanto el rendimiento a CO<sub>2</sub> como la concentración de O<sub>2</sub> disminuyen cuando el cociente entre el transportador de oxígeno y el carbón disminuye por debajo de 50. Este comportamiento es debido a que el transportador no es capaz de generar oxígeno lo suficientemente rápido para quemar por completo el carbón a CO<sub>2</sub>, aunque se trabajara en condiciones sobre-estequiométricas, es decir, por encima de 30 kg de transportador de oxígeno por kg de carbón. Por lo tanto, en la **Región II**, aparecen simultáneamente O<sub>2</sub> y CO en los gases de salida del reactor. Esta región está limitada por valores del cociente entre el transportador de oxígeno y el carbón entre 25 y 50. Además, en esta región se encontraron juntos CO y O<sub>2</sub> a la salida del reactor debido a que la concentración de O<sub>2</sub> en los gases era demasiado baja para permitir la completa combustión de CO a CO<sub>2</sub>. La cantidad de O<sub>2</sub> en los gases de combustión debería haber sido suficiente para convertir el CO remanente a CO<sub>2</sub> con cocientes superiores a 35, pero esto no ocurrió en el reactor.

Finalmente, se define la **Región III** como aquella donde aparecía CO inquemado sin O<sub>2</sub> presente en los gases de salida. En esta región se alcanza la máxima velocidad de transferencia de oxígeno, y disminuyendo el inventario de sólidos no es posible suministrar el oxígeno necesario para convertir por completo el carbón en el reactor de reducción a la velocidad demandado por el carbón. Este hecho determina un cambio en el proceso limitante durante la conversión del carbón, pasando de estar controlado por la reactividad del char a ser controlado por la velocidad de producción de oxígeno por parte del transportador de oxígeno, y determinado por la reactividad del transportador de oxígeno. Esta región fue observada para valores del cociente transportador de oxígeno/carbón inferiores a 25.

Se puede relacionar la velocidad de transferencia de oxígeno con el inventario de sólido necesario para suministrar el oxígeno para la combustión del combustible en el reactor de reducción. Así, el inventario de sólidos,  $m_{TO,RR}$ , depende del flujo de carbón que se puede procesar con el transportador de oxígeno a la velocidad de transferencia de oxígeno supuesta,  $r_{O_2,red}$ , y se calcula como:

$$m_{TO,RR} = 10^3 \frac{\Omega_{SF}}{r_{O_2,red} PCI} \quad (3.1)$$

siendo  $\Omega_{SF}$  la masa de oxígeno requerida por kg de carbón y  $PCI$  es el valor de poder calorífico inferior del combustible sólido. Del análisis del carbón mostrado en la Tabla 2.2, se calculó un valor de  $\Omega_{SF} = 2.1$  por kg de carbón, donde el  $PCI$  del carbón “El Cerrejón” pre-tratado es de 25878 kJ/kg. Por lo tanto, usando la Ecuación (3.1) y con los valores de velocidad de transferencia de oxígeno mostrados en la Figura 3.21 se puede calcular el inventario de sólidos en el reactor de reducción correspondiente a cada velocidad de transferencia de oxígeno. La Figura 3.23 muestra las tres regiones de combustión encontradas relacionando el inventario de sólidos en el reactor de reducción con el cociente entre el transportador de oxígeno y el carbón. Como se puede observar, al disminuir el cociente disminuye el inventario de sólidos en el reactor de reducción, hasta alcanzar un valor estable en el cual se ha alcanzado la máxima velocidad de transferencia de oxígeno, y por lo tanto aunque se siga disminuyendo el cociente transportador de oxígeno/carbón no disminuye el inventario de sólidos necesario.

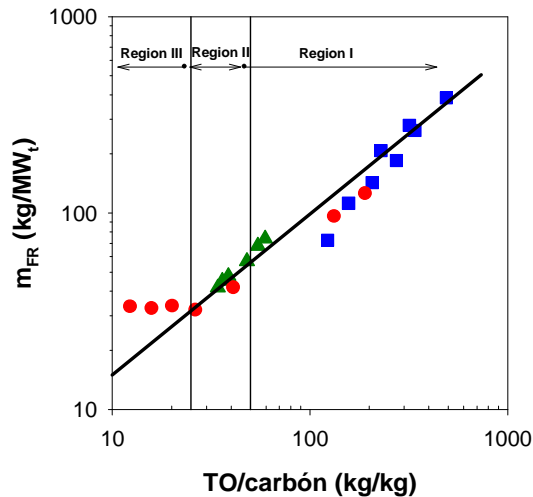


**Figura 3.23.** Inventario de sólidos en el reactor de reducción calculado para el transportador de oxígeno Cu60MgAl\_SD en función del cociente másico entre el transportador de oxígeno y el carbón.  $T_{max}=955^{\circ}\text{C}$ . Fracción másica del transportador de oxígeno Cu60MgAl\_SD en el reactor: (■) 100%; (▲) 10%; (●) 2.5%.

La Figura 3.23 también muestra los inventarios que separa cada región a la  $T_{max} = 955^{\circ}\text{C}$ . Un inventario de  $58 \text{ kg/MW}_t$  separaría las Regiones I y II. La Región II se dividiría en dos sub-regiones en función de si existe en el reactor suficiente  $\text{O}_2$  para quemar el CO generado o no. Así, dentro de la Región II y entre  $32$  y  $43 \text{ kg/MW}_t$  no habría suficiente  $\text{O}_2$  libre para quemar el CO, mientras que en el rango  $43$ - $58 \text{ kg/MW}_t$  se podría obtener combustión completa del combustible corriente abajo en una etapa posterior por medio de una combustión catalítica sin la necesidad de añadir  $\text{O}_2$  adicional. Finalmente, la Región III comienza a partir de inventario de sólidos inferiores a  $32 \text{ kg/MW}_t$ . Con este inventario no había  $\text{O}_2$  en la corriente de salida del reactor, y no se lograría la combustión completa.

Por otra parte, el inventario de sólidos en el reactor de reducción depende de la temperatura del reactor, ya que la velocidad de transferencia de oxígeno depende de la temperatura. En la Tabla 3.8 se muestran los inventarios de sólidos calculados a las tres temperaturas utilizadas. Así, a  $930^{\circ}\text{C}$  serían necesarios  $39 \text{ kg/MW}_t$  en el reactor de reducción, disminuyendo hasta  $29 \text{ kg/MW}_t$  al aumentar la temperatura hasta  $980^{\circ}\text{C}$ . Estos valores de inventario de sólidos corresponden a la cantidad mínima de sólido necesario para generar el oxígeno necesario para la combustión del carbón. Sin embargo, de los resultados experimentales se deduce que es necesario tener un exceso de oxígeno en los gases de salida del reactor para alcanzar la combustión completa del combustible a  $\text{CO}_2$  y  $\text{H}_2\text{O}$ .

### 3.2.3 Determinación de la velocidad máxima de generación de oxígeno durante la combustión de char

La conversión de carbón incluye una primera etapa de desvolatilización y la posterior combustión de la materia volátil y el residuo carbonoso (char). Según el esquema CLOU, la conversión de char es clave para obtener elevadas eficacias de captura de CO<sub>2</sub> en el proceso. Para evaluar de manera independiente la conversión del char se realizaron experimentos usando cargas de char en vez de carbón. El cociente entre el transportador de oxígeno y el char se varió entre 150 a 14. Igual que en el caso de los experimentos con carbón, a altos valores del cociente transportador de oxígeno/char se obtenía una concentración de O<sub>2</sub> igual a la de equilibrio. La concentración de oxígeno descendía con valores del cociente inferiores a 130, llegando a ser 0 con cocientes inferiores a 50. En todos los experimentos realizados con char no se detectó la presencia de CO en los gases de salida del reactor durante la combustión, incluso cuando no había O<sub>2</sub> en los gases de salida. Este hecho sugiere que el CO detectado en los experimentos con carbón y cocientes transportador de oxígeno/carbón inferiores a 50 provenía de los volátiles inquemados, los cuales tienen un peor contacto con el O<sub>2</sub> generado en el lecho fluidizado.

La Figura 3.21 muestra también la velocidad de generación de oxígeno en función del cociente másico entre el transportador de oxígeno y el char con partículas de Cu60MgAl\_SD diluidas al 2.5% en alúmina. Se puede observar una tendencia similar a la obtenida con carbón, aunque la velocidad máxima de transferencia de oxígeno fue menor que cuando se usó char. La mayor velocidad de transferencia de oxígeno obtenida cuando se quemaba carbón podría ser explicada por la reducción directa del CuO por los volátiles. En este caso, la reacción gas-sólido entre los volátiles y el transportador de oxígeno podría ser más rápida que la velocidad de generación de oxígeno gaseoso. La velocidad de transferencia de oxígeno con carbón es más cercana a la que se tendrá en una unidad CLOU. No obstante, la máxima velocidad de transferencia de oxígeno usando char en el reactor lecho fluidizado discontinuo es la máxima velocidad de generación de oxígeno gaseoso por parte de las partículas, siendo ésta similar a la obtenida en la TGA. De este modo, se obtuvo una velocidad de

transferencia de oxígeno  $2.6 \cdot 10^{-3}$  kg O<sub>2</sub>/s con carbón y  $1.2 \cdot 10^{-3}$  kg O<sub>2</sub>/s con char, ambas a 955°C los cuales pueden compararse con la velocidad de generación de oxígeno de  $1.57 \cdot 10^{-3}$  kg O<sub>2</sub>/s en la TGA a 1000°C y sin combustible.

Por otro lado, con los resultados obtenidos durante la combustión del char se puede calcular su velocidad de combustión. La Figura 3.24 muestra la velocidad de combustión del char en función del cociente másico entre el transportador de oxígeno y el char. La velocidad de combustión del char se incrementa al incrementarse el cociente transportador de oxígeno/char hasta alcanzar un máximo con cocientes superiores a 100. A cocientes menores la velocidad de combustión del char está limitada por la velocidad de suministro de oxígeno por parte del transportador de oxígeno. A cocientes transportador de oxígeno/char mayores a 100 la disponibilidad de oxígeno no está limitada por la reactividad del transportador de oxígeno. En consecuencia, todo el oxígeno demandado para la combustión del char es suministrado a una velocidad suficientemente alta por el transportador de oxígeno. Por tanto, la velocidad de combustión está fijada por la propia reactividad del char y por la concentración de O<sub>2</sub> en el reactor, la cual se encuentra determinada por el equilibrio termodinámico de la descomposición del CuO a Cu<sub>2</sub>O.

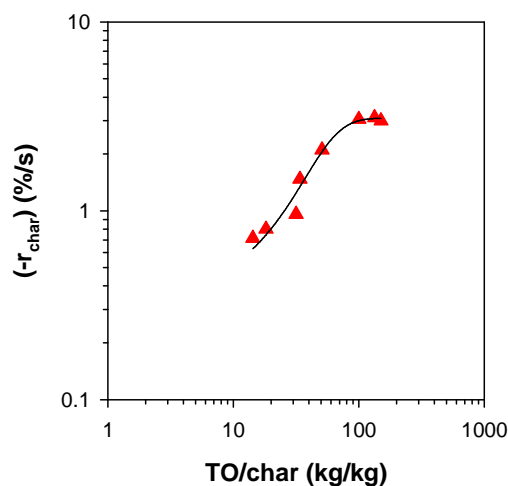


**Figura 3.24.** Velocidad de combustión de char,  $(-r_{char})$ , para el transportador de oxígeno Cu60MgAl\_SD en función del cociente másico entre el transportador de oxígeno y el char.  $T_{max} = 955$  °C. Fracción másica del transportador de oxígeno Cu60MgAl\_SD en el reactor: 2.5%.

De los resultados obtenidos en este apartado se puede concluir que es deseable una pequeña cantidad de oxígeno en la corriente gaseosa a la salida del reactor de reducción para conseguir combustión completa del carbón, correspondiente a la Región I en la

Figura 3.23. De esta forma, se evita la necesidad de instalar una etapa con un post-quemador para completar la combustión de los gases de salida. Es necesario mencionar que esto no significa que se convierta todo el carbón, sino que la cantidad de transportador de oxígeno es suficiente para aportar la cantidad de  $O_2$  demandada a la velocidad requerida. Hay que tener en cuenta que dependiendo de la reactividad del char y del tiempo de residencia en el reactor de reducción, una parte del char será transferido al reactor de oxidación, lo cual afectara a la captura de  $CO_2$ . Este hecho se considerará más adelante en esta Tesis Doctoral.

### **3.3 Demostración del proceso en una planta en continuo de 1.5 kW<sub>t</sub> con diferentes combustibles sólidos**

El proceso CLOU presenta grandes ventajas para la combustión de carbón con transportadores de oxígeno, entre las que destaca la posible combustión completa del carbón con inventarios de sólidos reducidos, tal y como se ha visto en la sección anterior. Debido a ello, en los últimos años ha existido un importante interés en el desarrollo de materiales con capacidad de generar O<sub>2</sub> en el reactor de reducción, como se muestra en la Tabla 1.8. Sin embargo, a día de hoy, todavía hay pocos estudios del proceso CLOU en continuo con combustibles sólidos, y todos ellos han sido realizados en la presente Tesis Doctoral.

En el apartado anterior se ha seleccionado un transportador de oxígeno basado en CuO con excelentes cualidades para su uso en el proceso CLOU con combustibles sólidos. Este material presentó alta resistencia a la aglomeración, baja velocidad de atrición y alta reactividad en la generación de oxígeno. Con este transportador de oxígeno se va a demostrar la viabilidad del proceso en continuo. Para ello, se ha utilizado una planta en continuo de 1.5 kW<sub>t</sub>. La unidad CLOU consta de dos reactores de lecho fluidizado interconectados (el reactor de reducción y el reactor de oxidación), con el transportador de oxígeno circulando continuamente entre ambos. Se llevó a cabo el estudio del proceso CLOU con el transportador de oxígeno Cu<sub>60</sub>MgAl\_SD con diferentes carbones, así como con biomasa. Además, se estudió la presencia de compuestos de azufre tanto en la corriente de CO<sub>2</sub> capturada como en la del aire agotado, analizándose la posible emisión de productos contaminantes como el SO<sub>2</sub> a la atmósfera.

#### **3.3.1 Evaluación preliminar de la capacidad para transferir oxígeno del transportador de oxígeno en continuo**

Antes de operar en continuo en la planta con alimentación de carbón, se estudió la capacidad del transportador Cu<sub>60</sub>MgAl\_SD para transferir oxígeno desde el reactor de oxidación hasta el reactor de reducción durante la operación en continuo sin alimentación de carbón (Artículo II). Se llevaron a cabo un total de 40 h de operación a

altas temperaturas, durante las cuales se analizó el efecto de la temperatura del reactor de reducción, la velocidad de circulación del sólido y la velocidad del gas de fluidización en la velocidad de generación de oxígeno. Además, se estudió el efecto de la concentración de oxígeno en el reactor de oxidación sobre la capacidad de regeneración del transportador de oxígeno en dicho reactor a diferentes temperaturas. En este apartado se usó CO<sub>2</sub> como gas de fluidización en el reactor de reducción, tal y como ocurriría en un sistema CLOU industrial; ver Figura 1.18. Sin embargo, la mayor parte de los experimentos realizados en esta Tesis Doctoral se llevaron a cabo usando N<sub>2</sub> como gas de fluidización en el reactor de reducción para poder evaluar la eficacia de combustión y de captura de CO<sub>2</sub> cuando se alimenta un combustible sólido. Para evaluar el efecto del gas de fluidización se realizó un test usando N<sub>2</sub> en vez de CO<sub>2</sub>. No se encontraron diferencias en la concentración de O<sub>2</sub> ni en la velocidad de generación de O<sub>2</sub> cuando se usaban N<sub>2</sub> o CO<sub>2</sub> como gases de fluidización. Por lo tanto, los resultados descritos en secciones posteriores no están afectados por realizar los experimentos con N<sub>2</sub> en vez de CO<sub>2</sub>.

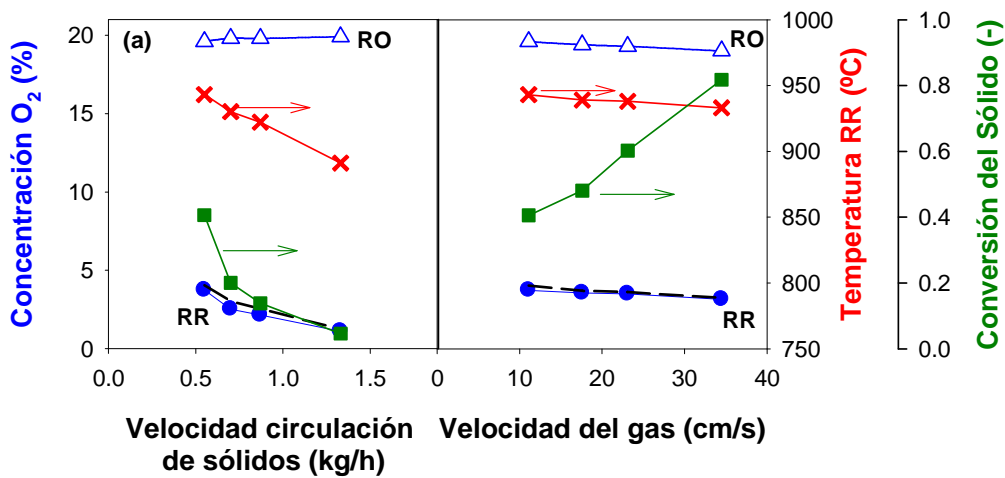


**Figura 3.25.** Concentración de O<sub>2</sub> en los reactores de reducción (-●-) y oxidación (-△-) y variación de la conversión del sólido (-■-) obtenidos en función de: (a) velocidad de circulación de los sólidos; y (b) velocidad del gas de fluidización en el reactor de reducción. Concentración de O<sub>2</sub> en las condiciones del equilibrio: - - -; Temperatura en el reactor de reducción: -X-.

Las Figuras 3.25(a) y (b) muestran la concentración de O<sub>2</sub> en los reactores de reducción y oxidación y la temperatura del reactor de reducción durante los periodos de estado estacionario en función de la velocidad del gas en el reactor de reducción y de la velocidad de circulación de los sólidos. También se muestra la correspondiente concentración de O<sub>2</sub> en el equilibrio en el reactor de reducción y la variación de la conversión del transportador de oxígeno,  $\Delta X_{TO}$ .



Durante los experimentos se pudo observar que el transportador de oxígeno era capaz de generar oxígeno en el reactor de reducción en todas las condiciones experimentales. Además en todos los casos la concentración de  $O_2$  estaba muy cercana a la concentración de equilibrio. En consecuencia, la reducción del transportador de oxígeno era lo suficientemente rápida para alcanzar las condiciones de equilibrio. Se puede observar que al aumentar la velocidad de circulación de sólidos disminuía la concentración de oxígeno en el reactor y, por tanto, la conversión del transportador de oxígeno. También, disminuye la temperatura del reactor de reducción, ya que se recircula una mayor cantidad de sólidos a menor temperatura.

Al aumentar la velocidad del gas en el reactor de reducción, ver Figura 3.25(b), al aumenta el flujo de  $O_2$  transferido en el reactor de reducción. Consecuentemente, la variación de la conversión de los sólidos también aumenta. Este resultado muestra que el transportador de oxígeno es capaz de liberar oxígeno en condiciones de equilibrio en un amplio rango de conversiones del sólido, es decir  $\Delta X_{TO} = 0.05-0.82$ . Además, también aumenta el oxígeno demandado por el transportador de oxígeno para su regeneración en el reactor de oxidación, y consecuentemente, disminuye la concentración de  $O_2$  en el reactor de oxidación.

Para maximizar el uso del aire en un sistema a escala industrial, la concentración de  $O_2$  a la salida del reactor debería ser cercana a la del equilibrio. Para simular las condiciones de operación en un reactor industrial, se disminuyó la concentración de  $O_2$  a la entrada del reactor de oxidación hasta obtener valores cercanos a los del equilibrio, a dos temperaturas diferentes del reactor de oxidación: 900 y 950°C. mayores temperaturas en el reactor de oxidación podrían disminuir el uso del  $O_2$  en el reactor de oxidación. Es necesario indicar que la concentración de  $O_2$  en el reactor de oxidación deberá ser mayor que la concentración en equilibrio a la temperatura del reactor. En todos los casos, el transportador de oxígeno se puede regenerar en el reactor de oxidación y la concentración de oxígeno medida en el reactor de reducción se mantuvo muy próxima a la concentración de equilibrio incluso cuando la temperatura del reactor de oxidación era mayor que en el reactor de reducción. Así, en un sistema CLOU no es necesario trabajar a menores temperaturas en el reactor de oxidación, lo cual sería posible industrialmente debido a que la reacción en el reactor de reducción es exotérmica.

En las series experimentales llevadas a cabo en la planta en continuo sin carbón se comprobaron tres características del transportador de oxígeno fundamentales para el proceso CLOU: (1) era capaz de liberar oxígeno a concentraciones de equilibrio en el reactor de reducción a diferentes temperaturas; (2) se regeneraba en el reactor de oxidación con diferentes concentraciones de O<sub>2</sub> y diferentes temperaturas; y (3) mostraba un buen comportamiento fluidodinámico, sin tendencia a la aglomeración.

### **3.3.2 Demostración del proceso en una planta en continuo de 1.5 kW<sub>t</sub> con carbón**

En este apartado se describen los resultados obtenidos durante la combustión de carbón en una planta piloto compuesto de dos lechos fluidizados interconectados. Esta fue la primera vez en la literatura que se llevó a cabo el proceso CLOU en un sistema en continuo, demostrándose la viabilidad del proceso CLOU para realizar la combustión de carbón con captura de CO<sub>2</sub>. Posteriormente, el proceso CLOU se llevó a cabo con distintos combustibles sólidos, incluyendo carbones de distinto rango y biomasa. Esta extensa campaña experimental fue fundamental para comprender el proceso CLOU, sus ventajas y desventajas, su flexibilidad en función del combustible y de las condiciones de operación, así como sus posibles problemas operacionales.

Para demostrar la viabilidad del proceso CLOU (Artículo V) se realizaron 3 series experimentales con el transportador de oxígeno Cu60MgAl\_SD usando como combustible el carbón colombiano “El Cerrejón” pre-tratado (un bituminoso alto en volátiles, ver Tabla 2.2). La Tabla 3.9 muestra una recopilación de las principales variables usadas en cada experimento. Las partículas de transportador de oxígeno se usaron durante 30 horas con fluidización a alta temperatura, de las cuales 18 h corresponden a la combustión de carbón.

**Tabla 3.9.** Datos de las principales variables usadas en los experimentos en la planta en continuo de 1.5 kW<sub>t</sub> para CLOU.

Test	T <sub>RR</sub> (°C)	φ (-)	λ (-)	$\dot{m}_{TO}$ (kg/h)	$\dot{m}_{SF}$ (kg/h)	Potencia (W)	m <sub>TO,RR</sub> (g)	m* <sub>TO,RR</sub> (kg/MW <sub>t</sub> )	τ <sub>RR</sub> (min)
CLOU01	<b>903</b>	1.2	2.8	<b>4.2</b>	0.112	681	412	605	5.9
CLOU02	<b>917</b>	1.2	2.8	4.2	0.112	681	412	605	5.9
CLOU03	<b>941</b>	1.2	2.8	4.2	0.112	681	373	547	5.3
CLOU04	<b>960</b>	1.2	2.8	4.2	0.112	681	393	577	5.6
CLOU05	924	4.3	4.7	9.0	<b>0.067</b>	410	471	1150	3.1
CLOU06	929	3.2	3.5	9.0	<b>0.089</b>	541	452	835	3.0
CLOU07	917	2.6	2.8	9.0	<b>0.112</b>	681	412	605	2.7
CLOU08	920	2.1	2.3	9.0	<b>0.135</b>	821	373	454	2.5
CLOU09	925	1.1	1.2	9.0	<b>0.256</b>	1560	368	235	2.5
CLOU10	901	1.1	2.8	<b>3.7</b>	0.112	681	452	663	7.3
CLOU11	901	2.0	2.8	<b>7.0</b>	0.112	681	452	663	3.9
CLOU12	898	4.0	2.8	<b>13.9</b>	0.112	681	491	721	2.1

Durante las diferentes series experimentales se variaron la temperatura del reactor de reducción (CLOU01-CLOU04), la velocidad de alimentación de carbón (CLOU05-CLOU09) y la velocidad de circulación de sólidos (CLOU01 y CLOU10-CLOU12). El estado estacionario para cada condición de operación se mantuvo al menos 60 minutos. La planta en continuo de 1.5 kW<sub>t</sub> fue operada de forma estable sin graves problemas operacionales durante la experimentación. Además, el cambio de condiciones de operación se realizaba suavemente y se alcanzaba el nuevo estado estacionario en un corto periodo de tiempo. Durante las 30 horas de operación no se detectó ninguna pérdida de fluidización ni problemas de aglomeración con el transportador de oxígeno utilizado, incluso cuando la temperatura del reactor de reducción fue tan alta como 960°C.

Durante la combustión de carbón en la unidad CLOU se analizaron los gases a la salida de ambos reactores de forma continua. Como ejemplo, la Figura 3.26 muestra la concentración de los gases medidos en base seca en función del tiempo de operación para la serie experimental CLOU01-CLOU04, donde la temperatura del reactor de reducción se varió entre los 900 y los 960°C. La velocidad de circulación de los sólidos se mantuvo en un valor medio de 4.2 kg/h, con un valor de la alimentación de carbón de 0.11 kg/h, lo que corresponde a un ratio transportador de oxígeno a combustible, φ, de 1.2 calculado según la Ecuación 2.19.

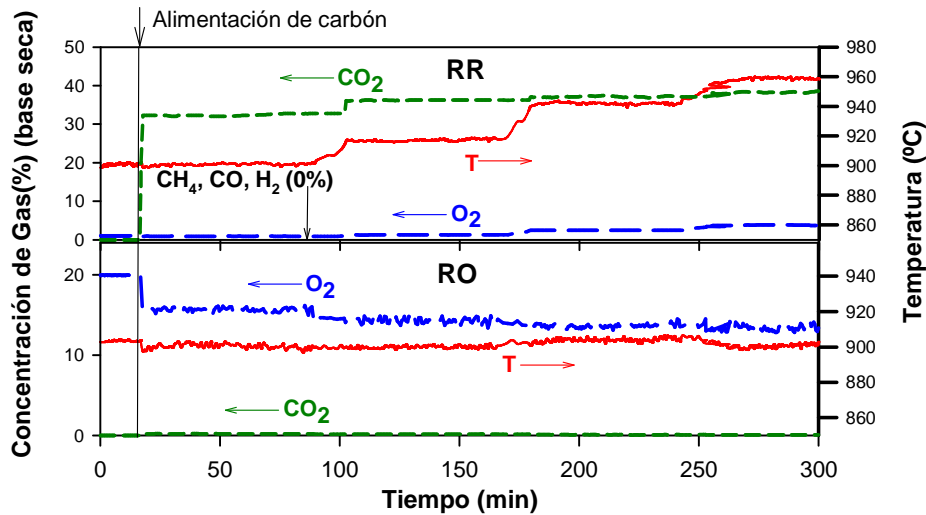


**Figura 3.26.** Evolución de la composición de los gases a la salida de los reactores de reducción (RR) y oxidación (RO) para diferentes temperaturas del reactor de reducción. Experimentos CLOU01-CLOU04.

$$\dot{m}_{\text{TO}} = 4.2 \text{ kg/h}; \phi = 1.2.$$

En la Figura 3.26 no se muestra el periodo de calentamiento. Una vez alcanzadas las condiciones de operación deseadas, la alimentación de carbón comenzó a  $t = 17$  min. Después de comenzar a alimentar carbón se observó un corto periodo de transición en el que aumentaba la concentración de  $\text{CO}_2$  en el reactor de reducción y disminuía la concentración de  $\text{O}_2$  en el reactor de reducción. Este hecho indicaba la combustión del carbón alimentado en el reactor de reducción, mientras que el transportador de oxígeno reducido consumía  $\text{O}_2$  en el reactor de oxidación al regenerarse. Una vez se alcanzó el estado estacionario, la concentración de los gases a la salida de los reactores, así como la temperatura, se mantuvo uniforme durante todo el periodo de combustión. Cuando se variaba la temperatura del reactor de reducción, el nuevo estado estacionario se alcanzaba en menos de 10 minutos, donde la combustión volvía a mantenerse estable.

En todos los casos, no se detectaron gases inquemados ( $\text{CH}_4$ ,  $\text{CO}$  o  $\text{H}_2$ ) a la salida del reactor de reducción. En algunos experimentos, se analizó la posible presencia de alquitranes a la salida del reactor de reducción usando un protocolo para la captura y medida de los alquitranes [76], ver apartado 2.4.5. No se detectaron alquitranes ni hidrocarburos pesados ( $>\text{C}_5$ ) a la salida del reactor de reducción. Además, el análisis de muestras de gas a la salida del reactor de reducción por cromatografía de gases mostró la ausencia también de hidrocarburos ligeros ( $\text{C}_2\text{-C}_4$ ). Por lo tanto, los compuestos mayoritarios presentes a la salida del reactor de reducción fueron  $\text{CO}_2$ ,  $\text{H}_2\text{O}$  y  $\text{O}_2$ , junto al  $\text{N}_2$  introducido como gas de fluidización. El uso de  $\text{N}_2$  permite mejorar la evaluación

de los datos experimentales obtenidos sin afectar al proceso de generación de  $O_2$  en el reactor de reducción. Debe resaltarse que además se detectaron pequeñas cantidades de  $SO_2$  y  $NO_x$  a la salida del reactor de reducción, pero en este momento estos gases no se evaluaron. Por lo tanto, los volátiles presentes en el carbón se convertían por completo a  $CO_2$  y  $H_2O$  en el reactor de reducción mediante la reacción con el oxígeno liberado en la descomposición del  $CuO$  a  $Cu_2O$  presente en el transportador de oxígeno. Además, la velocidad de generación de oxígeno era lo suficientemente elevada como para suministrar un exceso de oxígeno gas ( $O_2$ ) que salía del reactor junto a los gases de combustión. Por otro lado, en el reactor de oxidación la concentración de  $CO_2$  y  $O_2$  disminuía al aumentar la temperatura del reactor de reducción.

Las Figuras 3.27(a-f) muestran las concentraciones de  $CO_2$  y  $O_2$  (en base seca) a la salida de los reactores de reducción y oxidación en función de la temperatura del reactor de reducción, la velocidad de alimentación de carbón o la velocidad de circulación de los sólidos, según las condiciones de operación mostradas en la Tabla 3.9.

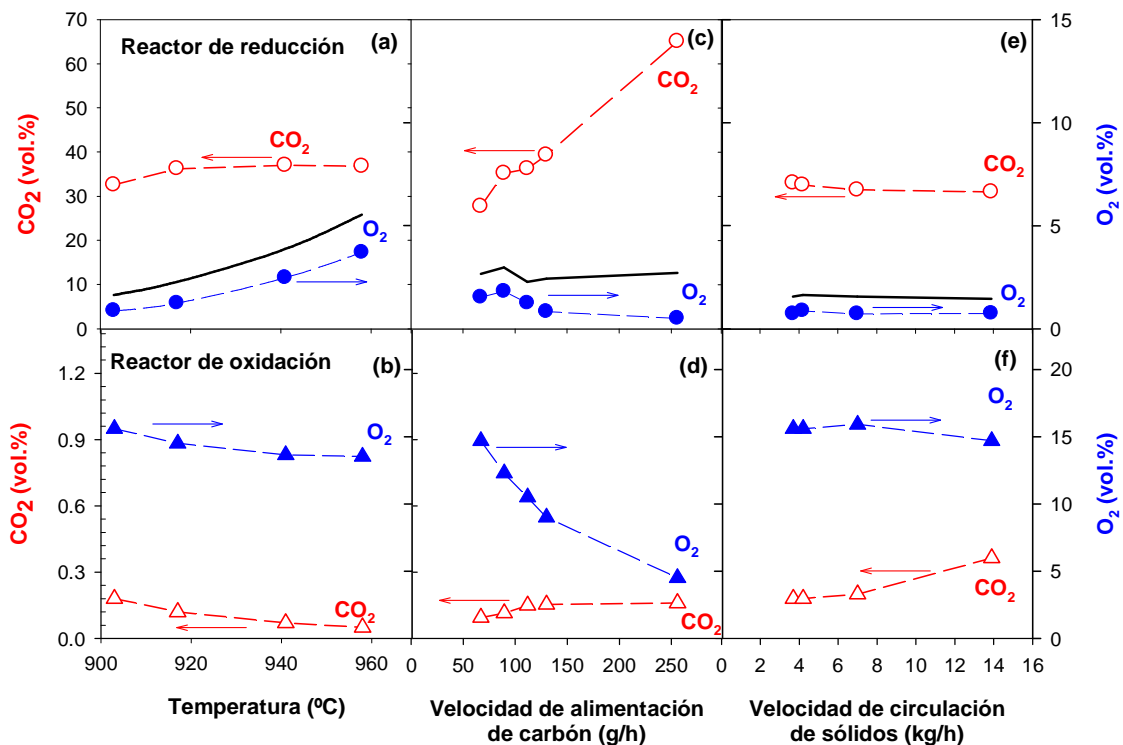


**Figura 3.27.** Concentraciones de  $CO_2$  y  $O_2$  a la salida de los reactores de reducción y oxidación obtenidas a diferentes: (a) y (b) temperatura del reactor de reducción; (c) y (d) velocidad de alimentación de carbón; y (e) y (f) velocidad de circulación de sólidos. Concentración de oxígeno en el equilibrio en el reactor de reducción; —.

El efecto de la temperatura del reactor de reducción sobre las concentraciones de  $\text{CO}_2$  y  $\text{O}_2$  se muestran en la Figura 3.27(a) y (b). Por un lado, tanto la concentración de  $\text{O}_2$  como de  $\text{CO}_2$  aumentan al aumentar la temperatura del reactor de reducción. Se puede observar que la concentración de  $\text{O}_2$  era ligeramente inferior a la concentración de equilibrio, probablemente debido a la reacción del  $\text{O}_2$  gas con partículas de char o volátiles en la zona superior del reactor de reducción (*freeboard*). Por otro lado, la concentración de  $\text{CO}_2$  en el reactor de oxidación disminuía al aumentar la temperatura del reactor de reducción, ver Figura 3.27(b). Este hecho indica que la cantidad de char transferido al reactor de oxidación disminuía con el aumento de la temperatura del reactor de reducción porque aumentaba la velocidad de combustión del char en él. Sin embargo, la concentración de  $\text{O}_2$  en el reactor de oxidación también descendía al aumentar la temperatura del reactor de reducción. Este hecho es evidente si se considera que al aumentar la temperatura se libera más  $\text{O}_2$  en el reactor de reducción.

Las Figuras 3.27(c-d) muestran el efecto de la velocidad de alimentación del carbón sobre la concentración de los diferentes gases. Se varió la alimentación de carbón entre 67 y 256 g/h, lo que corresponde a una potencia térmica entre 410 a 1560 W<sub>t</sub>. En este caso, se observó un importante aumento de la concentración de  $\text{CO}_2$  en el reactor de reducción al aumentar la velocidad de alimentación del carbón, y la correspondiente disminución de la concentración de  $\text{O}_2$  en el reactor de oxidación debido al incremento de la demanda de oxígeno por parte del carbón alimentado. El transportador de oxígeno muestra una velocidad de generación de oxígeno lo suficientemente alta para quemar completamente el carbón en todos los casos y además generar un exceso de oxígeno gaseoso en el reactor. Por lo tanto, la reactividad del transportador de oxígeno no limitaba la conversión del carbón. No obstante, se observó la disminución de la concentración de  $\text{O}_2$  en el reactor de reducción al aumentar la velocidad de alimentación de carbón al sistema. A la mayor velocidad de alimentación de carbón, 256 g/h, algunas partículas del transportador de oxígeno se elutriaban fuera del reactor de reducción debido a la gran cantidad de gases generados en el lecho del reactor. Sin embargo, durante el corto periodo de tiempo de operación estable durante este test (alrededor de 15 min) se obtuvo conversión completa del carbón a  $\text{CO}_2$  y  $\text{H}_2\text{O}$ , sin la presencia de gases inquemados y con un exceso de  $\text{O}_2$ . La operación a mayores velocidades de alimentación de carbón no era posible debido a la elutriación de las partículas por la expansión del gas. No obstante, esta limitación desaparecería en un reactor industrial, en

el que el régimen de fluidización podría ser turbulento. Aun así, el transportador de oxígeno Cu60MgAL\_SD podría suministrar el oxígeno demandado por el carbón.

En la última serie experimental, se estudió el efecto de la velocidad de circulación de sólidos en el rendimiento del proceso; ver Figuras 3.27 (e) y (f). La velocidad de circulación de sólidos se varió entre 3.7 y 13.9 kg/h, lo que correspondía a valores de  $\phi$  entre 1.1 hasta 4.0. Por lo tanto, la velocidad de circulación de sólidos se mantuvo siempre por encima del flujo estequiométrico de sólidos. La temperatura del reactor de reducción se mantuvo en 900°C. La concentración de CO<sub>2</sub> en el reactor de reducción disminuyó ligeramente al aumentar la velocidad de circulación de sólidos, con el correspondiente aumento de la concentración de CO<sub>2</sub> en el reactor de oxidación. Este hecho se debía a que al aumentar la velocidad de circulación de sólidos disminuye el tiempo de residencia de los sólidos en el reactor de reducción y por lo tanto se transfiere mayor cantidad de char al reactor de oxidación. No se detectaron gases inquemados en ninguno de los experimentos, incluso en el caso del menor valor de  $\phi$  usado (1.1), y en todos los casos sólo se observaron H<sub>2</sub>O, CO<sub>2</sub> y O<sub>2</sub> en los gases producto a la salida del reactor de reducción.

Para evaluar el proceso se calcularon las eficacias de combustión y de captura de CO<sub>2</sub> según las Ecuaciones (2.29) y (2.35). Las Figuras 3.28(a), (b) y (c) muestran la eficacia de captura de CO<sub>2</sub>, la conversión del char y la eficacia de combustión en función de la temperatura del reactor de reducción, la velocidad de alimentación de carbón y la velocidad de circulación de sólidos. También muestran la variación de la conversión de los sólidos. Se observó combustión completa del carbón a CO<sub>2</sub> y H<sub>2</sub>O en todos los experimentos, es decir  $\eta_{comb,RR} = 100\%$ . Sin embargo, la conversión del char en el reactor de reducción determina la eficacia de captura de CO<sub>2</sub> en el sistema CLOU, ya que el char que no se convierte en el reactor de reducción lo hará en el de oxidación, emitiendo CO<sub>2</sub> a la atmosfera.

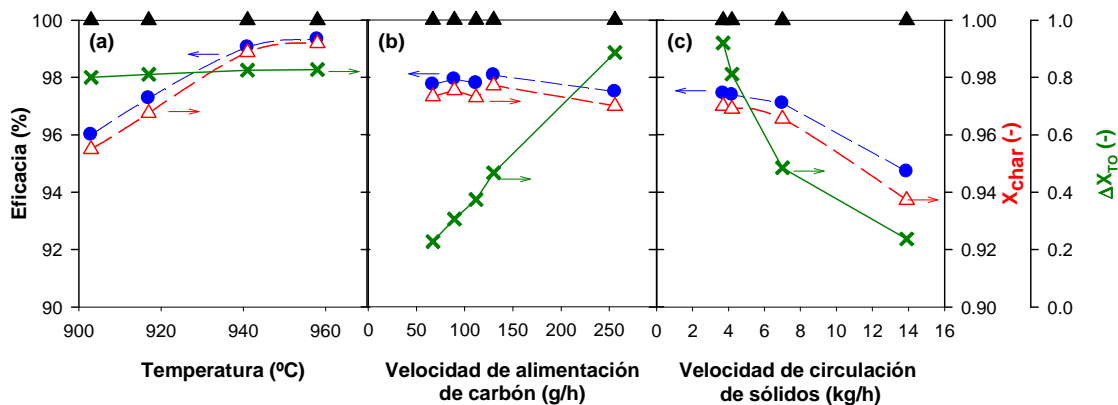


**Figura 3.28.** Eficacia de captura de CO<sub>2</sub> (---●---), conversión de char (---△---), eficacia de combustión (▲) y variación de la conversión del transportador de oxígeno (-X-) a diferentes: (a) temperaturas del reactor de reducción; (b) velocidad de alimentación de carbón; y (c) velocidad de circulación de los sólidos.

Se puede observar que se obtuvieron altos valores de captura de CO<sub>2</sub> en todos los casos. Es notable el efecto positivo que tiene la temperatura del reactor de reducción en la captura de CO<sub>2</sub>; ver Figura 3.28(a). Así, cuando la temperatura del reactor de reducción era de 960°C, el 99% del carbono en el carbón se capturaba, es decir, solamente el 1% del carbono entrante salía con los gases del reactor de oxidación. La razón para esta alta eficacia de captura de CO<sub>2</sub> es la elevada conversión del char, por encima del 96% a todas las temperaturas, la cual aumentaba con la temperatura. Este hecho sugiere una rápida conversión del char en el reactor de reducción por la combustión directa con el oxígeno gaseoso generado in-situ por el transportador de oxígeno, lo cual es característico del proceso CLOU.

La velocidad de alimentación de carbón no tenía un efecto relevante sobre la eficacia de captura de CO<sub>2</sub>; ver Figura 3.28(b), dado que la velocidad de circulación de los sólidos y la temperatura se mantuvieron constantes. Además, como había oxígeno en exceso en el reactor de reducción en todos los casos, la eficacia de captura de CO<sub>2</sub> resultante para las diferentes velocidades de alimentación de carbón no varió sustancialmente. Así, en las condiciones usadas en el sistema CLOU, el oxígeno generado en el reactor de reducción no estaba limitado por la reactividad del transportador de oxígeno; es decir, cuanto más oxígeno se demandaba, más oxígeno era suministrado por el transportador de oxígeno. Esto se puede apreciar en el aumento de la variación de conversión del sólido entre el 23 y el 90%, lo que indicaba que se transfería más oxígeno entre ambos reactores; ver Figura 3.28(b).



Finalmente, la Figura 3.28(c) muestra que el incremento de la velocidad de circulación de sólidos causa un descenso de la conversión del char en el reactor de reducción y por lo tanto una reducción de la eficacia de captura de CO<sub>2</sub>. Además, al aumentar la velocidad de circulación de los sólidos desciende acusadamente la variación de conversión del transportador de oxígeno. El efecto negativo que tiene la velocidad de circulación de sólidos sobre la conversión del char se debe a que disminuye el tiempo de residencia de los sólidos en el reactor de reducción, como se muestra en la Tabla 3.9. Los resultados mostraron que son necesarios más de 300 s de tiempo de residencia en el reactor de reducción para obtener conversiones de char superiores del 97% con este carbón a 900°C. Hay que tener en cuenta que el tiempo de residencia necesario para convertir una cierta fracción de char disminuye cuando la temperatura del reactor de reducción aumenta, ya que aumenta la velocidad de conversión del char. Así, se obtuvo una conversión de char del 99% a 960°C con un tiempo de residencia de 470 s. Esta tendencia encontrada es la opuesta a la observada en procesos CLC cuando el combustible utilizado es gas [79, 80]. En ese caso, los factores determinantes para la conversión de un gas son la disponibilidad de oxígeno y la reactividad media de los sólidos en el lecho, los cuales aumentan al aumentar la circulación de sólidos [81].

La Tabla 3.10 muestra un resumen de los parámetros de rendimientos (es decir, eficacia de combustión, eficacia de captura de CO<sub>2</sub> y conversión de char) obtenidos en los experimentos mostrados en la Tabla 3.9.

**Tabla 3.10.** Principales resultados para los experimentos realizados en la planta en continuo para CLOU de 1.5 kW<sub>t</sub> con el carbón colombiano “El Cerrejón”.

Experimento	Eficacia de Combustión (%)	Eficacia de Captura de CO <sub>2</sub> (%)	Conversión de Char (-)
CLOU01	100	96.0	0.96
CLOU02	100	97.3	0.97
CLOU03	100	99.1	0.99
CLOU04	100	99.3	0.99
CLOU05	100	97.8	0.97
CLOU06	100	97.9	0.98
CLOU07	100	97.8	0.97
CLOU08	100	98.1	0.98
CLOU09	100	97.5	0.97
CLOU10	100	97.5	0.97
CLOU11	100	97.1	0.97
CLOU12	100	94.7	0.94

La velocidad de generación de oxígeno, definida en la Ecuación (2.10), para el transportador de oxígeno Cu60MgAl\_SD se calculó en función de la velocidad de alimentación de carbón, la temperatura del reactor de reducción y el flujo de circulación de sólidos, ver Figura 3.29. Se encontró un ligero efecto sobre la velocidad de generación de oxígeno cuando se variaba la temperatura o el flujo de circulación de sólidos, incluso a altas conversiones del sólido (0.92). Por el contrario, se encontró que el oxígeno transferido aumentaba proporcionalmente al incremento de la velocidad de alimentación del carbón, ver Figura 3.29. Hay que considerar que la alimentación de carbón afecta al inventario de sólidos en el reactor de reducción, calculado como  $\text{kg}/\text{MW}_t$ , como se puede ver en la Tabla 3.9. Así, cuando mayor es la alimentación de carbón menor inventario de transportador de oxígeno existía en el reactor. Aunque se llegó a usar un inventario de sólidos bajo ( $235 \text{ kg}/\text{MW}_t$ ), no se alcanzó el valor máximo de la velocidad de generación de oxígeno determinado en el Apartado 3.2.2. Estos datos confirman que se estaba operando dentro de la Región I donde se obtiene conversión completa del combustible y la velocidad de generación de oxígeno está limitada por la demanda de  $\text{O}_2$  por el combustible, ver Figura 3.23.

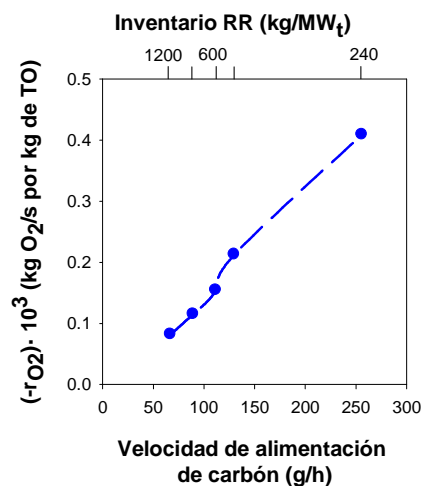


**Figura 3.29.** Velocidad de generación de oxígeno por el transportador de oxígeno Cu60MgAl\_SD e inventario de transportador de oxígeno en el reactor de reducción en función de la velocidad de alimentación de carbón. Temperatura: 925 °C.

La alta eficacia de combustión obtenida en el proceso CLOU podría estar influenciada por el buen contacto entre los volátiles procedentes del combustible sólido y el oxígeno, en forma de oxígeno gaseoso. Por tanto, este proceso es más efectivo para oxidar los compuestos volátiles que cuando la combustión de carbón se realiza mediante la gasificación *in-situ*, iG-CLC [32]. En el proceso CLOU, el oxígeno es liberado en la

fase emulsión y debe mezclarse con los volátiles como en la combustión en lecho fluidizado normal. Además, las altas eficacias de captura de CO<sub>2</sub> se debían a la rápida conversión del char en el reactor de reducción.

En conclusión, estos satisfactorios resultados demuestran que el proceso CLOU es viable tecnológicamente para la combustión de carbón, obteniéndose eficacias de captura de CO<sub>2</sub> cercanas al 100% y combustión completa del carbón a CO<sub>2</sub> y H<sub>2</sub>O.

### **3.3.3 Evaluación del proceso en la combustión de carbones de diferente rango**

En el apartado anterior se ha demostrado en una planta en continuo de 1.5 kW<sub>t</sub> que el proceso CLOU es capaz de obtener una eficacia de combustión del 100% junto a eficacias de captura de CO<sub>2</sub> cercanas a 100% usando el transportador de oxígeno Cu60MgAl\_SD. Cabe notar que el carbón utilizado fue un carbón bituminoso alto en volátiles muy reactivo tras su pre-oxidación. Por lo tanto, la elevada conversión del char obtenida se debió a su alta reactividad. No obstante, la reactividad del char va a depender del tipo de carbón, afectando a la conversión del char en el proceso y por tanto a la eficacia de captura de CO<sub>2</sub>. Por lo tanto, es necesario saber cuál es el efecto que tiene el tipo de carbón en la eficacia de combustión y de captura de CO<sub>2</sub>. Para ello se investigó la combustión de 4 carbones de diferente rango (un lignito, dos bituminosos y una antracita) a diferentes temperaturas del reactor de reducción usando el transportador de oxígeno Cu60MgAl\_SD en la unidad CLOU en continuo de 1.5 kW<sub>t</sub> (Artículo VI). Se llevaron a cabo un total de 40 horas de operación. La temperatura del reactor de reducción se varió entre 900 y 950°C, manteniendo la temperatura en el reactor de oxidación y en el *freeboard* en 900°C. En la Tabla 3.11 se muestra un resumen de las variables de operación usadas para cada carbón. La velocidad de circulación de sólidos se mantuvo en un valor promedio de 3-4 kg/h. Se varió la velocidad de alimentación de carbón desde 0.08 hasta 0.13 kg/h en función del carbón utilizado, manteniéndose el ratio transportador de oxígeno a carbón,  $\phi$ , definido en la Ecuación 2.29, entre 1 y 1.2. Cada condición experimental se mantuvo estable durante al menos 60 minutos.

**Tabla 3.11.** Condiciones de operación durante la combustión de carbones de distinto rango por el proceso CLOU en la planta en continuo de 1.5 kW<sub>t</sub>.

Carbón	$\dot{m}_{SF}$ (kg/h)	$\dot{m}_{TO}$ (kg/h)	$\phi$ (-)	$\lambda$ (-)	Potencia (W)	$m_{TO,RR}$ (kg/MW <sub>t</sub> )
Antracita	0.10	3.1	1.1	3.1	583	894
Bituminoso BV	0.10	3.7	1.0	2.7	805	709
Bituminoso MV	0.08	3.2	1.1	3.6	592	1003
Lignito	0.13	3.0	1.2	3.6	582	845

La Figura 3.30(a) muestra las eficacias de combustión y captura de CO<sub>2</sub> obtenidas para los diferentes carbones en función de la temperatura del reactor de reducción. Se encontró que para todas las condiciones de operación y todos los carbones usados se obtenían combustión completa del carbón a CO<sub>2</sub> y H<sub>2</sub>O. Al igual que en el caso de la combustión del carbón colombiano “El Cerrejón”, en ningún caso se detectó CH<sub>4</sub>, CO o H<sub>2</sub> en los gases provenientes del reactor de reducción. Tampoco se detectaron alquitranes ni hidrocarburos en la corriente de salida del reactor de reducción. Los únicos gases presentes fueron CO<sub>2</sub>, H<sub>2</sub>O y O<sub>2</sub>, junto al N<sub>2</sub> introducido como gas de fluidización. Además, se detectaron pequeñas cantidades de SO<sub>2</sub> y NO<sub>x</sub> a la salida del reactor de reducción, pero en este momento estos gases no se evaluaron. Hay que resaltar que, al no detectarse inquemados, los volátiles generados en todos los tests y con todos los carbones, se convertían completamente a CO<sub>2</sub> y H<sub>2</sub>O en el reactor de reducción por la reacción con el O<sub>2</sub> generado por el transportador de oxígeno. Por lo tanto, igual que con el carbón colombiano, la velocidad de generación de oxígeno era lo suficientemente alta como para suministrar un exceso de O<sub>2</sub> junto a los gases de combustión. Además, la concentración de oxígeno se encontraba cercana al equilibrio a cada temperatura probada y con cada combustible.

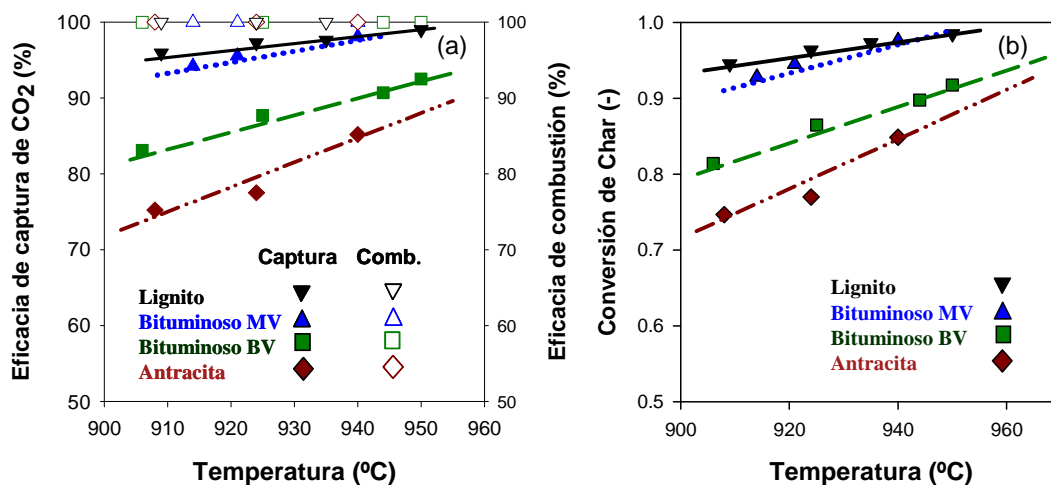


**Figura 3.30.** Efecto de la temperatura del reactor de reducción para varios carbones sobre: (a) eficacia de combustión en el reactor de reducción y eficacia de captura de CO<sub>2</sub>; y (b) conversión del char.

No obstante, el tipo de carbón afectaba a la eficacia de captura de CO<sub>2</sub>. La eficacia de captura de CO<sub>2</sub> descendía en el siguiente orden: lignito > bituminoso medio en volátiles > bituminoso bajo en volátiles > antracita. Para todos los carbones, la eficacia de captura de CO<sub>2</sub> aumentaba al aumentar la temperatura del reactor de reducción, siendo este efecto más relevante para los carbones con bajo contenido en volátiles como la antracita y el carbón bituminoso bajo en volátiles. Se obtuvieron eficacias de captura de CO<sub>2</sub> similares para el lignito y el carbón bituminoso medio en volátiles a temperaturas superiores a los 940°C. En estos casos, la eficacia de captura de CO<sub>2</sub> estaba por encima del 99%, pero se obtuvieron valores inferiores para el caso del carbón bituminoso bajo en volátiles (90%) y de la antracita (83%).

Las eficacias de captura de CO<sub>2</sub> dependen de la cantidad de carbono que se transfiere al reactor de oxidación desde el reactor de reducción. Como todo el carbono presente en los volátiles se captura (se convierten por completo a CO<sub>2</sub> y H<sub>2</sub>O), la captura de CO<sub>2</sub> depende del char inquemado en el reactor de reducción, es decir, de la conversión de char, la cual depende de la temperatura del reactor de reducción y de la velocidad de circulación de los sólidos, como se vio en el apartado 3.3.2. No obstante, en este estudio se mantuvo constante la velocidad de recirculación de sólidos en el sistema. La Figura 3.30(b) muestra la conversión de char en función de la temperatura del reactor de reducción para los diferentes carbones. Se encontraron tendencias similares a las encontradas para el caso de la eficacia de captura de CO<sub>2</sub>. La conversión de char aumentaba cuando aumentaba la temperatura del reactor de reducción para todos los carbones, y este incremento era más relevante para los carbones de bajo rango.

Por tanto, puede concluirse que el rango del carbón mostraba un importante efecto sobre la eficacia de captura de CO<sub>2</sub>. Además, si se desea aumentar la captura de CO<sub>2</sub> del proceso para carbones poco reactivos podría implementarse un *carbon stripper*. Esta unidad es un sistema de recuperación del char inquemado para recircularlo al reactor de reducción. Este sistema es similar al propuesto por Cao y Pan para el proceso *iG-CLC* [29]. La necesidad de un *carbon stripper* en el proceso CLOU dependerá principalmente de la reactividad del carbón utilizado en la combustión.

### 3.3.4 Combustión de biomasa

La biomasa tiene unas propiedades muy interesantes a la hora de su utilización como combustible en el proceso CLOU. Por una parte, si se implementa un sistema de captura de CO<sub>2</sub> con combustión de biomasa, el balance global de carbono en la atmósfera sería negativo, ya que el dióxido de carbono capturado durante la combustión habría sido previamente retirado de la atmósfera por parte de la biomasa. Por lo tanto, sería posible obtener emisiones negativas de CO<sub>2</sub> a la atmósfera. Hasta el trabajo realizado en esta Tesis Doctoral, se habían realizado unos pocos estudios usando biomasa como combustible en procesos *iG-CLC* [82-84] pero ninguno usando el proceso CLOU. Además, otra característica de la biomasa es su alto contenido en volátiles, lo cual puede suponer un comportamiento muy diferente a los carbones, o al comportamiento obtenido en el proceso *iG-CLC* [83]. En el proceso *iG-CLC*, la eficacia de combustión con biomasa [83] es menor que la obtenida con combustión de carbón, debido a su alto contenido en volátiles y al mal contacto de éstos con el transportador de oxígeno.

Para investigar la combustión de biomasa por el proceso CLOU, se han llevado a cabo diferentes experimentos en la planta en continuo usando el transportador de oxígeno Cu60MgAl\_SD y biomasa de pino como combustible (Artículo VII). Durante los experimentos se estudió el efecto de la temperatura del reactor de reducción sobre las eficacias de combustión y de captura de CO<sub>2</sub>. Se llevaron a cabo un total de 10 horas de operación. La temperatura del reactor de reducción se varió entre 860 y 935°C, manteniendo la temperatura en el reactor de oxidación a 900°C. La velocidad de circulación de sólidos se mantuvo en un valor promedio de 4.1 kg/h, mientras que la velocidad de alimentación de biomasa era de 0.22 kg/h, correspondiente a una potencia térmica de 1.2 kW<sub>t</sub>. El inventario de sólidos en el reactor de reducción se mantuvo constante en 565 kg/MW<sub>t</sub> en todos los experimentos. El ratio transportador de oxígeno a carbón,  $\phi$ , según Ecuación 2.19, se fijó en alrededor de 1.2. Durante el periodo experimental se analizaron los gases a la salida de ambos reactores de forma continua.

La Figura 3.31 muestra la concentración de los gases medidos en base seca en función del tiempo de operación cuando la temperatura del reactor de reducción se fue

incrementando desde 860 hasta 935°C. En estado estacionario, la temperatura se mantuvo constante durante al menos 120 minutos para cada condición experimental.

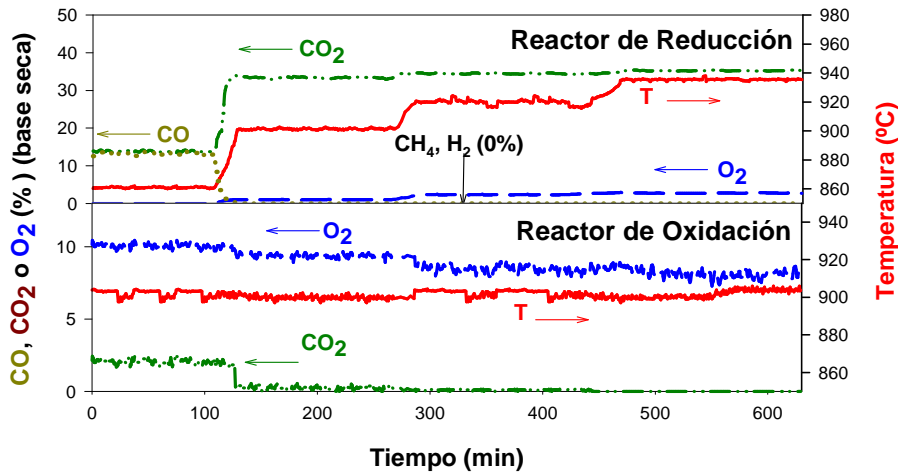


**Figura 3.31.** Evolución de la composición de los gases de los reactores de reducción y oxidación cuando se variaba la temperatura del reactor de reducción.  $\dot{m}_{SF} = 0.22 \text{ kg} / \text{h}$ . Combustible: biomasa de pino.

Para el experimento llevado a cabo a la menor temperatura en el reactor de reducción, 860°C, no se detectaron ni CH<sub>4</sub> ni H<sub>2</sub> pero sí CO en los gases de salida del reactor de reducción, y además la concentración de oxígeno era cercana a 0. Hay que considerar que el CO ha sido referido como producto principal durante la desvolatilización de astillas de pino [85]. Además se tomaron muestras a diferentes temperaturas de acuerdo con el protocolo de medida de alquitranes [76], ver apartado 2.4.5. Se detectaron alquitranes en un concentración de 0.31 g/Nm<sup>3</sup> (base seca). La composición de los alquitranes medidos fue naftaleno (61.7%), fenantreno (13.1%), acenaftileno (12.5%), indeno (7.2%) y estireno (5.5%).

La presencia de inquemados (CO y alquitranes) en la corriente de salida del reactor de reducción en la combustión de biomasa se debe a la baja temperatura de operación empleada en el reactor de reducción. Tal y como se esperaba por la termodinámica de la reacción de generación de O<sub>2</sub> por el transportador de oxígeno, el oxígeno generado no permitía quemar los volátiles completamente. A 860 °C, la concentración de O<sub>2</sub> en el equilibrio es 0.5%. Además, a esta temperatura la velocidad de generación de O<sub>2</sub> del transportador de oxígeno es extremadamente baja, ver apartado 4.1. Por lo tanto, a bajas temperaturas podría ser más relevante el mecanismo de reacción gas-sólido entre los volátiles y el transportador de oxígeno de forma similar al proceso *iG-CLC*. Por ejemplo, la combustión de biomasa en el proceso *iG-CLC* usando un transportador

basado en hierro, es de  $\eta_{\text{comb,RR}} = 80\%$  a  $880^\circ\text{C}$  con  $1550 \text{ kg/MW}_t$  [83]. Sin embargo, para el material usado durante esta Tesis Doctoral se obtuvo un  $\eta_{\text{comb,RR}} = 82\%$  pero con un inventario de sólidos mucho menor ( $565 \text{ kg/MW}_t$ ), lo que resalta la alta reactividad del transportador de oxígeno Cu60MgAl\_SD.

Además, en estas condiciones de operación, se transfería gran cantidad de char inquemado al reactor de oxidación junto al transportador de oxígeno. Así que aparecía una cantidad importante de  $\text{CO}_2$  como producto de combustión en los gases de salida del reactor de oxidación. Por lo tanto, esta temperatura no era adecuada para operar en el proceso CLOU.

Cuando la temperatura del reactor de reducción se fijó a  $900^\circ\text{C}$ , la cantidad de  $\text{O}_2$  generado aumentó y no se detectaron  $\text{CH}_4$ ,  $\text{CO}$  o  $\text{H}_2$  en los gases a la salida del reactor de reducción. Tampoco se detectaron ni alquitranes ni hidrocarburos ligeros en los gases de combustión. Por lo tanto, los únicos gases detectados fueron  $\text{CO}_2$ ,  $\text{H}_2\text{O}$  y  $\text{O}_2$ , junto al  $\text{N}_2$  introducido como gas de fluidización. Resultados similares se obtuvieron a mayores temperaturas. La Figura 3.32(a) muestra las eficacias de combustión y eficacia de captura de  $\text{CO}_2$  obtenidas en la planta en continuo en función de la temperatura del reactor de reducción. Como se ha comentado, para temperaturas inferiores a  $900^\circ\text{C}$ , la eficacia de combustión era baja con presencia de  $\text{CO}$  y alquitranes en los gases de salida del reactor de reducción. Para temperaturas superiores a  $900^\circ\text{C}$  en el reactor de reducción, se obtuvo combustión completa de la biomasa a  $\text{CO}_2$  y  $\text{H}_2\text{O}$ .

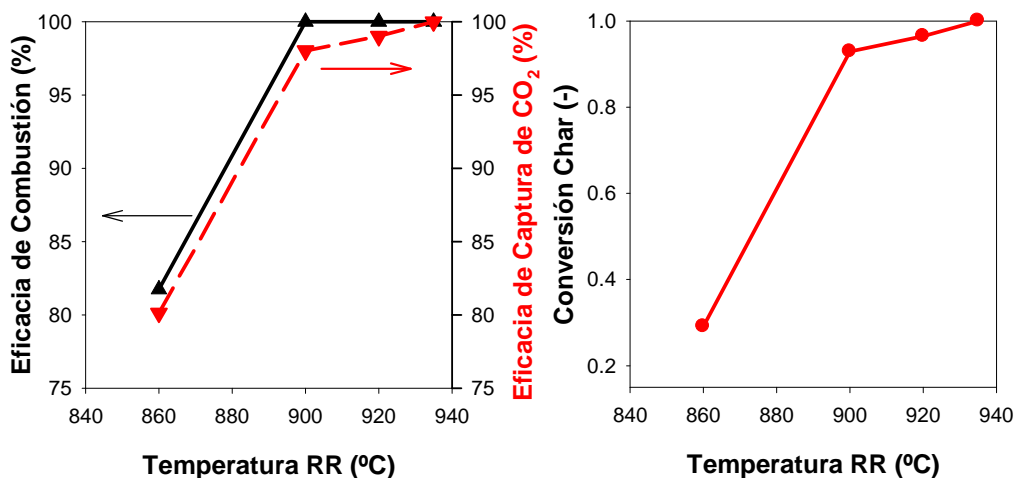


**Figura 3.32.** Efecto de la temperatura del reactor de reducción en: (a) Eficacias de combustión y captura de  $\text{CO}_2$ ; y (b) conversión del char.



La eficacia de captura de  $\text{CO}_2$  indica la fracción de carbono transferido al reactor de oxidación, donde se genera  $\text{CO}_2$  no capturado. En la Figura 3.32(a) se puede observar que la eficacia de captura aumenta con la temperatura del reactor de reducción, alcanzándose el 100% de captura a  $935^\circ\text{C}$ . Como todo el carbono contenido en los volátiles se captura en el reactor de reducción al ser completamente quemados a  $\text{CO}_2$  y  $\text{H}_2\text{O}$ , la eficacia de captura de  $\text{CO}_2$  únicamente depende del char no convertido en el reactor de reducción. La Figura 3.32(b) muestra la conversión de char en función de la temperatura del reactor de reducción. A la menor temperatura, solamente se alcanzaba una conversión del char del 29 % en el reactor de reducción. No obstante, a esa temperatura se obtenía una eficacia de captura del  $\text{CO}_2$  del 80% debido a la alta cantidad de volátiles que contiene la biomasa. Sin embargo, la conversión de char aumentaba cuando aumentaba la temperatura del reactor de reducción debido al aumento de la velocidad de conversión del char. Este importante aumento en la conversión del char es atribuido a un cambio de mecanismo. A la menor temperatura,  $860^\circ\text{C}$ , la disponibilidad de oxígeno gaseoso es baja y la conversión del char debe ser principalmente mediante gasificación. No obstante, en las condiciones utilizadas (en las que se usó  $\text{N}_2$  como gas de fluidización) la reacción de gasificación del char es lenta debido a la baja concentración de  $\text{H}_2\text{O}$  y  $\text{CO}_2$  presente en el reactor de reducción. A temperaturas mayores, la conversión del char llega a ser elevada, e incluso completa a  $935^\circ\text{C}$ , debido a la rápida generación de  $\text{O}_2$  por parte del transportador de oxígeno. Por lo tanto, este intervalo de temperaturas se considera adecuado para el proceso CLOU.

Como conclusión de la combustión de biomasa mediante el proceso CLOU, se puede decir que se requieren temperaturas superiores a los  $900^\circ\text{C}$  en el reactor de reducción para obtener los beneficios del efecto CLOU, y en consecuencia no obtener productos inquemados en los gases de combustión del reactor de reducción. A  $935^\circ\text{C}$  se logró tener combustión completa de la biomasa junto a una eficacia de captura de  $\text{CO}_2$  del 100%.

### 3.4 Estudio del efecto del azufre del combustible

El azufre presente en un combustible sólido, tal como el carbón, puede aparecer en las corrientes gaseosas procedentes de un proceso CLOU. Los problemas que puede generar y las soluciones a tomar dependerán de dónde se encuentren los compuestos de azufre. Desde el punto de vista de la captura de CO<sub>2</sub>, el azufre presente en el combustible puede emitirse en el reactor de reducción, que es donde mayoritariamente se convierte el combustible afectando a la calidad del CO<sub>2</sub> y con importantes consecuencias para su compresión, transporte y almacenamiento [12, 86, 87]. Desde el punto de vista medioambiental, el azufre alimentado con el combustible al sistema puede ser liberado como SO<sub>2</sub> a la atmósfera junto a la corriente de gases de salida del reactor de oxidación y por lo tanto se deberá cumplir con la legislación existente en materia de emisiones contaminantes.

Desde el punto de vista operacional, los compuestos de azufre podrían reaccionar con el transportador de oxígeno, los cuales pueden reducir la reactividad del transportador de oxígeno y generar problemas operacionales. Por ejemplo, el óxido de cobre podría reaccionar formando sulfuros los cuales presentan un bajo punto de fusión, por ejemplo 1100°C para el Cu<sub>2</sub>S, lo que podría producir problemas de aglomeración y afectar negativamente a la circulación de los sólidos entre ambos lechos fluidizados interconectados.

Sólo existen un pequeño número de estudios analizando el efecto del S sobre transportadores de oxígeno basados en CuO en plantas en continuo de CLC (con combustión de gases), bajo diferentes condiciones de operación. Forero y col. [88] estudiaron el efecto del S en la combustión de gas natural en el proceso CLC usando un transportador de oxígeno basado en CuO, con concentraciones de H<sub>2</sub>S hasta 1300 ppm. Se encontró que la mayor parte del S en el combustible se liberaba como SO<sub>2</sub> en la corriente de salida del reactor de reducción en condiciones normales de operación. No se detectó la formación de Cu<sub>2</sub>S o CuSO<sub>4</sub> en el reactor de reducción incluso cuando había un alto grado de reducción a Cu. Sin embargo, incluso en las condiciones más favorables para la formación de Cu<sub>2</sub>S, es decir, casi total reducción del CuO a Cu, no se

detectaron problemas de aglomeración en los lechos fluidizados. Recientemente, de Diego y col. [89] investigaron la combustión de gases con altas concentraciones de H<sub>2</sub>S (sour gas) entre 0.3 y 15% con transportadores de cobre, encontrando que el transportador de oxígeno era capaz de quemar completamente tanto el CH<sub>4</sub> como el H<sub>2</sub>S. El S se encontraba mayoritariamente como SO<sub>2</sub> a la salida del reactor de reducción, aunque se desprendían diferentes cantidades de SO<sub>2</sub> en el reactor de oxidación que disminuían al aumentar la relación transportador/combustible ( $\phi$ ). En este estudio, debido a la elevada concentración de H<sub>2</sub>S, se formaba Cu<sub>2</sub>S que generaba SO<sub>2</sub> en el reactor de oxidación, no pudiéndose conseguir emisiones de SO<sub>2</sub> inferiores a los límites de la UE para grandes centrales térmicas [90].

Para la combustión de carbón, no se encontró ningún estudio disponible en la literatura sobre el efecto del S en el rendimiento del proceso CLOU con transportadores de oxígeno basados en óxido de cobre. Por lo tanto, se consideró necesario desarrollar este estudio sobre el efecto del S presente en el combustible en el comportamiento del transportador de oxígeno y su distribución en el sistema CLOU, así como para comprender las consecuencias reales en el proceso CLOU del uso de un combustible con contenidos importantes en azufre.

Para investigar el efecto del azufre en el proceso CLOU, se han llevado a cabo diferentes experimentos en la planta en continuo de CLOU usando el transportador de oxígeno Cu60MgAl\_SD (Artículo VIII). Como combustible se utilizó un lignito con alto contenido en azufre (5.2%, ver Tabla 2.2). Durante los experimentos se estudió el efecto de la temperatura del reactor de reducción sobre la distribución del azufre en el sistema. Se llevaron a cabo un total de 15 horas de operación. La temperatura del reactor de reducción se varió entre 900 y 935°C, manteniendo la temperatura en el reactor de oxidación en 900°C. La velocidad de circulación de sólidos se mantuvo en un valor promedio de 3 kg/h, mientras que la velocidad de alimentación de carbón era de 0.12 kg/h, correspondiente a un ratio transportador de oxígeno a carbón,  $\phi$ , de 1.2. Se analizaron en continuo los gases a la salida de los reactores tanto para los productos de combustión (CH<sub>4</sub>, CO, H<sub>2</sub>, CO<sub>2</sub>) como las distintas formas de azufre (H<sub>2</sub>S, SO<sub>2</sub>, COS, etc.)

El análisis sobre las eficacias de combustión y de captura de  $\text{CO}_2$  usando este combustible se ha mostrado en el Apartado 3.3.3. Hay que recordar que durante las 15 h de operación se obtuvo la combustión completa del carbón, por lo tanto, los únicos productos de la combustión fueron  $\text{CO}_2$  y  $\text{H}_2\text{O}$ , junto con  $\text{O}_2$  procedente del transportador de oxígeno y al  $\text{N}_2$  introducido como gas de fluidización. En cuanto al azufre, se detecta  $\text{SO}_2$  a la salida del reactor de reducción y del reactor de oxidación. No se detecta ni  $\text{H}_2\text{S}$ , ni  $\text{COS}$  en ningún experimento.

Por otro lado, la eficacia de captura de  $\text{CO}_2$  aumentaba al aumentar la temperatura del reactor de reducción, debido al aumento de la velocidad de combustión del char y por lo tanto menos char sin convertir se transfería al reactor de oxidación. Por lo tanto, es de esperar que la variación de la conversión de char con la temperatura afecte a la distribución del azufre entre los dos reactores. La Figura 3.33 muestra la distribución del S a la salida de ambos reactores en función de la temperatura del reactor de reducción. Se puede observar que el azufre es emitido principalmente como  $\text{SO}_2$  en la corriente de salida reactor de reducción y aumenta al aumentar la temperatura del reactor de reducción, con la correspondiente disminución del  $\text{SO}_2$  en el reactor de oxidación. Este efecto se debía al aumento de la conversión de char en el reactor de reducción con el consiguiente aumento del azufre convertido en dicho reactor y la disminución del azufre transferido al reactor de oxidación.

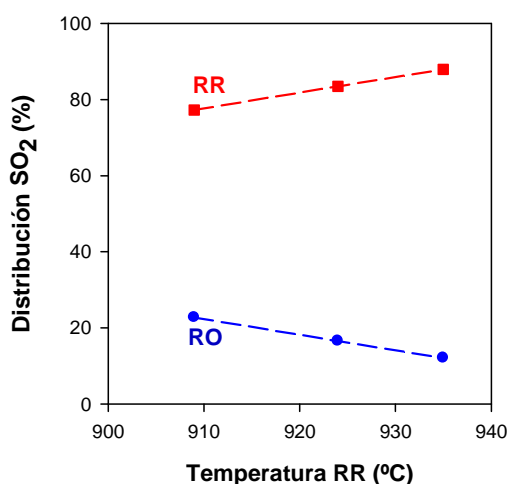


**Figura 3.33.** Distribución del  $\text{SO}_2$  en la planta en continuo para el proceso CLOU en las corrientes de salida del: reactor de reducción (■) y reactor de oxidación (●).

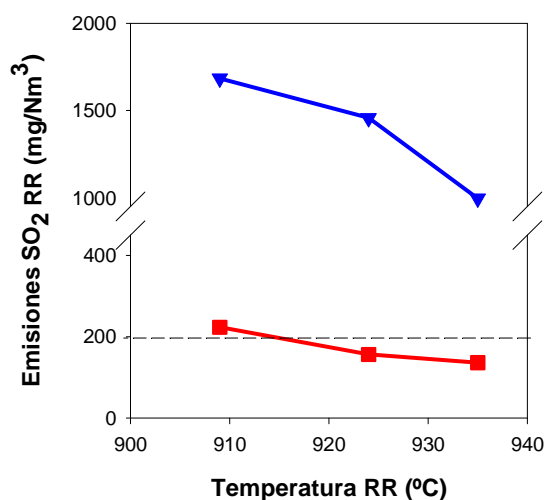


**Figura 3.34.** Efecto de la temperatura del reactor de reducción sobre las emisiones de SO<sub>2</sub> normalizadas al 6% de O<sub>2</sub> en el reactor de oxidación: (▼) medidas en la planta en continuo para el proceso CLOU y (■) calculada usando un ratio S/C constante durante la conversión del char; límite legal de emisiones según la UE (- - -).

La Figura 3.34 muestra las emisiones de SO<sub>2</sub> a la salida del reactor de oxidación normalizadas con un 6% de O<sub>2</sub> en función de la temperatura del reactor de reducción. También se muestra el límite de emisión de SO<sub>2</sub> impuesto por la UE para nuevas plantas de energía eléctrica por combustión de carbón (>300 MW<sub>t</sub>) [90]. Se puede observar que las emisiones de SO<sub>2</sub> procedentes del reactor de oxidación disminuían al aumentar la temperatura, como se ha comentado anteriormente. Aunque la cantidad de SO<sub>2</sub> a la salida del reactor de oxidación era inferior al 10% del S total alimentado a 935°C, el valor de la emisión de SO<sub>2</sub> era demasiado alto y excedía el límite legal establecido de 200 mg/Nm<sup>3</sup>. Resaltar que la combustión directa de este carbón con aire produciría una emisión de SO<sub>2</sub> a la atmosfera >20000 mg/Nm<sup>3</sup> debido al alto contenido de azufre. Otros carbones con menores contenidos podrían cumplir los límites de emisión.

Por medio de los valores de conversión del char medidos en el reactor de reducción, se puede calcular el S emitido como SO<sub>2</sub> en el reactor de oxidación suponiendo un ratio S/C constante durante la combustión e igual a la del análisis del char naciente. La Figura 3.34 muestra las emisiones de SO<sub>2</sub> calculadas correspondientes en el reactor de oxidación. Como se puede observar, las emisiones de SO<sub>2</sub> calculadas son mucho menores que las medidas. Este hecho podría ser debido a dos efectos diferentes: (i) que el S estuviera más concentrado respecto a la fracción de carbono en el char inquemado y transferido al reactor de oxidación; (ii) o que el transportador de oxígeno transfiriera parte del S al reactor de oxidación por reacción del S con el mismo.

Para analizar si se concentraba el azufre en el char, se llevó a cabo un detallado estudio de la liberación del S durante la combustión del char en lecho fluidizado. Para ello se cargaron 20 g de carbón en un lecho de arena con un tamaño de partícula de +0.2-0.3 mm y se calentó usando N<sub>2</sub> como gas de fluidización hasta los 925°C. Posteriormente, se realizó la combustión del char a 925°C con aire diluido (2.5% O<sub>2</sub>). Se usó esta baja concentración de O<sub>2</sub> para simular las condiciones de operación del reactor de reducción en el proceso CLOU. Todos los productos gaseosos se oxidaron completamente en un post-combustor corriente abajo del reactor y se midieron de forma continua las concentraciones de SO<sub>2</sub> y CO<sub>2</sub> en el gas. La Figura 3.35 muestra la evolución de la concentración de CO<sub>2</sub> y SO<sub>2</sub> en el flujo de salida del reactor de lecho fluidizado discontinuo durante la pirólisis y la posterior combustión del char.

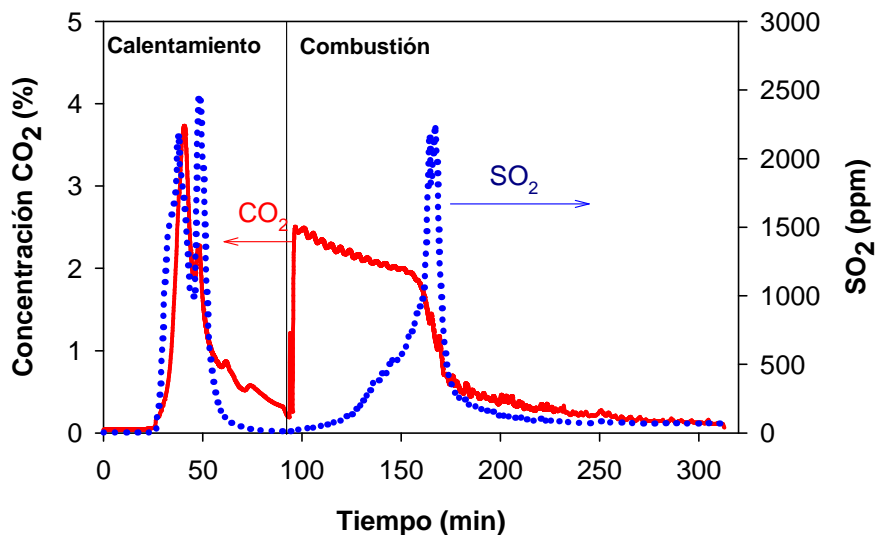


**Figura 3.35.** Concentración de las especies gaseosas de CO<sub>2</sub> (-) y SO<sub>2</sub> (•••) en el flujo de salida del reactor de lecho fluidizado discontinuo. Calentamiento: N<sub>2</sub>. Combustión: 2.5% O<sub>2</sub> en N<sub>2</sub>.

El balance másico al flujo de gases de salida indica que el 43% del S salía en la desvolatilización y el 57% durante la combustión del char. Por un lado, se puede observar que el S y el C en los volátiles evolucionan a la misma velocidad durante la desvolatilización del carbón. Sin embargo, los perfiles de C y S eran diferentes durante la combustión del char. Durante la combustión del char, la velocidad de generación de SO<sub>2</sub> alcanzaba su máximo cuando casi todo el C del char se había quemado. Como consecuencia de ello, el ratio S/C en el char aumentaba por un factor de 10 con respecto al medido en el análisis del char naciente. Este comportamiento podría ser explicado como resultado del alto contenido en azufre pirítico (2%) presente en este lignito. En un

ambiente de baja concentración de  $O_2$ , como es el caso del proceso CLOU, existe una competición por el oxígeno entre el C y el azufre pirítico. Como consecuencia, se favorece la combustión del C sobre la oxidación de la pirita [91]. Este hecho concuerda con el análisis realizado a los finos recogidos de los diferentes filtros de la planta, donde se observó que el ratio S/C cambiaba desde 0.09 (char analizado) hasta 1 en el char inquemado que salía del reactor de reducción, debido a la presencia de S pirítico. Estos resultados muestran que el S pirítico presente en el combustible puede afectar a las emisiones de azufre del reactor de oxidación en el sistema CLOU. Así, el ratio S/C en el char transferido al reactor de oxidación era mayor que el correspondiente al análisis elemental del char, y la emisión de S en el reactor de oxidación era mayor a lo esperado.

Con estos resultados, se puede realizar un balance al azufre considerando todas las fracciones (sólidas y gaseosas) que salen del sistema CLOU. Estos resultados se muestran en la Figura 3.36. La mayor emisión de S proviene de la corriente de salida del reactor de reducción en forma de  $SO_2$ . El balance de S en las corrientes gaseosas de salida de los reactores de reducción y oxidación se corresponde con el 50-55% del total. Entre el 8 y el 11% del total de azufre alimentado estaba en forma de S pirítico inquemado. Además, se conoce que la presencia de CaO en las cenizas del lignito permite la auto-retención de S durante la combustión a través de la formación de  $CaSO_4$  [92]. Por ello, en la Figura 3.36 también se ha considerado el S retenido por las cenizas por auto-retención. Teniendo en cuenta el azufre en ambas fases, sólida y gaseosa, el balance de S cierra aproximadamente al 80%.

Un posible destino del resto el S podría ser su acumulación en las partículas del transportador de oxígeno. Por lo tanto, se extrajeron muestras de partículas de transportador de oxígeno tanto del reactor de reducción como del de oxidación y se analizaron en busca de compuestos de azufre por XRD y SEM-EDX. En estos análisis no se detectó ningún compuesto de azufre en las partículas de transportador de oxígeno analizadas. Además, se analizó la reactividad de las partículas en la TGA obteniéndose que el transportador de oxígeno no había perdido reactividad, lo que indica que no se había formado ningún compuesto de azufre asociado al CuO.

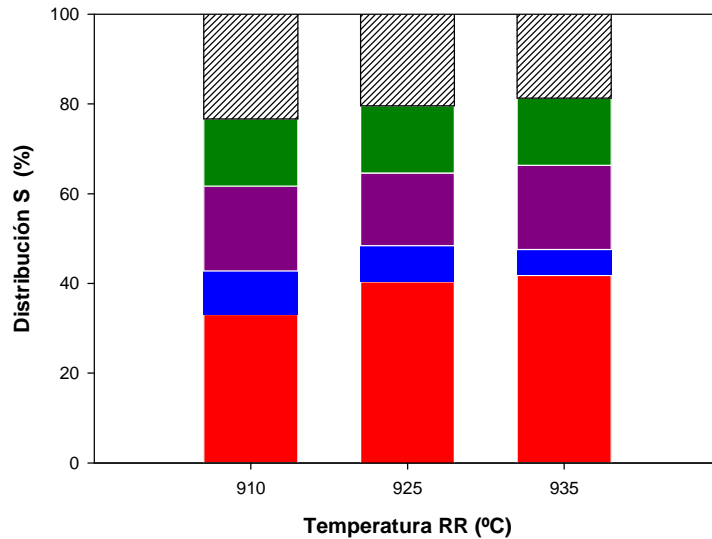


**Figura 3.36.** Distribución del S en la planta en continuo para el proceso CLOU. ■: Gas a la salida del reactor de reducción, y ■: reactor de oxidación; ■: S pirítico en las cenizas; ■: auto-retención por las cenizas.

Finalmente la Tabla 3.12 resume los resultados obtenidos respecto a emisiones de SO<sub>2</sub> a la atmósfera (aire empobrecido) y en la corriente de CO<sub>2</sub> destinada a transporte y almacenamiento obtenidos en esta sección a 915°C. En la Tabla 3.12 también se muestra el límite de emisiones de SO<sub>2</sub> impuesto por la UE para nuevas plantas de combustión con una potencia igual o mayor a 300 MW [90]. Respecto a la corriente de CO<sub>2</sub>, Pipitone y Bollard [93] dieron algunos ejemplos de las especificaciones sobre la calidad del CO<sub>2</sub> actualmente en vigor para su transporte y almacenamiento. A día de hoy, el proyecto Dynamis marca una primera directriz sobre la calidad de la corriente de CO<sub>2</sub> destinada a transporte y almacenamiento [12].

**Tabla 3.12:** Concentraciones de SO<sub>2</sub> medidas a la salida de los reactores de reducción y oxidación a 915°C.

	Aire empobrecido <sup>1</sup>	Corriente de CO <sub>2</sub>
<b>Límite</b>	<b>200 (mg/Nm<sup>3</sup>)<sup>2</sup></b>	<b>100 ppm<sup>3</sup></b>
CLOU	1580 (mg/Nm <sup>3</sup> ) <sup>2</sup>	32000 ppm

<sup>1</sup>Normalizado al 6% de O<sub>2</sub>

<sup>3</sup>Dynamis

<sup>2</sup>Límite legal UE

Respecto a las emisiones de SO<sub>2</sub> a la atmósfera, se puede ver en la Tabla 3.12, que las emisiones con este carbón son superiores al límite legal de la UE (200 mg/Nm<sup>3</sup>) como ya se ha comentado en esta sección. También se puede observar en esta Tabla 3.12 que hay un exceso de SO<sub>2</sub> en la corriente de salida del reactor de reducción comparada con la concentración recomendada para un transporte y almacenamiento seguro. Por lo tanto es necesario purificar ambas corrientes gaseosas para reducir la cantidad de SO<sub>2</sub> y



cumplir con ambos requisitos. Para disminuir la cantidad de  $\text{SO}_2$  presente en las corrientes de salida de ambos reactores, existen diferentes técnicas industriales. En el caso del  $\text{SO}_2$  presente en el reactor de oxidación la cantidad de éste se podría reducir con la instalación de un *carbon stripper* entre ambos reactores, ya que al transferirse menos char quemado al reactor de oxidación es esperable que se redujera la cantidad de  $\text{SO}_2$  emitido desde dicho reactor [63]. Por otro lado, para disminuir la cantidad de  $\text{SO}_2$  en la corriente gaseosa de salida tanto en el reactor de reducción como en el de oxidación, se podría usar un proceso industrial de desulfuración de gases por vía húmeda con  $\text{CaCO}_3$ . La ventaja de la desulfuración por vía húmeda en la corriente de  $\text{CO}_2$  previa al transporte (proveniente del reactor de reducción) es la alta concentración del  $\text{SO}_2$  en el gas y el menor volumen de gases a tratar respecto a la combustión convencional, ya que se ha eliminado el  $\text{N}_2$  en la corriente de  $\text{CO}_2$  capturado.

### 3.5 Caracterización del transportador de oxígeno

El uso del transportador de oxígeno a alta temperatura, la presencia de azufre en el combustible y de cenizas son factores que puede afectar a las propiedades del material. Por ello, se realizó un análisis de las propiedades del transportador de oxígeno tanto en la serie de experimentos sin combustible (Sección 3.3.1) como después de haber usado diferentes carbones (Sección 3.3.3). En ambos casos, los resultados obtenidos fueron similares. Los resultados obtenidos para las partículas tras los experimentos sin carbón se muestran en el Artículo II. La Tabla 3.13 muestra las propiedades más relevantes de las partículas usadas del transportador de oxígeno comparadas con las partículas frescas.

**Tabla 3.13.** Propiedades de las partículas del transportador de oxígeno CU60MgAl\_SD tanto frescas como usadas.

	<i>Frescas</i>	<i>Usadas<sup>a</sup></i>
Contenido en CuO (%)	60	<b>60</b>
Capacidad de transporte de oxígeno, $R_{OC}$ (%)	6	<b>6</b>
Velocidad de transferencia de oxígeno (kg O <sub>2</sub> /s kg TO)x10 <sup>3</sup>	1.66	<b>1.70</b>
Resistencia mecánica (N)	2.4	<b>0.7</b>
Densidad de partícula (kg/m <sup>3</sup> )	3860	<b>2815</b>
Porosidad (%)	16.1	<b>40.3</b>
Área superficial específica, BET (m <sup>2</sup> /g)	< 0.5	<b>0.73</b>
Fases principales, XRD	CuO, MgAl <sub>2</sub> O <sub>4</sub>	<b>CuO, MgAl<sub>2</sub>O<sub>4</sub></b>

a: 40 h en la planta en continuo para el proceso CLOU

Se determinó el contenido de Cu en todas las muestras por reducción completa en la TGA usando una corriente gaseosa con el 15% de H<sub>2</sub> a 850°C. En todos los casos - partículas frescas y usadas- el contenido en CuO fue del 60%. Además, se determinó en la TGA la reactividad de las muestras tomadas tras 40 h de operación a 1000°C, (descomposición en N<sub>2</sub> y oxidación en aire). La Figura 3.37 muestra las curvas conversión vs. tiempo obtenidas para las reacciones de (a) descomposición y (b) oxidación para las muestras tanto frescas como usadas. Se puede observar claramente que se mantiene la reactividad inicial en las partículas usadas tanto para la reducción como para la oxidación. Este hecho justifica que no cambiara ni la eficacia de combustión ni de captura de CO<sub>2</sub> durante las 40h de operación quemando los diferentes tipos de carbones en la planta en continuo.

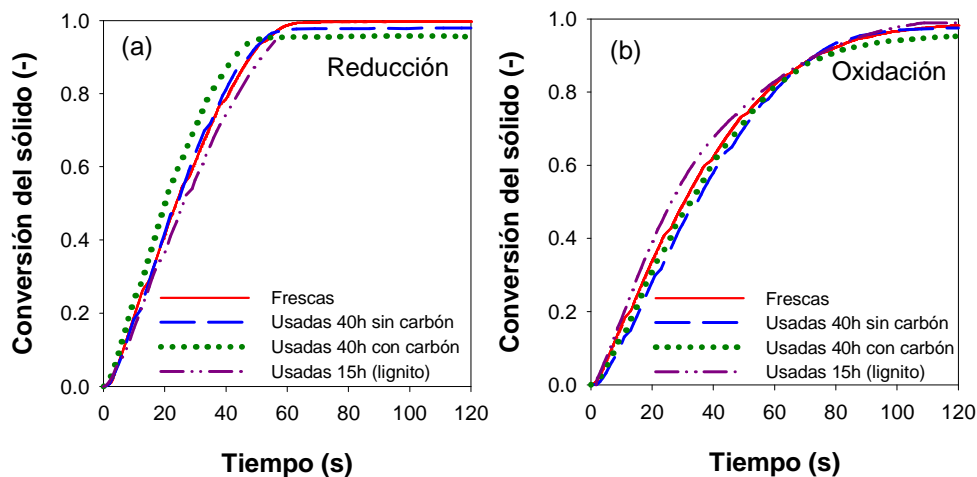


**Figura 3.37.** Curvas conversión vs. tiempo para las reacciones de (a) reducción y (b) oxidación, para las partículas tanto frescas como usadas en la planta en continuo con y sin carbón y tras 15h con lignito. Reducción en  $N_2$  y oxidación en aire a  $1000^\circ C$  en la TGA.

La Figura 3.37 también muestra la reactividad de partículas del transportador de oxígeno Cu60MgAl\_SD después de 15 h de operación en continuo con un lignito con alto contenido en azufre. Se puede ver que las muestras usadas exhiben la misma reactividad durante la reducción y la oxidación. Además, la capacidad de transporte de oxígeno no se vió afectada. Por lo tanto, la alta concentración de azufre durante las 15h de operación no afectó a la reactividad del transportador de oxígeno.

El análisis por XRD no reveló ningún cambio sustancial entre las fases presentes en las partículas usadas respecto a las frescas, siendo las principales fases cristalinas CuO y  $MgAl_2O_4$ . En muestras reducidas a la salida del reactor de reducción no se encontró Cu metálico, incluso en los experimentos en los que la variación de conversión de los sólidos era cercana a 1, y solo se encontró  $Cu_2O$  y  $MgAl_2O_4$ .

Se midieron valores de área superficial BET muy bajos para todas las partículas, tanto frescas como usadas, con un valor alrededor de  $0.5 \text{ m}^2/\text{g}$ . Sin embargo, las partículas frescas tenían una porosidad baja (16.1%), la cual se incrementó hasta el 40.3% después de 40 h de operación en la planta en continuo.

Además, se encontró una importante reducción de la resistencia mecánica de las partículas al aumentar el tiempo de operación, alcanzándose valores inferiores a 1 N después de las 40 h de operación en continuo. La reducción de la resistencia mecánica de las partículas estaba relacionada con el incremento de la porosidad al aumentar el

tiempo de operación en la planta; ver la Figura 3.38. Se encontró un comportamiento similar respecto a la porosidad y resistencia mecánica de las partículas usadas en el reactor de lecho fluidizado discontinuo (Apartado 3.1.4.2).

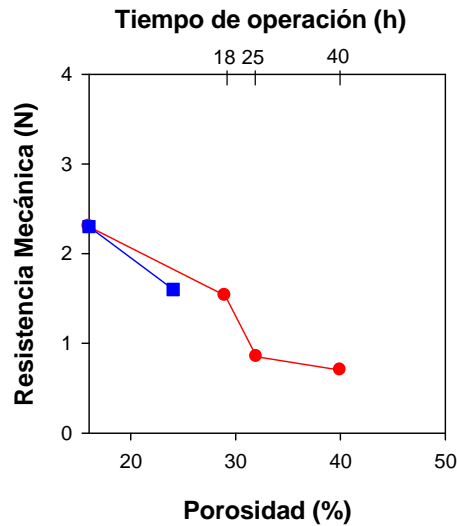


**Figura 3.38.** Resistencia mecánica en función de la porosidad para las partículas de Cu60MgAl\_SD: (●) usada en la planta en continuo para el proceso CLOU y (■) usada en el reactor de lecho fluidizado discontinuo. También se muestra el tiempo de operación en la planta en continuo.

La Figura 3.39 (derecha) muestra imágenes SEM de las partículas usadas extraídas del reactor de oxidación tras 40 h de operación en la planta en continuo. Los análisis EDX mostraban que el Cu seguía distribuido uniformemente en el interior de las partículas, y no había sufrido cambios durante las 40 h de operación en continuo. Sin embargo, sí que se encontró un importante número de partículas fragmentadas. Hay que señalar que las partículas usadas en la Figura 3.39 (d), no muestran ningún signo de aglomeración, incluso después de 15 h de operación en continuo a alta temperatura y con un combustible con alto contenido en azufre.

No obstante, este hecho no invalida los buenos resultados obtenidos respecto a las eficacias de combustión y de captura de CO<sub>2</sub> en el proceso CLOU para la combustión de carbón o biomasa con captura de CO<sub>2</sub>.

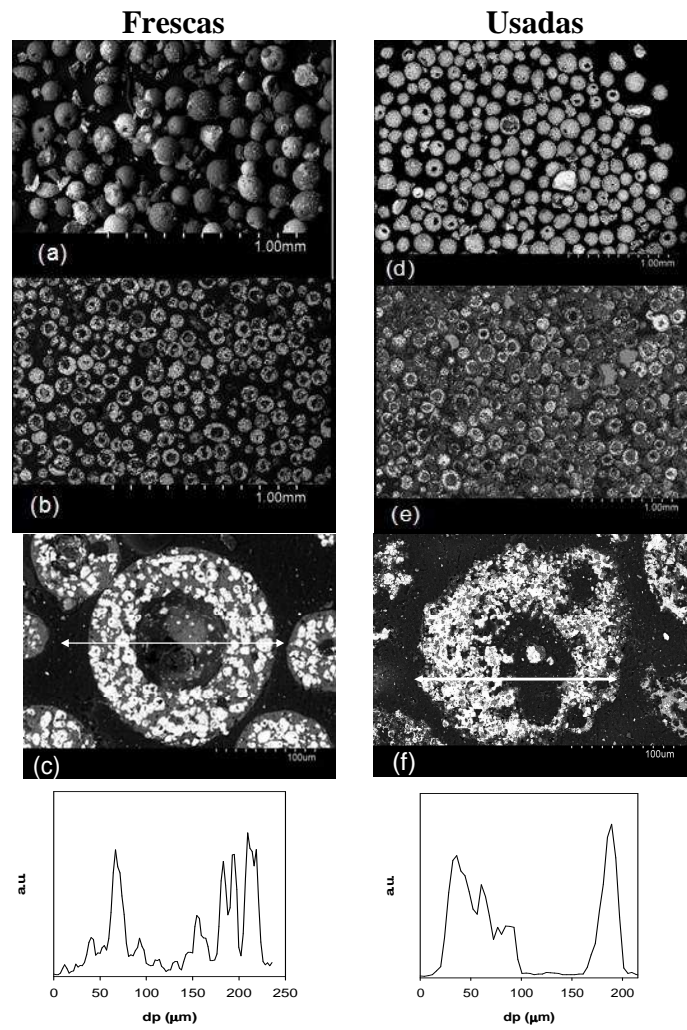


**Figura 3.39.** Imágenes SEM de partículas frescas (izquierda) y usadas (derecha) después de 40h de operación en la planta en continuo para el proceso CLOU: (a, d) imagen general de las partículas; (b, e) imágenes de la sección transversal de las partículas; (c, f) imagen y perfil EDX de Cu en la sección transversal de una partícula.

### 3.6 Comparación entre los procesos CLOU y *iG*-CLC

Como se ha comentado en el Capítulo 1, a día de hoy existen dos procesos diferentes basados en la tecnología CLC para la combustión de carbón: *iG*-CLC y CLOU. Ambos procesos tienen sus ventajas y sus desventajas a tener en cuenta; ver secciones 1.4.2 y 1.5. Por lo tanto, el objetivo de esta sección es realizar una comparación de ambos procesos basada en los resultados experimentales obtenidos con los mismos combustibles sólidos mediante experimentos de combustión realizados en la misma planta en continuo y obtenidos de la literatura para el *iG*-CLC [31, 83] y de esta Tesis Doctoral para el proceso CLOU (Artículo IX).

En los experimentos realizados para el proceso *iG*-CLC se utilizaron como transportadores de oxígeno ilmenita [31] en la combustión de carbones y un mineral de hierro [83] para la combustión de biomasa. En el caso del proceso CLOU se usó el transportador de oxígeno Cu60MgAl\_SD con todos los combustibles. Debido a las características específicas de cada proceso, se usaron diferentes inventarios de sólidos en el reactor de reducción, alrededor de 1500 kg/MW<sub>t</sub> en el proceso *iG*-CLC y entre 850 y 1000 kg/MW<sub>t</sub> para el proceso CLOU.

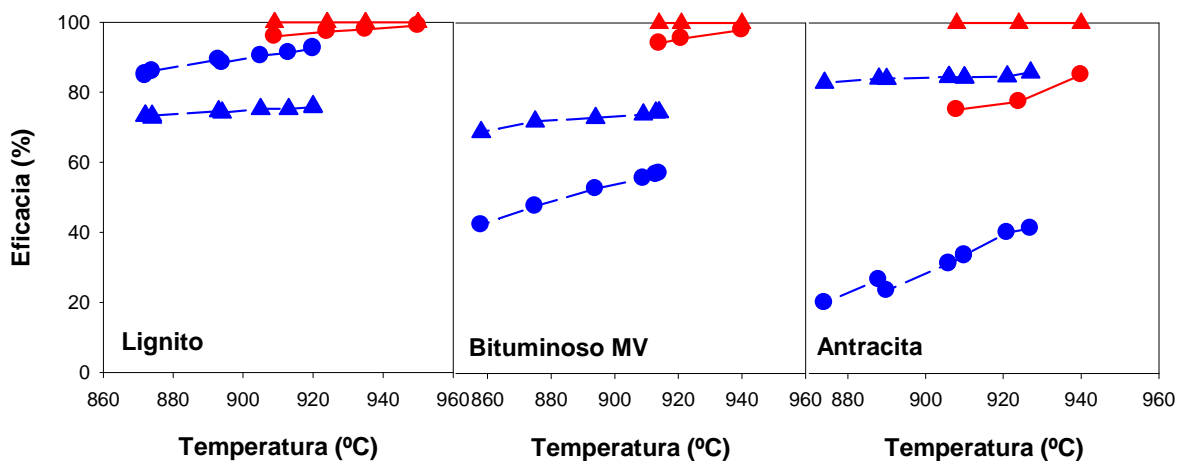


Figura 3.40. Eficacia de combustión (--▲--) y de captura de CO<sub>2</sub> (--●--) en función de la temperatura para los procesos CLOU (—) e *iG*-CLC (- -) con diferentes carbones.

La Figura 3.40 compara las eficacias de combustión y de captura de CO<sub>2</sub>, obtenidas para ambos procesos, a diferentes temperaturas del reactor de reducción usando diferentes carbones: un lignito, un carbón bituminoso medio en volátiles y una antracita. Las

diferencias entre el proceso *iG-CLC* y CLOU son evidentes cuando se comparan los resultados obtenidos. Respecto a la eficacia de combustión, se puede observar que para el proceso CLOU siempre se obtuvo combustión completa del combustible a CO<sub>2</sub> y H<sub>2</sub>O en el reactor de reducción. Sin embargo, en el proceso *iG-CLC* había productos inquemados a la salida del reactor de reducción (CH<sub>4</sub>, CO e H<sub>2</sub>). Por lo tanto la eficacia de combustión era inferior al 100%, y se encontró que era mayor para los carbones con menor contenido en volátiles. Además, la temperatura del reactor de reducción apenas afectaba a la eficacia de combustión. Resaltar el bajo inventario de transportador de oxígeno usado en el sistema CLOU (845 kg/MW<sub>t</sub> con lignito) en comparación con el proceso *iG-CLC*, donde se necesitaban alrededor de 1500 kg/MW<sub>t</sub> para obtener eficacias de combustión del 95% con lignito.

Además, en el proceso CLOU se obtuvieron mayores valores de eficacia de captura de CO<sub>2</sub> que en *iG-CLC*. La eficacia de captura de CO<sub>2</sub> sigue el orden lignito > bituminoso MV > antracita en ambos procesos. Por lo tanto, la eficacia de captura de CO<sub>2</sub> depende de la fracción de carbono en los volátiles y de la velocidad de conversión del char. Así, cuanto menos reactivo sea el carbón, se obtiene menor eficacia de captura de CO<sub>2</sub>. Por ejemplo, la eficacia de captura de CO<sub>2</sub> en *iG-CLC* a 920°C era un 93% con el lignito y esta se reducía a un 58% y 40% con el carbón bituminoso medio en volátiles y con antracita, respectivamente. Con el proceso CLOU para el lignito y el carbón bituminoso a 920°C se obtuvieron unas eficacias de captura de CO<sub>2</sub> del 97 y 95% respectivamente y se obtuvo un valor inferior para la antracita, un 77% a la misma temperatura.

La eficacia de captura de CO<sub>2</sub> es mayor en el proceso CLOU que en el *iG-CLC* porque es mayor la velocidad de conversión del char. El char se convierte más rápido porque se quema con O<sub>2</sub> gaseoso en vez de ser gasificado con H<sub>2</sub>O como en el proceso *iG-CLC*. Por lo tanto, se puede usar la velocidad de conversión del char por unidad de masa de carbono para realizar una comparación entre los diferentes combustibles, ya que la conversión del char en el interior del reactor de reducción depende directamente de esta velocidad. La Figura 3.41 muestra la velocidad de conversión del char en función de la temperatura del reactor de reducción calculada con la Ecuación 2.33 para los tres carbones utilizados en la planta en continuo durante los experimentos en CLOU o *iG-CLC*, usando los valores de conversión y tiempo medio de residencia del char obtenidos en la planta en continuo para cada carbón. Como era de esperar, la conversión del char

aumentó con la temperatura. Para el proceso CLOU, al aumentar la temperatura, aumenta la concentración de  $O_2$  en equilibrio y, lo que es más importante, aumenta la velocidad de generación de oxígeno. Como consecuencia, la velocidad de combustión del char se incrementa proporcionalmente.

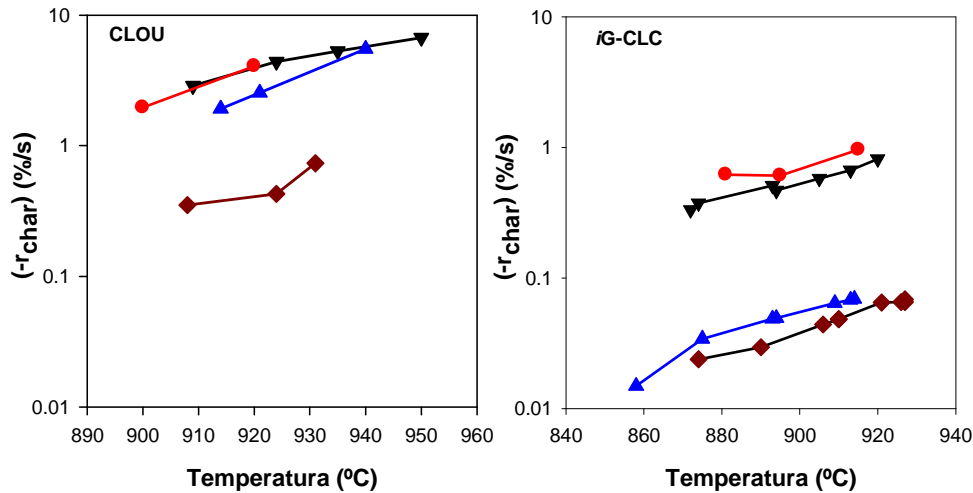


**Figura 3.41.** Velocidad de conversión del char para los diferentes combustibles en el proceso CLOU o *iG-CLC*: lignito (---▼---), bituminoso medio en volátiles (---▲---), antracita (---◆---) y biomasa (---●---), en función de la temperatura del reactor de reducción calculados a partir de los datos obtenidos en la planta en continuo.

Además se puede observar que la velocidad de conversión del char para el proceso CLOU es muy superior a la velocidad de conversión por gasificación del char en el proceso *iG-CLC*. Estos resultados explicarían la razón de la mayor eficacia de captura de  $CO_2$  obtenida para el proceso CLOU respecto al proceso *iG-CLC*. En la Figura 3.41 también se ha incluido la velocidad de conversión del char de biomasa para el proceso CLOU estudiado en el apartado 3.3.4 y para el proceso *iG-CLC* [83] con un mineral de hierro como transportador de oxígeno. Como se puede ver, la velocidad de conversión del char de biomasa para el proceso CLOU era muy similar a la obtenida para el lignito, uno de los carbones más reactivos utilizados en la planta. Esta alta velocidad de conversión del char, junto a la gran cantidad de volátiles que contiene la biomasa, permite alcanzar eficacias muy altas de captura de  $CO_2$ , incluso superiores a las obtenidas con lignito bajo las mismas condiciones de operación; ver Figura 3.32. Comparando la velocidad de conversión del char de biomasa por el proceso CLOU e *iG-CLC* se puede observar que a temperaturas de  $900^\circ C$  o superiores, la velocidad de conversión de char en el proceso CLOU es entre 3 y 4 veces superior a la obtenida con el *iG-CLC*. Esto es debido al diferente mecanismo de conversión del char, como se ha comentado anteriormente. Esta alta velocidad de conversión del char en el proceso



CLOU explica los menores inventarios de sólido necesarios en el proceso CLOU (565 kg/MW<sub>t</sub>) comparados con los requeridos por el *iG-CLC* (1550 kg/MW<sub>t</sub>) [83], para obtener similares eficacias de captura de CO<sub>2</sub>.

Por lo tanto se puede concluir que con el proceso CLOU se obtienen mayores eficacias de combustión y conversión del char en el reactor de reducción que en el proceso *iG-CLC*, lo que revierte en mayores eficacias de captura de CO<sub>2</sub> para todos los combustibles sólidos estudiados, utilizando además menores inventarios de sólido. Estos resultados son debidos a dos causas fundamentales: la mejor combustión de los volátiles con el O<sub>2</sub> gaseoso generado por el transportador de oxígeno y a la mayor velocidad de conversión del char mediante la reacción con O<sub>2</sub> gaseoso frente a la gasificación con H<sub>2</sub>O.

Respecto al transportador de oxígeno necesario en ambos procesos existen claras diferencias entre los procesos que hacen que las necesidades sean diferentes. En el proceso *iG-CLC* son preferibles transportadores de oxígeno baratos, generalmente minerales de hierro [83], ilmenita [31] o residuos ricos en hierro [94]. Esto es debido a que no es crucial utilizar materiales muy reactivos debido a que la etapa controlante del proceso *iG-CLC* es la gasificación del char. Por lo tanto, se prefieren transportadores baratos, aunque no muy reactivos, donde la pérdida económica que se produciría al purgar las cenizas del proceso junto con el transportador de oxígeno no sea muy elevada. Por otro lado, en el proceso CLOU se necesitan transportadores de oxígeno altamente reactivos. Para ello, se ha propuesto utilizar materiales sintéticos de cobre tal y como se ha mostrado en esta Tesis Doctoral. Estos transportadores altamente reactivos son caros y, por tanto, será necesario minimizar las pérdidas al extraer las cenizas del carbón. Por ello, existirá la necesidad de desarrollar transportadores de oxígeno que sean fácilmente separables de las cenizas, ya que dado el alto contenido en CuO necesario en el transportador, estas pérdidas supondrían un coste notable para el proceso. Vistos los buenos resultados obtenidos con un transportador de cobre en el proceso CLOU, el trabajo futuro estará encaminado hacia el desarrollo de transportadores de oxígeno de base cobre con un mejor tiempo medio de vida de las partículas respecto al mostrado por el transportador de oxígeno usado en esta Tesis Doctoral (Cu60MgAL\_SD) y que sean fácilmente separables de las cenizas.

## **4 Modelado del proceso CLOU**



## 4.1 Introducción al diseño de un proceso CLOU

Para realizar un diseño básico de un sistema CLOU es necesario determinar la cantidad de sólidos en los reactores de oxidación y reducción, así como la velocidad de circulación del transportador de oxígeno entre ambos reactores necesaria para la combustión completa del combustible.

El equilibrio termodinámico del transportador de oxígeno elegido determina las temperaturas y las concentraciones de oxígeno adecuadas para el proceso CLOU. Así, la concentración de oxígeno en las condiciones de equilibrio a la temperatura fijada en el reactor de reducción deberá ser lo suficientemente alta para permitir la liberación de  $O_2$  en el reactor de reducción y, además, la combustión del combustible sin que exista un gran exceso de  $O_2$  junto a los productos de combustión. Por otra parte, el transportador de oxígeno deberá de ser capaz de oxidarse en el reactor de oxidación a la concentración de oxígeno a la salida del mismo, la cual debería ser lo más baja posible para maximizar el uso del oxígeno del aire. Experimentalmente, se ha comprobado que las temperaturas de interés para este proceso se encuentran en el intervalo de entre 900 y 950 °C.

Para determinar el inventario de sólidos requerido en cada reactor es necesario conocer la cinética de reacción del transportador de oxígeno, tanto de la reacción de reducción, como de su reacción de oxidación posterior. En la literatura existen diferentes estudios sobre las cinéticas de las reacciones de liberación de oxígeno y posterior oxidación de materiales basados en CuO. La Tabla 4.1 muestra un resumen de los principales parámetros cinéticos obtenidos en la literatura para las reacciones de reducción y oxidación que ocurren en el proceso CLOU. Como puede verse, se han utilizado distintos modelos cinéticos para determinar dichos parámetros. Además también se muestra el contenido de metal, el tipo de soporte, el método de preparación utilizado, así como el diámetro de partícula analizado.

**Tabla 4.1.** Estudios cinéticos relevantes sobre las reacciones de reducción del CuO y la oxidación del Cu<sub>2</sub>O en condiciones CLOU en la literatura.

Transportador de oxígeno (% CuO)	Soporte	Método preparación <sup>a</sup>	dp (µm)	Instalación <sup>b</sup>	T (°C)	E <sub>A</sub> (kJ/mol)		Modelo <sup>c</sup>	Ref.
						Global (E <sub>1</sub> )	Cinética (E <sub>2</sub> )		
<b>Reducción</b>									
Puro	----	----	10	TGA	760-910	313	----	Primer orden	[95]
Puro	----	----	104-152	TGA	850-960	327	----	Primer orden	[43]
40	MgAl <sub>2</sub> O <sub>4</sub>	FG	125-180	LFD	850-900	139	----	A-E (N=2)	[64]
42	SiC	I	105-150	TGA	850-950	220	----	Primer orden	[96]
60	SiO <sub>2</sub>	MM	200-315	TGA	800-950	145	----	A-E (N=3)	[97]
20	SiO <sub>2</sub>	IH	< 45	TGA	900-1000	170	----	Primer orden	[69]
			75-125	LFD					
			125-210	LF					
18	SiO <sub>2</sub>	I	106-150	TGA	800-900	315	----	A-E (N=2)	[98]
						176			
60	TiO <sub>2</sub>	MM	200-315	TGA	900-975	155	----	A-E (N=3)	[97]
50	TiO <sub>2</sub>	MM	< 45	TGA	800-950	180	----	Primer orden	[69]
			75-125	LFD					
			125-210	LF					
50	TiO <sub>2</sub>	MM	< 45	TGA	900-1000	284	58	Primer orden	[99]
60	ZrO <sub>2</sub>	MM	200-315	TGA	800-1000	153	----	A-E (N=3)	[97]
55	ZrO <sub>2</sub>	FG	< 45	TGA	800-950	147	----	Primer orden	[69]
			75-125	LFD					
			125-210	LF					
45	ZrO <sub>2</sub>	FG	< 45	TGA	800-1000	264	67	Primer orden	[99]
40	ZrO <sub>2</sub>	FG	125-180	LF	775-925	281	20	Primer orden	[100]
<b>Oxidación</b>									
Puro	----	----	disco (5 mm) <sup>c</sup>	TGA	>900	173-98	----	Primer orden	[101]
Puro	----	----	10	TGA	400-500	76.5	----	Primer orden	[95]
18	SiO <sub>2</sub>	I	106-150	TGA	800-900	3	----	Reacción en	[98]
						-43	los límites de fase (N=2)		
55	ZrO <sub>2</sub>	FG	< 45	TGA	900-975	----	202	Primer orden	[69]
			75-125	LFD					
			125-210	LF					

<sup>a</sup>Método de preparación:  
 FG = Freeze granulation  
 I = Impregnación.  
 IH = Impregnación húmeda  
 MM = Mezcla mástica

<sup>b</sup>Instalación de laboratorio:  
 LFD = Lecho fluidizado discontinuo  
 LF = Lecho fijo  
 TGA = Termobalanza

<sup>c</sup>Modelo  
 A-E: Avrami-Erofeev

La mayoría de los trabajos se centran en la evaluación de los efectos de la temperatura sobre la velocidad de reacción y el cálculo, por lo tanto, de la energía de activación del proceso. Se han usado dos tipos de ecuaciones de velocidad para representar la liberación de O<sub>2</sub> por parte del CuO y la oxidación del Cu<sub>2</sub>O para el proceso CLOU [99, 100].

$$(-r_{Red})_{TO} = k_1 \cdot f(X) \quad (4.1)$$

$$(-r_{Red})_{TO} = k_2 \cdot (C_{O_2,eq} - C_{O_2})^{n'} \cdot f(X) \quad (4.2)$$

Se puede observar que en la Ecuación (4.1) la velocidad de reducción solamente depende de la temperatura (incluida en la constante cinética) y de la conversión del transportador de oxígeno,  $f(X)$ . Por otro lado, en la Ecuación (4.2) la velocidad de

reacción también depende del gradiente de oxígeno entre la concentración en el gas reaccionante y la de equilibrio. La concentración de oxígeno en el equilibrio es una función de la temperatura, descrita en la siguiente ecuación:

$$C_{O_2,eq} = \frac{101325}{R_g T} K_{eq} = \frac{101325}{R_g T} \exp(22 - 2.993 \cdot 10^4 T^{-1} - 1.048 \cdot 10^6 T^{-2}) \quad (4.3)$$

En función de la ecuación (4.1 o 4.2) considerada se obtienen diferentes valores para la energía de activación. Así, se calcula una energía de activación global,  $E_1$  de la constante cinética aparente  $k_1$ , cuando se considera el efecto de la temperatura tanto en la barrera para la reacción química como en la barrera termodinámica. Usando la Ecuación (4.2), se calcula una energía de activación en la barrera de la reacción química,  $E_2$ , de la constante cinética  $k_2$ , la cual no incluye la energía en la barrera termodinámica ( $E_1$ ) del efecto de la temperatura sobre la concentración de  $O_2$  en equilibrio.

Como se puede ver en la Tabla 4.1, se encontraron valores muy dispersos de las energías de activación. Además, los parámetros se determinaron analizando la dependencia únicamente de la temperatura. En aquellos trabajos que analizaron también el efecto de la concentración de  $O_2$ , las condiciones analizadas quedaban lejos de las condiciones de equilibrio. Por estas razones, se consideró necesario analizar el efecto de la temperatura y de la concentración de oxígeno en las reacciones de reducción y oxidación en un amplio rango de valores de operación, incluso aquellos próximos a la concentración de  $O_2$  en equilibrio, ya que estas condiciones son las esperadas en un sistema CLOU (Artículo X). Los experimentos se llevaron a cabo bajo atmósfera controlada en un analizador termogravimétrico CI electronics (TGA).

## **4.2 Cinética de las reacciones de reducción y oxidación del transportador de oxígeno Cu60MgAl\_SD**

Para obtener la cinética de las reacciones de reducción y oxidación, se realizaron múltiples experimentos en TGA a varias temperaturas. Además se varió la

concentración de oxígeno en un amplio rango de valores para obtener velocidades de reacción en condiciones tanto alejadas como próximas a las condiciones de equilibrio termodinámico. La Tabla 4.2 muestra las condiciones experimentales para los experimentos realizados en la TGA para el cálculo de la cinética de reducción y oxidación del transportador de oxígeno Cu60MgAl\_SD, junto con la concentración de O<sub>2</sub> en equilibrio para cada condición.

**Tabla 4.2.** Condiciones experimentales para los experimentos realizados en la TGA. También se muestra las concentraciones de O<sub>2</sub> en condiciones de equilibrio.

Reducción			Oxidación		
T (°C)	y <sub>O<sub>2</sub></sub> (%) *	y <sub>O<sub>2</sub>,eq</sub> (%)	T (°C)	y <sub>O<sub>2</sub></sub> (%) *	y <sub>O<sub>2</sub>,eq</sub> (%)
			850	21	0.4
875	0	0.8	875	21	0.8
900	0	1.4	900	21, 11, 9, 4, 2.5	1.4
925	0	2.4	925	21	2.4
950	0, 1.5, 2.5	4.2	950	21	4.2
975	0, 1.5, 4	7.0	975	21	7.0
1000	0, 1.5, 4, 6, 8, 9	11.6	1000	21	11.6

\* N<sub>2</sub> para balance

#### 4.2.1 Reducción del CuO a Cu<sub>2</sub>O

La Figura 4.1(a) muestra las curvas conversión vs. tiempo para el transportador de oxígeno Cu60MgAl\_SD obtenidas a diferentes temperaturas entre 875 y 1000°C, usando N<sub>2</sub> puro (concentración de O<sub>2</sub> del 0%) en la reacción de reducción. Se puede observar que cuando la temperatura aumenta, la velocidad de reducción aumenta.

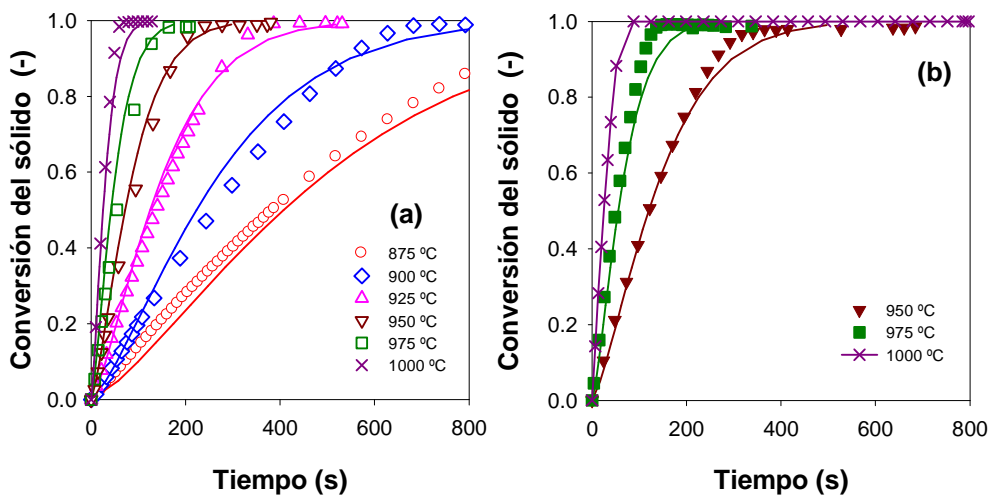


**Figura 4.1.** Efecto de la temperatura en la reacción de reducción del transportador de oxígeno en N<sub>2</sub> en TGA con: (a) y<sub>O<sub>2</sub></sub> = 0%, y (b) y<sub>O<sub>2</sub></sub> = 1.5%. Símbolos, datos experimentales; línea continua, predicciones del modelo.

Considerando la velocidad de reducción dada por la Ecuación (4.2), la velocidad de reacción aumentó con la temperatura porque aumentó la constante cinética y la fuerza impulsora. A menudo, este efecto se expresa por medio de la diferencia entre la concentración de oxígeno en el equilibrio y la concentración de oxígeno en el sistema alrededor de las partículas, es decir  $(C_{O_2,eq} - C_{O_2})$ . Por lo tanto, la velocidad de reducción depende de la concentración de oxígeno en la superficie externa de las partículas y de la concentración de  $O_2$  en equilibrio, la cual también aumenta con la temperatura siguiendo la Ecuación (4.3)

La Figura 4.1(b) muestra las curvas conversión vs. tiempo obtenidas para el transportador de oxígeno Cu60MgAl\_SD para tres temperaturas diferentes durante la reacción de reducción, usando una concentración de  $O_2$  del 1.5% en  $N_2$ . Se puede observar en estas curvas, que la velocidad era más lenta que la correspondiente a la misma temperatura pero sin oxígeno. Esta figura confirma que la velocidad de reacción disminuye cuando la fuerza impulsora disminuye debido a la aproximación de la concentración de  $O_2$  a la de equilibrio.

Para analizar el efecto de la concentración de oxígeno en la velocidad de reacción, la Figura 4.2 muestra las curvas conversión vs. tiempo obtenidas para el transportador de oxígeno Cu60MgAl\_SD con concentraciones de oxígeno entre 0 y el 9% a 1000°C. Este intervalo de concentraciones de  $O_2$  se eligió debido a que la máxima concentración de  $O_2$  está limitada por la concentración de  $O_2$  en el equilibrio, por ejemplo un 11.6% a 1000°C; así que la concentración de oxígeno durante los experimentos en la TGA debe ser inferior a la concentración de equilibrio. La velocidad de generación de oxígeno disminuye cuando la concentración de oxígeno aumenta debido a que disminuye la fuerza impulsora de la reacción. Este descenso era más pronunciado cuando la concentración de  $O_2$  estaba cercana a la concentración de equilibrio. Además, no se pudo detectar un cambio en el peso de la muestra en la TGA cuando la concentración de  $O_2$  era muy cercana a la de equilibrio ( $y_{O_2} > 9\%$ ), porque la velocidad de reacción era muy lenta. Un comportamiento similar fue descrito por Clayton y Whitty [99], durante la reducción cuando la fuerza impulsora estaba cercana a 0.



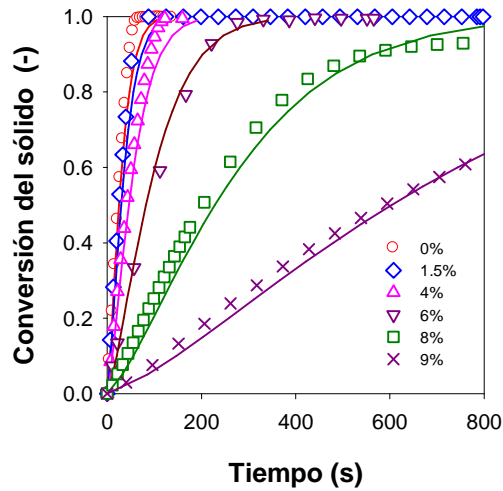


**Figura 4.2.** Efecto de la concentración de oxígeno a 1000°C en la reducción del transportador de oxígeno en TGA, usando mezclas  $N_2+O_2$ . Símbolos, datos experimentales; línea continua, predicciones del modelo cinético.

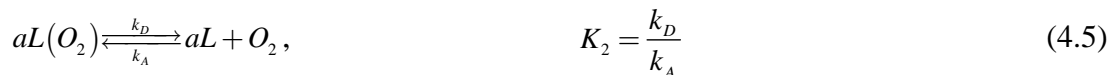
#### *Cinética de la reacción de reducción de CuO a Cu<sub>2</sub>O*

Para describir la reacción de reducción de CuO a Cu<sub>2</sub>O con generación de O<sub>2</sub> se propone un modelo de reacción en la superficie de las partículas usando un mecanismo de Langmuir-Hinshelwood mostrado en las Ecuaciones (4.4) y (4.5). El CuO en la superficie se descompone en Cu<sub>2</sub>O por reacción en los sitios activos  $a$  dando O<sub>2</sub> adsorbido en la superficie de la partícula. A continuación el O<sub>2</sub> desorbe, regenerando los sitios activos  $a$  en la superficie [102]. Aplicando este modelo a la descomposición del CuO, se obtienen las siguientes ecuaciones:

1. Reacción química de descomposición del CuO en Cu<sub>2</sub>O y O<sub>2</sub> adsorbido, la cual es un equilibrio dinámico entre la reacción directa e inversa:



2. Desorción del O<sub>2</sub> adsorbido



Cuando la reacción está controlada por la descomposición química, Ecuación (4.4), la velocidad de reacción viene dada por:

$$\frac{dX_{Red}}{dt} = k_{Red} S_{CuO} (1 - \theta) \left( 1 - \frac{C_{O_2}}{C_{O_2,eq}} \right) \cdot f(X_{Red}) \quad (4.6)$$

donde  $\theta$  es la fracción de sitios activos ocupados por el  $O_2$ . En estas condiciones, es posible usar diferentes isothermas de adsorción para obtener el valor de  $\theta$ . García-Labiano y col. [103] seleccionaron la isoterma de Freundlich para describir adecuadamente la calcinación del  $CaCO_3$ , cuyo efecto en la concentración de  $CO_2$  sobre la velocidad de calcinación del  $CaCO_3$  fue similar al mostrado para la concentración de  $O_2$  en la descomposición del  $CuO$ . Así, se seleccionó la isoterma de Freundlich para describir la fracción de sitios activos ocupados, es decir, el parámetro  $\theta$ , el cual se calcula con la siguiente ecuación:

$$\theta = cC_{O_2}^{1/n} \quad (4.7)$$

$$c = c_0 e^{-E_c/R_s T} \quad (4.8)$$

Combinando las Ecuaciones (4.6) y (4.7), la expresión para la velocidad de reacción es la siguiente:

$$\frac{dX_{Red}}{dt} = k_{Red} f(X_{Red}) S_{CuO} \left(1 - cC_{O_2}^{1/n}\right) \left(1 - \frac{C_{O_2}}{C_{O_2,eq}}\right) \quad (4.9)$$

Se han usado diferentes modelos para definir la función  $f(X_{Red})$  en la Ecuación (4.9), incluyendo mecanismos de nucleación [64, 97, 98] o de reacción química de primer orden [95, 100]. El mecanismo de Langmuir-Hinshelwood es un modelo de reacción en la superficie ampliamente utilizado para reacciones gas-sólido catalíticas. Debido a esta reacción de superficie, se propone el uso del modelo de nucleación para describir la dependencia de la conversión en la reacción sobre la superficie de las partículas de transportador de oxígeno.

La ecuación de Avrami-Erofeev [104] correspondiente al mecanismo de nucleación es la siguiente:

$$f(X_{Red}) = N^{-1} (1 - X_{Red}) \left[-\ln(1 - X_{Red})\right]^{1-N} \quad (4.10)$$

La expresión final para la velocidad de reducción, incluyendo la Ecuación (4.10) para la función de conversión, es la siguiente:

$$\frac{dX_{Red}}{dt} = k_{Red} S_{CuO} \left(1 - cC_{O_2}^{1/n}\right) \left(1 - \frac{C_{O_2}}{C_{O_2,eq}}\right) \left(N^{-1} (1 - X_{Red}) \left[-\ln(1 - X_{Red})\right]^{1-N}\right) \quad (4.11)$$

Integrando la Ecuación (4.11), se obtiene la siguiente ecuación para calcular la evolución de la conversión con el tiempo:

$$\left[-\ln(1 - X_{\text{Red}})\right]^N = k_{\text{Red}} S_{\text{CuO}} \left(1 - c C_{\text{O}_2}^{1/n}\right) \left(1 - \frac{C_{\text{O}_2}}{C_{\text{O}_2, \text{eq}}}\right) t \quad (4.12)$$

Se define una constante cinética efectiva como:

$$k'_{\text{Red}} = k_{\text{Red}} S_{\text{CuO}} = k'_{\text{Red},0} e^{-E_{\text{Red}}/R_s T} \quad (4.13)$$

El modelo cinético tiene cuatro parámetros ( $N$ ,  $n$ ,  $k'_{\text{Red}}$  and  $c$ ), los cuales deben de ser calculados en función de la temperatura de reacción. El valor de  $N$  representa el tipo de modelo de nucleación y crecimiento de los núcleos. Dicho valor oscila generalmente entre 1/4 y 3. Para calcular el mejor valor de  $N$ , en la Figura 4.3(a) se muestra el grafico  $(-\ln(1 - X_{\text{Red}}))^N$  vs. tiempo para diferentes valores de  $N$ , usando los datos experimentales de conversión vs. tiempo de la Figura 4.1. La Tabla 4.3 muestra los coeficientes de correlación para los diferentes valores de  $N$  para la regresión lineal de cada curva. El mejor ajuste corresponde a un valor de  $N$  de 3/4. Este procedimiento se ha realizado para cada curva de conversión a cada temperatura y concentración de  $\text{O}_2$  estudiadas, obteniéndose el mismo resultado de  $N$  para cada una de ellas.

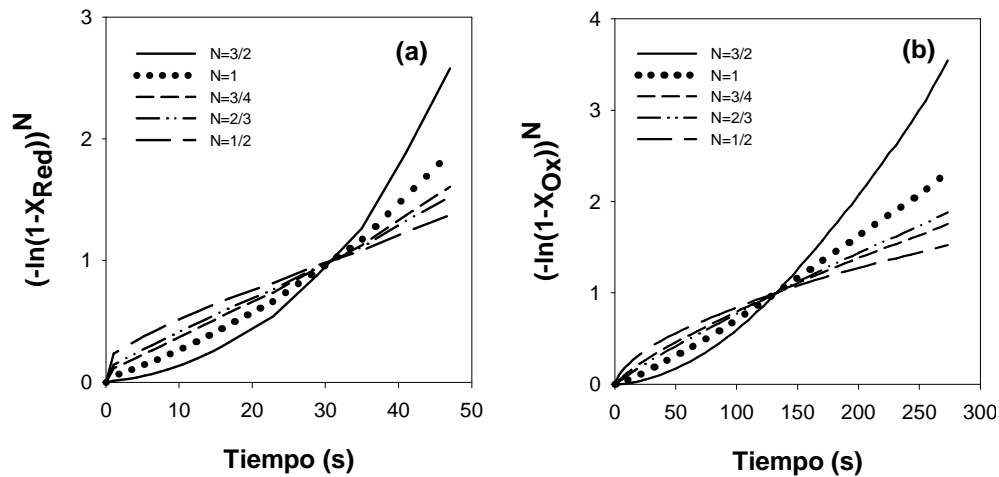


**Figura 4.3.** Determinación del parámetro  $N$  usando datos de conversión para calcular  $(-\ln(1-X))^N$  vs. tiempo (Ecuación (4.12)) a (a) 1000°C, 4%  $\text{O}_2$  para la reducción; y (b) 900°C, 6%  $\text{O}_2$  para la oxidación.

**Tabla 4.3.** Coeficientes de correlación para la dependencia lineal de las curvas  $(-\ln(1-X_{red}))^N$  vs. tiempo para diferentes valores de N para el transportador de oxígeno Cu60MgAl\_SD.  $T_{Red} = 1000^\circ\text{C}$ ;  $y_{O_2,Red} = 4\%$ ;  $T_{Ox} = 900^\circ\text{C}$ ;  $y_{O_2,Ox} = 6\%$

N	Reducción	Oxidación
3/2	0.9017	0.9570
1	0.9769	0.9970
3/4	0.9961	0.9977
2/3	0.9951	0.9926
1/2	0.9838	0.9703

Para determinar los valores de la constante de velocidad por la reacción química,  $k'_{Red}$ , y su variación con la temperatura, se consideraron los experimentos realizados a diferentes temperaturas (entre 875 y 1000°C) con una atmósfera con el 100% de  $N_2$ . En este caso, la Ecuación (4.12) se simplifica a  $[-\ln(1-X_{Red})]^N = k'_{Red}t$ . La Figura 4.4 muestra las representaciones de Arrhenius para la reacción de reducción, y la Tabla 4.4 muestra los parámetros cinéticos obtenidos para el factor pre-exponencial y la energía de activación.

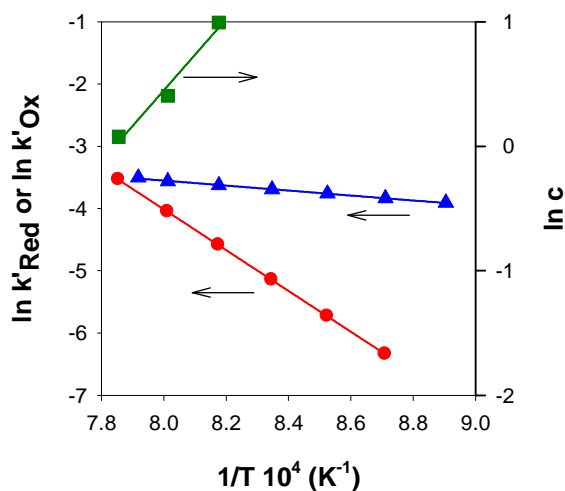


**Figura 4.4.** Dependencia de la temperatura de los parámetros cinéticos para el transportador de oxígeno Cu60MgAl\_SD: constante cinética para la liberación de oxígeno (●); constante cinética para la oxidación (▲); y parámetro de adsorción c para la reducción (■).

El valor obtenido de la energía de activación era de  $270 \text{ kJ}\cdot\text{mol}^{-1}$ . No se puede comparar este valor con los valores de energía de activación de la literatura porque el modelo cinético aquí propuesto es diferente. La energía de activación depende del número de parámetros dependientes de la temperatura considerados en el modelo cinético. Así, la energía de activación global se calcula únicamente con el parámetro  $k_I$  dependiente de la temperatura, ver Ecuación (4.1). La energía de activación cinética se calcula con 2

parámetros dependientes de la temperatura, es decir  $k_2$  y  $C_{O_2,eq}$ ; ver Ecuación (4.2). En este apartado la energía de activación tiene un parámetro adicional afectado por la temperatura,  $c$ , en el modelo cinético propuesto.

Los parámetros  $n$  y  $c$  en la Ecuación (4.12) se calcularon considerando el efecto de la concentración de oxígeno sobre la velocidad de reducción del transportador de oxígeno. Después de integrar y realizar algunas operaciones algebraicas sobre la Ecuación (4.11), se obtiene la siguiente expresión:

$$Y_R = \ln \left\{ 1 - \frac{1}{k'_{Red} \left( 1 - \frac{C_{O_2}}{C_{O_2,eq}} \right) \left( N^{-1} (1 - X_{Red}) [-\ln(1 - X_{Red})]^{1-N} \right)} \left[ \frac{dX_{Red}}{dt} \right]_{X_{Red}=0.2} \right\} = \ln(c) + \frac{1}{n} \ln(C_{O_2}) \quad (4.14)$$

Se calculó la velocidad de reacción cuando  $X_{Red} = 0.2$ , es decir, cuando se obtiene la máxima velocidad de reacción en el modelo de nucleación con el valor de  $N = 3/4$ .

**Tabla 4.4.** Parámetros cinéticos determinados para el transportador de oxígeno Cu60MgAl\_SD.

Reducción		Oxidación	
$k'_{Red,0}$ (s <sup>-1</sup> )	3.6 · 10 <sup>9</sup>	$k'_{Ox,0}$ ((m <sup>3</sup> · mol <sup>-1</sup> ) <sup>1/n</sup> · s <sup>-1</sup> )	6.2 · 10 <sup>-1</sup>
$E_{Red}$ (kJ mol <sup>-1</sup> )	270	$E_{Ox}$ (kJ mol <sup>-1</sup> )	32
$c_0$ ((m <sup>3</sup> mol <sup>-1</sup> ) <sup>1/n</sup> )	1.8 · 10 <sup>-10</sup>		
$E_C$ (kJ mol <sup>-1</sup> )	-240		
$n$	0.5	$n$	1.2

Trazando el lado izquierdo de la Ecuación (4.14),  $Y_R$ , frente al  $\ln(C_{O_2})$ , se pueden calcular los parámetros  $c$  y  $n$  calculando la ordenada en el origen y la pendiente de la curva obtenida; ver Figura 4.5(a). De esta forma se obtiene, para todas las temperaturas estudiadas, un valor de  $n$  de 0.5 (ver Tabla 4.4). Considerando una dependencia de  $c$  con la temperatura del tipo Arrhenius, la Figura 4.4 muestra el ajuste de  $c$  con la temperatura para la reacción de reducción, y la Tabla 4.4 muestra los parámetros cinéticos obtenidos para el factor pre-exponencial y la energía de activación obtenida para  $c$  usando la Ecuación (4.8). El valor de la energía de activación para el parámetro  $c$  es -240 kJ · mol<sup>-1</sup>, negativo, como corresponde a un proceso de adsorción.

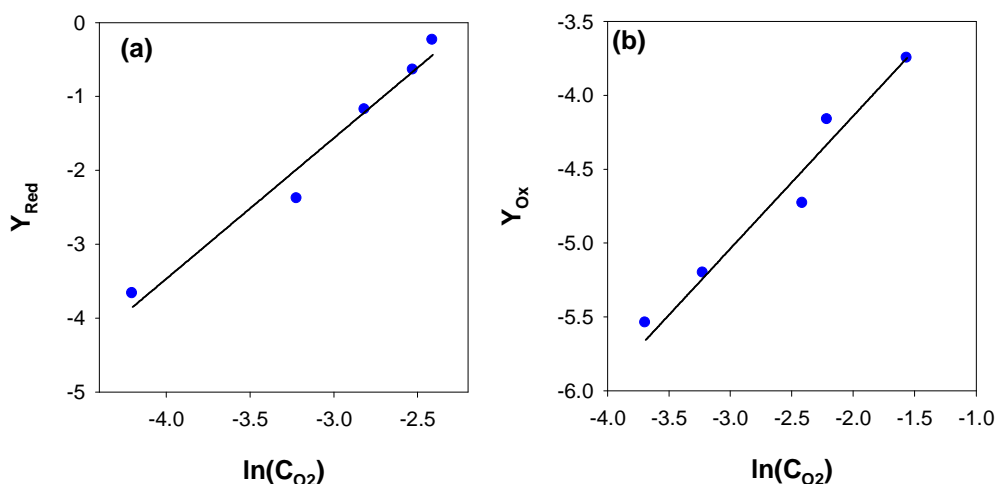


**Figura 4.5.** Determinación de (a) parámetros  $n$  y  $c$  usando la Ecuación (4.14) para la reacción de reducción a 1000°C; y (b) parámetro  $n$  usando la Ecuación (4.21) para la reacción de oxidación a 900°C.

El modelo desarrollado con los parámetros cinéticos obtenidos se utilizó para obtener las curvas teóricas a diferentes temperaturas de operación, las cuales se comparan con las curvas experimentales de conversión vs. tiempo para diferentes concentraciones de  $O_2$  y temperaturas. En las Figuras 4.1 y 4.2 se puede observar un buen ajuste entre las curvas experimentales y las teóricas resultantes del modelo cinético propuesto para todas las temperaturas y los intervalos de concentración de oxígeno usados, incluyendo condiciones de reacción con concentraciones de  $O_2$  tanto lejanas como cercanas al equilibrio. Este resultado indica que la isoterma de Freundlich junto con el modelo de nucleación con  $N = 3/4$  es válido para describir la descomposición del  $CuO$  en un amplio rango de concentraciones de  $O_2$ . Por lo tanto, el modelo propuesto predice apropiadamente las velocidades de reacción cuando las concentraciones de  $O_2$  están cercanas al equilibrio, donde modelos anteriores encontrados en la literatura habían fallado [99]. Esta condición es necesaria en el reactor de reducción de una planta de CLOU para evitar compuestos inquemados en los gases de salida del reactor de reducción; ver apartados 3.2.2 y 3.3.2.

#### 4.2.2 Oxidación del $Cu_2O$ a $CuO$

La Figura 4.6(a) muestra las curvas conversión vs. tiempo obtenidas para la oxidación del  $Cu_2O$  en el transportador de oxígeno para valores de concentración de oxígeno desde el 21% al 2.5% a 900°C. La velocidad de oxidación era rápida cuando la

concentración de oxígeno era mucho mayor que la concentración de oxígeno en el equilibrio. Sin embargo, descendía rápidamente cuando la concentración de oxígeno se aproximaba a la concentración de equilibrio.

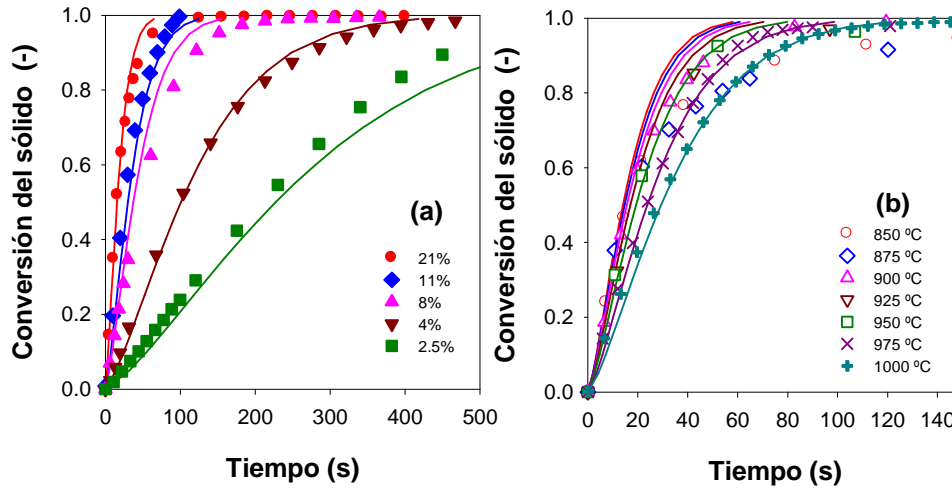


**Figura 4.6.** Efecto de (a) concentración de  $O_2$  a  $900^\circ C$  y (b) la temperatura con  $y_{O_2} = 21\%$  en TGA, en la oxidación del transportador de oxígeno. Símbolos, datos experimentales; línea continua, predicciones del modelo.

Este efecto también fue observado por Whitty y Clayton [69] cuando disminuía la fuerza impulsora de la reacción de oxidación. La Figura 4.6(b) muestra las curvas conversión vs. tiempo para el transportador de oxígeno  $Cu_{60}MgAl_{SD}$  para diferentes temperaturas entre  $850$  y  $1000^\circ C$ , usando aire como gas reactivo. Se puede observar que la velocidad de reacción disminuía cuando aumentaba la temperatura, siendo la reacción más lenta a  $1000^\circ C$ , debido a que la fuerza impulsora de la reacción disminuía, ya que aumenta el valor de la concentración de  $O_2$  en equilibrio,  $C_{O_2,eq}$ .

#### Cinética de reacción de oxidación de $Cu_2O$ a $CuO$

Se ha usado un modelo mecanístico de Langmuir-Hinshelwood para describir la reacción química de oxidación del  $Cu_2O$  en el proceso CLOU.

1. Adsorción del  $O_2$  sobre la superficie de  $Cu_2O$ :



2. Reacción química de oxidación de  $Cu_2O$  para formar  $CuO$ :



Cuando la reacción está controlada por la descomposición química, Ecuación (4.16), la velocidad de reacción viene dada por:

$$\frac{dX_{Ox}}{dt} = k_{Ox} S_{Cu_2O} c C_{O_2}^{1/n} \left( 1 - \frac{C_{O_2,eq}}{C_{O_2}} \right) f(X_{Ox}) \quad (4.17)$$

De manera similar al análisis para la reducción, el valor de  $\theta$  se calcula con la isoterma de Freundlich, es decir con la Ecuación (4.7). Además, el modelo de nucleación también fue considerado para la reacción de oxidación. La expresión para la velocidad de la reacción de oxidación, incluyendo la función de la evolución de la conversión, es la siguiente:

$$\frac{dX_{Ox}}{dt} = k_{Ox} S_{Cu_2O} \cdot c C_{O_2}^{1/n} \left( 1 - \frac{C_{O_2,eq}}{C_{O_2}} \right) \cdot \left( N^{-1} (1 - X_{Ox}) [-\ln(1 - X_{Ox})]^{1-N} \right) \quad (4.18)$$

Integrando la Ecuación (4.18) se obtiene la siguiente expresión para calcular la evolución de la conversión del transportador de oxígeno con el tiempo:

$$[-\ln(1 - X_{Ox})]^N = k_{Ox} S_{Cu_2O} c C_{O_2}^{1/n} \left( 1 - \frac{C_{O_2,eq}}{C_{O_2}} \right) t \quad (4.19)$$

Los parámetros  $k_{Ox}$  y  $c$  no se pueden calcular separadamente para la reacción de oxidación. En este caso, se define una constante cinética efectiva para la reacción de oxidación como:

$$k'_{Ox} = k_{Ox} S_{Cu_2O} c = k'_{Ox,0} e^{-E_{Ox}/R_s T} \quad (4.20)$$

Por lo tanto, es necesario determinar tres parámetros:  $N$ ,  $n$  y  $k'_{Ox}$ . Para determinar el valor de  $N$ , en la Figura 4.3 se muestra el gráfico  $(-\ln(1 - X_{Ox}))^N$  vs. tiempo para diferentes valores de  $N$ , usando los datos experimentales de conversión vs. tiempo de la Figura 4.6. La Tabla 4.3 muestra los coeficientes de correlación para los diferentes valores de  $N$  para la regresión lineal de cada curva. El mejor corresponde a un valor de  $N$  de 3/4. Este procedimiento se ha realizado para cada curva de conversión a cada temperatura y concentración de  $O_2$  estudiadas, obteniéndose el mismo resultado de  $N$  para cada una de ellas.

Los parámetros  $n$  y  $k'_{Ox}$  para la reacción de oxidación se obtuvieron representando  $Y_{Ox}$  vs.  $\ln(C_{O_2})$  a 900°C, como se describe en la siguiente ecuación derivada de las Ecuaciones (4.18) y (4.20), para  $X_{Ox} = 0.2$ , igual que para la reacción de reducción.



$$Y_{Ox} = \ln \left\{ \frac{1}{\left(1 - \frac{C_{O_2,eq}}{C_{O_2}}\right) \left(N^{-1}(1 - X_{Ox})[-\ln(1 - X_{Ox})]^{1-N}\right)} \left[ \frac{dX_{Ox}}{dt} \right]_{X_{Ox}=0.2} \right\} = \ln(k'_{Ox}) + \frac{1}{n} \ln(C_{O_2}) \quad (4.21)$$

La Figura 4.5(b) muestra la regresión lineal de  $Y_{Ox}$  vs.  $\ln(C_{O_2})$ . Se obtuvo un valor de  $n$  igual a 1.2. Se realizaron experimentos a diferentes temperaturas entre 850 y 1000°C y un 21% de  $O_2$  para calcular la dependencia de la constante cinética frente a la temperatura. Considerando la dependencia de Arrhenius de  $k'_{Ox}$ , la Figura 4.4 muestra las curvas de Arrhenius para la reacción de oxidación, y la Tabla 4.4 muestra los parámetros cinéticos obtenidos para el factor pre-exponencial y la energía de activación. Se obtuvo un valor de la energía de activación de 32 kJ·mol<sup>-1</sup> para la constante cinética de oxidación.

Finalmente, la Figura 4.6(a) muestra la comparación entre las curvas experimentales y las predicciones del modelo para diferentes concentraciones de  $O_2$  a temperatura constante. Se puede observar un buen ajuste entre las curvas experimentales y las teóricas resultantes del modelo cinético propuesto para todas las temperaturas y los intervalos de concentración de oxígeno usados. Este resultado indica que la isoterma de Freundlich junto con el modelo de nucleación con  $N = 3/4$  es válido para describir la oxidación del  $Cu_2O$  en un amplio rango de concentraciones de  $O_2$ , incluso con concentraciones de oxígeno cercanas al equilibrio. Por otro lado, la Figura 4.6(b) muestra las curvas conversión vs. tiempo tanto experimentales como teóricas a diferentes temperaturas. Se puede observar que también se obtuvo buen ajuste con el modelo propuesto.

Se puede concluir que con el modelo cinético propuesto en este apartado, es posible predecir las velocidades de reducción y oxidación a diferentes concentraciones de oxígeno y diferentes temperaturas en un amplio rango de condiciones de operación adecuadas para la operación del proceso CLOU.

### 4.3 Modelado simplificado del proceso CLOU

Para realizar el diseño de los reactores del proceso CLOU es necesario realizar el modelado del proceso. A la hora de diseñar un sistema CLOU, los parámetros más importantes son el inventario de sólidos en el sistema y la velocidad de circulación del transportador de oxígeno entre los reactores. Ambos parámetros están altamente influenciados por la reactividad del transportador de oxígeno y su capacidad de transporte de oxígeno. En este trabajo se va a realizar el modelado simplificado de los reactores de reducción y oxidación utilizando la cinética determinada previamente. Con este modelo se podrá evaluar el efecto de las variables más importantes del proceso sobre la eficacia de captura de CO<sub>2</sub> cuando se utilizan diferentes combustibles sólidos.

#### 4.3.1 Circulación de sólidos e inventarios mínimos de transportador de oxígeno

Uno de los parámetros fundamentales en un proceso CLC es la velocidad de circulación de sólidos entre ambos reactores, ya que es la causante de que se suministre el oxígeno necesario para la combustión del combustible. Se calculó la velocidad de circulación de los sólidos con un balance de materia al sistema. Abad y col. [81] desarrollaron un modelo simplificado para el proceso CLC y que posteriormente fue modificado para el proceso *i*G-CLC con combustibles sólidos [105]. En este modelo la velocidad de circulación de sólidos por MW<sub>t</sub>,  $\dot{m}_{TO}$ , la cual depende de la composición y el poder calorífico del combustible sólido, se puede calcular de la siguiente forma

$$\dot{m}_{TO} = \frac{10^3 \Omega_{SF}}{PCI \cdot R_{TO} \cdot \Delta X_{TO}} \quad (4.22)$$

siendo  $\Omega_{SF}$  la masa de oxígeno necesario por kg de combustible sólido para obtener combustión completa de combustible;  $PCI$  el poder calorífico inferior del combustible sólido; y  $\Delta X_{TO}$  la variación de la conversión del transportador de oxígeno en cada reactor.

Se calculó la velocidad de circulación de sólidos entre ambos reactores en función de la variación de la conversión del transportador de oxígeno. La Figura 4.7 muestra la

velocidad de circulación del sólido cuando se usa un lignito como combustible, con un valor de  $\Omega_{SF} = 1.2$  kg de oxígeno por kg de carbón y un  $PCI$  de 16250 kJ/mol. La variación de la conversión del sólido,  $\Delta X_{TO}$ , es mayor para valores bajos de circulación del sólido, y disminuye rápidamente cuando aumenta la velocidad de circulación, alcanzado valores cercanos a 0 cuando la velocidad es muy alta. Abad y col. [81] estimaron que la máxima velocidad de circulación de sólidos posible a costes razonables en una planta de CLC era de  $16 \text{ kg}\cdot\text{s}^{-1}$  por  $\text{MW}_t$ , basado en el desarrollo comercial de unidades de lecho fluidizado circulante. Esto significa que el mínimo valor de  $\Delta X_{TO}$  debería ser 0.1.

En cuanto al inventario de sólidos en los reactores, se necesita una cantidad mínima para transferir el  $\text{O}_2$  a la velocidad demandada y tomar el oxígeno necesario en el reactor de oxidación. Se calculó el inventario mínimo de sólidos en los reactores de reducción y oxidación por  $\text{MW}_t$  de combustible,  $m_{TO}$ , para la combustión de combustibles sólidos haciendo un balance al reactor [105]:

$$m_{TO} = \frac{10^3 \Omega_{SF}}{PCI \cdot R_{TO} \left( \frac{dX_i}{dt} \right)} \quad (4.23)$$

Se obtuvo la reactividad promedio para cada reactor considerando la concentración de gases promedio en cada uno, junto a la distribución del tiempo de residencia de los sólidos.

Se calculó una concentración promedio de  $\text{O}_2$  diferente en cada reactor. En un proceso CLOU, el inventario mínimo de sólidos en el reactor de reducción, para transferir el oxígeno requerido por el combustible, corresponde a la condición donde la velocidad de generación de oxígeno es maximizada. Se alcanza esta condición cuando se considera que la concentración de oxígeno en la Ecuación (4.11) es 0, lo que corresponde con el límite asintótico en el cual todo el  $\text{O}_2$  liberado se consume por el combustible y no hay exceso de  $\text{O}_2$  en los gases; ver Apartado 3.2.2. Por otro lado, se calculó el inventario de sólidos en el reactor de oxidación considerando un exceso de aire del 20%. La concentración promedio de  $\text{O}_2$  en el reactor de oxidación era aquella que cumplía la Ecuación (4.24), en este caso el 11% [81].

$$\left[ \frac{\Delta X_g}{dt} \right]_{O_2} = \int_{X_{g,in}}^{X_{g,out}} \left[ \frac{dX_g}{dt} \right] \quad (4.24)$$

Se consideró también la distribución de tiempos de residencia de las partículas en el reactor para calcular la velocidad de reacción promedio. Suponiendo mezcla perfecta en los reactores, se calculó la velocidad de reacción promedio como [81]:

$$\left( \overline{\frac{dX_i}{dt}} \right) = \int_0^{t_c} \left[ \frac{dX_i}{dt} \right] \frac{e^{-t/\tau_{RR}}}{\tau_{RR}} dt \quad (4.25)$$

donde  $\tau_{RR}$  es el tiempo medio de residencia de las partículas de transportador de oxígeno en el reactor de reducción, el cual depende de la velocidad de circulación de sólidos y del tamaño del reactor.

$$\tau_{RR} = \frac{m_{TO,RR}}{\dot{m}_{TO}} = \frac{\Delta X_{Red}}{\left[ \frac{dX_{Red}}{dt} \right]} \quad (4.26)$$

Esta ecuación considera que las partículas entran en el reactor parcialmente convertidas. El tiempo necesario para alcanzar la conversión completa será  $t_c$ , siendo este valor el límite superior de la integral de la Ecuación (4.25). Siguiendo el método presentado por Abad y col. [81], se puede calcular  $t_c$  en función de la conversión media de los sólidos a la entrada del reactor para el modelo de nucleación con la siguiente ecuación:

$$t_c = \frac{1}{k} \left( -\ln \bar{X}_{Red,inRR} \right)^{3/4} \quad (4.27)$$

De este modo, la velocidad de reacción inicial de las partículas entrantes se corresponde a la de las partículas completamente oxidadas, para  $X_{red} = 0$ , y  $t_c$  es el tiempo necesario para alcanzar la reducción completa, correspondiente en este caso a  $X_{red} = 1 - \bar{X}_{Red,inRR}$ , ya que las partículas pueden haber sido parcialmente oxidadas en el reactor de oxidación.

La expresión que describe la reactividad usando el modelo de nucleación es la siguiente:

$$\left[ \frac{dX_{Red}}{dt} \right] = \frac{4}{3} k \cdot t^{1/3} \cdot e^{-(k \cdot t)^{4/3}} \quad (4.28)$$

El parámetro  $k$  incluye la constante cinética y la función de la concentración de oxígeno.

$$k = k'_{Red} \left( 1 - cC_{O_2}^{1/n} \right) \left( 1 - \frac{C_{O_2}}{C_{eq}} \right) \quad (4.29)$$

La Figura 4.7 muestra los inventarios mínimos de transportador de oxígeno para los reactores de reducción y oxidación en función de la variación de la conversión del transportador de oxígeno a 950°C. Se puede observar, que con bajos valores de variación de conversión del transportador de oxígeno se necesitan bajos inventarios de sólidos en ambos reactores pero con altos valores de velocidad de circulación de sólidos, y viceversa. Si se supone un valor de  $\Delta X_{TO} = 0.1$ , los valores de inventarios de transportador de oxígeno son de 160 kg/MW<sub>t</sub> y 95 kg/MW<sub>t</sub> para los reactores de reducción y oxidación, respectivamente, mientras que si  $\Delta X_{TO} = 0.7$  los inventarios son 300 y kg/MW<sub>t</sub>. Hay que destacar que en los experimentos realizados en la planta en continuo de 1.5 kW<sub>t</sub> se trabajó en estado estacionario con un inventario de sólidos en el reactor de reducción de 454 kg/MW<sub>t</sub>, ver Apartado 3.3.2. Sin embargo, en ese caso había exceso de O<sub>2</sub> en los gases de salida del reactor de reducción. Por lo tanto, hubiera sido posible trabajar con menores inventarios de sólidos en la planta en continuo consiguiendo combustión completa del combustible.

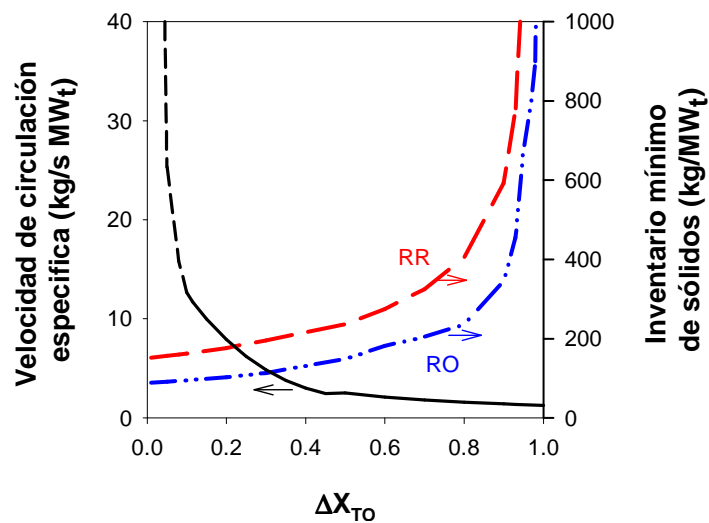


**Figura 4.7.** Inventario mínimo de sólidos por MW<sub>t</sub> en función de la variación de la conversión del transportador de oxígeno entre los reactores de reducción y oxidación: reactor de reducción (- - -), reactor de oxidación (- · · · - · · ·); velocidad específica de circulación de sólidos posible (—) y velocidad específica de circulación superior al límite hidrodinámico (- - -), usando lignito como combustible. Temperatura: 950°C. Límite hidrodinámico para el flujo de sólidos: 16 kg/s por MW<sub>t</sub>.

Hay que considerar, que el inventario mínimo de transportador de oxígeno calculado en esta sección depende de la reactividad del transportador de oxígeno, y corresponde a la cantidad de sólidos necesarios para suministrar el oxígeno a la velocidad requerida, determinada por la velocidad de alimentación del carbón. Más adelante, en el Apartado

4.3.2, se analizará el consumo de oxígeno por el combustible, el cual dependerá de su reactividad.

### 4.3.2 Eficacia de captura de CO<sub>2</sub> para diferentes combustibles

Una vez determinados los inventarios mínimos necesarios para transferir el oxígeno requerido por el combustible es necesario determinar los inventarios para suministrar el tiempo de residencia necesario para alcanzar altas eficiencias de captura. Así, el tiempo de residencia de los sólidos en el reactor de reducción deberá permitir la conversión del char alimentado, que está directamente relacionado con la reactividad del carbón. Hay que recordar que el char inquemado en el reactor de reducción alcanza el reactor de oxidación, donde se quemará, generando CO<sub>2</sub> que no se captura. Por lo tanto, la eficacia de captura de CO<sub>2</sub> dependerá del inventario de sólidos en el reactor de reducción.

Para calcular la conversión del char en el reactor de reducción, es necesario considerar los procesos que tienen lugar en él. En el reactor de reducción de un sistema CLOU se alcanza un pseudo-equilibrio entre el O<sub>2</sub> liberado por el transportador de oxígeno y el oxígeno consumido por el combustible. Por lo tanto, en el balance de oxígeno en el reactor de reducción se deben considerar tanto el oxígeno generado por el transportador de oxígeno como los diferentes destinos de ese oxígeno: conversión del char y los volátiles, y el O<sub>2</sub> en exceso presente en la corriente gaseosa.

$$\left(-r_{O_2}\right)_{TO} = \left(r_{O_2}\right)_{Char} + \left(r_{O_2}\right)_{vol} + \left(r_{O_2}\right)_{gas} \quad (4.30)$$

La velocidad de generación de oxígeno dependerá del inventario de transportador de oxígeno en el reactor de reducción, de su capacidad de transporte de oxígeno y de la velocidad de reducción del transportador de oxígeno, que depende a su vez de su reactividad, de la temperatura del reactor y de la concentración de oxígeno en el reactor:

$$\left(-r_{O_2}\right)_{TO} = R_{TO} m_{TO,RR} \left[ \frac{dX_{Red}}{dt} \right] \quad (4.31)$$

El oxígeno generado por el transportador de oxígeno se usa para:

1. Quemar las partículas de char. Durante los experimentos de combustión de char con  $O_2$  gaseoso, se observó que la velocidad de reacción era constante con el tiempo [29, 61]. Así, se puede calcular la velocidad de reacción como:

$$(r_{O_2})_{Char} = \frac{M_{O_2}}{M_C} \frac{m_{C,RR}}{1 - X_{Char}} \left[ \frac{dX_{Char}}{dt} \right] \quad (4.32)$$

2. Quemar los volátiles. Se supone combustión completa de los volátiles. El oxígeno que reacciona con los volátiles es la diferencia entre la demanda de oxígeno del combustible sólido y la demanda de oxígeno del carbono fijo.

$$(r_{O_2})_{vol} = \dot{m}_{SF} \left\{ \Omega_{SF} - \frac{M_{O_2}}{M_C} [C_{fix}] \right\} \quad (4.33)$$

3. Se acumula en el flujo de gases de salida del reactor. El oxígeno puede estar presente en el flujo de gases que salen del reactor de reducción, pero con una concentración siempre por debajo de la concentración de equilibrio a la temperatura del reactor. La velocidad de generación de oxígeno en la corriente gaseosa depende del gas a la salida del reactor de reducción, que a su vez depende de la corriente de gas que entra en el reactor de reducción.

$$(r_{O_2})_{gas} = M_{O_2} [F_{gas} y_{O_2}]_{outRR} \quad (4.34)$$

La velocidad de combustión del char,  $(r_{O_2})_{Char}$ , depende de la masa de char en el reactor de reducción. Para calcularlo se realizó un balance al carbono considerando los diferentes flujos donde existe carbono: carbono en el combustible, carbono en los volátiles, carbono en el char convertido en el reactor de reducción, y carbono en el flujo de sólidos que salen del reactor de reducción.

$$F_{C,SF} = F_{C,vol} + X_{Char} F_{C,char} + (1 - X_{Char}) F_{C,char} \quad (4.35)$$

Cada flujo de carbono se calcula como:

$$F_{C,SF} = \frac{1}{M_C} \dot{m}_{SF} [f_{C,SF}] \quad (4.36)$$

$$F_{C,vol} = \frac{1}{M_C} \dot{m}_{SF} [f_{C,SF} - f_{C,fix}] \quad (4.37)$$

$$F_{C,char} = \frac{1}{M_C} \dot{m}_{SF} [f_{C,fix}] \quad (4.38)$$

$$(1 - X_{Char}) F_{C,char} = \frac{1}{M_C} \dot{m}_{TO} \frac{x_{C,RR}}{1 - x_{C,RR}} (1 - \eta_{SSC}) \quad (4.39)$$

siendo  $x_c$  la fracción de carbono en los sólidos en el reactor de reducción:

$$x_C = \frac{m_{C,RR}}{m_{TO,RR} - m_{C,RR}} \quad (4.40)$$

La fracción de char  $x_C$  afecta al flujo de char transferido al reactor de oxidación y al oxígeno consumido en el reactor de reducción. En la Ecuación (4.39) también se considera el efecto de la eficacia de separación de un posible sistema de separación de char,  $\eta_{SSC}$ , sobre la conversión del char. Un sistema de separación de char permite la recirculación selectiva de partículas de char inquemadas al reactor de reducción desde la corriente de sólidos que sale del mismo con el fin de minimizar el flujo de carbono inquemado que llega al reactor de oxidación [29]. El objetivo de su utilización es, por tanto, obtener altas eficacias de captura de CO<sub>2</sub> [29, 61].

Fijando la masa de transportador de oxígeno en el reactor de reducción, se puede realizar un proceso iterativo modificando la concentración de O<sub>2</sub> y la fracción másica de carbono en el reactor de reducción para obtener la velocidad de generación de oxígeno y la velocidad de consumo de éste en las Ecuaciones (4.31) y (4.32). El objetivo de este proceso iterativo es cumplir simultáneamente los balances de oxígeno y carbono mostrados en las Ecuaciones (4.30) y (4.35). Una vez que se conoce cada flujo de carbono, se puede obtener la eficacia de captura de CO<sub>2</sub>,  $\eta_{CC}$ , para el inventario de sólidos supuesto.

$$\eta_{CC} = \frac{F_{C,vol} + X_{Char} F_{C,char}}{F_{C,SF}} \quad (4.41)$$

Cabe señalar que la eficacia de captura de CO<sub>2</sub> también depende de la velocidad de circulación de los sólidos porque: (1) la velocidad de circulación de sólidos afecta al tiempo de residencia de los sólidos, y por lo tanto, a la reactividad del transportador de oxígeno; y (2) afecta a la conversión de char y al flujo de carbono que sale del reactor de reducción.



En este apartado, se han considerado dos combustibles para la simulación y diseño: un carbón bituminoso bajo en volátiles (BV) y un lignito; ver Tabla 2.2. Estos carbones fueron previamente utilizados en la planta en continuo de 1.5 kW<sub>t</sub> mostrando diferentes comportamientos durante los experimentos de combustión; ver Apartado 3.3.3. Se calculó la velocidad de conversión de char con la siguiente ecuación:

$$\left[ \frac{dX_{Char}}{dt} \right] = k_{Char} C_{O_2}^p \quad (4.42)$$

donde la constante de conversión de char se calcula como:

$$k_{Char} = k_{Char,0} e^{-E_0/R_s T} \quad (4.43)$$

Los parámetros cinéticos de reactividad del char necesarios para este estudio se tomaron del trabajo de Hurt y Mitchell [106]. La Tabla 4.5 muestra los parámetros cinéticos correspondientes para cada carbón.

**Tabla 4.5.** Parámetros cinéticos considerados para cada carbón, obtenidos de [106].

Parámetros cinéticos	Lignito	Bituminoso Bajo en Volátiles
$k_{char,0}$ (m <sup>3</sup> ·mol <sup>-1</sup> ·s <sup>-1</sup> )	2.7·10 <sup>7</sup>	1.8·10 <sup>7</sup>
$E_0$ (kJ mol <sup>-1</sup> )	91.5	94.1
$p$	0.5	0.5

Los principales resultados del modelo son la concentración de O<sub>2</sub> en el reactor de reducción y la eficacia de captura de CO<sub>2</sub>. La Figura 4.8(a) muestra la concentración de O<sub>2</sub> a la salida del reactor de reducción en función de la conversión del transportador de oxígeno usando lignito como combustible y diferentes valores del inventario de sólidos en el reactor de reducción (150, 250, 500 y 1500 kg/MW<sub>t</sub>). La temperatura del reactor de reducción se fijó en 950°C y no se consideró el uso del sistema de separación de char ( $\eta_{SSC} = 0$ ). También se muestra la concentración de O<sub>2</sub> en el equilibrio. Se puede observar que la concentración de oxígeno disminuye cuando la variación de la conversión aumenta. Esto es debido al hecho de que se quema más carbón en el reactor de reducción y disminuye la reactividad promedio del transportador de oxígeno al incrementarse  $\Delta X_{TO}$ ; ver Ecuación (4.30). También se puede ver que la concentración de O<sub>2</sub> aumenta cuando aumenta el inventario de sólidos en el reactor de reducción, porque hay disponible más oxígeno en los sólidos que puede ser liberado. Resaltar que hay O<sub>2</sub> libre en la corriente gaseosa que sale del reactor de reducción. Esto significa que el

transportador de oxígeno es altamente reactivo y puede liberar  $O_2$  aunque en ocasiones el tiempo de residencia en el reactor de reducción no sea lo suficiente para convertir por completo el char.

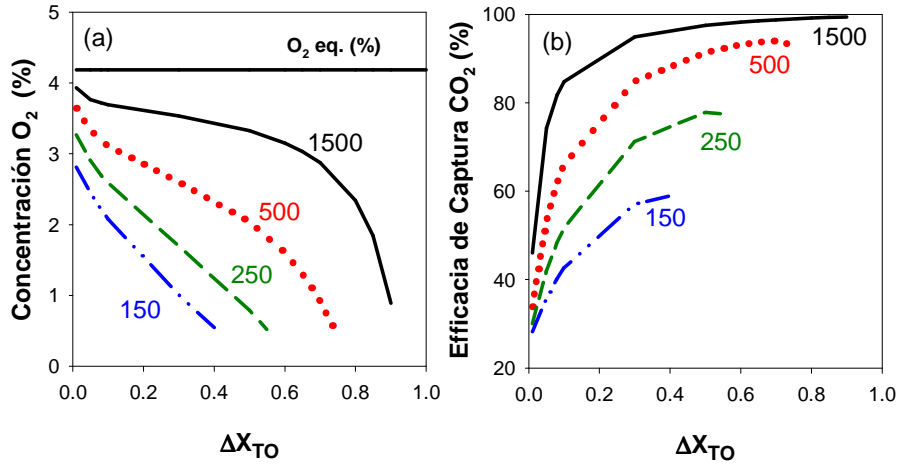


**Figura 4.8.** (a) Concentración de  $O_2$  a la salida del reactor de reducción y (b) eficacia de captura de  $CO_2$ , en función de la variación de conversión del transportador de oxígeno en el reactor de reducción usando lignito como combustible para diferentes inventarios de sólidos en el reactor de reducción: 1500(—), 500 (•••••), 250 (- - -) and 150 (- · - ·) kg/MW<sub>T</sub>. Temperatura: 950°C,  $\eta_{SSC} = 0$ .

La Figura 4.8(b) muestra la eficacia de captura de  $CO_2$  en función de la variación de conversión del transportador de oxígeno para las mismas condiciones que la Figura 4.8(a). La eficacia de captura de  $CO_2$  aumenta cuando aumenta el inventario de sólidos en el reactor de reducción, debido al asociado incremento del tiempo de residencia de los sólidos. Resaltar que todas las líneas convergen a un valor de captura de  $CO_2$  mínimo del 24% cuando  $\Delta X_{TO} = 0$ , el cual corresponde al contenido de carbono en los volátiles de este carbón que son siempre quemados en el reactor de reducción. Para altos valores de conversión del transportador de oxígeno, el incremento de la eficacia de captura de  $CO_2$  es más suave. Este comportamiento es debido a dos razones aditivas: 1) el tiempo de residencia en el reactor de reducción es inversamente proporcional a la variación de conversión, produciendo que la conversión de char no es directamente proporcional a la variación de la conversión del transportador de oxígeno; 2) a menor concentración de  $O_2$  en el reactor de reducción disminuye la velocidad de conversión del char en dicho reactor. De hecho, la eficacia de captura de  $CO_2$  puede disminuir ligeramente a altos valores de  $\Delta X_{TO}$ . Por lo tanto, se observó un máximo en la eficacia de captura de  $CO_2$  para cada inventario de sólidos en el reactor de reducción al variar la conversión de sólidos. Este máximo se debe a que la concentración de oxígeno disminuye a valores cercanos a 0, y el efecto de la baja concentración de  $O_2$  en la

disminución de la velocidad de conversión del char es mayor que el efecto positivo debido al incremento del tiempo de residencia.

Con este combustible y a 950 °C, sólo se alcanzan eficacias de captura de CO<sub>2</sub> superiores al 90% con inventarios de transportador de oxígeno superiores a 500 kg/MW<sub>t</sub> y  $\Delta X_{TO} > 0.5$ , sin el uso de un sistema de separación de char ( $\eta_{SSC} = 0$ ). Por lo tanto, se recomienda trabajar con altos valores de  $\Delta X_{TO}$ , es decir con bajas velocidades de circulación de sólidos, para obtener altas eficacias de captura de CO<sub>2</sub>.

Señalar que el inventario de sólidos mínimo en el reactor de reducción, determinado para suministrar el flujo de oxígeno estequiométrico para quemar un lignito (por ejemplo de 300 kg/MW<sub>t</sub>, con un  $\Delta X_{TO} = 0.7$ ; ver Figura 4.7), es inferior al inventario de sólidos necesario para alcanzar eficacias de captura de CO<sub>2</sub> superiores al 95% (600 kg/MW<sub>t</sub>, con un  $\Delta X_{TO} = 0.7$ ; ver Figura 4.9). Por lo tanto, la conversión de carbón está limitada por el tiempo de residencia en el reactor de reducción, ya que el transportador de oxígeno es capaz de transferir todo el O<sub>2</sub> necesario en estas condiciones. Este hecho concuerda con los resultados previos obtenidos en el análisis de la reactividad del transportador de oxígeno (Apartado 3.2.3) y los resultados obtenidos en la planta en continuo para el proceso CLOU (Apartado 3.3.3).

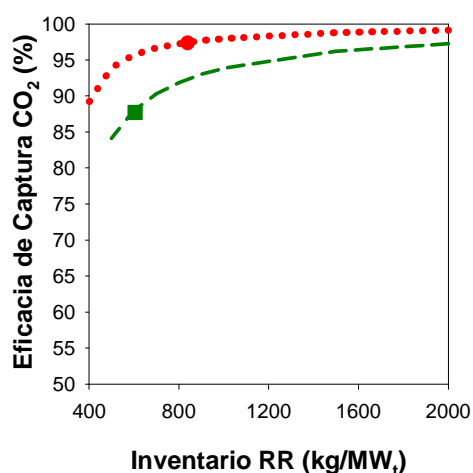


**Figura 4.9.** Eficacia de captura de CO<sub>2</sub>, en función del inventario de sólidos en el reactor de reducción para dos carbones diferentes: lignito (●●●), y bituminoso BV (---); Temperatura: 950°C,  $\eta_{SSC} = 0\%$ ,  $\Delta X_{TO} = 0.7$ . Puntos experimentales obtenidos en la planta en continuo para el proceso CLOU de 1.5 kW<sub>t</sub>: lignito (●) y carbón bituminoso BV (▲): Apartado 3.3.3.

Se puede analizar el efecto del inventario de sólidos en el reactor de reducción sobre la eficacia de captura de CO<sub>2</sub> predicha para diferentes carbones. El efecto del inventario de sólidos en la eficacia de captura de CO<sub>2</sub> para los diferentes carbones se muestra en la Figura 4.9 considerando una variación de la conversión del sólido de  $\Delta X_{TO} = 0.7$ . En todos los casos la eficacia de captura de CO<sub>2</sub> aumenta con el inventario de sólidos debido al mayor tiempo de residencia de los sólidos y la mayor disponibilidad de oxígeno. Se puede observar que para el carbón más reactivo, es decir el lignito, es posible alcanzar altas eficacias de captura de CO<sub>2</sub> ( $\geq 95\%$ ) con aproximadamente 600 kg/MW<sub>t</sub> en el reactor de reducción. Sin embargo, para un carbón menos reactivo como es el bituminoso BV, son necesarios mayores inventarios de sólidos para alcanzar altas eficacias de captura de CO<sub>2</sub>, con valores cercanos a 1500 kg/MW<sub>t</sub>. Además, la Figura 4.9 muestra los resultados experimentales obtenidos en la planta en continuo para el proceso CLOU de 1.5 kW<sub>t</sub> para los diferentes carbones estudiados; ver Apartado 3.3.3. Como se puede ver las eficacias predichas por el modelo para cada carbón simulado coinciden con los resultados experimentales obtenidos. Este hecho valida el modelo desarrollado en esta Tesis Doctoral y permite utilizarlo como herramienta de simulación y diseño.

En esta simulación no se ha considerado la presencia de una unidad de separación de char o *carbon stripper*. Aunque se alcanzan altas eficacias de captura de CO<sub>2</sub> con ambos carbones sería necesario un sistema de separación de char para lograr elevadas eficacias de captura de CO<sub>2</sub> con bajos inventarios. Así, el modelo se ha utilizado para predecir las eficacias de captura de CO<sub>2</sub> cuando se utiliza un sistema de separación de char.

Las Figuras 4.10 y 4.11 muestran la eficacia de captura de CO<sub>2</sub> en función del inventario en el reactor de reducción cuando se considera un sistema de separación de char con diferentes eficacias ( $\eta_{SSC} = 0, 50$  y  $90\%$ ), diferentes temperaturas: 900 (a), 925 (b) y 950 °C (c) y bien lignito o un carbón bituminoso bajo en volátiles como combustible.

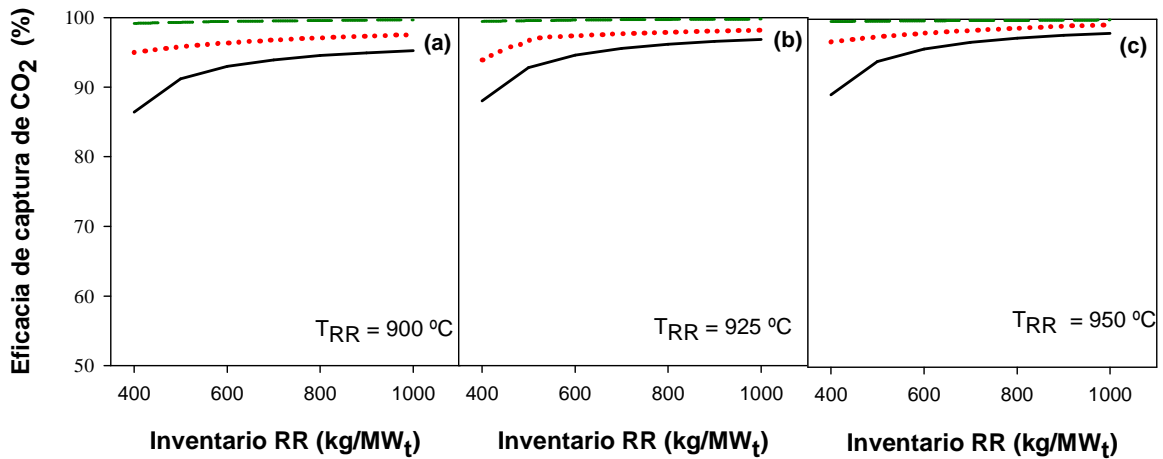


**Figura 4.10.** Eficacia de captura de CO<sub>2</sub>, en función del inventario de sólidos en el reactor de reducción para el lignito para tres diferentes eficacias de un sistema de separación de char y tres temperaturas: (a) 900, (b) 925 y (c) 950°C.  $\eta_{SSC}$ : 0 (—), 50% (••••) y 90% (-----).

La eficacia de captura de CO<sub>2</sub> aumenta al aumentar el inventario del reactor de reducción para una determinada eficacia del sistema de separación de char, debido al aumento en la conversión de char en el reactor de reducción. Como se puede observar en las figuras, el efecto del sistema de separación de char es muy alto especialmente a menores temperaturas y a bajos inventarios en el reactor de reducción. También es más relevante cuando se utilizan combustibles poco reactivos para obtener altas eficacias de captura de CO<sub>2</sub> con bajos valores de inventario de sólidos. Así, el efecto obtenido es superior con el carbón bituminoso bajo en volátiles que para el lignito debido a la diferencia de la reactividad entre ambos carbones. Por lo tanto, para los carbones con reactividades bajas se hace necesario el uso de un sistema de separación de char para alcanzar altos valores de eficacia de captura de CO<sub>2</sub> cuando se diseñe un proceso CLOU.

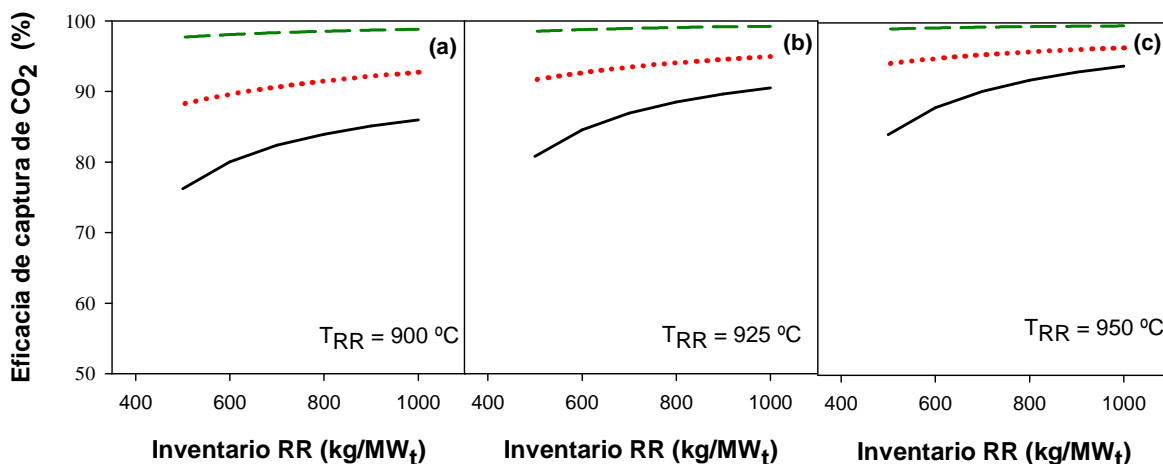


**Figura 4.11.** Eficacia de captura de CO<sub>2</sub>, en función del inventario de sólidos en el reactor de reducción para carbón bituminoso bajo en volátiles para tres diferentes eficacias de un sistema de separación de char y tres temperaturas: (a) 900, (b) 925 y (c) 950°C.  $\eta_{SSC}$ : 0 (—), 50% (••••) y 90% (-----).

**Tabla 4.6.** Inventarios de sólidos necesarios para alcanzar un 95% de eficacia de captura de CO<sub>2</sub> con diferentes eficacias del sistema de separación del char.

Combustible	Temperatura (°C)	$\eta_{CC}$ (%)	$\eta_{SSC}$ (%)	$m_{TO,RR}$ (kg/MW <sub>t</sub> )
Lignito	925	95	0	<b>700</b>
Bituminoso BV	925	95	75	<b>500</b>

Finalmente, la Tabla 4.6 muestra un resumen de los inventarios de sólidos necesarios para alcanzar una eficacia de captura de CO<sub>2</sub> del 95% con los dos combustibles simulados a 925 °C. Como se puede observar, con el lignito no es necesario el uso de un sistema de separación de char para alcanzar valores altos de eficacia de captura de CO<sub>2</sub> con inventarios de sólidos bajos. Este valor se podría incluso reducirse, aumentando la temperatura del reactor de reducción, pasando de 700 kg/MW<sub>t</sub> a 925°C a 600 kg/MW<sub>t</sub> a 950°C. Pero este aumento de la temperatura supondría un aumento del O<sub>2</sub> en exceso en la corriente de salida del reactor de reducción (del 2.5% al 4%) que posteriormente habría que eliminar de la corriente de CO<sub>2</sub> a almacenar. Si se utilizara un sistema de separación de char, el inventario de sólidos en el reactor de reducción se reduciría (ver Figura 4.10), pero esta reducción se vería amortiguada por la cantidad de sólidos que serían necesarios emplear en el propio *carbon stripper*, junto al aumento de costes de mantenimiento y de operación de un nuevo reactor de lecho fluidizado en el sistema.

Por otro lado, para el carbón bituminoso es necesaria la implementación de un sistema de separación de char en el sistema si se quieren utilizar valores de inventarios de sólidos similares al lignito. Así, un *carbon stripper* con una eficacia del 75%, conseguiría una eficacia de captura de CO<sub>2</sub> del 95% con 500 kg/MW<sub>t</sub> en el reactor de reducción. En este caso, la reducción tan elevada del inventario de sólidos en el reactor de reducción sí que sería ventajosa, ya que muy probablemente, la suma de los inventarios de sólidos en el sistema de separación de char y en el reactor de reducción sería inferior al inventario necesario en el reactor de reducción sin el *carbon stripper* (>1700 kg/MW<sub>t</sub> a 925 °C) para obtener una eficacia de captura de CO<sub>2</sub> similar.



## **5 Conclusiones**





### *Selección del transportador de oxígeno*

Durante el desarrollo de esta Tesis Doctoral se realizó una intensa campaña experimental para profundizar en el conocimiento sobre el proceso *Chemical-Looping with Oxygen Uncoupling* (CLOU). Para ello se prepararon y caracterizaron más de 50 transportadores de oxígeno por diferentes métodos y con diferentes composiciones. En todos ellos se ha usado como fase activa óxido de cobre.

Tras la investigación realizada se concluyó que un material con un 60% de CuO y como soporte inerte un 40% de MgAl<sub>2</sub>O<sub>4</sub> preparado por un método de preparación industrial como es el *spray drying* es adecuado para su uso como transportador de oxígeno para el proceso CLOU. Este material cumplía todos los requisitos necesarios para el proceso CLOU: alta reactividad, alta velocidad de generación de oxígeno, alta resistencia a la aglomeración y baja velocidad de atrición.

Se analizó la capacidad de generación de O<sub>2</sub> y de regeneración del transportador de oxígeno (sin combustión de carbón) del transportador de oxígeno seleccionado en una planta consistente en dos lechos fluidizados interconectados: el reactor de reducción y el de oxidación. Se encontró que el transportador de oxígeno era capaz de producir oxígeno en el reactor de reducción en condiciones de equilibrio en todas las condiciones operacionales analizadas, incluso cuando las conversiones del transportador de oxígeno eran altas. Respecto a la oxidación en el reactor de oxidación se encontró que el transportador de oxígeno era capaz de regenerarse en un amplio intervalo de temperaturas y con concentraciones de oxígeno cercanas al equilibrio termodinámico. Este hecho facilitaría la integración energética entre los dos reactores, debido a la flexibilidad para seleccionar la temperatura en el reactor de oxidación. De este modo, el material Cu60MgAl\_SD, mostró excelentes cualidades para ser usado como transportador de oxígeno en el proceso CLOU con carbón.

### *Combustión con carbón en un lecho fluidizado discontinuo*

El transportador de oxígeno seleccionado mostró una gran capacidad para quemar combustibles sólidos, debido a su elevada velocidad de generación de oxígeno. La velocidad de generación de oxígeno está relacionada con el inventario de sólidos en el reactor de reducción del proceso CLOU. Se identificaron tres regiones operativas dependiendo del inventario de sólidos y la temperatura.

- La Región I con inventarios de sólidos superiores a 58 kg/MW<sub>t</sub> para una temperatura del reactor de reducción de 955°C, se caracterizaba porque no había compuestos inquemados en los gases de salida del reactor. Los únicos productos de la combustión eran CO<sub>2</sub> y H<sub>2</sub>O junto con un exceso de O<sub>2</sub>, el cual estaba cercano a la concentración de equilibrio. En esas condiciones, la concentración de oxígeno a la salida del reactor aumentaba con la temperatura.
- La Región II estaba confinada para valores de inventario de sólidos entre 32 y 58 kg/MW<sub>t</sub>, donde en los gases de salida del reactor se encontraban tanto CO como O<sub>2</sub>, junto al CO<sub>2</sub>, siendo este el producto principal de la combustión. El CO fue el único producto inquemado presente en los gases, el cual procedía de la oxidación incompleta de los volátiles. No obstante con un inventario mínimo de 43 kg/MW<sub>t</sub> había suficiente oxígeno en el gas para convertir el CO a CO<sub>2</sub> en los gases de combustión.
- La Región III se caracteriza por la ausencia de oxígeno en los gases de combustión y la presencia de cierta cantidad de CO inquemado. En esta región se obtuvo la máxima velocidad de generación de oxígeno, la cual aumentaba de 2.1·10<sup>-3</sup> a 930°C a 2.8·10<sup>-3</sup> kg O<sub>2</sub>/s por kg de transportador de oxígeno a 980°C. Para estas velocidades de generación de oxígeno se estimó que el inventario de transportador de oxígeno necesario pasaba de 39 a 930°C a 29 kg/MW<sub>t</sub> a 980°C.

La velocidad máxima de generación de oxígeno obtenida con carbón era mayor (aproximadamente el doble) que la velocidad obtenida cuando se quemaba char, debido a la reacción directa gas-sólido entre los volátiles del carbón y el transportador de oxígeno. De este modo, los resultados obtenidos con el char fueron representativos de la velocidad de liberación de oxígeno gaseoso desde las partículas de transportador, mientras que los experimentos realizados con carbón podrían también incluir una rápida velocidad de reacción gas-sólido entre los volátiles del carbón y las partículas con la reducción directa del CuO.

#### *Demostración del proceso CLOU en continuo*

Se ha demostrado la viabilidad del proceso CLOU con combustibles sólidos. Este es uno de los principales logros de esta Tesis Doctoral. Para ello, se utilizó el material previamente seleccionado (Cu60MgAl\_SD) en una planta en continuo de 1.5 kW<sub>t</sub>,

consistente en dos lechos fluidizados interconectados construida en el Instituto de Carboquímica para la combustión de carbón con captura de CO<sub>2</sub>. En una primera campaña experimental se obtuvo una exitosa operación durante 18h de combustión y 30h de operación a altas temperaturas, usando carbón como combustible. Se investigó el efecto de las condiciones de operación (como la temperatura del reactor de reducción, la velocidad de circulación de sólidos y la velocidad de alimentación de carbón) sobre las eficacias de combustión y de captura de CO<sub>2</sub>. Se determinó que se requieren temperaturas superiores a los 900°C en el reactor de reducción para obtener los beneficios del efecto CLOU. En el intervalo de temperaturas utilizado (900-960 °C), el transportador de oxígeno mostró una excelente actividad para el proceso CLOU.

En ningún caso se detectaron compuestos inquemados en los gases de salida del reactor de reducción, siendo CO<sub>2</sub> y H<sub>2</sub>O los únicos productos de la combustión, incluso cuando las partículas del transportador de oxígeno estaban altamente convertidas. Además, se encontró O<sub>2</sub> junto al CO<sub>2</sub> en los gases de combustión a la salida del reactor de reducción, con lo que el reactor de reducción operaba en la Región I del proceso CLOU, descrita anteriormente. Esta concentración de O<sub>2</sub> aumentaba con la temperatura del reactor de reducción, y siempre se encontraba en concentraciones cercanas a la de equilibrio a cada temperatura.

En todos los experimentos se obtuvieron eficacias de captura de CO<sub>2</sub> muy altas, siendo siempre superiores al 95%. Además, la eficacia de captura de CO<sub>2</sub> dependía fuertemente de la temperatura del reactor de reducción. Así, la eficacia de captura de CO<sub>2</sub> aumentó del 97% a 900°C hasta el 99.3% a 960°C. Estas altas eficacias de captura de CO<sub>2</sub> se debían a la rápida conversión del char en el reactor de reducción.

La velocidad de circulación de sólidos afectó de forma importante a la eficacia de captura de CO<sub>2</sub>. Un aumento de la velocidad de circulación de los sólidos producía un descenso de la conversión del char en el reactor de reducción y, por lo tanto, la eficacia de captura de CO<sub>2</sub> descendía debido a una reducción del tiempo de residencia medio de los sólidos en el reactor. Se encontró que era necesario un tiempo de residencia por encima de 300 s en el reactor de reducción para obtener una conversión del char sobre el 97% a 900°C con el carbón utilizado.

Por el contrario, la velocidad de alimentación de carbón no afectaba significativamente a la eficacia de captura de CO<sub>2</sub>, debido a que el tiempo de residencia de los sólidos en el reactor de reducción no variaba. No obstante, un aumento del flujo de carbón afectaba al inventario de sólidos en kg/MW<sub>t</sub> en el reactor de reducción. Incluso con el inventario de sólidos más bajo usado en el reactor de reducción (240 kg/MW<sub>t</sub>), se obtenía una conversión completa del combustible, junto con altas eficacias de captura de CO<sub>2</sub>.

Estos resultados demostraron por primera vez en la literatura la viabilidad del proceso CLOU utilizando un transportador de oxígeno de base CuO en una planta en continuo de 1.5 kW<sub>t</sub>.

#### *Efecto del tipo de carbón*

A continuación se estudió el efecto de las características del combustible sobre el rendimiento del proceso CLOU. Para ello se utilizaron carbones de diferente rango: un lignito, dos bituminosos y una antracita. Se llevaron a cabo un total de 40 horas de operación, durante las cuales la temperatura del reactor de reducción se varió entre 900 y 950°C.

Independientemente del tipo de carbón se obtuvo combustión completa a CO<sub>2</sub> y H<sub>2</sub>O sin presencia de compuestos inquemados, con un exceso de O<sub>2</sub> en los gases de salida del reactor de reducción.

El rango del carbón mostró un importante efecto sobre la eficacia de captura de CO<sub>2</sub>. Las eficacias de captura de CO<sub>2</sub> fueron muy altas para el lignito y el carbón bituminoso medio en volátiles, alcanzándose valores del 99% a 950°C con el lignito. Por el contrario, para carbones poco reactivos (carbón bituminoso bajo en volátiles y la antracita) sería necesario un sistema de recirculación selectiva de char, *carbon stripper*, para alcanzar altos valores de eficacia de captura de CO<sub>2</sub>.

#### *Combustión de biomasa por el proceso CLOU*

Hasta el momento solo se habían probado combustibles fósiles en el proceso CLOU. Sin embargo los combustibles renovables, y más concretamente la biomasa, tienen unas propiedades muy interesantes a la hora de su utilización como combustible en el

proceso CLOU. Esta Tesis Doctoral presenta las primeras horas experimentales quemando biomasa mediante el proceso CLOU en la planta en continuo de 1.5 kW<sub>t</sub>.

Se logró combustión completa de la biomasa con ausencia de alquitranes en la salida de reactor de reducción, junto a una eficacia de captura de CO<sub>2</sub> del 100%. Esto demuestra que aun con el alto contenido en volátiles de la biomasa, estos se quemaban completamente en el reactor de reducción, lo cual demuestra un buen contacto entre los volátiles y el transportador de oxígeno. Se encontró que la velocidad de conversión del char de biomasa en el proceso CLOU es alta y similar a la obtenida para el lignito.

La combustión de biomasa por el proceso CLOU demostró las ventajas del proceso para su aplicación industrial con emisiones negativas de CO<sub>2</sub>.

#### *Efecto del azufre del combustible en el proceso CLOU*

El diseño de una planta industrial con captura de CO<sub>2</sub> puede verse afectado por la presencia de compuestos de azufre presentes en el combustible. En un sistema CLOU, la presencia de azufre puede originar emisiones de SO<sub>2</sub> a la atmósfera, problemas operacionales o afectar a la calidad del CO<sub>2</sub> capturado. La operación en continuo en la planta de 1.5 kW<sub>t</sub> quemando lignito con alto contenido en azufre (5.2%), demostró que la mayoría del azufre presente en el carbón se liberaba como SO<sub>2</sub> en el reactor de reducción. No obstante, una fracción menor se transfería al reactor de oxidación, encontrándose que las emisiones normalizadas a la atmósfera serían superiores a los 200 mg/Nm<sup>3</sup>, límite establecido por la UE. Estas emisiones se atribuyen a la liberación no uniforme del SO<sub>2</sub> durante la combustión del char, resultante de la presencia de azufre pirítico en el carbón (2%).

#### *Caracterización del transportador de oxígeno*

Tras 40 h de operación en continuo quemando distintos tipos de carbones, el transportador de oxígeno mantuvo su reactividad y su contenido en CuO. Además, el transportador de oxígeno no mostró ningún problema de aglomeración.

No obstante, se encontró una importante reducción de la resistencia mecánica de las partículas relacionada con un aumento de la porosidad durante los experimentos realizados en la planta en continuo. Este hecho indica que es necesario una mejora de

las propiedades mecánicas del transportador de oxígeno que aumenten su tiempo de vida medio junto a la necesidad de preparar partículas que sean fácilmente separables de las cenizas.

#### *Evaluación comparativa entre los procesos CLOU e iG-CLC*

Utilizando datos de la literatura se realizó una comparación entre los procesos *iG-CLC* y *CLOU* en la combustión de combustibles sólidos con similares combustibles y en la misma planta piloto. Se encontró que con el proceso *CLOU* se obtienen mayores eficiencias de combustión y mayores eficiencias de captura de  $\text{CO}_2$  para todos los combustibles sólidos estudiados y con menores inventarios de sólidos. Estos resultados son debidos a dos causas fundamentales: la mejor combustión de los volátiles con el  $\text{O}_2$  gaseoso generado por el transportador de oxígeno y a la mayor velocidad de conversión del char con el  $\text{O}_2$  gaseoso frente a la gasificación con  $\text{H}_2\text{O}$ . La velocidad de conversión de char en el proceso *CLOU* era entre 1.5 y 4 veces superior a la obtenida con el *iG-CLC* en función del combustible usado.

#### *Modelado del proceso CLOU*

Para poder desarrollar el modelado del proceso se estudió la cinética de las reacciones de reducción de  $\text{CuO}$  a  $\text{Cu}_2\text{O}$  y su oxidación para el transportador de oxígeno  $\text{Cu60MgAl}_{\text{SD}}$  mediante termogravimetría. Los parámetros cinéticos se obtuvieron utilizando un modelo de nucleación para la variación de la conversión del sólido con el tiempo con control cinético en la superficie de las partículas, junto con un modelo mecanístico del tipo Langmuir-Hinshelwood con isoterma de Freundlich para la adsorción/desorción de  $\text{O}_2$ . Con este modelo y los parámetros cinéticos determinados, se obtuvo un buen ajuste de los resultados experimentales en un amplio intervalo de concentraciones de  $\text{O}_2$  y de temperaturas, incluso cuando la concentración de  $\text{O}_2$  estaba muy cercana a la de equilibrio.

Se desarrolló un modelo simplificado utilizando la cinética determinada para el transportador de oxígeno  $\text{Cu60MgAl}_{\text{SD}}$  con el objetivo de determinar los parámetros básicos del diseño y el efecto de las condiciones de operación del proceso *CLOU* sobre la eficacia de captura de  $\text{CO}_2$ .

Se determinó que el inventario mínimo de sólidos necesario para transferir el oxígeno demandado para la completa combustión del carbón era de 160 kg/MW<sub>t</sub> en el reactor de reducción y 95 kg/MW<sub>t</sub> en el reactor de oxidación a 950°C y una velocidad de circulación de sólidos de 16 kg·s<sup>-1</sup> por MW<sub>t</sub>. El modelo permite evaluar el efecto del inventario de sólidos sobre la eficacia de captura de CO<sub>2</sub> para distintos combustibles. Se determinó que la eficacia de captura de CO<sub>2</sub> depende de forma importante de la reactividad del combustible sólido, de la velocidad de circulación de sólidos y del inventario de sólidos en el reactor de reducción.

Así, para carbones altamente reactivos (carbón bituminoso alto en volátiles y el lignito), es posible alcanzar altas eficacias de captura de CO<sub>2</sub> (>95%) con 700 kg/MW<sub>t</sub> a 925°C. Sin embargo, para carbones poco reactivos, como el carbón bituminoso bajo en volátiles, son necesarios inventarios de 1700 kg/MW<sub>t</sub> para lograr altas eficacias de captura de CO<sub>2</sub> a 925°C. Sin embargo, utilizando un *carbon stripper* con una eficacia del 75% se lograría reducir el inventario necesario a 500 kg/MW<sub>t</sub>. Estos resultados resaltan la necesidad de usar un sistema de separación y recirculación del char con carbones poco reactivos, *carbon stripper*, con el que se podrían alcanzar eficacias de captura de CO<sub>2</sub> mayores del 95% con bajos inventarios de sólidos.

Analizando los resultados mostrados en esta Tesis Doctoral, se puede concluir que se pueden obtener excelentes resultados respecto a las eficacias de combustión y de captura de CO<sub>2</sub> en el proceso CLOU para la combustión de carbón o biomasa con bajos inventarios de un transportador de oxígeno basados en CuO. De este modo, el trabajo futuro nos anima a seguir con el desarrollo de transportadores de oxígeno adecuados para su uso en CLOU, con una mejora en el tiempo de vida de las partículas. Además, los parámetros cinéticos obtenidos junto a la herramienta de simulación desarrollada, configuran un útil instrumento de diseño y optimización para el proceso CLOU.





## **6 Acrónimos, notaciones y símbolos**



## Símbolos

$a$	Sitios activos en la superficies de las partículas (-)
$C_i$	Concentración de carbono en el reactor de reducción ( $\text{mol}\cdot\text{s}^{-1}$ )
$C_{coal}$	Concentración de carbono en el carbón ( $\text{kg}\cdot\text{kg}^{-1}$ )
$C_{fix}$	Concentración de carbono en el carbono fijo ( $\text{kg}\cdot\text{kg}^{-1}$ )
$C_{O_2}$	Concentración de oxígeno ( $\text{mol}\cdot\text{m}^{-3}$ )
$C_{O_2,eq}$	Concentración de oxígeno en condiciones de equilibrio ( $\text{mol}\cdot\text{m}^{-3}$ )
$C_{O_2,Ox}$	Concentración de oxígeno durante la reacción de oxidación ( $\text{mol}\cdot\text{m}^{-3}$ )
$C_{O_2,Red}$	Concentración de oxígeno durante la reacción de reducción ( $\text{mol}\cdot\text{m}^{-3}$ )
$c$	Constante de la velocidad de adsorción ( $(\text{m}^3\cdot\text{mol}^{-1})^{1/n}$ )
$c_0$	Factor pre-exponencial de la constante de velocidad de adsorción ( $(\text{m}^3\cdot\text{mol}^{-1})^{1/n}$ )
$E_1$	Energía de activación global ( $\text{J}\cdot\text{mol}^{-1}$ ), Ecuación (4.1)
$E_2$	Energía de activación cinética ( $\text{J}\cdot\text{mol}^{-1}$ ), Ecuación (4.2)
$E_C$	Energía de activación del parámetro $c$ ( $\text{J}\cdot\text{mol}^{-1}$ )
$E_0$	Energía de activación de la reacción de combustión del char ( $\text{J}\cdot\text{mol}^{-1}$ )
$E_{Ox}$	Energía de activación de la reacción de oxidación ( $\text{J}\cdot\text{mol}^{-1}$ )
$E_{Red}$	Energía de activación de la reacción de reducción ( $\text{J}\cdot\text{mol}^{-1}$ )
$E_t$	Energía de activación termodinámica ( $\text{J}\cdot\text{mol}^{-1}$ ), Eq. (4.3)
$F_i$	Flujo molar del compuesto $i$ ( $\text{mol}\cdot\text{s}^{-1}$ )
$f_{C,fix}$	Fracción másica de carbono fijo en el carbón (-)
$f_{C,SF}$	Fracción másica de carbono en el combustible sólido (-)
$f_{C,vol}$	Fracción másica de carbono en los volátiles (-)
$f_i$	Fracción másica del elemento o componente $i$ en el carbón (-)
$f_{H/C}$	Ratio molar hidrógeno-carbono en el combustible (-)
$f_{O/C}$	Ratio molar oxígeno-carbono en el combustible (-)
$f_{S,char}$	Fracción másica de azufre en el char (-)
$K_1$	Constante de equilibrio de la descomposición química y adsorción del $O_2$ (-)
$K_2$	Constante de equilibrio de la desorción del $O_2$ adsorbido (-)
$K_3$	Constante de equilibrio de la adsorción del $O_2$ sobre la superficie del $Cu_2O$ (-)
$K_4$	Constante de equilibrio de la oxidación de $Cu_2O$ a $CuO$ (-)

$k$	Parámetro cinético para el proceso de simulación ( $s^{-1}$ ), Ecuación (4.28)
$k_{Char}$	Constante de la velocidad de la reacción química de la combustión del char ( $s^{-1}$ ), Ecuación (4.42)
$k_1$	Constante cinética ( $s^{-1}$ ), Ecuación (4.2)
$k_2$	Constante cinética ( $m^{-3} \cdot mol^{-1} \cdot s^{-1}$ ), Ecuación (4.3)
$k_f$	Constante de la velocidad de la reacción química del proceso directo en el equilibrio CuO-Cu <sub>2</sub> O ( $mol \cdot m^{-2} \cdot s^{-1}$ )
$k_b$	Constante de la velocidad de la reacción química del proceso inverso en el equilibrio CuO-Cu <sub>2</sub> O ( $s^{-1}$ )
$k_A$	Constante de la velocidad de desorción del O <sub>2</sub> adsorbido ( $s^{-1}$ )
$k_D$	Constante de la velocidad de adsorción del O <sub>2</sub> sobre la superficie del Cu <sub>2</sub> O ( $s^{-1}$ )
$k_{Ox}$	Constante de la velocidad de reacción química para la oxidación de Cu <sub>2</sub> O en CuO ( $kg \cdot m^{-2} \cdot s^{-1}$ )
$k_{Red}$	Constante de la velocidad de reacción química para la reducción de CuO en Cu <sub>2</sub> O ( $kg \cdot m^{-2} \cdot s^{-1}$ )
$k_{Char,0}$	Factor pre-exponencial de la constante de la velocidad de la reacción química de la combustión del char ( $m^3 \cdot mol^{-1} \cdot s^{-1}$ )
$k'_{Ox}$	Constante efectiva de la velocidad de reacción química para la oxidación de Cu <sub>2</sub> O en CuO ( $(m^3 \cdot mol^{-1})^{1/n} \cdot s^{-1}$ )
$k'_{Red}$	Constante efectiva de la velocidad de reacción química para la reducción de CuO en Cu <sub>2</sub> O ( $s^{-1}$ )
$k'_{Ox,0}$	Factor pre-exponencial de la constante de la velocidad de la reacción química de la oxidación de Cu <sub>2</sub> O a CuO ( $(m^3 \cdot mol^{-1})^{1/n} \cdot s^{-1}$ )
$k'_{Red,0}$	Factor pre-exponencial de la constante de la velocidad de la reacción química de la reducción de CuO a Cu <sub>2</sub> O ( $s^{-1}$ )
$M_i$	Peso atómico o molecular del elemento o compuesto $i$ ( $kg \cdot mol^{-1}$ )
$m$	Masa de la muestra a cada tiempo en la TGA (kg)
$\dot{m}_{SF}$	Flujo másico de combustible alimentado al reactor de reducción ( $kg \cdot s^{-1}$ )
$m_{C,RR}$	Inventario de carbono en el reactor de reducción ( $kg \cdot MW_{th}^{-1}$ )
$m_{char}$	masa de char en la carga de combustible (kg)
$\dot{m}_{TO}$	Velocidad de circulación de sólidos ( $kg \cdot s^{-1} \cdot MW_{th}^{-1}$ )
$m_{TO}$	Inventario de transportador de oxígeno en el reactor (kg)

$m_{TO,i}$	Inventario de transportador de oxígeno en el reactor $i$ ( $\text{kg} \cdot \text{MW}_{\text{th}}^{-1}$ )
$m_{\text{ox}}$	Masa de la muestra de transportador de oxígeno completamente oxidada (kg)
$m_{\text{red}}$	Masa de la muestra de transportador de oxígeno completamente reducida (kg)
$N$	Orden de la reacción de nucleación (-)
$N_{\text{O}_2}$	Moles de oxígeno que puede liberar el transportador de oxígeno (mol)
$n$	Orden de la reacción Langmuir-Hinshelwood (-)
$n'$	Orden de reacción (-)
$p$	Orden de reacción para la combustión de char (-)
$R_g$	Constante de los gases ( $8.314 \text{ J} \cdot \text{mol}^{-1} \cdot \text{K}^{-1}$ )
$R_{\text{O}}$	Capacidad de transporte de oxígeno del óxido metálico (-)
$R_{\text{TO}}$	Capacidad de transporte de oxígeno del transportador de oxígeno (-)
$(-r_{\text{Char}})$	Velocidad de conversión del char ( $\% \cdot \text{s}^{-1}$ )
$(-r_{\text{O}_2})_{\text{Char}}$	Velocidad de consumo de oxígeno por parte del char ( $\text{s}^{-1}$ )
$(-r_{\text{O}_2})_{\text{gas}}$	Velocidad de liberación de oxígeno en la corriente de gas ( $\text{s}^{-1}$ )
$(-r_{\text{O}_2})_{\text{TO}}$	Velocidad de generación de oxígeno por el transportador de oxígeno ( $\text{s}^{-1}$ )
$r_{\text{O}_2,ox}$	Velocidad de consumo de de oxígeno en la oxidación (kg $\text{O}_2/\text{s}$ por kg de transportador de oxígeno)
$r_{\text{O}_2,red}$	Velocidad instantánea de generación de oxígeno (kg $\text{O}_2/\text{s}$ por kg de transportador de oxígeno)
$(-r_{\text{O}_2})_{\text{vol}}$	Velocidad de conversión de los volátiles ( $\text{s}^{-1}$ )
$(r_{\text{Ox}})_{\text{TO}}$	Velocidad de oxidación del transportador de oxígeno ( $\text{s}^{-1}$ )
$(-r_{\text{Red}})_{\text{TO}}$	Velocidad de reducción del transportador de oxígeno ( $\text{s}^{-1}$ )
$S_{\text{ash}}$	Azufe en las cenizas (kg/s)
$S_{\text{CuO}}$	Área superficial específica del CuO ( $\text{m}^2 \cdot \text{kg}^{-1}$ )
$T$	Temperatura (K)
$t$	Tiempo (s)
$t_c$	Tiempo de reacción necesario para alcanzar la completa conversión del transportador de oxígeno (s)

$\tau_{\text{char}}$	Tiempo de residencia promedio de las partículas de char en el reactor de reducción (s)
$\tau_{\text{RR}}$	Tiempo de residencia promedio de las partículas del transportador de oxígeno en el reactor de reducción (s)
$X$	Conversión del sólido (-)
$X_i$	Conversión instantánea del sólido (-)
$X_f$	Conversión del sólido final (-)
$X_{\text{char}}$	Conversión del char (-)
$X_g$	Conversión del gas en el reactor de oxidación (-)
$X_{g,\text{in}}$	Conversión del gas en el flujo de entrada al reactor de oxidación (-)
$X_{g,\text{out}}$	Conversión del gas el flujo de salida del reactor de oxidación (-)
$\overline{X}_{\text{Red},\text{inRR}}$	Conversión media de reducción del transportador de oxígeno a la entrada al reactor de reducción (-)
$X_{\text{Red}}$	Conversión de reducción del transportador de oxígeno (-)
$X_{\text{Ox}}$	Conversión de oxidación del transportador de oxígeno (-)
$x_{C,i}$	Fracción másica de carbono en los sólidos en el reactor $i$ (-)
$x_{\text{MeO}}$	Fracción de óxido metálico activo en el transportador de oxígeno (-)
$y_i$	Fracción molar del compuesto $i$ (-)
$y_{i,\text{outRR}}$	Fracción molar del gas $i$ en los gases de salida del reactor de reducción(-)
$y_{i,\text{outRO}}$	Fracción molar del gas $i$ en los gases de salida del reactor de oxidación(-)
$\Delta X_g$	Variación de la conversión de los gases (-)
$\Delta X_{\text{TO}}$	Variación de la conversión del transportador de oxígeno (-)

#### Letras griegas

$\eta_{\text{CC}}$	Eficacia de captura de $\text{CO}_2$ (-)
$\eta_{\text{SSC}}$	Eficacia del sistema de separación de char (-)
$\eta_{\text{comb,RR}}$	Eficacia de combustión en el reactor de reducción (-)
$\gamma_{\text{CO}_2}$	Rendimiento a $\text{CO}_2$ (-)
$\gamma_{\text{CO}_2,\text{ave}}$	Rendimiento a $\text{CO}_2$ promedio (-)
$\lambda$	Ratio de exceso de aire (-)

$v_{\text{atrición}}$	Velocidad de atrición (%/h)
$\phi$	Ratio transportador de oxígeno/combustible (-)
$\theta$	Fracción de sitios activos ocupados por O <sub>2</sub> (-)
$\Omega_{SF}$	Masa estequiométrica de O <sub>2</sub> par convertir 1 kg de carbón (kg·kg <sup>-1</sup> )
$\omega$	Conversión másica del transportador de oxígeno (-)

#### Acrónimos

AV	Carbón Bituminoso Alto en Volátiles
ASTM	Sociedad Americana para Pruebas y Materiales
BET	Brunauer-Emmett-Teller
BV	Carbón Bituminoso Bajo en Volatices
CAC	Captura y Almacenamiento de CO <sub>2</sub>
CFB	Caldera de Lecho Fluidizadasdo Circulante
CLC	<i>Chemical Looping Combustion</i>
CLOU	<i>Chemical Looping with Oxygen Uncoupling</i>
EOR	
EEUU	Estados Unidos de America
GN	Gas Natural
LF	Reactor de Lecho Fijo
LFD	Reactor de Lecho Fluidizado Discontinuo
IEA	Agencia Internacional de la Energía
IPCC	Panel Intergubernamental para el Cambio Climático
MV	Carbón Bituminoso Medio en Volátiles
PCI	Poder Calorífico Inferior (kJ·kg <sup>-1</sup> )
RO	Reactor de oxidación
RR	Reactor de reducción
SD	<i>Spray drying</i>
TGA	Termobalanza
TO	Transportador de oxígeno
UE	Unión Europea
WGS	<i>Water gas sift</i>
XRD	Difractometro de rayos-X



## Subíndices

C,char	Carbono en el char
C,coal	Carbono en el carbón
C,vol	Carbono en los volátiles
inRO	Corriente de entrada del reactor de oxidación
inRR	Corriente de entrada del reactor de reducción
RO	Reactor de oxidación
RR	Reactor de reducción
TO	Transportador de oxígeno
outRO	Corriente de salida del reactor de oxidación
outRR	Corriente de salida del reactor de reducción
Ox	Reacción de oxidación
Red	Reacción de reducción

## **7 Bibliografía**



- [1] IPCC, The fifth Assessment Report Climate Change 2014: Mitigation of Climate Change, Cambridge University Press, Cambridge, UK, 2014.
- [2] IPCC, IPCC Climate Change 2007: Synthesis Report, 2007.
- [3] IPCC, Climate Change and biodiversity, 2002.
- [4] IEA, World Energy Outlook, in, International Energy Agency, Paris, France, 2013.
- [5] COP15, in: XV Conferencia Internacional sobre el Cambio Climatico, Copenhagen, Dinamarca, 2009.
- [6] COP18, in: XVIII Conferencia Internacional sobre el Cambio Climatico, Doha , Qatar, 2012.
- [7] NOAA, CO2Now.org, in, Institution of Oceanography in San Diego (La Jolla) California, USA, Mauna Loa Observatory, Hawaii, USA, 2014.
- [8] IEA, Energy technology perspectives: Pathways to a clean energy system, in, International Energy Agency, Paris, France, 2012.
- [9] L. Strömberg, G. Lindgren, J. Jacoby, R. Giering, M. Anheden, U. Burchhardt, H. Altmann, F. Kluger, G.N. Stamatelopoulos, Update on Vattenfall's 30 MW<sub>th</sub> oxyfuel pilot plant in Schwarze Pumpe, in: Energy Procedia, 2009, pp. 581-589.
- [10] A.F. Ghoniem, Needs, resources and climate change: Clean and efficient conversion technologies, Progr. Energy Combust. Sci., 37 (2011) 15-51.
- [11] Pteco2, Transporte de CO<sub>2</sub>: estado del arte, alternativas y retos, Asociación de la Plataforma Tecnológica Española del CO<sub>2</sub>, 2013.
- [12] E. de Visser, C. Hendriks, M. Barrio, M.J. Mølnevik, G. de Koeijer, S. Liljemark, Y. Le Gallo, Dynamis CO<sub>2</sub> quality recommendations, International Journal of Greenhouse Gas Control, 2 (2008) 478-484.
- [13] C. Hermanrud, T. Andresen, O. Eiken, H. Hansen, A. Janbu, J. Lippard, H.N. Bolås, T.H. Simmenes, G.M.G. Teige, S. Østmo, Storage of CO<sub>2</sub> in saline aquifers–Lessons learned from 10 years of injection into the Utsira Formation in the Sleipner area, Energy Procedia, 1 (2009) 1997-2004.
- [14] F. Riddiford, I. Wright, C. Bishop, T. Espie, A. Tourqui, Monitoring geological storage the In Salah Gas CO<sub>2</sub> storage project, in, 2005, pp. 1353-1359.
- [15] S.D. Hovorka, S.M. Benson, C. Doughty, B.M. Freifeld, S. Sakurai, T.M. Daley, Y.K. Kharaka, M.H. Holtz, R.C. Trautz, H.S. Nance, L.R. Myer, K.G. Knauss, Measuring permanence of CO<sub>2</sub> storage in saline formations: The Frio experiment, Environmental Geosciences, 13 (2006) 105-121.
- [16] S. Mito, Z. Xue, Geochemical trapping of CO<sub>2</sub> in saline aquifer storage: Results of repeated formation fluid sampling at the Nagaoka site, in, 2013, pp. 5449-5455.
- [17] Pteco2, Almacenamiento de CO<sub>2</sub>: tecnologías, oportunidades y expectativas, Asociación de la Plataforma Tecnológica Española del CO<sub>2</sub>, Madrid, 2012.
- [18] ZEP, Cost of CSS-CO<sub>2</sub> Capture and Storage, in, European Technology Platform for Zero Emission Fossil Fuel Power Plants, 2011.
- [19] ZEP, CO<sub>2</sub> Capture and Storage for Gas, in: Sustainable, low-carbon power for Europe, European Technology Platform for Zero Emissions Fossil Fuel Power Plants, Brussels, Belgium, 2014.
- [20] ZEP, The Cost of CO<sub>2</sub> Capture, in: Post-demonstration CCS in the EU, European Technology Platform for Zero Emissions Fossil Fuel Power Plants, Brussels. Belgium, 2011.
- [21] H.J. Richter, K.F. Knoche, Reversibility of combustion processes, ACS Symp. Ser., (1983) 71-85.
- [22] M. Ishida, D. Zheng, T. Akehata, Evaluation of a chemical-looping-combustion power-generation system by graphic exergy analysis, Energy, 12 (1987) 147-154.

- [23] J. Adanez, A. Abad, F. Garcia Labiano, P. Gayan, L. de Diego, Progress in Chemical-Looping Combustion and Reforming technologies, *Progr. Energy Combust. Sci.*, 38 (2012) 215-282.
- [24] A. Lyngfelt, B. Leckner, T. Mattisson, A fluidized-bed combustion process with inherent CO<sub>2</sub> separation; Application of chemical-looping combustion, *Chem. Eng. Sci.*, 56 (2001) 3101-3113.
- [25] L.F. de Diego, F. García-Labiano, J. Adánez, P. Gayán, A. Abad, B.M. Corbella, J. María Palacios, Development of Cu-based oxygen carriers for chemical-looping combustion, *Fuel*, 83 (2004) 1749-1757.
- [26] F. García-Labiano, P. Gayán, J. Adánez, L.F. De Diego, C.R. Forero, Solid waste management of a chemical-looping combustion plant using Cu-based oxygen carriers, *Environ. Sci. Technol.*, 41 (2007) 5882-5887.
- [27] A. Lyngfelt, H. Thunman, Construction and 100 h of Operational Experience of A 10-kW Chemical-Looping Combustor, in, 2005, pp. 625-645.
- [28] A. Lyngfelt, Oxygen carriers for chemical looping combustion -4000 h of operational experience, *Transporteurs d'oxygène pour la combustion en boucle chimique: Experience accumulée pendant 4000 h d'opération*, 66 (2011) 161-172.
- [29] Y. Cao, W.P. Pan, Investigation of chemical looping combustion by solid fuels. 1. Process analysis, *Energy and Fuels*, 20 (2006) 1836-1844.
- [30] J.S. Dennis, S.A. Scott, A.N. Hayhurst, In situ gasification of coal using steam with chemical looping: A technique for isolating CO<sub>2</sub> from burning a solid fuel, *J. Energy Inst.*, 79 (2006) 187-190.
- [31] A. Cuadrat, A. Abad, F. García-Labiano, P. Gayán, L.F. de Diego, J. Adánez, Relevance of the coal rank on the performance of the in situ gasification chemical-looping combustion, *Chem. Eng. J. (Lausanne)*, 195-196 (2012) 91-102.
- [32] P. Gayán, A. Abad, L.F. de Diego, F. García-Labiano, J. Adánez, Assessment of technological solutions for improving chemical looping combustion of solid fuels with CO<sub>2</sub> capture, *Chem. Eng. J. (Lausanne)*, 233 (2013) 56-69.
- [33] S. Bryant, L.W. Lake, Effect of Impurities on Subsurface CO<sub>2</sub> Storage Processes, in, 2005, pp. 983-996.
- [34] A. Abad, A. Cuadrat, T. Mendiara, F. García Labiano, P. Gayán, L.F. de-Diego, J. Adánez, Low-Cost Fe-Based Oxygen Carrier Materials for the *iG-CLC* Process with Coal. 2, *Ind. Eng. Chem. Res.*, 51 (2012) 16230-16241.
- [35] T. Mattisson, A. Lyngfelt, H. Leion, Chemical-looping with oxygen uncoupling for combustion of solid fuels, *International Journal of Greenhouse Gas Control*, 3 (2009) 11-19.
- [36] T. Mattisson, H. Leion, A. Lyngfelt, Chemical-looping with oxygen uncoupling using CuO/ZrO<sub>2</sub> with petroleum coke, *Fuel*, 88 (2009) 683-690.
- [37] O.R. Oy, HSC Chemistry 6.1. Chemical reaction and equilibrium software with thermochemical database and simulation module. , in, 2008.
- [38] E. Eyring, Chemical looping with copper oxide as carrier and coal as fuel Proceedings of 1st International Conference on Chemical Looping, 2010.
- [39] A. Shulman, E. Cleverstam, T. Mattisson, A. Lyngfelt, Manganese/Iron, Manganese/Nickel, and Manganese/Silicon Oxides Used in Chemical-Looping With Oxygen Uncoupling (CLOU) for Combustion of Methane, *Energy Fuels*, 23 (2009) 5269-5275.
- [40] H. Leion, Y. Larring, E. Bakken, R. Bredesen, T. Mattisson, A. Lyngfelt, Use of CaMn<sub>0.875</sub>Ti<sub>0.125</sub>O<sub>3</sub> as oxygen carrier in chemical-looping with oxygen uncoupling, *Energy Fuel*, 23 (2009) 76-83.

- [41] Y.-y. Wen, Z.-s. Li, L. Xu, N.-s. Cai, Experimental Study of Natural Cu Ore Particles as Oxygen Carriers in Chemical Looping with Oxygen Uncoupling (CLOU), *Energy Fuels*, 26 (2012) 3919-3927.
- [42] H. Zhao, K. Wang, Y. Fang, J. Ma, D. Mei, C. Zheng, Characterization of natural copper ore as oxygen carrier in chemical-looping with oxygen uncoupling of anthracite, *International Journal of Greenhouse Gas Control*, 22 (2014) 154-164.
- [43] E.M. Eyring, G. Konya, J.S. Lighty, A.H. Sahir, A.F. Sarofim, K. Whitty, Chemical Looping with Copper Oxide as Carrier and Coal as Fuel, *Oil Gas Sci. Technol.*, 66 (2011) 209-221.
- [44] D. Jing, T. Mattisson, M. Ryden, P. Hallberg, A. Hedayati, J. Van Noyen, F. Snijkers, A. Lyngfelt, Innovative Oxygen Carrier Materials for Chemical-Looping Combustion, *Energy Procedia*, 37 (2013) 645-653.
- [45] M. Rydén, D. Jing, M. Källén, H. Leion, A. Lyngfelt, T. Mattisson, CuO-based oxygen-carrier particles for chemical-looping with oxygen uncoupling - Experiments in batch reactor and in continuous operation, *Industrial and Engineering Chemistry Research*, 53 (2014) 6255-6267.
- [46] A.-M. Azad, A. Hedayati, M. Rydén, H. Leion, T. Mattisson, Examining the Cu–Mn–O Spinel System as an Oxygen Carrier in Chemical Looping Combustion, *Energy Technology*, 1 (2013) 59-69.
- [47] N. Mohammad Pour, H. Leion, M. Rydén, T. Mattisson, Combined Cu/Mn oxides as an oxygen carrier in chemical looping with oxygen uncoupling (CLOU), *Energy and Fuels*, 27 (2013) 6031-6039.
- [48] Q. Imtiaz, M. Broda, C.R. Müller, Structure-property relationship of co-precipitated Cu-rich, Al<sub>2</sub>O<sub>3</sub>- or MgAl<sub>2</sub>O<sub>4</sub>-stabilized oxygen carriers for chemical looping with oxygen uncoupling (CLOU), *Appl. Energy*, 119 (2014) 557-565.
- [49] P. Gayán, I. Adánez-Rubio, A. Abad, L. de Diego, F. García Labiano, J. Adánez, Development of Cu-based oxygen carriers for Chemical-Looping with Oxygen Uncoupling (CLOU) process, *Fuel*, 96 (2012) 226-238.
- [50] M. Arjmand, A.-M. Azad, H. Leion, A. Lyngfelt, T. Mattisson, Prospects of Al<sub>2</sub>O<sub>3</sub> and MgAl<sub>2</sub>O<sub>4</sub>-Supported CuO Oxygen Carriers in Chemical-Looping Combustion (CLC) and Chemical-Looping with Oxygen Uncoupling (CLOU), *Energy Fuels*, 25 (2011) 5493-5502.
- [51] Q. Song, W. Liu, C. Bohn, R. Harper, E. Sivaniah, S. Scott, J. Dennis, A high performance oxygen storage material for chemical looping processes with CO<sub>2</sub> capture, *Energy & environmental science*, 6 (2013) 288-298.
- [52] A. Hedayati, A.-M. Azad, M. Rydén, H. Leion, T. Mattisson, Evaluation of Novel Ceria-Supported Metal Oxides As Oxygen Carriers for Chemical-Looping Combustion, *Ind. Eng. Chem. Res.*, 51 (2012) 12796-12806.
- [53] Q. Imtiaz, A. Kierzkowska, M. Broda, C. Muller, Synthesis and performance of Al<sub>2</sub>O<sub>3</sub>, CeO<sub>2</sub> or MgAl<sub>2</sub>O<sub>4</sub>-supported CuO-based materials for chemical looping with oxygen uncoupling, *Proceedings of the 2nd International Conference on Chemical Looping*, Darmstadt, Germany, (2012).
- [54] L. Xu, J. Xu, Z. Wang, N. Li, Cai, Experimental Study of Cement-Supported CuO Oxygen Carriers in Chemical Looping with Oxygen Uncoupling (CLOU), *Energy Fuels*, 27 (2013) 1522-1530.
- [55] D. Mei, H. Zhao, Z. Ma, Y. Fang, C. Zheng, Fluidized bed reactor investigation of copper-based oxygen carrier in chemical looping with oxygen uncoupling, *Ranshao Kexue Yu Jishu/Journal of Combustion Science and Technology*, 19 (2013) 15-20.

- [56] D. Mei, H. Zhao, Z. Ma, C. Zheng, Using the sol-gel-derived CuO/CuAl<sub>2</sub>O<sub>4</sub> oxygen carrier in chemical looping with oxygen uncoupling for three typical coals, *Energy and Fuels*, 27 (2013) 2723-2731.
- [57] I. Adánez-Rubio, P. Gayán, F. García-Labiano, L. de Diego, J. Adánez, A. Abad, Development of CuO-based oxygen-carrier materials suitable for Chemical-Looping with Oxygen Uncoupling (CLOU) process, *Energy Procedia*, 4 (2011) 417-424.
- [58] A. Abad, I. Adánez-Rubio, P. Gayán, F. García Labiano, L. de Diego, J. Adánez, Demonstration of chemical-looping with oxygen uncoupling (CLOU) process in a 1.5 kW<sub>th</sub> continuously operating unit using a Cu-based oxygen-carrier, *International journal of greenhouse gas control*, 6 (2012) 189-200.
- [59] I. Adánez-Rubio, A. Abad, P. Gayán, L. de Diego, F. García Labiano, J. Adánez, Identification of operational regions in the Chemical-Looping with Oxygen Uncoupling (CLOU) process with a Cu-based oxygen carrier, *Fuel*, 102 (2012) 634-645.
- [60] I. Adánez-Rubio, P. Gayán, A. Abad, L. de Diego, F. García Labiano, J. Adánez, Evaluation of a Spray-Dried CuO/MgAl<sub>2</sub>O<sub>4</sub> Oxygen Carrier for the Chemical Looping with Oxygen Uncoupling Process, *Energy Fuels*, 26 (2012) 3069-3081.
- [61] I. Adánez-Rubio, A. Abad, P. Gayán, L.F. de Diego, F. García Labiano, J. Adánez, Performance of CLOU process in the combustion of different types of coal with CO<sub>2</sub> capture, *International journal of greenhouse gas control*, 12 (2013) 430-440.
- [62] I. Adánez-Rubio, A. Abad, P. Gayán, L.F. de Diego, F. García-Labiano, J. Adánez, Biomass combustion with CO<sub>2</sub> capture by chemical looping with oxygen uncoupling (CLOU), *Fuel Process. Technol.*, 124 (2014) 104-114.
- [63] I. Adánez-Rubio, A. Abad, P. Gayán, F. García Labiano, L. de Diego, J. Adánez, The fate of sulphur in the Cu-based Chemical Looping with Oxygen Uncoupling (CLOU) Process, *Appl. Energy*, 113 (2014) 1855-1862.
- [64] M. Arjmand, M. Keller, H. Leion, T. Mattisson, A. Lyngfelt, Oxygen Release and Oxidation Rates of MgAl<sub>2</sub>O<sub>4</sub>-Supported CuO Oxygen Carrier for Chemical-Looping Combustion with Oxygen Uncoupling (CLOU), *Energy Fuels*, 26 (2012) 6528-6539.
- [65] I. Adánez-Rubio, M. Arjmand, H. Leion, P. Gayán, A. Abad, T. Mattisson, A. Lyngfelt, Investigation of Combined Supports for Cu-Based Oxygen Carriers for Chemical-Looping with Oxygen Uncoupling (CLOU), *Energy Fuels*, 27 (2013) 3918-3927.
- [66] M. Keller, M. Arjmand, H. Leion, T. Mattisson, Interaction of mineral matter of coal with oxygen carriers in chemical-looping combustion (CLC), *Chem. Eng. Res. Des.*, (2014).
- [67] S.B. Peterson, G. Konya, C.K. Clayton, R.J. Lewis, B.R. Wilde, E.M. Eyring, K.J. Whitty, Characteristics and CLOU performance of a novel SiO<sub>2</sub>-supported oxygen carrier prepared from CuO and β-SiC, *Energy and Fuels*, 27 (2013) 6040-6047.
- [68] G. Pu, P. Xu, L. Zhang, Study on the oxygen releasing and circulation reaction properties of two Cu-based oxygen carriers prepared by impregnation method using graphite as pore-forming agent, *Zhongguo Dianji Gongcheng Xuebao/Proceedings of the Chinese Society of Electrical Engineering*, 33 (2013) 67-72.
- [69] K. Whitty, C. Clayton, Measurement and Modeling of Kinetics for Copper-Based Chemical Looping with Oxygen Uncoupling, 2nd International Conference on Chemical Looping 26-28 September 2012, Darmstadt, Germany, (2012).
- [70] C. Clayton, K. Whitty, Measurement and modeling of decomposition kinetics for copper oxide-based chemical looping with oxygen uncoupling, *Appl. Energy*, 116 (2014) 416-423.

- [71] C.K. Clayton, H.Y. Sohn, K.J. Whitty, Oxidation kinetics of  $\text{Cu}_2\text{O}$  in oxygen carriers for chemical looping with oxygen uncoupling, *Industrial and Engineering Chemistry Research*, 53 (2014) 2976-2986.
- [72] M. Arjmand, H. Leion, T. Mattisson, A. Lyngfelt,  $\text{ZrO}_2$ -supported CuO oxygen carriers for chemical-looping with oxygen uncoupling (CLOU), in, 2013, pp. 550-559.
- [73] P. Moldenhauer, M. Rydén, T. Mattisson, A. Lyngfelt, Chemical-looping combustion and chemical-looping with oxygen uncoupling of kerosene with Mn- and Cu-based oxygen carriers in a circulating fluidized-bed 300 W laboratory reactor, *Fuel Process. Technol.*, 104 (2012) 378-389.
- [74] J.J. Pis, T.A. Centeno, M. Mahamud, A.B. Fuertes, J.B. Parra, J.A. Pajares, R.C. Bansal, Preparation of active carbons from coal part I. Oxidation of coal, *Fuel Process. Technol.*, 47 (1996) 119-138.
- [75] J. Adánez, L.F. De Diego, F. García-Labiano, P. Gayán, A. Abad, J.M. Palacios, Selection of oxygen carriers for chemical-looping combustion, *Energy and Fuels*, 18 (2004) 371-377.
- [76] P. Simell, P. Ståhlberg, E. Kurkela, J. Albrecht, S. Deutsch, K. Sjöström, Provisional protocol for the sampling and analysis of tar and particulates in the gas from large-scale biomass gasifiers. Version 1998, *Biomass and Bioenergy*, 18 (2000) 19-38.
- [77] A. Lyngfelt, B. Kronberger, J. Adanez, J.X. Morin, P. Hurst, The grace project: Development of oxygen carrier particles for chemical-looping combustion. Design and operation of a 10 kW chemical-looping combustor, in: *Greenhouse Gas Control Technologies*, 2005, pp. 115-123.
- [78] M. Rydén, P. Moldenhauer, S. Lindqvist, T. Mattisson, A. Lyngfelt, Measuring attrition resistance of oxygen carrier particles for chemical looping combustion with a customized jet cup, *Powder Technol.*, 256 (2014) 75-86.
- [79] L.F. de Diego, F. García-Labiano, P. Gayán, J. Celaya, J.M. Palacios, J. Adánez, Operation of a 10 kW<sub>th</sub> chemical-looping combustor during 200 h with a  $\text{CuO-Al}_2\text{O}_3$  oxygen carrier, *Fuel*, 86 (2007) 1036-1045.
- [80] J. Adánez, C. Dueso, L.F.D. Diego, F. García-Labiano, P. Gayán, A. Abad, Methane combustion in a 500 W<sub>th</sub> chemical-looping combustion system using an impregnated ni-based oxygen carrier, *Energy and Fuels*, 23 (2009) 130-142.
- [81] A. Abad, J. Adánez, F. García Labiano, L. de Diego, P. Gayán, J. Celaya, Mapping of the range of operational conditions for Cu-, Fe-, and Ni-based oxygen carriers in chemical-looping combustion, *Chem. Eng. Sci.*, 62 (2007) 533-549.
- [82] H. Gu, L. Shen, J. Xiao, S. Zhang, T. Song, Chemical Looping Combustion of Biomass/Coal with Natural Iron Ore as Oxygen Carrier in a Continuous Reactor, *Energy Fuels*, 25 (2011) 446-455.
- [83] T. Mendiara, A. Abad, L.F. de Diego, F. García Labiano, P. Gayán, J. Adánez, Biomass combustion in a CLC system using an iron ore as an oxygen carrier, *International Journal of Greenhouse Gas Control*, 19 (2013) 322-330.
- [84] L. Shen, J. Wu, J. Xiao, Q. Song, R. Xiao, Chemical-Looping Combustion of Biomass in a 10 kW<sub>th</sub> Reactor with Iron Oxide As an Oxygen Carrier, *Energy Fuels*, 23 (2009) 2498-2505.
- [85] J. Adánez, P. Gayán, L.F. De Diego, F. Garcia-Labiano, A. Abad, Combustion of wood chips in a CFBC. Modeling and validation, *Industrial and Engineering Chemistry Research*, 42 (2003) 987-999.
- [86] B. Sass, Carbon dioxide capture for storage in deep geologic formations results from the  $\text{CO}_2$  capture project, 2005.
- [87] S. Bryant, Carbon dioxide capture for storage in deep geologic formations e results from the  $\text{CO}_2$  capture project, 2005.



- [88] C.R. Forero, P. Gayán, F. García Labiano, L.F. de Diego, A. Abad, J. Adánez, Effect of gas composition in Chemical-Looping Combustion with copper-based oxygen carriers: Fate of sulphur, *International Journal of Greenhouse Gas Control*, 4 (2010) 762-770.
- [89] L.F. De Diego, F. García-Labiano, P. Gayán, A. Abad, A. Cabello, J. Adánez, G. Sprachmann, Performance of Cu- and Fe-based oxygen carriers in a 500 W<sub>th</sub> CLC unit for sour gas combustion with high H<sub>2</sub>S content, *International Journal of Greenhouse Gas Control*, 28 (2014) 168-179.
- [90] O.J.E. Commun, On the limitation of emissions of certain pollutants into the air from large combustion plants, in: E.C. Directive (Ed.) 2001/80/EC, 2001, pp. 1–21
- [91] R.G. Benito, Emissions of SO<sub>2</sub> during batch fluidized bed combustion of Rundle retorted shale, *Fuel*, 72 (1993) 869-872.
- [92] L.F. de Diego, A. Rufas, F. García-Labiano, M. de las Obras-Loscertales, A. Abad, P. Gayán, J. Adánez, Optimum temperature for sulphur retention in fluidised beds working under oxy-fuel combustion conditions, *Fuel*, 114 (2013) 106-113.
- [93] G. Pipitone, O. Bolland, Power generation with CO<sub>2</sub> capture: Technology for CO<sub>2</sub> purification, *International Journal of Greenhouse Gas Control*, 3 (2009) 528-534.
- [94] T. Mendiara, L.F. de Diego, F. García-Labiano, P. Gayán, A. Abad, J. Adánez, Behaviour of a bauxite waste material as oxygen carrier in a 500W<sub>th</sub> CLC unit with coal, *International Journal of Greenhouse Gas Control*, 17 (2013) 170-182.
- [95] D. Chadda, J.D. Ford, M.A. Fahim, Chemical energy storage by the reaction cycle CuO/Cu<sub>2</sub>O, *International Journal of Energy Research*, 13 (1989) 63-73.
- [96] S. Peterson, G. Konya, C. Clayton, R. Lewis, B. Wilde, E. Eyring, K. Whitty, Characteristics and CLOU Performance of a Novel SiO<sub>2</sub>-Supported Oxygen Carrier Prepared from CuO and β-SiC, *Energy Fuels*, 27 (2013) 6040-6047.
- [97] K. Wang, Q. Yu, Q. Qin, Reduction Kinetics of Cu-Based Oxygen Carriers for Chemical Looping Air Separation, *Energy Fuels*, 27 (2013) 5466-5474.
- [98] H. Song, K. Song, E. Shah, T. Doroodchi, B. Wall, Moghtaderi, Analysis on Chemical Reaction Kinetics of CuO/SiO<sub>2</sub>Oxygen Carriers for Chemical Looping Air Separation, *Energy Fuels*, 28 (2014) 173-182.
- [99] C. Clayton, K. Whitty, Measurement and modeling of decomposition kinetics for copper oxide-based chemical looping with oxygen uncoupling, *Appl. Energy*, (2013).
- [100] A. Sahir, H. Sohn, H. Leion, J. Lighty, Rate Analysis of Chemical-Looping with Oxygen Uncoupling (CLOU) for Solid Fuels, *Energy Fuels*, 26 (2012) 4395-4404.
- [101] Y. Zhu, K. Mimura, J.W. Lim, M. Isshiki, Q. Jiang, Brief review of oxidation kinetics of copper at 350 °C to 1050 °C, *Metall. Mater. Trans. A*, 37 (2006) 1231-1237.
- [102] C.N. Hinshelwood, The Kinetics of Heterogeneous Reactions, in: *Kinetics of Chemical Change* Clarendon Press, Oxford, 1940, pp. 178-234.
- [103] F. García-Labiano, A. Abad, L.F. de Diego, P. Gayán, J. Adánez, Calcination of calcium-based sorbents at pressure in a broad range of CO<sub>2</sub> concentrations, *Chem. Eng. Sci.*, 57 (2002) 2381-2393.
- [104] B.V. Erofe'Ev, *Comptes Rendus de l'Académie des Sciences de l'Urss*, (1946) 511.
- [105] A. Abad, J. Adánez, A. Cuadrat, F. García Labiano, P. Gayán, L. de Diego, Kinetics of redox reactions of ilmenite for chemical-looping combustion, *Chem. Eng. Sci.*, 66 (2011) 689-702.
- [106] R. Hurt, R. Mitchell, Unified high-temperature char combustion kinetics for a suite of coals of various rank, *Symposium, International, on Combustion*, 24 (1992) 1243-1250.

## **Apéndice - Artículos**



**Paper I**





## Development of Cu-based oxygen carriers for Chemical-Looping with Oxygen Uncoupling (CLOU) process

Pilar Gayán\*, Iñaki Adánez-Rubio, Alberto Abad, Luis F. de Diego, Francisco García-Labiano, Juan Adánez

*Instituto de Carboquímica (C.S.I.C.), Dept. of Energy & Environment, Miguel Luesma Castán, 4, Zaragoza 50018, Spain*

### ARTICLE INFO

#### Article history:

Received 25 April 2011

Received in revised form 10 January 2012

Accepted 11 January 2012

Available online 26 January 2012

#### Keywords:

CLOU

Oxygen carrier

Carbon capture

Coal

### ABSTRACT

The Chemical-Looping with Oxygen Uncoupling (CLOU) process is a Chemical-Looping Combustion (CLC) technology that allows the combustion of solid fuels with inherent CO<sub>2</sub> separation using oxygen carriers. This technology has low energy penalty for CO<sub>2</sub> separation and thus low CO<sub>2</sub> capture costs. The CLOU process is a new option, when the direct use of a solid fuel in a CLC technology is considered. The CLOU process uses oxygen carriers based on some metal oxides that have the capability to evolve gaseous oxygen at high temperatures. The oxygen generated by the metal oxide reacts directly with the solid fuel, which is mixed with the oxygen carrier in the fuel reactor. The selection of a suitable oxygen carrier is a key factor for the CLOU technology development. The aim of this work was to produce and characterize oxygen carrier materials based on CuO with high oxygen transfer capability, high oxygen generation rates and good fluidization properties. Several oxygen carriers were prepared with different CuO contents, inert supports and preparation methods (incipient wet impregnation, mechanical mixing following by pelletizing by extrusion, or pelletizing by pressure). The reaction rates for oxygen generation (reduction) and regeneration were determined carrying out successive cycles in a TGA system. In this way, it was determined the chemical suitability of the materials. Selected oxygen carriers were tested by redox cycles in a batch fluidized-bed reactor working at different temperatures and reacting atmospheres. The fluidization behavior against agglomeration and attrition during a high number of cycles was determined. Oxygen carriers with 60 wt.% of CuO on MgAl<sub>2</sub>O<sub>4</sub> and with 40 wt.% CuO on ZrO<sub>2</sub> prepared by mechanical mixing following by pelletizing by pressure were identified as suitable materials for CLOU process.

© 2012 Elsevier Ltd. All rights reserved.

### 1. Introduction

In order to stabilize the CO<sub>2</sub> concentration in the atmosphere between 450 and 750 ppm CO<sub>2</sub> several measures must be taken. Among them Carbon Capture and Storage (CCS) would contribute with 15–55% to the cumulative mitigation effort worldwide until 2100 [1]. CCS is a process involving the separation of CO<sub>2</sub> emitted by industry and energy-related sources, and the storage for its isolation from the atmosphere over a long term. Chemical-Looping Combustion process (CLC) has been suggested among the best alternatives to reduce the economic cost of CO<sub>2</sub> capture using flue gas [2] and to increase the efficiency with respect to other CO<sub>2</sub> capture process [3]. In this process, CO<sub>2</sub> is inherently separated from other combustion products, N<sub>2</sub> and unused O<sub>2</sub>, through the use of a solid oxygen carrier and thus no energy is expended for the separation. The CLC process has been demonstrated for combustion of gaseous fuel such as natural gas and syngas in 10–140 kW<sub>th</sub> units using oxygen carrier materials based on Ni [4,5], Cu [6], Fe

[7,8]. All these oxygen carriers have been reviewed in Adánez et al. [9]. However, solid fuels are considerably more abundant and less expensive than natural gas, and it would be highly advantageous if the CLC process could be adapted for these types of fuels. One option to use solid fuels in a CLC process is to use syngas from a previous gasifying stage in the fuel reactor. In this technology, it is necessary to use pure oxygen for the gasification of the solid fuel. This stage has a significant energy penalty due to the oxygen separation from the air. A second option of development is the Chemical-Looping Coal Combustion, where the solid fuel is directly introduced to the fuel reactor. The solid–solid reaction between the char and the metal oxide is not very likely to occur at an appreciable rate in a fluidized bed [10] and the in situ gasification of solid fuel followed by combustion of products (IG-CLC), has been proposed as a solution, where the conversion of solid fuel goes via a gasifying agent, e.g. H<sub>2</sub>O. Because of the slow gasification reaction rate, a carbon stripper is necessary to separate the unreacted char particles from the oxygen carrier, before it is regenerated with air, to avoid CO<sub>2</sub> emission in this reactor [11,12]. To increase the gasification rate, temperature higher than 1000 °C has been proposed in the fuel reactor [13]. As partial loss of oxygen carrier in the purge stream of ash particle is likely to occur, low

\* Corresponding author. Tel.: +34 976 733977; fax: +34 976 733318.

E-mail address: [pgayan@icb.csic.es](mailto:pgayan@icb.csic.es) (P. Gayán).

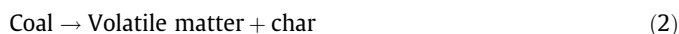
cost materials are preferred in this CLC option, e.g. ilmenite, hematite or anichite [14–17].

In order to overcome the low reactivity of the char gasification stage in the direct solid fueled Chemical-Looping Combustion, an alternative process was recently proposed [18,19]. The Chemical-Looping with Oxygen Uncoupling (CLOU) process is based on the strategy of using oxygen carriers which release gaseous oxygen in the fuel reactor thereby allowing the solid fuel to burn with gas phase oxygen. In this way, the slow gasification step on the direct solid fuel Chemical-Looping Combustion is avoided, giving a much faster solid conversion [19,20]. In the CLOU process, the fluidization gas can be recycled  $\text{CO}_2$ , reducing in this way the steam duty of the plant and associated energy penalties.

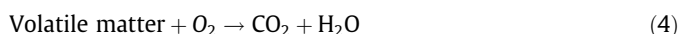
Fig. 1 shows a schematic diagram of a CLOU system. In the fuel reactor  $\text{CO}_2$  and steam are produced by different reactions. First the oxygen carrier releases oxygen according to:



and the solid fuel begins devolatilization producing a solid residue (char) and volatile matter as a gas product:

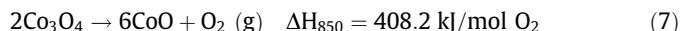
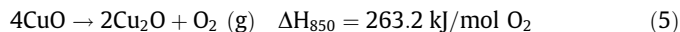


Then, char and volatiles are burnt as in usual combustion according to reactions (3) and (4):



After steam condensation, a pure  $\text{CO}_2$  stream can be obtained. The reduced oxygen carrier is transported to the air reactor, where the oxygen carrier is regenerated to the initial oxidation stage with the oxygen of the air, and thus becomes ready for a new cycle. The exit stream of the air reactor contains only  $\text{N}_2$  and unreacted  $\text{O}_2$ . Therefore CLOU process has a low energy penalty for  $\text{CO}_2$  separation and low  $\text{CO}_2$  capture costs are expected. The heat release over the fuel and air reactors is the same as for conventional combustion.

The possible metal oxides that have the property of release oxygen are limited; moreover, this  $\text{O}_2$  release must be reversible in order to oxidize the oxygen carrier in the air reactor. Thus a special requirement is needed for the oxygen carrier to be used in the CLOU process in comparison to oxygen carriers for normal CLC, where the fuel must be able to react directly with the oxygen carrier without any release of gas phase oxygen. Only those metal oxides that have a suitable equilibrium partial pressure of oxygen at temperatures of interest for combustion (800–1200 °C) can be used as CLOU oxygen carriers. Three such metal oxide systems have been identified:  $\text{CuO}/\text{Cu}_2\text{O}$ ,  $\text{Mn}_2\text{O}_3/\text{Mn}_3\text{O}_4$ , and  $\text{Co}_3\text{O}_4/\text{CoO}$  [19]. These systems can release oxygen in the gas phase through the following reversible reactions:



Although the transport capacity of the cobalt oxide is high (6.6 g  $\text{O}_2$ /100 g  $\text{Co}_3\text{O}_4$ ), the great endothermicity of the reaction (7) makes this metal oxide hardly attractive for the CLOU process. The most promising metal oxide systems for the CLOU process have found to be  $\text{CuO}/\text{Cu}_2\text{O}$  and  $\text{Mn}_2\text{O}_3/\text{Mn}_3\text{O}_4$  [19].

Table 1 shows the different oxygen carriers developed for the CLOU process found in the literature. Mn-based oxygen carrier particles have been prepared by mixing  $\text{Mn}_2\text{O}_3$  with different materials, as  $\text{Fe}_2\text{O}_3$ ,  $\text{NiO}$  and  $\text{SiO}_2$ . Shulman et al. [21] found some Mn/Fe oxygen carriers with very high reactivity towards methane, a quality that authors employ to open the possibility to combine benefits of CLOU and CLC processes with gaseous fuel. Another Mn-based oxygen carrier with a spinel perovskite-like structure is  $\text{CaMn}_{0.875}\text{Ti}_{0.125}\text{O}_3$  [24,25]. In this case, the oxygen transport capacity is improved due to the inclusion of Ca and Ti in the metal structure allowing  $\text{Mn}_2\text{O}_3$  reduction to MnO. Uncoupling properties of this oxygen carrier were tested in continuous experiments [25] showing the oxygen release at temperatures higher than 720 °C with an oxygen concentration around 4% at the fuel reactor outlet at 950 °C. This oxygen carrier was also tested in a continuously operated CLC system for natural gas which includes both CLOU and standard CLC by Mn oxides during 70 h. During these experiments oxygen carrier presented a combustion efficiency about 99.8% for natural gas at 950 °C using bed inventories of 1900 kg/MW<sub>th</sub> of which about 30% was located in the fuel reactor. [25].

Copper has the highest oxygen transport capacity (10 g  $\text{O}_2$ /100 g  $\text{CuO}$  compared to 3 g  $\text{O}_2$ /100 g  $\text{Mn}_2\text{O}_3$ ) and the reaction with C is exothermic in the fuel reactor, as shown in reaction (8). Fig. 2 shows the partial pressure of oxygen as a function of temperature for the  $\text{CuO}/\text{Cu}_2\text{O}$  and the  $\text{CuAl}_2\text{O}_4/\text{CuAlO}_2$  systems, calculated using HSC software [27] and data from reference [28], respectively.  $\text{CuAl}_2\text{O}_4$  was also included because this compound can be formed when  $\text{Al}_2\text{O}_3$  is used as supporting material. The oxygen concentration at equilibrium conditions greatly depends on the temperature. An equilibrium concentration of 1.5 vol.%  $\text{O}_2$  can be reached in the fuel reactor at 900 °C for  $\text{CuO}/\text{Cu}_2\text{O}$  system, whereas the equilibrium concentration increases up to 12.4 vol.% at 1000 °C. Moreover, it is desirable to have a low concentration of oxygen from the fuel reactor in order to obtain a high purity  $\text{CO}_2$  stream. In the air reactor, the metal oxide is stable below 950 °C if the maximum oxygen concentration from the air reactor is 4.5 vol.%.



Mattisson et al. [19,26] developed oxygen carriers with 60 and 40 wt.% of  $\text{CuO}$ . Cyclic testing with solid fuels verified that oxygen was released close to the equilibrium pressure in the temperature

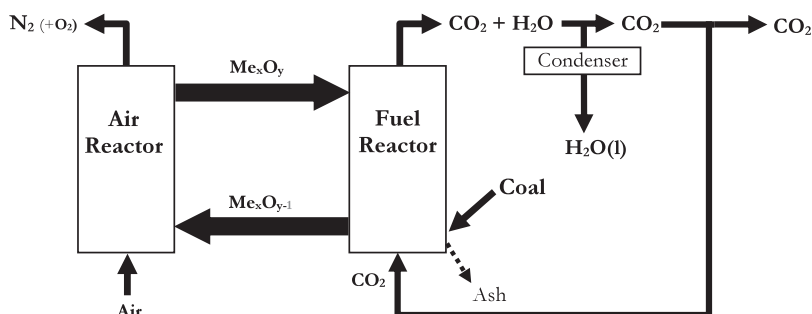


Fig. 1. Schematic diagram of the CLOU process.

**Table 1**  
Oxygen carriers in the literature for CLOU process.

MeO (wt.%)	Other metal (wt.%)	Support material	Preparation method <sup>a</sup>	Facility <sup>b</sup>	Reference
Mn <sub>3</sub> O <sub>4</sub> (80)		SiO <sub>2</sub>	FG	bFB	[21]
Mn <sub>3</sub> O <sub>4</sub> (80–20)	Fe <sub>2</sub> O <sub>3</sub> (20–800)		FG and SD	bFB, CLC	[21–23]
Mn <sub>3</sub> O <sub>4</sub> (80)	NiO (20)		FG	bFB	[21]
Mn-ore				bFB	[23]
CaMn <sub>0.875</sub> Ti <sub>0.125</sub> O <sub>3</sub>			SD + FG	TGA, bFB, CLC	[24,25]
CuO (60)		Al <sub>2</sub> O <sub>3</sub>	FG	bFB	[19]
CuO (40)		ZrO <sub>2</sub>	FG	bFB	[26]
CuO (n.a.)		SiO <sub>2</sub>	n.a	TGA, bFB	[20]

<sup>a</sup> Key for preparation method: FG = freeze granulation, SD = spray drying, n.a. = non-available.

<sup>b</sup> Key for facility: CLC = continuously operated CLC system, bFB = batch fluidized bed, TGA = thermogravimetric analyzer.

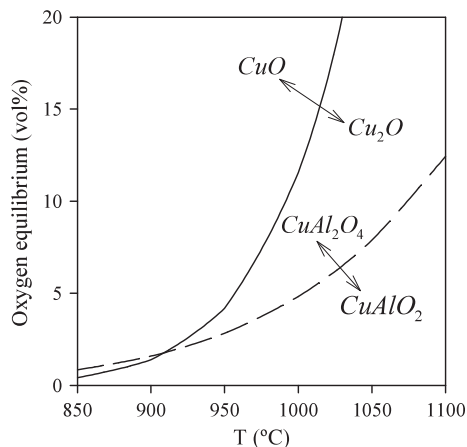


**Fig. 2.** Equilibrium oxygen concentrations over the CuO/Cu<sub>2</sub>O and the CuAl<sub>2</sub>O<sub>4</sub>/CuAlO<sub>2</sub> systems as a function of temperature.

range of 880–985 °C, and the material could also be regenerated close to equilibrium. When solid fuel particles were added to a bed of oxygen carrier particles, a very rapid release of oxygen and combustion of fuel started. Thus, the conversion rate of the fuel could be increased by almost two orders of magnitude, compared to coal gasification in a Chemical-Looping Combustion system with steam [26].

Our research group at the Instituto de Carboquímica (CSIC) has undertaken several studies using oxygen carriers based on copper. These Cu-based oxygen carriers were, so far, developed for gaseous fueled CLC. In those studies, the oxidized form was CuO, whereas the reduced form was metallic Cu. In previous works, potential Cu-based oxygen carriers were prepared using different supports [29]. The effect of oxygen carrier composition and preparation method on the reactivity and durability of the material was also investigated in a TGA [30]. It was found that the optimum preparation method for Cu-based oxygen carriers was impregnation on a support. Later, the preparation conditions and oxygen carrier characteristics were optimized to avoid the agglomeration of the Cu-based materials during their operation in a fluidized bed [31]. Based on these findings, an oxygen carrier was selected to test its behavior in a 10 kW<sub>th</sub> CLC prototype using methane as fuel. The results obtained during 200 h of continuous operation were very successful [6]. Additional work has been recently carried out to test the behavior of this oxygen carrier in a CLC continuous unit of 500 W<sub>th</sub> using syngas as fuel [32] or methane containing variable amounts of light hydrocarbons (LHC) or H<sub>2</sub>S [33,34]. From these works, it was concluded that a Cu-based material containing 15 wt.% CuO impregnated on Al<sub>2</sub>O<sub>3</sub> was a promising material to be used as oxygen carrier in CLC. Nevertheless, oxygen carriers developed for CLC process should be tested for the specific characteristics required for CLOU process. In this sense, a preliminary

development of suitable materials was carried out by Adánez-Rubio et al. [35] for the CLOU process.

In this work, a full screening of several Cu-based oxygen carriers prepared by different methods on several supports for the CLOU process was carried out. The rate of oxygen release during oxygen carrier reduction and the rate of oxidation were analyzed by TGA. The fluidization properties of the materials such as attrition and agglomeration were evaluated in a batch fluidized-bed reactor. Different operating conditions, such as temperature and oxygen concentration were tested and analyzed. Moreover, physical and chemical characteristics of particles were also analyzed after consecutive redox cycles.

## 2. Experimental

### 2.1. Preparation of materials

Oxygen carriers were composed of copper oxide as oxygen source for the combustion process, and an inert binder for increasing the mechanical strength and improving the fluidization properties. Several oxygen carriers were prepared with different CuO contents and using different supports:  $\gamma$ -Al<sub>2</sub>O<sub>3</sub>,  $\alpha$ -Al<sub>2</sub>O<sub>3</sub>, MgAl<sub>2</sub>O<sub>4</sub>, sepiolite, SiO<sub>2</sub>, TiO<sub>2</sub>, ZrO<sub>2</sub> and MgO. In addition different preparation methods were used.

#### 2.1.1. Incipient wet impregnation

Commercial  $\gamma$ -Al<sub>2</sub>O<sub>3</sub> (Puralox NWA-155, Sasol Germany GmbH),  $\alpha$ -Al<sub>2</sub>O<sub>3</sub> obtained by calcination of the  $\gamma$ -Al<sub>2</sub>O<sub>3</sub> at 1150 °C during 2 h, and MgAl<sub>2</sub>O<sub>4</sub> (obtained by impregnation of  $\gamma$ -Al<sub>2</sub>O<sub>3</sub> with magnesium nitrate and calcinated at 800 °C) were used as support to prepare oxygen carriers by incipient wet impregnation.  $\alpha$ -Al<sub>2</sub>O<sub>3</sub>,  $\gamma$ -Al<sub>2</sub>O<sub>3</sub> and MgAl<sub>2</sub>O<sub>4</sub> particles had densities of 1300, 2000 and 1800 kg/m<sup>3</sup> and porosities of 55.4%, 47.3% and 50.0%, respectively. The particle size used was +0.1–0.3 mm. Cu-based oxygen carriers were prepared by addition of a volume of an aqueous solution of copper nitrate corresponding to the total pore volume of the support particles. The aqueous solution was slowly added to the support particles, with thorough stirring at room temperature. The desired active phase loading was achieved by applying successive impregnations followed by calcinations at 550 °C, in air atmosphere for 30 min, to decompose the impregnated metal nitrates into insoluble metal oxide. Finally, the oxygen carriers were sintered for 1 h at 850 °C. Oxygen carriers with different copper contents were prepared ranging from 15 wt.% (1 impregnation step) to 33 wt.% (3 impregnation steps).

#### 2.1.2. Mechanical mixing followed by pelletizing by extrusion

The oxygen carriers were prepared from commercial pure copper oxide as powder of particle size <10  $\mu$ m (Panreac, PRS). Al<sub>2</sub>O<sub>3</sub> (Sigma Aldrich, purum), sepiolite (Mg<sub>4</sub>Si<sub>6</sub>O<sub>15</sub>(OH)<sub>2</sub>·6H<sub>2</sub>O, Panreac, QP), SiO<sub>2</sub> (Sigma Aldrich, purum), TiO<sub>2</sub> (Sigma Aldrich, purum) or



ZrO<sub>2</sub> (Sigma Aldrich, purum) were used as inert materials. Graphite (Sigma Aldrich, purum,  $d_p$ : 1–2  $\mu\text{m}$ ) as a high-temperature pore forming additive was also added during preparation. A powder mixture including the active metal oxide and the inert in the desired concentration, and 10 wt.% of graphite, was converted by water addition into a paste of suitable viscosity to be extruded in a syringe, obtaining cylindrical extrudates of about 2 mm diameter. These extrudates were gently dried at 80 °C overnight, cut at the desired length, and sintered at 950 or 1100 °C for 6 h in a muffle furnace. The extrudates were ground and sieved to obtain the desired particle size of 0.1–0.3 mm.

### 2.1.3. Mechanical mixing followed by pelletizing by pressure

The oxygen carriers were prepared from commercial pure copper oxide as powder of particle size <10  $\mu\text{m}$  (Panreac, PRS). MgAl<sub>2</sub>O<sub>4</sub> (Baikowski, S30CR), sepiolite (Panreac, QP), MgO (Panreac, PRS) or ZrO<sub>2</sub> (Sigma Aldrich, purum) were used as support. A powder mixture including the active metal oxide and the inert in the desired concentration, and 10 wt.% of graphite (Sigma Aldrich, purum,  $d_p$ : 1–2  $\mu\text{m}$ ), was ball-milled for 2 h and pelletized by pressure in a hydraulic press at 160 bar obtaining cylindrical pellets of about 1 mm in diameter. These pellets were calcined at different temperatures (950, 1100 or 1300 °C) to increase the mechanical strength during 6 h. After that, pellets were crushed and sieved to obtain the desired particle diameter (+0.1–0.3 mm). In some cases, the graphite content was reduced to 0.5 wt.% and the calcination time was extended to 12 h.

Table 2 shows all the oxygen carriers prepared with their main properties, as the density and the mechanical strength of particles.  $R_0$  is the oxygen carrier capacity of the oxygen carrier particles and was calculated as:

$$R_0 = \frac{m_{\text{ox}} - m_{\text{red}}}{m_{\text{ox}}} \quad (9)$$

$m_{\text{ox}}$  being the mass of full oxidized oxygen carrier material, whereas  $m_{\text{red}}$  is the mass at the reduction state, i.e. when all the CuO was reduced to Cu<sub>2</sub>O. The oxygen generation rate, define in Eq. (12) was also shown in Table 2.

## 2.2. Experimental set-up

### 2.2.1. Thermogravimetric analyzer

Multicycle tests to analyze the reactivity of the oxygen carriers during successive reduction–oxidation cycles were carried out in a TGA CI Electronics type described elsewhere [29]. The desired mass of oxygen carrier (about 50 mg) was loaded in a platinum wired mesh basket (14 mm diameter and 8 mm height) to reduce mass transfer resistance around the solid sample. The sample was heated to the set operating temperature in air atmosphere. After stabilization, the experiment started by exposing the oxygen carrier to alternating inert and oxidizing conditions. The inert gas was nitrogen and the gas used for oxidation was air, both flow rates being 25 nL/h. The experiments were usually carried out at 1000 °C for the reduction and oxidation reaction. However, in some cases other oxygen concentrations (4 or 11 vol.%) and oxidation temperatures (900 or 950 °C) were used to analyze the oxidation reaction in more detail. These temperatures were selected as a function of the thermodynamic equilibrium of the CuO/Cu<sub>2</sub>O system, as shown in Fig. 2.

Initially, to establish whether thermodynamic limitations, external film mass transfer and/or inter-particle diffusion were affecting the reaction rate, the sample weight and the gas flow rate were varied in the range of 40–100 mg and from 10–40 nL/h,

**Table 2**

Physical properties and reactivity ( $r_{\text{O}_2}$  at 1000 °C in N<sub>2</sub>) of the oxygen carriers prepared by different methods.

Oxygen carrier	Support	Density of particle (kg/m <sup>3</sup> )	Crushing strength (N)	$R_0$ (%)	$(r_{\text{O}_2}) \times 10^3 \left( \frac{\text{kgO}_2}{\text{s kgOC}} \right)$
<i>Incipient wet impregnation</i>					
Cu15 $\gamma$ -Al_I850	$\gamma$ -Al <sub>2</sub> O <sub>3</sub>	1600	2.5 ± 0.5	1.5	0.64
Cu33 $\gamma$ -Al_I850	$\gamma$ -Al <sub>2</sub> O <sub>3</sub>	1900	3.0 ± 0.4	3.3	1.03
Cu15 $\alpha$ -Al_I850	$\alpha$ -Al <sub>2</sub> O <sub>3</sub>	2200	4.6 ± 0.5	1.5	0.52
Cu15MgAl_I850	MgAl <sub>2</sub> O <sub>4</sub>	1900	2.1 ± 0.3	1.5	1.32
Cu21MgAl_I850	MgAl <sub>2</sub> O <sub>4</sub>	2000	0.8 ± 0.2	2.1	1.25
<i>Mechanical mixing following by pelletizing by extrusion</i>					
Cu60Al_E1100	Al <sub>2</sub> O <sub>3</sub>	3000	<0.5	6	1.67
Cu80Al_E1100	Al <sub>2</sub> O <sub>3</sub>	3900	2.6 ± 0.5	8	0.99
Cu80Se_E950	Sepiolite	2300	0.8 ± 0.3	8	1.76
Cu60Si_E950	SiO <sub>2</sub>	2000	1.1 ± 0.2	6	1.43
Cu80Si_E950	SiO <sub>2</sub>	2900	0.9 ± 0.2	8	1.75
Cu40Ti_E950	TiO <sub>2</sub>	3400	2.3 ± 0.4	4	1.19
Cu60Ti_E950	TiO <sub>2</sub>	4000	2.2 ± 0.2	6	–
Cu80Ti_E950	TiO <sub>2</sub>	5200	2.2 ± 0.4	8	0.64
Cu60Zr_E950	ZrO <sub>2</sub>	3000	<0.5	6	1.10
Cu80Zr_E950	ZrO <sub>2</sub>	3800	0.7 ± 0.2	8	1.64
<i>Mechanical mixing following by pelletizing by pressure</i>					
Cu60MgAl_P950	MgAl <sub>2</sub> O <sub>4</sub>	3900	<0.5	6	–
Cu60MgAl_P1100	MgAl <sub>2</sub> O <sub>4</sub>	3800	1.2 ± 0.3	6	1.47
Cu60MgAl_P1300	MgAl <sub>2</sub> O <sub>4</sub>	–	Melt	6	–
Cu60MgAl_P1100a	MgAl <sub>2</sub> O <sub>4</sub>	3700	1.7 ± 0.3	6	1.50
Cu60MgAl_P1100b	MgAl <sub>2</sub> O <sub>4</sub>	3700	2.2 ± 0.3	6	1.57
Cu60Zr_P950a	ZrO <sub>2</sub>	5400	<0.5	6	–
Cu40Zr_P1100a	ZrO <sub>2</sub>	4900	4.0 ± 0.4	4	1.01
Cu60Zr_P1100a	ZrO <sub>2</sub>	5400	3.0 ± 0.5	6	1.40
Cu60Mg_P1100a	MgO	4100	2.2 ± 0.4	6	0.89
Cu60Se_P1100	Sepiolite	3900	2.2 ± 0.5	6	1.45
Cu60Si_P950	SiO <sub>2</sub>	2000	<0.5	6	–
Cu60Si_P950	SiO <sub>2</sub>	–	Melt	6	–

Example of nomenclature of the oxygen carriers: Cu60MgAl\_P950:Cu60, 60 wt.% CuO; MgAl, inert binder (Al:Al<sub>2</sub>O<sub>3</sub>; Se:Sepiolite; Si:SiO<sub>2</sub>; Ti:TiO<sub>2</sub>; Zr:ZrO<sub>2</sub>; MgAl:MgAl<sub>2</sub>O<sub>4</sub>; Mg:MgO); P, pelletizing by pressure (I: Incipient wet impregnation, E: pelletizing by extrusion); 950, sintering temperature (°C); a = 0.5 wt.% graphite, b = 0.5 wt.% graphite + 12 h sintering time.

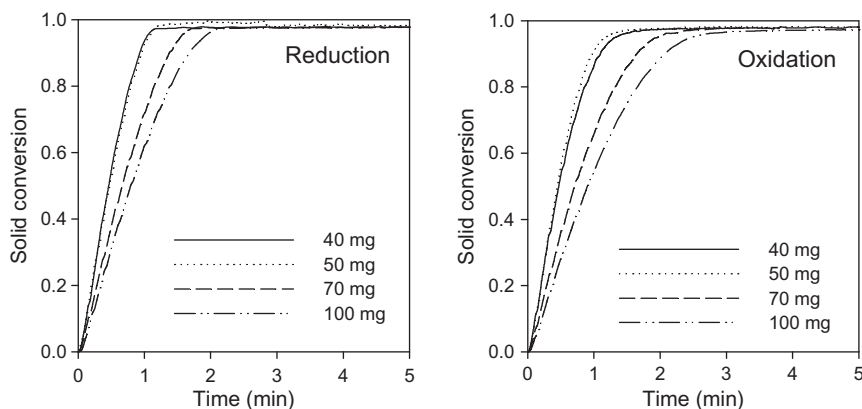


**Fig. 3.** Effect of mass load in TGA experiments (25 L<sub>N</sub>/h) on the reaction rate during the reduction and oxidation period with Cu60MgAl\_P1100b oxygen-carrier.  $T = 1000\text{ }^{\circ}\text{C}$ . Reduction: 100 vol.% N<sub>2</sub>. Oxidation: air.

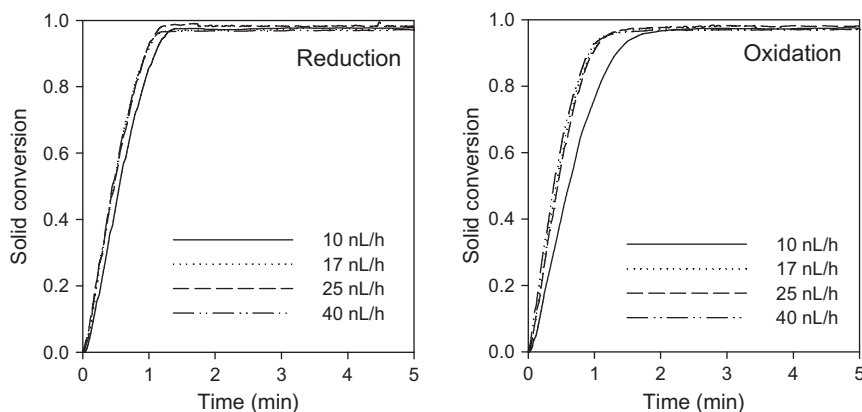


**Fig. 4.** Effect of inlet gas flow in TGA experiments (50 mg) on the reaction rate during the reduction and oxidation period with Cu60MgAl\_P1100b oxygen-carrier.  $T = 1000\text{ }^{\circ}\text{C}$ . Reduction: 100 vol.% N<sub>2</sub>. Oxidation: air.

respectively (see Figs. 3 and 4). Fig. 3 shows the conversion-time curves obtained during the reduction and oxidation with different mass loaded in TGA for Cu60MgAl\_P1100b with mass from 40 to 100 mg in the third redox cycle. It can be seen that with a mass lower than 70 mg, gas diffusion inside the particles did not control the global reaction rate. The reduction and oxidation reactivities with different nitrogen flows are depicted in Fig. 4. The reaction rates with gas flows higher than 17 nL/h were similar. As a consequence, it is considered that the reaction rate was not controlled by inter-particle diffusion or diffusion through the gas film around the particle when N<sub>2</sub> flow was higher than 20 nL/h.

### 2.2.2. Fluidized bed facility

Reduction–oxidation multi-cycles were carried out in a fluidized-bed reactor to understand the oxygen release behavior of the oxygen carrier under operating conditions similar to that existing in the CLOU process. The fluidization behavior of the materials with respect to agglomeration phenomena and attrition rate could also be observed.

Fig. 5 shows the experimental set-up used for testing the oxygen carriers. It consisted of a system for gas feeding, a fluidized-bed reactor, a parallel filter system to recover the solids elutriated from the fluidized-bed reactor, and a gas analysis system. The gas feeding system had different mass flow controllers for the different gases. The composition of the gas during reduction was 100 vol.% N<sub>2</sub> or CO<sub>2</sub>, and during oxidation different oxygen concentrations were used ranging from 5 to 21 vol.% O<sub>2</sub> in N<sub>2</sub>. The fluidized-bed reactor has 54 mm inner diameter and 500 mm height,

with a preheating zone just under the distributor plate. The entire system was inside an electrically heated furnace. The fluidized-bed reactor was fed with a batch of 0.2–0.4 kg (depend of the oxygen carrier density) of oxygen carrier to ensure a bed height of at least 55 mm (with this bed height ensure that the thermopar is in the middle of the bed). The tests were carried out at 900, 950 and 1000 °C with an inlet superficial gas velocity of 0.15 m/s (the minimum fluidization velocity of the different materials varied from 0.02 to 0.04 m/s). The reactor had two connected pressure taps in order to measure the differential pressure drop in the bed. Agglomeration problems, causing defluidization of the bed, could be detected by a sharp decrease in the bed pressure drop during operation. Two hot filters located downstream from the fluidized-bed reactor recovered the solids elutriated from the bed during the successive reduction–oxidation cycles. An on line paramagnetic gas analyzer measured the O<sub>2</sub> concentration during the test. The reduction periods varied from 300 to 1800 s, depending on the material and operation conditions. The oxidation periods necessary for complete oxygen carrier regeneration varied between 120 and 1800 s. Those suitable materials were exposed to more than 40 redox cycles corresponding to more than 40 h of operation.

### 2.3. Characterization techniques

Some samples, both fresh and used, were physically and chemically characterized by different techniques. The mechanical strength, determined using a Shimpo FGN-5X crushing strength

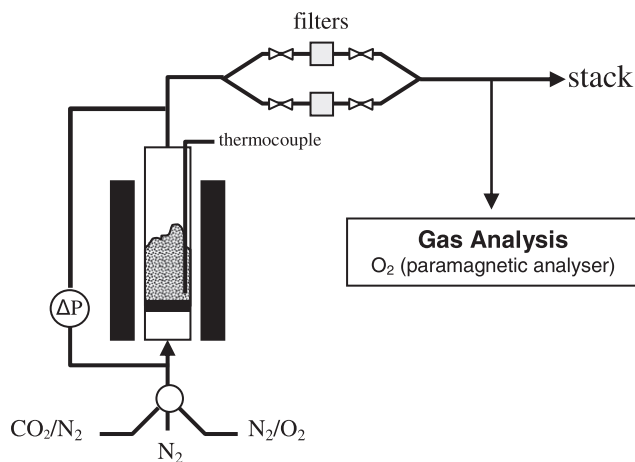


Fig. 5. Experimental setup used for multi-cycle tests in a batch fluidized bed reactor.

apparatus, was taken as the average value of 20 measurements of the force needed to fracture a particle. The surface area of the oxygen carrier particles was determined by the Brunauer–Emmett–Teller (BET) method in a Micromeritics ASAP-2020, whereas the pore volume was measured by Hg intrusion in a Quantachrome PoreMaster 33. The identification of crystalline chemical species was carried out using a powder X-ray diffractometer Bruker AXS graphite monochromator. The oxygen carrier particles were also analyzed in a scanning electron microscope (SEM) ISI DS-130 coupled to an ultra thin window PGT Prism detector for energy-dispersive X-ray (EDX) analysis.

### 3. Results and discussion

#### 3.1. Oxygen carrier reactivity in TGA

TGA experiments allowed analysis of the reactivity of the oxygen carriers under well-defined conditions, and in the absence of complex fluidizing factors such as those derived from particle attrition and interphase mass transfer processes. For screening purposes, at least five cycles of reduction and oxidation were carried out with each carrier. Usually the reactivity changed during the initial redox cycle and then stabilized during subsequent cycles. Reactivity data were obtained in TGA tests from the weight variations during the reduction and oxidation cycles as a function of time. The oxygen carrier conversion was calculated as:

$$\text{For reduction: } X_{red} = \frac{m_{ox} - m}{m_{ox} - m_{red}} \quad (10)$$

$$\text{For oxidation: } X_{ox} = 1 - \frac{m_{ox} - m}{m_{ox} - m_{red}} \quad (11)$$

$m$  being the mass of sample at each time,  $m_{ox}$  is the mass of the sample fully oxidized and  $m_{red}$  is the mass of the sample in the reduced form. Oxygen generation rates  $r_{O_2}$  were calculated with Eq. (12) and are shown in Table 2

$$r_{O_2} = R_O \cdot \frac{dX_{red}}{dt} \quad (12)$$

$R_O$  being the oxygen transport capacity for the oxygen carrier particles (Eq. (9)).

The oxygen release rate of impregnated oxygen carriers was first investigated using  $\gamma$ - $Al_2O_3$ ,  $\alpha$ - $Al_2O_3$  and  $MgAl_2O_4$  support with different copper contents ranging from 15 to 33 wt.%. Fig. 6 shows the oxygen carrier conversion vs. time of impregnated oxygen carriers at 1000 °C and 100 vol.%  $N_2$ . The Cu-based oxygen carrier impregnated on  $\gamma$ - $Al_2O_3$  showed the lowest conversion during the reduction reaction and a decrease of the reactivity as the number of cycles increased. Similar patterns were found for oxidation reactions of this impregnated material. This behavior is related to the formation of a copper aluminate in the oxygen carrier, with low reactivity during  $CuAl_2O_4$  reduction. Thus, the formation of the copper aluminate produced a deactivation of the oxygen carrier for the CLOU process. Similar results were found for the materials prepared with  $\alpha$ - $Al_2O_3$  or with higher copper content, indicating that the copper content did not improve the oxygen use in the impregnated samples.

On the contrary, oxygen carrier impregnated on  $MgAl_2O_4$  showed the highest reactivity during the reduction reaction and did not present any deactivation with cycles due to the minimized interaction of CuO with the  $MgAl_2O_4$  support. The maximum conversion reached with this oxygen carrier was increased to 60%, and the reactivity, as  $r_{O_2}$ , was higher than for  $\gamma$ - $Al_2O_3$  and  $\alpha$ - $Al_2O_3$  (see Table 2). However, the oxygen transport capacity is only 0.9%. Higher values are desired for the CLOU process. Here, the oxygen transport capacity was defined as  $R_{OC} = R_O \cdot X_{max}$ ,  $X_{max}$  being the maximum conversion reached in TGA experiments. To increase the transport capacity, an oxygen carrier with higher CuO content was prepared by increasing the number of impregnations (Cu21MgAl\_I850). Similar results (regarding oxygen transport capacity) were found in this case. Therefore, to have an oxygen carrier with sufficient  $O_2$  transport capacity, a high number of impregnations steps should be carried out. To increase the copper content of the materials in a more direct manner, the mechanical mixing followed

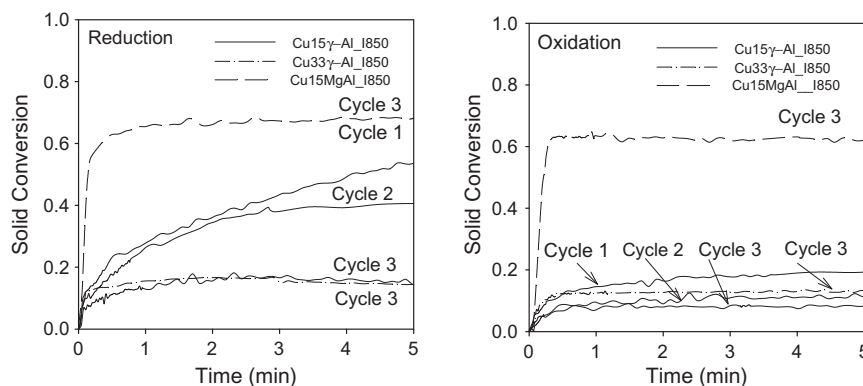


Fig. 6. Conversion vs. time curves from TGA tests of different oxygen carriers prepared by impregnation on different supports.  $T = 1000$  °C. Reduction: 100 vol.%  $N_2$ . Oxidation: air.

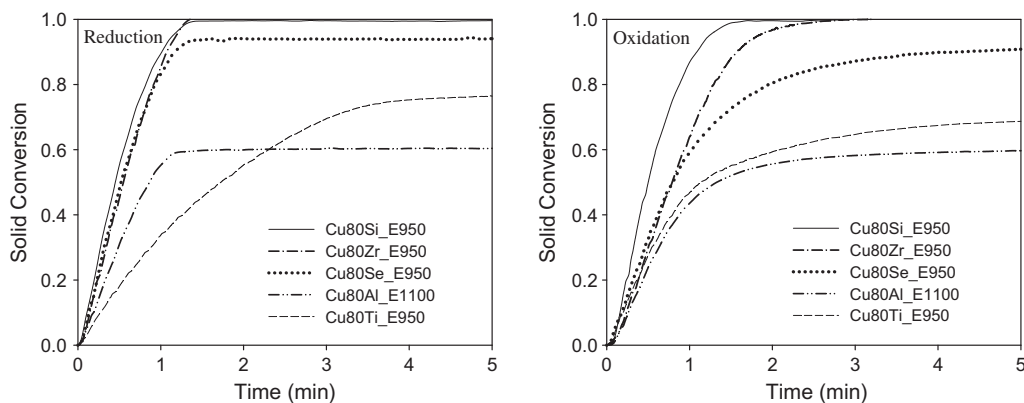


Fig. 7. Conversion vs. time curves for the third redox cycle from TGA tests of different oxygen carriers prepared by mechanical mixing followed by extrusion with different supports.  $T = 1000$  °C. Reduction: 100 vol.%  $N_2$ . Oxidation: air.

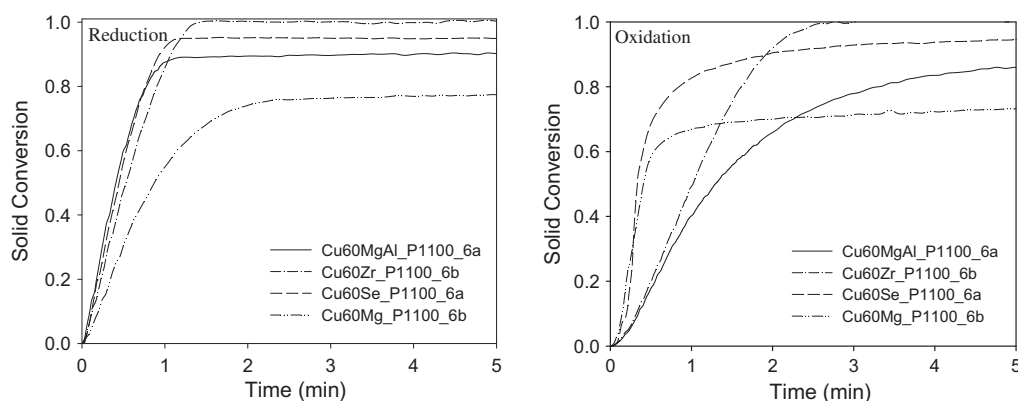


Fig. 8. Conversion vs. time curves for the third redox cycle from TGA tests of different oxygen carrier prepared by mechanical mixing followed by pelletizing by pressure.  $T = 1000$  °C. Reduction: 100 vol.%  $N_2$ . Oxidation: air.

by pelletizing by extrusion method was used for particle preparation.

Fig. 7 shows the reduction and oxidation reactivities of the samples prepared by the mechanical mixing followed by extrusion using different supports. Firstly, the oxygen carriers were prepared with 80 wt.% of copper content and were calcined at 950 °C, except oxygen carrier with  $Al_2O_3$  as support that were calcined at 1100 °C. As it can be seen, the results with the oxygen carriers prepared with this method depended on the support. Those prepared with  $ZrO_2$ , sepiolite, or  $SiO_2$  as support showed high oxygen generation rates and both reduction and oxidation reaction rates were stable with cycles. Oxygen carriers supported on alumina and  $TiO_2$  had lower reaction rates, both for reduction and oxidation reactions, and lower conversion values were reached.

For some samples agglomeration problems occurred in the TGA set-up. Oxygen carriers supported on  $Al_2O_3$ ,  $ZrO_2$  and  $TiO_2$  with high CuO contents (80 wt.%) agglomerated. For this reason, oxygen carriers with lower copper contents (60 or 40 wt.%) were also prepared and tested. Oxygen carrier prepared with  $TiO_2$  as support always agglomerated even with CuO contents of 40 wt.%. However, oxygen carriers with  $ZrO_2$  as support and 60 wt.% of CuO did not present any agglomeration in the TGA and showed high reduction and oxidation reactivities.

Cu-based oxygen carriers supported on  $MgAl_2O_4$ ,  $ZrO_2$ ,  $SiO_2$  and sepiolite were selected as a result of this preliminary reactivity screening, since they showed high reactivity and stability with the redox cycles. However, the mechanical strength of these oxygen carriers were too low to be used in a fluidized bed (values

above 1 N are recommended) [36]. As it can be seen in Table 2, low values (<1 N) of this parameter were measured for these samples. In order to increase the mechanical strength of the oxygen carriers another pelletizing method was used. Samples using  $MgAl_2O_4$ ,  $ZrO_2$ ,  $SiO_2$  and sepiolite as support were prepared by mechanical mixing followed by pelletizing by pressure with 60 wt.% of copper content. Also MgO as support was used with this method. Different graphite contents and calcination temperatures were analyzed to have oxygen carriers with high reaction rates and also high mechanical strength. In general, particles calcined at 950 °C showed low mechanical strength, whereas an increase in sintering temperature to 1300 °C caused the melting of particles. However, particles sintered at 1100 °C showed adequate mechanical strength to be used in a fluidized-bed. Nevertheless particles prepared with  $SiO_2$  and sintered at 1100 °C melted, so  $SiO_2$  was rejected as inert in this screening.

Fig. 8 shows the reduction reactivities of the samples prepared by the mechanical mixing followed by pelletizing by pressure. As can be seen, high reactivity was observed with these oxygen carriers. The oxygen generation rates determined with these materials are shown in Table 2. These reaction rates showed by these oxygen carriers for CLOU are in the same order as the rate of oxygen transference for highly reactive oxygen carriers developed for CLC [37–38]. Although the oxygen carrier prepared using MgO as support had high reduction and oxidation rates, full conversion was not reached, reducing in this way its oxygen transport capacity. This fact can be attributed to the deactivation of copper through the formation of  $Cu_2MgO_3$ , which was detected by XRD. Moreover, the

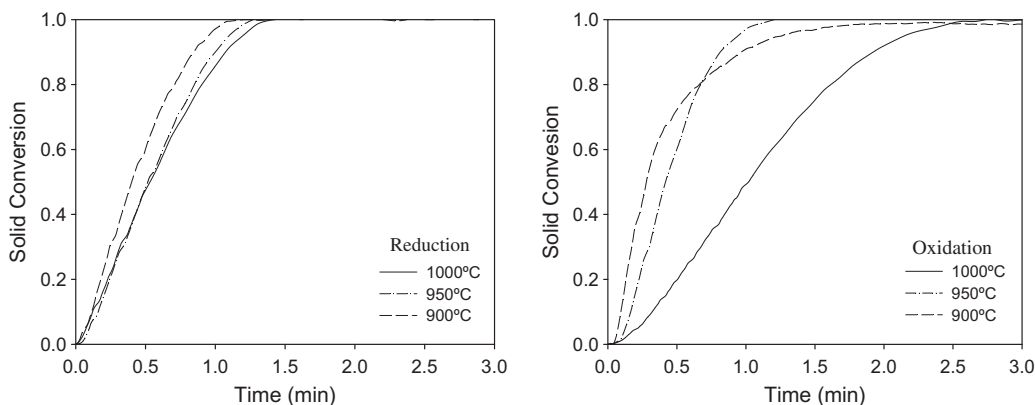


Fig. 9. Conversion vs. time curves for the third redox cycle at different reacting temperatures for Cu60Zr\_P1100a. Reduction: 100 vol.% N<sub>2</sub>. Oxidation: air.

oxidation reactions showed similar results as for reduction with these oxygen carriers.

The effect of reaction temperature on the reduction and oxidation reactivities was analyzed in the TGA with these materials. Fig. 9 shows the effect of temperature on the reduction and oxidation reaction for Cu60Zr\_P1100a oxygen carrier. Similar results were found with the other materials. As it can be seen, the reduction temperature hardly affected to the reduction reaction rate, reaching full solid conversion in less than 1 min for the different temperatures used. It must be pointed out that TGA reduction cycles were carried out using 100% N<sub>2</sub> and therefore O<sub>2</sub> release was not limited by the O<sub>2</sub> concentration equilibrium in the gas stream. On the contrary, the higher the oxidation temperature, the lower the oxidation reaction rate was. This result was due to the effect of the equilibrium oxygen concentration in the reduction reaction of CuO to Cu<sub>2</sub>O, which implies that the oxidation reaction rate is carried out with the driving force of the difference between the inlet oxygen concentration (21 vol.% in this case) and the oxygen concentration at equilibrium at that temperature. As it was shown in Fig. 2, at 1000 °C the oxygen concentration at equilibrium is 12.4 vol.%, and the oxygen concentration at equilibrium at 900 °C is only 1.5 vol.%. This fact will have important consequences on the operating temperatures needed for the combustion and regeneration reactions in the CLOU process.

The effect of the oxygen concentration on the oxidation reaction was also analyzed by TGA for materials prepared by pelletizing by pressure. Fig. 10 shows the effect of the oxygen concentration on the oxidation reaction rate for Cu60Zr\_P1100a oxygen carrier at 900 °C. As can be seen, the higher the oxygen concentration, the higher the oxidation reaction rate is. This fact is explained as the oxidation reaction is carried out with the driving force of the difference between the inlet oxygen concentration and the oxygen concentration at equilibrium (1.5 vol.% at 900 °C). Similar results were found with the other materials.

In view of these satisfactory results obtained in TGA with the oxygen carriers prepared by mechanical mixing followed by pelletizing by pressure, it was decided to prepare some batches of these oxygen carriers, to be used in the batch fluidized-bed reactor. Batches of 0.5 kg of the oxygen carriers with MgAl<sub>2</sub>O<sub>4</sub>, MgO, ZrO<sub>2</sub> and sepiolite as support were prepared.

### 3.2. Oxygen carrier behavior in batch fluidized bed

Reduction–oxidation multi-cycles were carried out in a fluidized-bed reactor to understand the oxygen release behavior of the oxygen carrier and the fluidization behavior of the material with respect to agglomeration phenomena and attrition rate.

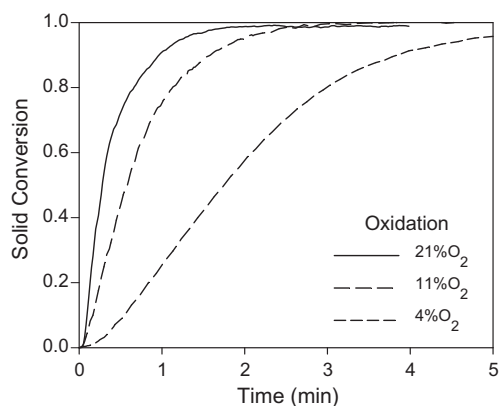


Fig. 10. Conversion vs. time curves for the third cycle at different reacting oxygen concentrations for Cu60Zr\_P1100a. T = 900 °C.

#### 3.2.1. Reduction and oxidation reactions

Several reduction–oxidation cycles using N<sub>2</sub> or CO<sub>2</sub> as fluidization media were carried out in this facility to determine the oxygen release behavior as a function of the operating conditions. The conversion of the oxygen carrier as a function of time was calculated from the oxygen outlet concentration by the equations:

$$\text{Reduction } X_{\text{red}} = \int_{t_0}^{t_{\text{red}}} \frac{Q_{\text{out}}}{n_0 P_{\text{tot}}} (P_{O_2, \text{out}}) dt \quad (13)$$

$$\text{Oxidation } X_{\text{oxi}} = \int_{t_0}^{t_{\text{oxi}}} \frac{Q_{\text{in}} \cdot P_{O_2, \text{in}} - Q_{\text{out}} \cdot P_{O_2, \text{out}}}{n_0 P_{\text{tot}}} dt \quad (14)$$

X being the conversion of the oxygen carrier,  $Q_{\text{in}}$  is the molar flow rate of the gas incoming to the reactor,  $Q_{\text{out}}$  is the molar flow rate of the gas leaving the reactor,  $P_{\text{tot}}$  is the total pressure,  $P_{O_2, \text{in}}$  is the partial pressure of O<sub>2</sub> incoming to the reactor,  $P_{O_2, \text{out}}$  is the partial pressure of O<sub>2</sub> exiting the reactor,  $n_0$  are the moles of molecular oxygen which can be released from fully oxidized oxygen carrier, and t is the time.

Fig. 11 shows the oxygen concentration measured at the outlet of the reactor and the bed temperature measured during a typical reduction and oxidation cycle at 1000 °C. The fluidizing medium was pure nitrogen during reduction and during oxidation the inlet oxygen concentration was 21 vol.% in nitrogen. At the beginning of the reduction period, a rapid oxygen release occurred close to the oxygen concentration equilibrium for the measured bed temperature. After 10 min, the outlet oxygen concentration fell near zero indicating an important decrease in the oxygen release rate. After

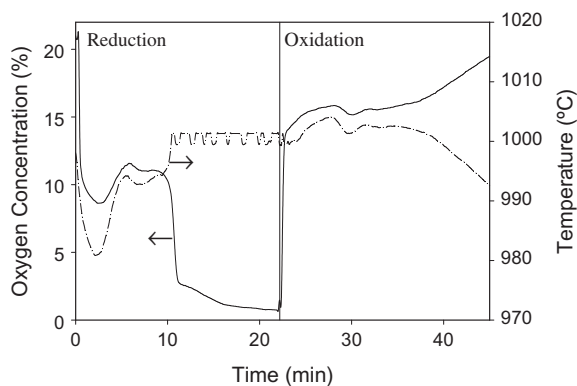


**Fig. 11.** Evolution with time of oxygen concentration and bed temperature during a typical reduction and oxidation cycle with Cu60MgAl\_P1100.  $T = 1000\text{ }^{\circ}\text{C}$ . Reduction: 100 vol.%  $\text{N}_2$ . Oxidation: air.

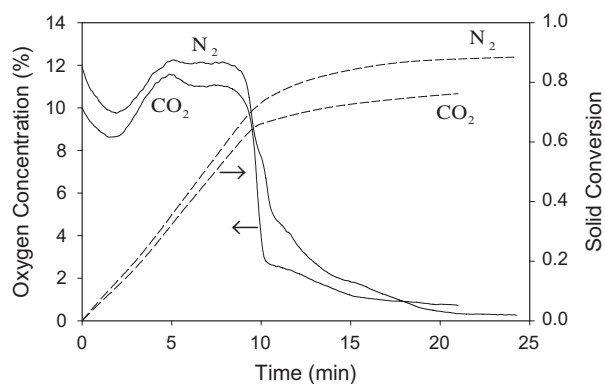


**Fig. 12.** Evolution of oxygen concentration with time and calculated solids conversions during a reduction period with Cu60MgAl\_P1100 using different fluidization gases.  $T = 1000\text{ }^{\circ}\text{C}$ .

20 min the oxidation started. The oxidation reaction took place at an oxygen concentration near the equilibrium oxygen concentration for this temperature. As can also be observed in Fig. 11, there are relevant temperature disturbances during the tests that can be explained by the heats of reduction and oxidation reactions. The set point temperature,  $1000\text{ }^{\circ}\text{C}$ , is defined as the fluidized-bed reactor temperature measured at the end of the oxidation period prior to the reduction period, when no reaction occurs. A temperature drop occurred due to the endothermic release of oxygen in the reduction reaction of CuO. Once the main part of the oxygen had been released, an increase in temperature occurred due to the gradually slower oxygen reduction reaction. When the oxidation began, a quick increase of temperature occurred due to the exothermic oxidation reaction.

In the CLOU process a carrier gas composed of recirculated  $\text{CO}_2$  is most likely used for the case of solid fuel combustion, as shown in Fig. 1. However, during oxygen carrier testing  $\text{N}_2$  is commonly used as a carrier gas [21,26]. The effect of fluidization gas was analyzed using pure nitrogen and pure  $\text{CO}_2$  as fluidization medium. Fig. 12 shows the evolution of the oxygen concentration with time and the calculated solids conversion during a reduction period with Cu60MgAl\_P1100 and using different fluidization gases ( $\text{N}_2$  or  $\text{CO}_2$ ) in a typical cycle at  $1000\text{ }^{\circ}\text{C}$ . As it can be seen, similar results were found independently of the gas used. Small differences in the profiles could be due to slight changes in the reaction temperature, probably due to the different heat capacity of these gases. For this reason, pure nitrogen was used as fluidization medium in the batch experiments.

The effect of reaction temperature in the batch fluidized bed was analyzed using 900, 950 and  $1000\text{ }^{\circ}\text{C}$  for the test. Fig. 13 shows oxygen concentration profiles and the solid conversion during a reduction period using different bed temperatures for two different oxygen carriers. The oxygen equilibrium concentration at each temperature is also shown. As can be seen in Fig. 13a, the oxygen carrier prepared using  $\text{MgAl}_2\text{O}_4$  as support gave oxygen concentration close to the equilibrium condition at each temperature. Thus, at all temperatures the oxygen release rate was limited by thermodynamic restrictions. At the lowest temperature, the solid decomposition is highly limited due to the low oxygen concentration at equilibrium and at the highest temperature ( $1000\text{ }^{\circ}\text{C}$ ), the solid reached a high conversion value in less than 15 min. These results of the effect of the reduction temperature are very different of those found by TGA. As was explained above, in the fluidized bed the  $\text{O}_2$  concentration equilibrium limits the  $\text{O}_2$  release rate since the gas flow has reached an  $\text{O}_2$  concentration close to the equilibrium one at each temperature, whereas the reaction rate in TGA was not limited by the equilibrium concentrations. Fig. 13b shows the solid conversion and oxygen concentration profiles during a reduction period with Cu60Zr\_P1100a using different bed temperatures. In this case, the oxygen concentration measured was much lower than the predicted by thermodynamics. These worse results are due to a defluidization of the bed, observed by a low pressure drop in the reactor. After extracting the solid from the reactor, the presence of agglomerated particles was confirmed.

The effect of the oxygen concentration in the oxidation reaction was analyzed using 21% and 10 vol.% of oxygen during oxidation at different temperatures. Fig. 14 shows the solid conversion and oxygen profile measured in a typical oxidation period of the Cu60MgAl\_P1100 oxygen carrier. An important effect of the oxygen concentration was found. The oxidation reaction rate was very low when the oxygen concentration in the gas flow was close to the oxygen concentration equilibrium, i.e. 9.5 vol.% at  $975\text{ }^{\circ}\text{C}$ , and thus the solid conversion after 20 min was very low. In these conditions, the oxidation of the solid was not completed. However, increasing the oxygen concentration to 21% and temperature to  $1010\text{ }^{\circ}\text{C}$  ( $\text{O}_2$  concentration at equilibrium = 14.5%), the regeneration of the oxygen carrier is almost completed in 25 min. Note that from TGA experiments, conversion of 90% was reached in less than 1 min (see Fig. 8) with air. Thus, although the oxygen carrier showed very high reactivity for the redox reactions, the higher time needed for complete conversion in batch fluidized-bed reactor experiments was due to the limitation in the oxygen flow supplied to the reactor. The equilibrium concentration was also reached during the oxidation period. These results confirmed those pointed out in the TGA analysis about the important dependency of the operating temperatures in the reduction and oxidation reactors for the successful development of the process.

### 3.2.2. Attrition and agglomeration behavior of oxygen carrier particles

The multi-cycle tests carried out in the fluidized bed were also useful to determine the fluidization behavior of the different oxygen carriers with respect to the attrition and agglomeration phenomena.

An important parameter for the selection of a suitable oxygen carrier material for the CLOU process is the agglomeration behavior during fluidization. Different behavior of the oxygen carriers with respect to these phenomena was found to depend on the CuO content and support used. Oxygen carriers prepared with MgO and sepiolite as inert resulted in formation of hard agglomerates and thus were rejected. Agglomeration took place during reduction to  $\text{Cu}_2\text{O}$  and made difficult the oxidation of the oxygen carrier. The test must be stopped due to the sticking of the particles causing defluidization and it was detected by an abrupt decrease of the bed pressure drop in the reactor. Oxygen carrier prepared with

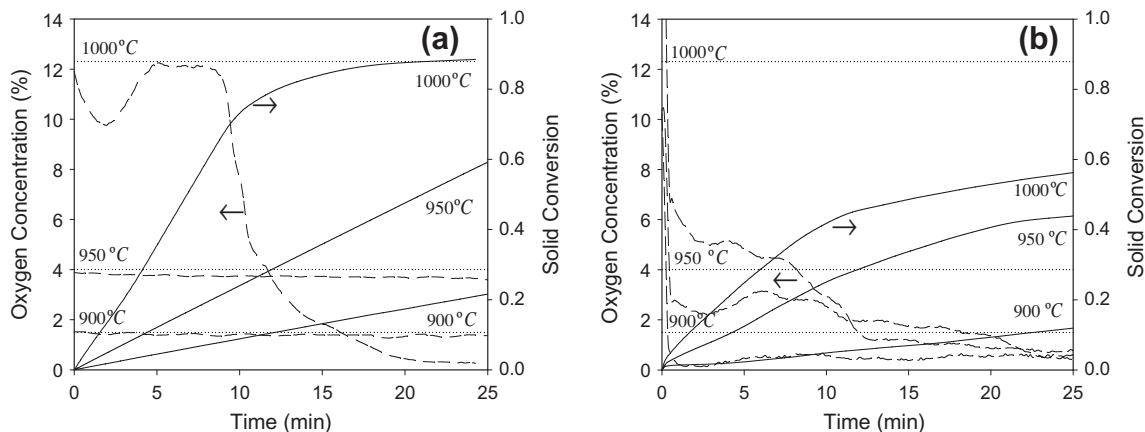


**Fig. 13.** Oxygen concentration and solid conversion profiles during a reduction period using different bed temperatures. (a) Cu60MgAl\_P1000; (b) Cu60Zr\_P1000a. (...) oxygen equilibrium concentration at each temperature.

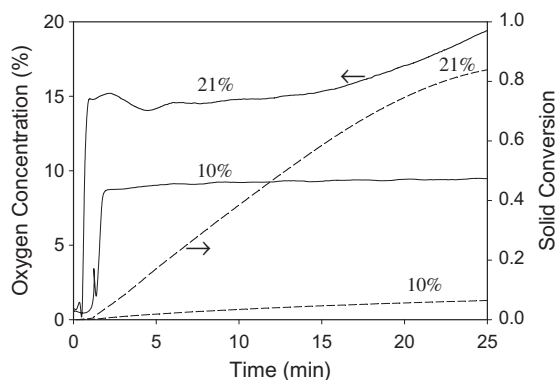


**Fig. 14.** Evolution of oxygen concentration with time and calculated solids conversions during an oxidation period with Cu60MgAl\_P1100 using different oxygen concentrations.  $[O_2]=10\%$  at  $T = 975^\circ\text{C}$ ,  $[O_2]=21\%$  at  $T = 1010^\circ\text{C}$ .

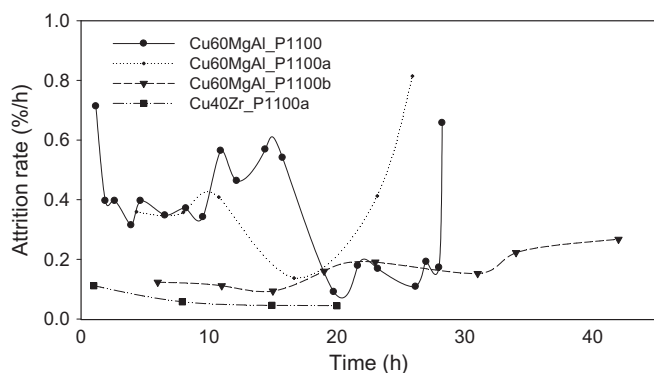


**Fig. 15.** Attrition rate of selected Cu-based oxygen carriers during multi-cycle operation in the fluidized bed. Temperature was varied in the range 900–1000 °C.

60 wt.% CuO and ZrO<sub>2</sub> as inert presented moderate agglomeration behavior, causing low oxygen release rate (see Fig. 13b). However, an oxygen carrier with 40 wt.% CuO and ZrO<sub>2</sub> as inert did not present agglomeration phenomena at any conditions. Similarly, carriers prepared using MgAl<sub>2</sub>O<sub>4</sub> as support with 60 wt.% of CuO did not present any agglomeration problem at any temperature.

Another important parameter for the selection of a suitable oxygen carrier material for the CLOU process is the attrition behavior during fluidization. The attrition rate of the oxygen carrier was

evaluated as the weight of particles elutriated from the bed recovered in the filters with a  $d_p < 40\ \mu\text{m}$  during a measured time, corresponding to several reduction–oxidation cycles. Fig. 15 shows the attrition rates for the different oxygen carriers as a function of time. As it can be seen, the attrition rate in the case of Cu40Zr\_1100 was very low and stable during more than 20 h. A value of 0.045%/h, which corresponds to a particle lifetime of 2220 h, was measured. The attrition rate for Cu60MgAl\_P1100 was high and unstable after 25 h of operation. In order to decrease the attrition rate of this material, two different oxygen carriers were prepared with higher mechanical strength. Firstly, particles with lower porosity were prepared by decreasing the graphite content (Cu60MgAl\_P1100a). As can be seen, the oxygen carrier presented similar behavior to previous oxygen carrier (Cu60MgAl\_P1100). Further, the mechanical strength of particles was increased by increasing the sintering time to 12 h (Cu60MgAl\_P1100b). The attrition rate of this material was now stable during more than 40 h, although with a relatively high value (0.2%/h), which corresponds to a particle lifetime of 500 h.

### 3.3. Characterization of CLOU materials

A physical and chemical characterization was carried out, both for fresh and used particles in the batch fluidized bed. In addition, the CuO content of fine particles elutriated from the fluidized-bed reactor was determined by reduction with 15 vol.% H<sub>2</sub> at 800 °C in TGA. Table 3 shows the characterization results of the different oxygen carriers. All samples had low initial porosity and surface area due to the preparation method used. The surface area was lower than 0.5 m<sup>2</sup>/g in all cases. However, the reactivity of these samples was high.

The crystallite phases found by XRD analysis of the oxygen carriers prepared using MgAl<sub>2</sub>O<sub>4</sub> and ZrO<sub>2</sub> as supports were mainly CuO and the corresponding support. New compounds were not detected in any of the samples after being used, even for the monoclinic phase of the ZrO<sub>2</sub>. Thus, interaction of the CuO with the corresponding support was neither found, indicating the stability of the material. In addition, the chemical stability was analyzed by comparing reactivity of fresh and used particles. The oxygen release rate ( $r_{O_2}$ ) determined from TGA experiments was not affected by the cycle number.

The mechanical strength of the used samples was, in the majority cases, similar to the fresh ones, excepting for Cu60MgAl\_P1100 particles. These particles have an initial low value for mechanical strength, which correspond to high attrition values, but it was further decreased after 30 h of operation. Changes both in porosity

**Table 3**  
Characterization of the fresh and after-used oxygen carrier particles.

Oxygen carrier	Time being fluidized (h)	Porosity (%)		Mechanical strength (N)		Crystallite phases	
		Fresh	Used	Fresh	Used	Fresh	Used
Cu60MgAl_P1100	28	13.0	26.4	$1.2 \pm 0.3$	$0.6 \pm 0.3$	CuO, MgAl <sub>2</sub> O <sub>4</sub>	CuO, MgAl <sub>2</sub> O <sub>4</sub>
Cu60MgAl_P1100a	25	11.2	22.5	$1.7 \pm 0.3$	$1.6 \pm 0.4$	CuO, MgAl <sub>2</sub> O <sub>4</sub>	CuO, MgAl <sub>2</sub> O <sub>4</sub>
Cu60MgAl_P1100b	42	10.5	30.0	$2.2 \pm 0.3$	$2.0 \pm 0.4$	CuO, MgAl <sub>2</sub> O <sub>4</sub>	CuO, MgAl <sub>2</sub> O <sub>4</sub>
Cu60Zr_P1100	10	7.9	9.1	$3.0 \pm 0.5$	$2.6 \pm 0.5$	CuO, ZrO <sub>2</sub> (M)	CuO, ZrO <sub>2</sub> (M)
Cu40Zr_P1100	15	9.0	12.1	$4.0 \pm 0.4$	$4.2 \pm 0.4$	CuO, ZrO <sub>2</sub> (M)	CuO, ZrO <sub>2</sub> (M)

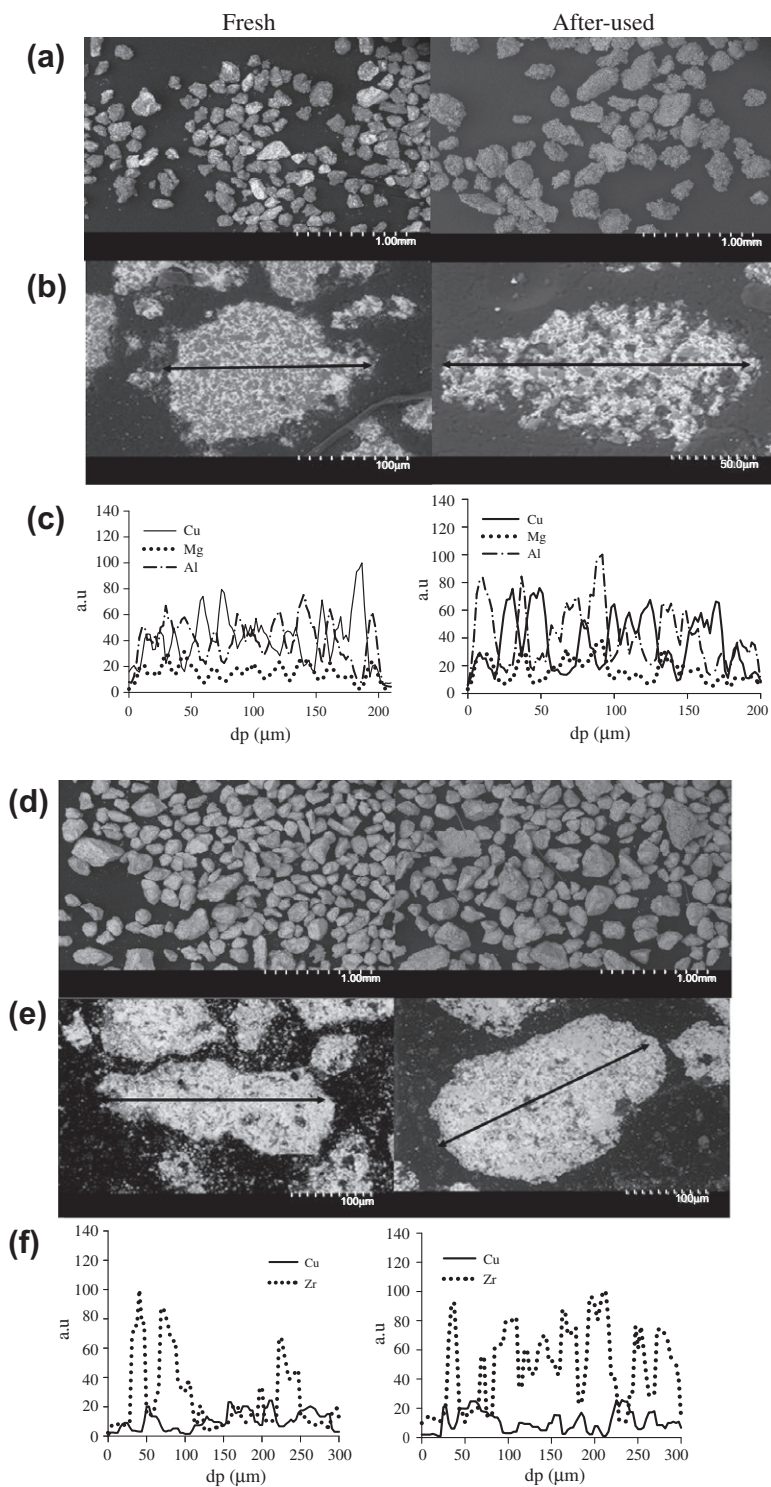


**Fig. 16.** SEM images and EDX analysis of Cu60MgAl\_P1100b (a–c) and Cu40Zr\_P1100 (d–f) particles both fresh (left) and after used (right). General view of the particles (a and d) and image of a cross section of a particle (b and e). EDX line profiles of Cu, Al, Mg and Zr (c and f) in a cross section of a particle.



and mechanical strength were low for particles prepared with  $ZrO_2$ . However, for particles prepared with  $MgAl_2O_4$  as inert material an important increase of particle porosity after cycles was found. The surface area remained low in all cases.

For the material Cu60MgAl\_P1100 with an initial low mechanical strength, the attrited fines contained mainly  $MgAl_2O_4$  during the initial 10 h. Only during the last period, oxygen carrier started losing CuO. For other materials, the compositions of attrited fines were similar to the composition of fresh particles.

Fig. 16 shows an example of the SEM–EDX analysis carried out with the different samples. SEM image of the particles show an irregular shape due to the milling process required in the preparation method (see Fig. 16a and d). The general appearance of the used particles using  $ZrO_2$  as inert was similar to the fresh particles (see Fig. 16e). No important changes in the surface texture were detected and the solid structure was maintained. On the contrary, the increase in the porosity of oxygen carriers prepared with  $MgAl_2O_4$  as support can be clearly seen in the SEM image of cross section of a particle (see Fig. 16b). The copper distribution inside the particles was also analyzed by EDX in some cut and polished particles. It was found in fresh particles for both oxygen carriers a uniform distribution of copper existed through the particles. Moreover there was not evidence of redistribution or migration during the redox cycles for both materials.

These results indicated that oxygen carriers prepared with a 40 wt.% of CuO and  $ZrO_2$  as support and 60 wt.% of CuO and  $MgAl_2O_4$  as support had satisfactory results both regarding reactivity, attrition and agglomeration behavior during repeated redox cycles, properties required for the CLOU process.

#### 4. Conclusions

The potential of different Cu-based oxygen carriers for the Chemical-Looping with Oxygen Uncoupling (CLOU) process was determined through thermogravimetric analysis and batch fluidized bed testing. Materials prepared using three different methods (incipient wet impregnation, mechanical mixing following by extrusion and mechanical mixing following by pelletizing by pressure), supports ( $\gamma-Al_2O_3$ ,  $\alpha-Al_2O_3$ ,  $MgAl_2O_4$ , sepiolite,  $SiO_2$ ,  $TiO_2$ ,  $MgO$  and  $ZrO_2$ ) and different CuO fractions from 15 to 80 wt.% were characterized.

Oxygen carriers prepared by impregnation on  $Al_2O_3$  were rejected due to their low reactivity which decreased with the cycles.

Particles prepared by mechanical mixing following by pelletizing using  $Al_2O_3$ ,  $MgAl_2O_4$ ,  $MgO$ ,  $SiO_2$ , sepiolite and  $ZrO_2$  with 80 wt.% CuO showed high reactivity but low mechanical strength if extrusion was used. However mechanical strength increased when pelletizing by pressure was used.

Highly resistant particles were obtained by mechanical mixing followed by pelletizing by pressure using  $MgAl_2O_4$ ,  $ZrO_2$ , sepiolite and  $MgO$ . Oxygen carriers prepared with 60 wt.% CuO content and these supports showed high reaction rates both for oxygen release and oxidation reactions.

Agglomeration and attrition behavior of the oxygen carriers prepared by pelletizing depended on the support used. Materials prepared with  $MgAl_2O_4$  as inert and 60 wt.% of CuO and 40 wt.% CuO and  $ZrO_2$  as inert did not present any agglomeration problem at any temperature. Oxygen carriers prepared with  $MgO$  and sepiolite as inerts were rejected due to agglomeration problems. The attrition rate measured for the oxygen carrier prepared using  $ZrO_2$  as support was very low and stable (0.045%/h). The oxygen carrier prepared using  $MgAl_2O_4$  as inert had a stable attrition rate (0.2%/h), during more than 40 h of redox cycling.

Experiments in batch fluidized bed show that the oxygen release rate is nearly constant at each temperature and it was limited

because oxygen concentration reached the thermodynamic equilibrium. A negligible effect of the fluidization gas ( $CO_2$  or  $N_2$ ) was found during oxygen carrier decomposition. Moreover, an important effect of the oxygen concentration in the gas flow was found in the oxidation reaction.

The results indicated that oxygen carriers prepared with a 40 wt.% of CuO and  $ZrO_2$  as support and 60 wt.% of CuO with  $MgAl_2O_4$  have satisfactory results both regarding reactivity and fluidization behavior, properties required for the CLOU process.

#### Acknowledgments

This work was partially supported by the European Commission, under the RFCS program (ECLAIR Project, Contract RFCP-CT-2008-0008), ALSTOM Power Boilers (France) and by the Spanish Ministry of Science and Innovation (PN, ENE2010-19550). I. Adánez-Rubio thanks CSIC for the JAE fellowship.

#### References

- [1] IPCC. Mitigation of climate change. Contribution of working group III to the fourth assessment report of the Intergovernmental panel on climate change. Cambridge, UK: Cambridge University Press; 2008. <<http://www.ipcc.ch>>.
- [2] Kerr HR. Capture and separation technology gaps and priority research needs. Carbon dioxide capture for storage in deep geologic formations. Amsterdam: Elsevier Science; 2005. p. 655–60.
- [3] Kvamsdal HM, Jordal K, Bolland O. A quantitative comparison of gas turbine cycles with  $CO_2$  capture. Energy 2007;32(1):10–24.
- [4] Kolbitsch P, Bolhär-Nordenkamp J, Pröll T, Hofbauer H. Comparison of two Ni-based oxygen carriers for chemical looping combustion of natural gas in 140 kW continuous looping operation. Ind Eng Chem Res 2009;48(11):42–7.
- [5] Linderholm C, Mattisson T, Lyngfelt A. Long-term integrity testing of spray-dried particles in a 10 kW chemical-looping combustor using natural gas as fuel. Fuel 2009;88:2083–96.
- [6] Adánez J, Gayán P, Celaya J, de Diego LF, García-Labiano F, Abad A. Chemical looping combustion in a 10 kW<sub>th</sub> prototype using a CuO/ $Al_2O_3$  oxygen carrier: effect of operating conditions on methane combustion. Ind Eng Chem Res 2006;45(17):75–80.
- [7] Lyngfelt A, Thunman H. Construction and 100 h of operational experience of a 10-kW chemical-looping combustor. In: Thomas DC, Benson SM, editors. Carbon dioxide capture for storage in deep geologic formations – results from the  $CO_2$  capture project, vol. 1. Oxford, UK: Elsevier; 2005 [Chapter 36].
- [8] Pröll T, Mayer K, Bolhär-Nordenkamp J, Kolbitsch P, Mattisson T, Lyngfelt A, et al. Natural minerals as oxygen carriers for chemical looping combustion in a dual circulating fluidized bed system. Energy Procedia 2009;1:27–34.
- [9] Adánez J, Abad A, García-Labiano F, Gayán P, de Diego LF. Progress in chemical-looping combustion and reforming technologies. Prog Energy Combust Sci 2012;38:215–82.
- [10] Brown TA, Dennis JS, Scott SA, Davidson JF, Hayhurst AN. Gasification and chemical looping combustion of a lignite char in a fluidized bed of iron oxide. Energy Fuels 2010;24:3034–48.
- [11] Cao Y, Pan WP. Investigation of chemical looping combustion by solid fuels. 1. Process analysis. Energy Fuel 2006;20:57–68.
- [12] Berguerand N, Lyngfelt A. Design and operation of a 10 kW<sub>th</sub> chemical-looping combustor for solid fuels – testing with South African coal. Fuel 2008;87:2713–26.
- [13] Berguerand N, Lyngfelt A. Chemical-Looping combustion of petroleum coke using ilmenite in a 10 kW<sub>th</sub> unit-high-temperature operation. Energy Fuel 2009;23:57–68.
- [14] Leion H, Lyngfelt A, Johansson M, Jerndal E, Mattisson T. The use of ilmenite as an oxygen carrier in chemical-looping combustion. Chem Eng Res Des 2008;86:1017–26.
- [15] Leion H, Mattisson T, Lyngfelt A. Use of ores and industrial products as oxygen carriers in chemical-looping combustion. Energy Fuels 2009;23:2307–15.
- [16] Shen L, Wu J, Xiao J, Song Q, Xiao R. Chemical-looping combustion of biomass in a 10 kW reactor with iron oxide as an oxygen carrier. Energy Fuels 2009;23:2498–505.
- [17] Wang J, Anthony EJ. Clean combustion of solid fuels. Appl Energy 2008;85:73–9.
- [18] Lyngfelt A, Mattisson T. Three stages combustion for  $CO_2$  capture. Patent SE200500249; 2006 [in Swedish].
- [19] Mattisson T, Lyngfelt A, Leion H. Chemical-looping oxygen uncoupling for combustion of solid fuels. Int J Greenhouse Gas Control 2009;3:11–9.
- [20] Eyring E, Konya G, Lighty JA, Sahir A, Sarofim A, Whitty K. Chemical looping with copper oxide as carrier and coal as fuel. In: Proceedings of 1st international conference on chemical looping; 2010, Lyon, France.
- [21] Shulman A, Cleverstam E, Mattisson T, Lyngfelt A. Manganese/iron, manganese/nickel, and manganese/silicon oxides used in chemical-looping with oxygen uncoupling (CLOU) for combustion of methane. Energy Fuel 2009;23:69–75.

- [22] Azimi G, Leion H, Mattisson T, Lyngfelt A. Chemical-looping with oxygen uncoupling using combined Mn–Fe oxides, testing in batch fluidized bed. *Energy Procedia* 2011;4:370–7.
- [23] Rydén M, Lyngfelt A, Mattisson T. Combined manganese/iron oxides as oxygen carrier for chemical-looping combustion with oxygen uncoupling (CLOU) in a circulating fluidized bed reactor system. *Energy Procedia* 2011;4:341–8.
- [24] Leion H, Larring Y, Bakken E, Bredesen R, Mattisson T, Lyngfelt A. Use of  $\text{CaMn}_{0.875}\text{Ti}_{0.125}\text{O}_3$  as oxygen carrier in chemical-looping with oxygen uncoupling. *Energy Fuel* 2009;23:76–83.
- [25] Rydén M, Lyngfelt A, Mattisson T.  $\text{CaMn}_{0.875}\text{Ti}_{0.125}\text{O}_3$  as oxygen carrier for chemical-looping with oxygen uncoupling (CLOU) – experiments in a continuously operating fluidized-bed reactor system. *Int J Greenhouse Gas Control* 2010;5:356–66.
- [26] Mattisson T, Leion H, Lyngfelt A. Chemical-looping with oxygen uncoupling using  $\text{CuO/ZrO}_2$  with petroleum coke. *Fuel* 2009;88:683–90.
- [27] HSC Chemistry 6.1. Chemical reaction and equilibrium software with thermochemical database and simulation module. Outotec Research Oy; 2008.
- [28] Jacob KT, Alcock CB. Thermodynamics of  $\text{CuAlO}_2$  and  $\text{CuAl}_2\text{O}_4$  and Phase equilibria in the system  $\text{Cu}_2\text{O–CuO–Al}_2\text{O}_3$ . *J Am Ceram Soc* 1975;58:192–5.
- [29] Adánez J, de Diego LF, García-Labiano F, Gayán P, Abad A, Palacios JM. Selection of oxygen carriers for chemical-looping combustion. *Energy Fuels* 2004;18(2):71–7.
- [30] de Diego LF, García-Labiano F, Adánez J, Gayán P, Abad A, Corbella BM, et al. Development of Cu-based oxygen carriers for chemical-looping combustion. *Fuel* 2004;83(13):49–57.
- [31] de Diego LF, Gayán P, García-Labiano F, Celaya J, Abad A, Adánez J. Impregnated  $\text{CuO/Al}_2\text{O}_3$  oxygen carriers for chemical-looping combustion: avoiding fluidized bed agglomeration. *Energy Fuels* 2005;19(5):1850–6.
- [32] Forero CR, Gayán P, de Diego LF, Abad A, García-Labiano F, Adánez J. Syngas combustion in a 500 W<sub>th</sub> chemical-looping combustion system using an impregnated Cu-based oxygen carrier. *Fuel Process Technol* 2009;90(12):71–9.
- [33] Forero CR, Gayán P, García-Labiano F, de Diego LF, Abad A, Adánez J. Effect of gas composition in chemical-looping combustion with copper-based oxygen carriers: fate of sulphur. *Int J Greenhouse Gas Control* 2010;4(5):62–70.
- [34] Gayán P, Forero CR, de Diego LF, Abad A, García-Labiano F, Adánez J. Effect of gas composition in chemical-looping combustion with copper-based oxygen carriers: fate of light hydrocarbons. *Int J Greenhouse Gas Control* 2010;4(1):13–22.
- [35] Adánez-Rubio I, Gayán P, García-Labiano F, de Diego LF, Adánez J, Abad A. Development of CuO-based oxygen-carrier materials suitable for chemical-looping with oxygen uncoupling (CLOU) process. *Energy Procedia* 2011;4:417–24.
- [36] Johansson M, Mattisson T, Lyngfelt A. Investigation of  $\text{Fe}_2\text{O}_3$  with  $\text{MgAl}_2\text{O}_4$  for chemical-looping combustion. *Ind Eng Chem Res* 2004;43:6978–87.
- [37] Johansson M, Mattisson T, Lyngfelt A. Comparison of oxygen carriers for chemical-looping combustion. *Thermal Sci* 2006;10:93–107.
- [38] Gayán P, de Diego LF, García-Labiano F, Adánez J, Abad A, Dueso C. Effect of support on reactivity and selectivity of Ni-based oxygen carriers for chemical-looping combustion. *Fuel* 2008;87:2641–50.



## **Paper II**



# Evaluation of a Spray-Dried CuO/MgAl<sub>2</sub>O<sub>4</sub> Oxygen Carrier for the Chemical Looping with Oxygen Uncoupling Process

Iñaki Adánez-Rubio, Pilar Gayán,\* Alberto Abad, Luis F. de Diego, Francisco García-Labiano, and Juan Adánez

Department of Energy and Environment, Instituto de Carboquímica (ICB), Consejo Superior de Investigaciones Científicas (CSIC), Miguel Luesma Castán, 4, Zaragoza 50018, Spain

**ABSTRACT:** The chemical looping with oxygen uncoupling (CLOU) process is a chemical looping combustion (CLC) technology that allows for the combustion of solid fuels with inherent CO<sub>2</sub> separation. As in CLC technology, in the CLOU process, the oxygen necessary for fuel combustion is supplied by a solid oxygen carrier, which is moving between two reactors: the fuel and air reactors. The CLOU technology uses the property of some metal oxides (CuO, Mn<sub>2</sub>O<sub>3</sub>, and Co<sub>3</sub>O<sub>4</sub>), which can generate gaseous oxygen at high temperatures. The oxygen generated by the oxygen carrier reacts directly with the solid fuel, which is mixed with the oxygen carrier in the fuel reactor. The reduced oxygen carrier is transported to the air reactor, where it is oxidized by air. In this work, a material prepared by spray drying containing 60 wt % CuO and 40 wt % MgAl<sub>2</sub>O<sub>4</sub> as supporting material was evaluated as an oxygen carrier for the CLOU process using different installations. First, the oxygen release rate and the fluidization behavior, with regard to the agglomeration and attrition rate, were analyzed in a thermogravimetric analyzer (TGA) and in a batch fluidized bed, respectively. Then, the effects of the main operating conditions, such as the temperature, solids flow rate, and gas velocity in the fuel reactor, on the oxygen-carrier capability to release gaseous oxygen were analyzed in a continuous CLOU unit using N<sub>2</sub> and CO<sub>2</sub> as fluidization media. In addition, the effect of the oxygen concentration in the air reactor on the capability of the oxygen carrier to be regenerated was evaluated. The results obtained showed that this oxygen carrier has suitable characteristics for the CLOU process. Nevertheless, after 40 h of continuous operation at high temperatures, the particle integrity decreased significantly, indicating the need to improve the lifetime of this kind of material for use in an industrial CLOU process.

## 1. INTRODUCTION

To stabilize the CO<sub>2</sub> concentration in the atmosphere, several measures must be taken. Among them, the carbon capture and storage (CCS) would contribute 15–55% to the cumulative mitigation effort worldwide until 2100.<sup>1</sup> The CCS is a process involving the separation of CO<sub>2</sub> emitted by industry and energy-related sources and then storage of it for a long period of time. The chemical looping combustion (CLC) process has been suggested among the best alternatives to reduce the economic cost of CO<sub>2</sub> capture in power plants<sup>2</sup> and to increase the efficiency with respect to other CO<sub>2</sub> capture processes.<sup>3</sup> In this process, CO<sub>2</sub> is inherently separated from other combustion products, N<sub>2</sub> and unused O<sub>2</sub>, through the use of a solid oxygen carrier, and thus, no energy is expended for the separation. The CLC process has been demonstrated for gaseous fuel combustion, such as natural gas and syngas, in 10–140 kW<sub>th</sub> units using oxygen-carrier materials based on Ni,<sup>4,5</sup> Cu,<sup>6,7</sup> or Fe.<sup>8,9</sup> A huge number of oxygen carriers have been proposed for CLC with gaseous fuels, which have been reviewed by Adánez et al.<sup>10</sup> Because solid fuels are considerably more abundant and less expensive than natural gas, it would be highly advantageous if the CLC process could be adapted for these types of fuels. The first option to use solid fuels in a CLC process was to use syngas in the fuel reactor coming from a previous gasifying stage. In this technology, experience gained in the development of CLC for syngas can be useful,<sup>11,12</sup> but it is necessary to use pure oxygen for the gasification of the solid fuel, causing an important energy penalty because of oxygen

separation from air. The second option of development is the CLC with solids fuels, where the solid fuel is directly introduced to the fuel reactor. Devolatilization of coal particles happen in the CLC system, and the remaining char must be gasified. Thus, a gasification agent, e.g., H<sub>2</sub>O or CO<sub>2</sub>, must be used as the fluidization gas. The oxygen carrier reacts with volatiles and the gas product of coal gasification. Because of the slow gasification reaction rate, the residence time of char particles must be high in the gasification step to have high CO<sub>2</sub> capture efficiencies.<sup>13,14</sup> To increase the gasification rate, temperatures higher than 1000 °C have been proposed.<sup>14</sup> Because a partial loss of the oxygen carrier is expected in the purge stream of ash, low-cost and environmental friendly materials are preferred in this CLC option, e.g., natural minerals or industrial/waste products.<sup>15–19</sup>

To overcome the low reactivity of the char gasification stage in the direct solid-fueled CLC, an alternative process was very recently proposed.<sup>20</sup> The chemical looping with oxygen uncoupling (CLOU) process is based on the strategy of using oxygen carriers that release gaseous oxygen at high temperatures, thereby allowing the solid fuel to burn with gas-phase oxygen. In this way, the slow gasification step of the direct solid-fueled CLC is avoided, giving a much faster solid conversion.<sup>20–22</sup>

Received: February 8, 2012

Revised: April 2, 2012

Published: April 12, 2012

Figure 1 shows a schematic diagram of a CLOU system. As proposed by Mattisson et al.,<sup>20</sup> the CLOU process is composed

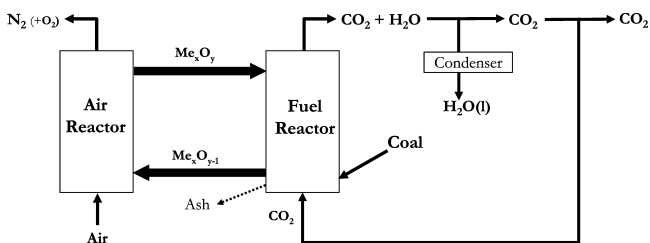
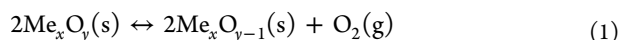
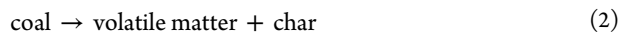


Figure 1. Schematic diagram of the CLOU process for solid fuels.

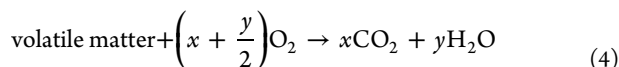
of two interconnected fluidized-bed reactors: the fuel reactor and the air reactor. In the fuel reactor, CO<sub>2</sub> and steam are produced by different reactions. First, the oxygen carrier releases oxygen according to



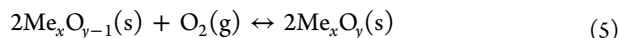
and the solid fuel begins devolatilization, producing a solid residue (char) and volatile matter as gas products.



Then, char and volatiles are burnt as in usual combustion according to reactions 3 and 4.



In the air reactor, the oxygen carrier is regenerated by oxygen from the air, following the next reaction.



After steam condensation, a pure CO<sub>2</sub> stream can be obtained. In the CLOU process, the fluidization gas can be recycled CO<sub>2</sub>. In this way, the steam duty of the plant for the gasification step and energy penalties related are reduced. The reduced oxygen carrier (Me<sub>x</sub>O<sub>y-1</sub>) is transported to the air reactor, where the oxygen carrier is regenerated to the initial oxidation stage with oxygen of the air according to reaction 5, and ready for a new cycle. The exit stream of the air reactor contains only N<sub>2</sub> and unreacted O<sub>2</sub>. Therefore, the CLOU process has a low-energy penalty for CO<sub>2</sub> separation, and low CO<sub>2</sub> capture costs are expected. The heat release over the fuel and air reactors is the same as for conventional combustion.

Thus, metal oxides used in oxygen carriers for CLOU must evolve gaseous oxygen at high temperatures. Besides, this O<sub>2</sub> release must be reversible to oxidize the oxygen carrier in the air reactor. Thus, a special requirement is needed for the oxygen carrier to be used in the CLOU process in comparison to oxygen carriers for normal CLC, where the fuel must be able to react directly with the oxygen carrier without any release of gas-phase oxygen. Only those metal oxides that have a suitable equilibrium partial pressure of oxygen at temperatures of interest for combustion (800–1200 °C) can be used as CLOU oxygen carriers. The possible metal oxides that have the property of release oxygen are limited: CuO, Mn<sub>2</sub>O<sub>3</sub>, and Co<sub>3</sub>O<sub>4</sub>.<sup>20</sup> Copper has the highest oxygen transport capacity (10 g of O<sub>2</sub>/100 g of CuO compared to 3 g of O<sub>2</sub>/100 g of Mn<sub>2</sub>O<sub>3</sub> and 6 g of O<sub>2</sub>/100 g of Co<sub>3</sub>O<sub>4</sub>). Moreover, for the CuO/Cu<sub>2</sub>O system, the reaction with C is exothermic in the fuel reactor, as

shown in reaction 6, which can be advantageous for the heat balance of the CLOU system.

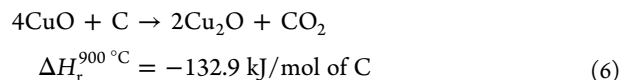


Figure 2 shows the partial pressure of oxygen as a function of the temperature for the CuO/Cu<sub>2</sub>O system, calculated using

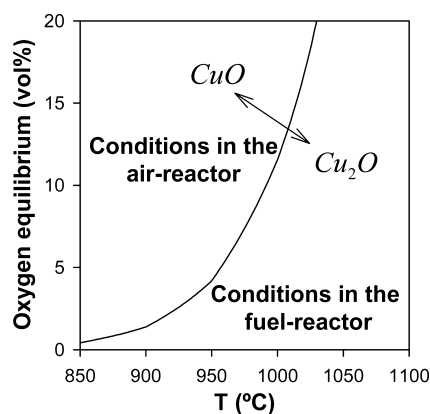


Figure 2. Equilibrium oxygen concentrations over the CuO/Cu<sub>2</sub>O system as a function of the temperature.

HSC software.<sup>23</sup> The oxygen concentration at equilibrium conditions greatly depends upon the temperature. It is clear from this figure that the air- and fuel-reactor temperatures in the process must be adjusted to the thermodynamic equilibrium of the system. On the one hand, the metal oxide is stable in the air reactor below 950 °C if the maximum oxygen concentration from the air reactor is 4.5 vol %. A higher temperature must be avoided in the air reactor if high use of oxygen in the air is desirable. On the other hand, it would be desirable to have a low oxygen concentration at the exit of the fuel reactor to obtain a high-purity CO<sub>2</sub> stream. However, in a previous work,<sup>22</sup> it was found that an oxygen concentration in the fuel-reactor outlet close to the thermodynamic equilibrium was necessary to avoid unburnt compounds. An equilibrium concentration of 1.5 vol % O<sub>2</sub> can be reached in the fuel reactor at 900 °C for the CuO/Cu<sub>2</sub>O system, whereas the equilibrium concentration increases up to 12.4 vol % at 1000 °C. Therefore, it could be advantageous to operate the fuel reactor at lower temperatures than the air-reactor temperatures, if the oxygen-carrier reactivity is high enough for full combustion.

Mattisson et al.<sup>20,21</sup> developed oxygen carriers with 60 and 40 wt % CuO. Cyclic testing with solid fuels verified that oxygen was released close to the equilibrium pressure in the temperature range of 880–985 °C, and the material could also be regenerated close to equilibrium. When solid fuel particles were added to a bed of oxygen-carrier particles, a very rapid release of oxygen and combustion of fuel started. Thus, the conversion rate of the fuel could be increased by almost 2 orders of magnitude compared to coal gasification in a CLC system with steam.<sup>21</sup> Although no permanent agglomeration was detected, some defluidization phenomena were reported.

On the basis of previous experience<sup>24–26</sup> on the development of Cu-based materials for the CLC process, an analysis about the suitability of several Cu-based materials was carried out at ICB, CSIC.<sup>27,28</sup> Particles prepared by several methods with different supports and metal oxide contents were tested in a

thermogravimetric analyzer (TGA) and batch fluidized bed. Impregnated particles on  $\text{Al}_2\text{O}_3$  were suitable for CLC but not for CLOU because they lost the oxygen release property when  $\text{CuAl}_2\text{O}_4$  is formed. It was found that particles with 60 wt % CuO and using  $\text{MgAl}_2\text{O}_4$  as the supporting material prepared by mechanical mixing were adequate for use as an oxygen carrier for the CLOU process. This material showed high reactivity and oxygen transport capacity and suitable attrition resistance and does not have a tendency to agglomerate during operation in a batch fluidized-bed reactor.

After the screening tests, a batch of 60 wt % CuO supported on  $\text{MgAl}_2\text{O}_4$  was prepared by spray drying (Cu60MgAl). The proof of the concept of the CLOU process was demonstrated using this material as an oxygen carrier,<sup>29</sup> burning coal in a 1.5 kW<sub>th</sub> continuously operated unit consisting of two interconnected fluidized-bed reactors. The effects of the fuel-reactor temperature, coal feeding rate, and solids circulation flow rate on the combustion and  $\text{CO}_2$  capture efficiencies were investigated. Fast reaction rates of oxygen generation were observed with the oxygen carrier, and full combustion of coal was attained in the plant using a solids inventory of  $\approx 235$  kg/MW<sub>th</sub> in the fuel reactor. In addition, values close to 100% in carbon capture efficiency were obtained at 960 °C. An assessment about the suitability of this material during long-term operation in a CLOU system is necessary.

The aim of this work was focused on the oxygen-carrier behavior during long-term operation in a continuous CLOU unit. The effect of operating conditions, such as the temperature and gas velocity in the fuel reactor, solids circulation rate, and oxygen concentration in the air reactor, on the oxygen-carrier capability to release gaseous oxygen has been evaluated without fuel feeding. The evolution of the physical and chemical characteristics of the Cu60MgAl oxygen carrier was also analyzed.

## 2. EXPERIMENTAL SECTION

**2.1. Oxygen-Carrier Material.** The material used was a Cu-based oxygen carrier prepared by spray drying. Oxygen-carrier particles were manufactured by VITO (Flemish Institute for Technological Research, Belgium) using  $\text{MgAl}_2\text{O}_4$  spinel (Baikowski, S30CR) and CuO (Panreac, PRS) as raw materials. The CuO content was 60 wt %. After particle formation by spray drying, the particles were calcined for 12 h at 1100 °C. Nevertheless, after material reception, particles were calcined for a second time to increase the mechanical strength. The oxygen-carrier particles had a total calcination time of 24 h at 1100 °C. The particle size of the oxygen carrier was +0.1–0.2 mm. From now on, the oxygen carrier was named as Cu60MgAl.

Physical and chemical characterizations were carried out with these particles. The copper content was determined by complete reduction in TGA using 15 vol %  $\text{H}_2$  at 850 °C. The oxygen transport capability,  $R_{\text{OC}}$ , was also calculated in TGA as  $R_{\text{OC}} = 1 - m_{\text{red}}/m_{\text{ox}}$ , with  $m_{\text{ox}}$  being the mass of fully oxidized particles and  $m_{\text{red}}$  being the mass of fully reduced particles, i.e., when all CuO have been reduced to  $\text{Cu}_2\text{O}$ .<sup>28</sup> The crushing strength was determined by measuring the force needed to fracture a particle using a Shimpo FGN-5X crushing strength apparatus. The crushing strength was taken as the average value of at least 20 measurements. The real density was determined by He pycnometry in a Micromeritics AccuPyc II 1340. The surface area of the oxygen carrier was determined by the Brunauer–Emmett–Teller (BET) method by adsorption/desorption of nitrogen at 77 K in a Micromeritics ASAP-2020 (Micromeritics Instruments, Inc.), whereas the pore volumes were measured by Hg intrusion in a Quantachrome PoreMaster 33. The identification of crystalline chemical species was carried out by a powder X-ray diffractometer (XRD) Bruker AXS graphite monochromator. The oxygen-carrier particles were also analyzed in a scanning electron microscope (SEM) ISI DS-130

coupled to an ultrathin window PGT Prism detector for energy-dispersive X-ray (EDX) analysis.

Table 1 shows the main properties of this oxygen carrier. It has a low porosity and a very low superficial area. The crushing strength of

**Table 1. Properties of the Fresh and Used Oxygen-Carrier Particles of Cu60MgAl**

	fresh	used batch <sup>a</sup>	used CLOU unit <sup>a</sup>
CuO content (wt %)	60	60	60
oxygen transport capacity, $R_{\text{OC}}$ (wt %)	6	6	6
crushing strength (N)	2.4	1.6	0.7
real density (kg/m <sup>3</sup> )	4600	4712	4713
porosity (%)	16.1	24.0	40.3
specific surface area, BET (m <sup>2</sup> /g)	<0.5	0.54	0.73
XRD main phases	CuO and $\text{MgAl}_2\text{O}_4$	CuO and $\text{MgAl}_2\text{O}_4$	CuO and $\text{MgAl}_2\text{O}_4$

<sup>a</sup>After 40 h.

the particles after 24 h of calcination was high enough for fluidization. The crystalline phases detected by XRD were only CuO and  $\text{MgAl}_2\text{O}_4$ . Moreover, Figure 3 shows SEM images and EDX analysis of the fresh oxygen-carrier particles. A very regular spherical shape with a hole in the core of the particles, which is characteristic of particles prepared by spray drying, was found. EDX analysis confirmed a uniform distribution of CuO inside the particles.

**2.2. Experimental Setup.** **2.2.1. TGA and Batch Fluidized-Bed Facilities.** A TGA was used for the determination of the oxygen-carrier reactivity during reduction and oxidation reactions. A detailed description of the TGA can be found elsewhere.<sup>25</sup> The reduction step of CuO to  $\text{Cu}_2\text{O}$  was carried out in a  $\text{N}_2$  atmosphere, and different oxygen concentrations for the oxidation reaction were used (4, 11, and 21 vol %). The experiments were carried out at different temperatures for both the reduction and oxidation reactions (900, 950, and 1000 °C).

A batch fluidized-bed reactor was used to know the oxygen release behavior in a fluidization environment and the behavior with respect to agglomeration and attrition phenomena. A detailed description of the facility can be found elsewhere.<sup>28</sup> The tests were carried out at 950 °C with an inlet superficial gas velocity in the reactor at 0.15 m/s. A batch of 250 g of oxygen-carrier particles was used as the bed material. Gas during reduction was 100 vol %  $\text{N}_2$ , and during oxidation, air was used.  $\text{O}_2$  was continuously analyzed at the outlet stream of the reactor with a paramagnetic analyzer (Maihak S710/OXOR-P) to determine the  $\text{O}_2$  concentration evolution with time.

The reactor had two connected pressure taps to measure the differential pressure drop along the bed. Agglomeration problems, causing defluidization of the bed, could be detected by a sharp decrease in the bed pressure drop during operation. The attrition rate of the oxygen carrier was evaluated in the batch fluidized-bed facility as the weight of particles with a  $d_p < 40$   $\mu\text{m}$  elutriated from the bed and recovered in the filter system during a measured time, corresponding to several reduction–oxidation cycles.

**2.2.2. Experimental Setup ICB-CSIC-s1.** A schematic view of the CLOU unit is shown in Figure 4. The setup was basically composed of two interconnected fluidized-bed reactors, the air and fuel reactors, joined by a loop seal, a riser for solids transport from the air reactor to the fuel reactor, a cyclone, and a solids valve to control the solids circulation flow rate in the system. The fuel reactor consisted of a bubbling fluidized bed of 50 mm inner diameter and 200 mm bed height.  $\text{N}_2$  or  $\text{CO}_2$  can be used as fluidizing gas. The gas flow was varied from 186 to 552 L<sub>N</sub>/h, corresponding to a gas velocity of 0.1 and 0.3 m/s, respectively. The oxygen carrier is reduced in the fuel reactor evolving gaseous oxygen to the surroundings. Reduced oxygen-carrier particles overflowed into the air reactor through a U-shaped fluidized-bed loop seal of 50 mm inner diameter, to avoid gas mixing



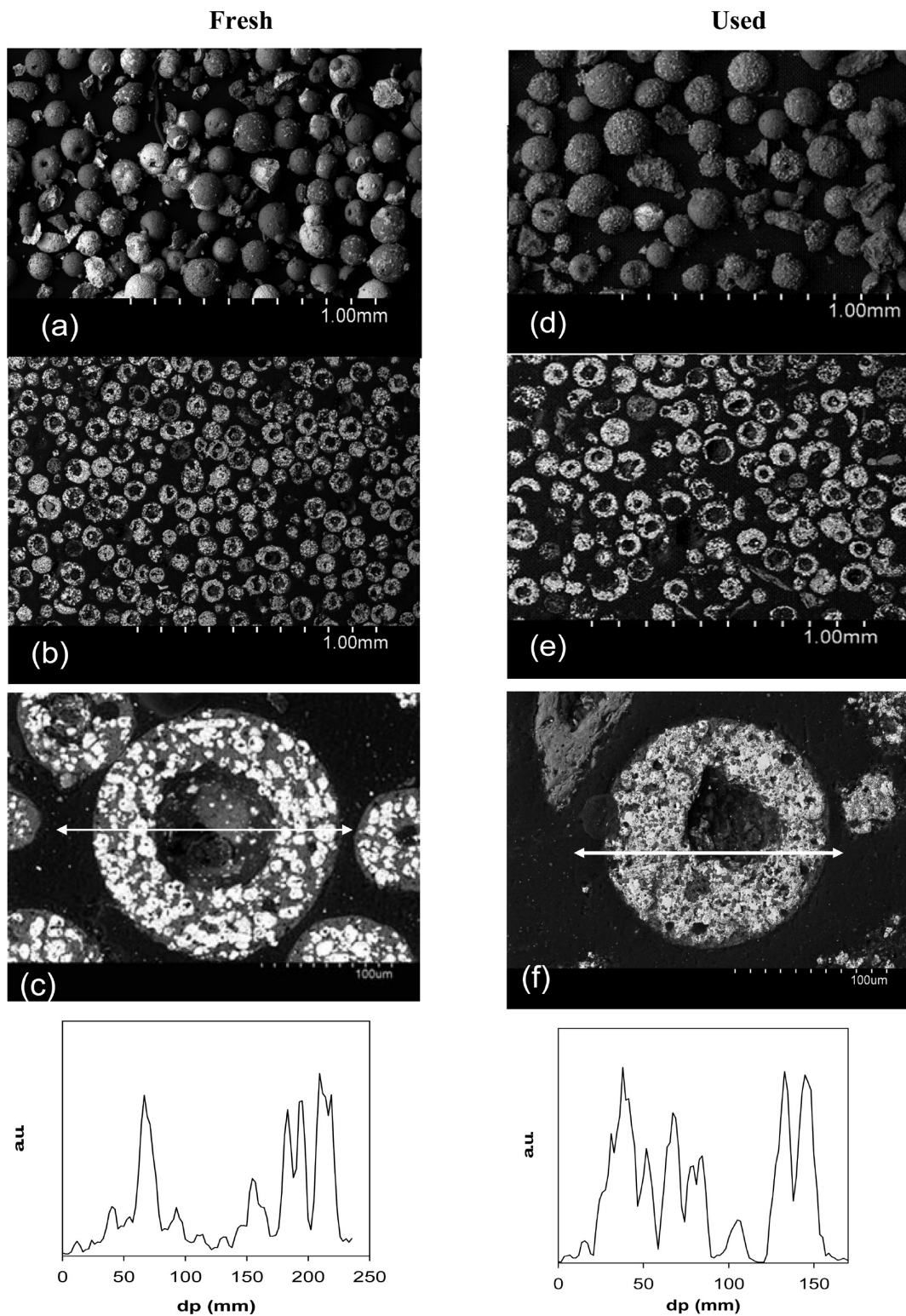


**Figure 3.** SEM images of fresh (right) and used (left) particles after 40 h in the CLOU unit: (a and d) SE image of the particles, (b and e) BSE of cross-section particles, and (c and f) SE image and EDX line profile of Cu in a cross-section of a particle.

between fuel and air. A  $N_2$  flow of 60  $L_N/h$  was introduced in the loop seal. The oxidation of the carrier took place in the air reactor, consisting of a bubbling fluidized bed of 80 mm inner diameter and 100 mm bed height, followed by a riser. The gas flow was varied from 1740 to 1980  $L_N/h$ . To know the effect of the oxygen concentration in the air reactor on the regenerability of the oxygen carrier, different oxygen concentrations in the air reactor were used. In these cases, a flow of air mixed with nitrogen was used, keeping a total gas flow in

the air reactor of 1980  $L_N/h$ . In addition, a secondary air flow (240  $L_N/h$ ) was introduced at the top of the air reactor to help particle entrainment.  $N_2$  and unreacted  $O_2$  left the air reactor passing through a high-efficiency cyclone and a filter before the stack. Entrained oxidized solid particles were recovered by the cyclone and sent to a solids reservoir, setting the oxygen carrier ready to start a new cycle. In addition, this reservoir acts as a loop seal, avoiding the leakage of gas between the fuel reactor and the riser. The regenerated oxygen-carrier

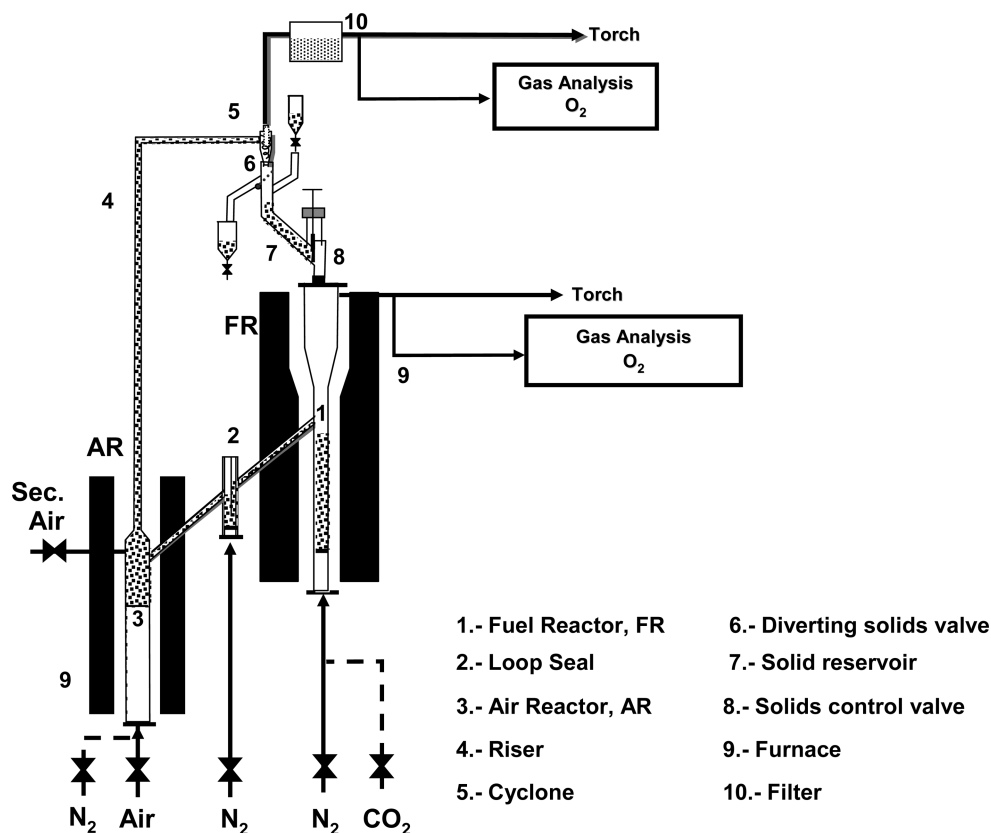


Figure 4. Schematic view of the ICB-CSIC-s1 unit for CLOU.

particles returned to the fuel reactor by gravity from the solids reservoir through a solids valve, which controlled the flow rates of solids entering the fuel reactor. In addition, diverting the solids valve located below the cyclone allowed for the measurement of the solids flow rates at any time. Therefore, this design allows for the control and measurement of the solids circulation flow rate between both reactors.

The unit was heated by means of various independent ovens to obtain independent temperature control of the air and fuel reactors. During operation,  $O_2$  was analyzed at the outlet stream from fuel and air reactors. A paramagnetic analyzer (Maihak S710/OXOR-P) was used to determine the  $O_2$  concentration. Also, temperatures in the fuel reactor, air reactor, and riser were monitored as well as the pressure drops in different locations of the system, such as the fuel-reactor bed, the air-reactor bed, and the loop seal.

The oxygen carrier,  $Cu_6O/MgAl$ , was prepared by spray drying. In a previous work, this material was used to prove the concept of the CLOU process for coal combustion.<sup>29</sup> In the present work, a deeper investigation on the behavior of oxygen-carrier particles is performed. For this purpose, the continuous unit was used without feeding coal.

**2.3. Experimental Planning in the Continuous ICB-CSIC-s1 CLOU Unit.** Different experimental tests were carried out using the same batch of oxygen-carrier particles. The total oxygen-carrier inventory in the system was around 2.0 kg, being about 0.7 kg in the fuel reactor. The exact amount of solids in the fuel reactor was calculated from pressure-drop measurements along the fuel reactor for each test.

Table 2 shows a compilation of the main variables used in each test. The capability of the oxygen carrier to evolve gaseous oxygen and to be regenerated in a cyclic manner was tested in a continuous way.  $CO_2$  was used as fluidizing gas in the fuel reactor. However, test A01 was carried out using  $N_2$  as fluidizing media to determine the possible effect of the surrounding gas on the oxygen-carrier behavior. As in previous tests, burning coal  $N_2$  was used to fluidize the fuel reactor.<sup>29</sup>

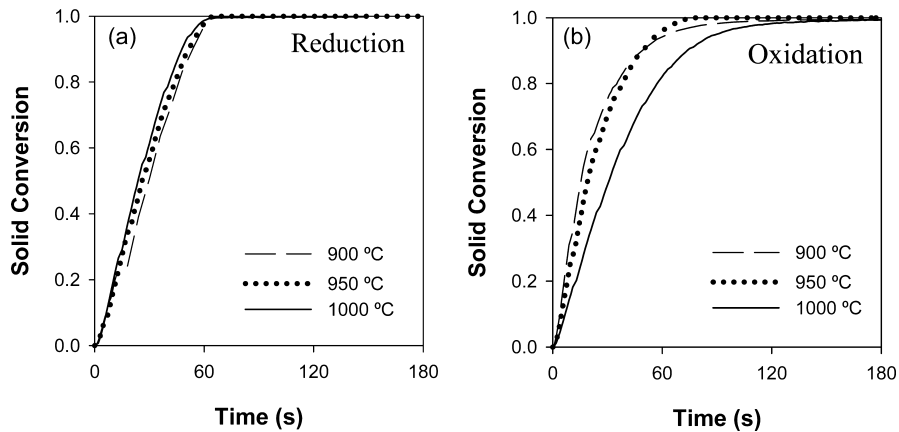
The effects of the fuel-reactor temperature (A02–A04), the solids circulation flow rate (A04–A07), and the gas velocity in the fuel reactor (A04 and A08–A10) on the oxygen release rate were analyzed.

Table 2. Main Data for Experimental Tests in the ICB-CSIC-s1 Plant

test	$T_{FR}$ (°C)	$T_{AR}$ (°C)	$Q_{inFR}$ (L <sub>N</sub> /h)	$u_{g,inFR}$ (m/s)	$\dot{m}_s$ (kg/h)	$[O_2]_{inAR}$ (%)	$m_{FR}$ (g)
A01	915	900	186	0.11	0.6	21.0	690
A02	915	900	186	0.11	0.6	21.0	690
A03	927	900	186	0.11	0.6	21.0	690
A04	943	900	186	0.11	0.6	21.0	690
A05	930	900	186	0.11	0.7	21.0	722
A06	922	900	186	0.11	0.9	21.0	737
A07	891	900	186	0.11	1.3	21.0	740
A08	939	900	280	0.17	0.6	21.0	713
A09	938	900	368	0.23	0.6	21.0	713
A10	933	900	552	0.35	0.6	21.0	713
A11	939	908	552	0.35	0.8	21.0	713
A12	939	900	552	0.35	0.8	10.5	713
A13	937	899	552	0.35	0.8	5.3	713
A14	944	900	552	0.35	0.8	2.7	713
A15	943	899	552	0.35	0.8	2.0	713
A16	937	949	552	0.35	0.9	5.3	713
A17	936	950	552	0.35	0.9	10.5	713
A18	936	951	552	0.35	0.9	21.0	713

In addition, the regeneration capacity using different  $O_2$  concentrations and air-reactor temperatures were analyzed (A11–A18).

**2.4. Data Evaluation.** TGA experiments allowed us to determine the reactivity of the oxygen carriers under well-defined conditions and in the absence of complex fluidizing factors, such as those derived from particle attrition and interphase mass-transfer processes. Reactivity data were obtained in TGA tests from the weight variations during the reduction and oxidation cycles as a function of time. At least five cycles of reduction and oxidation were carried out. The oxygen-carrier conversion was calculated as



**Figure 5.** Effect of the (a) reduction and (b) oxidation temperatures on the reactivity of Cu60MgAl (reduction with  $N_2$  and oxidation with air in TGA).

$$\text{for reduction: } X_{\text{red}} = \frac{m_{\text{ox}} - m}{m_{\text{ox}} - m_{\text{red}}} \quad (7)$$

$$\text{for oxidation: } X_{\text{ox}} = 1 - X_{\text{red}} = \frac{m - m_{\text{red}}}{m_{\text{ox}} - m_{\text{red}}} \quad (8)$$

with  $m$  being the mass of the sample at each time,  $m_{\text{ox}}$  being the mass of the sample fully oxidized, and  $m_{\text{red}}$  being the mass of the sample in the reduced form.

Initially, to establish whether thermodynamic limitations, external film mass transfer, and/or interparticle diffusion were affecting the reaction rate, the gas flow rate and the sample weight were varied in the range of 10–40  $L_N/h$  and 40–100 mg, respectively. It was observed that the reaction rate was not affected by the amount of sample used or the flow rate, indicating that external and interparticle diffusion was not of importance.<sup>28</sup> Moreover,  $O_2$  evolved to the  $N_2$  atmosphere was swept away, avoiding the buildup of  $O_2$  around the particles.

In the batch fluidized-bed facility, the oxidation degree of the oxygen carrier was calculated from the oxygen concentration at the reactor outlet. Taking as reference  $X_{\text{ox}} = 1$  for the fully oxidized oxygen carrier, the variation in  $X_{\text{ox}}$  with the reacting time was calculated for both the reduction and oxidation steps as

$$\text{reduction } X_{\text{ox}} = 1 - \int_{t_0}^{t_1} \frac{F_{\text{out}}}{n_0 P_{\text{tot}}} (P_{O_2, \text{out}}) dt \quad (9)$$

$$\text{oxidation } X_{\text{ox}} = X_{\text{ox}}|_{t_1} + \frac{1}{n_0 P_{\text{tot}}} - \int_{t_1}^{t_2} (F_{\text{in}} P_{O_2, \text{in}} - F_{\text{out}} P_{O_2, \text{out}}) dt \quad (10)$$

with  $F_{\text{in}}$  being the gas molar flow rate in the reactor,  $F_{\text{out}}$  being the gas molar flow rate leaving the reactor,  $P_{\text{tot}}$  being the total pressure,  $P_{O_2, \text{in}}$  being the  $O_2$  partial pressure in the reactor,  $P_{O_2, \text{out}}$  being the  $O_2$  partial pressure exiting the reactor,  $n_0$  being the moles of molecular oxygen that can be released from the fully oxidized oxygen carrier,  $t_0$  being the time at the beginning of the reduction,  $t_1$  being the time at the end of the reduction, and  $t_2$  being the time at the end of oxidation.

In the continuous CLOU unit, mass balances were found to be accurate using the measurements of the oxygen concentration from the air and fuel reactors. The flow of oxygen exiting both reactors was calculated as

$$F_{O_2, \text{outFR}} = y_{O_2, \text{outFR}} F_{\text{outFR}} \quad (11)$$

$$F_{O_2, \text{outAR}} = y_{O_2, \text{outAR}} F_{\text{outAR}} \quad (12)$$

The gas flow,  $F_{\text{outFR}}$ , was calculated using the inlet flow to the reactors,  $F_{\text{inFR}}$  and  $F_{\text{inAR}}$ . Thus, the following mass balance is applied

$$F_{\text{outFR}} = F_{\text{inFR}} + y_{O_2, \text{outFR}} F_{\text{outFR}} \quad (13)$$

$$F_{\text{outAR}} = F_{\text{inAR}} - (y_{O_2, \text{inAR}} F_{\text{inAR}} - y_{O_2, \text{outAR}} F_{\text{outAR}}) \quad (14)$$

The inlet flow to the air reactor includes the primary and secondary air, besides the nitrogen flow coming from the loop seal. In the same way, the inlet flow to the fuel reactor accounts for the fluidizing gas and the nitrogen flow coming from the loop seal. Preliminary results showed that 40 vol %  $N_2$  introduced to fluidize the loop seal went to the fuel reactor and the rest went to the air reactor.

When eqs 11 and 13 were combined, the oxygen flow from the fuel reactor is calculated as

$$F_{O_2, \text{outFR}} = \frac{y_{O_2, \text{outFR}}}{1 - y_{O_2, \text{outFR}}} F_{\text{inFR}} \quad (15)$$

Similarly, the oxygen flow exiting the air reactor was calculated by combining eqs 12 and 14 as

$$F_{O_2, \text{outAR}} = \frac{1 - y_{O_2, \text{inAR}}}{1 - y_{O_2, \text{outAR}}} y_{O_2, \text{outAR}} F_{\text{inAR}} \quad (16)$$

From these results, it is possible to calculate the stoichiometric index,  $\Phi_{\text{ox}}$ , defined as the ratio between oxygen reacted in the air and fuel reactors

$$\Phi_{\text{ox}} = \frac{F_{O_2, \text{inAR}} - F_{O_2, \text{outAR}}}{F_{O_2, \text{outFR}}} \quad (17)$$

A stoichiometric index lower than unity means that a fraction of the oxygen released in the fuel reactor comes from the oxygen initially present in the oxygen carrier. This was the case in non-stationary periods, when operational conditions were varied. After a few minutes, the stoichiometric index was around unity, which can be considered a good verification of the steady-state operation. This means that the amount of oxygen taken from the air is equal to the amount of oxygen released in the fuel reactor.

The variation of the solids conversion was calculated from an oxygen balance in the reactor.

$$M_{O_2} F_{O_2, \text{outFR}} = \dot{m}_s R_{OC} \Delta X_s \quad (18)$$

The rate of oxygen generation per unit of mass of solids in the fuel reactor can be calculated from the  $O_2$  flow exiting the fuel reactor as

$$r_{O_2} = \frac{F_{O_2, \text{outFR}} M_{O_2}}{m_{FR}} \quad (19)$$

### 3. RESULTS AND DISCUSSION

**3.1. Oxygen-Carrier Reactivity in TGA.** The oxygen carrier was first characterized using a TGA to analyze the oxygen release and regeneration rates as a function of the

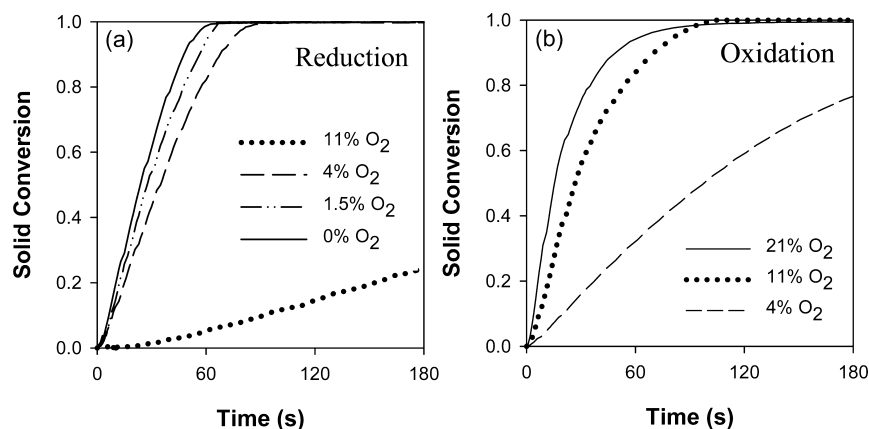


**Figure 6.** Effect of the oxygen concentration on the (a) reduction and (b) oxidation rates of Cu60MgAl (reduction at 1000 °C and oxidation at 900 °C with different oxygen concentrations in TGA).

number of cycles, temperature, and oxygen concentration. It was found that both reduction and oxidation reaction rates were stable with cycles.

Panels of a and b of Figure 5 show the oxygen-carrier conversion versus time at different reduction and regeneration temperatures, respectively. The oxygen carrier showed high oxygen generation rates, reaching full solid conversion in less than 1 min for the different temperatures used. The effect of the temperature on the reduction rate was very poor. On the contrary, the higher the oxidation temperature, the lower the oxidation reaction rate. This result was due to the effect of the equilibrium oxygen concentration in the reduction reaction of CuO to Cu<sub>2</sub>O, which implies that the oxidation reaction rate is carried out with the driving force of the difference between the inlet oxygen concentration (21 vol % in this case) and the oxygen concentration at equilibrium at that temperature. It is necessary to take into account that the reaction rate ( $r_{O_2}$ ) in this type of process depends upon both the actual partial pressure of oxygen,  $P_{O_2}$ , and the partial pressure of oxygen at equilibrium conditions,  $P_{O_2,eq}$ .

$$(r_{O_2}) = k(P_{O_2,eq} - P_{O_2}) \quad (20)$$

As shown in Figure 2, the oxygen concentration at equilibrium is 12.4 vol % at 1000 °C and only 1.5 vol % at 900 °C. In addition, the sinterization of the CuO layer formed during oxidation can affect the reaction rate at different temperatures.<sup>30,31</sup>

The effect of the oxygen concentration in the reduction reaction was also analyzed by TGA. Figure 6a shows the effect of the oxygen concentration on the reduction reaction at 1000 °C. The oxidation was always carried out using air at 1000 °C for all of the cycles. As seen, the lower the oxygen concentration, the higher the reduction reaction rate. On the other hand, the effect of the oxygen concentration in the oxidation reaction was shown in Figure 6b at 900 °C. The reduction was always carried out in N<sub>2</sub> at 1000 °C for all of the cycles. The higher the oxygen concentration, the higher the oxidation reaction rate. These effects are due to the driving force in the reduction and oxidation reactions, which are the difference between the oxygen concentration in the reacting gas and the oxygen concentration at equilibrium (1.5 vol % at 900 °C and 12 vol % at 1000 °C).

**3.2. Oxygen-Carrier Behavior in the Batch Fluidized Bed.** Reduction–oxidation multicycles were carried out in the

batch fluidized-bed reactor to know the oxygen release and behavior with respect to agglomeration and attrition phenomena during fluidization. A total of 40 h of fluidization at 950 °C was carried out during 22 consecutive redox periods. As an example, Figure 7 shows the oxygen concentration at the outlet

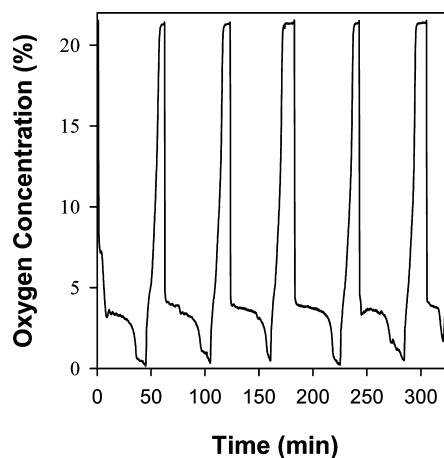
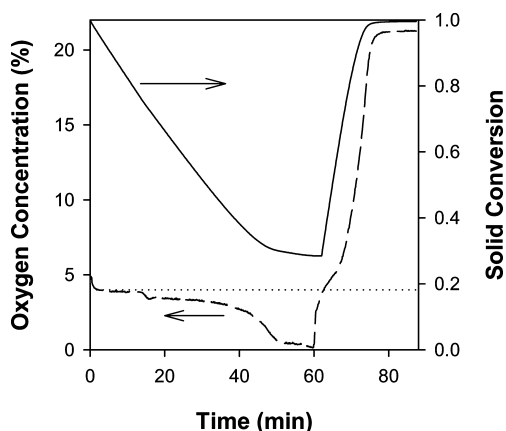


**Figure 7.** O<sub>2</sub> concentration as a function of time for 6 consecutive cycles of reduction–oxidation in the batch fluidized-bed reactor for Cu60MgAl at 950 °C (reduction with N<sub>2</sub> and oxidation with air).

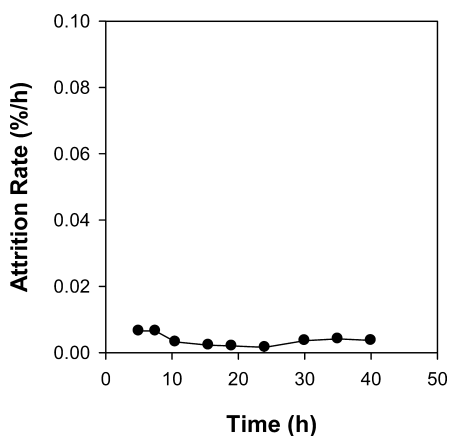
of the reactor for 6 consecutive redox periods of the Cu60MgAl oxygen carrier. A constant reactivity can be seen for both reduction and oxidation reactions.

Figure 8 shows the solid conversion and oxygen concentration profile during a reduction and regeneration period in a typical cycle. The equilibrium oxygen concentration at 950 °C is also shown. As seen, the oxygen carrier showed an oxygen release rate nearly constant until solid conversion reached 0.7. During this period, the oxygen release rate was limited by the thermodynamic equilibrium of oxygen.

The multicycle test carried out in the fluidized bed was also useful to determine the fluidization behavior of the oxygen carrier with respect to the attrition and agglomeration phenomena. Figure 9 shows the attrition rate for the Cu60MgAl oxygen carrier as a function of the operation time. The attrition rate of this material was stable, with a very low value (0.004% h<sup>-1</sup>), which corresponds to a particle lifetime of 25 000 h. Moreover, despite the high CuO content of the material and the high temperature used during



**Figure 8.** Solid conversion and oxygen concentration profile during a reduction and regeneration period in the batch fluidized-bed reactor with Cu60MgAl at 950 °C (reduction with N<sub>2</sub> and oxidation with air). (···) Oxygen equilibrium concentration.



**Figure 9.** Attrition rate of Cu60MgAl during multicycle operation in the batch fluidized bed.

fluidization, the oxygen carrier prepared by spray drying did not present any agglomeration problems in any of the tests.

**3.3. Continuous ICB-CSIC-s1 CLOU Unit.** Continuous operation in the CLOU unit using the Cu60MgAl oxygen carrier without coal addition was performed to evaluate the oxygen release behavior without other combustion effects. A total amount of 40 h in hot fluidization operation using the same batch of particles was carried out. The effects of the fuel-reactor temperature, fluidizing gas velocity, and solids circulation flow rate on the oxygen release rate were analyzed. In addition, the effect of the oxygen concentration in the air reactor at different temperatures on the regeneration capability of the oxygen carrier was studied.

As an example, the evolution with time of the temperature and oxygen concentration from the air and fuel reactors is shown in Figure 10 for experimental tests A02–A04. The temperature was varied in the range of 915–943 °C. At steady state, the gas outlet concentration and temperature were maintained uniform during the whole time, which was about 120 min for each experimental condition. A change in the fuel-reactor temperature affected the oxygen concentration exiting both the air and fuel reactors. When the temperature was varied, a transition period appeared and steady state was reached usually in less than 10 min.

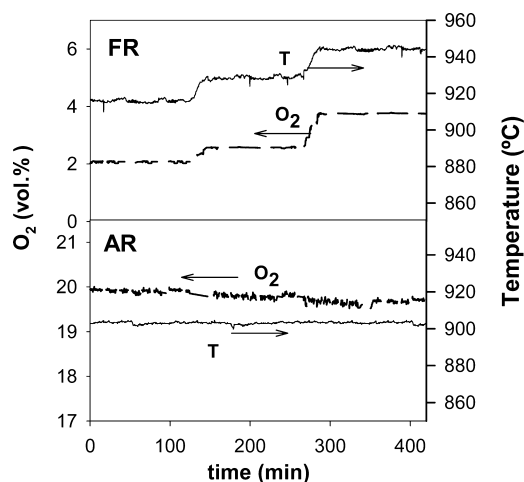


**Figure 10.** Evolution of the oxygen concentration in the air and fuel reactors as the temperature in the fuel reactor was varied for experimental tests A02–A04.  $\dot{m}_s = 0.6$  kg/h, and  $u_g = 0.11$  m/s.

Panels a, b, and c of Figure 11 show the oxygen concentration in the air and fuel reactors during the steady-state period as a function of the fuel-reactor temperature, the solids circulation flow rate, and the gas velocity in the fuel reactor, respectively. The oxygen concentration at equilibrium conditions are also shown in Figure 11. In addition, panels a, b, and c of Figure 12 show the oxygen flow exiting both the air and fuel reactors in each experimental test calculated using eqs 14 and 15 as a function of the fuel-reactor temperature, the solids circulation flow rate, and the gas velocity in the fuel reactor, respectively. In addition, the variation of the solids conversion in the reactor,  $\Delta X_s$ , was also depicted in Figure 12.

Figure 11a shows that the oxygen concentration in the fuel reactor increased with the fuel-reactor temperature. In all cases, the oxygen concentration is close to the equilibrium concentration (see Figure 11a). Thus, the oxygen-carrier reduction is fast enough to reach the equilibrium condition. The oxygen release rate was limited by the thermodynamic equilibrium of oxygen in the fuel reactor. Higher rates were obtained in previous works using the same oxygen carrier<sup>22,29</sup> when experiments were carried out with fuel feeding, because an oxygen sink was there. Figure 12a shows that more O<sub>2</sub> is generated in the fuel reactor with the consequent decrease of the O<sub>2</sub> concentration in the air-reactor exit (Figure 11a). Therefore, as the temperature increased, more oxygen is transferred in each reactor and the variation of the solids conversion increased correspondingly.

In an industrial CLOU process of solid fuel combustion, a carrier gas composed of recirculated CO<sub>2</sub> is most likely used, as shown in Figure 1. However, in previous works of CLOU oxygen-carrier evaluations, N<sub>2</sub> was commonly used as a carrier gas.<sup>20,28,29</sup> To evaluate the effect of the fluidization media, test A01 was carried out using N<sub>2</sub> as a fluidizing gas instead of CO<sub>2</sub> (test A02; see Table 2). No differences in the oxygen concentration and oxygen release rate when CO<sub>2</sub> or N<sub>2</sub> was used as a fluidizing gas were observed. Therefore, previous experimental results obtained using N<sub>2</sub> as the fluidization media are comparable to the results obtained when CO<sub>2</sub> is used.

Experimental test series A04–A07 were carried out varying the solids circulation flow rate to analyze the effect of  $\Delta X_s$  on the average reactivity of the oxygen-carrier particles and its capability to release oxygen. Figure 11b shows the oxygen

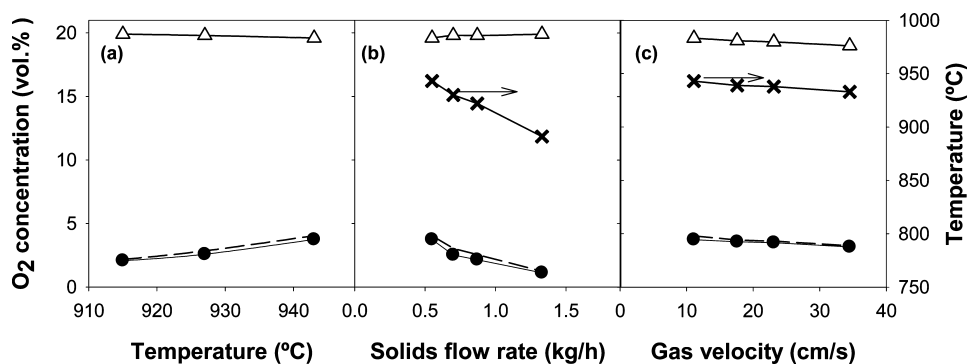


**Figure 11.** Oxygen concentration from the fuel (●) and air (△) reactor obtained at (a) different fuel-reactor temperatures, (b) solids circulation rate, and (c) fuel-reactor fluidizing gas velocities. (---) O<sub>2</sub> concentration at equilibrium condition; (×) temperature in the fuel reactor.

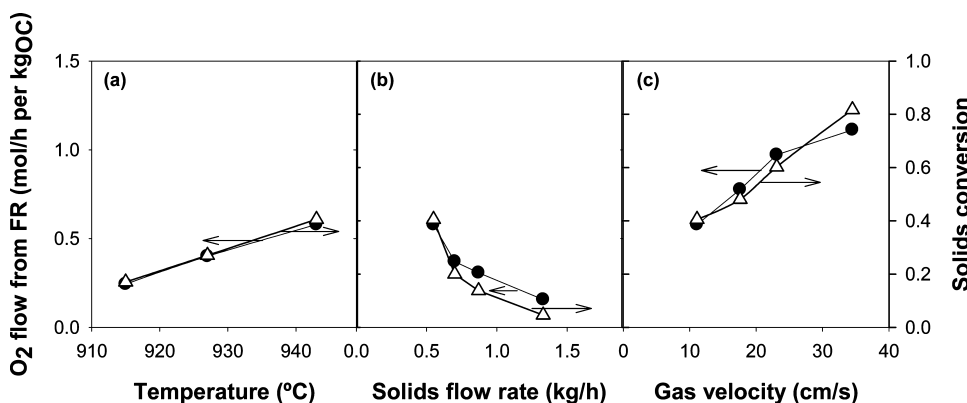


**Figure 12.** Flow of oxygen exiting the fuel reactor (●) and variation of the solids conversion (△) at (a) different fuel-reactor temperatures, (b) solids circulation rate, and (c) fuel-reactor fluidizing gas velocities.

concentration as a function of the solids circulation flow rate. Unfortunately, it was not possible to maintain a constant temperature in the fuel reactor when the solids circulation rate was varied to analyze its effect independent of the variation of the temperature. The solids coming from the solids reservoir above the fuel reactor were at a lower temperature than that existing in the fuel reactor. Thus, a higher amount of solids must be heated as the solids flow increased and the fuel-reactor temperature decreased. Nevertheless, it can be seen in Figure 11b that the oxygen concentration in the fuel reactor was close to the equilibrium concentration in all cases. The oxygen release rate was shown in Figure 12b as a function of the solids flow, but again, it was limited by the thermodynamic equilibrium. A decrease in the solid flow rate increased the O<sub>2</sub> flow exiting the fuel reactor and, therefore, the solid conversion because the fuel-reactor temperature increased. However, a maximum solid conversion of 0.4 was only reached. This fact is due to the chosen amount of gas flow used in the tests that limit the maximum amount of O<sub>2</sub> exiting the fuel reactor.

To enhance the oxygen release rate and the solid conversion, tests A08–A10 were carried out by increasing the gas velocity in the fuel reactor. Figure 11c shows that the oxygen concentration in the fuel reactor slightly decreased with the gas velocity. Nevertheless, this decrease in the oxygen concentration was due to a decrease in the reactor temperature related with an increase in the gas velocity (see Table 2). Oxygen concentrations close to the equilibrium conditions were reached in all cases. Even so, the oxygen flow from the fuel reactor increased as the gas flow increased (see Figure 12c). On

the contrary, the oxygen concentration in the air reactor decreased as the gas velocity increased (see Figure 11c). Indeed, the flow of oxygen transferred in both reactors increased with the gas velocity in the fuel reactor, and more oxygen is demanded for regeneration of the oxygen carrier. Therefore, the rate of reduction of the oxygen carrier is promoted by increasing the gas velocity in the fuel reactor. This fact is indicated by the increase in the variation of solids conversion,  $\Delta X_s$  (see Figure 12c). The results shown in this work indicate that the oxygen carrier can release oxygen at equilibrium conditions in a wide range of the solids conversion, i.e.,  $\Delta X_s = 0.05\text{--}0.82$ .

The gas velocity was increased until a value close to the terminal velocity of the smallest oxygen-carrier particles used. A further increase of the gas velocity was prevented to avoid the elutriation of particles from the fluidized bed. The highest value of the oxygen release rate obtained in the tests was  $1 \times 10^{-5}$  kg of O<sub>2</sub> s<sup>-1</sup> (kg of oxygen carrier)<sup>-1</sup>. This value is much lower than the value obtained in a batch fluidized bed using coal as fuel [ $2.6 \times 10^{-3}$  kg of O<sub>2</sub> s<sup>-1</sup> (kg of oxygen carrier)<sup>-1</sup> at 955 °C].<sup>22</sup> Because the oxygen concentration was close to the equilibrium condition, the oxygen release rate was limited by the existing oxygen concentration (eq 20), even at the highest gas velocity. Higher values of the oxygen release rate could be obtained if an increase in the gas velocity was carried out in the plant.

Other imperative characteristics of the CLOU process, in comparison to normal CLC, are the especially constrained operating conditions for the air reactor because of the thermodynamic limitations of the oxidation of the oxygen

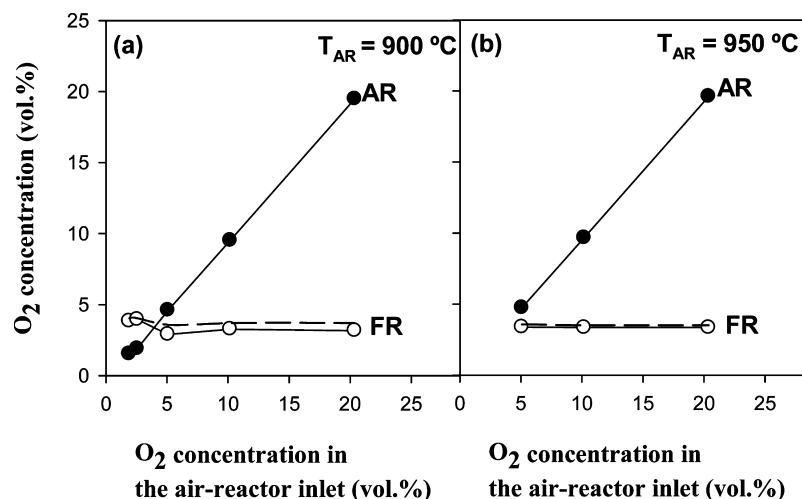


**Figure 13.** Oxygen concentration from the fuel- (○) and air- (●) reactor outlet obtained at different oxygen concentrations in the air-reactor inlet. (---) O<sub>2</sub> concentration at equilibrium conditions in the fuel reactor.  $T_{FR} = 940$  °C.

carrier. The equilibrium concentration of oxygen in the air reactor will be given by the temperature in the reactor; which is determined by the temperature of the incoming particles, the circulation rate, and the heat of reaction in the fuel reactor.<sup>32</sup>

In experiments A01–A10, there was an important oxygen excess in the air-reactor inlet flow with respect to the oxygen necessary to oxidize the oxygen carrier. Therefore, the oxygen concentration at the air-reactor outlet hardly changed during experiments. However, to maximize the use of air in an industrial scale, the oxygen concentration at the outlet must be near equilibrium. To simulate the operation conditions in an industrial reactor, the oxygen concentration in the air-reactor inlet was reduced to values near the corresponding equilibrium at two different air-reactor temperatures.

Experimental tests A11–A15 analyze the effect of the oxygen concentration in the air-reactor inlet on the oxygen concentration outlet stream of the air and fuel reactors. Panels a and b of Figure 13 show the effect of the oxygen concentration in the air-reactor inlet on the regeneration behavior and the capability of the oxygen carrier to release oxygen in the fuel reactor at different air-reactor temperatures, 900 and 950 °C. The fuel reactor was fixed at 940 °C. In both cases, the oxygen flow in the air reactor was enough to complete oxidization of the oxygen carrier. The oxygen concentration in the fuel-reactor outlet was close to the equilibrium concentration in all tests. At the lowest oxygen concentration in the air-reactor inlet, a small variation was found because of small changes in the fuel-reactor temperature. These results demonstrate that it is possible to completely regenerate the oxygen carrier with oxygen concentrations in the air reactor near equilibrium concentrations. Although the oxidation rate decreased as the oxygen concentration in the air-reactor inlet decreased, as found in TGA experiments (Figure 6), the oxidation rate was still fast enough to regenerate the oxygen carrier in the air reactor and did not affect to the oxygen release in the fuel reactor.

Finally, experimental tests A16–A18 analyze the effect of the oxygen concentration of the air-reactor inlet at the temperature of 950 °C in the air reactor, which is higher than the temperature in the fuel reactor (940 °C). Apparently, this operation condition is unfavorable because the reaction in the fuel reactor<sup>20,32</sup> is exothermic. However, this condition can be

feasible depending upon the energetic integration of the CLOU system with the heat recovery system of the whole plant. At 950 °C in the air reactor, the effect of the inlet oxygen concentration in the air reactor is the same as observed at a lower temperature in the air reactor.

These results reveal that the system can be operated under these conditions, at least regarding the capability of the oxygen carrier to transfer oxygen from air to fuel. These results are unique and very relevant because they indicate that it is not necessary to work at a lower air-reactor temperature than the fuel-reactor temperature or with a high oxygen excess in the air reactor. There are no restricted operation conditions in the air reactor other than the thermodynamic equilibrium, if the oxygen-carrier reactivity is high enough for oxidation, as found with the Cu60MgAl oxygen carrier. However, a higher temperature in the air reactor could decrease the O<sub>2</sub> use in the air reactor.

**3.4. Characterization of Used Cu60MgAl Oxygen-Carrier Particles.** Solids samples extracted from batch reactor tests after 40 h of fluidization and from the fuel and air reactors after 20 and 40 h of continuous operation in the CLOU unit were characterized by different techniques. Table 1 shows relevant properties for used particles compared to the fresh particles.

The XRD analysis of used particles revealed the presence of CuO and MgAl<sub>2</sub>O<sub>4</sub> as major components. Thus, no changes in the chemical structure of the material were observed. In addition, XRD results of some reduced samples taken from the fuel reactor of the CLOU unit at different times showed only Cu<sub>2</sub>O and MgAl<sub>2</sub>O<sub>4</sub> as main components. That is, metallic Cu was never detected in the samples, even in those tests where the variation of the solids conversion was close to unity.

SEM images of used particles from the air reactor after 40 h of operation in the CLOU unit are shown in Figure 3 (left). Cu60MgAl particles showed an increase of the superficial (Figure 3d) and internal (Figure 3e) porosity. EDX analysis showed that internal CuO distribution inside the particles was uniform and has not changed after 40 h of continuous operation in the CLOU unit. However, an important amount of broken particles can be observed.

The copper content of all samples was determined by complete reduction in TGA using 15 vol % H<sub>2</sub> at 850 °C. In all

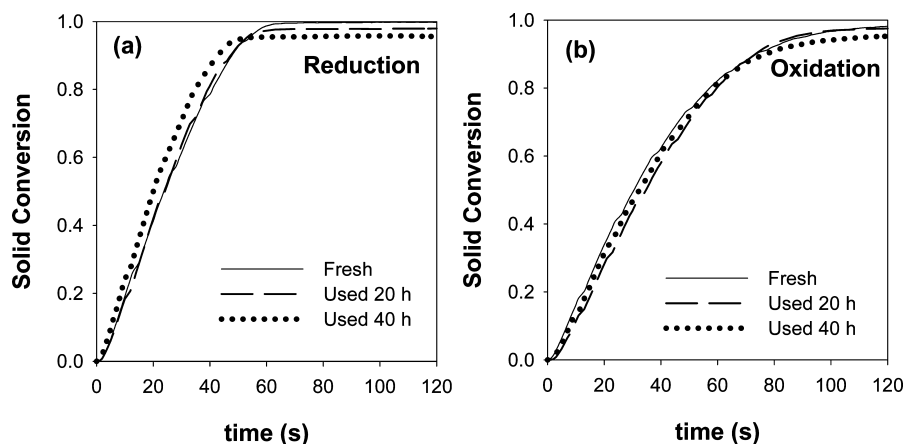


**Figure 14.** Conversion versus time curves for (a) reduction and (b) oxidation reactions for fresh and used after 20 and 40 h in the CLOU unit particles (reduction in  $N_2$  and oxidation in air at 1000 °C in TGA).

cases, fresh and used particles, the CuO content was 60 wt %. In addition, the reactivity of samples taken after 20 and 40 h of operation in the CLOU unit was determined by TGA at 1000 °C in  $N_2$  for the decomposition reaction and in air for the re-oxidation. A similar behavior was found for fresh and used particles of Cu60MgAl. Figure 14 shows the conversion versus time curves obtained for the decomposition and oxidation reactions for the used samples, as well as for fresh oxygen carrier. The maintenance of the initial reactivity can be clearly seen for used particles in both decomposition and oxidation reactions. This fact justifies the unchanged capability to release oxygen at equilibrium conditions and to be re-oxidized by air observed in the CLOU unit after the high number of reduction–oxidation cycles suffered by the oxygen-carrier particles.

Very low values of the BET surface area were measured for all samples, fresh and used, around 0.5  $m^2/g$ . However, fresh particles had a low-porosity development (16.1%) that was increased until 40.3% after 40 h of operation in the continuous CLOU unit. In addition, an important reduction in the crushing strength of the particles as the operation time increased was found. Values lower than 1 N were reached after continuous operation. The reduction in the crushing strength of the particles was related to an increase in the porosity as the operation time in the CLOU unit increased (see Figure 15). A similar behavior can also be observed in Figure 15 with the porosity and the crushing strength of the particles used in the batch fluidized-bed reactor. The particle integrity in the ICB-CSIC-s1 plant after 40 h of continuous operation was very low. The formation of an important amount of fine particles entrained from the air reactor forced the stoppage of the operation. This clearly indicates the need to improve the lifetime of this kind of material for its use in a CLOU process of coal combustion.

However, with regard to the agglomeration behavior, it must be pointed out that, in both the batch fluidized-bed reactor (40 h) and during continuous operation in the CLOU unit (40 h), the oxygen-carrier particles never showed agglomeration problems, even when the oxygen carrier was highly reduced, i.e.,  $\Delta X_s = 0.7\text{--}0.82$ .

#### 4. CONCLUSION

In this work, an oxygen carrier prepared by spray drying containing 60 wt % CuO and  $MgAl_2O_4$  as supporting material

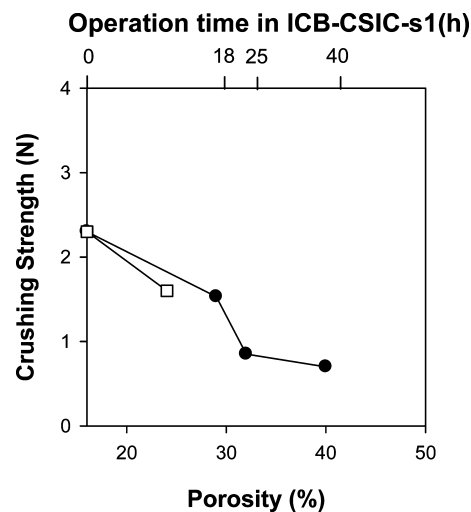


**Figure 15.** Crushing strength as a function of porosity for Cu60MgAl particles: (●) used in the ICB-CSIC-s1 unit and (□) used in the batch fluidized-bed reactor. The operation time in the ICB-CSIC-s1 unit is also shown.

was evaluated. First, the oxygen release rate and the fluidization behavior, with regard to the agglomeration and attrition rate, were analyzed in a TGA and a batch fluidized bed, respectively. High reaction rates for both oxygen release and oxidation were found.

The effects on the oxygen release rate of the fuel-reactor temperature, the solids circulation flow rate, and the fluidizing gas velocity in the fuel reactor were then analyzed in a continuous CLOU unit. It was found that the flow of oxygen transferred in both reactors increased with the fuel-reactor temperature and the gas velocity in the fuel reactor. The oxygen carrier was able to produce oxygen at equilibrium conditions in all of the operational conditions analyzed, even at high conversion of the oxygen carrier.

In addition, the regeneration capacity using different  $O_2$  concentrations and temperatures in the air reactor was analyzed. A decreased in the oxygen concentration in the air-reactor inlet did not produce a variation in the oxygen concentration in the fuel-reactor outlet independent of the air-reactor temperature (higher or lower than the fuel-reactor temperature). These results are very relevant because they indicate that it is not necessary to work at a lower air-reactor



temperature than the fuel-reactor temperature or with a high oxygen excess in the air reactor.

During 40 h of continuous operation, the oxygen-carrier particles never showed agglomeration problems. In addition, the CuO content and the oxygen-carrier reactivity were maintained constant. However, an important reduction in the crushing strength of the particles related to an increase in the porosity as the operation time in the CLOU unit increased was found. The formation of an important amount of fine particles entrained from the air reactor forced the stoppage of the operation after 40 h of operation in the ICB-CSIC-s1 plant. This fact indicates the need to improve the lifetime of this oxygen carrier for its use in coal combustion by the CLOU process.

## AUTHOR INFORMATION

### Corresponding Author

\*Telephone: +34-976-733977. Fax: +34-976-733318. E-mail: pgrayan@icb.csic.es.

### Notes

The authors declare no competing financial interest.

## ACKNOWLEDGMENTS

This work was partially supported by the European Commission, under the RFCS Program (ECLAIR Project, Contract RFCP-CT-2008-0008), ALSTOM Power Boilers (France), and the Spanish Ministry of Science and Innovation (ENE2010-19550). Iñaki Adánez-Rubio thanks CSIC for the JAE fellowship.

## NOMENCLATURE

- $k$  = kinetic constant ( $\text{mol atm}^{-1} \text{s}^{-1}$ )  
 $F_{\text{O}_2}$  = molar flow of oxygen ( $\text{mol/s}$ )  
 $F_{\text{inFR}}$  = gas flow introduced in the fuel reactor ( $\text{mol/s}$ )  
 $F_{\text{inAR}}$  = gas flow introduced in the air reactor ( $\text{mol/s}$ )  
 $F_{\text{outAR}}$  = gas flow exiting the air reactor ( $\text{mol/s}$ )  
 $F_{\text{outFR}}$  = gas flow exiting the fuel reactor ( $\text{mol/s}$ )  
 $M_{\text{O}_2}$  = molecular weight of oxygen ( $\text{kg/mol}$ )  
 $m$  = mass of oxygen ( $\text{kg}$ )  
 $m_{\text{ox}}$  = mass of the sample fully oxidized ( $\text{kg}$ )  
 $m_{\text{red}}$  = mass of the sample fully reduced ( $\text{kg}$ )  
 $\dot{m}_s$  = solids circulation rate ( $\text{kg/s}$ )  
 $m_{\text{FR}}$  = mass of solids in the fuel reactor ( $\text{kg}$ )  
 $n_0$  = moles of molecular oxygen ( $\text{mol}$ )  
 $P_{\text{tot}}$  = total pressure ( $\text{atm}$ )  
 $P_{\text{O}_2, \text{in}}$  = partial pressure of  $\text{O}_2$  incoming to the reactor ( $\text{atm}$ )  
 $P_{\text{O}_2, \text{out}}$  = partial pressure of  $\text{O}_2$  exiting the reactor ( $\text{atm}$ )  
 $P_{\text{O}_2}$  = partial pressure of  $\text{O}_2$  ( $\text{atm}$ )  
 $P_{\text{O}_2, \text{eq}}$  = partial pressure of  $\text{O}_2$  at equilibrium conditions ( $\text{atm}$ )  
 $Q_{\text{inFR}}$  = volumetric gas flow ( $\text{m}^3/\text{s}$ )  
 $r_{\text{O}_2}$  = rate of oxygen generation [ $\text{kg of O}_2 \text{s}^{-1} (\text{kg of OC})^{-1}$ ]  
 $R_{\text{OC}}$  = oxygen transport capability  
 $T$  = temperature ( $^\circ\text{C}$ )  
 $t_0$  = time at the beginning of the reduction period ( $\text{s}$ )  
 $t_1$  = time at the end of the reduction period ( $\text{s}$ )  
 $t_2$  = time at the end of the oxidation period ( $\text{s}$ )  
 $u_g$  = gas velocity ( $\text{m/s}$ )  
 $u_{\text{mf}}$  = minimum fluidizing velocity ( $\text{m/s}$ )  
 $X_{\text{red}}$  = oxygen carrier conversion during the reduction period

$X_{\text{ox}}$  = oxygen carrier conversion during the oxidation period  
 $y_{\text{O}_2}$  = molar fraction of oxygen

## Greek Letters

$\Delta H_r$  = enthalpy of reaction ( $\text{kJ/mol}$ )  
 $\Delta X_s$  = variation of oxygen carrier conversion between the air and fuel reactors  
 $\Phi_{\text{ox}}$  = stoichiometric index

## Acronyms

AR = air reactor  
 BET = Brunauer–Emmett–Teller  
 CLC = chemical looping combustion  
 CLOU = chemical looping with oxygen uncoupling  
 FR = fuel reactor  
 in = inlet  
 IPCC = Intergovernmental Panel on Climate Change  
 OC = oxygen carrier  
 out = outlet  
 XRD = X-ray diffractometer

## REFERENCES

- (1) Intergovernmental Panel on Climate Change (IPCC). *Mitigation of Climate Change. Contribution of Working Group III to the Fourth Assessment Report of the Intergovernmental Panel on Climate Change*; Cambridge University Press: Cambridge, U.K., 2008; <http://www.ipcc.ch>.
- (2) Kerr, H. R. Capture and separation technology gaps and priority research needs. *Carbon Dioxide Capture for Storage in Deep Geologic Formations*; Elsevier: Amsterdam, The Netherlands, 2005; pp 655–660.
- (3) Kvamsdal, H. M.; Jordal, K.; Bolland, O. *Energy* **2007**, *32* (1), 10–24.
- (4) Kolbitsch, P.; Bolh ar-Nordenkamp, J.; Pr oll, T.; Hofbauer, H. *Ind. Eng. Chem. Res.* **2009**, *48* (11), 42–47.
- (5) Linderholm, C.; Mattisson, T.; Lyngfelt, A. *Fuel* **2009**, *88*, 2083–2096.
- (6) Ad anez, J.; Gay an, P.; Celaya, J.; de Diego, L. F.; Garc a-Labiano, F.; Abad, A. *Ind. Eng. Chem. Res.* **2006**, *45* (17), 75–80.
- (7) de Diego, L. F.; Garc a-Labiano, F.; Gay an, P.; Celaya, J.; Palacios, J. M.; Ad anez, J. *Fuel* **2007**, *86*, 1036–1045.
- (8) Lyngfelt, A.; Thunman, H. Construction and 100 h of operational experience of a 10-kW chemical-looping combustor. *Carbon Dioxide Capture for Storage in Deep Geologic Formations— Results from the CO<sub>2</sub> Capture Project*; Elsevier: Amsterdam, The Netherlands, 2005; Vol. 1, Chapter 36.
- (9) Pr oll, T.; Mayer, K.; Bolh ar-Nordenkamp, J.; Kolbitsch, P.; Mattisson, T.; Lyngfelt, A.; Hofbauer, H. *Energy Procedia* **2009**, *1*, 27–34.
- (10) Ad anez, J.; Abad, A.; Garc a-Labiano, F.; Gay an, P.; de Diego, L. F. *Prog. Energy Combust. Sci.* **2012**, *38*, 215–282.
- (11) Mattisson, T.; Garc a-Labiano, F.; Kronberger, B.; Lyngfelt, A.; Ad anez, J.; Hofbauer, H. *Int. J. Greenhouse Gas Control* **2007**, *1*, 158–169.
- (12) Ryu, H.-J.; Jo, S.-H.; Park, Y.; Bae, D. H.; Kim, S. *Proceedings of the 1st International Conference on Chemical Looping*; Lyon, France, March 17–19, 2010.
- (13) Cao, Y.; Pan, W. P. *Energy Fuels* **2006**, *20*, 57–68.
- (14) Berguerand, N.; Lyngfelt, A. *Energy Fuels* **2009**, *23*, 57–68.
- (15) Wang, J.; Anthony, E. J. *Appl. Energy* **2008**, *85*, 73–79.
- (16) Cuadrat, A.; Abad, A.; Garc a-Labiano, F.; Gay an, P.; de Diego, L. F.; Ad anez, J. *Int. J. Greenhouse Gas Control* **2011**, *5*, 1630–1642.
- (17) Leon, H.; Mattisson, T.; Lyngfelt, A. *Energy Fuels* **2009**, *23*, 2307–2315.
- (18) Shen, L.; Wu, J.; Xiao, J.; Song, Q.; Xiao, R. *Energy Fuels* **2009**, *23*, 2498–2505.
- (19) Mendiara, T.; Abad, A.; de Diego, L. F.; Garc a-Labiano, F.; Gay an, P.; Ad anez, J. *Energy Fuels* **2012**, *26*, 1420–1431.

- (20) Mattisson, T.; Lyngfelt, A.; Leion, H. *Int. J. Greenhouse Gas Control* **2009**, *3*, 11–19.
- (21) Mattisson, T.; Leion, H.; Lyngfelt, A. *Fuel* **2009**, *88*, 683–690.
- (22) Adánez-Rubio, I.; Abad, A.; Gayán, P.; de Diego, L. F.; García-Labiano, F.; Adánez, J. *Proceedings of the International Conference on Coal Science and Technology (ICCS&T)*; Oviedo, Spain, Oct 9–13, 2011.
- (23) Outotec Research Oy. *HSC Chemistry 6.1. Chemical Reaction and Equilibrium Software with Thermochemical Database and Simulation Module*; Outotec Research Oy: Pori, Finland, 2008.
- (24) Adánez, J.; de Diego, L. F.; García-Labiano, F.; Gayán, P.; Abad, A.; Palacios, J. M. *Energy Fuels* **2004**, *18* (2), 71–77.
- (25) de Diego, L. F.; García-Labiano, F.; Adánez, J.; Gayán, P.; Abad, A.; Corbella, B. M.; Palacios, J. M. *Fuel* **2004**, *83* (13), 49–57.
- (26) de Diego, L. F.; Gayán, P.; García-Labiano, F.; Celaya, J.; Abad, A.; Adánez, J. *Energy Fuels* **2005**, *19* (5), 1850–1856.
- (27) Adánez-Rubio, I.; Gayán, P.; García-Labiano, F.; de Diego, L. F.; Adánez, J.; Abad, A. *Energy Procedia* **2011**, *4*, 417–424.
- (28) Gayán, P.; Adánez-Rubio, I.; Abad, A.; de Diego, L. F.; García-Labiano, F.; Adánez, J. *Fuel* **2012**, *96*, 226–238.
- (29) Abad, A.; Adánez-Rubio, I.; Gayán, P.; García-Labiano, F.; de Diego, L. F.; Adánez, J. *Int. J. Greenhouse Gas Control* **2012**, *6*, 189–200.
- (30) Zhu, Y.; Mimura, K.; Isshiki, M. *Oxid. Met.* **2003**, *59* (5–6), 575–590.
- (31) Zhu, Y.; Mimura, K.; Lim, J. W.; Isshiki, M.; Jiang, Q. *Metall. Mater. Trans. A* **2006**, *37*, 1231–1237.
- (32) Eyring, E.; Konya, G.; Lighty, J.; Sahir, A.; Sarofim, A.; Whitty, K. *Oil Gas Sci. Technol.* **2011**, *2*, 209–221.



## **Paper III**



# Investigation of Combined Supports for Cu-Based Oxygen Carriers for Chemical-Looping with Oxygen Uncoupling (CLOU)

Iñaki Adánez-Rubio,<sup>†</sup> Mehdi Arjmand,<sup>\*,‡</sup> Henrik Leion,<sup>‡</sup> Pilar Gayán,<sup>†</sup> Alberto Abad,<sup>†</sup> Tobias Mattisson,<sup>§</sup> and Anders Lyngfelt<sup>§</sup>

<sup>†</sup>Instituto de Carboquímica (ICB-CSIC), Department of Energy & Environment, Miguel Luesma Castán, 4, Zaragoza, 50018, Spain

<sup>‡</sup>Department of Chemical and Biological Engineering, Division of Environmental Inorganic Chemistry, Chalmers University of Technology, SE-412 96 Göteborg, Sweden

<sup>§</sup>Department of Energy and Environment, Division of Energy Technology, Chalmers University of Technology, SE-412 96 Göteborg, Sweden

**ABSTRACT:** The chemical-looping with oxygen uncoupling (CLOU) process is a novel solution for efficient combustion with inherent separation of carbon dioxide. The process uses a metal oxide as an oxygen carrier to transfer oxygen from an air to a fuel reactor. In the fuel reactor, the metal oxide releases gas phase oxygen, which oxidizes the fuel through normal combustion. In this study, Cu-based oxygen carrier materials that combine different supports of MgAl<sub>2</sub>O<sub>4</sub>, TiO<sub>2</sub>, and SiO<sub>2</sub> are prepared and characterized with the objective of obtaining highly reactive and attrition resistant particles. The oxygen carrier particles were produced by spray-drying and were calcined at different temperatures ranging from 950 to 1030 °C for 4 h. The chemical-looping performance of the oxygen carriers was examined in a batch fluidized-bed reactor in the temperature range of 900–950 °C under alternating reducing and oxidizing conditions. The mechanical stability of the oxygen carriers was tested in a jet-cup attrition rig. All of the oxygen carriers showed oxygen uncoupling behavior with oxygen concentrations close to equilibrium. During reactivity tests with methane, oxygen carriers with lower mechanical stability showed higher reactivity, yielding almost complete fuel conversion. Oxygen carrier materials based on support mixtures of MgAl<sub>2</sub>O<sub>4</sub>/TiO<sub>2</sub>, MgAl<sub>2</sub>O<sub>4</sub>/SiO<sub>2</sub>, and TiO<sub>2</sub>/SiO<sub>2</sub> showed a combination of high mechanical stability, low attrition rates, good reactivity with methane, and oxygen uncoupling behavior.

## 1. INTRODUCTION

The intergovernmental panel on climate control (IPCC) has suggested that a 50–85% reduction in total CO<sub>2</sub> emission is necessary by 2050 to restrict the predicted global temperature rise to 2 °C.<sup>1</sup> In order to mitigate the increasing levels of carbon dioxide in the atmosphere, several technologies have been proposed. Among suggested alternatives, one solution is to reduce the CO<sub>2</sub> emissions in combustion processes by means of a scheme, generally called Carbon Capture and Storage (CCS). However, the greatest drawback with most of the proposed processes is that there are large costs and energy penalties incurred due to gas separation steps needed in order to obtain CO<sub>2</sub> in a pure form. Consequently, the overall efficiency of the power generation process may decrease by approximately 7–15%, when using conventional capture techniques in comparison to combustion without carbon capture. One solution for this problem is chemical-looping combustion (CLC).<sup>2</sup>

The principle concept of the chemical-looping combustion process is based on two interconnected reactors, an air and a fuel reactor, with an oxygen carrier circulating between them.<sup>3–5</sup> The scheme of the CLC process is shown in Figure 1. When fuel and air are introduced into the respective reactors, the following reactions occur, i.e., reaction 1 in the fuel reactor and reaction 2 in the air reactor:

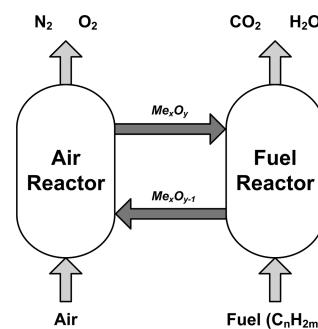
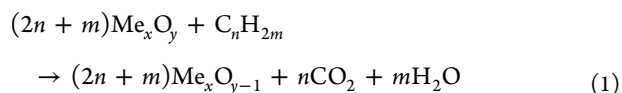
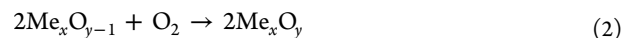


**Figure 1.** Schematic of the chemical-looping combustion (CLC) process.



Here, Me<sub>x</sub>O<sub>y</sub> and Me<sub>x</sub>O<sub>y-1</sub> are the oxidized and the reduced forms of an oxygen carrier. C<sub>n</sub>H<sub>2m</sub> is the fuel, which could be gas, liquid, or solid. In the event of complete fuel conversion, the exhaust stream from the fuel reactor would ideally consist of only CO<sub>2</sub> and water steam, from which pure CO<sub>2</sub> could be obtained after condensing the water. The reduced oxygen carrier (Me<sub>x</sub>O<sub>y-1</sub>) would then be circulated back to the air reactor to reoxidize with air, thus becoming ready for the next cycle. The reaction in the fuel reactor can be either endothermic or exothermic depending on the fuel and the oxygen carrier;

Received: April 16, 2013

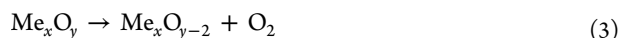
Published: June 24, 2013



however, the oxidation of the oxygen carrier in the air reactor is always exothermic.<sup>6</sup> By combining the reduction, eq 1, with the oxidation, eq 2, it is seen that the overall reaction becomes identical with the conventional combustion process, which shows that the CLC process does not entail any direct energy penalty for CO<sub>2</sub> separation.

The chemical-looping combustion (CLC) process was initially introduced by Lewis and co-workers<sup>7</sup> to produce a pure stream of CO<sub>2</sub>. In 1994, Ishida and Jin<sup>8</sup> suggested that this technique could be used for CO<sub>2</sub>-capture from power plants. In 2001, Lyngfelt et al.<sup>3</sup> proposed a unit consisting of two interconnected fluidized-bed units to implement the chemical-looping combustion process. The process was first demonstrated for gaseous fuels in 2003.<sup>9</sup> Later, Kolbitsch et al.<sup>10</sup> designed, built, and operated a 120 kW unit consisting of two circulating fluidized bed reactors. To date, CLC has been successfully demonstrated in a number of units of sizes up to 120 kW<sup>11</sup> and overviews of current achievements in CLC are given by Lyngfelt,<sup>11,12</sup> Hossain and de Lasa,<sup>13</sup> and Adanez et al.<sup>14</sup>

In general, the use of solid fuels, such as coal, in CLC requires one more step than the combustion of gaseous fuels. Solid fuel conversion through direct solid–solid contact between the oxygen carrier and the fuel is not expected to occur at an appreciable rate. Hence, there are two options for using solid fuels in this case, CLC with gasification of solid fuels<sup>15</sup> and chemical-looping with oxygen uncoupling (CLOU).<sup>16</sup> The first approach involves gasifying the char that remains after devolatilization in the presence of steam, which produces CO and H<sub>2</sub>. These gases can then react with the oxygen carrier to produce CO<sub>2</sub> and H<sub>2</sub>O similar to eq 1. However, in the case of CLOU, an oxygen carrier provides gaseous oxygen during the reduction phase, according to eq 3, and the char reacts directly with the uncoupled gaseous oxygen:



The reduced oxygen carrier is then transferred to the air reactor for reoxidation. The overall heat of reaction for the CLOU process is the same as for CLC, and only the mechanism by which the fuel accesses the oxygen in the carrier is different. Furthermore, the CLOU process benefits from avoiding the slow gasification of the solid fuel that is needed to produce the synthesis gas that can react with the oxygen carrier.<sup>16</sup> It should be emphasized that the oxygen carrier in CLOU must be able to both react with O<sub>2</sub> (oxidize) and release O<sub>2</sub> at temperatures suitable for the process, i.e., 800 to 1200 °C.

The most commonly proposed approach to realizing CLC is to use interconnected fluidized-bed reactors in a fashion similar to the circulating fluidized-bed boiler (CFB),<sup>3</sup> the difference being that CLC will require an active oxygen carrier rather than inert sand as the bed material. Conventional CFB boilers often operate at an air to fuel ratio of about 1.2, which in the case of CLC corresponds to an outlet oxygen concentration from the air reactor close to 5%. It is important to note that this concentration is somewhat higher than in normal combustion since the flue gas from the air reactor does not contain CO<sub>2</sub>. As a result of this, oxide systems with an equilibrium oxygen partial pressure lower than 5% at temperatures typical of the air reactor are desirable. Otherwise, a higher air ratio than in the conventional combustion process will be required, which would result in a higher heat loss due to a larger flue gas stream. Moreover, the oxygen carrier should also be able to release a sufficiently large amount of oxygen in the fuel reactor and at a sufficiently high rate. Thus, the choice of oxygen carriers for the CLOU process is limited by

these kinds of considerations. Demonstration of the CLOU process<sup>17</sup> has proven the advantage of this technology over the CLC process, where slow gasification is an imperative step.<sup>18</sup> Moreover, the solids inventory in the fuel reactor of the CLOU process would be lower than in CLC,<sup>19,20</sup> which means avoiding the need for a carbon stripper for reaching a high CO<sub>2</sub> capture rate.<sup>20</sup>

An essential aspect in the development of the CLC and the CLOU processes is the selection of oxygen carrier materials with reasonable reactivity. Oxygen carriers consisting of oxides of transition metals (Mn, Fe, Co, Ni, and Cu), their mixtures, and a number of natural minerals (ores), industrial wastes, and byproducts have been investigated in CLC and CLOU.<sup>11–14</sup> In general, important characteristics of the oxygen carriers are reactivity during oxidation and reduction over a large number of cycles and the ability to fully convert the fuel. Furthermore, thermal and mechanical stability, proper fluidization characteristics, and resistance to attrition and agglomeration are sought-after properties. One way of achieving these properties in oxygen carriers is to combine the active phase (carrier oxide) with an inert support such as TiO<sub>2</sub>, SiO<sub>2</sub>, ZrO<sub>2</sub>, Al<sub>2</sub>O<sub>3</sub>, or MgAl<sub>2</sub>O<sub>4</sub> during particle fabrication and/or heat-treating the oxygen carriers.<sup>13</sup>

Considerable attention has been given to copper-oxide materials as efficient oxygen carriers, owing to their high oxygen transport capacity, high reactivity, and absence of thermodynamic limitation, for the complete conversion of the fuel.<sup>11–14</sup> Among various investigated supports for CuO oxygen carriers, Al<sub>2</sub>O<sub>3</sub> has been extensively used.<sup>21–32</sup> However, when Al<sub>2</sub>O<sub>3</sub> is used as the support, there is a facile interaction between CuO and Al<sub>2</sub>O<sub>3</sub>, during either fabrication or operation, which results in the partial loss of CuO and CLOU behavior due to the formation of copper(II) aluminate (CuAl<sub>2</sub>O<sub>4</sub>) and copper(I) aluminate (CuAlO<sub>2</sub>; delafossite) phases.<sup>21–32</sup> Since the copper-aluminate phases are highly reducible,<sup>21–32</sup> this interaction does not necessarily create any obstacle with respect to CLC application. For application in CLOU, however, this interaction should be hindered in order to preserve CuO as the active phase, for instance by using other supports such as TiO<sub>2</sub>, ZrO<sub>2</sub>, SiO<sub>2</sub>, or MgAl<sub>2</sub>O<sub>4</sub>.

Most of the studies using Cu-based oxygen carriers have been carried out at low temperatures (~800 °C) where the CLOU effect is minor, i.e., the application for CLC.<sup>11–14</sup> However, at higher temperatures (~950 °C), an increase in the carbon conversion rate in the presence of CuO particles has been reported and has been associated with the direct oxidation of char.<sup>7</sup> It is now well established that CuO decomposes to Cu<sub>2</sub>O when the actual concentration of oxygen is lower than the equilibrium concentration.<sup>16</sup> Consequently, oxygen is released, which allows CLOU to take effect. For temperatures of 900 and 925 °C, this occurs at oxygen concentrations below 1.5 and 2.7%, respectively.<sup>16</sup> Thus, from a CLOU point of view, the optimum temperature of the air reactor is most likely in the range of 900 to 925 °C for Cu-based oxygen carriers. Research has also been conducted on Cu-based oxygen carriers in the temperature regime applicable for CLOU in fluidized-bed batch reactors,<sup>16,19,20,23,33–39</sup> continuous operations,<sup>17,34,40,41</sup> and thermogravimetric studies,<sup>35,42–44</sup> with and without supports.

The major issue in the development of Cu-based oxygen carriers for CLOU has been the mechanical stability of the carriers during continuous operation. One suitable and often-used criterion for characterizing the mechanical integrity of oxygen carriers has been the crushing strength (CS), i.e., the

Table 1. Oxygen Carriers Prepared in This Work

oxygen carrier <sup>a</sup>	active phase (content [wt %])	support phase (content [wt %])	crushing strength (CS) [N]	comments
C4T6_950			3.2	
C4T6_970		TiO <sub>2</sub> (60)	4.1	
C4T6_1000			—	formation of melt
C4MA6_1000		MgAl <sub>2</sub> O <sub>4</sub> (60)	0.6	
C4MA6_1030			0.8	
C4S6_1000		SiO <sub>2</sub> (60)	0.7	
C4S6_1030			0.5	
C4MA4T2_970			1.0	
C4MA4T2_1000		MgAl <sub>2</sub> O <sub>4</sub> (40), TiO <sub>2</sub> (20)	1.5	
C4MA4T2_1030			—	formation of melt
C4MA2T4_970			1.3	
C4MA2T4_1000		MgAl <sub>2</sub> O <sub>4</sub> (20), TiO <sub>2</sub> (40)	1.0	
C4MA2T4_1030			—	formation of melt
C4MA4S2_970	CuO (40)		—	formation of soft particles
C4MA4S2_1000		MgAl <sub>2</sub> O <sub>4</sub> (40), SiO <sub>2</sub> (20)	1.4	
C4MA4S2_1030			1.7	
C4MA2S4_1000		MgAl <sub>2</sub> O <sub>4</sub> (20), SiO <sub>2</sub> (40)	—	formation of soft particles
C4MA2S4_1030			—	
C4T4S2_950			1.7	
C4T4S2_970		TiO <sub>2</sub> (40), SiO <sub>2</sub> (20)	1.8	
C4T4S2_1000			—	formation of melt
C4T2S4_1000			1.1	
C4T2S4_1030		TiO <sub>2</sub> (20), SiO <sub>2</sub> (40)	1.0	
C4MA2T2S2_950			—	
C4MA2T2S2_970			—	
C4MA2T2S2_1000		MgAl <sub>2</sub> O <sub>4</sub> (20), TiO <sub>2</sub> (20), SiO <sub>2</sub> (20)	—	formation of melt
C4MA2T2S2_1030			—	

<sup>a</sup>Example of nomenclature for the oxygen carriers. C4MA4T2\_1000: C4, 40 wt % CuO; MA4, 40 wt % MgAl<sub>2</sub>O<sub>4</sub>; T2, 20 wt % TiO<sub>2</sub>; 1000, sintering temperature [°C].

force needed to fracture a single particle. Oxygen carriers with a crushing strength above 1 N have generally shown better performance with respect to attrition in continuous operation. A recent investigation has shown that oxygen carrier particles with a crushing strength above 2 N are more likely to resist attrition than softer particles.<sup>45</sup> For Cu-based oxygen carriers, MgAl<sub>2</sub>O<sub>4</sub>-supported CuO materials have been successfully used as the CLOU oxygen carrier in continuous operation,<sup>17,40</sup> showing complete fuel conversion and high carbon capture efficiency.<sup>40</sup> Although the crushing strength of the fresh particles has been reported above 1 N, their mechanical stability has been found to decrease substantially after 40 h in continuous operation.<sup>34</sup> Nevertheless, the oxygen uncoupling behavior and fuel conversion of these particles was not affected.

The aim of this study is to investigate whether combining different supports of MgAl<sub>2</sub>O<sub>4</sub>, TiO<sub>2</sub>, and SiO<sub>2</sub> could potentially increase the mechanical stability of Cu-based oxygen carriers for the CLOU application. The oxygen uncoupling property of these oxygen carriers during N<sub>2</sub> exposure and their reactivity with methane in the temperature range of 900–950 °C has been assessed. In addition, the oxygen carriers have been evaluated in a jet-cup attrition rig with regard to their attrition resistance and mechanical integrity.

## 2. EXPERIMENTAL SECTION

**2.1. Preparation and Fabrication of the Oxygen Carriers.** The oxygen carriers prepared in this investigation are summarized in Table 1. The particles were manufactured by spray-drying at VITO (Flemish Institute for Technological Research, Belgium). In this technique, a water-based slurry of CuO (Sigma Aldrich) and the intended combination of support powders of MgAl<sub>2</sub>O<sub>4</sub> (S30CR, Baikowski),

TiO<sub>2</sub> (Alfa Aesar), and SiO<sub>2</sub> (SilverBond M800, Sibelco) were prepared. All particles were prepared to obtain 40 wt % CuO and 60 wt % support material, but the support materials were combined in different ratios of 20/40 wt % (or 40/20 wt %) and 20/20/20 wt %. The powder mixtures were then ball milled, and organic binders were added prior to spray-drying. During continuous stirring, the slurry was pumped through a spray-drying nozzle to form spherical particles which were then injected into the hot spray-drying chamber. After drying and collecting, the fraction between 106 and 212 μm was separated from the rest of the batch by sieving. This was followed by calcination of the material at the selected temperature indicated in Table 1 for 4 h. The calcined material was sieved through stainless steel screens to yield particles in the range of 125–180 μm. It should be mentioned that it was not possible to obtain any materials with a combination of all three supports, i.e. C4AM2T2S2, because the materials melted during calcination, even at lower temperatures. Also, the C4AM2S4 formulation failed because the calcined particles were too soft. It may be possible that the combination of the different supports and the active phase with the given composition resulted in mixtures with a lower melting point than the pure substances. This is a phenomenon common in solid mixtures consisting of different oxides when heat-treated at high temperatures.

**2.2. Characterization of the Oxygen Carriers.** The crystalline phases of the oxygen carriers were identified using powder X-ray diffraction (Bruker AXS, D8 Advanced) with Cu Kα1 radiation. The bulk (tapped) density was obtained for particles in the size range of 125–180 μm with a graduated cylinder. The Brunauer–Emmett–Teller (BET) specific surface area was determined using N<sub>2</sub>-adsorption (Micromeritics, TriStar 3000). The particle size distribution (PSD) was calculated using a light microscope (Nikon, SMZ800) and ImageJ software,<sup>46</sup> which measured the area of an ellipse fitted to a large number of particles. The crushing strength, i.e., the force needed to fracture a single particle, was found by using a digital force gauge (Shimpo, FGN-5) for particles in the size range of 180–250 μm. Thirty measurements were made for every sample, and the average measurement was chosen



as the representative crushing strength. The morphology of the particles was examined with an environmental scanning electron microscope (ESEM) fitted with a field emission gun (FEI, Quanta 200).

The attrition rate of the particles sized 125–180  $\mu\text{m}$  was measured using a customized jet-cup attrition rig,<sup>45</sup> which simulates the effects of grid jet attrition and cyclone attrition in a circulating fluidized-bed combustor. The jet-cup attrition rig consisted of a conical cup located at the bottom of the apparatus with a nozzle that was tangentially introduced in relation to the cup wall. The cup was placed at the bottom of a gravitational particle-gas separator, which was an additional cone. Due to the increasing cross-section area in the upper cone, the gas velocity in the settling chamber was much lower compared to the inlet. Therefore, the low gas velocity in this upper region allowed the elutriated particles to fall back into the cup, while the produced fines were allowed to exit. At the top of the apparatus, a particle filter with a mesh size of 0.01  $\mu\text{m}$  was mounted to collect the fines. Approximately, 5 g of a fresh sample was placed inside the cup, and the apparatus was assembled. Air at 10 L/min was introduced at the nozzle, which corresponds to an air jet velocity of approximately 94 m/s. In order to avoid static electricity, which otherwise would cause particles to adhere to the inner walls of the apparatus, the air was humidified by bubbling it through a column of water. Six measurements at 10 min intervals were made for every sample. These experiments were carried out at room temperature and near atmospheric pressure.<sup>45</sup>

**2.3. Experimental Setup and Procedure in the Fluidized-Bed Reactor.** A laboratory-scale fluidized-bed reactor system was used for examining the oxygen uncoupling behavior and the reactivity of the oxygen carriers. The scheme of the experimental setup used in this investigation is shown in Figure 2. The dimensions of the quartz reactor

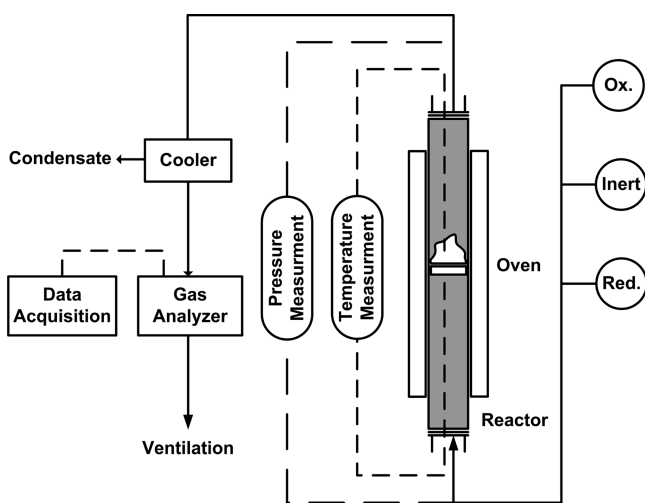


Figure 2. Schematic of the experimental setup used in this investigation.

were as follows: 870 mm high and 22 mm in inner diameter with a porous quartz plate located at a height of 370 mm from the bottom. The reactor temperature was measured with chromel-alumel (type K) thermocouples sheathed in inconel-600 located about 5 mm below and 25 mm above the plate. Pressure transducers (Honeywell) were used to measure the pressure drop over the bed of particles and the quartz plate at a frequency of 20 Hz. The pressure drop over the quartz plate was approximately constant for constant flows. Thus, it was possible to determine if the particles were fluidized or not, by measuring the fluctuations in the pressure drop; i.e., a defluidization would be noted from a decrease in pressure fluctuations. The exit gas stream from the reactor was led into a condenser to remove the water that was generated during the oxidation of the fuel. The composition of the dry gas was measured using a Rosemount NGA-2000 analyzer which measured the concentration of  $\text{O}_2$  through a paramagnetic channel and  $\text{CO}_2$ , CO, and  $\text{CH}_4$  through infrared channels with correction for other measured gases.

Fifteen grams of the sample was placed on the porous plate, and the reactor was heated to 900  $^\circ\text{C}$  in an 11%  $\text{O}_2$ –balance  $\text{N}_2$  mixture, in order to oxidize the oxygen carrier fully, prior to experiments. In previous investigations using the same experimental setup,<sup>23,47</sup> a 5%  $\text{O}_2$  stream was used during the oxidation phase. This was done in order to determine whether the oxygen carrier could be oxidized under oxygen deficient conditions similar to those at the outlet of the air reactor in a realistic CLC unit. The rationale of using an 11%  $\text{O}_2$  stream instead, in this study, was to accelerate the oxidation process, particularly at 950  $^\circ\text{C}$ , at which point the equilibrium oxygen concentration over  $\text{CuO}$ – $\text{Cu}_2\text{O}$  is approximately 4.5%. Hereinafter, the term “cycle” will be used to mean a redox cycle involving the reduction of the oxygen carrier sample in inert gas or fuel, followed by oxidation with the aforementioned 11%  $\text{O}_2$  mixture. A set of three inert gas ( $\text{N}_2$ ) cycles was carried out at 900, 925, and 950  $^\circ\text{C}$  for 360 s, to investigate the oxygen release. Subsequent to the inert cycles, fuel cycles with 100% methane for 20 s during the reduction period were carried out at 900, 925, and 950  $^\circ\text{C}$ . Nitrogen was used as an inert purge for 60 s in between the oxidation and reduction periods. Each cycle was repeated three times to establish reproducibility of the performance. Thus, the performance of the oxygen carriers was evaluated in a total of 18 cycles corresponding to approximately 8 h of operation under hot conditions in the fluidized-bed reactor. Flow rates of 450, 600, and 900  $\text{mL}_{\text{N}}/\text{min}$  were used during reduction, inert, and oxidation, respectively. These flow rates were chosen to achieve a value of the superficial gas velocity,  $U$ , in the reactor approximately 4–12, 8–23, and 13–35 times higher than the calculated minimum fluidization gas velocity,  $U_{\text{mf}}$  of the oxygen carrier particles during reduction (with methane), inert, and oxidation periods, respectively. The minimum fluidization velocity,  $U_{\text{mf}}$ , was calculated by using the correlation given by Kunii and Levenspiel.<sup>48</sup> However, it should be noted that due to gas expansion during reduction, the actual velocity in the bed was higher, as 1 mol of  $\text{CH}_4$  was converted to 1 mol of  $\text{CO}_2$  and 2 mol of  $\text{H}_2\text{O}$ . There was no carbon deposition during the reduction period, which would have been identified by way of carbon burnoff in the subsequent oxidation period. This was due to the fact that the oxygen available in the oxygen carriers was more than the stoichiometric demand of the fuel.

**2.4. Data Analysis.** The reactivity of a given oxygen carrier has been quantified in terms of gas yield or conversion efficiency,  $\gamma$ , and has been defined as the fraction of fully oxidized fuel divided by the carbon containing gases in the outlet stream, in this study  $\text{CO}_2$ , CO, and  $\text{CH}_4$ .

$$\gamma_{\text{CH}_4} = \frac{y_{\text{CO}_2}}{y_{\text{CO}_2} + y_{\text{CH}_4} + y_{\text{CO}}} \quad (4)$$

Here,  $y_i$  denotes the concentration (vol %) of the respective gas measured with the gas analyzer.

In order to facilitate a comparison between different oxygen carriers at varying temperatures,  $\gamma_{\text{CH}_4, \text{ave}}$  is used, which is defined as the average of gas yield in eq 5 for the entire reduction period.

The mass-based conversion of the oxygen carrier,  $\omega$ , is defined as

$$\omega = \frac{m}{m_{\text{ox}}} \quad (5)$$

where  $m$  is the actual mass of the oxygen carrier during the experiments.

Equation 6 is employed for calculating  $\omega$  as a function of time during the reduction period from the measured concentrations of various gaseous species:

$$\omega_i = 1 - \int_{t_0}^{t_1} \frac{\dot{n}_{\text{out}} M_{\text{O}}}{m_{\text{ox}}} (4y_{\text{CO}_2} + 2y_{\text{O}_2} - y_{\text{H}_2}) dt \quad (6)$$

where  $\omega_i$  is the instantaneous mass-based conversion at time  $t_1$ ,  $\dot{n}_{\text{out}}$  is the molar flow rate of the dry gas at the reactor outlet as measured with the analyzer,  $M_{\text{O}}$  is the molar mass of oxygen, and  $t_0$  and  $t_1$  are the initial and final times of measurement.

## 3. RESULTS

**3.1. Oxygen Uncoupling of the Carriers.** Reduction–oxidation multicycles were carried out in a fluidized-bed reactor

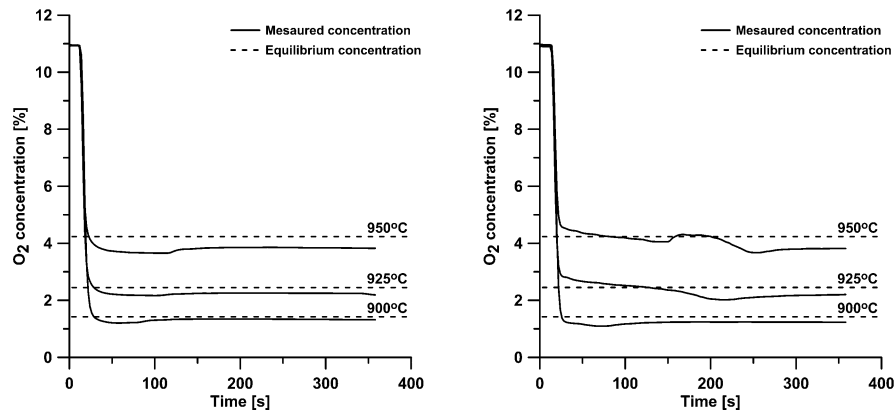


Figure 3. Measured and equilibrium oxygen concentrations during the inert period at different bed temperatures for (left) C4S6\_1000 and (right) C4MA4T2\_970.

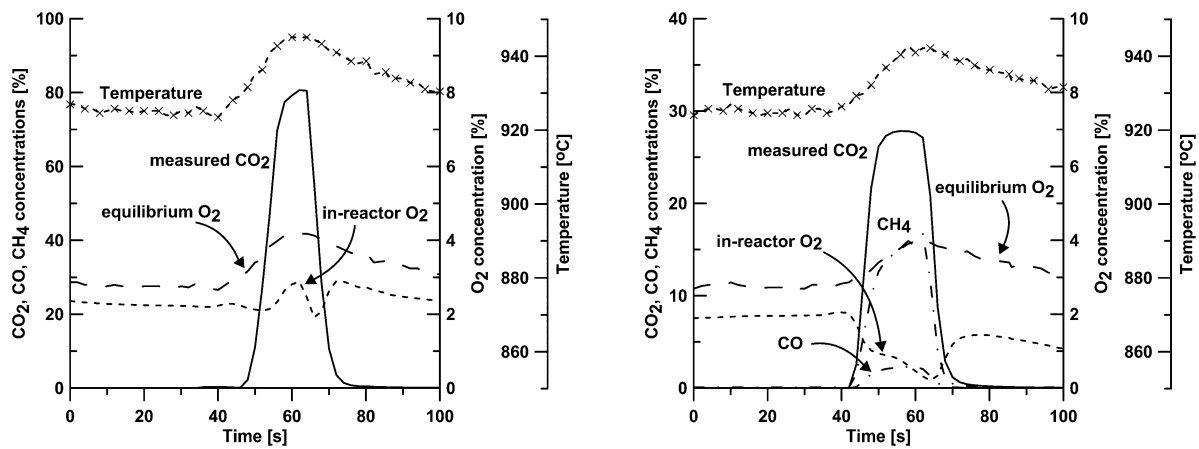


Figure 4. Concentration and temperature profiles for C4MA6\_1030 (left) and C4MA4S2\_1030 (right) during reduction cycle with methane at 925 °C.

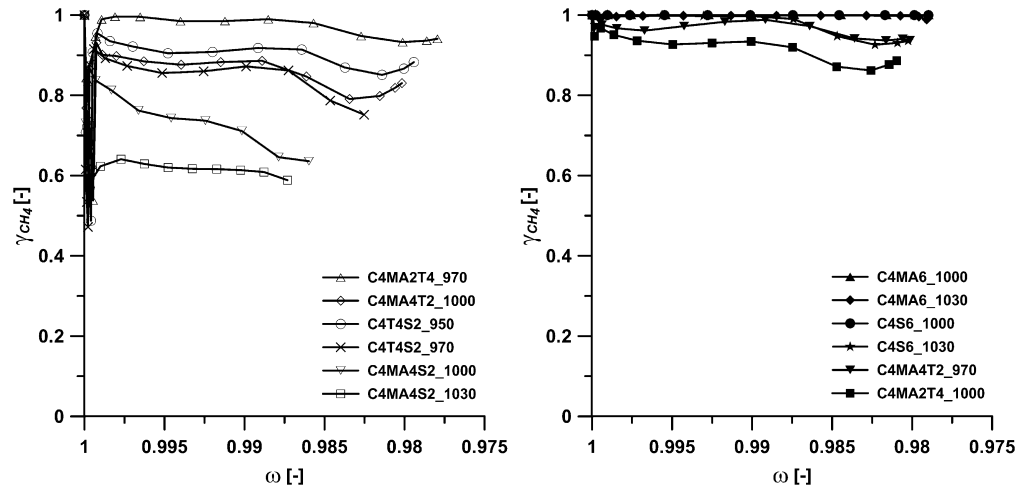
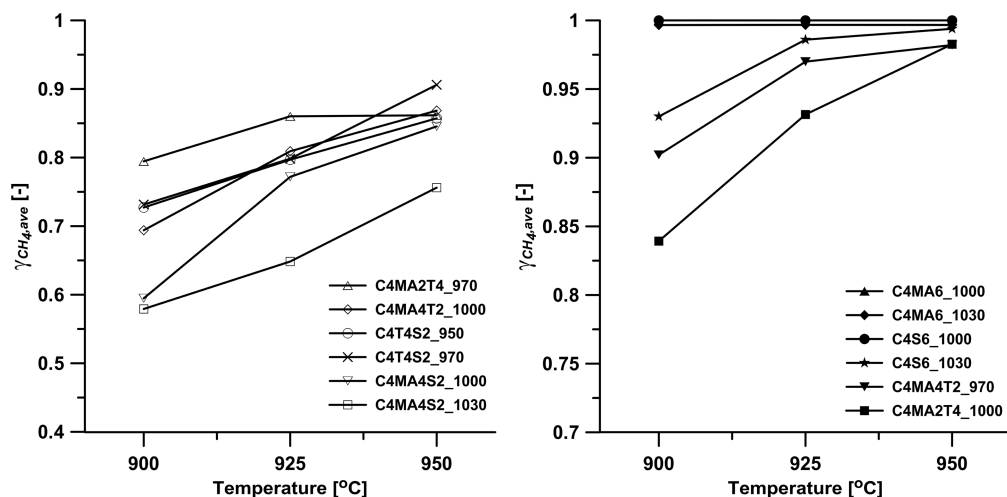


Figure 5. Reactivity (gas yield,  $\gamma$ , vs. mass based conversion,  $\omega$ ) of oxygen carriers with methane as the fuel at 950 °C for oxygen carriers with CS > 1 (left) and oxygen carriers with CS  $\leq$  1 (right).

to investigate the oxygen release behavior of the oxygen carriers, the reactivity with methane, and the fluidization behavior of the materials with respect to agglomeration and/or defluidization. The oxygen carriers with only TiO<sub>2</sub> (C4T6) and with a combination of 20 wt % TiO<sub>2</sub> and 40 wt % SiO<sub>2</sub> (C4T2S4) as the support agglomerated during the first inert cycle and thus were not further investigated. As an example, Figure 3 shows the oxygen concentration in the outgoing gas from the reactor for the

C4S6\_1000 and C4MA4T2\_970 oxygen carriers and the corresponding equilibrium oxygen concentration at three different temperatures, i.e. 900, 925, and 950 °C. During the inert period, the majority of the oxygen carriers investigated in this study released oxygen close to the corresponding equilibrium concentration at the different temperatures studied.

**3.2. Reactivity of the Oxygen Carriers.** Figure 4 shows the gas concentration and the temperature profiles during the



**Figure 6.** Average gas yield,  $\gamma_{CH_4,ave}$ , as a function of temperature for oxygen carriers with CS > 1 (left) and oxygen carriers with CS ≤ 1 (right). Note: For reasons of clarity, the scale of  $\gamma_{CH_4,ave}$  is different in the figures.

reactivity test with methane at 925 °C for the C4MA6\_1030 and C4MA4S2\_1030 oxygen carriers. It can be seen that for C4MA6\_1030 as the oxygen carrier, Figure 4 (left), there is complete conversion of fuel to CO<sub>2</sub> and H<sub>2</sub>O. During reduction, the temperature in the bed increased by approximately 25 °C, and thus the oxygen carrier released more oxygen. This and the complete fuel conversion obtained here are primarily due to the fast rate of oxygen release from this carrier. The high reactivity of the C4MA6\_1030 formulation is also in conformity with previous investigations using the MgAl<sub>2</sub>O<sub>4</sub>-supported CuO oxygen carrier.<sup>17,20,23,34,35,40</sup> Subsequent to reduction, the oxygen carrier continued releasing oxygen close to equilibrium concentration. It should be noted that the in-reactor O<sub>2</sub> concentration accounts for the dilution created by water produced during the conversion of methane, which was later removed in the condenser. For C4MA4S2\_1030 as the oxygen carrier, Figure 4 (right), there was incomplete conversion of methane and unconverted products, such as CO and CH<sub>4</sub>, observed at the reactor's outlet stream. Moreover, during the reduction, the release of O<sub>2</sub> from the oxygen carrier decreased. These effects could be attributed to the much slower rate of oxygen release for this carrier than for the C4MA6\_1030 material.

Figure 5 shows the gas yield as a function of the mass-based conversion of all of the investigated oxygen carriers at 950 °C using methane as the fuel for the third repeated cycle. It can be observed that, in general, oxygen carriers with a higher crushing strength, as shown in Figure 5 (left), exhibited a lower reactivity or slower rate of oxygen release than those with a lower crushing strength, as illustrated in Figure 5 (right). Thus, most of the oxygen carriers with a crushing strength of 1 or lower exhibited close to complete conversion of the fuel. For instance, oxygen carriers prepared with only MgAl<sub>2</sub>O<sub>4</sub> (C4MA6) or SiO<sub>2</sub> (C4S6) as the support showed the highest reactivity during methane conversion with  $\gamma$  close to 1 and a change in the mass-based conversion,  $\omega$ , of the carriers of approximately 2%. However, when mixtures of these supports were used (C4MA4S2), the reactivity of the oxygen carriers decreased substantially. It may be possible that the addition of SiO<sub>2</sub> resulted in lowered gas diffusion in the oxygen carriers in comparison to their counterparts with single-phase supports. However, this was not the case for oxygen carriers based on MgAl<sub>2</sub>O<sub>4</sub>/TiO<sub>2</sub>

(C4MA2T4\_970 and C4MA4T2\_1000) and TiO<sub>2</sub>/SiO<sub>2</sub> (C4T4S2) as the support. Despite having crushing strengths higher than 1, the latter oxygen carriers also showed reasonably high fuel conversion with  $\gamma$  higher than 0.9 and a change in the mass-based conversion,  $\omega$ , of the carriers of approximately 2%.

Figure 6 shows the average gas yield,  $\gamma_{CH_4,ave}$ , as a function of temperature for the investigated oxygen carriers that used methane as the fuel and for the third repeated cycle. It can be observed that for most of the oxygen carriers, the average gas yield for methane rose with the temperature, likely due to a faster rate of oxygen release at higher temperatures. Table 2 summarizes the overall functionality of the oxygen carriers

**Table 2. Overall Functionality of the Oxygen Carriers during the Reactivity Tests**

oxygen carrier	agglomeration during inert cycles	oxygen concentration during inert gas periods	gas conversion
C4T6_950	yes		
C4T6_970	yes		
C4MA6_1000	no	very close to equilibrium	very high
C4MA6_1030	no	very close to equilibrium	very high
C4S6_1000	no	very close to equilibrium	very high
C4S6_1030	no	very close to equilibrium	very high
C4MA4T2_970	no	slightly lower than equilibrium	high
C4MA4T2_1000	no	slightly lower than equilibrium	high
C4MA2T4_970	no	slightly lower than equilibrium	high
C4MA2T4_1000	no	slightly lower than equilibrium	high
C4MA4S2_1000	no	lower than equilibrium	average
C4MA4S2_1030	no	lower than equilibrium	average
C4T4S2_950	no	slightly lower than equilibrium	high
C4T4S2_970	no	slightly lower than equilibrium	high
C4T2S4_1000	yes		
C4T2S4_1030	yes		

Table 3. Physical and Chemical Properties and Characteristics of the Tested Oxygen Carriers As Prepared and Used

oxygen carrier	bulk density [ $\text{g}/\text{cm}^3$ ] <sup>a</sup>			BET specific surface area [ $\text{m}^2/\text{g}$ ] <sup>a</sup>			crystalline phases detected by XRD
	fresh	trend	used	fresh	trend	used	
C4MA6_1000	0.97	↓	0.80	8.81	↓	7.99	CuO, $\text{MgAl}_2\text{O}_4$
C4MA6_1030	1.03	↓	0.79	7.05	—	7.09	
C4S6_1000	0.93	—	0.91	1.10	↑	1.58	CuO, $\text{SiO}_2$ (quartz), $\text{SiO}_2$ (cristobalite)
C4S6_1030	0.96	↓	0.88	0.71	—	0.71	
C4MA4T2_970	1.54	↓	1.34	0.21	↑	0.67	$\text{MgAl}_2\text{O}_4$ , $\text{MgTi}_2\text{O}_5$ , CuO
C4MA4T2_1000	1.71	↓	1.30	0.04	↑	0.67	
C4MA2T4_970	1.55	↓	1.30	0.25	↑	0.74	$\text{MgAl}_2\text{O}_4$ , $\text{TiO}_2$ , CuO, $\text{MgTi}_2\text{O}_5$
C4MA2T4_1000	1.54	↓	1.18	0.04	↑	0.58	
C4MA4S2_1000	1.67	↓	1.10	0.25	↑	0.68	$\text{CuMgSi}_2\text{O}_6$ , CuO, $\text{MgAl}_2\text{O}_4$
C4MA4S2_1030	1.66	↓	1.15	0.16	↑	0.77	
C4T4S2_950	1.81	↓	1.46	0.38	—	0.35	CuO, $\text{TiO}_2$ , $\text{SiO}_2$ (tridymite), $\text{SiO}_2$ (quartz)
C4T4S2_970	1.93	↓	1.44	0.04	↑	0.22	

<sup>a</sup>The mean particle size in the measurement of bulk density and BET specific area was approximately 152.5  $\mu\text{m}$ .

during the inert gas and reactivity cycles. For oxygen carriers with high rates of oxygen release, i.e., those reaching closer to equilibrium concentration of oxygen, the methane conversion was most likely dominated by the CLOU mechanism. However, for oxygen carriers with a lower rate of oxygen release, i.e., in which the oxygen concentration was considerably lower than the equilibrium concentration, the CLC mechanism was dominant.

**3.3. Attributes of the Oxygen Carriers before and after Reactivity Tests.** Table 3 summarizes the study of oxygen carrier particles with respect to the physical and chemical changes that these materials undergo during the redox processes. For the majority of the samples, there was a decrease in the density and an increase in the BET specific surface area of the particles. However, there was no change in the crystalline phase of any of the oxygen carriers after the reactivity test compared to their fresh counterparts, as determined with the XRD analysis. Figure 7 shows the XRD signatures of fresh as well as used samples for C4MA4S2\_1000 and C4MA4T2\_1000 as an example. It should be mentioned that in the case of the used samples, the reactivity cycles were ended with an oxidation (11%  $\text{O}_2$ ) stream. In the case of C4MA4S2\_1000, it could be observed that the active CuO phase had reacted with both the  $\text{MgAl}_2\text{O}_4$  and the  $\text{SiO}_2$  support phases, which resulted in the formation of  $\text{CuMgSi}_2\text{O}_6$ . This could result in an oxygen carrier conversion lower than theoretically expected, should the  $\text{CuMgSi}_2\text{O}_6$  be unreactive. In the case of the  $\text{MgAl}_2\text{O}_4/\text{TiO}_2$  as the support, an interaction could be seen between the supports, which resulted in the formation of  $\text{MgTi}_2\text{O}_5$ .

Some of the oxygen carriers prepared here showed reasonable mechanical stability, as indicated by the crushing strength measured prior to the reactivity tests shown in Table 1. It should be noted that the crushing strength might not correlate linearly with attrition and fragmentation behavior in a real CLC system. Dust formation or particle fragmentation was not observed for any of the particles after the reactivity tests. However, given that the total number of cycles and the gas velocities employed in this study were rather low, further long-term tests in continuous operation will be needed in order to confirm the mechanical stability of these materials. Figure 8 shows the rate of attrition of the fresh oxygen carriers during testing in a jet-cup attrition rig for 1 h. In Table 4, the attrition index,  $A_r$ , defined as the slope of the attrition in the last 30 min of the test period, is shown for the investigated oxygen carriers. It can be seen that, except for the C4S6 materials, which had high attrition rates and turned into dust, the rest of the oxygen carriers had very similar attrition

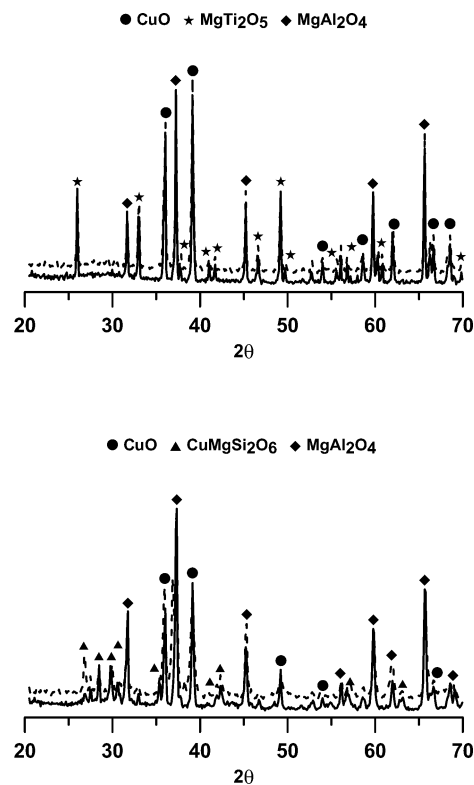


Figure 7. Comparative XRD signatures of fresh and used oxygen carriers for (top) C4MA4T2\_1000 and (bottom) C4MA4S2\_1000. Solid lines represent fresh and dashed lines represent materials after the reactivity test.

rates. The attrition rates of the materials used here are much lower than previously investigated spray-dried Cu-based oxygen carriers<sup>45</sup> with  $\text{ZrO}_2$  as the support, which were tested in the same apparatus and had shown reasonable functionality in continuous operation in a 300 W reactor.<sup>41</sup> Therefore, the combination of supports has indeed resulted in the formation of oxygen carriers with high mechanical resistance while maintaining sufficiently high reactivity and oxygen release ability for the CLOU application. The attrition rates for the oxygen carriers prepared with  $\text{MgAl}_2\text{O}_4/\text{TiO}_2$ ,  $\text{MgAl}_2\text{O}_4/\text{SiO}_2$ , and  $\text{TiO}_2/\text{SiO}_2$  as the support are comparable to those for  $\text{CaMn}_{0.9}\text{Mg}_{0.1}\text{O}_{3-\delta}$ , which has shown excellent functionality in continuous operation in a 10 kW unit.<sup>49</sup> Thus, equally good results could be expected

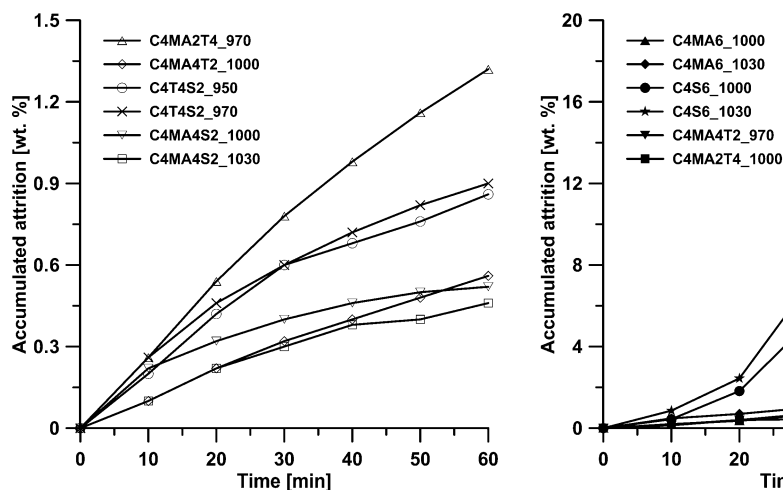


Figure 8. Accumulated attrition as a function of time for oxygen carriers with CS > 1 (left) and (b) CS ≤ 1 (right). Note: For reasons of clarity, the scale of accumulated attrition is different in the figures.

Table 4. Attrition Rates of the Tested Oxygen Carriers and Their Corresponding Crushing Strength (CS) in the Fresh State

oxygen carrier	attrition rate, $A_i$ [wt %/h]	crushing strength (CS) [N]
C4MA6_1000	1.2	0.6
C4MA6_1030	1.4	0.8
C4S6_1000	19.4	0.7
C4S6_1030	25.6	0.5
C4MA4T2_970	1.4	1.0
C4MA4T2_1000	0.5	1.5
C4MA2T4_970	1.1	1.3
C4MA2T4_1000	0.6	1.0
C4MA4S2_1000	0.2	1.4
C4MA4S2_1030	0.3	1.7
C4T4S2_950	0.5	1.7
C4T4S2_970	0.6	1.8

for these materials; nevertheless, experiments in continuous operation are required for confirmation.

The particle size distribution (PSD) of the oxygen carriers before and after the reactivity test for particles with an attrition rate below 1 wt %/h are shown in Figure 9. It can be seen that these materials exhibit an overall increase in particle size for these materials. This factor, together with the decrease in density and the increase in BET specific surface area of the particles (Table 4), indicates that the majority of the oxygen carriers investigated here experienced some degree of swelling during the reactivity tests.

The ESEM images of the fresh and used C4T4S2\_950 oxygen carrier are shown in Figure 10, as an example. The porosity of the particles seems to have increased after the reactivity test compared to the fresh samples. This was the case for most of the oxygen carriers investigated here. Thus, the slight increase in size distribution shown in Figure 9 is most likely associated with the increase in the porosity of the particles. Similar observations have been made previously for MgAl<sub>2</sub>O<sub>4</sub>-supported CuO materials after reactivity tests.<sup>23,34</sup>

Figure 11 shows the average gas yield,  $\gamma_{CH_4,ave}$  at 925 °C for the investigated oxygen carriers, as a function of their attrition rate,  $A_i$ . It can be observed that oxygen carriers with a higher gas yield are also more prone to attrition. Thus, there may be a trade-off between the reactivity of the oxygen carriers and their resistance

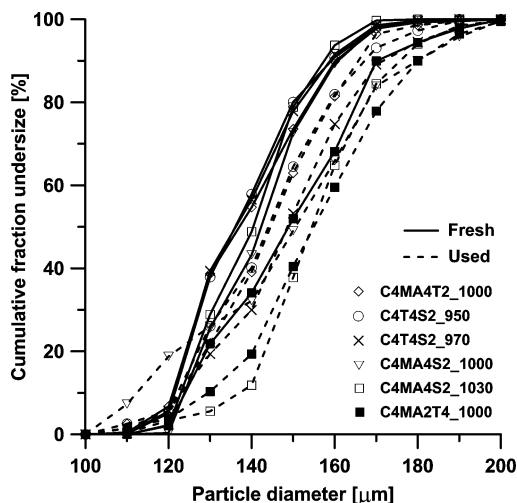


Figure 9. Particle size distributions (PSD) of fresh and used oxygen carriers, with attrition rate,  $A_i$ , less than 1 wt %/h.

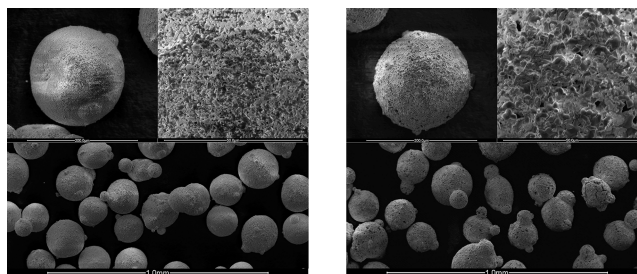
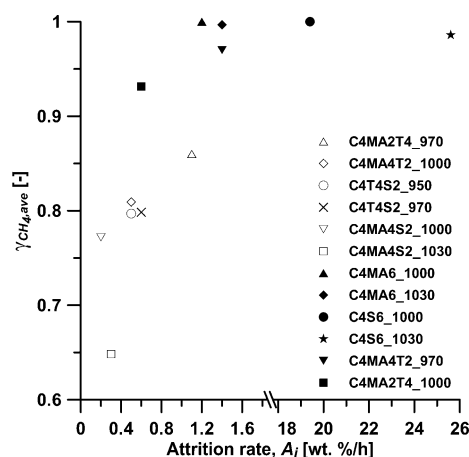


Figure 10. ESEM images of (left) fresh and (right) used C4T4S2\_950 particles after the reactivity tests. The size bars for the images with higher magnification are 200 and 50 μm, while those of the images with lower magnification are 1 mm.

to attrition. For application in a full scale plant, oxygen carriers with high attrition resistance are required, as they will be circulated for many cycles. In particular, C4MA2T4\_1000 features high reactivity, CLOU behavior, and a low attrition rate. The C4MA4S2 materials achieve the lowest attrition rates but remain fairly reactive.



**Figure 11.** Average gas yield,  $\gamma_{CH_4,ave}$ , at 925 °C as a function of attrition rate,  $A_j$ , for the investigated oxygen carriers.

#### 4. CONCLUSION

Several oxygen carriers based on CuO as the active phase and a combination of  $MgAl_2O_4$ ,  $SiO_2$ , and  $TiO_2$  as the support were investigated for the CLOU application. The particles were prepared by spray drying, and the experiments were carried out in a fluidized-bed batch reactor in the temperature range of 900–950 °C. Their CLOU behavior was assessed in an  $N_2$  environment, and their reactivity was tested with methane. Most of the oxygen carriers exhibited oxygen uncoupling behavior reaching that reached close to the equilibrium concentration of oxygen over  $CuO/Cu_2O$ , at the corresponding experimental temperature. In terms of methane conversion, oxygen carriers with a crushing strength below 1 generally had a higher rate of oxygen release and higher fuel conversion. However, by combining different supports, it was possible to obtain oxygen carriers with high mechanical stability, with oxygen release behavior and high reactivity with methane.

On the basis of the results from the reactivity and jet-cup attrition rig experiments, oxygen carriers prepared with  $MgAl_2O_4/TiO_2$ ,  $MgAl_2O_4/SiO_2$ , and  $TiO_2/SiO_2$  as the support exhibited a combination of high mechanical stability, low attrition rates, good reactivity with methane, and oxygen uncoupling behavior.

#### AUTHOR INFORMATION

##### Corresponding Author

\*Telephone: +46-31-772-2822. E-mail: arjmand@chalmers.se.

##### Notes

The authors declare no competing financial interest.

#### ACKNOWLEDGMENTS

I.A.-R. thanks CSIC for the JAE fellowship cofunded by the European Social Fund and the project PN-ENE2010-19550 supported by the Spanish Ministry of Science and Innovation. The authors also wish to acknowledge Vattenfall and Chalmers University of Technology via the Energy Area of Advance for the financial support for this study.

#### REFERENCES

(1) Pachauri, R. K.; Reisinger, A. *Fourth Assessment Report: Climate Change (Synthesis Report)*; Intergovernmental Panel on Climate Change: Geneva, 2007.

(2) Herzog, H. J.  $CO_2$  capture and storage: Costs and market potential. In *Greenhouse Gas Control Technologies 7*; Rubin, E. S., Keith, D. W., Gilboy, C. F., Wilson, M., Morris, T., Gale, J., Thambimuthu, K., Thambimuthu, K., Eds.; Elsevier Science Ltd: Oxford, 2005; pp 21–28.

(3) Lyngfelt, A.; Leckner, B.; Mattisson, T. A fluidized-bed combustion process with inherent  $CO_2$  separation; application of chemical-looping combustion. *Chem. Eng. Sci.* **2001**, *56* (10), 3101–3113.

(4) Ishida, M.; Jin, H. A Novel Chemical-Looping Combustor without  $NO_x$  Formation. *Ind. Eng. Chem. Res.* **1996**, *35* (7), 2469–2472.

(5) Kronberger, B.; Johansson, E.; Löffler, G.; Mattisson, T.; Lyngfelt, A.; Hofbauer, H. A Two-Compartment Fluidized Bed Reactor for  $CO_2$  Capture by Chemical-Looping Combustion. *Chem. Eng. Technol.* **2004**, *27* (12), 1318–1326.

(6) Jerndal, E.; Mattisson, T.; Lyngfelt, A. Thermal Analysis of Chemical-Looping Combustion. *Chem. Eng. Res. Des.* **2006**, *84* (9), 795–806.

(7) Lewis, K. W.; Gilliland, E. R.; Sweeney, M. P. Gasification of Carbon Metal Oxides in a Fluidized Powder Bed. *Chem. Eng. Prog.* **1951**, *47* (5), 251–256.

(8) Ishida, M.; Jin, H. A new advanced power-generation system using chemical-looping combustion. *Energy* **1994**, *19* (4), 415–422.

(9) Lyngfelt, A.; Thunman, H. Construction and 100 h of operational experience of a 10 kW chemical looping combustor. In *The  $CO_2$  Capture and Storage Project (CCP) for Carbon Dioxide Storage in Deep Geologic Formations For Climate Change Mitigation*; Thomas, D., Ed.; Elsevier Science: London, 2003; Vol. 1—Capture and Separation of Carbon Dioxide From Combustion Sources.

(10) Kolbitsch, P.; Pröll, T.; Bolhar-Nordenkamp, J.; Hofbauer, H. Design of a Chemical Looping Combustor using a Dual Circulating Fluidized Bed (DCFB) Reactor System. *Chem. Eng. Technol.* **2009**, *32* (3), 398–403.

(11) Lyngfelt, A. Oxygen Carriers for Chemical Looping Combustion - 4000 h of Operational Experience. *Oil Gas Sci. Technol.* **2011**, *66* (2), 161–172.

(12) Lyngfelt, A.; Mattisson, T. Materials for Chemical-Looping Combustion. *Efficient Carbon Capture for Coal Power Plants*; Stolten, D., Sherer, V., Eds.; WILEY-VCH Verlag GmbH & Co. KGaA: Weinheim, Germany, 2011; Chapter 17.

(13) Hossain, M. M.; de Lasa, H. I. Chemical-looping combustion (CLC) for inherent  $CO_2$  separations—a review. *Chem. Eng. Sci.* **2008**, *63* (18), 4433–4451.

(14) Adanez, J.; Abad, A.; Garcia-Labiano, F.; Gayan, P.; de Diego, L. F. Progress in Chemical-Looping Combustion and Reforming technologies. *Prog. Energy Combust. Sci.* **2012**, *38* (2), 215–282.

(15) Scott, S. A.; Dennis, J. S.; Hayhurst, A. N.; Brown, T. In situ gasification of a solid fuel and  $CO_2$  separation using chemical looping. *AIChE J.* **2006**, *52* (9), 3325–3328.

(16) Mattisson, T.; Lyngfelt, A.; Leion, H. Chemical-looping with oxygen uncoupling for combustion of solid fuels. *Int. J. Greenhouse Gas Control* **2009**, *3* (1), 11–19.

(17) Abad, A.; Adánez-Rubio, I.; Gayán, P.; García-Labiano, F.; de Diego, L. F.; Adánez, J. Demonstration of chemical-looping with oxygen uncoupling (CLOU) process in a 1.5  $kW_{th}$  continuously operating unit using a Cu-based oxygen-carrier. *Int. J. Greenhouse Gas Control* **2012**, *6*, 189–200.

(18) Gayán, P.; Adánez-Rubio, I.; Cuadrat, A.; Mendiara, T.; Abad, A.; García-Labiano, F.; De Diego, L.; Adánez, J. Use of Chemical-Looping processes for coal combustion with  $CO_2$  capture. *Energy Procedia* **2013**, In Press.

(19) Arjmand, M.; Keller, M.; Leion, H.; Mattisson, T.; Lyngfelt, A. Oxygen Release and Oxidation Rates of  $MgAl_2O_4$ -Supported CuO Oxygen Carrier for Chemical-Looping Combustion with Oxygen Uncoupling (CLOU). *Energy Fuels* **2012**, *26* (11), 6528–6539.

(20) Adánez-Rubio, I.; Abad, A.; Gayán, P.; de Diego, L. F.; García-Labiano, F.; Adánez, J. Identification of operational regions in the Chemical-Looping with Oxygen Uncoupling (CLOU) process with a Cu-based oxygen carrier. *Fuel* **2012**, *102*, 635–645.

(21) Chuang, S. Y.; Dennis, J. S.; Hayhurst, A. N.; Scott, S. A. Development and performance of Cu-based oxygen carriers for

chemical-looping combustion. *Combust. Flame* **2008**, *154* (1–2), 109–121.

(22) Dennis, J. S.; Müller, C. R.; Scott, S. A. In situ gasification and CO<sub>2</sub> separation using chemical looping with a Cu-based oxygen carrier: Performance with bituminous coals. *Fuel* **2010**, *89* (9), 2353–2364.

(23) Arjmand, M.; Azad, A.-M.; Leion, H.; Lyngfelt, A.; Mattisson, T. Prospects of Al<sub>2</sub>O<sub>3</sub> and MgAl<sub>2</sub>O<sub>4</sub>-Supported CuO Oxygen Carriers in Chemical-Looping Combustion (CLC) and Chemical-Looping with Oxygen Uncoupling (CLOU). *Energy Fuels* **2011**, *25* (11), 5493–5502.

(24) Forero, C. R.; Gayán, P.; García-Labiano, F.; de Diego, L. F.; Abad, A.; Adánez, J. High temperature behaviour of a CuO/γAl<sub>2</sub>O<sub>3</sub> oxygen carrier for chemical-looping combustion. *Int. J. Greenhouse Gas Control* **2011**, *5* (4), 659–667.

(25) Gayán, P.; Forero, C. R.; Abad, A.; de Diego, L. F.; García-Labiano, F.; Adánez, J. Effect of Support on the Behavior of Cu-Based Oxygen Carriers during Long-Term CLC Operation at Temperatures above 1073 K. *Energy Fuels* **2011**, *25* (3), 1316–1326.

(26) Mattisson, T.; Järnäs, A.; Lyngfelt, A. Reactivity of Some Metal Oxides Supported on Alumina with Alternating Methane and Oxygen Application for Chemical-Looping Combustion. *Energy Fuels* **2003**, *17* (3), 643–651.

(27) de Diego, L. F.; Gayán, P.; García-Labiano, F.; Celaya, J.; Abad, A.; Adánez, J. Impregnated CuO/Al<sub>2</sub>O<sub>3</sub> Oxygen Carriers for Chemical-Looping Combustion: Avoiding Fluidized Bed Agglomeration. *Energy Fuels* **2005**, *19* (5), 1850–1856.

(28) de Diego, L. F.; García-Labiano, F.; Gayán, P.; Celaya, J.; Palacios, J. M.; Adánez, J. Operation of a 10 kW<sub>th</sub> chemical-looping combustor during 200 h with a CuO-Al<sub>2</sub>O<sub>3</sub> oxygen carrier. *Fuel* **2007**, *86* (7–8), 1036–1045.

(29) Arjmand, M.; Azad, A.-M.; Leion, H.; Mattisson, T.; Lyngfelt, A. Evaluation of CuAl<sub>2</sub>O<sub>4</sub> as an Oxygen Carrier in Chemical-Looping Combustion. *Ind. Eng. Chem. Res.* **2012**, *51* (43), 13924–13934.

(30) Wang, B.; Zhao, H.; Zheng, Y.; Liu, Z.; Yan, R.; Zheng, C. Chemical looping combustion of a Chinese anthracite with Fe<sub>2</sub>O<sub>3</sub>-based and CuO-based oxygen carriers. *Fuel Process. Technol.* **2012**, *96* (0), 104–115.

(31) de Diego, L. F.; García-Labiano, F.; Adánez, J.; Gayán, P.; Abad, A.; Corbella, B. M.; María Palacios, J. Development of Cu-based oxygen carriers for chemical-looping combustion. *Fuel* **2004**, *83* (13), 1749–1757.

(32) Chuang, S. Y.; Dennis, J. S.; Hayhurst, A. N.; Scott, S. A. Kinetics of the chemical looping oxidation of H<sub>2</sub> by a co-precipitated mixture of CuO and Al<sub>2</sub>O<sub>3</sub>. *Chem. Eng. Res. Des.* **2011**, *89* (9), 1511–1523.

(33) Mattisson, T.; Leion, H.; Lyngfelt, A. Chemical-looping with oxygen uncoupling using CuO/ZrO<sub>2</sub> with petroleum coke. *Fuel* **2009**, *88* (4), 683–690.

(34) Adánez-Rubio, I.; Gayán, P.; Abad, A.; de Diego, L. F.; García-Labiano, F.; Adánez, J. Evaluation of a Spray-Dried CuO/MgAl<sub>2</sub>O<sub>4</sub> Oxygen Carrier for the Chemical Looping with Oxygen Uncoupling Process. *Energy Fuels* **2012**, *26* (5), 3069–3081.

(35) Gayán, P.; Adánez-Rubio, I.; Abad, A.; de Diego, L. F.; García-Labiano, F.; Adánez, J. Development of Cu-based oxygen carriers for Chemical-Looping with Oxygen Uncoupling (CLOU) process. *Fuel* **2012**, *96*, 226–238.

(36) Arjmand, M.; Leion, H.; Mattisson, M.; Lyngfelt, A. ZrO<sub>2</sub>-Supported CuO Oxygen Carriers for Chemical-Looping with Oxygen Uncoupling (CLOU). *Energy Procedia* **2013**, In press.

(37) Arjmand, M.; Azad, A.-M.; Leion, H.; Rydén, M.; Mattisson, M. CaZrO<sub>3</sub> and SrZrO<sub>3</sub>-supported CuO Oxygen Carriers for Chemical-looping with Oxygen Uncoupling (CLOU). *Energy Procedia* **2013**, In press.

(38) Leion, H.; Mattisson, T.; Lyngfelt, A. Using chemical-looping with oxygen uncoupling (CLOU) for combustion of six different solid fuels. *Energy Procedia* **2009**, *1* (1), 447–453.

(39) Hedayati, A.; Azad, A.-M.; Rydén, M.; Leion, H.; Mattisson, T. Evaluation of Novel Ceria-Supported Metal Oxides As Oxygen Carriers for Chemical-Looping Combustion. *Ind. Eng. Chem. Res.* **2012**, *51* (39), 12796–12806.

(40) Adánez-Rubio, I.; Abad, A.; Gayán, P.; de Diego, L. F.; García-Labiano, F.; Adánez, J. Performance of CLOU process in the combustion of different types of coal with CO<sub>2</sub> capture. *Int. J. Greenhouse Gas Control* **2013**, *12* (0), 430–440.

(41) Moldenhauer, P.; Rydén, M.; Mattisson, T.; Lyngfelt, A. Chemical-looping combustion and chemical-looping with oxygen uncoupling of kerosene with Mn- and Cu-based oxygen carriers in a circulating fluidized-bed 300W laboratory reactor. *Fuel Process. Technol.* **2012**, *104* (0), 378–389.

(42) Xu, L.; Wang, J.; Li, Z.; Cai, N. Experimental Study of Cement-Supported CuO Oxygen Carriers in Chemical Looping with Oxygen Uncoupling (CLOU). *Energy Fuels* **2013**, *27* (3), 1522–1530.

(43) Eyring, E. M.; Konya, G.; Lighty, J. S.; Sahir, A. H.; Sarofim, A. F.; Whitty, K. Chemical Looping with Copper Oxide as Carrier and Coal as Fuel. *Oil Gas Sci. Technol.* **2011**, *66* (2), 209–221.

(44) Wen, Y.-y.; Li, Z.-s.; Xu, L.; Cai, N.-s. Experimental Study of Natural Cu Ore Particles as Oxygen Carriers in Chemical Looping with Oxygen Uncoupling (CLOU). *Energy Fuels* **2012**, *26*, 3919–3927.

(45) Rydén, M.; Moldenhauer, P.; Lindqvist, S.; Mattisson, M.; Lyngfelt, A. Measuring attrition resistance of oxygen carrier particles for chemical-looping combustion with the jet cup method. Submitted for publication, 2012.

(46) Rasband, W. S. *ImageJ*; National Institutes of Health: Bethesda, MD, 1997.

(47) Arjmand, M.; Hedayati, A.; Azad, A.-M.; Leion, H.; Rydén, M.; Mattisson, T. Ca<sub>x</sub>La<sub>1-x</sub>Mn<sub>1-y</sub>M<sub>y</sub>O<sub>3-δ</sub> (M = Mg, Ti, Fe, or Cu) as Oxygen Carriers for Chemical-Looping with Oxygen Uncoupling (CLOU). *Energy Fuels* **2013**, DOI: 10.1021/ef3020102.

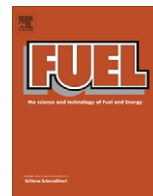
(48) Kunii, D.; Levenspiel, O. *Fluidization Engineering*; Butterworth-Heinemann: Boston, 1991.

(49) Källén, M.; Rydén, M.; Dueso, C.; Mattisson, T.; Lyngfelt, A. CaMn<sub>0.9</sub>Mg<sub>0.1</sub>O<sub>3-δ</sub> as Oxygen Carrier in a Gas-Fired 10 kW<sub>th</sub> Chemical-Looping Combustion Unit. *Ind. Eng. Chem. Res.* **2013**, In press.

## **Paper IV**







## Identification of operational regions in the Chemical-Looping with Oxygen Uncoupling (CLOU) process with a Cu-based oxygen carrier

Iñaki Adáñez-Rubio, Alberto Abad\*, Pilar Gayán, Luis F. de Diego, Francisco García-Labiano, Juan Adáñez

*Instituto de Carboquímica (ICB-CSIC), Dept. of Energy & Environment, Miguel Luesma Castán, 4, Zaragoza 50018, Spain*

### HIGHLIGHTS

- ▶ New experimental method to determine the maximum oxygen generation rate of an oxygen carrier.
- ▶ Method to determine the minimum solids inventory that must be used in the fuel reactor.
- ▶ Three different regions were identified depending on the oxygen carrier to coal mass ratio.
- ▶ A maximum rate of oxygen generation was  $2.8 \times 10^{-3}$  as kg O<sub>2</sub>/s per kg of OC at 980 °C.
- ▶ From this value the estimated solids inventory in the fuel reactor was 29 kg/MW<sub>th</sub>.

### ARTICLE INFO

#### Article history:

Received 27 September 2011

Received in revised form 24 April 2012

Accepted 14 June 2012

Available online 27 June 2012

#### Keywords:

Carbon capture

Combustion

Coal

CLOU

Copper

### ABSTRACT

Chemical-Looping with Oxygen Uncoupling (CLOU) is an alternative chemical-looping process for the combustion of solid fuels with inherent CO<sub>2</sub> capture. The CLOU process demands a material as oxygen carrier with the ability to decompose with O<sub>2</sub> release at suitable temperatures for solid fuel combustion, e.g. copper oxide. This article presents an experimental method to determine the maximum oxygen generation rate of an oxygen carrier as well as to determine the minimum solid inventory that must be used in the fuel reactor. The method here proposed can be used as basis for comparison of the use of different oxygen carriers or type of coals. In this work, the combustion of coal by using a promising Cu-based oxygen carrier prepared by the spray drying method was tested. The oxygen carrier (Cu60MgAl) was composed of 60 wt.% CuO and MgAl<sub>2</sub>O<sub>4</sub> was used as supporting material. Experiments were carried out in a batch fluidized-bed reactor at temperatures ranging from 900 to 980 °C. Three different regions were identified depending on the oxygen carrier to coal mass ratio. For oxygen carrier to coal ratios higher than 50 (Region I), coal was fully converted to CO<sub>2</sub> and H<sub>2</sub>O. In addition, an excess of oxygen was present in the flue gases, which was close to the equilibrium concentration. When this ratio was in the range 50–25 (Region II), the concentration of oxygen was decreasing whereas some CO was observed as the only unconverted gas. Further decrease in the oxygen carrier to coal ratio below 25 (Region III) caused the depletion of oxygen in the exhaust gases but CO remained as the only unconverted gas. CH<sub>4</sub> or H<sub>2</sub> were never detected at the reactor outlet in any case and agglomeration problems were never observed. These regions were related to the solids inventory in the fuel reactor by the rate of oxygen generation calculated in every case. A maximum rate of oxygen generation for the oxygen carrier was determined as kg O<sub>2</sub>/s per kg of oxygen carrier, which increased with the temperature from  $2.1 \times 10^{-3}$  at 930 °C to  $2.8 \times 10^{-3}$  at 980 °C. From these values, the estimated solids inventory in the fuel reactor was changed from 39 at 930 °C to 29 kg/MW<sub>th</sub> at 980 °C. The results obtained in this work showed that in the CLOU process it is possible to reach full conversion of the solid fuel with very low solids inventory and avoiding the oxygen polishing step.

© 2012 Elsevier Ltd. All rights reserved.

### 1. Introduction

According to the IPCC report on mitigation of climate change [1], which considers different possible growing scenarios, Carbon

\* Corresponding author. Tel.: +34 976 733977; fax: +34 976 733318.

E-mail address: [abad@icb.csic.es](mailto:abad@icb.csic.es) (A. Abad).

Capture and Storage (CCS) would contribute with 15–55% to the cumulative mitigation effort worldwide until 2100 in order to stabilize CO<sub>2</sub> concentration in the atmosphere. CCS is a process involving the separation of CO<sub>2</sub> emitted by industry and energy-related sources, and its storage for isolation from the atmosphere over a long term. Chemical-Looping Combustion process (CLC) has been suggested among the best alternatives to reduce the

**Nomenclature**

$f_{C, char}$	mass fraction in char of carbon (-)	$r_{O_2, max}$	maximum rate of oxygen generation (kg O <sub>2</sub> /s per kg of oxygen carrier)
$f_{H/C}$	hydrogen to carbon molar ratio in the coal (-)	$R_{OC}$	oxygen transport capability (-)
$f_{O/C}$	oxygen to carbon molar ratio in the coal (-)	$t$	time (s)
$F_{air}$	molar flow of air (mol/s)	$T$	temperature (°C)
$F_i$	molar flow of gas $i$ (mol/s)	$T_0$	initial temperature in the experiment (°C)
$F_{out}$	molar flow at the reactor exit (mol/s)	$T_{max}$	maximum temperature reached during experiment (°C)
$F_{O, coal}$	molar flow of oxygen from the existing oxygen in the coal (mol/s)	$X_o$	oxygen carrier conversion (-)
$m_{char}$	mass of char fed to the fuel reactor (kg)	$X_{o, f}$	oxygen carrier conversion at the end of the reducing period (-)
$m_{FR}$	mass of oxygen carrier in the fuel reactor (kg/MW <sub>th</sub> )	$y_i$	molar fraction of gas $i$ (-)
$m_O$	mass of oxygen required per kg of coal to complete combustion (kg O <sub>2</sub> /kg coal)		
$m_{ox}$	mass of fully oxidized oxygen carrier (kg)		
$m_{OC}$	mass of oxygen carrier in the reactor (kg)	<i>Greek symbols</i>	
$m_{red}$	mass of reduced oxygen carrier, as Cu <sub>2</sub> O (kg)	$\Delta H_r$	enthalpy of reaction (kJ/mol)
$M_C$	molecular weight of carbon (=12 × 10 <sup>-3</sup> kg/mol)	$\gamma_{CO_2}$	CO <sub>2</sub> yield (-)
$M_{O_2}$	molecular weight of oxygen (=32 × 10 <sup>-3</sup> kg/mol)		
$r_{char}$	rate of char combustion (kg C/s per kg C)	<i>Acronyms</i>	
$r_{O_2, red}$	rate of oxygen generation in the reduction (kg O <sub>2</sub> /s per kg of oxygen carrier)	<i>LHV</i>	Low Heating Value (kJ/kg)
$r_{O_2, ox}$	rate of oxygen consumption in the oxidation (kg O <sub>2</sub> /s per kg of oxygen carrier)	<i>OC</i>	oxygen carrier

economic cost of CO<sub>2</sub> capture using fuel gas [2] and to increase the efficiency with respect to other CO<sub>2</sub> capture process [3]. In this process, CO<sub>2</sub> is inherently separated from other combustion products, N<sub>2</sub> and unused O<sub>2</sub>, through the use of a solid oxygen carrier and thus no energy is expended for the separation. The CLC process has been demonstrated for gaseous fuel combustion such as natural gas and syngas in 10–140 kW<sub>th</sub> units using oxygen carrier materials based on Ni [4,5], Cu [6] and Fe [7,8]. A review of the materials developed to be used as oxygen carrier is found in Adanez et al. [9].

Solid fuels are considerably more abundant and less expensive than natural gas. Thus, the use of the CLC concept for coal combustion can be highly relevant. First option to use solid fuels in a CLC process was to use syngas in the fuel reactor coming from a previous gasifying step. However, it is necessary to use pure oxygen for gasification of the solid fuel to apply this technology. This step has an important energy penalty due to the oxygen separation from the air. The second option of development is the Chemical-Looping Combustion with coal, where the solid fuel is directly introduced to the fuel reactor. Even other kinds of solid fuels could be used, e.g. biomass or solid wastes [10]. Here, the solid fuel is physically mixed with the oxygen carrier in the fuel reactor, which is fed with a gaseous stream of a gasifying agent, e.g. steam or CO<sub>2</sub>. Thus, volatiles and the gas products from coal gasification are converted to CO<sub>2</sub> and H<sub>2</sub>O by reaction with the oxygen carrier particles in the fuel reactor. The limitation in the solid fuel conversion in the CLC with coal comes from the slow gasification process [10–12]. To increase the gasification rate, temperatures higher than 1000 °C have been proposed to be used in the fuel reactor [12].

An alternative process, Chemical-Looping with Oxygen Uncoupling (CLOU), was recently proposed by Mattisson and coworkers [13] making use of the idea first proposed by Lewis and Gilliland [14] to produce CO<sub>2</sub> from solid carbonaceous fuels by using gaseous oxygen produced by the decomposition of CuO. The CLOU process is based on the strategy of using oxygen carrier materials which release gaseous oxygen in the fuel reactor and thereby allowing the solid fuel to burn with gas phase oxygen. These mate-

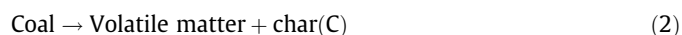
rials can be also regenerated at high temperatures. In this way, the slow gasification step on the CLC process with solid fuels is not necessary, giving a much faster fuel conversion [15,16]. In CLOU process, fluidization gas can be recycled CO<sub>2</sub>. In this process, the use of steam is not necessary, contrary to the case of CLC with coal [11].

Leion et al. [17] using six different solid fuels show that the differences in reactivity between fuels were more pronounced in CLC with solid fuels using steam as gasification agent than in CLOU process. This fact was explained by the difference in the reaction paths between CLC and CLOU processes. In CLC the limiting reaction is the slow coal gasification, which is strongly affected by the temperature and coal type. However, they stated that the rate of oxygen release from the oxygen carrier particles becomes the limiting step in the CLOU process. Thus, the type of fuel used has lower relevance in the conversion rate. Experiments carried out at 980 °C using petroleum coke as fuel [15] showed that CLOU process can increase the fuel conversion by a factor of 45 with respect to the conversion found when the same fuel was gasified with steam and using Fe-based oxygen carriers which do not release oxygen in the fuel reactor. A quantification of the role of oxygen uncoupling in accelerating the gasification of solid fuels was also confirmed by Eyring et al. [18] and Abad et al. [16] using Cu-based oxygen carrier materials.

Fig. 1 shows a schematic diagram of a CLOU system. In the fuel reactor the fuel conversion is produced by different reactions. First the oxygen carrier releases oxygen according to:



and the solid fuel begins devolatilization producing a carbonaceous solid (char, mainly composed by carbon and ash) and volatile matter as gas product:



Then, char and volatiles are burnt as in usual combustion with gaseous oxygen according to reactions:



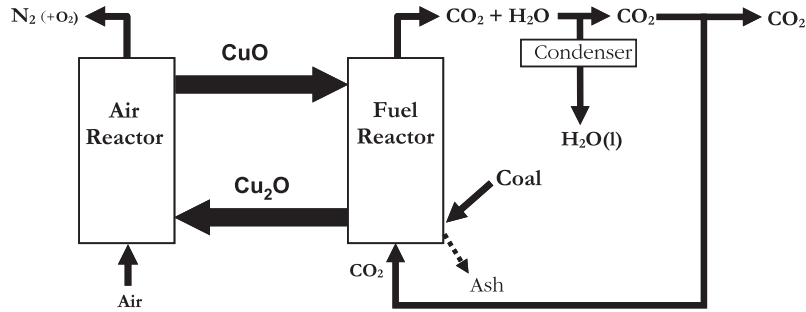
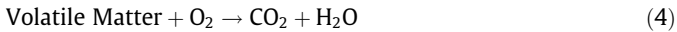


Fig. 1. Schematic design of the CLOU system using copper oxide as oxygen carrier.



After steam condensation, a pure  $\text{CO}_2$  stream can be obtained. The reduced oxygen carrier is transported to the air reactor, where the oxygen carrier is regenerated to the initial oxidation stage with the oxygen of the air, and being ready for a new cycle. Ideally, the exit stream of the air reactor contains only  $\text{N}_2$  and unreacted  $\text{O}_2$ . The heat release over the fuel and air reactors is the same as for conventional combustion. Therefore,  $\text{CO}_2$  is inherently captured in the CLOU process, and a low energy penalty for  $\text{CO}_2$  separation and low  $\text{CO}_2$  capture costs are expected as in the CLC process.

About the oxygen carrier, only those metal oxides that have a suitable equilibrium partial pressure of oxygen at temperatures of interest for combustion (800–1200 °C) can be used as CLOU oxygen carriers for solid fuel combustion. Besides, this  $\text{O}_2$  release must be reversible in order to oxidize the oxygen carrier in the air reactor and regenerate the material. Thus a special requirement is needed for the oxygen carrier to be used in the CLOU process in comparison to oxygen carriers for normal CLC, where the fuel must be able to react directly with the oxygen carrier without any release of gas phase oxygen.  $\text{CuO}/\text{Cu}_2\text{O}$ ,  $\text{Mn}_2\text{O}_3/\text{Mn}_3\text{O}_4$ , and  $\text{Co}_3\text{O}_4/\text{CoO}$  have been identified as redox pairs with capacity to evolve oxygen at high temperature [13].

The temperature in the air and fuel reactors in the CLOU process must be adjusted according to the thermodynamic equilibrium and reaction kinetics in order to optimize the process [18]. Thus, the operating conditions for the air reactor are constrained due to the thermodynamics of the oxidation of the oxygen carrier. As example, Fig. 2 shows the partial pressure of oxygen as a function of the temperature for the  $\text{CuO}/\text{Cu}_2\text{O}$  system, calculated using HSC software [19]. The oxygen concentration at equilibrium conditions greatly depends on the temperature. Thus, the equilibrium concen-

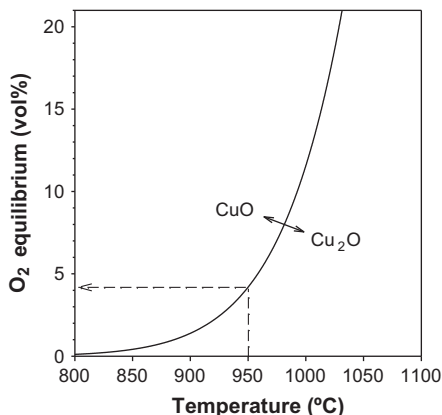
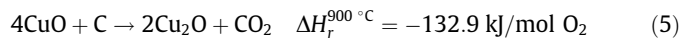


Fig. 2. Equilibrium oxygen concentration over the  $\text{CuO}/\text{Cu}_2\text{O}$  system as a function of temperature.

tration at 900 °C is 1.5 vol.%  $\text{O}_2$  for  $\text{CuO}/\text{Cu}_2\text{O}$  system, whereas it increases up to 12.4 vol.% at 1000 °C. Therefore, if the acceptable oxygen concentration from the air reactor was maximum 4.5 vol.%,  $\text{Cu}_2\text{O}$  should be oxidized to  $\text{CuO}$  below 950 °C. Higher temperature in the air reactor would cause a higher fraction of unused oxygen.

Moreover, the equilibrium concentration of oxygen in the fuel reactor will be given by the temperature in the reactor; which is determined by the temperature of the incoming particles, the circulation rate, as well as the heat of reaction in the fuel reactor. For example, the overall reaction with C is exothermic in the fuel reactor for copper oxide, as it is showed in reaction (5). Thus it is possible to have a temperature increase in the fuel reactor, which results in a significantly higher partial pressure of  $\text{O}_2$  at equilibrium conditions.



A high equilibrium partial pressure of oxygen together with a very reactive oxygen carrier will promote the overall conversion rate of the solid fuel in the fuel reactor. In addition, the combustion of the fuel will decrease the oxygen concentration in the reactor and can improve the decomposition reaction of the metal oxide particles. However, it should be desirable to get low concentration of oxygen from the fuel reactor in order to obtain a high purity  $\text{CO}_2$  stream. Similar conclusions can be inferred from thermodynamics of other materials.

There are only a small number of materials proposed in the literature dealing with the use of Cu- [16–18,20,21], and Mn-based [22–26] based materials for CLOU process. An overview of the characteristics of these materials can be found in [9,20,21].

In the research group at Chalmers University of Technology, 20 different CLOU materials were tested in batch fluidized bed for combustion of gaseous ( $\text{CH}_4$ ) or solid fuels [13,15,17,22,23,25]. Good results were obtained using an oxygen carrier based on  $\text{CuO}$  and  $\text{ZrO}_2$  as support [13,17]. Although there were some defluidization phenomena during some parts of the experiments, no permanent agglomerations were detected. Cyclic testing with solid fuels in the temperature range of 880–985 °C verified a very rapid release of oxygen and combustion of fuel started with a high conversion rate. Regarding the use of manganese oxides for CLOU process, Shulman et al. [22] analyzed the CLOU properties of different Mn-based materials combined with  $\text{Fe}_2\text{O}_3$ ,  $\text{NiO}$  or  $\text{SiO}_2$  prepared by freeze granulation. They found that some Mn/Fe oxygen carriers showed very high reactivity towards methane. Further, other Mn/Fe materials prepared by spray drying were tested by the same research group [23]. One of them was successfully applied for the combustion of methane in a continuously operated unit [24]. The authors apply this quality to open the possibility to combine benefits of CLOU and CLC processes in the future for the combustion of gaseous fuels. A manganese ore was also tested for CLOU by Rydén et al. [24] in a continuous unit using  $\text{CH}_4$ , but this material was much less

reactive than synthetic Mn/Fe particles. Other material with a spinel perovskite-like type structure,  $\text{CaMn}_{0.875}\text{Ti}_{0.125}\text{O}_3$ , [25,26] was also evaluated as an oxygen carrier for CLOU process. Conversion rates were lower than those found for Cu-based CLOU materials, although it was still higher compared to normal CLC with solid fuels.

In the research group of ICB-CSIC [20,21], a screening study was carried out considering more than 25 different Cu-based oxygen carriers prepared by different methods, using several supporting materials and varying the copper content. The reaction rates for oxygen release and oxygen carrier regeneration were determined carrying out successive cycles in a TGA system at different reaction temperatures and oxygen concentrations. Selected materials were tested by redox decomposition–regeneration cycles in a batch fluidized-bed reactor working at different temperatures and reacting atmospheres. The fluidization behavior against agglomeration and attrition during a high number of cycles was determined. Two promising Cu-based oxygen carriers prepared by pelletizing by pressure (60 wt.% CuO supported on  $\text{MgAl}_2\text{O}_4$ , and 40 wt.% CuO supported on  $\text{ZrO}_2$ ) were selected for further studies using coal as fuel. These materials exhibited high reactivity during successive redox cycles. In addition, a low attrition rate was measured and agglomeration was never detected.

After the screening tests, it was decided to prepare a Cu-based material (60 wt.%) supported on  $\text{MgAl}_2\text{O}_4$  by the industrial preparation method spray drying (Cu60MgAl). Similar particles to those previously prepared by pelletization by pressure were obtained. So, new spray dried particles were tested in a continuously operated CLOU unit using coal as fuel [16]. In this work it was demonstrated the proof of the concept of CLOU process for coal combustion using a Cu-based oxygen carrier. The fuel reactor temperature was varied from 900 °C to 960 °C and the solids inventory was decreased from 1150 to 235 kg/MW<sub>th</sub>. In all experiments complete combustion to  $\text{CO}_2$  and  $\text{H}_2\text{O}$  of fuel and high carbon capture efficiency was measured. The carbon capture efficiency depended on the fuel reactor temperature ranging from 97% at 900 °C to 99.3% at 960 °C. These findings suggested that good performance in coal combustion could be obtained even if the solids inventory was lower than 235 kg/MW<sub>th</sub>. However, further decrease of the solids inventory was not possible due to operational limitations of CLOU unit.

The aim of this work was to investigate the performance of the Cu60MgAl material as oxygen carrier for the CLOU process. The minimum solids inventory to get full combustion of coal was determined by a new method applied to CLOU process. The rate of oxygen release was determined when batches of “El Cerrejón” coal particles were added to a fluidized-bed reactor containing the oxygen carrier material. Different oxygen carrier to fuel ratios were used, as well as several temperatures between 900 and 950 °C were tested. The minimum solids inventory in the fuel reactor was inferred from the maximum rate of oxygen release obtained at every temperature

## 2. Experimental

### 2.1. Cu-based oxygen carrier

The oxygen carrier used was a Cu-based material prepared by spray drying. Oxygen carrier particles were manufactured by VITO (Flemish Institute for Technological Research, Belgium) using  $\text{MgAl}_2\text{O}_4$  spinel from Baikowski, grade S30CR and CuO from PRS PANRE-AC (96% CuO) as raw materials. The CuO content was 60 wt.%. After particles were formed by spray drying the particles were calcined for 12 h at 1100 °C and sieved (100–300 μm). Particles were calcined for a second time to increase the mechanical strength. Thus, oxygen carrier particles had a total calcination time of 24 h at 1100 °C. These particles are referred to as Cu60MgAl.

**Table 1**  
Properties of the Cu60MgAl oxygen carrier particles.

CuO content (wt.%)	60
Oxygen transport capability, $R_{OC}$ (wt.%)	6.0
Crushing strength (N)	2.4
Density of particles ( $\text{kg/m}^3$ )	3860
XRD main phases	CuO, $\text{MgAl}_2\text{O}_4$

Oxygen carrier particles were physically and chemically characterized by different techniques. Main characteristics are shown in Table 1. The mechanical strength, determined using a Shimpo FGN-5X crushing strength apparatus, was taken as the average value of the force needed to fracture a particle obtained in 20 measurements. Identification of crystalline chemical species was carried out by powder X-ray diffractometer Bruker AXS graphite monochromator.

The mechanical strength of the particles after 24 h of calcination was adequate for its use in a fluidized bed. The compounds found by XRD analysis were CuO and  $\text{MgAl}_2\text{O}_4$ . The oxygen transport capability,  $R_{OC}$ , was calculated as  $R_{OC} = (m_{ox} - m_{red})/m_{ox}$ ,  $m_{ox}$  being the mass of completely oxidized particles and  $m_{red}$  the mass in the reduced form, i.e. when all CuO has been reduced to  $\text{Cu}_2\text{O}$ .

### 2.2. Fuel

The fuels used were a bituminous Colombian coal “El Cerrejón” and char prepared with this coal. This is the same fuel used in previous work in a continuous CLOU unit [16]. The coal particle size used in this study was +200 to 300 μm. This coal showed a high swelling behavior, which could promote agglomeration of the fluidized bed. In order to avoid coal swelling, the coal was subjected to a thermal pre-treatment for pre-oxidation. Coal was heated at 180 °C in air atmosphere for 28 h [27]. Elemental and proximate analyses of the fresh and pre-treated coal are shown in Table 2. The pre-oxidation causes an increase in the oxygen content from 7% to 17.6%.

The char was produced by devolatilization of pre-treated bituminous Colombian coal “El Cerrejón”. To produce the char, a batch of 500 g of coal particles was devolatilized in a fluidized-bed reactor. The reactor was fluidized by  $\text{N}_2$  and it was heated up from room temperature to 900 °C with a temperature ramp of 20 °C/min and afterwards cooled down. Since the gas velocity increases with the temperature, the  $\text{N}_2$  flow was correspondingly reduced as the temperature increased to ensure bubbling bed conditions and to avoid elutriation of particles. The proximate and ultimate analysis of the obtained char is also shown in Table 2. The particle size of char was in the range +200 to 300 μm, and the density of the particles was about 1000  $\text{kg/m}^3$ .

### 2.3. Experimental setup: batch fluidized-bed reactor

Reduction–oxidation multi-cycles were carried out in a fluidized-bed reactor to know the oxygen release behavior of the oxygen carrier in similar operating conditions to that existing in the CLOU process. The experimental work was carried out in a setup consisting of a fluidized-bed reactor, a system for gas feeding, a solid fuel feeding system, and the gas analysis system. A schematic layout of the laboratory setup is presented in Fig. 3. The reactor – 55 mm inner diameter and 700 mm height – is electrically heated by a furnace, and had a preheating zone just under the distributor plate.

The reactor was loaded with 240 g of solid material. Solids are placed above the distributor plate, ensuring a bed height about 50 mm at static conditions. In order to have good fluidizing behavior, a particle size fraction of +100 to 200 μm was used in the bed.

**Table 2**  
Properties of fresh and pre-treated “El Cerrejón” coal and the char prepared.

	Fresh Colombian coal	Pre-treated Colombian coal	Char coal
C	70.8%	65.8 %	79.8%
H	3.9%	3.3%	0.7%
N	1.7%	1.6%	1.3%
S	0.5%	0.6%	0.6%
O <sup>a</sup>	7.0	17.6	0.8
Moisture	7.5%	2.3%	6.4%
Volatile matter	34.0%	33.0%	3.0%
Fixed carbon	49.9%	55.9%	80.2%
Ash	8.6%	8.8%	10.4%

<sup>a</sup> Oxygen to balance.

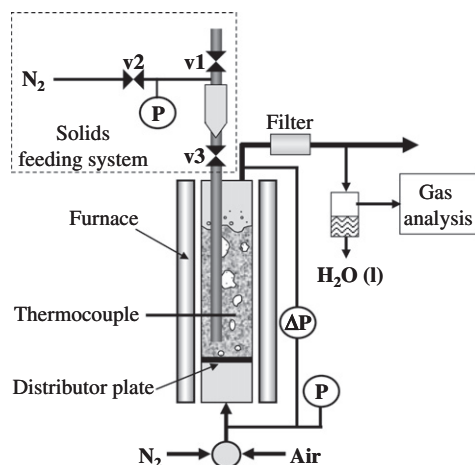


**Fig. 3.** Schematic layout of the laboratory setup.

The minimum fluidizing velocity was  $4 \times 10^{-3}$  m/s for the smallest particle size and  $1.5 \times 10^{-3}$  m/s for the biggest one. The terminal velocity was 0.33 m/s and 1.15 m/s, respectively. In some test, the oxygen carrier was diluted in alumina particles (+200 to 400  $\mu\text{m}$ ). In these test the total mass of solids was 240 g, but it was possible to operate with lower amount of oxygen carrier.

The temperature inside the bed was measured and used to control the reaction temperature. The reactor had pressure taps in order to measure the absolute pressure in the bed and the pressure drop. Agglomeration and defluidization problems could be detected by a sharp decrease in the bed pressure drop during operation. The pressure tap was also useful to detect possible blocking in the downstream pipes due to possible elutriated particles or tar condensation in cold points.

The gas feeding system had different mass flow controllers connected to an automatic three-way valve. In this way, it was possible to feed alternatively air or nitrogen. The total fluidizing flow was 200 L<sub>N</sub>/h, which corresponds to a gas velocity of 0.1 m/s at 900 °C in the reactor. Different gas analyzers measured continuously the gas composition at the reactor exit after water condensation. CO, CO<sub>2</sub> and CH<sub>4</sub> dry basis concentrations were determined using non-dispersive infrared analysis (NDIR) and H<sub>2</sub> by thermal gas conductivity. The O<sub>2</sub> concentration was determined in a paramagnetic analyzer.

The feeding system of the solid fuel consisted of a fuel chute which ends 20 mm above the distributor plate and about 50–60 mm below the upper level of the fluidizing particles. So, solid fuel particles are fed inside the fluidized bed. The upper part of the chute has a valve system that creates a reservoir in which

the fuel is placed. Coal particles were fed by valve v1 to a small reservoir placed in the upper part of the fuel chute, see Fig. 3. After that, the deposit was over-pressurized 1 bar with N<sub>2</sub> by valve v2. Once the reservoir was pressurized, valve v2 was closed and v3 was opened and quickly closed. Then, coal particles fall down to the fluidized bed through the fuel chute as the reservoir is unpressurized. Thus, it was ensured that coal particles were forced to enter to the fluidized bed, whereas a continuous flow of nitrogen through the fuel chute is avoided.

The oxygen carrier particles were exposed sequentially to reducing and oxidizing conditions. During reduction periods, batches of “El Cerrejón” coal were fed to the reactor through the solids feeding system whereas the reactor was fluidized with N<sub>2</sub>. Every load was left till coal combustion was complete or the oxygen carrier was fully reduced, which usually happened in less than 120 s. After every reducing period, oxygen carrier particles were fully re-oxidized with air before starting a new cycle.

#### 2.4. Experimental planning

The experimental work was carried out at temperatures between 900 and 950 °C, which is the intended temperature interval in the fuel reactor in a CLOU process with Cu-based materials [16]. The temperature of the reactor was fixed before starting the reducing or oxidizing period, but during reaction the temperature could increase up to 50 °C because the exothermic reaction when coal is burnt or the Cu<sub>2</sub>O was oxidized.

Three series of experiments were performed to increase the oxygen carrier to coal ratio in the range covered. The first tests were done with an amount of 240 g of oxygen carrier material in the bed. This batch of particles was exposed to a total number of 35 reduction/oxidation cycles, corresponding to 31 h of hot fluidization in order to evaluate possible variations in the oxygen carrier reactivity during redox cycles or the appearance of operational problems during fluidization using coal as fuel. The temperature was fixed to 925 °C at the starting of the reduction period. In this case, the loads of coal between 0.2 and 2 g were added. Thus, very high oxygen carrier to coal mass ratios were used (in the range 1200–120), but the fluidization behavior of the oxygen carrier could be analyzed without interference of using a diluting material.

The second and third series were carried out with the oxygen carrier diluted in alumina particles. Thus, the mass fraction of the oxygen carrier in the bed was 10 wt.% and 2.5 wt.%, respectively. In the second series, with 24 g of oxygen carrier in the bed, the reducing periods consisted of introducing loads of coal from 0.4 to 1.2 g, i.e. the oxygen carrier to coal ratio was in the range 60–20. Further, in the third series (with only 6 g of oxygen carrier in the bed) the loads of coal change from 0.03 to 0.5 g, corresponding to oxygen carrier to coal ratios of 200 and 12, respectively. In this way, the oxygen carrier to carbon mass ratio was decreased but a mass of coal higher than 2 g was not used. Two grams was the highest amount of coal that could be fed to obtain repetitive and useful results. Higher mass of coal resulted in relevant entrainment of solids originated by the big amount of gases generated.

For the coal and oxygen carrier material used in this work the stoichiometric oxygen carrier to coal ratio is 30. At this condition, the exact amount of oxygen to fully convert coal to CO<sub>2</sub> and H<sub>2</sub>O is present in the particles. For lower oxygen carrier to coal ratios, some char will remain unconverted at the end of the reduction period. However, tests working with lower ratios were accomplished to evaluate the maximum value of the instantaneous oxygen generation rate of the oxygen carrier. In the batch fluidized bed, the unconverted char was burnt during the oxidation period. However, in a continuously operated CLOU system, the depleted oxygen particles should be replaced with particles coming from the air

reactor, thus avoiding the limitation in the oxygen availability happening in a batch fluidized-bed reactor. But the behavior of the oxygen carrier against coal combustion in the batch reactor would be similar to that in a CLOU unit.

An additional series was done using char instead of coal as fuel. This series of experiments was carried out with an oxygen carrier mass fraction of 2.5 wt.%. The char loads changed from 0.04 to 0.4 g, corresponding to oxygen carrier to char mass ratios of 150 and 14, respectively.

### 3. Data evaluation

To analyze the oxygen uncoupling properties of the Cu60MgAl oxygen carrier, consecutive redox cycles have been done in a batch fluidized-bed reactor. During the reduction period a batch of coal was added to the bed, whereas oxidation with air was accomplished during the oxidation period. The instantaneous rate of oxygen generation per amount of oxygen carrier,  $r_{O_2,red}(t)$ , was calculated from a mass balance to the oxygen atoms in the reactor.

$$r_{O_2,red}(t) = \frac{M_{O_2}}{m_{OC}} [F_{O_2} + F_{CO_2} + 0.5(F_{CO} + F_{H_2O}) - 0.5F_{O,coal}] \quad (6)$$

The molar gas flow of each component exiting the fuel reactor,  $F_i$ , is calculated as:

$$F_i = F_{out} \cdot y_i \quad (7)$$

$F_{out}$  being total dry basis outlet flow calculated by using the  $N_2$  flow to the reactor,  $F_{N_2}$ .

$$F_{out} = \frac{F_{N_2}}{(1 - \sum_i y_i)} \quad (8)$$

$y_i$  is the molar fraction of the component  $i$  in the product gas analyzed in every experimental condition. Possible gas  $i$  includes  $O_2$ ,  $CO_2$ ,  $CO$ ,  $H_2$  and  $CH_4$ . Nevertheless, methane and hydrogen were not considered in the balance because they were not detected in any case. The water concentration was not measured. However, to consider the oxygen exiting with  $H_2O$  coming from oxidation of hydrogen in the coal, it was assumed that the hydrogen evolution was proportional to the carbon evolution, maintaining the same C/H ratio in the gases than in the coal. Thus, the  $H_2O$  flow was calculated as:

$$F_{H_2O} = 0.5f_{H/C}(F_{CO_2} + F_{CO}) \quad (9)$$

$f_{H/C}$  being the hydrogen to carbon molar ratio in coal ( $f_{H/C} = 0.61$ , for Colombian pre-treated coal). Equally, the evolution of oxygen from coal was assumed to be proportional to coal evolution. Thus, the flow of oxygen coming from coal,  $F_{O,coal}$  in Eq. (7), was calculated as:

$$F_{O,coal} = f_{O/C}(F_{CO_2} + F_{CO}) \quad (10)$$

$f_{O/C}$  being the oxygen to carbon molar ratio in the coal ( $f_{O/C} = 0.20$ , for Colombian pre-treated coal).

When char was used as fuel, a conversion rate of char per mass of reacting char in the reactor was calculated as the rate of carbon combustion to give  $CO_2$  or  $CO$ :

$$(-r_{char}(t)) = \frac{F_{CO_2} + F_{CO}}{\frac{m_{char} \cdot f_{C, char}}{M_C} - \int_0^t (F_{CO_2} + F_{CO}) dt} \quad (11)$$

$m_{char}$  being the mass of char in the fuel batch and  $f_{C, char}$  the carbon content in char. Before starting a reducing period, the oxygen carrier particles were fully oxidized, i.e. the oxygen carrier conversion was  $X_o = 1$ . As the oxygen carrier particles were reacting during reduction period, the oxidation degree decreased. Thus, the oxygen carrier conversion was calculated from the integration of  $r_{O_2,red}$  with time:

$$X_o(t) = 1 - \frac{1}{R_{OC}} \int_0^t r_{O_2,red}(t) dt \quad (12)$$

Thus, the final conversion of the particles,  $X_o$ , was calculated by integrating Eq. (12) for the time spent in reduction conditions. In the same way, an oxygen balance was done to calculate the oxidation rate with air – Eq. (13) – and the evolution with time of the oxygen carrier conversion,  $X_o$  Eq. (14). In some cases, char was not completely converted during the reduction period because the depletion of oxygen in the particles was reached. Thus,  $CO_2$  and  $CO$  can appear during the oxidation period as the remaining char is burned with oxygen in air, being the oxygen for char combustion considered in:

$$(-r_{O_2,ox}(t)) = \frac{M_{O_2}}{m_{OC}} [0.21F_{air} - F_{O_2} - (F_{CO_2} + 0.5F_{CO})] \quad (13)$$

$$X_o(t) = X_{of} + \frac{1}{R_{OC}} \int_0^t (-r_{O_2,ox}(t)) dt \quad (14)$$

Finally, the  $CO_2$  yield was defined as the carbon fraction as  $CO_2$  in the outgoing gases, calculated as:

$$\gamma_{CO_2} = \frac{F_{CO_2}}{F_{CO_2} + F_{CO}} \quad (15)$$

### 4. Results

Reduction–oxidation multi-cycles with Cu60MgAl oxygen carrier were carried out in a batch fluidized-bed reactor to determine the oxygen release behavior as a function of the operating conditions in similar environment to that found in a CLOU process with solid fuels. Moreover, the fluidization behavior of the solid particles with respect to the agglomeration phenomena could be observed.

Test series were carried out by using different bed materials: first, the bed material was Cu60MgAl particles; second, the bed material was 10 wt.% oxygen carrier diluted in alumina particles; and third, only 2.5 wt.% Cu60MgAl diluted in alumina. All these tests were carried out with a total mass of particles in the reactor of 240 g. The oxygen carrier was subjected to about 34 redox cycles which last during 31 h between 900 and 950 °C. The oxygen carrier never showed agglomeration problems, even when the oxygen carrier was highly reduced to  $Cu_2O$  during the reduction period.

Fig. 4 shows the concentration of  $O_2$ ,  $CO_2$  and  $CO$  measured at the outlet of the reactor and the bed temperature during a typical reduction and oxidation cycle at 925 °C with an oxygen carrier inventory in the reactor of 240 g. The fluidizing medium was pure nitrogen during reduction and during oxidation the inlet oxygen concentration was 21 vol.%. The time  $t = 0$  corresponds to the initial time of the reduction period, i.e. when air during oxidation was replaced by nitrogen. At the beginning a rapid oxygen release occurred close to the oxygen concentration equilibrium for the measured bed temperature. After a short period, a batch of 2 g of coal particles were fed to the reactor, and only  $CO_2$  and  $O_2$  were observed in the outgoing gases, indicating full combustion of the volatiles and char. The  $CO_2$  concentration in this case was as high as 76 vol.% which was maintained constant during ~8 s, and eventually decreased to zero when the complete coal combustion was reached. This result suggests a fast combustion of coal where it is not differentiated a first period of fast combustion of volatiles from a subsequent slower period of combustion of the remaining char. At this condition, the gas flow at the reactor exit was increased by a factor of 5 with regard to the inlet  $N_2$  flow because the  $CO_2$  and  $H_2O$  generated during coal combustion.

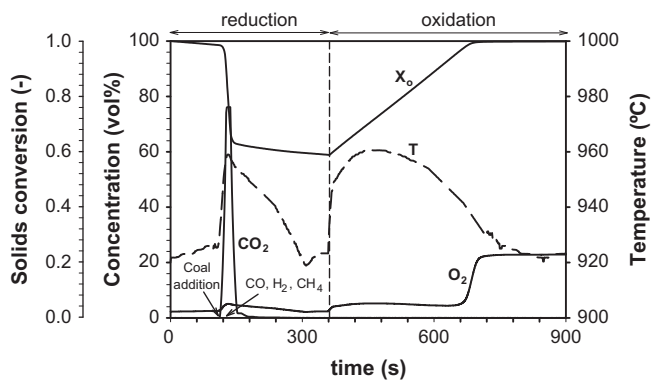


**Fig. 4.** Concentration of  $O_2$ ,  $CO_2$ ,  $CO$ ,  $H_2$  and  $CH_4$  during a typical reduction and oxidation cycle with Cu60MgAl. The variation in the oxygen carrier conversion,  $X_o$ , and temperature during the reduction and oxidation periods also is shown.  $T_0 = 925$  °C; reduction in  $N_2$  and oxidation with air; mass fraction of oxygen carrier: 100 wt.%; Coal batch: 2 g.

In addition, the oxygen release rate was high enough to supply an excess of gaseous oxygen ( $O_2$ ) exiting together the combustion gases. During coal combustion the bed temperature increased about 30 °C due to the exothermic reaction of CuO with coal, see Eq. (5). The oxygen concentration was correspondingly increased, remaining close to the equilibrium condition when temperature varied. This fact indicates that the oxygen carrier was able to transfer the oxygen demanded by the coal combustion and even more gaseous oxygen until equilibrium was reached. Therefore, the conversion of coal was limited by the coal reactivity, i.e. by the coal combustion rate at the existing oxygen concentration in the bed. It must be taking into account that in the fuel reactor two processes in series are happening: oxygen generation and coal combustion with the oxygen generated. If oxygen generation rate is higher than rate of coal combustion, oxygen at equilibrium is reached, and the coal combustion rate depends on the coal reactivity. On contrary, the oxygen at equilibrium is not reached and the coal combustion rate will be limited by the oxygen generation rate.

In Fig. 4, the variation of oxygen carrier conversion,  $X_o$ , with reacting time is also shown. It can be seen that the oxygen carrier was slowly converted during the initial period before coal addition. Besides, the oxygen carrier was able to produce gaseous oxygen until the equilibrium concentration was reached. Therefore, the oxygen generation rate was limited by the fact that the equilibrium concentration is reached in absence of fuel. A sharp decrease in the oxygen carrier conversion was happening when coal was fed to the reactor because the fast oxygen transference from oxygen carrier to fuel. After coal was completely burnt the temperature decreased until the set point value. As the oxygen carrier was not completely reduced after coal combustion, still oxygen was generated up to equilibrium concentration was reached. The variation in the solids conversion during the reducing period was 41%. Then, oxidation period starts at  $t = 360$  s and a quick increase in the temperature occurred due to the highly exothermic reaction. Equally to reduction period, oxygen concentration was close to the equilibrium condition until the oxygen carrier was fully oxidized, which is in accordance to highly reactive materials observed in TGA experiments [20,21].

Similar behavior was observed in redox cycles when different amounts of coal were added to the bed in the range 0.2–2.0 g, corresponding to oxygen carrier to coal ratios between 1200 and 120. As expected, the  $CO_2$  concentration from fuel reactor increased with the coal mass added because more fuel is burnt. Also, more oxygen is transferred to gases.  $CH_4$ ,  $CO$  or  $H_2$  were not observed in any case, indicating the full combustion of volatiles in the bed, as well as carbon in char. From the  $CO_2$  and  $O_2$  evolution in the

gas phase, it was possible to calculate the instantaneous oxygen generation rate,  $r_{O_2,red}$ , from Eq. (6). The higher value of  $r_{O_2,red}$  was obtained when coal was added to the bed, and it was maintained roughly constant while the coal combustion proceeds. Fig. 5 shows the instantaneous oxygen generation rate during the coal combustion period,  $r_{O_2,red}$ , as a function of the oxygen carrier to coal mass ratio. In all cases the ratio of oxygen carrier to coal is above the stoichiometric value to convert coal to  $CO_2$  and  $H_2O$ . The effect of the oxygen carrier to coal ratio is evident on the oxygen generation rate. In this case it is observed that  $r_{O_2,red}$  is inversely proportional to the oxygen carrier to coal ratio. The incremental oxygen requirements when the batch of coal increases (i.e. the oxygen carrier to coal is decreased) is fully provided by the oxygen carrier. Thus, at the CLOU conditions used in these experiments, the oxygen generated in the reactor was not limited by the reactivity of the oxygen carrier but for the demand of oxygen by coal; i.e. the more oxygen is demanded, the more oxygen is supplied. This fact suggests that a decrease in the oxygen carrier to coal ratio would allow increasing the oxygen generation rate provided by the Cu60MgAl oxygen carrier. Thus, the maximum in the instantaneous oxygen generation rate by this material could not be observed during these series of experiments, being necessary to work with higher values of oxygen carrier to coal ratios. However, the reproducibility of results in the fluidized bed failed with coal batches higher than 2 g which conducted to a loss in the confidence of the calculated oxygen generation rate.

In order to decrease the oxygen carrier to coal ratio but still maintain the confidence on the results obtained, the following tests were carried out diluting the oxygen carrier in alumina particles, but keeping the total mass of solids in the reactor to be 240 g. Firstly, batches of coal in the range 0.4–1.2 g were used at 925 °C using an oxygen carrier mass fraction of 10 wt.% in alumina. Then, the oxygen carrier to coal ratio was in the range 60–20. During the experimental work it was observed that for oxygen carrier to coal ratios lower than 35 the oxygen carrier was fully reduced after coal addition whereas char remained unburnt. Thus, some unconverted char was burnt in the subsequent oxidation period, which was evidenced by the presence of  $CO_2$  in the gases when air was introduced to the bed. The value of oxygen carrier to coal of 35 was close to the stoichiometric oxygen available in the bed material to convert the coal to  $CO_2$  and  $H_2O$ , which was an oxygen carrier to coal ratio of 30. The oxygen carrier to coal value observed during experimental work was some higher because some oxygen in particles was evolved to gas before coal addition to the bed.

During the time converting coal, similar behavior to that found when using only Cu60MgAl particles as bed material was observed

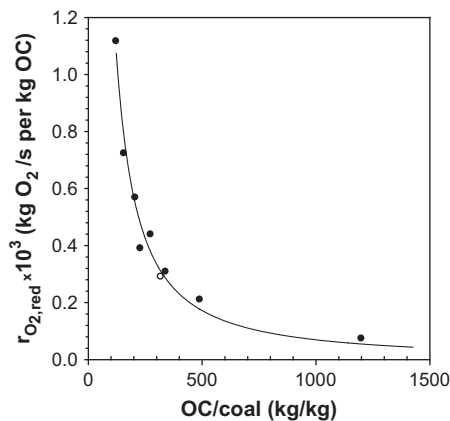


**Fig. 5.** Instantaneous oxygen generation rate,  $r_{O_2,red}$ , for the Cu60MgAl material as a function of the oxygen carrier to coal mass ratio.  $T_0 = 925$  °C. Mass fraction of Cu60MgAl oxygen carrier in the reactor: 100 wt.%.



in the oxygen carrier to coal range of 60–50. Further decrease in the oxygen carrier to coal ratio below 50 caused the appearance of CO together with CO<sub>2</sub> in the exhaust gases during the reduction period, as well as lower oxygen concentration compared to the equilibrium concentration. Nevertheless, CH<sub>4</sub> or H<sub>2</sub> were not found in any case. This fact indicates that the instantaneous oxygen generation rate is approaching to the maximum value given by the reactivity of the oxygen carrier.

Fig. 6a shows the CO<sub>2</sub> yield,  $\gamma_{\text{CO}_2}$ , whereas the ratio between the oxygen concentration at the reactor exit and that present at equilibrium conditions,  $\text{O}_2/\text{O}_{2,\text{eq}}$ , was plotted in Fig. 6b. It can be seen as both the CO<sub>2</sub> yield and the oxygen concentration decreases when the oxygen carrier to coal mass ratio was lower than ~50. This behavior is due to that the oxygen carrier is not able to release oxygen fast enough to fully burnt coal to CO<sub>2</sub>, although over-stoichiometric conditions are used.

O<sub>2</sub> and CO were both found in the gaseous stream exiting the reactor, because the oxygen concentration in the gases was too low to allow the full combustion of CO to CO<sub>2</sub>. The amount of oxygen in the flue gases would be enough to convert the remaining CO to CO<sub>2</sub> for oxygen carrier to coal ratios higher than 35, but this has not happened in the reactor. However, an excess of CO regarding the O<sub>2</sub> present in gases was found for oxygen carrier to coal ratios lower than 35. At these conditions, if conversion of CO to CO<sub>2</sub> was desired in a down-stream step, addition of oxygen should be done to the exiting stream.

Fig. 7 shows the oxygen generation rate as a function of the oxygen carrier to coal ratio when the Cu60MgAl particles were 10 wt.% diluted in alumina. In the same way that in the previous tests, the oxygen generation rate increased as the oxygen carrier to coal ratio decreased. This fact suggests that the presence of CO in the outgoing gases was not due to a limitation of the oxygen carrier to supply the required oxygen by the fuel, but rather to an inefficient combustion of char or volatiles at the low oxygen concentrations. The lower oxygen concentration than the equilibrium value would indicate that the oxygen generation rate is reaching its maximum value given by the oxygen carrier reactivity.

An attempt to determine the maximum oxygen generation rate of the Cu60MgAl material was done in a third series of experiments. In these tests an additional dilution of the oxygen carrier material in alumina was done. So, the mass fraction of the Cu60MgAl was 2.5 wt.%, whereas the loads of coal were between 0.03 and 0.5 g, corresponding to oxygen carrier to coal ratios from 200 to 12. Fig. 8 shows the oxygen generation rate as a function of the oxygen carrier to coal ratio in a double logarithmic scale. To observe the global trend of the oxygen generation rate, the previous results

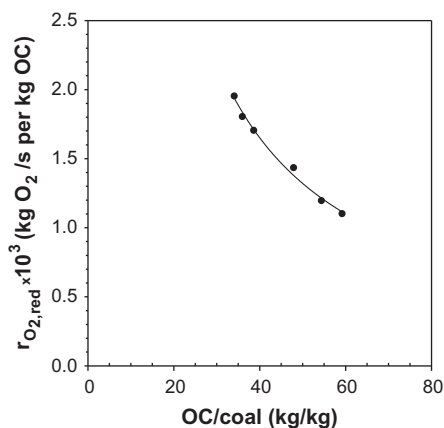


Fig. 7. Instantaneous oxygen generation rate,  $r_{\text{O}_2,\text{red}}$ , for the Cu60MgAl oxygen carrier as a function of the oxygen carrier to coal mass ratio.  $T_0 = 925$  °C. Mass fraction of Cu60MgAl oxygen carrier in the reactor: 10 wt.%.

obtained with different dilutions of the oxygen carrier in alumina, i.e. 100 wt.% and 10 wt.%, were included. It can be observed a similar trend of the data obtained with different oxygen carrier dilutions at similar oxygen carrier to coal ratios. When the oxygen carrier to coal ratio decreased from high values until a value of 25, the oxygen generation rate increased. However, at lower oxygen carrier to coal values it seemed that the oxygen generation rate reached a maximum, and no further incremental in the oxygen generation rate was obtained by decreasing the oxygen carrier to coal ratio. Thus, for oxygen carrier to coal <25 – where the maximum rate for oxygen generation was reached – the coal conversion was limited by the oxygen generation rate from the oxygen carrier. The calculated value for the maximum oxygen generation rate was  $2.6 \times 10^{-3}$  kg O<sub>2</sub>/s per kg of oxygen carrier when the temperature during the reduction period increased up to 955 °C.

The CO<sub>2</sub> yield and the  $\text{O}_2/\text{O}_{2,\text{eq}}$  ratio obtained for the third experimental series were also shown in Fig. 6a and b, respectively. Both, the CO<sub>2</sub> yield and the  $\text{O}_2/\text{O}_{2,\text{eq}}$  ratio followed a downward trend when the oxygen carrier to coal ratio decreased. Moreover, the oxygen concentration becomes zero when the maximum rate of oxygen generation was reached. This fact determines a change in the limiting process during conversion of coal from the rate of coal combustion determined by the char reactivity towards the rate of oxygen production by the oxygen carrier determined by the oxygen carrier reactivity.

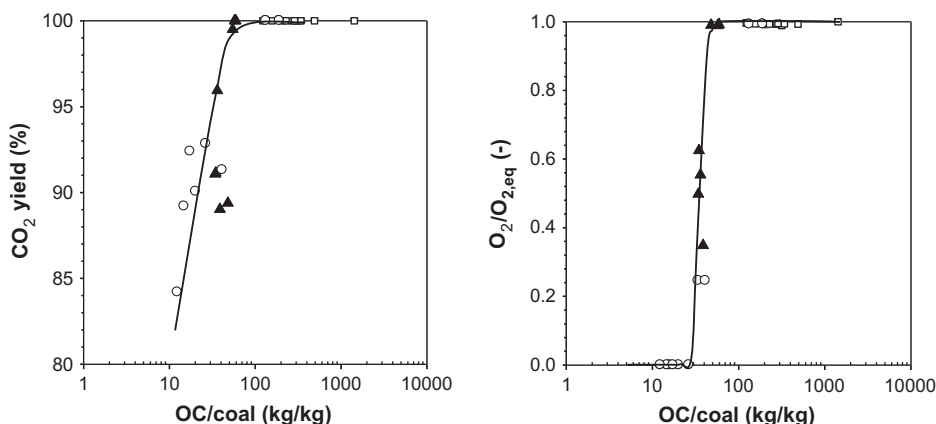
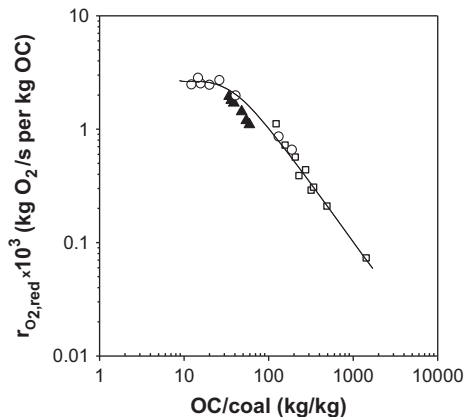


Fig. 6. (a) CO<sub>2</sub> yield and (b) ratio between the oxygen concentration at the reactor exit and at equilibrium conditions,  $\text{O}_2/\text{O}_{2,\text{eq}}$ , as a function of the oxygen carrier to coal mass ratio.  $T_0 = 925$  °C. Mass fraction of Cu60MgAl oxygen carrier in the reactor: (□) 100 wt.%; (▲) 10 wt.%; (○) 2.5 wt.%.



**Fig. 8.** Instantaneous oxygen generation rate,  $r_{O_2,red}$ , for the Cu60MgAl oxygen carrier as a function of the oxygen carrier to coal mass ratio.  $T_0 = 925$  °C. Mass fraction of Cu60MgAl oxygen carrier in the reactor: (□) 100 wt.%; (▲) 10 wt.%; (○) 2.5 wt.%.

Analogous experiments were carried out at initial temperatures,  $T_0$ , of 900 °C and 950 °C. In these cases, temperature increased until  $T_{max}$  of 930 °C and 980 °C, respectively, when coal was added to the bed. Similar trend was found for the oxygen generation rate with the oxygen carrier to coal ratio. Nevertheless, the maximum oxygen generation rate increased with the reacting temperature, as showed in Table 3.

In the second and third experimental series, it can be observed that with an oxygen carrier to coal ratio lower than 50, CO was present in the outlet gases from the reactor. The presence of CO could come from unconverted volatiles in the bed or from char combustion, since a relevant amount of CO can appear as combustion product of solid fuels in an oxygen lean atmosphere [28]. To evaluate the CO source an experimental series was done using char instead of coal. The oxygen carrier to char mass ratios varied from 150 to 14. Similar to experiments with coal, gaseous oxygen was in the gases at equilibrium concentration for high oxygen carrier to coal mass ratios. But in this case, the oxygen concentration decreased for oxygen carrier to char mass ratio below 130 becoming zero at oxygen carrier to char ratios lower than 50. In all the experiments carried out with char no CO was present in the outlet gases even if oxygen was not present in the exhaust gases. This fact suggests that the CO detected in test with coal at oxygen carrier to coal ratios lower than 50, was due to unburnt volatiles. The presence of CO could be due to the oxygen transference rate from the oxygen carrier was not fast enough to fully convert carbon in volatiles to  $CO_2$ , but oxygen remaining in the oxygen carrier is able to burn char fast enough to  $CO_2$ .

Fig. 9 shows the oxygen generation rate as a function of oxygen carrier to fuel mass ratio when coal or char were burnt with Cu60MgAl particles 2.5 wt.% diluted in alumina. It can be observed that at oxygen carrier to fuel ratios higher than 100 oxygen generation rates were similar both for coal and char. However, when the oxygen carrier to fuel ratio decreased, oxygen generation rate in the case of coal is two times higher than when the fuel is char.

**Table 3**

Maximum value of the oxygen generation rate,  $r_{O_2,max}$ , for the Cu60MgAl material and calculated solids inventory in the fuel reactor for coal combustion,  $m_{FR}$ , as a function of the temperature.

$T_0$ (°C)	$T_{max}$ (°C)	$r_{O_2,max} \times 10^3$ (kg O <sub>2</sub> /s per kg OC)	$m_{FR}$ (kg OC/MW <sub>th</sub> )
900	930	2.1	39
925	955	2.6	32
950	980	2.8	29

When char was used as fuel, the maximum oxygen generation rate obtained was the same than the value found by thermo-gravimetric analysis during CuO decomposition in  $N_2$  [20,21]. Thus, the maximum reaction rate using char in the fluidized bed looks to be the maximum rate of generation of gaseous oxygen from particles, which is the same than that obtained in TGA. At low oxygen carrier to coal ratios, oxygen was not present. So, the maximum rate of oxygen generation was reached for this condition due to the driving force, i.e. the difference between the partial pressure of oxygen at equilibrium and the oxygen in the phase, is maximum. The highest oxygen generation rate obtained when coal was burnt could be explained by the direct reduction of CuO by the volatile matter. In this case, gas–solid reaction between volatile matter and oxygen carrier could be faster than oxygen generation rate. In this way, the rate of transference of oxygen from solid particles to gaseous compounds ( $O_2$ ,  $CO_2$ ,  $H_2O$  or  $CO$ ) is faster when coal is used instead of char. More studies are needed to confirm this explanation.

In the fuel reactor of a CLOU process, two processes should happen in series: oxygen generation and coal combustion with the oxygen generated. Also, the gas–solid reaction between reacting gases, e.g. volatile compounds, and the solid oxygen carrier could be relevant. The oxygen generation rate has been analyzed as much with coal as char. Differences were attributed to the presence of volatiles in coal. Now, an analysis about the rate of char combustion is done. With the results obtained using char as fuel it can be calculated the char combustion rate. Fig. 10 shows the char combustion rate as a function of the oxygen carrier to char ratio at 925 °C when Cu60MgAl particles were 2.5 wt.% diluted in alumina. The char combustion rate increased with the oxygen carrier to char ratio up to a maximum. This maximum in the char combustion rate was reached at oxygen carrier to char ratios higher than 100. At lower ratios the conversion rate of char was limited by the rate of oxygen supply from the oxygen carrier. At oxygen carrier to char ratios higher than 100 the oxygen availability is not limited by oxygen carrier reactivity. Thus, all the oxygen demanded for char combustion is supplied by the oxygen carrier at enough high rate, and the combustion rate of char is fixed by its own reactivity with oxygen and the oxygen concentration in the reactor. The oxygen concentration during char combustion is determined by thermodynamic equilibrium of CuO decomposition to  $Cu_2O$ . The maximum char combustion rate reached was 3.12%/s at the maximum temperature reached during the experiment, i.e.  $T_{max} = 955$  °C. This value is 10 times lower to that obtained during coal continuous combustion in a CLOU unit [16] (27%/s at 960 °C).

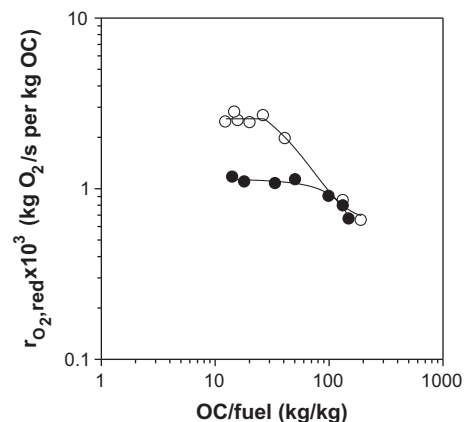


**Fig. 9.** Instantaneous oxygen generation rate,  $r_{O_2,red}$ , for the Cu60MgAl oxygen carrier as a function of the oxygen carrier to coal mass ratio.  $T_0 = 925$  °C. Mass fraction of Cu60MgAl oxygen carrier in the reactor: 2.5 wt.%. Fuel: (○) coal; (●) char.

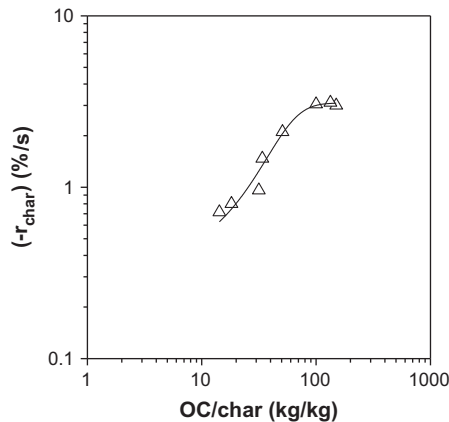


**Fig. 10.** Char combustion rate,  $(-r_{char})$ , for the Cu60MgAl oxygen carrier as a function of the oxygen carrier to char mass ratio.  $T_0 = 925$  °C. Mass fraction of Cu60MgAl oxygen carrier in the reactor: 2.5 wt.%.

This fact may be explained due to the char used in this work is much less reactive than the nascent char produced in the direct combustion of the coal. The relevance of the thermal treatment on the char reactivity in combustion or gasification processes is a well known behavior [29–32], which supports these results.

## 5. Discussion

The rate of oxygen generation calculated by the procedure above described can be related to the solids inventory needed to fully convert the fuel in the fuel reactor of a CLOU system. Assuming that the solids circulation rate in a CLOU system is high enough to transport the required oxygen in the fuel reactor, the coal combustion would be not limited by the availability of oxygen transported from the air reactor. Thus, the solids inventory,  $m_{FR}$ , depends on the flow of coal that the oxygen carrier is able to process at the rate of oxygen generation assumed,  $r_{O_2,red}$ , and it can be calculated as:

$$m_{FR} = 10^3 \frac{m_O}{r_{O_2} LHV} \quad (16)$$

being  $m_O$  the mass of oxygen required per kg of coal to fully convert it to  $CO_2$  and  $H_2O$ , as for the case of the conventional combustion with air.  $LHV$  is the lower heating value of the solid fuel. From coal analysis showed in Table 2, a value for  $m_O = 2.1$  kg  $O_2$  per kg of coal was calculated, whereas the  $LHV$  was 25878 kJ/kg for pre-treated “El Cerrejón” coal. Notice that the solids inventory does not depends on the oxygen carrier to coal ratio in experiments, but depends on the oxygen generation rate obtained.

The calculated solids inventories for the maximum oxygen generation,  $r_{O_2}$ , are shown in Table 3. The solids inventory in the fuel reactor was dependent on the reactor temperature because the increase of the oxygen generation rate with the temperature. Thus, 39 kg/ $MW_{th}$  would be necessary in the fuel reactor at a reacting temperature of 930 °C, decreasing to 29 kg/ $MW_{th}$  if temperature increases up to 980 °C. Here, the temperature is the maximum temperature reached during the reduction period.

These values of solids inventory corresponds to the minimum amount of solids that generate the required oxygen for coal combustion but not having an excess of oxygen in the gases. However, from the experimental results it seems that an excess of oxygen in the exhaust gases must be necessary in order to reach complete combustion of fuel to  $CO_2$  and  $H_2O$ . Thus, the maximum generation rate of oxygen was obtained for oxygen carrier to coal ratios lower than 25, but incomplete combustion of coal can happen with CO at

the outlet stream for oxygen carrier to coal ratios lower than 50. This fact would reduce the combustion efficiency if solids inventories showed in Table 3 were used, which corresponded to the calculated values using the maximum oxygen generation rate. In order to increase the combustion efficiency, the complete combustion of gases can be addressed improving the contact time between the oxygen carrier and unburnt CO in gases, e.g. increasing the solids inventory in the fuel reactor. Thus, higher solids inventory than that calculated using the maximum rate of oxygen generation could be necessary in order to get complete combustion of fuel to  $CO_2$  and  $H_2O$ .

From the results obtained in this work, three different regions for coal combustion in the CLOU process can be identified depending on the oxygen carrier to coal ratio. Fig. 11 shows the delimiting conditions for these regions and the calculated solids inventory. The solids inventory depends on the instantaneous rate of oxygen generation obtained for every value of oxygen carrier to carbon mass ratio. The Region I was defined as the region where CO was not present in the exhaust gases, corresponding to oxygen carrier to coal ratios higher than 50. The oxygen generation rate for the delimiting border was about  $1.4 \times 10^{-3}$  kg  $O_2/s$  per kg of oxygen carrier corresponding to a solid inventory of 58 kg/ $MW_{th}$ . In the Region II,  $O_2$  and CO simultaneously appeared in the outgoing gases. This region is limited between values of oxygen carrier to coal ratios of 25 and 50, and it can be divided in two: at higher oxygen carrier to coal ratios than 35, the fraction of oxygen in gases was enough to convert the existing CO to  $CO_2$ , and even an excess of oxygen remained in gases. At this condition, the oxygen generation rate was about  $1.9 \times 10^{-3}$  kg  $O_2/s$  per kg of oxygen carrier corresponding to a solid inventory of 43 kg/ $MW_{th}$  at 955 °C. Thus, in the range 43–58 kg/ $MW_{th}$  complete combustion could be accomplished downstream in a subsequent step by catalytic combustion without addition of new  $O_2$ . Finally, in the Region III no oxygen was present in the exhaust gases. The maximum rate for oxygen generation of the oxygen carrier is reached, and lowering the solids inventory does not allow supplying oxygen to fully convert the coal in the fuel reactor at the rate that is demanded by the coal feeding rate. This region was observed for oxygen carrier to coal ratios lower than 25.

In this work, the dependence of the oxygen generation rate on the oxygen carrier to coal ratio was analyzed to obtain the maximum rate of  $O_2$  release. The numbers of the oxygen carrier to coal ratios defining the regions in this work are for the Colombian pre-treated coal. These numbers could be different as function of the fuel, that is, the ratio needed to reach the maximum rate would de-

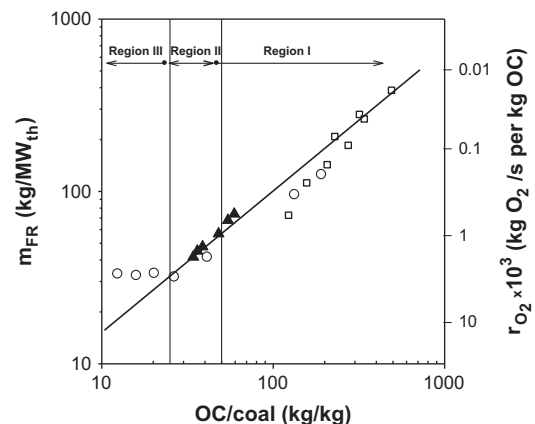


**Fig. 11.** Calculated solids inventory in the fuel reactor for the Cu60MgAl oxygen carrier as a function of the oxygen carrier to coal mass ratio.  $T_0 = 925$  °C. Mass fraction of Cu60MgAl oxygen carrier in the reactor: (□) 100 wt.%; (▲) 10 wt.%; (○) 2.5 wt.%.

depends on reactivity of coal and its composition. Thus, the more reactive is a coal, the more oxygen carrier to coal ratio would be needed to reach this maximum. This fact is explained because as the solid fuel is more reactive, a lower amount of solid fuel would be needed to demand oxygen at the same rate.

From the results showed in this work, it can be concluded that a small oxygen amount is desirable in the flue gases coming from the fuel reactor if complete combustion wants to be reached. In this way, the necessity of an oxygen polishing step would be avoided. Thus, it can be suggested that a CLOU system should be operated in the Region I, where complete combustion of coal can be obtained. It is necessary to notice that this does not mean all coal would be converted to gas, but all gas produced from coal is oxidized to CO<sub>2</sub> and H<sub>2</sub>O. Depending on the char reactivity and the residence time in the reactor, some char will be transferred to the air reactor before it was converted. If a relevant fraction of char was bypassed to the air reactor, a higher mean residence time of solids should be necessary in the fuel reactor. This can be accomplished or (1) by increasing the solids inventory in the fuel reactor; or (2) by introducing a carbon separation system between the fuel reactor and the air reactor, which separates char from oxygen carrier particles to be recirculated to the fuel reactor. In this case, the solids inventory calculated in this work should be the lowest amount of solids required to fully convert coal.

The excess of oxygen in Region I should decrease as the fuel reactor temperature was lower because the oxygen concentration at equilibrium is reduced. It is remarkable that the excess of oxygen could be problematic for the transport and storage of the CO<sub>2</sub>, and it must be removed from the exhaust gas stream. This situation is similar to that present in coal oxy-combustion units. To address the excess of oxygen, one option would be to separate the oxygen in the purification and compression process of the CO<sub>2</sub> before being transported [33].

## 6. Conclusions

A Cu-based oxygen carrier prepared by spray drying was tested for the CLOU process in a batch fluidized-bed reactor. The oxygen carrier containing CuO (60 wt.%) and MgAl<sub>2</sub>O<sub>4</sub> was used as inert material, whereas the bituminous Colombian coal “El Cerrejón” was used as fuel. The capability of particles to evolve gaseous oxygen in the fuel reactor was evaluated as a function of the oxygen carrier to coal mass ratio and reactor temperature. The oxygen carrier was subjected to about 34 redox cycles which last during 31 h between 900 and 950 °C. The oxygen carrier never showed agglomeration problems during all the experimental work.

A decrease in the oxygen carrier to coal mass ratio caused a continuous increase in the oxygen generation rate of the Cu60MgAl material until the maximum rate of oxygen generation was reached. The maximum generation rate obtained with coal was higher (about twice) the reaction rate obtained with char. Results obtained with char were representative of the rate of evolution of gaseous oxygen from particles, whereas experiments with coal also could include a fast gas–solid reaction rate between volatile matter and solid particles with direct reduction of CuO.

The oxygen generation rate was related to the solids inventory in the fuel reactor in a CLOU process. Three operating regions were identified depending on the solids inventory. Unburnt compounds were not present in the outgoing gases in Region I when the calculated solids inventory was higher than 58 kg/MW<sub>th</sub> at 955 °C. CO<sub>2</sub> and H<sub>2</sub>O were the only products of coal combustion and an excess of O<sub>2</sub> was observed, which was found to be close to the equilibrium concentration. At these conditions, the oxygen concentration at the reactor outlet increased with the temperature. The Region II was confined between 32 and 58 kg/MW<sub>th</sub>, where both CO and O<sub>2</sub> were

present in the exhaust gases together CO<sub>2</sub> as main product. CO was the only unconverted product present in gases, which came from incomplete oxidation of volatile matter. The maximum rate of oxygen generation was found in the so-called Region III. Oxygen was not present in the flue gases, and a certain concentration of CO was present as unburnt compound. Maximum oxygen generation rates from  $2.1 \times 10^{-3}$  at 930 °C to  $2.8 \times 10^{-3}$  kg O<sub>2</sub>/s per kg of oxygen carrier at 980 °C were found. The estimated solids inventory in the fuel reactor changed from 39 at 930 °C to 29 kg/MW<sub>th</sub> at 980 °C. However, for full combustion of coal to CO<sub>2</sub> and H<sub>2</sub>O a minimum bed inventory of 43 kg/MW<sub>th</sub> at 930 °C was necessary, corresponding to a zone in Region II where oxygen released from the reactor is enough to convert CO to CO<sub>2</sub> in the exhaust gases.

The results obtained in this work showed that the reactivity of the Cu60MgAl oxygen carrier allows the complete conversion of the solid fuel in a CLOU process with very low solids inventory and avoiding the oxygen polishing step. The method proposed in this work can be used for other oxygen carrier materials and coals in order to compare the behavior of different materials in the CLOU process.

## Acknowledgements

This work was partially supported by the European Commission, under the RFCS Program (ECLAIR Project, Contract RFCP-CT-2008-0008), ALSTOM Power Boilers (France) and by the Spanish Ministry of Science and Innovation (PN, ENE2010-19550). I. Adánez-Rubio thanks CSIC for the JAE fellowship co-funded by the European Social Fund.

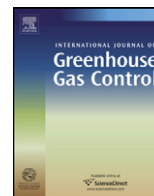
## References

- [1] IPCC. IPCC special report on carbon dioxide capture and storage. Working group III of the intergovernmental panel on climate change. Cambridge: Cambridge University Press, UK; 2005. <<http://www.ipcc.ch>>.
- [2] Kerr HR. Capture and separation technology gaps and priority research needs. Carbon dioxide capture for storage in deep geologic formations. Amsterdam: Elsevier Science; 2005. p. 655–60.
- [3] Kvamsdal HM, Jordal K, Bolland O. A quantitative comparison of gas turbine cycles with CO<sub>2</sub> capture. Energy 2007;32(1):10–24.
- [4] Kolbitsch P, Bolhär-Nordenkamp J, Pröll T, Hofbauer H. Comparison of two Ni-based oxygen carriers for chemical looping combustion of natural gas in 140 kW continuous looping operation. Ind Eng Chem Res 2009;48(11):42–7.
- [5] Linderholm C, Mattisson T, Lyngfelt A. Long-term integrity testing of spray-dried particles in a 10 kW chemical-looping combustor using natural gas as fuel. Fuel 2009;88:2083–96.
- [6] Adánez J, Gayán P, Celaya J, de Diego LF, García-Labiano F, Abad A. Chemical looping combustion in a 10 kW<sub>th</sub> prototype using a CuO/Al<sub>2</sub>O<sub>3</sub> oxygen carrier: effect of operating conditions on methane combustion. Ind Eng Chem Res 2006;45(17):75–80.
- [7] Lyngfelt A, Thunman H. Construction and 100 h of operational experience of a 10-kW chemical-looping combustor. In: Thomas DC, Benson SM, editors. Carbon dioxide capture for storage in deep geologic formations – results from the CO<sub>2</sub> capture project, vol. 1. Oxford, UK: Elsevier; 2005 [chapter 36].
- [8] Pröll T, Mayer K, Bolhär-Nordenkamp J, Kolbitsch P, Mattisson T, Lyngfelt A, et al. Natural minerals as oxygen carriers for chemical looping combustion in a dual circulating fluidized bed system. Energy Proc 2009;1:27–34.
- [9] Adánez J, Abad A, García-Labiano F, Gayán P, de Diego LF. Progress in chemical-looping combustion and reforming technologies. Prog Energy Combust Sci 2012;38:215–82.
- [10] Cao Y, Pan WP. Investigation of chemical looping combustion by solid fuels. 1. Process analysis. Energy Fuel 2006;20:57–68.
- [11] Cuadrat A, Abad A, García-Labiano F, Gayán P, de Diego LF, Adánez J. Effect of operating conditions in chemical-looping combustion of coal in a 500 W<sub>th</sub> unit. Int J Greenhouse Gas Control 2012;6:153–63.
- [12] Berguerand N, Lyngfelt A. Chemical-looping combustion of petroleum coke using ilmenite in a 10 kW<sub>th</sub> unit-high-temperature operation. Energy Fuel 2009;23:57–68.
- [13] Mattisson T, Lyngfelt A, Leion H. Chemical-looping oxygen uncoupling for combustion of solid fuels. Int J Greenhouse Gas Control 2009;3:11–9.
- [14] Lewis WK, Gilliland ER. Production of pure carbon dioxide. Patent 2665972; 1954.
- [15] Mattisson T, Leion H, Lyngfelt A. Chemical-looping with oxygen uncoupling using CuO/ZrO<sub>2</sub> with petroleum coke. Fuel 2009;88:683–90.
- [16] Abad A, Adánez-Rubio I, Gayán P, García-Labiano F, de Diego LF, Adánez J. Demonstration of chemical-looping with oxygen uncoupling (CLOU) process in

- a 1.5 kWth continuously operating unit using a Cu-based oxygen-carrier. *Int J Greenhouse Gas Control* 2012;6:189–200.
- [17] Leion H, Mattisson T, Lyngfelt A. Using chemical-looping with oxygen uncoupling (CLOU) for combustion of six different solid fuels. *Energy Proc* 2009;1:447–53.
- [18] Eyring E, Konya G, Lighty J, Sahir A, Sarofim A, Whitty K. Chemical looping with copper oxide as carrier and coal as fuel. *Oil Gas Sci Technol – Revue IFP Nouv Technol* 2011;2:209–21.
- [19] HSC Chemistry 6.1<sup>®</sup>. Chemical reaction and equilibrium software with thermochemical database and simulation module. Outotec Research Oy; 2008.
- [20] Adáñez-Rubio I, Gayán P, García-Labiano F, de Diego LF, Adáñez J, Abad A. Development of CuO-based oxygen-carrier materials suitable for chemical-looping with oxygen uncoupling (CLOU) process. *Energy Proc* 2011;4:417–24.
- [21] Gayán P, Adáñez-Rubio I, Abad A, de Diego LF, García-Labiano F, Adáñez J. Development of CuO-based oxygen-carrier materials suitable for chemical-looping with oxygen uncoupling (CLOU) process. *Fuel* 2012;6:226–38.
- [22] Shulman A, Cleverstam E, Mattisson T, Lyngfelt A. Manganese/iron, manganese/nickel, and manganese/silicon oxides used in chemical looping with oxygen uncoupling (CLOU) for combustion of methane. *Energy Fuels* 2009;23:5269–75.
- [23] Azimi G, Leion H, Mattisson T, Lyngfelt A. Chemical-looping with oxygen uncoupling using combined Mn–Fe oxides, testing in batch fluidized bed. *Energy Proc* 2011;4:370–7.
- [24] Rydén M, Lyngfelt A, Mattisson T. Combined manganese/iron oxides as oxygen carrier for chemical-looping combustion with oxygen uncoupling (CLOU) in a circulating fluidized bed reactor system. *Energy Proc* 2011;4:341–8.
- [25] Leion H, Larring Y, Bakken E, Bredesen R, Mattisson T, Lyngfelt A. Use of  $\text{CaMn}_{0.875}\text{Ti}_{0.125}\text{O}_3$  as oxygen carrier in chemical looping with oxygen uncoupling. *Energy Fuels* 2009;23:5276–83.
- [26] Rydén M, Lyngfelt A, Mattisson T.  $\text{CaMn}_{0.875}\text{Ti}_{0.125}\text{O}_3$  as oxygen carrier for chemical oxygen combustion with oxygen uncoupling (CLOU) – experiments in a continuously operating fluidized-bed reactor system. *Int J Greenhouse Gas Control* 2010;5:356–66.
- [27] Pis JJ, Centeno TA, Mahamund M, Fuertes AB, Parra JB, Pajares JA, et al. Preparation of active carbons from coal – Part I. Oxidation of coal. *Fuel Process Technol* 1996;47:19–38.
- [28] Laurendeau NM. Heterogeneous kinetics of coal char gasification and combustion. *Prog Energy Combust Sci* 1978;4:221–70.
- [29] Jenkins SP, Nandi SP, Walker Jr PL. Reactivity of heat-treated coals in air at 500 °C. *Fuel* 1973;52:288–93.
- [30] Walker Jr PL. *Advances in coal utilization technology*. Chicago: Institute of Gas Technology; 1979.
- [31] Johnson JL. *Kinetics of coal gasification*. New York: Wiley; 1980.
- [32] Blake JH, Bopp GR, Jones JF, Miller MG, Tambo W. Aspects of the reactivity of porous carbons with carbon dioxide. *Fuel* 1967;46:115–25.
- [33] Allam R, White V, Ivens N, Simmonds M. The oxyfuel baseline: revamping heaters and boilers to oxyfiring by cryogenic air separation and flue gas recycle. In: Thomas DC, Benson SM, editors. *Carbon dioxide capture for storage in deep geologic formations – results from the CO<sub>2</sub> capture project*, vol. 1. Oxford, UK: Elsevier; 2005 [chapter 26].

## **Paper V**





## Demonstration of chemical-looping with oxygen uncoupling (CLOU) process in a 1.5 kW<sub>th</sub> continuously operating unit using a Cu-based oxygen-carrier

Alberto Abad\*, Iñaki Adánez-Rubio, Pilar Gayán, Francisco García-Labiano, Luis F. de Diego, Juan Adánez

*Instituto de Carboquímica (ICB-CSIC), Dept. of Energy & Environment, Miguel Luesma Castán, 4, Zaragoza, 50018, Spain*

### ARTICLE INFO

#### Article history:

Received 30 June 2011

Received in revised form 10 October 2011

Accepted 28 October 2011

#### Keywords:

CLOU

Copper oxide

Carbon capture

Coal

Combustion

CLC

### ABSTRACT

Chemical-looping with oxygen uncoupling (CLOU) process is a chemical-looping combustion (CLC) technology that allows the combustion of solid fuels with inherent CO<sub>2</sub> separation. As in the CLC technology, in the CLOU process the oxygen necessary for the fuel combustion is supplied by a solid oxygen-carrier, which contains a metal oxide. The CLOU technology uses the property of the copper oxide which can generate gaseous oxygen at high temperatures. The oxygen generated by the oxygen-carrier reacts directly with the solid fuel, which is mixed with the oxygen-carrier in the fuel-reactor. The reduced oxygen-carrier is transported to the air-reactor where it is oxidized by air. The flue gases from the fuel-reactor are only CO<sub>2</sub> and H<sub>2</sub>O, since fuel is not mixed with air. This work demonstrates the proof of the concept of the CLOU technology burning coal in a 1.5 kW<sub>th</sub> continuously operated unit consisting of two interconnected fluidized-bed reactors. A bituminous coal was used as fuel. An oxygen-carrier prepared by spray drying containing 60 wt.% CuO and MgAl<sub>2</sub>O<sub>4</sub> as supporting material was used as oxygen-carrier. The effects of fuel-reactor temperature, coal feeding rate, and solids circulation flow rate on the combustion and on the CO<sub>2</sub> capture efficiencies were investigated. Fast reaction rates of oxygen generation were observed with the oxygen-carrier and full combustion of coal was attained in the plant using a solids inventory ≈ 235 kg/MW<sub>th</sub> in the fuel-reactor. In addition, values close to 100% in carbon capture efficiency were obtained at 960 °C. Results obtained are analyzed and discussed in order to be useful for the scale-up of a CLOU process fuelled with coal.

© 2011 Elsevier Ltd. All rights reserved.

### 1. Introduction

According to the IPCC report on mitigation of climate change (IPCC, 2005), carbon capture and storage (CCS) would contribute with 15–55% to the cumulative mitigation effort worldwide until 2100 in order to stabilize CO<sub>2</sub> concentration in the atmosphere. CCS is a process involving the separation of CO<sub>2</sub> emitted by industry and energy-related sources, and its storage for isolation from the atmosphere over a long term. Chemical-looping combustion process (CLC) has been suggested among the best alternatives to reduce the economic cost of CO<sub>2</sub> capture using fuel gas (Kerr, 2005) and to reduce energy penalty compared with other CO<sub>2</sub> capture process (Kvamsdal et al., 2007). In this process, CO<sub>2</sub> is inherently separated from other combustion products, N<sub>2</sub> and unused O<sub>2</sub>, through the use of a solid oxygen-carrier and thus no energy is expended for its separation. A CLC system usually consists of two interconnected fluidized-bed reactors, designated as air-reactor and fuel-reactor, with the oxygen-carrier circulating between them. The CLC process has been demonstrated for gaseous fuel combustion such as

natural gas and syngas in 10–140 kW<sub>th</sub> units using oxygen-carrier materials based on Ni (Linderholm et al., 2009; Kolbitsch et al., 2009), Cu (Adánez et al., 2006) and Fe (Lyngfelt and Thunman, 2005; Pröll et al., 2009). All these oxygen-carriers have been reviewed by Adánez et al. (2011).

The use of the CLC concept for energy generation by coal combustion is more relevant for solid fuels, due to coal is considerably more abundant and less expensive than natural gas. It would be highly advantageous if the CLC process could be adapted to coal, as well as other kind of solid fuels. The first option to use solid fuels in a CLC process was to use syngas in the fuel-reactor coming from a previous gasifying step. However it is necessary to use pure oxygen for gasification of the solid fuel to apply this technology. This step has an important energy penalty due to the oxygen separation from the air. The second option of development is the chemical-looping solid fuel combustion, where the solid fuel is directly introduced to the fuel-reactor which is fluidized by a gasifying agent, e.g. H<sub>2</sub>O or CO<sub>2</sub>. Because of the slow gasification reaction rate, a carbon stripper is necessary to separate the unreacted char particles from the oxygen-carrier, before it is regenerated with air, to avoid CO<sub>2</sub> emissions in this reactor (Berguerand and Lyngfelt, 2008; Cao and Pan, 2006). To increase the gasification rate, temperatures higher than 1000 °C have been proposed to be used in the fuel-reactor (Berguerand and

\* Corresponding author. Tel.: +34 976 733977; fax: +34 976 733318.  
E-mail address: [abad@icb.csic.es](mailto:abad@icb.csic.es) (A. Abad).



### Nomenclature

$f_{C,fix}$	carbon fraction as fixed carbon in the coal
$f_C$	carbon fraction in the coal
$F_i$	molar flow of compound $i$ (mol/s)
$F_{in,FR}$	dry basis gas flow introduced in the fuel-reactor (mol/s)
$f_i$	mass fraction in coal of element or compound $i$
$F_{out,AR}$	dry basis exiting gas flow in the air-reactor (mol/s)
$F_{out,FR}$	dry basis gas flow exiting from the fuel-reactor (mol/s)
$\dot{m}_{coal}$	mass-based flow of coal fed-in to the fuel-reactor (kg/s)
$\dot{m}_{C,vol}$	mass flow of carbon contained in the volatile matter (kg/s)
$M_i$	molecular weight of compound $i$ (kg/mol)
$\dot{m}_s$	solids circulation rate (kg/s)
$m_{s,FR}$	mass of solids in the fuel-reactor (kg)
$(-r_C)$	fractional conversion rate of char (%/s)
$r_{O_2}$	rate of oxygen generation (kg O <sub>2</sub> /s per kg of OC)
$X_{char}$	conversion of char in the fuel-reactor
$y_i$	molar fraction in dry basis of the $i$ product

### Greek letters

$\Delta H_r$	enthalpy of reaction (kJ/mol)
$\Delta X_{OC}$	difference of oxygen-carrier conversion in the air- and fuel-reactors
$\eta_{CC}$	carbon capture efficiency (%)
$\eta_{comb}$	combustion efficiency in the fuel-reactor (%)
$\lambda$	stoichiometric air ratio
$\tau_{FR}$	mean residence time of solids in the fuel-reactor (s)
$\phi$	oxygen-carrier to fuel ratio
$\Omega_{coal}$	stoichiometric moles of O <sub>2</sub> to convert 1 kg of coal (mol/kg)

### Acronyms

AR	air-reactor
CLC	chemical-looping combustion
CLOU	chemical-looping with oxygen uncoupling
FR	fuel-reactor
in	inlet
IPCC	intergovernmental panel on climate change
OC	oxygen-carrier
out	outlet

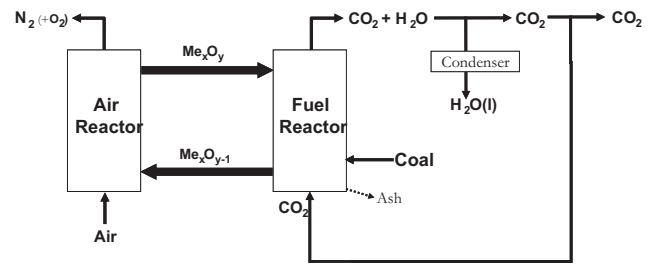
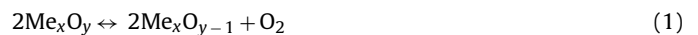


Fig. 1. Schematic diagram of the CLOU process.

CLOU process, fluidization gas can be recycled CO<sub>2</sub>, reducing in this way the steam duty of units in which steam is used to accelerate gasification kinetics.

Fig. 1 shows a schematic diagram of a CLOU system. In the fuel-reactor CO<sub>2</sub> and H<sub>2</sub>O are produced by different reactions. First the oxygen-carrier releases oxygen according to:



and the solid fuel begins devolatilization producing a solid residue (char) and volatile matter as gas product:



Then, char and volatiles are burnt as in usual combustion according to reactions (3) and (4):



After steam condensation, a pure CO<sub>2</sub> stream can be obtained in the fuel-reactor. The reduced oxygen-carrier is transported to the air-reactor, where the oxygen-carrier is regenerated to the initial oxidation stage by reverse reaction (1) with the oxygen of the air, and being ready for a new cycle. The exit stream of the air-reactor contains only N<sub>2</sub> and unreacted O<sub>2</sub>. Therefore, CLOU process such as CLC technology has a low energy penalty for CO<sub>2</sub> separation and low CO<sub>2</sub> capture costs would be expected. The heat release over the fuel- and air-reactors is the same as for conventional combustion.

A special requirement is needed for the oxygen-carrier to be used in the CLOU process in comparison to oxygen-carriers for normal CLC, where the fuel must be able to react directly with the oxygen-carrier without any release of gas phase oxygen. Only those metal oxides that have a suitable equilibrium partial pressure of oxygen at temperatures of interest for combustion (800–1200 °C) can be used as CLOU oxygen-carriers for solid fuel combustion. CuO/Cu<sub>2</sub>O, Mn<sub>2</sub>O<sub>3</sub>/Mn<sub>3</sub>O<sub>4</sub>, and Co<sub>3</sub>O<sub>4</sub>/CoO have been identified as redox pairs with capacity to evolve oxygen at those temperatures (Mattisson et al., 2009a). Copper, manganese and cobalt oxides have an oxygen transport capacity of 10, 3 and 6.6 g O<sub>2</sub> per 100 g of metal oxide, respectively.

In the CLOU process, the O<sub>2</sub> release (reaction (1)) must be reversible in order to oxidize the oxygen-carrier in the air-reactor and regenerate the material, which depends on the thermodynamic of the metal oxide used. Fig. 2 shows the partial pressure of oxygen as a function of the temperature for the systems CuO/Cu<sub>2</sub>O, Mn<sub>2</sub>O<sub>3</sub>/Mn<sub>3</sub>O<sub>4</sub>, and Co<sub>3</sub>O<sub>4</sub>/CoO, calculated using HSC software (HSC Chemistry 6.1, 2008). The respective reactions are endothermic for the three metal oxides, as it is shown in reactions (5)–(7). Operating conditions in the air-reactor and fuel-reactor would be determined by the thermodynamics of reaction (1) with the specific oxygen-carrier. On the one hand, the partial pressure of O<sub>2</sub> at equilibrium conditions must be low (4 kPa or lower) at the air-reactor temperature, in order to have a high use of the oxygen in air. On the other hand, the equilibrium concentration of oxygen in the fuel-reactor will be given by the temperature in the reactor determined

Lyngfelt, 2009). Moreover, there is a partial loss of oxygen-carrier in the purge stream of ash particles and low cost materials are preferred in this CLC option, e.g. ilmenite, hematite or anhydrite (Leon et al., 2008, 2009a; Shen et al., 2009; Wang and Anthony, 2008).

An alternative process, chemical-looping with oxygen uncoupling (CLOU), was recently proposed (Mattisson et al., 2009a) to overcome the low reactivity of the char gasification stage in the direct solid fuelled chemical-looping combustion. Mattisson and co-workers (Mattisson et al., 2009a) made use of the idea first proposed by Lewis and Gilliland (1954) to produce CO<sub>2</sub> from solid carbonaceous fuels by using gaseous oxygen produced by the decomposition of CuO.

Chemical-looping with oxygen uncoupling (CLOU) process is based on the strategy of using oxygen-carrier materials which release gaseous oxygen in the fuel-reactor and thereby allowing the solid fuel to burn with gas phase oxygen. These materials can be also regenerated at high temperatures. In this way, the slow gasification step in the chemical-looping combustion with solid fuels is avoided, giving a much faster solid conversion (Mattisson et al., 2009b). In

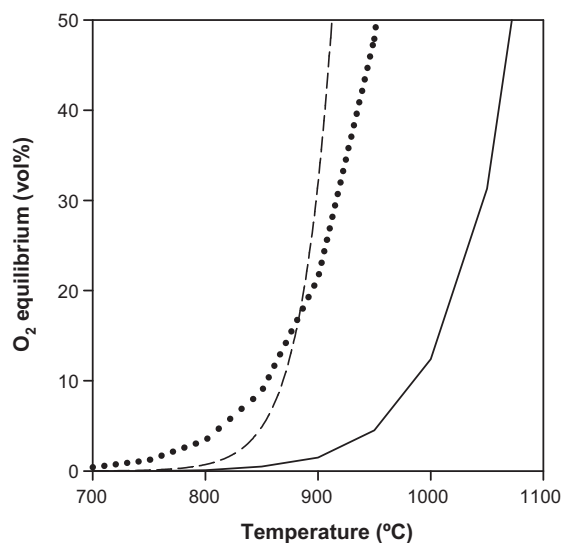
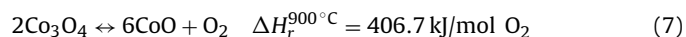
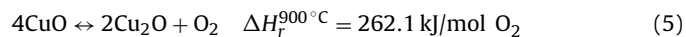
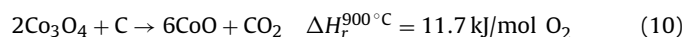
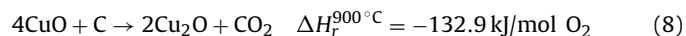


Fig. 2. Equilibrium oxygen concentration over the CuO/Cu<sub>2</sub>O (—), Mn<sub>2</sub>O<sub>3</sub>/Mn<sub>3</sub>O<sub>4</sub> (···) and Co<sub>3</sub>O<sub>4</sub>/CoO (---) systems as a function of temperature.

by the energy balance to CLOU system. A high equilibrium partial pressure of oxygen together with a very reactive oxygen-carrier will promote the overall conversion rate of the solid fuel in the fuel-reactor. In addition, the combustion of the fuel will decrease the oxygen concentration in the reactor and can improve the decomposition reaction of the metal oxide particles. The temperature at which the air- and fuel-reactor will operate is determined by the temperature of the incoming particles, the circulation rate and energy extraction, as well as the heat of reaction in both reactors, as it was analyzed by Eyring et al. (2011) for a CLOU process.



In the case of copper and manganese oxides, the overall reaction with carbon is exothermic in the fuel-reactor, as it is shown in reactions (8) and (9). Thus it is possible to have a temperature increase in the fuel-reactor, which results in a significantly higher partial pressure of O<sub>2</sub> at equilibrium conditions. In addition to heat release, overall heat balances to include heat losses (or heat inputs) and heat withdrawals (either in oxygen-carrier or fluidizing gas) are needed to obtain the temperatures in the reactors. In the other hand the reaction of the cobalt oxide with carbon is an endothermic reaction, see reaction (10).



There are only a small number of works in the literature for CLOU process dealing with the use of Cu-, Mn-, and Co-based based materials.

Regarding the use of manganese oxides for CLOU process, several Mn-based particles supported on Fe<sub>2</sub>O<sub>3</sub>, NiO, SiO<sub>2</sub> or MgO have been tested in a batch fluidized bed at Chalmers University of Technology (Azimi et al., 2011; Rydén et al., 2011b; Shulman et al., 2009, 2011). Good oxygen uncoupling and mechanical properties, as well as high reactivity with methane were showed for a Mn/Fe material after repeated redox cycles (Shulman et al., 2009). The formation of the Fe<sub>x</sub>Mn<sub>1-x</sub>O<sub>3</sub> iron manganate improves the oxygen uncoupling properties with respect to the manganese oxides. Later, the

optimum molar ratio Fe:Mn was determined to be 2:1 (Azimi et al., 2011). Tests in a batch fluidized bed with coal or petcoke as fuel revealed a high conversion of char, although the oxygen released was found to be around 0.5% of the mass. This material has also been tested in a continuous facility with methane as fuel (Rydén et al., 2011b), showing much better oxygen uncoupling properties than a manganese ore. However, the authors pointed out that much of the synthetic particles turned into a fine dust after 4 h of operation and collapsed material formed very soft agglomerations in the fuel-reactor.

Physical mixing of oxygen-carriers with Mn<sub>2</sub>O<sub>3</sub> and Co<sub>3</sub>O<sub>4</sub> (60 wt.%) supported on three different binders (yttria-stabilized zirconia (YSZ; 92 wt.% ZrO<sub>2</sub> and 8 wt.% Y<sub>2</sub>O<sub>3</sub>), Al<sub>2</sub>O<sub>3</sub> and TiO<sub>2</sub>) were investigated with promising results on oxygen release rate (Moghtaderi, 2010). However, these materials were proposed for oxygen production in the chemical-looping air separation process (CLAS), where coal is not mixed with the oxygen-carrier.

Perovskite type materials based on Mn and Ca oxides (CaMn<sub>x</sub>Ti<sub>1-x</sub>O<sub>3</sub>) has also been tested in a batch fluidized facility (Leion et al., 2009c; Rydén et al., 2011a). The oxygen uncoupling properties of perovskite type materials caused a fast conversion of petcoke (Leion et al., 2009c). The perovskite material CaMn<sub>0.875</sub>Ti<sub>0.125</sub>O<sub>3</sub> was later examined for 70 h in a small circulating fluidized-bed reactor using natural gas as fuel (Rydén et al., 2011a). Particles retained most of their physical properties and reactivity over the course of the experiments. In addition, high reactivity with CH<sub>4</sub> was found, although complete conversion of natural gas was not obtained during the experimental tests.

In general, Cu-based materials have faster release of oxygen than Mn-based particles (Leion et al., 2009c). Preliminary experiments were conducted using Al<sub>2</sub>O<sub>3</sub> or ZrO<sub>2</sub> as supporting materials (Leion et al., 2009b; Mattisson et al., 2009a,b). The results showed the relevance of the oxygen uncoupling properties on increasing the char conversion, which was the starting point for the proposal of the CLOU process. These experiments were done in a batch fluidized-bed reactor, and a high rate of char conversion was found for several carbonaceous materials, including petcoke, coal, and biomass (Leion et al., 2009b). It was found a 50 times increase in the conversion rate of petroleum coke at CLOU conditions with CuO relative to those measured with Fe-based oxygen-carrier in a CLC system with solid fuels (Mattisson et al., 2009a). It is noteworthy that Fe-based materials do not have oxygen uncoupling properties. A solids inventory between 120 and 200 kg/MW<sub>th</sub> was estimated for CLOU process using Cu-based particles (Mattisson et al., 2009a; Eyring et al., 2011), which was much lower than the amount of solids required in a CLC system 2000 kg/MW<sub>th</sub> for Fe-based particles (Leion et al., 2007; Mattisson et al., 2009b). However, they found some defluidization phenomena with Cu-based particles during some parts of the experiments (Mattisson et al., 2009b).

Avoiding agglomeration with Cu-based oxygen-carriers has been a major concern in the past. Thus, for CLC conditions where CuO can be reduced to Cu agglomeration is avoided by using CuO fractions lower than 20 wt.% in the particle (de Diego et al., 2005). However, the condition is different for CLOU, where CuO is reduced to Cu<sub>2</sub>O. In the research group of ICB-CSIC (Adánez-Rubio et al., 2011; Gayán et al., submitted for publication), a screening study considering 25 different Cu-based oxygen-carriers was done to select appropriate materials for CLOU process. Particles prepared by different methods and using several CuO contents and supporting materials were tested. Reactivity of materials was analyzed in a TGA, whereas mechanical stability and fluidization properties were studied in a batch fluidized bed. Two promising Cu-based oxygen-carriers prepared by pelletizing by pressure (60 wt.% CuO supported on MgAl<sub>2</sub>O<sub>4</sub>, and 40 wt.% CuO supported on ZrO<sub>2</sub>) were selected according to their high reactivity, low attrition rate and avoidance

**Table 1**  
Properties of the oxygen-carrier Cu60MgAl.

CuO content (wt.%)	60
Oxygen transport capacity, $R_{OC}$ (wt.%)	6
Crushing strength (N)	2.4
Real density (kg/m <sup>3</sup> )	4600
Porosity (%)	16.1
Specific surface area, BET (m <sup>2</sup> /g)	<0.5
XRD main phases	CuO, MgAl <sub>2</sub> O <sub>4</sub>

of agglomeration during successive redox cycles by alternating nitrogen and air.

To summarize, some works using oxygen-carriers with oxygen uncoupling properties have been done mainly in batch operation mode. The oxygen uncoupling properties of carrier materials were determined by analyzing the break off of oxygen in nitrogen and the conversion of CH<sub>4</sub> or solid fuels (petcoke, coal, biomass). However, the CLOU concept is based on the use of two interconnected fluidized beds, the oxygen-carrier being continuously circulating between them. In continuously operated units, only limited information about the oxygen uncoupling properties of two Mn-based materials using a gaseous fuel (CH<sub>4</sub>) in the fuel-reactor can be found (Rydén et al., 2011a,b). Up to the present, no experimental evidence has been found in the literature about the CLOU concept with solid fuels in continuously operated systems.

The aim of this work was to investigate the proof of the concept of the CLOU process in a continuously operated CLOU plant using coal as fuel. In this work, particles prepared by spray drying containing 60 wt.% CuO and using MgAl<sub>2</sub>O<sub>4</sub> as supporting material were used as oxygen-carrier for the CLOU process. This is the first time that the CLOU concept is demonstrated in a system composed by two interconnected fluidized-bed reactors using a solid fuel (bituminous coal). The effect of operating conditions – such as temperature of the fuel-reactor, the solids circulation rate and the coal feeding rate – on the combustion and CO<sub>2</sub> capture efficiencies were investigated. The results obtained were analyzed and discussed in order to be useful for the scale-up of a CLOU process fuelled with coal.

## 2. Experimental

### 2.1. Oxygen-carrier material

The oxygen-carrier was a Cu-based material prepared by spray drying. Oxygen-carrier particles were manufactured by VITO (Flemish Institute for Technological Research, Belgium) using MgAl<sub>2</sub>O<sub>4</sub> spinel (Baikowski, S30CR) and CuO (PANREAC, PRS) as raw materials. The CuO content was 60 wt.%. The particles were calcined 24 h at 1100 °C. The particle size of the oxygen-carrier was +0.1 to 0.2 mm. From now on, the oxygen-carrier was named as Cu60MgAl. Table 1 shows the main properties of this material.

The mechanical strength, determined using a Shimpo FGN-5X crushing strength apparatus, was taken as the average value of 20 measurements of the force needed to fracture a particle. The surface area of the oxygen-carrier particles was determined by the Brunauer–Emmett–Teller (BET) method in a Micromeritics ASAP-2020, whereas the pore volume was measured by Hg intrusion in a Quantachrome PoreMaster 33. The identification of crystalline chemical species was carried out by powder X-ray diffractometer Bruker AXS graphite monochromator.

The fresh material has a very low porosity and a very low superficial area. The mechanical strength of the particles after 24 h of calcination was adequate for its use in a fluidized bed. The crystalline phases found by XRD analysis were only CuO and MgAl<sub>2</sub>O<sub>4</sub>. The oxygen transport capability,  $R_{OC}$ , was calculated in a TGA as  $R_{OC} = 1 - m_{red}/m_{ox}$ ,  $m_{ox}$  being the mass of fully oxidized particles

**Table 2**  
Properties of fresh and pre-treated “El Cerrejón” coal.

	El Cerrejón	
	Fresh	Pre-treated
Proximate analysis (wt.%)		
Moisture	7.5%	2.3%
Volatile matter	34.0%	33.0%
Fixed carbon	49.9%	55.9%
Ash	8.6%	8.8%
Ultimate analysis (wt.%)		
C	70.8%	65.8%
H	3.9%	3.3%
N	1.7%	1.6%
S	0.5%	0.6%
LHV (kJ/kg)	25,880	21,899

and  $m_{red}$  in the reduced form, i.e. when all CuO has been reduced to Cu<sub>2</sub>O.

Preliminary results showed that similar material prepared by mechanical mixing has adequate values of reactivity and oxygen transport capacity, high attrition resistance and does not have tendency to agglomerate during operation in a fluidized-bed reactor (Adánez-Rubio et al., submitted for publication-a).

### 2.2. Coal fuel

The fuel was a bituminous Colombian coal “El Cerrejón”. Proximate and ultimate analysis and the low heating value of this coal were determined. The properties of this coal are shown in Table 2. The coal particle size used for this study was +200 to 300 μm.

Bed agglomeration problems with pipes clogging were found when “El Cerrejón” coal was fed into the system because this coal showed a high swelling behaviour. In order to avoid coal swelling and bed agglomeration, the coal was subjected to a thermal pre-treatment for pre-oxidation. Coal was heated at 180 °C in air atmosphere for 28 h (Pis et al., 1996). Proximate and ultimate analyses of the pre-treated coal are shown in Table 2. The pre-oxidation causes an increase in the oxygen content from 7.2 to 17.6% and a decrease in the heating value. Despite the decrease in the heating value, the swelling properties of this coal were eliminated and agglomeration problems were not observed in any experiment carried out with this pre-treated coal.

### 2.3. Experimental set-up ICB-CSIC-s1

A schematic view of the experimental set-up used is shown in Fig. 3. The set-up was basically composed of two interconnected fluidized-bed reactors – the air- and fuel-reactors – joined by a loop seal and a riser for solids transport from the air-reactor to the fuel-reactor, a cyclone and a solids valve to control the solids circulation flow rate in the system. The reactors operate slightly higher than atmospheric pressure, taking into consideration the pressure drops in the bed and pipes to stack. The fuel-reactor (1) consisted of a bubbling fluidized bed with 50 mm of inner diameter and 200 mm bed height. N<sub>2</sub> or CO<sub>2</sub> can be used as fluidizing gas. The gas flow was 186 L<sub>N</sub>/h, corresponding to a gas velocity of 0.11 m/s at 900 °C. The minimum fluidizing velocities of the oxygen-carrier particles are 0.006 m/s for the smallest particle size and 0.023 m/s for the biggest one. The terminal velocities of the oxygen-carrier particles are 0.40 m/s and 1.45 m/s, for the smallest and biggest particles, respectively.

Coal (9) was fed in by a screw feeder (10) at the bottom of the bed just above the fuel-reactor distributor plate in order to maximize the time that the fuel and volatile matter are in contact with the bed material. The screw feeder has two stages: the

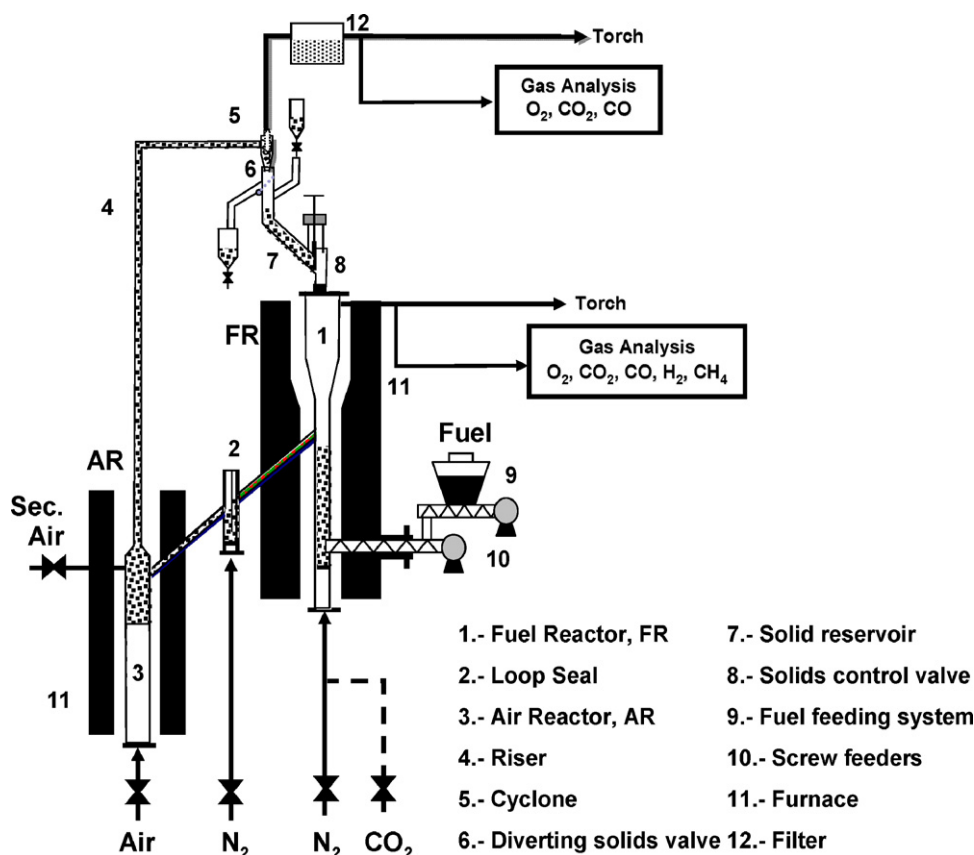


Fig. 3. Schematic view of the ICB-CSIC-s1 unit for CLOU (1.5 kW<sub>th</sub>).

first one with variable speed to control the coal flow rate, and the second one has high rotating velocity to avoid coal pyrolysis inside the screw. A small N<sub>2</sub> flow (24 L<sub>N</sub>/h) is introduced at the beginning of the screw feeder to avoid any possible volatile reverse flow.

The oxygen-carrier is decomposed in the fuel-reactor, evolving gaseous oxygen to the surroundings. The oxygen burns the volatiles and char proceeding from coal pyrolysis in the fuel-reactor. Reduced oxygen-carrier particles overflowed into the air-reactor through a U-shaped fluidized bed loop seal (2) with 30 mm of inner diameter, to avoid gas mixing between fuel and air. A N<sub>2</sub> flow of 60 L<sub>N</sub>/h was introduced in the loop seal. Preliminary experiments were carried out to observe the distribution of gas fed to the loop seal. In experimental conditions used in this work, the gas in the loop-seal was distributed approximated at 50% in each reactor (air- and fuel-reactor).

The oxidation of the carrier took place in the air-reactor (3), consisting of a bubbling fluidized bed with 80 mm of inner diameter and 100 mm bed height, and followed by a riser with 30 mm of inner diameter. The air flow was 1740 L<sub>N</sub>/h ( $u_g = 0.40$  m/s). In addition, a secondary air flow (240 L<sub>N</sub>/h) was introduced at the top of the bubbling bed to help particle entrainment through a riser (4). N<sub>2</sub> and unreacted O<sub>2</sub> left the air-reactor passing through a high-efficiency cyclone (5) and a filter before the stack. The oxidized solid particles recovered by the cyclone were sent to a solids reservoir (7), setting the oxygen-carrier ready to start a new cycle. The regenerated oxygen-carrier particles returned to the fuel-reactor by gravity from the solids reservoir through a solids valve (8) which controls the flow rates of solids entering to the fuel-reactor. A diverting solids valve (6) located below the cyclone allowed the measurement of the solids flow rates at any time. Therefore, this design allows to control and measure the solids circulation flow

rate between both reactors. The ash particles from char combustion were not recovered by the cyclone and were collected in a filter down-stream. Thus, ash particles were not accumulated in the system. Finally, it is worthy of consideration that leakage of gas between both reactors was avoided by the presence of oxygen in the fuel-reactor solely should come from oxygen released by reaction (5).

The total oxygen-carrier inventory in the system was around 2.0 kg, being about 0.4 kg in the fuel-reactor. The exact amount of solids in the fuel-reactor was calculated from pressure drop measurements in the reactor for each test.

CO<sub>2</sub>, CO, H<sub>2</sub>, CH<sub>4</sub>, and O<sub>2</sub> were analyzed at the outlet stream from fuel-reactor, whereas CO<sub>2</sub>, CO and O<sub>2</sub> were analyzed from the flue gases of the air-reactor. Non-dispersive infrared (NDIR) analyzers (Maihak S710/UNOR) were used for CO, CO<sub>2</sub>, and CH<sub>4</sub> concentration determination; a paramagnetic analyzer (Maihak S710/OXOR-P) was used to determine O<sub>2</sub> concentration; and a thermal conductivity detector (Maihak S710/THERMOR) was used for H<sub>2</sub> concentration determination. In some selected experiments, the tar amount present in fuel-reactor product gas was determined following the tar protocol (Simell et al., 2000), as well as higher C<sub>2</sub>–C<sub>4</sub> hydrocarbons were analyzed off-line by a gas chromatograph (HP5890 Serie II).

Because of heat losses, the system is not auto-thermal and is heated up by means of various independent ovens to get independent temperature control of the air-reactor, fuel-reactor, and freeboard above the bed in the fuel-reactor. During operation, temperatures in the bed and freeboard of the fuel-reactor, air-reactor bed and riser were monitored as well as the pressure drops in important locations of the system, such as the fuel-reactor bed, the air-reactor bed and the loop seal.

**Table 3**  
Main data for experimental tests in the continuous CLOU prototype ICB-CSIC-s1 (bold values correspond to the variable changed in every test series).

Test	$T_{FR}$ (°C)	$\phi$	$\lambda$	$\dot{m}_s$ (kg/h)	$\dot{m}_{coal}$ (g/h)	Power (W)	$m_{s,FR}$ (g)	$m_{s,FR}^*$ (kg/MW <sub>th</sub> )
CLOU01	<b>903</b>	1.2	2.8	<b>4.2</b>	112	681	412	605
CLOU02	<b>917</b>	1.2	2.8	4.2	112	681	412	605
CLOU03	<b>941</b>	1.2	2.8	4.2	112	681	373	547
CLOU04	<b>960</b>	1.2	2.8	4.2	112	681	393	577
CLOU05	924	4.3	4.7	9.0	<b>67</b>	410	471	1150
CLOU06	929	3.2	3.5	9.0	<b>89</b>	541	452	835
CLOU07	917	2.6	2.8	9.0	<b>112</b>	681	412	605
CLOU08	920	2.1	2.3	9.0	<b>135</b>	821	373	454
CLOU09	925	1.1	1.2	9.0	<b>256</b>	1560	368	235
CLOU10	901	1.1	2.8	<b>3.7</b>	112	681	452	663
CLOU11	901	2.0	2.8	<b>7.0</b>	112	681	452	663
CLOU12	898	4.0	2.8	<b>13.9</b>	112	681	491	721

#### 2.4. Experimental planning

Three different experimental test series were carried out using the same batch of oxygen-carrier particles. Table 3 shows a compilation of the main variables used in each test. Oxygen-carrier particles were used during 30 h of hot fluidization conditions, whereof 18 h corresponded to coal combustion.

The fuel-reactor temperature (CLOU01–CLOU04), the coal feeding rate (CLOU05–CLOU09) and the solid circulation flow rate (CLOU01 and CLOU10–CLOU12) were varied during experimental work using “El Cerrejón” coal. The temperature in the freeboard was maintained at 900 °C in all cases. The coal fed in was varied from 67 to 256 g/h, which corresponded to a thermal power of 410–1560 W<sub>th</sub>. N<sub>2</sub> was used as fluidizing gas in the fuel-reactor in order to improve the evaluation of experimental results. A parameter  $\phi$  was defined to calculate the stoichiometric solid circulation rate needed for combustion of each coal feeding rate. A value of  $\phi = 1$  corresponds to the stoichiometric flow of CuO to fully convert coal to CO<sub>2</sub> and H<sub>2</sub>O through reactions (1)–(4), being the CuO reduced to Cu<sub>2</sub>O. The oxygen-carrier to fuel ratio ( $\phi$ ) was defined by the following equation:

$$\phi = \frac{0.25F_{CuO}}{\Omega_{coal}\dot{m}_{coal}} \quad (11)$$

$F_{CuO}$  being the molar flow rate of CuO and  $\dot{m}_{coal}$  the mass-based flow of coal fed-in to the reactor.  $\Omega_{coal}$  is the stoichiometric mols of oxygen, as O<sub>2</sub>, needed to convert 1 kg of coal to CO<sub>2</sub> and H<sub>2</sub>O, as well as NO and SO<sub>2</sub>. This value was calculated from the proximate and ultimate analysis of coal, see Table 2, yielding a value of  $\Omega_{coal} = 59$  mol O<sub>2</sub> per kg of coal.

$$\Omega_{coal} = \frac{f_C}{M_C} + 0.25\frac{f_H}{M_H} + 0.5\frac{f_N}{M_N} + \frac{f_S}{M_S} - 0.5\frac{f_O}{M_O} \quad (12)$$

The temperature in the air-reactor was maintained at 900 °C. Air flow into the air-reactor was maintained constant for all tests, always remaining in excess over the stoichiometric oxygen demand of the fuel. The stoichiometric air ratio,  $\lambda$ , was defined by Eq. (13). Depending on the fuel flow, the value of  $\lambda$  ranged from 1.2 to 4.7.

$$\lambda = \frac{\text{oxygen flow in air}}{\text{oxygen demand}} = \frac{0.21F_{air}}{\Omega_{coal}\dot{m}_{coal}} \quad (13)$$

#### 2.5. Data evaluation

To analyze the confidence of the results, a mass balance to oxygen and carbon was carried out using the measurements of the analyzers from the air- and fuel-reactors. The dry basis product gas flow in the fuel-reactor,  $F_{out,FR}$ , was calculated as

$$F_{out,FR} = \frac{F_{in,FR}}{1 - (Y_{CO_2,out,FR} + Y_{CO,out,FR} + Y_{H_2,out,FR} + Y_{CH_4,out,FR})} \quad (14)$$

$y_{i,out,FR}$  being the concentration in dry basis exiting from the fuel-reactor, where  $i$  can be: CO<sub>2</sub>, CO, H<sub>2</sub> or CH<sub>4</sub>.

The outlet air-reactor gas flow,  $F_{out,AR}$ , was calculated through the introduced N<sub>2</sub>,  $F_{N_2,AR}$ .

$$F_{out,AR} = \frac{F_{N_2,AR}}{1 - (Y_{O_2,out,AR} + Y_{CO_2,out,AR})} \quad (15)$$

Thus, the exiting flows of O<sub>2</sub> and CO<sub>2</sub> from the air- and fuel-reactors can be easily calculated using the actual concentration of every gas  $i$ .

$$F_{i,out} = y_{i,out}F_{out} \quad (16)$$

Notice that nitrogen is used as fluidizing agent in the fuel-reactor during experimental work, thus CO<sub>2</sub> comes uniquely from the coal combustion. The mass balances for oxygen and carbon were found to be accurate by using the measurements of the analyzers from the air- and fuel-reactors. The mass balance to carbon can be done as:

$$\begin{aligned} f_C \cdot \dot{m}_{coal} &= f_{C,fix} \cdot \dot{m}_{coal} + \dot{m}_{C,vol} \\ &= M_C(F_{CO_2,out,FR} + F_{CO,out,FR} + F_{CH_4,out,FR} + F_{CO_2,out,AR}) \end{aligned} \quad (17)$$

$f_{C,fix}$  being the carbon fraction as fixed carbon in the coal, and  $\dot{m}_{C,vol}$  the mass flow of carbon contained in the volatile matter calculated as

$$\dot{m}_{C,vol} = (f_C - f_{C,fix})\dot{m}_{coal} \quad (18)$$

Eq. (18) assumes that the volatiles evolved in the fuel-reactor are the same as in a proximate analysis measurement. The elutriation of char particles from the fuel-reactor was negligible regarding the carbon balance in the system.

From the flow of CO<sub>2</sub> and O<sub>2</sub> exiting from the fuel-reactor, the rate of oxygen generation per unit of mass of solid in the fuel-reactor can be calculated as:

$$r_{O_2} = \frac{(F_{CO_2,out,FR} + F_{O_2,out,FR} + 0.5(F_{CO,out,FR} + F_{H_2O,out,FR}) - 0.5\dot{m}_{coal}((f_{H_2O}/M_{H_2O}) + (f_O/M_O)))M_{O_2}}{m_{s,FR}} \quad (19)$$

The variation of the oxygen-carrier conversion in the fuel-reactor was calculated as:

$$\Delta X_{OC} = \frac{r_{O_2} \cdot m_{s,FR}}{0.25F_{CuO}} \quad (20)$$

The evaluation of the CLOU performance was carried out by studying the effect of the operational variables on the carbon capture efficiency, the char conversion and the combustion efficiency in the fuel-reactor.

The carbon capture efficiency,  $\eta_{CC}$ , was defined as the fraction of carbon initially present in the coal fed in which is actually at the

outlet of fuel-reactor as CO<sub>2</sub>. This is the actual CO<sub>2</sub> captured in the CLOU system, the remaining is CO<sub>2</sub> exiting together with nitrogen from the air-reactor.

$$\eta_{CC} = \frac{M_C F_{CO_2, out, FR}}{f_C \cdot \dot{m}_{coal}} \quad (21)$$

The carbon capture efficiency depends on the conversion of char in the fuel-reactor. The conversion of char in the fuel-reactor,  $X_{char}$ , was calculated considering the carbon contained in the coal fed remaining in the char, i.e. fixed carbon, and the carbon not converted in the fuel-reactor, which exits as CO<sub>2</sub> from the air-reactor.

$$X_{char} = \frac{f_{C, fix} \cdot \dot{m}_{coal} - M_C \cdot F_{CO_2, out, AR}}{f_{C, fix} \cdot \dot{m}_{coal}} \quad (22)$$

The conversion of char in the fuel-reactor was related to the temperature and the mean residence time of solids in the fuel-reactor,  $\tau_{FR}$ .  $\tau_{FR}$  is calculated by the following equation:

$$\tau_{FR} = \frac{m_{s, FR}}{\dot{m}_s} \quad (23)$$

$m_{s, FR}$  being the mass of solids in the fuel-reactor and  $\dot{m}_s$  the solids circulation rate between the air- and fuel-reactors.

Finally, the combustion efficiency in the fuel-reactor,  $\eta_{comb}$ , evaluates the combustion degree of coal only converted in the fuel-reactor. The combustion efficiency in the fuel-reactor was calculated through the quotient between the oxygen required to fully burn unconverted gases (CH<sub>4</sub>, CO and H<sub>2</sub>) and the oxygen demanded by coal converted to gas only in the fuel-reactor. Therefore, the combustion efficiency in the fuel-reactor was calculated as:

$$\eta_{comb, FR} = 1 - \frac{4F_{CO_4, out, FR} + F_{CO, out, FR} + F_{H_2, out, FR}}{(\Omega_{coal}/M_O)\dot{m}_{coal} - 2F_{CO_2, out, AR}} \quad (24)$$

### 3. Results

To demonstrate the proof of the concept of the CLOU process, several tests under continuous operation were carried out in the ICB-CSIC-s1 experimental unit using coal as fuel. A Cu-based material (Cu60MgAl) was used as oxygen-carrier. Although CO<sub>2</sub> should be the fluidizing gas in a CLOU unit, in this work N<sub>2</sub> was fed to the fuel-reactor to use measurements of CO<sub>2</sub> concentration to carry out the carbon balance. In other work, it was determined that the fluidization agent does not have any influence on the oxygen uncoupling behaviour of a Cu-based oxygen-carrier (Gayán et al., submitted for publication).

Different fuel-reactor temperatures, coal feeding rates and solid circulation flow rates were used, see Table 3. The CLOU prototype was easy to operate and control, and steady state for each operating condition was maintained for at least 60 min. Around of 30 h of continuous hot CLOU operation were accomplished. Agglomeration or defluidization was never detected with this Cu-based oxygen-carrier, even though the fuel-reactor temperature was as high as 960 °C.

The exit gas compositions of fuel- and air-reactors exit gases were analyzed. As an example, Fig. 4 shows the concentration of gases (dry basis) measured as a function of the operating time for test series CLOU01–CLOU04 where the fuel-reactor temperature was varied from 900 °C to 960 °C. The solids circulation rate was maintained at a mean value of 4.2 kg/h, whereas the coal feeding rate was 0.11 kg/h, corresponding to a oxygen-carrier to fuel ratio,  $\phi$ , of 1.2, as defined by Eq. (11). Carbon feeding started at  $t = 17$  min. Before carbon feeding, the oxygen concentration in the fuel-reactor was at equilibrium conditions at the reactor temperature. Thus, the oxygen uncoupling effect of the oxygen-carrier is showed. After carbon feeding, a short transitional period it is shown until steady state is reached. At steady state, the gas outlet concentration and temperature were maintained uniform during the whole combustion

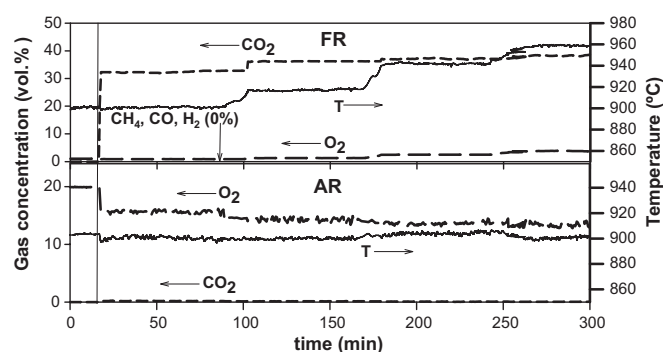


Fig. 4. Evolution of the gas composition in the air- and fuel-reactor at different fuel-reactor temperatures. Experimental tests CLOU01–CLOU04.  $\dot{m}_s = 4.2$  kg/h;  $\phi = 1.2$ . Fuel feeding to the system after vertical line,  $t = 17$  min.

time. When temperature was varied, a transition period appeared and stable combustion was reached usually in less than 10 min.

In all cases, no CH<sub>4</sub>, CO or H<sub>2</sub> were detected in the outlet gas stream of the fuel-reactor. The possible presence of tars or light hydrocarbons (C<sub>2</sub>–C<sub>4</sub>) was also analyzed. For some experiments, tar measurements were done using tar protocol (Simell et al., 2000) at the fuel-reactor outlet stream. Tar was not detected in the fuel-reactor outlet flow, that is, no hydrocarbons heavier than C<sub>5</sub>. In addition, gas from the fuel-reactor outlet stream was collected in bags and analyzed off line using a gas chromatograph. The analysis showed that there were no C<sub>2</sub>–C<sub>4</sub> hydrocarbons in the gases. Thus, CO<sub>2</sub>, H<sub>2</sub>O and O<sub>2</sub> were the only gases at the fuel-reactor outlet together with the N<sub>2</sub> introduced as fluidizing gas. It must be pointed out that small amounts of SO<sub>2</sub> and NO<sub>x</sub> were also present at the fuel-reactor gas stream, but these components were not evaluated in this work. Therefore, volatiles were fully converted into CO<sub>2</sub> and H<sub>2</sub>O in the fuel-reactor by reaction with the oxygen released from the CuO decomposition. In addition, the oxygen release rate was high enough to supply an excess of gaseous oxygen (O<sub>2</sub>) exiting together with the combustion gases. In the air-reactor the CO<sub>2</sub> and O<sub>2</sub> concentration decreased when the temperature increased in the fuel-reactor.

The corresponding performance parameters (i.e. combustion efficiency, carbon capture efficiency and char conversion) to the tests shown in Table 3 are summarized in Table 4. Fig. 5(a)–(c) shows the O<sub>2</sub> and CO<sub>2</sub> concentration (dry basis) exiting from the fuel- and air-reactors as a function of the fuel-reactor temperature, the coal feeding rate and the solids circulation flow rate, respectively.

The effect of the fuel-reactor temperature on the CO<sub>2</sub> and O<sub>2</sub> concentration in the air- and fuel-reactors are shown in Fig. 5(a). On the one hand, both O<sub>2</sub> and CO<sub>2</sub> concentrations from the fuel-reactor slightly increased with the temperature. The oxygen concentration

Table 4

Main results for experimental tests in the continuous CLOU prototype ICB-CSIC-s1.

Test	Combustion efficiency	Carbon capture efficiency
CLOU01	100	96.0
CLOU02	100	97.3
CLOU03	100	99.1
CLOU04	100	99.3
CLOU05	100	97.8
CLOU06	100	97.9
CLOU07	100	97.8
CLOU08	100	98.1
CLOU09	100	97.5
CLOU10	100	97.5
CLOU11	100	97.1
CLOU12	100	94.7

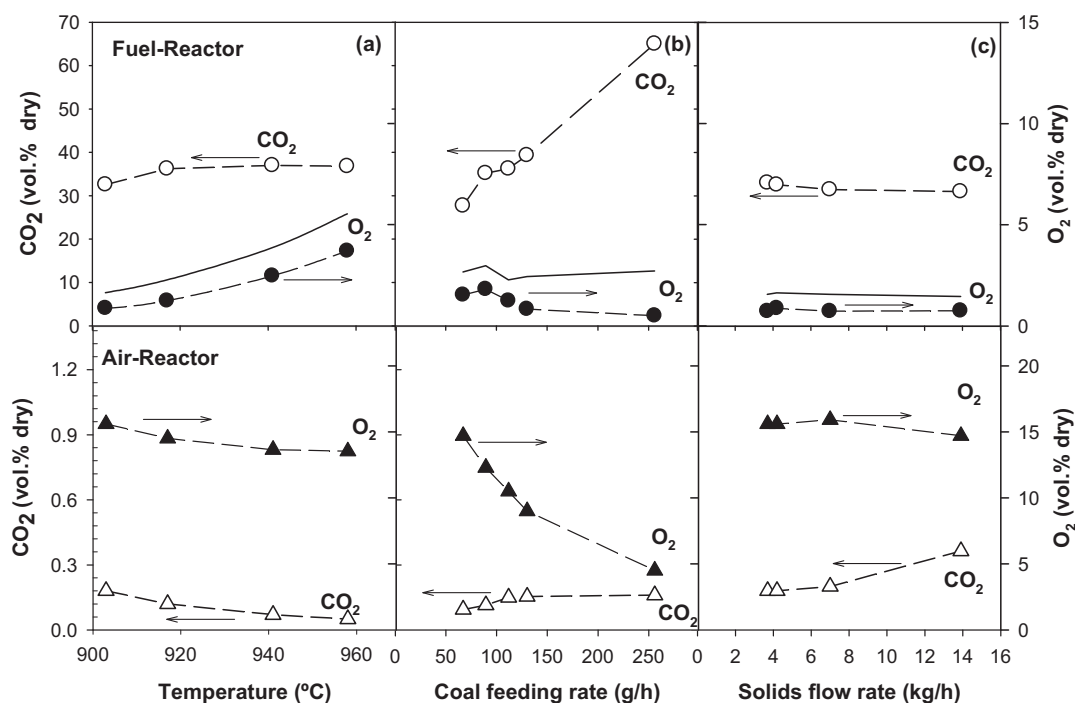


Fig. 5. CO<sub>2</sub> and O<sub>2</sub> concentration from the fuel- and air-reactors obtained at different (a) fuel-reactor temperatures, (b) coal feeding rates, and (c) solids circulation flow rate. Fuel-reactor: CO<sub>2</sub> (○) and O<sub>2</sub> (●). Air-reactor: CO<sub>2</sub> (△) and O<sub>2</sub> (▲). Oxygen concentration at equilibrium in the fuel-reactor (---).

was slightly lower than the equilibrium concentration, likely due to O<sub>2</sub> reaction in the freeboard with char particles or un-burnt gases. This fact was in contrast to the O<sub>2</sub> equilibrium concentration observed when coal was not fed to the reactor ( $t < 17$  min). On the other hand, CO<sub>2</sub> concentration in the air-reactor decreased as the fuel-reactor temperature increased. This fact indicates that the amount of char transferred to the air-reactor decreased with the fuel-reactor temperature because of the higher char combustion rates present in fuel-reactor. However, the oxygen concentration in the air-reactor decreased with the fuel-reactor temperature. This fact is evident if it is considered that in addition to the oxygen used to burn coal, which is constant, also oxygen is released from the fuel-reactor. The decrease observed in O<sub>2</sub> concentration from the air-reactor was due to a higher CuO conversion in the fuel-reactor when increasing the fuel-reactor temperature, as more gaseous oxygen is released.

The effects of the coal feeding rate on the concentration of gases are shown in Fig. 5(b). In this case, it is observed an important CO<sub>2</sub> concentration increase in fuel-reactor with the coal feeding rate, and the oxygen concentration in the air-reactor decreases correspondingly to the increase in the oxygen demanded by the coal fed. The oxygen concentration in the fuel-reactor decreases as the coal feeding rate increases. Nevertheless, the oxygen-carrier shows high enough rate of oxygen generation to burn all the coal in all cases and still gives an excess of gaseous oxygen. Thus, the oxygen-carrier reactivity did not limit the O<sub>2</sub> concentration release. Likely, the decrease in the oxygen concentration observed was due to a higher amount of oxygen reacting in the freeboard. If the oxygen concentration at the fuel-reactor outlet was constrained by the rate of oxygen generation of the oxygen-carrier, a sharp decrease in the oxygen concentration until values close to zero should be observed as the coal feeding rate was increased (Adánez-Rubio et al., submitted for publication-b).

In the last series of experiments, it was studied the effect of the solids circulation flow rate on the process performance. Solids circulation flow rates from 3.7 to 13.9 kg/h were used, corresponding to  $\phi$  values from 1.1 to 4.0, and the fuel-reactor temperature

was 900 °C. The stoichiometric flow of solids to supply the oxygen needed to burn the coal was 3.5 kg/h. Thus the solids circulation rate was maintained above the stoichiometric flow of solids, although values close to the stoichiometric flow were used in test CLOU10, where the oxygen-carrier to fuel ratio was 1.1. Fig. 5(c) shows the O<sub>2</sub> and CO<sub>2</sub> concentration obtained in the fuel- and air-reactors with different solids circulation flow rates. CO<sub>2</sub> concentration in the fuel-reactor decreased with the circulation rate with the corresponding increase in the CO<sub>2</sub> concentration in the air-reactor. In spite of the low  $\phi$  ratio used in this experiment, no unburnt gases were detected. In all cases, H<sub>2</sub>O, CO<sub>2</sub> and O<sub>2</sub> were observed as the only product gases from the fuel-reactor. Minor variation in the concentration of gases was observed when the oxygen-carrier flow rates change.

Fig. 6(a)–(c) shows the variation of solids conversion as a function of the fuel-reactor temperature, coal feeding rate and solids circulation flow rate, respectively. The molar flow of CO<sub>2</sub> exiting from the fuel-reactor is also shown in these Figures.

Fig. 6(a) shows that the increase in the fuel-reactor temperature produced an increase in the CO<sub>2</sub> flow at the outlet of the fuel-reactor. Moreover, as higher is O<sub>2</sub> concentration and more char is burning in the fuel-reactor, the variation of solids conversion slightly increases with fuel-reactor temperature. Although, the variation of solids conversion in the fuel-reactor was very high,  $\approx 80\%$  in all cases, there were not problems with the fluidization behaviour.

Fig. 6(b) shows the CO<sub>2</sub> molar flow from the fuel-reactor and the oxygen-carrier conversion as a function of coal feeding rate. In all cases the ratio of oxygen-carrier to fuel is above the stoichiometric value. At these conditions, there was an excess of oxygen in the circulating solids and the coal combustion was not limited by the availability of reactant. As expected, the CO<sub>2</sub> flow from fuel-reactor increased with the coal feeding rate because more fuel is burnt. Also, more oxygen is transferred between the two reactors, as it is indicated by the increase of the variation of solids conversion between 23 and 90%. The highest coal feeding rate tested was 0.256 kg/h (test CLOU09). The solids inventory in the fuel-reactor at

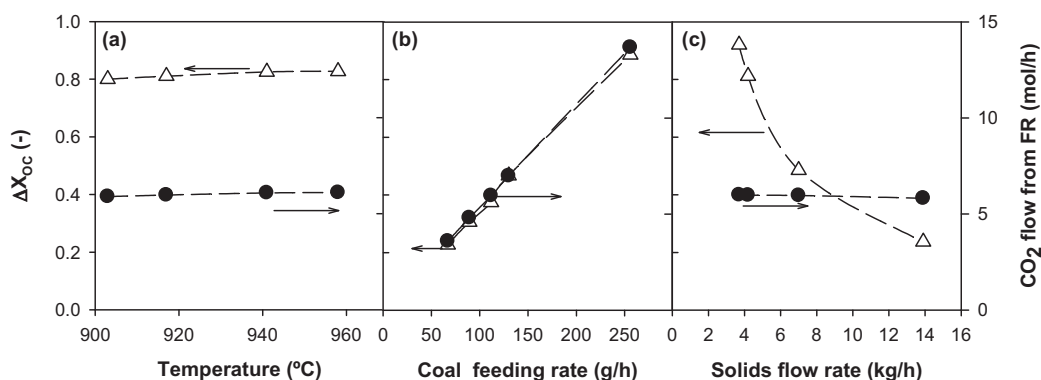


**Fig. 6.** Variation of the oxygen-carrier conversion ( $\Delta$ ) and flow of CO<sub>2</sub> exiting from the fuel-reactor ( $\bullet$ ) at different (a) fuel-reactor temperatures, (b) coal feeding rates, and (c) solids circulation flow rate.

this condition was 235 kg/MW<sub>th</sub>. At this condition, oxygen-carrier particles were elutriated from the fuel-reactor because the high amount of gases generated in the bed. Nevertheless, during the short time of stable operation (about 15 min) full conversion of coal to CO<sub>2</sub> and H<sub>2</sub>O was observed, unburnt gases were not detected and there was an excess of O<sub>2</sub> present. Unfortunately, the growth up of gas velocity in the bed prevented to work with larger coal feeding rates, although the Cu60MgAl oxygen-carrier would be able to supply the oxygen demanded by coal.

Fig. 7 shows the rate of oxygen generation, defined in Eq. (19), by Cu60MgAl oxygen-carrier as a function of the coal feeding rate, corresponding to the flows of CO<sub>2</sub>, H<sub>2</sub>O and O<sub>2</sub> exiting from the fuel-reactor. It can be seen that the oxygen transferred increases proportionally to the increase in the coal feeding rate. The upper limit for the oxygen generation rate using Cu60MgAl oxygen-carrier was not reached in the CLOU facility, although a low solid inventory was used (235 kg/MW<sub>th</sub>). This confirms the statement made that in this system the oxygen evolved in the fuel-reactor is not limited by the reaction rate of oxygen-carrier, but for the demand of oxygen by coal.

As a consequence, limited effect on the oxygen generation rate, i.e. the sum of O<sub>2</sub> and CO<sub>2</sub> flows, was observed when the temperature or the solids circulation flow rate (Fig. 6(c)) was varied, even though the variation of the solids conversion was as

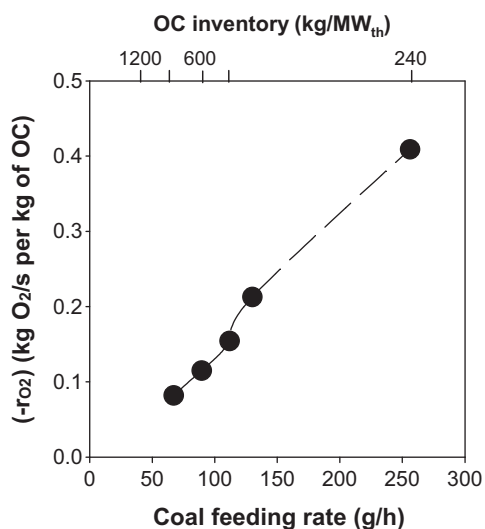


**Fig. 7.** Rate of oxygen transferred by Cu60MgAl oxygen-carrier as a function of the coal feeding rate and the oxygen-carrier inventory.

high as 0.92. Thus, high reactivity of the oxygen-carrier was found in a wide range of variation of the solids conversion.

Fig. 8(a)–(c) shows the carbon capture efficiency, char conversion and the combustion efficiency as a function of the fuel-reactor temperature, the coal feeding rate and the solids circulation flow rate. Complete combustion to CO<sub>2</sub> and H<sub>2</sub>O of the coal was observed either in the fuel-reactor or the air-reactor, i.e.  $\eta_{comb} = 100\%$ . However, the char conversion in the fuel-reactor determines the carbon capture efficiency in the CLOU system by the undesirable CO<sub>2</sub> emissions in the air-reactor outlet.

It can be seen that high values of CO<sub>2</sub> capture efficiency were obtained in all cases. It is noteworthy the positive effect of fuel-reactor temperature on the CO<sub>2</sub> capture efficiency, see Fig. 8(a). Thus, when the fuel-reactor temperature was 960 °C, 99% of carbon in coal is captured, i.e. only 1% of carbon is exiting in the air-reactor outlet gas stream. The reason for this high CO<sub>2</sub> capture efficiency is a fast conversion of char in the fuel-reactor by combustion with gaseous oxygen. Fig. 8(a) also shows values of char conversion above 96%, which increases with the temperature. In that sense, the CO<sub>2</sub> flow from the air-reactor decreased with the fuel-reactor temperature because more char is burned in the fuel-reactor. There is a lower char concentration in fuel-reactor due to the higher char combustion rates and a lower amount of carbon is transferred to the air-reactor.

The fuel load had no relevant effect on the CO<sub>2</sub> capture efficiency; see Fig. 8(b). Since the circulation rate and the temperature are kept constant and there is an oxygen excess in all cases, the resulting CO<sub>2</sub> capture efficiency for the different coal feeding rates does not change substantially. Thus, at the conditions used in the CLOU system, the oxygen generated in the fuel-reactor was not limited by the reactivity of this oxygen-carrier, i.e. the more oxygen is demanded, more oxygen is supplied.

Finally, Fig. 8(c) shows that an increase in the solids circulation flow causes a decrease in the char conversion and in the CO<sub>2</sub> capture efficiency. This result for CLOU with solid fuels is opposite to the trend found for CLC with gaseous fuels, for which it was found that higher solids circulation rate leads to better performance of the system (Adánez et al., 2011). For gaseous fuels the determining factor is to have oxygen available to fully oxidize the fuel, whereas for solid fuels more factors come into consideration. The fact that there must be enough residence time for char combustion determines this resulting trend for solid fuels in this facility. Therefore, the negative effect of the solids circulation rate on the char conversion was due to the decrease in the residence time of solids in the fuel-reactor.

Both char and oxygen-carrier conversions were plotted in Fig. 9 against mean residence time in the fuel-reactor. Obviously, the greater is the residence time in the fuel-reactor, which is inversely



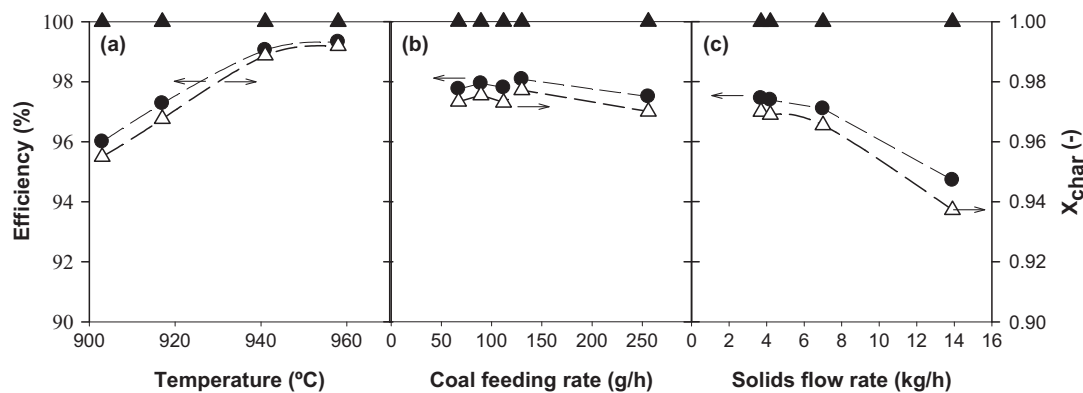


Fig. 8. Carbon capture efficiency (●), char conversion (Δ) and combustion efficiency (▲) at different (a) fuel-reactor temperatures, (b) coal feeding rates, and (c) solids circulation flow rate.

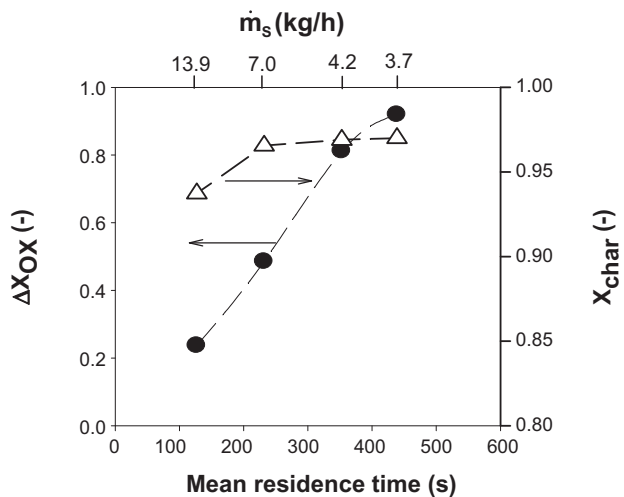


Fig. 9. Variation of the oxygen-carrier conversion (●) and char conversion (Δ) as a function of the mean residence time of solids in the fuel-reactor. Experimental test series CLOU01 and CLOU10–CLOU12.  $T_{FR} = 900^\circ\text{C}$ .

proportional to the solids circulation flow rate, the higher are the oxygen-carrier and char conversion. A residence time above 300 s is needed to get a char conversion about 97% at  $900^\circ\text{C}$  with this coal. Notice that the mean residence time to convert a certain fraction of char will decrease when the fuel-reactor temperature increases. Thus, a char conversion of 99% was obtained of  $960^\circ\text{C}$  with a residence time of 470 s.

## 4. Discussion

### 4.1. Operating temperature in the reactors

The operating temperature in each reactor is a key parameter in the CLOU process, since the oxygen concentration at equilibrium condition is highly dependent on temperature.

When fuel-reactor temperature increases, carbon capture and char conversion also increase. This is due to a faster combustion rate of char at higher temperatures together with a high equilibrium partial pressure of oxygen by oxygen-carrier. Thus, an equilibrium concentration of 1.5 vol%  $\text{O}_2$  can be reached in the fuel-reactor at  $900^\circ\text{C}$  for CuO/Cu<sub>2</sub>O system, whereas the equilibrium concentration increases up to 12.4 vol% at  $1000^\circ\text{C}$ . In addition, the consumption of oxygen by combustion of the fuel improves the decomposition reaction of the metal oxide particles.

In order to optimize the power plant efficiency it is important to keep the outlet partial pressure of  $\text{O}_2$  from the air-reactor as low

as possible while combustion products are only  $\text{CO}_2$  and  $\text{H}_2\text{O}$ . This concentration will depend on the oxygen-carrier reactivity for oxidation reaction and the  $\text{O}_2$  equilibrium concentration with CuO at the actual air-reactor temperature. In the air-reactor, CuO is stable below  $950^\circ\text{C}$  if the maximum oxygen concentration from the air-reactor is 4.5 vol%, whereas will be stable below  $900^\circ\text{C}$  at 1.5 vol%. Thus, the use of  $\text{O}_2$  in air is higher as the temperature is lower. This is the reason for fixing the air-reactor temperature at  $900^\circ\text{C}$  during the experimental work.

It is clear that the air- and fuel-reactor temperatures in the process must be adjusted according with the thermodynamic equilibrium and reaction kinetics in order to optimize the process. In fact, reaction kinetics of CuO decomposition (reaction (5)) could be more relevant than the oxygen concentration at equilibrium conditions in the fuel-reactor.

The high temperature dependency of the oxygen concentration in the CLOU process makes the thermal integration between fuel-reactor and air-reactor a key aspect in the development of the technology. According to the energy balance to the CLOU system, it was thought that to reach the thermal integration in the CLOU system, the fuel-reactor temperature should be higher than air-reactor temperature (Eyring et al., 2011; Mattisson et al., 2009a). As example, Eyring et al. (2011) showed a design of a CLOU system where the air-reactor was at  $850^\circ\text{C}$  and the fuel-reactor was at  $950^\circ\text{C}$ . Thus, high temperatures, near  $950^\circ\text{C}$ , in the fuel-reactor allow a better combustion and an increase in the carbon capture efficiency, because there is more oxygen to burn the fuel. A lower temperature in the air-reactor allows a high oxidation reaction rate. This is due to the oxidation reaction rate is carried out with the driving force of the difference between the inlet oxygen concentration (21 vol% in this case) and the oxygen concentration at equilibrium (1.5 vol% at  $900^\circ\text{C}$ ). Nevertheless, in this work it has been shown that it is possible to work with both fuel- and air-reactors, at the same temperature ( $900^\circ\text{C}$ ), keeping fuel combustion in the CLOU system. Even uncoupling behaviour was demonstrated to work at fuel-reactor temperature lower than air-reactor temperature (Adánez-Rubio et al., submitted for publication-a). This fact permits to increase the degree of freedom in the design of a CLOU system. For example, the required energy extraction from the air- and fuel-reactors can be fitted to obtain desired temperatures in both reactors (Eyring et al., 2011).

### 4.2. Performance of the CLOU system

From results showed in this work during CLOU operation, char conversions from 96 to 99% were obtained in the fuel-reactor with losses from 4 to 1% of carbon in the air-reactor as  $\text{CO}_2$ . No un-burnt gases were observed, being the combustion efficiency

in the fuel-reactor 100% using Cu60MgAl as oxygen-carrier. In all CLOU tests, coal was fully converted either or in the fuel-reactor or in the air-reactor. A carbon capture of 97.5% was reached using an oxygen-carrier inventory in the fuel-reactor of  $\approx 235 \text{ kg/MW}_{\text{th}}$ . Likely, a lower inventory of solids could be used in the plant reaching also full conversion of fuel to  $\text{CO}_2$  and  $\text{H}_2\text{O}$ . However, at the highest coal load, the gases generated during combustion in the fuel-reactor caused an increase in the gas velocity (3–4 times the inlet velocity), which was responsible of particle elutriation from the bed. To make possible to operate at high velocity a design of the fuel-reactor as a circulating fluidized bed itself can be used.

Some gas phase oxygen was present together with the  $\text{CO}_2$  stream, which should be treated in a similar way that in the exhaust gases in an oxyfuel system. It should be desirable to get low concentration of oxygen from the fuel-reactor in order to obtain a high purity  $\text{CO}_2$  stream. It must be considered in the CLOU process that two different reactions take place in the fuel-reactor, namely the reaction rate of oxygen release by the oxygen-carrier and the combustion rate of the fuel, and the relation between must be considered. Thus, the CLOU system must be designed having enough amount of oxygen-carrier to release oxygen to burn the fuel, and high enough amount of solid fuel to avoid an excess of oxygen in the outlet stream from the fuel-reactor. The optimum oxygen concentration in the fuel-reactor will be a compromise between the  $\text{O}_2$  generation by the oxygen-carrier and the oxygen consumption by the fuel. Thus, it has been showed in this work that increasing the coal feeding the oxygen concentration approach to zero, while the good performance of the system is not modified. This situation can be beneficial in order to obtain a  $\text{CO}_2$  stream with low oxygen concentration.

A comparison between the CLOU process and the CLC with coal using Fe-based oxygen-carrier can be done. In the CLC with coal, char is gasified by steam and/or  $\text{CO}_2$  in the fuel-reactor. Cuadrat et al. (2011) showed that in the same ICB-CSIC-s1 facility a char conversion of 80% and a combustion efficiency of 96% were obtained with ilmenite inventory of about  $1800 \text{ kg/MW}_{\text{th}}$  at temperature of  $950^\circ\text{C}$ . The fuel was the same Colombian coal, but ilmenite does not have oxygen uncoupling properties. So, the char was converted by steam gasification in the fuel-reactor. An oxygen polishing step has been proposed (Berguerand and Lyngfelt, 2008, 2009) to convert the un-burnt gases in the fuel-reactor outlet stream, which demands from 5 to 10% of total oxygen required for coal combustion.

Rates of char conversion per unit of carbon mass in char can be used to carry out a comparison between both CLC options with solid fuels. The fractional conversion rate of the char,  $(-r_C)$ , depends on the char conversion in the fuel-reactor and the mean residence time of char particles in this reactor,  $\tau_{\text{char}}$ . The rate of char conversion was calculated as follow:

$$(-r_C) = \frac{X_{\text{char}}}{\tau_{\text{char}}} \quad (25)$$

$\tau_{\text{char}}$  is related with the mean residence time of solids in the fuel-reactor with the following equation:

$$\tau_{\text{char}} = \tau_{\text{FR}} \cdot (1 - X_{\text{char}}) \quad (26)$$

The flow of carbon exiting from the fuel-reactor is equal to carbon entering to air-reactor, which is emitted as  $\text{CO}_2$  in the air-reactor.

Fig. 10 shows the fractional conversion rate of the char calculated with this simplified model as a function of the fuel-reactor temperature with CLOU process. As expected, it can be seen that char conversion rate increases with temperature. Char conversion rates are 60 times faster than those obtained by Cuadrat et al. (2011) using ilmenite for chemical-looping combustion of coal were found. Experiments carried out at  $900^\circ\text{C}$  showed that the char conversion

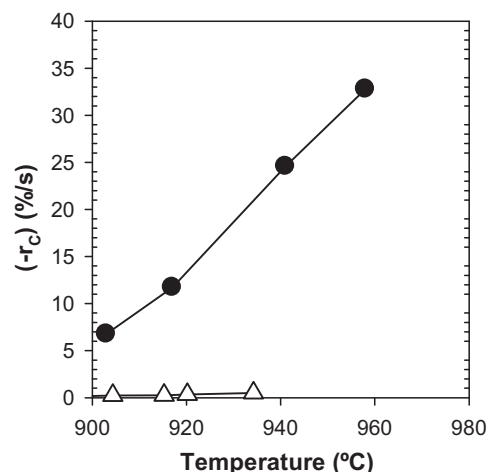


Fig. 10. Fractional conversion rate of char for Cu60MgAl (●) and ilmenite (△) as a function of fuel-reactor temperature. Data obtained with ilmenite taken from (Cuadrat et al., 2011).

rate remained constant with increasing mean residence times of the char in the fuel-reactor.

The main reason for this important difference in the carbon capture performance between CLC with coal and CLOU is the different way which char is converted. In CLC with coal, char is converted through gasification by  $\text{H}_2\text{O}$  and/or  $\text{CO}_2$  which is slower than combustion with  $\text{O}_2$  happening in the CLOU process. As the char conversion is fast for the CLOU process, the carbon capture efficiency was high with the Colombia “El Cerrejón” coal: above 97% in all cases, and reached 99% at the higher temperature tested ( $960^\circ\text{C}$ ). Nevertheless, values somewhat lower could be obtained if less reactive coals were used as fuel. If required, a system to separate chars from oxygen-carrier particles in the exiting stream of solids from the fuel-reactor could be used, e.g. a carbon stripper. Nevertheless, the amount of unconverted char recovered by the carbon stripper in the CLOU will be always lower than in CLC with coal.

The combustion efficiency in CLOU and CLC process could be influenced by the differences in contact between the volatiles evolved from the solid fuel and the oxygen in the form of gaseous  $\text{O}_2$  in CLOU or metal oxide in CLC. Thus, volatiles must diffuse to emulsion phase to react with the oxygen-carrier in the CLC with solids fuels. In this case, the gas–solid contact efficiency is low. On the contrary, in the CLOU process, gaseous oxygen is evolved in emulsion, and must mix with volatiles as in common fluidized bed combustion. It seems that this process is more effective oxidizing volatile compounds.

In short, very good behaviour during coal combustion has been showed by the CLOU process. Carbon capture efficiency can be close to 100% and full combustion of fuel to  $\text{CO}_2$  and  $\text{H}_2\text{O}$  was obtained, which avoids the need of an oxygen polishing step downstream.

## 5. Conclusions

Coal Combustion in a continuous  $1.5 \text{ kW}_{\text{th}}$  CLOU unit system was carried out during 18 h with combustion of coal and 30 h of hot fluidization operation, using an oxygen-carrier prepared by spray drying with 60 wt.% of  $\text{CuO}$  and  $\text{MgAl}_2\text{O}_4$  as inert. The effect of operating conditions – such as temperature of the fuel-reactor, solids circulation rate and the coal feeding rate – on the carbon capture efficiency, and the combustion efficiency were investigated.

It was stated that no special measures must be taken because the complete combustion of fuel and high carbon capture efficiency measured. In all cases, unburnt compounds were not present in the

fuel-reactor outlet, being CO<sub>2</sub> and H<sub>2</sub>O the only products of combustion even if the oxygen-carrier particles were highly converted. Thus, the CLOU process should not require special measures such as an oxygen polishing step. In all cases, oxygen was found together with CO<sub>2</sub> in the gaseous stream from the fuel-reactor. The oxygen concentration from the fuel-reactor increased with the temperature of the fuel-reactor. At higher fuel-reactor temperatures, the capability of Cu<sub>60</sub>MgAl particles to release oxygen is enhanced by increases in the temperature of the fuel-reactor because the increase of the oxygen concentration at equilibrium conditions. To decrease the fraction of O<sub>2</sub> in the CO<sub>2</sub> stream the solid inventory must be optimized. The carbon capture efficiency depended of the fuel-reactor temperature ranging from 97% at 900 °C to 99.3% at 960 °C. Fast conversion of char was evidenced and increased with temperature. The rate of char conversion was as high as 33%/s at 960 °C.

Not significant effect on the CO<sub>2</sub> capture efficiency was observed varying the carbon feeding rate, which affects the calculated solid inventory. Even, at the lowest solids inventory in the fuel-reactor (240 kg/MW<sub>th</sub>) full combustion of coal was observed. The maximum capability of the oxygen-carrier to produce oxygen was not reached during operation. Therefore, lower solid inventories would be needed to obtain full conversion of fuel.

An increase of solid circulation rate produced a decrease in the mean residence time of solids in the fuel-reactor, which slightly decreased the char conversion and the efficiency of carbon capture. A residence time above 300 s is needed to get a char conversion of about 97% at 900 °C with this coal.

The results obtained in this work demonstrated the proof of the concept of CLOU process for coal combustion using a Cu-based oxygen-carrier and important conclusions for the scale-up of the CLOU process were obtained.

## Acknowledgements

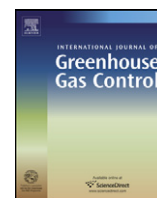
This work was partially supported by the European Commission, under the RFCS program (ECLAIR Project, Contract RFCP-CT-2008-0008), ALSTOM Power Boilers (France) and by the Spanish Ministry of Science and Innovation (Project ENE2010-19550). I. Adánez-Rubio thanks CSIC for the JAE fellowship.

## References

- Adánez, J., Gayán, P., Celaya, J., de Diego, L.F., García-Labiano, F., Abad, A., 2006. Chemical looping combustion in a 10 kW<sub>th</sub> prototype using a CuO/Al<sub>2</sub>O<sub>3</sub> oxygen carrier: effect of operating conditions on methane combustion. *Ind. Eng. Chem. Res.* 45 (17), 75–80.
- Adánez, J., Abad, A., García-Labiano, F., Gayán, P., de Diego, L.F., 2011. Progress in chemical-looping combustion and reforming technologies: a review. *Prog. Eng. Comb. Sci.*, doi:10.1016/j.peccs.2011.09.001.
- Adánez-Rubio, I., Gayán, P., García-Labiano, F., de Diego, L.F., Adánez, J., Abad, A., 2011. Development of CuO-based oxygen carrier materials suitable for chemical-looping with oxygen uncoupling (CLOU). *Energy Procedia* 4, 417–424.
- Adánez-Rubio, I., Gayan, P., Abad, A., de Diego, L.F., Garcia-Labiano, F., Adanez, J. Evaluation of a spray dried CuO/MgAl<sub>2</sub>O<sub>4</sub> oxygen-carrier for CLOU, submitted for publication-a.
- Adánez-Rubio, I., Abad, A., Gayán, P., de Diego, L.F., García-Labiano, F., Adánez, J. Identification of operational regions in the chemical-looping with oxygen uncoupling (CLOU) process with a Cu-based oxygen-carrier, submitted for publication-b.
- Azimi, G., Leion, H., Mattisson, T., Lyngfelt, A., 2011. Chemical-looping with oxygen uncoupling using combined Mn–Fe oxides, testing in batch fluidized bed. *Energy Procedia* 4, 370–377.
- Bergerand, N., Lyngfelt, A., 2008. Design and operation of a 10 kW<sub>th</sub> chemical-looping combustor for solid fuels—testing with South African coal. *Fuel* 87, 2713–2726.
- Bergerand, N., Lyngfelt, A., 2009. Chemical-looping combustion of petroleum coke using ilmenite in a 10 kW<sub>th</sub> unit-high-temperature operation. *Energy Fuels* 23, 57–68.
- Cao, Y., Pan, W.P., 2006. Investigation of chemical looping combustion by solid fuels. 1. Process analysis. *Energy Fuels* 20, 57–68.
- Cuadrat, A., Abad, A., Adánez, J., de Diego, L.F., García-Labiano, F., Gayan, P., 2011. CO<sub>2</sub> capture by chemical-looping coal combustion using Ilmenite as oxygen carrier in a 500W<sub>th</sub> unit. In: Proceedings of the 5th International Conference on Clean Coal Technologies (CCT2011), Zaragoza, Spain.
- de Diego, L.F., Gayán, P., García-Labiano, F., Celaya, J., Abad, A., Adánez, J., 2005. Impregnated CuO/Al<sub>2</sub>O<sub>3</sub> oxygen carriers for chemical-looping combustion: avoiding fluidizing bed agglomeration. *Energy Fuels* 19, 1850–1856.
- Eyring, E., Konya, G., Lighty, J., Sahir, A., Sarofim, A., Whitty, K., 2011. Chemical looping with copper oxide as carrier and coal as fuel. *Oil Gas Sci. Technol.—Rev. IFP Nouvelles Technologies* 2, 209–221.
- Gayán, P., Adánez-Rubio, I., Abad, A., de Diego, L.F., García-Labiano, F., Adánez, J. Development of CuO-based oxygen-carrier materials suitable for chemical-looping with oxygen uncoupling (CLOU) process, submitted for publication.
- HSC Chemistry 6.1® 2008. Chemical Reaction and Equilibrium Software with Thermochemical Database and Simulation Module. Outotec Research Oy.
- IPCC, 2005. IPCC special report on carbon dioxide capture and storage. In: Metz, B., Davidson, O., de Coninck, H.C., Loos, M., Meyer, L.A. (Eds.), Working Group III of the Intergovernmental Panel on Climate Change. Cambridge University.
- Kerr, H.R., 2005. Capture and Separation Technology Gaps and Priority Research Needs. Carbon Dioxide Capture for Storage in Deep Geologic Formations. Elsevier Science, Amsterdam, pp. 655–660.
- Kolbitsch, P., Bolhär-Nordenkamp, J., Pröll, T., Hofbauer, H., 2009. Comparison of two Ni-based oxygen carriers for chemical looping combustion of natural gas in 140 kW continuous looping operation. *Ind. Eng. Chem. Res.* 48 (11), 42–47.
- Kvamsdal, H.M., Jordal, K., Bolland, O., 2007. A quantitative comparison of gas turbine cycles with CO<sub>2</sub> capture. *Energy* 32 (1), 10–24.
- Leion, H., Mattisson, T., Lyngfelt, A., 2007. The use of petroleum coke as fuel in chemical-looping combustion. *Fuel* 86, 1947–1958.
- Leion, H., Lyngfelt, A., Johansson, M., Jerndal, E., Mattisson, T., 2008. The use of ilmenite as an oxygen carrier in chemical-looping combustion. *Chem. Eng. Res. Des.* 86, 1017–1026.
- Leion, H., Mattisson, T., Lyngfelt, A., 2009a. Use of ores and industrial products as oxygen carriers in chemical-looping combustion. *Energy Fuels* 23, 2307–2315.
- Leion, H., Mattisson, T., Lyngfelt, A., 2009b. Using chemical-looping with oxygen uncoupling (CLOU) for combustion of six different solid fuels. *Energy Procedia* 1, 447–453.
- Leion, H., Larring, Y., Bakken, E., Bredesen, R., Mattisson, T., Lyngfelt, A., 2009c. Use of CaMn<sub>0.875</sub>Ti<sub>0.125</sub>O<sub>3</sub> as oxygen carrier in chemical looping with oxygen uncoupling. *Energy Fuels* 23, 5276–5283.
- Lewis, W.K., Gilliland, E.R., 1954. Production of pure carbon dioxide. Patent 2,665,972.
- Linderholm, C., Mattisson, T., Lyngfelt, A., 2009. Long-term integrity testing of spray-dried particles in a 10 kW chemical-looping combustor using natural gas as fuel. *Fuel* 88, 2083–2096.
- Lyngfelt, A., Thunman, H., 2005. Construction and 100 h of operational experience of a 10-kW chemical-looping combustor. In: Thomas, D.C., Benson, S.M. (Eds.), Carbon Dioxide Capture for Storage in Deep Geologic Formations—Results from the CO<sub>2</sub> Capture Project, vol. 1. Elsevier, Oxford, UK, Chapter 36.
- Mattisson, T., Lyngfelt, A., Leion, H., 2009a. Chemical-looping oxygen uncoupling for combustion of solid fuels. *Int. J. Greenhouse Gas Control* 3, 11–19.
- Mattisson, T., Leion, H., Lyngfelt, A., 2009b. Chemical-looping with oxygen uncoupling using CuO/ZrO<sub>2</sub> with petroleum coke. *Fuel* 88, 683–690.
- Moghtaderi, B., 2010. Application of chemical looping concept for air separation at high temperatures. *Energy Fuels* 24, 190–198.
- Pis, J.J., Centeno, T.A., Mahamund, M., Fuertes, A.B., Parra, J.B., Pajares, J.A., Bansal, R.C., 1996. Preparation of active carbons from coal part I. Oxidation of coal. *Fuel Process. Technol.* 47, 19–38.
- Pröll, T., Mayer, K., Bolhär-Nordenkamp, J., Kolbitsch, P., Mattisson, T., Lyngfelt, A., Hofbauer, H., 2009. Natural minerals as oxygen carriers for chemical looping combustion in a dual circulating fluidized bed system. *Energy Procedia* 1, 27–34.
- Rydén, M., Lyngfelt, A., Mattisson, T., 2011a. CaMn<sub>0.875</sub>Ti<sub>0.125</sub>O<sub>3</sub> as oxygen carrier for chemical oxygen combustion with oxygen uncoupling (CLOU)—experiments in a continuously operating fluidized-bed reactor system. *Int. J. Greenhouse Gas Control* 5, 356–366.
- Rydén, M., Lyngfelt, A., Mattisson, T., 2011b. Combined manganese/iron oxides as oxygen carrier for chemical-looping combustion with oxygen uncoupling (CLOU) in a circulating fluidized bed reactor system. *Energy Procedia* 4, 341–348.
- Shen, L., Wu, J., Xiao, J., Song, Q., Xiao, R., 2009. Chemical-looping combustion of biomass in a 10 kW reactor with iron oxide as an oxygen carrier. *Energy Fuels* 23, 2498–2505.
- Shulman, A., Cleverstam, E., Mattisson, T., Lyngfelt, A., 2009. Manganese/iron, manganese/nickel, and manganese/silicon oxides used in chemical looping with oxygen uncoupling (CLOU) for combustion of methane. *Energy Fuels* 23, 5269–5275.
- Shulman, A., Cleverstam, E., Mattisson, T., Lyngfelt, A., 2011. Chemical-looping with oxygen uncoupling using Mn/Mg-based oxygen-carriers—oxygen release and reactivity with methane. *Fuel* 90, 941–950.
- Simell, P., Stahlberg, P., Kurkela, E., Albrecht, J., Deutch, S., Sjöström, K., 2000. Provisional protocol for the sampling and analysis of tar and particles in the gas from large-scale biomass gasifiers. *Biomass Bioenergy* 18, 19–38.
- Wang, J., Anthony, E.J., 2008. Clean combustion of solid fuels. *Appl. Energy* 85, 73–79.

## **Paper VI**





## Performance of CLOU process in the combustion of different types of coal with CO<sub>2</sub> capture

I. Adánez-Rubio, A. Abad\*, P. Gayán, L.F. de Diego, F. García-Labiano, J. Adánez

*Instituto de Carboquímica (ICB-CSIC), Miguel Luesma Castán 4, 50018 Zaragoza, Spain*

### ARTICLE INFO

#### Article history:

Received 14 May 2012

Received in revised form

16 November 2012

Accepted 24 November 2012

Available online 31 December 2012

#### Keywords:

Carbon capture

Combustion

Coal

CLOU

Copper

Chemical-looping

### ABSTRACT

Chemical-looping with oxygen uncoupling (CLOU) process is a chemical-looping combustion (CLC) technology that allows the combustion of solid fuels using oxygen carriers with inherent CO<sub>2</sub> separation. The oxygen necessary for the fuel combustion is supplied by a solid oxygen carrier, which contains a metal oxide. The oxygen carrier circulates between two interconnected fluidized reactors: the fuel and the air reactor. In the CLOU process, the oxygen carrier releases gaseous oxygen in the fuel reactor which burns coal as in common combustion with air, so the CO<sub>2</sub> generated is undiluted with N<sub>2</sub>. The reduced oxygen carrier is oxidized by air to the initial metal oxide in the air reactor, then being ready to start a new cycle. The aim of this work is to study the performance of the CLOU process using coals of different rank. Experiments were carried out in a continuously operated 1.5 kW<sub>th</sub> unit. Particles prepared by spray drying containing 60 wt% CuO were used as oxygen carrier. Four coals of different rank (anthracite, low volatile bituminous, medium volatile bituminous and lignite) were used as fuel. Besides, the temperature in the fuel reactor was varied between 900 and 950 °C. In all the experiments there was complete combustion of the coal to CO<sub>2</sub> and H<sub>2</sub>O, without any unburnt product. The carbon capture efficiency greatly depends on the coal rank and fuel reactor temperature. High carbon capture efficiencies were obtained for lignite and medium volatile bituminous coals. The maximum capture efficiency was 99.3% at 950 °C with lignite. The analysis of the experimental results was used to evaluate the effect of the coal rank in a CLOU system when a carbon separation system is included. At 925 °C, the solid inventory needed to reach 95% of CO<sub>2</sub> capture efficiency with a carbon separation system of 90% of efficiency is 45 kg/MW<sub>th</sub> using lignite, 85 kg/MW<sub>th</sub> using MV bituminous, 140 kg/MW<sub>th</sub> using LV bituminous and 490 kg/MW<sub>th</sub> using anthracite. It must be pointed out the low solid inventories needed in the CLOU process for the different coal rank analyzed in this work.

© 2012 Elsevier Ltd. All rights reserved.

### 1. Introduction

According to the IPCC report on mitigation of climate change (IPCC, 2005), in order to stabilize CO<sub>2</sub> concentration in the atmosphere carbon capture and storage (CCS) would contribute with 15–55% to the cumulative mitigation effort worldwide until 2100. CCS is a process involving the separation of CO<sub>2</sub> emitted by industry and energy-related sources, and its storage for isolation from the atmosphere over a long term. chemical-looping combustion process (CLC) has been suggested among the best alternatives to reduce the economic cost of CO<sub>2</sub> capture (Kerr, 2005) and to reduce energy penalty compared with other CO<sub>2</sub> capture process (Kvamsdal et al., 2007). In this process, CO<sub>2</sub> is inherently separated from other combustion products, N<sub>2</sub> and unused O<sub>2</sub>, through the use of a solid

oxygen carrier. Thus no energy is expended for the CO<sub>2</sub> separation. The CLC process has been demonstrated for combustion of gaseous fuels such as natural gas or syngas in 10–140 kW<sub>th</sub> units using oxygen carrier materials based on Ni (Linderholm et al., 2009; Kolbitsch et al., 2009; Ryu et al., 2010), Cu (Adánez et al., 2006) and Fe (Pröll et al., 2009). All these oxygen carriers have been reviewed by Adánez et al. (2012).

However, for energy generation is highly relevant the direct use of solid fuels in the CLC concept because solid fuels are considerably more abundant and less expensive than natural gas. In the chemical-looping combustion with solid fuels, the fuel is physically mixed with the oxygen carrier in the fuel reactor. The in situ gasification of the solid fuel, e.g. coal, biomass or solid wastes, has been proposed using steam or CO<sub>2</sub> as gasification agent (Cao and Pan, 2006; Scott et al., 2006). This process has been demonstrated in units of 10 kW<sub>th</sub> with coal or biomass (Berguerand and Lyngfelt, 2008; Shen et al., 2009). The limitation in the solid fuel conversion in the CLC with solid fuels comes from the slow gasification process

\* Corresponding author.

E-mail address: [abad@icb.csic.es](mailto:abad@icb.csic.es) (A. Abad).

## Nomenclature

### Symbols

$F_i$	molar flow of compound $i$ (mol/s)
$f_c$	mass fraction of carbon in coal
$f_{C,fix}$	mass fraction of fix carbon in coal
$f_{C,vol}$	mass fraction of carbon in volatiles
$f_i$	mass fraction in coal of element or compound $i$
$M_i$	atomic or molecular weigh of $i$ elements or compound (kg/mol)
$m$	mass of the sample at each time in TGA (kg)
$m_0$	initial mass of char in TGA (kg)
$m_{ash}$	mass of ash remaining after full combustion in TGA (kg)
$\dot{m}_{coal}$	mass-based flow of coal fed-in to the fuel reactor (kg/s)
$\dot{m}_{OC}$	solids circulation rate (kg/s)
$m_{ox}$	mass of the oxygen carrier sample fully oxidized (kg)
$m_{red}$	mass of the oxygen carrier sample fully reduced (kg)
$m_{s,FR}$	mass of solids in the fuel reactor (kg)
$R_{OC}$	oxygen transport capability
$(-r_C)$	fractional conversion rate of the char ( $s^{-1}$ )
$\tau_{char}$	mean residence time of char particles in the fuel reactor (s)
$\tau_{FR}$	mean residence time of solids in the fuel reactor (s)
$X_{char}$	char conversion
$Y_{i,outFR}$	molar fraction of the gas $i$ exiting from the fuel reactor
$Y_{i,outAR}$	molar fraction of the gas $i$ exiting from the air reactor

### Greek letters

$\eta_{CC}$	carbon capture efficiency
$\eta_{comb,FR}$	combustion efficiency in the fuel reactor
$\eta_{CSS}$	efficiency of the carbon separation system
$\lambda$	air excess ratio
$\phi$	oxygen carrier to fuel ratio
$\Omega_{coal}$	stoichiometric mass of $O_2$ to convert 1 kg of coal (kg/kg)

### Subscripts

AR	air reactor
BET	Brunauer–Emmett–Teller
CLC	chemical-looping combustion
CLOU	chemical-looping with oxygen uncoupling
FR	fuel reactor
inAR	inlet stream from air reactor
inFR	inlet stream from fuel reactor
IPCC	Intergovernmental Panel on Climate Change
outAR	outlet stream from air reactor
outFR	outlet stream from fuel reactor
OC	oxygen carrier
TGA	thermogravimetric analyzer
XRD	X-ray diffractometer

(Berguerand and Lyngfelt, 2008; Cuadrat et al., 2012a). To increase the gasification rate, temperatures higher than 1000 °C has been proposed (Berguerand and Lyngfelt, 2009).

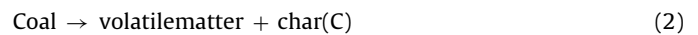
To overcome the low reactivity of the char gasification step in the direct solid fuelled chemical-looping combustion, an alternative process, chemical-looping with oxygen uncoupling (CLOU), was recently proposed by Mattisson et al. (2009a). They made use of the idea first proposed by Lewis and Gilliland (1954) to produce  $CO_2$  from solid carbonaceous fuels by using gaseous oxygen produced by the decomposition of CuO. chemical-looping with oxygen

uncoupling (CLOU) process is based on the strategy of using oxygen carrier materials which release gaseous oxygen and thereby allowing the solid fuel to burn with gas phase oxygen. These materials can be also regenerated at high temperatures.

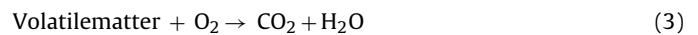
Fig. 1 shows a schematic diagram of a CLOU system. In the fuel reactor the fuel conversion is produced by different reactions. First the oxygen carrier releases oxygen according to:



and the solid fuel begins to devolatilize producing a carbonaceous solid residue (char, mainly composed by carbon and ash) and volatile matter as gas product:



Then, volatiles and char are burnt as in usual combustion with gaseous oxygen according to reactions (3) and (4):



After steam condensation, a pure  $CO_2$  stream can be obtained from the fuel reactor. The reduced oxygen carrier is transported to the air reactor, where the oxygen carrier is regenerated to the initial oxidation stage with the oxygen of the air, and being ready for a new cycle. Ideally, the exit stream of the air reactor contains only  $N_2$  and unreacted  $O_2$ . The heat release over the fuel and air reactors is the same as for conventional combustion. Therefore CLOU process has a low energy penalty for  $CO_2$  separation and low  $CO_2$  capture costs are expected.

In the CLOU process, the slow gasification step on the direct solid fuel CLC is avoided, giving a much faster solid conversion (Mattisson et al., 2009b; Eyring et al., 2011; Abad et al., 2012). It was found that the conversion rate of the solid fuel was increased by a factor of 45 for petroleum coke (Mattisson et al., 2009a) or by 60 for a bituminous coal (Abad et al., 2012) at CLOU conditions oxygen carriers in comparison to those measured with oxygen carrier which do not have oxygen uncoupling properties. Moreover, the combustion of the fuel consumes the oxygen generated by the oxygen carrier and improves the decomposition reaction of the metal oxide particles (Adáñez-Rubio et al., 2012a). As consequence, a solids inventory in the fuel reactor between 120 and 200 kg/MW<sub>th</sub> were estimated for CLOU process (Mattisson et al., 2009a; Eyring et al., 2011). A minimum solids inventory was estimated by Adáñez-Rubio et al. (2012a) as low as 50 kg/MW<sub>th</sub>. These solids inventories are much lower than the ones required in a CLC system with solid fuels, 2000 kg/MW<sub>th</sub> for Fe-based particles (Leion et al., 2007; Cuadrat et al., 2012b, c).

Thus, a special requirement is needed for the oxygen carrier to be used in the CLOU process in comparison to oxygen carriers for normal CLC, where the fuel reacts directly with the solid oxygen carrier without any release of gas phase oxygen. Only those metal oxides that have a suitable equilibrium partial pressure of oxygen at temperatures of interest for combustion (800–1200 °C) can be used as oxygen carrier materials in the CLOU process. Besides, this  $O_2$  release must be reversible in order to oxidize the oxygen carrier in the air reactor and regenerate the material. CuO/Cu<sub>2</sub>O, Mn<sub>2</sub>O<sub>3</sub>/Mn<sub>3</sub>O<sub>4</sub>, and Co<sub>3</sub>O<sub>4</sub>/CoO have been identified as redox pairs with capacity to evolve oxygen at high temperature (Mattisson et al., 2009a). Up to date, there are only a small number of works in the literature for CLOU process dealing with the use of Cu- and Mn-based materials.

Regarding the use of manganese oxides for CLOU process, several Mn-based particles supported on Fe<sub>2</sub>O<sub>3</sub>, NiO, SiO<sub>2</sub> or MgO and a perovskite type material (CaMn<sub>x</sub>Ti<sub>1-x</sub>O<sub>3</sub>) have been tested in a batch fluidized bed at Chalmers University of Technology (Azimi et al., 2011; Leion et al., 2009a; Shulman et al., 2009, 2011). Good

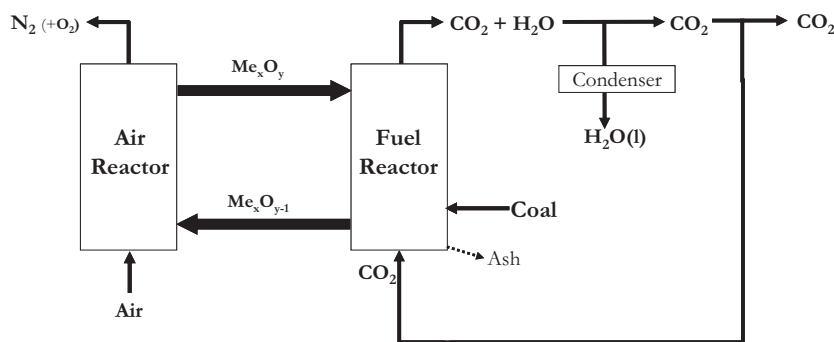


Fig. 1. Schematic layout of the CLOU system.

oxygen uncoupling and mechanical properties, as well as high reactivity with methane were showed for a Mn/Fe material and perovskite type material. These two promising materials were further tested in a continuous facility with methane as fuel (Rydén et al., 2011a, b).

In general, Cu-based materials have faster release of oxygen than Mn-based particles (Leion et al., 2009a). Preliminary experiments in a batch fluidized-bed reactor were conducted using Cu-based materials with  $\text{Al}_2\text{O}_3$  or  $\text{ZrO}_2$  as supporting materials (Leion et al., 2009b; Mattisson et al., 2009a, b), and a high fractional conversion rate of char was found for several carbonaceous materials, including petcoke, coal or biomass. However, they found some defluidization phenomena with Cu-based particles during some parts of the experiments.

In the research group of ICB-CSIC, a screening study considering 25 different Cu-based oxygen carriers was done to select appropriate materials for CLOU process (Adánez-Rubio et al., 2011; Gayán et al., 2012). Particles prepared by different methods and using several CuO contents and supporting materials were tested. Reactivity of materials was analyzed in a TGA, whereas mechanical stability and fluidization properties were studied in a batch fluidized bed. Two promising Cu-based oxygen carriers prepared by pelletizing by pressure (60 wt% CuO supported on  $\text{MgAl}_2\text{O}_4$ , and 40 wt% CuO supported on  $\text{ZrO}_2$ ) were selected according to their high reactivity, low attrition rate and avoidance of agglomeration during successive redox cycles by alternating nitrogen and air.

After the screening tests, a batch of 60 wt% of CuO supported on  $\text{MgAl}_2\text{O}_4$  was prepared by spray drying. The proof of the concept of the CLOU process was demonstrated using this material as oxygen carrier (Abad et al., 2012) burning a bituminous coal in a 1.5 kW<sub>th</sub> continuously operated unit consisting of two interconnected fluidized-bed reactors. The effects of fuel reactor temperature, coal feeding rate, and solids circulation flow rate on the combustion, and CO<sub>2</sub> capture efficiencies were investigated. Fast oxygen generation rate by the oxygen carrier and full combustion of coal was attained in the plant using a solids inventory in the fuel reactor of 235 kg/MW<sub>th</sub>. In conjunction, values close to 100% in carbon capture efficiency were obtained at 960 °C. An analysis about the evolution of physical and chemical characteristics of this oxygen carrier with the operational time is summarized in a previous work (Adánez-Rubio et al., 2012b).

Leion et al. (2009b) using six different solid fuels showed that the differences in reactivity between solid fuels were more pronounced in chemical-looping combustion than in CLOU process. This fact was explained by the difference in the reaction paths between both processes. In CLC, the limiting reaction is the slow gasification of the fuel, whereas in CLOU the release of oxygen from the oxygen carrier particle becomes rate limiting.

The aim of this work was to investigate the performance of the CLOU process for different type of coals ranging from lignite to

anthracite. The effect of the coal rank and the fuel reactor temperature on the combustion efficiency and carbon capture efficiency was investigated in a continuously operated CLOU unit. The results obtained are analyzed and discussed in order to be useful for the scale-up of a CLOU process fuelled with coal.

## 2. Experimental

### 2.1. The Cu-based oxygen carrier

The oxygen carrier was a Cu-based material prepared by spray drying. Oxygen carrier particles were manufactured by VITO (Flemish Institute for Technological Research, Belgium) using  $\text{MgAl}_2\text{O}_4$  spinel (Baikowski, S30CR) and CuO (Panreac, PRS) as raw materials. The CuO content was 60 wt%. The particles were calcined 24 h at 1100 °C. The particle size of the oxygen carrier was +0.1 to 0.2 mm. From now on, the oxygen carrier was named as Cu60MgAl. Table 1 shows the main properties of this material.

Physical and chemical characterization was carried out with these particles. The copper content was determined by complete reduction in TGA using 15 vol.% H<sub>2</sub> at 850 °C. The oxygen transport capability,  $R_{OC}$ , was calculated in TGA in nitrogen atmosphere as  $R_{OC} = (m_{ox} - m_{red})/m_{ox}$ , being  $m_{ox}$  the mass of fully oxidized particles and  $m_{red}$  in the reduced form, i.e. when all CuO has been reduced to Cu<sub>2</sub>O. The crushing strength was determined by measuring the force needed to fracture a particle using a Shimpo FGN-5X crushing strength apparatus. The crushing strength was taken as the average value of at least 20 measurements. The skeletal density, i.e. the density of solids excluding the pores, was determined by He picnometry in a Micromeritics AccuPyc II 1340. The surface area of the oxygen carrier was determined by the Brunauer–Emmett–Teller (BET) method by adsorption/desorption of nitrogen at 77 K in a Micromeritics ASAP-2020 (Micromeritics Instruments Inc.), whereas the pore volumes were measured by Hg intrusion in a Quantachrome PoreMaster 33. The identification of crystalline chemical species was carried out by powder X-ray diffractometer Bruker AXS graphite monochromator.

Preliminary results showed that this material had adequate values of reactivity and oxygen transport capacity in fluidized-bed conditions (Adánez-Rubio et al., 2012a). In tests carried out in a

Table 1  
Properties of the oxygen carrier Cu60MgAl.

CuO content (wt%)	60
Oxygen transport capacity, $R_{OC}$ (wt%)	6
Crushing strength (N)	2.4
Skeletal density (kg/m <sup>3</sup> )	4600
Porosity (%)	16.1
Specific surface area, BET (m <sup>2</sup> /g)	<0.5
XRD main phases	CuO, $\text{MgAl}_2\text{O}_4$



continuous CLOU unit burning coal with this material, high combustion rate with complete combustion to  $\text{CO}_2$  and  $\text{H}_2\text{O}$  were obtained using a low solids inventory in the fuel reactor (Abad et al., 2012).

## 2.2. Coals

Four different coals were used for CLOU experiments with the Cu60AlMg oxygen carrier. A lignite from Teruel basin (Spain), a medium volatile bituminous coal from South Africa, a low volatile bituminous coal from Checkia, and an anthracite from El Bierzo (Spain) were used with the aim to cover a wide range of coals. Main properties of selected coals (proximate and ultimate analysis and LHV) are shown in Table 2. Note the high ash contents of lignite (25.2%) and anthracite (31.6%) coals. The coal particle size used for this study was +0.2 to 0.3 mm with all fuels.

## 2.3. TGA facility

A thermogravimetric analyzer (TGA) was used for the determination of the coal combustion reactivity. A detailed description of the TGA can be found elsewhere (de Diego et al., 2004). The TGA consisted of a quartz tube (24 mm i.d.) placed in a mobile furnace. This furnace has two positions: upper position inside the reaction zone, and a lower position outside the reaction zone. The method developed by Adáñez et al. (2001) was used to obtain the intrinsic reactivity of coal combustion. Char was prepared for each coal in the TGA. For char preparation, 5 mg of the corresponding coal were well mixed in 45 g of silica sand and placed in a wire mesh basket inside the quartz reactor of the TGA at ambient temperature. A  $\text{N}_2$  flow of 25  $\text{L}_\text{N}/\text{h}$  was fed into the reactor. At the same time, the furnace was heated to 900 °C, but in the lower position. When the mass of the sample was stable, a quick heating was carried out using the mobile furnace. A flash devolatilization of coal occurred, in a similar way as in at CLOU unit. Devolatilization was carried out at 900 °C during 30 s. After that, the coal sample was cooled to ambient temperature. The char reactivity was determined at 500 °C in air atmosphere using 25  $\text{L}_\text{N}/\text{h}$ . Experimental conditions were selected to avoid film gas transfer and internal diffusion resistances as much as possible trying to obtain intrinsic reactivities.

## 2.4. ICB-CSIC-s1 unit for the CLOU process

A schematic view of the experimental set-up used is shown in Fig. 2. The set-up was basically composed of two interconnected fluidized-bed reactors – the air and fuel reactors – joined by a loop seal in the lower and a riser for solids transport from the air reactor to the fuel reactor. A cyclone recovers the solid entrained from the riser. A solids valve controls the solids circulation flow rate in the system. The reactors operate at slightly higher than atmospheric pressure, taking into consideration the pressure drops in the beds and pipes to stack. The fuel reactor (1) consisted of a bubbling fluidized bed with 50 mm of inner diameter and 200 mm bed height.  $\text{N}_2$  was used as fluidizing gas.  $\text{N}_2$  instead  $\text{CO}_2$  was used as fluidizing gas in order to improve the accuracy for calculation of carbon burnt in the fuel reactor. In a previous work it was determined that the fluidization agent does not have any influence on the oxygen carrier behaviour (Adáñez-Rubio et al., 2011; Gayán et al., 2012). The gas flow was 186  $\text{L}_\text{N}/\text{h}$ , corresponding to a gas velocity of 0.11 m/s at 900 °C. The minimum fluidizing velocities of the oxygen carrier particles are 0.006 m/s for the smallest particle size and 0.023 m/s for the biggest one while the terminal velocities of particles are 0.40 m/s and 1.45 m/s respectively.

Coal (9) was fed in by a screw feeder (10) at the bottom of the bed just above the fuel reactor distributor plate in order to maximize the time that the fuel and volatile matter are in contact with the

bed material. The screw feeder has two steps: the first one with variable speed to control the coal flow rate, and the second one is water cooled and it has high rotating velocity to avoid coal pyrolysis inside the screw. A small  $\text{N}_2$  flow (24  $\text{L}_\text{N}/\text{h}$ ) is introduced at the beginning of the screw feeder to avoid any possible volatile reverse flow.

The oxygen carrier is decomposed in the fuel reactor, evolving gaseous oxygen to the surroundings. The oxygen burns the volatiles and char proceeding from coal pyrolysis in the fuel reactor. Reduced oxygen carrier particles overflowed into the air reactor through a U-shaped fluidized bed loop seal (2) with 30 mm of inner diameter. A  $\text{N}_2$  flow of 60  $\text{L}_\text{N}/\text{h}$  was introduced in the loop seal. Preliminary experiments were carried out to observe the distribution of gas fed in to the loop seal. In the experimental conditions used in this work, the gas in the loop-seal was distributed approximated at 50% in each reactor (air and fuel reactor).

The oxidation of the carrier took place in the air reactor (3), being a bubbling fluidized bed with 80 mm of inner diameter and 100 mm bed height, and followed by a riser (4) with 30 mm of inner diameter. The air flow was 1740  $\text{L}_\text{N}/\text{h}$  ( $\mu_g = 0.40$  m/s). In addition, a secondary air flow (240  $\text{L}_\text{N}/\text{h}$ ) was introduced at the top of the bubbling bed to help particle entrainment through a riser.  $\text{N}_2$  and unreacted  $\text{O}_2$  left the air reactor passing through a high-efficiency cyclone (5) and a filter before the stack. The oxidized solid particles recovered by the cyclone were sent to a solids reservoir (7), setting the oxygen carrier ready to start a new cycle. The regenerated oxygen carrier particles returned to the fuel reactor by gravity from the solids reservoir through a solids valve (8) which controls the flow rates of solids entering to the fuel reactor. A diverting solids valve (6) located below the cyclone allowed the measurement of the solids flow rates at any time. Therefore, this design allows us to control and to measure the solids circulation flow rate between both reactors. The ash particles from char combustion were not recovered by the cyclone and were collected in a filter down-stream. Thus, ash particles were not accumulated in the system. The ashes recovered in the filter closed the mass balance difference above 80% with regard to the amount of ash fed to the system. Further investigation on oxygen carrier extracted from the diverting valve (6) showed no presence of ash particles, confirming that ashes are not accumulated in the system. Further investigation on oxygen carrier extracted from the CLOU system showed little presence of ash particles. Finally, it is worthy of consideration that leakage of gas between both reactors was avoided by the presence of the U-shaped loop seal (2) and the solids reservoir (7). Thus, the presence of oxygen in the fuel reactor solely came from oxygen released by reaction (1).

The total oxygen carrier inventory in the system was around 2.0 kg, being about 0.5–0.6 kg in the fuel reactor. The amount of solids in the fuel reactor was calculated from pressure drop measurements in the reactor for each test.

$\text{CO}_2$ , CO,  $\text{H}_2$ ,  $\text{CH}_4$ , and  $\text{O}_2$  were continuously analyzed at the outlet stream from fuel reactor, whereas  $\text{CO}_2$ , CO and  $\text{O}_2$  were analyzed from the flue gases of the air reactor. Non-dispersive infrared (NDIR) analyzers (Maihak S710/UNOR) were used for CO,  $\text{CO}_2$ , and  $\text{CH}_4$  concentration determination; a paramagnetic analyzer (Maihak S710/OXOR-P) was used to determine  $\text{O}_2$  concentration; and a thermal conductivity detector (Maihak S710/THERMOR) was used for  $\text{H}_2$  concentration determination. In some selected experiments, the tar amount present in fuel reactor product gas was determined following the tar protocol (Simell et al., 2000), as well as higher  $\text{C}_2$ ,  $\text{C}_3$  and  $\text{C}_4$  hydrocarbons were analyzed off-line by a gas chromatograph (HP5890 Series II).

Because of heat losses, the system is not auto-thermal and it is heated up by means of various independent ovens to get independent temperature control of the air reactor, fuel reactor, and freeboard above the bed in the fuel reactor. During operation,

**Table 2**  
Properties of coals used in this work.

	Anthracite	Low volatile bituminous	Medium volatile bituminous	Lignite
Proximate analysis (wt%)				
Moisture	1.0	2.0	4.2	12.6
Volatile matter	7.5	17.1	25.5	28.6
Fixed carbon	59.9	68.8	55.9	33.6
Ash	31.6	12.1	14.4	25.2
Ultimate analysis (wt%)				
C	60.7	75.8	69.3	45.4
H	2.1	3.7	3.9	2.5
N	0.9	1.9	1.9	0.6
S	1.3	0.4	0.9	5.2
O <sup>a</sup>	2.4	4.1	5.4	8.5
LHV (kJ/kg)	21,900	28,950	25,500	16,250
$\Omega_{\text{coal}}$ (kg O <sub>2</sub> /kg coal)	1.8	2.2	2.0	1.2

<sup>a</sup> Oxygen to balance.

temperatures in the bed and freeboard of the fuel reactor, air reactor bed and riser were monitored as well as the pressure drops in important locations of the system, such as the fuel reactor bed, the air reactor bed and the loop seal. The temperature in the fuel reactor was varied from 900 to 950 °C, whereas the freeboard temperature was 900 °C. The temperature in the air reactor was maintained at 900 °C.

In Table 3, a resume of the operational variables used in this work for all coals is shown. The solids circulation rate was maintained at a mean value of 3–4 kg/h, whereas the coal feeding rate was varied from 0.08 to 0.13 kg/h depending on the coal type. The oxygen carrier to fuel ratio,  $\phi$ , was around 1.0–1.2. The oxygen carrier to fuel ratio was defined as the ratio of the oxygen transported

by the oxygen carrier to the oxygen demanded by coal for complete combustion. A value of  $\phi = 1$  corresponds to the stoichiometric flow of CuO needed to fully convert coal to CO<sub>2</sub> and H<sub>2</sub>O, being CuO reduced to Cu<sub>2</sub>O. Thus,  $\phi$  was calculated with the following equation:

$$\phi = \frac{R_{\text{OC}} \dot{m}_{\text{OC}}}{\Omega_{\text{coal}} \dot{m}_{\text{coal}}} \quad (5)$$

$\dot{m}_{\text{OC}}$  being the solids circulation flow rate in the completely oxidized state and  $\dot{m}_{\text{coal}}$  the mass-based flow of coal fed in to the reactor.  $\Omega_{\text{coal}}$  is the stoichiometric kg of oxygen to convert 1 kg of coal to CO<sub>2</sub> and H<sub>2</sub>O. This value was calculated from the proximate

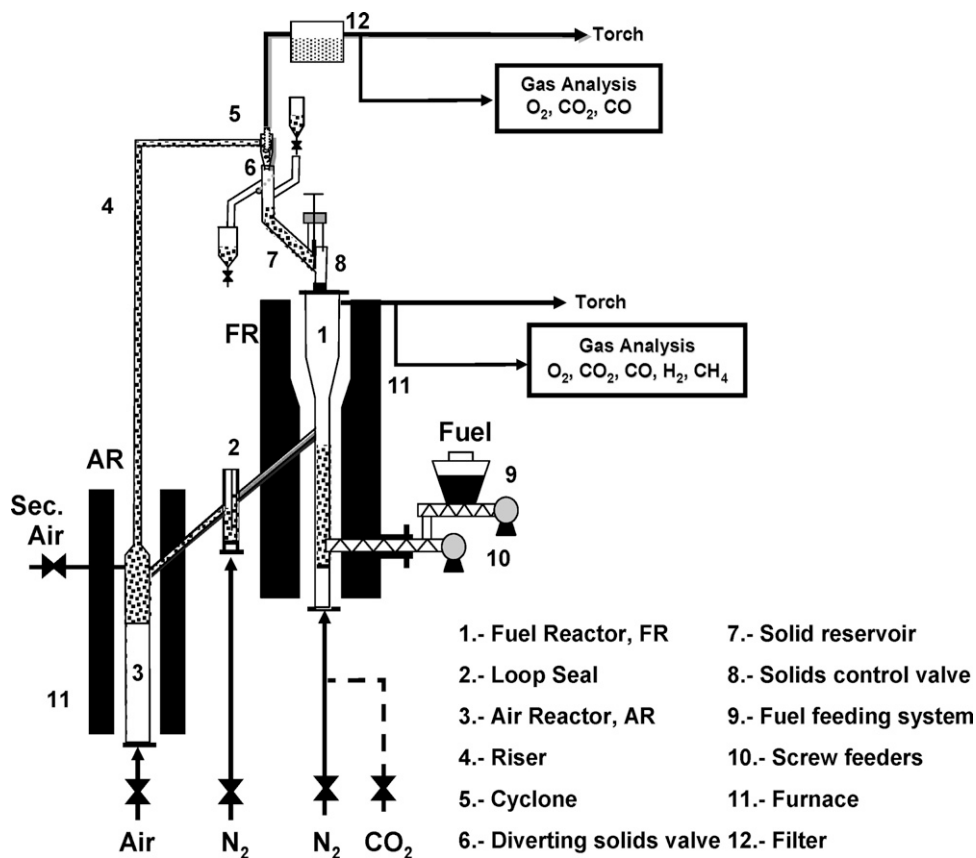


**Fig. 2.** Schematic view of the ICB-CSIC-s1 unit for the CLOU process (1.5 kW<sub>th</sub>).

**Table 3**  
Operational conditions during experimental work in ICB-CSIC-s1 unit.

Coal	$\dot{m}_{\text{coal}}$ (kg/h)	$\dot{m}_{\text{CuO}}$ (kg/h)	$\phi$	$\lambda$	Power(W)	$m_{\text{FR}}$ (kg/MW <sub>th</sub> )
Anthracite	0.10	3.1	1.1	3.1	583	894
LV bituminous	0.10	3.7	1.0	2.7	805	709
MV bituminous	0.08	3.2	1.1	3.6	592	1003
Lignite	0.13	3.0	1.2	3.6	582	845

and ultimate analysis of coal, see Table 2, by using the following equation:

$$\Omega_{\text{coal}} = \left( \frac{f_C}{M_C} + 0.25 \frac{f_H}{M_H} + 0.5 \frac{f_N}{M_N} + \frac{f_S}{M_S} - \frac{f_O}{M_{O_2}} \right) \cdot M_{O_2} \quad (6)$$

$f_i$  being the mass fraction of the element  $i$  in coal.

Air flow into the air reactor was maintained constant for all tests, always remaining in excess over the stoichiometric oxygen demanded by the fuel. The air excess ratio,  $\lambda$ , was defined in Eq. (7), and the values for the experimental work were always above 1, and are shown in Table 3.

$$\lambda = \frac{\text{Oxygen flow}}{\text{Oxygen demanded}} = \frac{0.21 F_{\text{air}} M_{O_2}}{\Omega_{\text{coal}} \dot{m}_{\text{coal}}} \quad (7)$$

### 2.5. Data evaluation

Char reactivity was obtained in TGA tests from the weight variations during reaction with air as a function of time. The char conversion was calculated as:

$$X_{\text{char}} = \frac{m_0 - m}{m_0 - m_{\text{ash}}} \quad (8)$$

being  $m$  the sample mass at each time,  $m_0$  the char sample mass fully devolatilized and  $m_{\text{ash}}$  the ash remaining mass in the char after reaction.

In the continuous CLOU unit, to analyze the confidence of the results, a mass balance to oxygen and carbon was carried out using the measurements of the gas stream coming from the air and fuel reactors. The product gas flow in dry basis in the fuel reactor,  $F_{\text{outFR}}$ , was calculated as:

$$F_{\text{outFR}} = \frac{F_{\text{inFR}}}{1 - (Y_{\text{CO}_2, \text{outFR}} + Y_{\text{CO}, \text{outFR}} + Y_{\text{H}_2, \text{outFR}} + Y_{\text{CH}_4, \text{outFR}} + Y_{\text{O}_2, \text{outFR}})} \quad (9)$$

$F_{\text{inFR}}$  being the inlet flow to the fuel reactor, i.e. the sum of  $N_2$  for fluidizing,  $N_2$  from loop seal and  $N_2$  from the screw-feeder, and  $y_{i, \text{outFR}}$  the  $i$  gas concentration exiting from the fuel reactor in dry basis.

The outlet gas flow from air reactor,  $F_{\text{outAR}}$ , was calculated through the introduced  $N_2$ .

$$F_{\text{outAR}} = \frac{F_{N_2, \text{inAR}}}{1 - (Y_{O_2, \text{outAR}} + Y_{CO_2, \text{outAR}})} \quad (10)$$

Thus, the exiting flows of  $O_2$  and  $CO_2$  from the air and fuel reactors can be easily calculated using the actual concentration of each gas  $i$ .

$$F_{i, \text{out}} = y_{i, \text{out}} F_{\text{out}} \quad (11)$$

Notice that nitrogen is used as fluidizing agent in the fuel reactor during experimental work, thus  $CO_2$  comes uniquely from the coal combustion.

With the gas flows, a mass balance to carbon and oxygen was done as:

$$f_C \cdot \dot{m}_{\text{coal}} = M_C (F_{\text{CO}_2, \text{outFR}} + F_{\text{CO}, \text{outFR}} + F_{\text{CH}_4, \text{outFR}} + F_{\text{CO}_2, \text{outAR}}) \quad (12)$$

$$M_{O_2} (F_{\text{CO}_2, \text{outFR}} + F_{O_2, \text{outFR}} + 0.5 F_{\text{CO}, \text{outFR}} + 0.5 F_{\text{H}_2O, \text{outFR}})_{\text{outFR}} - \left( \frac{f_{\text{H}_2O}}{M_{\text{H}_2O}} + \frac{f_O}{M_O} \right) \dot{m}_{\text{coal}} = M_{O_2} [F_{O_2, \text{inAR}} - (F_{O_2, \text{outAR}} + F_{\text{CO}_2, \text{outAR}} + 0.5 F_{\text{CO}, \text{outFR}})] \quad (13)$$

The water concentration was not measured. However, to consider the oxygen exiting with  $H_2O$  coming from oxidation of hydrogen in the coal, it was assumed that water came both from humidity and hydrogen content in coal.

$$F_{\text{H}_2O, \text{outFR}} = \left( 0.5 \frac{f_H}{M_H} + \frac{f_{\text{H}_2O}}{M_{\text{H}_2O}} \right) \dot{m}_{\text{coal}} \quad (14)$$

The evaluation of the CLOU performance with different coals was carried out by studying the effect of the operational variables on the carbon capture efficiency, the char conversion and the combustion efficiency in the fuel reactor.

The carbon capture efficiency,  $\eta_{\text{CC}}$ , was defined as the fraction of carbon present in the coal which is at the outlet of fuel reactor. This is the real carbon captured in the CLOU system, as the remaining carbon exit as  $CO_2$  exiting together with nitrogen at the air reactor outlet.

$$\eta_{\text{CC}} = 1 - \frac{F_{\text{CO}_2, \text{outAR}}}{F_{\text{CO}_2, \text{outFR}} + F_{\text{CO}, \text{outFR}} + F_{\text{CH}_4, \text{outFR}} + F_{\text{CO}_2, \text{outAR}}} \quad (15)$$

The carbon capture efficiency depends on the conversion of char in the fuel reactor,  $X_{\text{char}}$ . Its value was calculated considering that the carbon contained in the fuel reactor comes from the carbon in volatiles and carbon in char converted. Thus, the carbon from char was the exiting carbon minus the flow of carbon in volatiles,  $F_{\text{C,vol}}$ :

$$X_{\text{char}} = 1 - \frac{F_{\text{CO}_2, \text{outAR}}}{F_{\text{CO}_2, \text{outFR}} + F_{\text{CO}, \text{outFR}} + F_{\text{CH}_4, \text{outFR}} + F_{\text{CO}_2, \text{outAR}} - F_{\text{C,vol}}} \quad (16)$$

The molar flow of carbon contained in the volatile matter was calculated as:

$$F_{\text{C,vol}} = \frac{(f_C - f_{\text{C,fix}}) \dot{m}_{\text{coal}}}{M_C} \quad (17)$$

$f_{\text{C,fix}}$  being the fixed carbon given by coal analysis, see Table 2. Eq. (17) assumes that the volatiles evolved in the fuel reactor are the same as in a proximate analysis measurement.

The conversion of char in the fuel reactor was related to the temperature and the mean residence time of solids in the fuel reactor,  $\tau_{\text{FR}}$ , which is calculated by the following equation:

$$\tau_{\text{FR}} = \frac{m_{\text{s,FR}}}{\dot{m}_{\text{OC}}} \quad (18)$$

$m_{\text{s,FR}}$  being the mass of solids in the fuel reactor and  $\dot{m}_{\text{OC}}$  the solids circulation rate between the air and fuel reactors.

The fractional conversion rate of the char,  $(-r_C)$ , can be calculated from the values of the char conversion in the fuel reactor and

the mean residence time of char particles in this reactor,  $\tau_{\text{char}}$ . The fractional conversion rate of char was calculated as follows:

$$(-r_c) = \frac{X_{\text{char}}}{\tau_{\text{char}}} \quad (19)$$

$\tau_{\text{char}}$  is related to the mean residence time of solids in the fuel reactor with the following equation:

$$\tau_{\text{char}} = \tau_{\text{FR}} \cdot (1 - X_{\text{char}}) \quad (20)$$

Finally, the combustion efficiency in the fuel reactor,  $\eta_{\text{comb,FR}}$ , evaluates the combustion degree only to the fraction of coal converted in the fuel reactor. The combustion efficiency in the fuel reactor was calculated through the quotient between the oxygen required to fully burn unconverted gases ( $\text{CH}_4$ ,  $\text{CO}$  and  $\text{H}_2$ ) and the oxygen demanded for full combustion of the coal converted in the fuel reactor. Therefore, the combustion efficiency in the fuel reactor was calculated as:

$$\eta_{\text{comb,FR}} = 1 - \frac{4F_{\text{CH}_4,\text{outFR}} + F_{\text{CO,outFR}} + F_{\text{H}_2,\text{outFR}}}{2\Omega_{\text{coal}}\dot{m}_{\text{coal}} - 2F_{\text{CO}_2,\text{outAR}}} \quad (21)$$

### 3. Results

To investigate the performance of the CLOU system for the combustion of different coals, several tests under continuous operation were carried out in the ICB-CSIC-s1 experimental rig. The Cu60MgAl material was used as oxygen carrier. The effect of the coal rank and the fuel reactor temperature on the combustion efficiency and carbon capture efficiency was investigated. Thus, the fuel reactor temperature was varied from 900 to 950 °C. A total of 40 h of operation were carried out. Similarly to that found in a previous work (Adáñez-Rubio et al., 2012b), both reactivity and oxygen transport capacity of solids were maintained constant during the experimental work.

The gas composition of the exit gases of fuel and air reactor was determined for every experimental condition. As example, Fig. 3 shows the concentration of gases (dry basis) measured as a function of the operating time for experiments carried out with lignite. Several temperatures in the fuel reactor was tested, and at least 60 min was operated at constant temperature.

When temperature was varied, a transition period appeared and stable combustion was reached usually in less than 10 min. At steady state, the gas outlet concentration and temperature were maintained uniform during the whole combustion time. The mass balances for carbon and oxygen, see Eqs. (12) and (13), were found to be accurate. Thus, the loss of carbon by elutriation of char particles from the fuel reactor or carbon not recovered by cyclone was negligible regarding the carbon balance in the system. Moreover, when the oxygen transferred from the oxygen carrier to the fuel was equal to the oxygen transferred from the air to the oxygen carrier, the steady state was reached.

In all cases, no  $\text{CH}_4$ ,  $\text{CO}$  or  $\text{H}_2$  were detected in the gases exiting from the fuel reactor. The possible presence of tars or light hydrocarbons was also analyzed. In addition, in the experiments done at the lowest temperature for all the coals, tar measurements in the fuel reactor were done using a tar protocol. The results showed that there were not tars in the fuel reactor outlet flow, that is, no hydrocarbons heavier than  $\text{C}_5$ . Also in these experiments, gas from the outlet stream of fuel reactor was collected in bags and analyzed with a gas chromatograph. The analysis proved that there were no  $\text{C}_2$ – $\text{C}_4$  hydrocarbons in the gases. Thus,  $\text{CO}_2$ ,  $\text{H}_2\text{O}$  and  $\text{O}_2$  were the only gases, together with  $\text{N}_2$  introduced as fluidizing gas. Also, small fractions of  $\text{SO}_2$  and  $\text{NO}$  were present in the gases coming from sulphur and nitrogen present in the coal. However, these components were not evaluated in this work.

Therefore, it was found that volatiles were fully converted into  $\text{CO}_2$  and  $\text{H}_2\text{O}$  in the fuel reactor by reaction with the oxygen

released from the  $\text{CuO}$  decomposition. In addition, the oxygen release rate was high enough to supply an excess of gaseous oxygen ( $\text{O}_2$ ) exiting together with the combustion gases. Oxygen concentration was close to thermodynamic equilibrium for each reactor temperature, being the oxygen concentration at equilibrium conditions 1.7% at 910 °C, 2.4% at 925 °C, 3.0% at 935 °C and 4.2% at 950 °C. As temperature was increased, more  $\text{O}_2$  is released from the fuel reactor according to equilibrium of  $\text{CuO}$  decomposition. On the other hand, the  $\text{O}_2$  concentration at the outlet of the air reactor slightly decreased with temperature due to the oxygen carrier comes more reduced from the fuel reactor because more oxygen was released in the fuel reactor. Similar results were found with the other fuels.

Fig. 4(a) shows the combustion and carbon capture efficiency obtained for different coals as a function of the fuel reactor temperature. Complete combustion in the fuel reactor of coal to  $\text{CO}_2$  and  $\text{H}_2\text{O}$  was found for all the operating conditions and coals. Note the low solids inventory used in the CLOU system (see Table 3) compared to CLC with coal, where about 1800 kg/ $\text{MW}_{\text{th}}$  was necessary to obtain a combustion efficiency of 96% (Cuadrat et al., 2011). However, the type of coal affected to the carbon capture efficiency. The carbon capture efficiency decreased in the order lignite > medium volatile bituminous > low volatile bituminous > anthracite. For all coals,  $\text{CO}_2$  capture increased with temperature, being this effect more relevant for coals with low volatile matter content as anthracite and LV bituminous coal. Similar carbon capture efficiencies were obtained for lignite and medium volatile bituminous coal at temperatures above 940 °C. In these cases, the carbon capture efficiency was above 99%, but lower values were obtained for low volatile bituminous coal (90%) or anthracite (83%). This result clearly indicates the need of a carbon separation system when low reactive coals are used, to return unconverted char to the fuel reactor. This system is similar to the proposed for CLC with solid fuels (Cao and Pan, 2006). In this way it is possible to increase the char conversion and to reduce the amount of char transferred to the air reactor. The need of a carbon separation system will depend mainly on the coal reactivity in combustion with oxygen.

$\text{CO}_2$  capture efficiencies are dependent on the carbon transferred from the fuel to the air reactor. As the all carbon in volatiles were captured, the carbon capture depends on the unconverted char in the fuel reactor, i.e. the char conversion, which in a CLOU or a CLC system can be affected by the reactor temperature and the solids circulation flow rate (Cuadrat et al., 2012d). Nevertheless, the solids flow rate was maintained constant for all the tests. Fig. 4(b) shows the char conversion as a function of the fuel reactor temperature for different coals. Similar trends to that found for the  $\text{CO}_2$  capture efficiency were found for different coals. Char conversions increased when the temperature increased for all coals and the increase was more effective for low rank coals.

The differences observed in char conversion among the different fuel must be related with the intrinsic combustion reactivity of the coals. Thus, reactivity of the coal chars was determined in TGA. Fig. 5 shows the char conversion versus time obtained in TGA using air at 500 °C for the different fuels used in this study. It can be observed that lignite char is the most reactive which is attributed to the low amount of fixed carbon and high amount of oxygen. The reactivity of LV bituminous and anthracite are very similar and lower than MV bituminous and lignite. Thus, chars from LV bituminous coal and anthracite need elevated reaction times to reach a high conversion. Besides, the reactivity of the different fuels in TGA explains the tendency of the  $\text{CO}_2$  capture efficiency and the char conversion measured in the continuous CLOU unit. Thus, the highest  $\text{CO}_2$  capture efficiency was measured with the most reactive fuel, i.e. the lignite. However, the TGA reactivity for anthracite and LV bituminous char were similar, and the char conversion measured in the continuous CLOU unit of these coals was different.

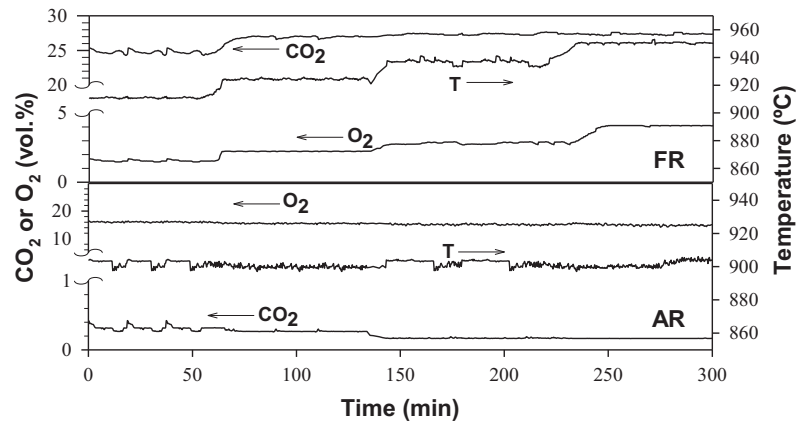


Fig. 3. Evolution of the gas composition in the air and fuel reactor as temperature in the fuel reactor was varied. Coal: lignite,  $\dot{m}_{\text{coal}} = 0.13$  kg/h.

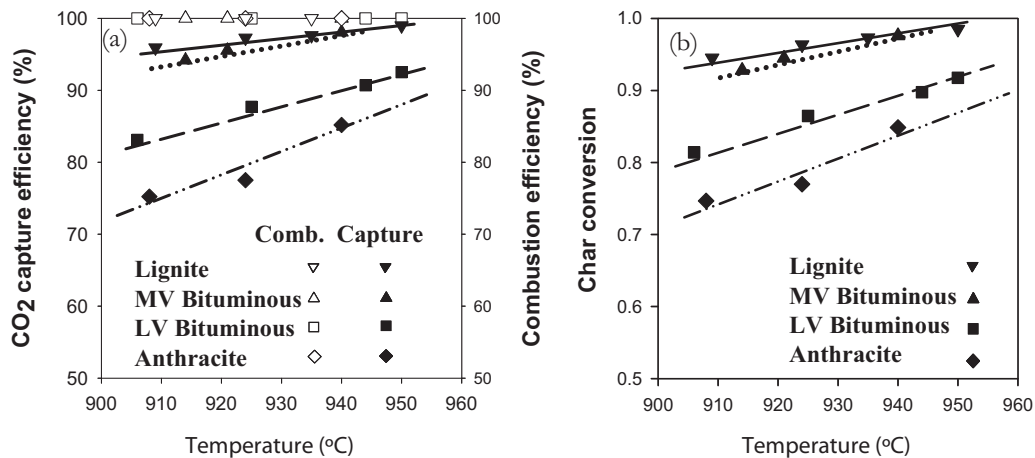


Fig. 4. (a) Combustion efficiency in the fuel reactor and carbon capture efficiency and (b) char conversion, as a function of the fuel reactor temperature obtained with different coals.

Fractional conversion rate of char per unit of carbon mass in char can be used to carry out a comparison between the different coals, because char conversion in the fuel reactor depends directly of this rate. Fig. 6 shows the fractional conversion rate of char as

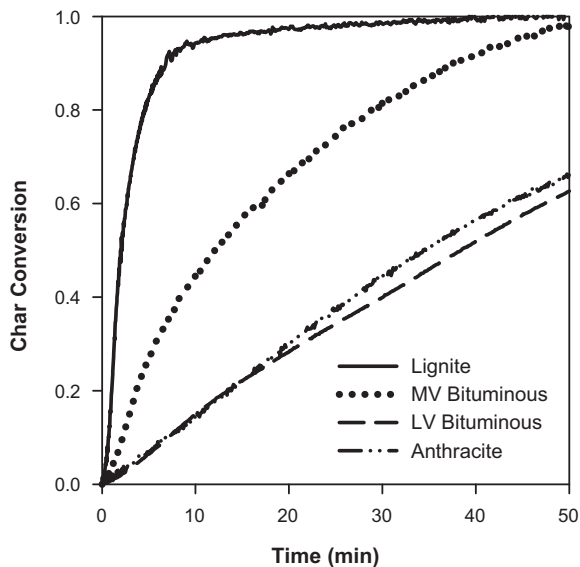


Fig. 5. Conversion vs. time curves for combustion in air at 500 °C of char from the coals used in this work.

a function of temperature calculated using Eq. (19) for the four coals used in the CLOU unit. As expected, the fractional conversion rate of char increases with temperature. The differences between fractional conversion rates showed in Fig. 6 for the different fuels are lower than the difference in reactivity measured in the TGA. It is necessary to consider that at the operating conditions used in the CLOU unit, the reaction rates are in a reaction regime II for porous solids (Walker et al., 1968), that is, the effect of char reactivity is smoothed by the mixed control of the diffusion and kinetic rates.

#### 4. Discussion

With the results obtained in the continuous CLOU unit, an optimization of the CLOU process has been carried out to maximize the CO<sub>2</sub> capture efficiency with the minimum solid inventory. Thus, the carbon capture efficiency was analyzed as a function of the fractional conversion rate of char of the different coals (Cuadrat et al., 2012b). The effect of using a carbon separation system is also analyzed in this section.

As carbon capture efficiency depends on the char conversion in the fuel reactor, a carbon separation system can be used to improve the char conversion and carbon capture in the system. This system allows the separation of char from the oxygen carrier by fluidized bed selective entrainment. In this way the char is transported to the fuel reactor to improve the char conversion, whereas oxygen carrier particles sent to the air reactor.

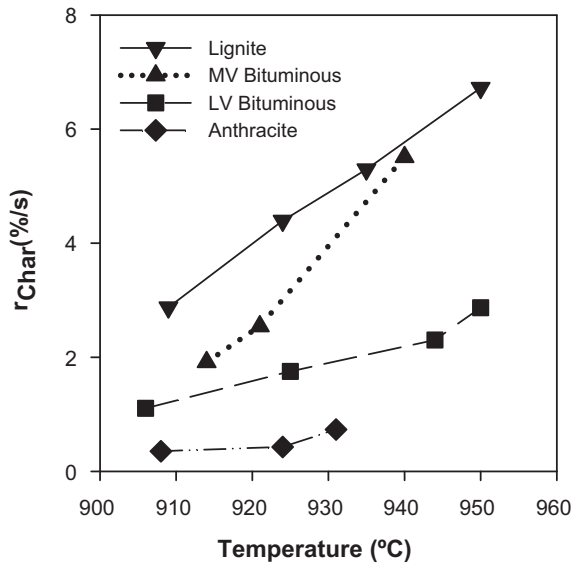


Fig. 6. Fractional conversion rate of char for the four different fuels: lignite (–▼–), medium volatile bituminous (–▲–), low volatile bituminous (–■–) and anthracite (–◆–), as a function of fuel reactor temperature.

Considering a carbon separation system, char conversion can be calculated as a function of the carbon separation system efficiency as follows (Cuadrat et al., 2012b):

$$X_{char} = 1 - \frac{\dot{m}_{OC}(1 - \eta_{CCS})}{(-r_C) \cdot m_{s,FR} + \dot{m}_{OC}(1 - \eta_{CCS})} \quad (22)$$

where  $\dot{m}_s$  is the oxygen carrier flow rate,  $\eta_{CCS}$  is the carbon separation system efficiency,  $(-r_C)$  the fractional conversion rate of char and  $m_{s,FR}$  the mass of oxygen carrier in the fuel reactor. The carbon capture efficiency is related to the char conversion with the following equation:

$$\eta_{CC} = \frac{f_{C,vol}}{f_C} + \frac{f_{C,char}}{f_C} \cdot X_{char} = \frac{f_C - f_{C,fix}}{f_C} + \frac{f_{C,fix}}{f_C} X_{char} \quad (23)$$

Using Eqs. (22) and (23), it is possible to analyze the effect of the oxygen carrier inventory and the efficiency of carbon separation system on char conversion and carbon capture efficiency in the system, once the value of  $(-r_C)$  is known.

Fig. 7(a)–(c) shows the char conversion as a function of the fuel reactor inventory for lignite when a carbon separation system with

different efficiency ( $\eta_{CCS} = 0, 50$  and  $90\%$ ) is considered at  $909$  (a),  $935$  (b) and  $950^\circ\text{C}$  (c). In this analysis, the residence time of solids was maximized by operating at a value of the oxygen carrier to fuel ratio,  $\phi = 1.1$  (Cuadrat et al., 2012c). Namely, the solid circulation flow rate per  $\text{MW}_{th}$  of fuel was fixed for every coal. As it can be seen in Fig. 7(a), if the carbon separation system efficiency ( $\eta_{CCS}$ ) is given, the char conversion increases with the oxygen carrier inventory due to the increase of the residence time of solids in the fuel reactor. For the same reason, if  $\eta_{CCS}$  increases more char returns to the fuel reactor increasing its residence time. As a consequence, the char conversion increases with  $\eta_{CCS}$ . The effect of carbon separation system was very high especially at the lower temperatures and lower oxygen carrier inventories in the fuel reactor.

It is possible to calculate the carbon capture efficiencies in the CLOU process by using Eq. (23). Fig. 8(a)–(c) shows the carbon capture efficiency as a function of the fuel reactor inventory for lignite when a carbon separation system with different efficiencies ( $\eta_{CCS} = 0, 50$  and  $90\%$ ) is considered at  $909$  (a),  $935$  (b) and  $950^\circ\text{C}$  (c). Carbon capture efficiency increases with the fuel reactor inventory for a fixed carbon separation system efficiency, due to the increase of the char conversion. As can be seen in the figures, the effect of carbon separation system was very high especially at the lower temperatures and lower oxygen carrier inventories in the fuel reactor.

Same trends were found for the different coals used in this work although values were dependent on coal reactivity which was related with the coal rank. With low reactivity coals higher oxygen carrier inventories were needed to obtain the same carbon capture efficiency using a carbon separation system with the same efficiency,  $\eta_{CCS}$ .

Fig. 9 shows the minimum fuel reactor inventory necessary to reach a carbon capture efficiency of  $95\%$  as a function of the temperature a carbon separation system with  $\eta_{CCS} = 90\%$  was also included with all different coals. Important differences were found depending on the coal rank. Lignite and MV bituminous, have a high char conversion rate and need very low fuel reactor inventories, with values of  $45$  and  $85 \text{ kg/MW}_{th}$  respectively to reach  $95\%$  carbon capture efficiency at  $925^\circ\text{C}$  respectively. At these conditions, the residence time of solids in the fuel reactor is  $31$  and  $58 \text{ s}$ , respectively. As opposite, for anthracite higher fuel reactor inventories are needed to reach high values of carbon capture efficiency, near  $490 \text{ kg/MW}_{th}$  at  $925^\circ\text{C}$ , with a residence time of  $365 \text{ s}$ . However, these inventories are much lower than those found to burn anthracite in the CLC process using ilmenite (Cuadrat et al., 2012b,

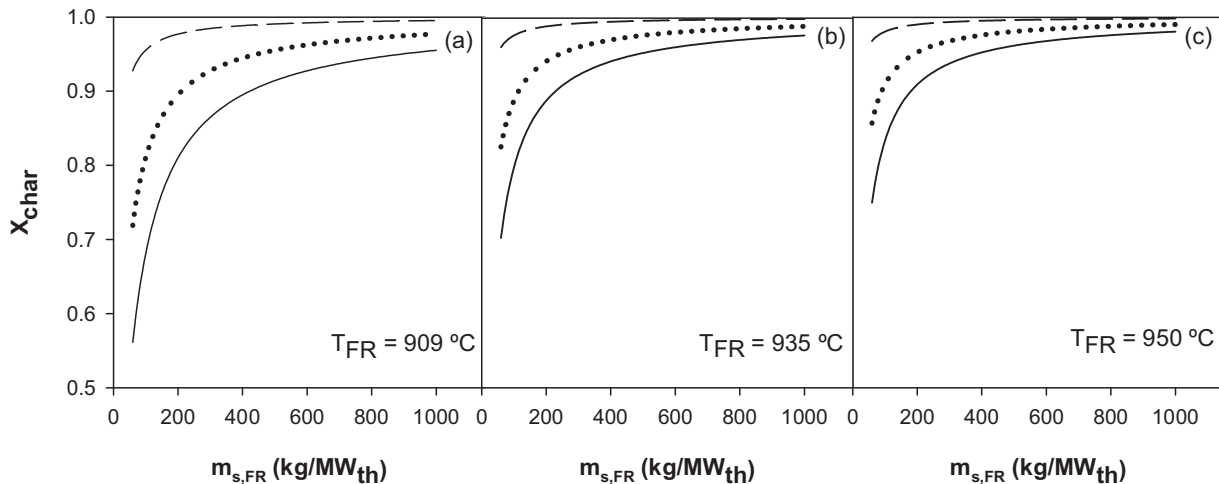
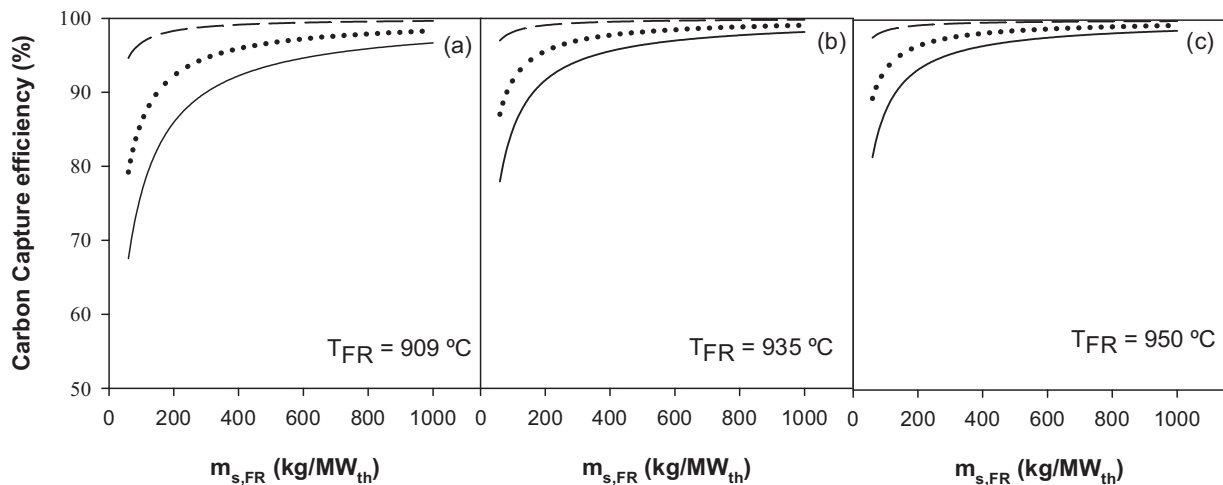


Fig. 7. Char conversion as a function of the fuel reactor inventory for lignite at three different efficiencies of the carbon separation system and three temperatures in the fuel reactor: (a)  $909^\circ\text{C}$ , (b)  $935^\circ\text{C}$  and (c)  $950^\circ\text{C}$ .  $\eta_{CCS} : 0$  (—),  $50\%$  (···),  $90\%$  (–·–).  $\phi = 1.1$ .  $\dot{m}_{OC} = 1.35 \text{ kg/s per MW}_{th}$ .



**Fig. 8.** Carbon capture efficiency as a function of the fuel reactor inventory for lignite at three different efficiencies of the carbon separation system and three temperatures in the fuel reactor: (a) 909 °C, (b) 935 °C and (c) 950 °C.  $\eta_{\text{CSS}} : 0$  (—), 50% (···), 90% (—).  $\phi = 1.1$ ;  $\dot{m}_{\text{oc}} = 1.35$  kg/s per  $\text{MW}_{\text{th}}$ .

c) as 1800  $\text{kg}/\text{MW}_{\text{th}}$  are needed. Moreover, the inventories needed for the different fuels showed an important decrease with temperature indicating the need of fuel reactor temperatures as higher as possible, especially for anthracite.

These inventories are calculated to reach high char conversion values. However, it must be taken into account the oxygen carrier reactivity. In a previous work using this oxygen carrier, Adáñez-Rubio et al. (2012a) defined three different regions of combustion behaviour depending on the solid inventory. The minimum oxygen carrier inventory necessary to reach complete combustion to  $\text{CO}_2$  and  $\text{H}_2\text{O}$  (Region I) was 58  $\text{kg}/\text{MW}_{\text{th}}$  at 955 °C. Therefore, a solid inventory of 35  $\text{kg}/\text{MW}_{\text{th}}$  (using lignite at 950 °C, see Fig. 9) represents operation in Region III, where incomplete combustion occurs. This fact indicates that in the case of highly reactive coals, e.g. lignite or medium volatiles bituminous coals, the solids inventory will be defined by the amount of solids necessary to reach complete combustion rather than to reach high char conversion values.

In other cases, i.e. low reactive coals or absence of a carbon separation system, the solids inventory in the fuel reactor will come defined to have solids residence time high enough to convert the

char. In this case, the absence of unburnt products would be guaranteed even if lower solid inventories were used. At these conditions (Region I defined by Adáñez-Rubio et al., 2012a), complete combustion is reached, although some oxygen at equilibrium conditions will be also present. This oxygen could limit the fuel reactor temperature if the oxygen concentration in the  $\text{CO}_2$  stream should be minimized, because this oxygen must be separated from  $\text{CO}_2$  before its transport and storage (Allam et al., 2005).

## 5. Conclusions

The performance of the CLOU process for combustion of coals of different rank with a Cu-based oxygen carrier (Cu60MgAl) prepared by spray-drying was determined in a continuously operated unit.

With all the coals used, unburnt compounds were not present in the fuel reactor outlet.  $\text{CO}_2$ ,  $\text{H}_2\text{O}$  and  $\text{O}_2$  were the only products present at the fuel reactor outlet. Very high carbon capture efficiencies were obtained for lignite and MV bituminous coals, reaching values of 99% with lignite at 950 °C. The carbon capture efficiency increased with fuel reactor temperature and this increase was more relevant for anthracite and LV bituminous.

The coal rank showed an important effect on the carbon capture efficiency. For low reactivity coals it is necessary the use of a carbon separation system to reach a  $\text{CO}_2$  capture efficiencies higher than 95%.

The analysis of the experimental results was used to evaluate the performance of the CLOU system when a carbon separation system is included using different coal rank. It was found very low solid inventories for all the different coal rank used. For example, at 925 °C the solid inventory needed to reach a 95% of  $\text{CO}_2$  capture efficiency with a carbon separation system of 90% of efficiency is 45  $\text{kg}/\text{MW}_{\text{th}}$  using Lignite, 85  $\text{kg}/\text{MW}_{\text{th}}$  using MV bituminous, 140  $\text{kg}/\text{MW}_{\text{th}}$  using LV bituminous and 490  $\text{kg}/\text{MW}_{\text{th}}$  using anthracite. The residence times corresponding to these inventory values are 31, 58, 140 and 365 s, respectively.

## Acknowledgements

This work was partially supported by the European Commission, under the RFCS programme (ECLAIR Project, Contract RFCP-CT-2008-0008), ALSTOM Power Boilers (France) and by the Spanish Ministry of Science and Innovation (PN, ENE2010-19550). I. Adáñez-Rubio thanks CSIC for the JAE fellowship co-funded by the European Social Fund.

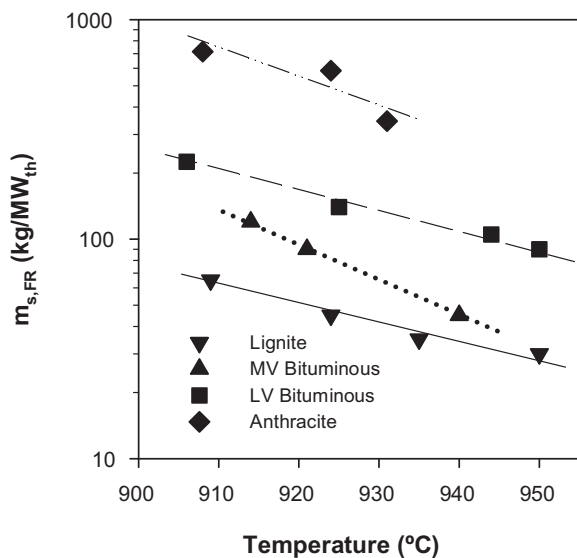


**Fig. 9.** Fuel reactor inventory as a function of the fuel reactor temperature of the different fuels: lignite ( $\nabla$ ), medium volatile bituminous ( $\blacktriangle$ ), low volatile bituminous ( $\blacksquare$ ) and anthracite ( $\blacklozenge$ ).  $\eta_{\text{CC}} = 95\%$ ;  $\eta_{\text{CSS}} = 90\%$ .  $\phi = 1.1$ .

## References

- Abad, A., Adánez-Rubio, I., Gayán, P., García-Labiano, F., de Diego, L.F., Adánez, J., 2012. Demonstration of chemical-looping with oxygen uncoupling (CLOU) process in a 1.5 kW<sub>th</sub> continuously operating unit using a Cu-based oxygen-carrier. *International Journal of Greenhouse Gas Control* 6, 189–200.
- Adánez, J., de Diego, L.F., García-Labiano, F., Abad, A., Abanades, J.C., 2001. Determination of biomass char combustion reactivities for FBC applications by a combined method. *Industrial and Engineering Chemistry Research* 40 (20), 4317–4323.
- Adánez, J., Gayán, P., Celaya, J., de Diego, L.F., García-Labiano, F., Abad, A., 2006. Chemical looping combustion in a 10 kW<sub>th</sub> prototype using a CuO/Al<sub>2</sub>O<sub>3</sub> oxygen carrier: effect of operating conditions on methane combustion. *Industrial and Engineering Chemistry Research* 45 (17), 75–80.
- Adánez, J., Abad, A., García-Labiano, F., Gayán, P., de Diego, L.F., 2012. Progress in chemical-looping combustion and reforming technologies. *Progress in Energy and Combustion Science* 38, 215–282.
- Adánez-Rubio, I., Gayán, P., García-Labiano, F., de Diego, L.F., Adánez, J., Abad, A., 2011. Development of CuO-based oxygen carrier materials suitable for chemical-looping with oxygen uncoupling (CLOU). *Energy Procedia* 4, 417–424.
- Adánez-Rubio, I., Gayán, P., Abad, A., de Diego, L.F., García-Labiano, F., Adánez, J., 2012a. Identification of operational regions in the chemical-looping with oxygen uncoupling (CLOU) process with a Cu-based oxygen-carrier. *Fuel*, <http://dx.doi.org/10.1016/j.fuel.2012.06.063>.
- Adánez-Rubio, I., Gayán, P., Abad, A., de Diego, L.F., García-Labiano, F., Adánez, J., 2012b. Evaluation of a spray-dried CuO/MgAl<sub>2</sub>O<sub>4</sub> oxygen carrier for the chemical looping with oxygen uncoupling process. *Energy and Fuels* 26 (5), 3069–3081.
- Allam, R., White, V., Ivens, N., Simmonds, M., 2005. The oxyfuel baseline: revamping heaters and boilers to oxyfiring by cryogenic air separation and flue gas recycle. In: Thomas, D.C., Benson, S.M. (Eds.), *Carbon Dioxide Capture for Storage in Deep Geologic Formations—Results from the CO<sub>2</sub> Capture Project*, vol. 1. Elsevier, Oxford, Chapter 26.
- Azimi, G., Leion, H., Mattisson, T., Lyngfelt, A., 2011. Chemical-looping with oxygen uncoupling using combined Mn–Fe oxides, testing in batch fluidized bed. *Energy Procedia* 4, 370–377.
- Berguerand, N., Lyngfelt, A., 2008. Design and operation of a 10 kW<sub>th</sub> chemical-looping combustor for solid fuels—testing with South African coal. *Fuel* 87, 2713–2726.
- Berguerand, N., Lyngfelt, A., 2009. Chemical-looping combustion of petroleum coke using ilmenite in a 10 kW<sub>th</sub> unit-high-temperature operation. *Energy and Fuels* 23, 57–68.
- Cao, Y., Pan, W.P., 2006. Investigation of chemical looping combustion by solid fuels. 1. Process analysis. *Energy Fuels* 20, 57–68.
- Cuadrat, A., Abad, A., García-Labiano, F., Gayán, P., de Diego, L.F., Adánez, J., 2011. The use of ilmenite as oxygen-carrier in a 500 W(th) chemical-looping coal combustion unit. *International Journal of Greenhouse Gas Control* 5, 1630–1642.
- Cuadrat, A., Abad, A., García-Labiano, F., Gayán, P., de Diego, L.F., Adánez, J., 2012a. Relevance of the coal rank on the performance of the in-situ gasification chemical-looping combustion. *Chemical Engineering Journal*, <http://dx.doi.org/10.1016/j.cej.2012.04.052>.
- Cuadrat, A., Abad, A., de Diego, L.F., García-Labiano, F., Gayán, P., Adánez, J., 2012b. Prompt considerations on the design of chemical-looping combustion of coal from experimental tests. *Fuel*, <http://dx.doi.org/10.1016/j.fuel.2012.01.050>.
- Cuadrat, A., Abad, A., Gayán, P., de Diego, L.F., García-Labiano, F., Adánez, J., 2012c. Theoretical approach on the CLC performance with solid fuels: optimizing the solids inventory. *Fuel*, <http://dx.doi.org/10.1016/j.fuel.2012.01.071>.
- Cuadrat, A., Abad, A., García-Labiano, F., Gayán, P., de Diego, L.F., Adánez, J., 2012d. Effect of operating conditions in chemical-looping combustion of coal in a 500 W<sub>th</sub> unit. *International Journal of Greenhouse Gas Control* 6, 153–163.
- de Diego, L.F., García-Labiano, F., Adánez, J., Gayán, P., Abad, A., Corbella, B., Palacios, J.M., 2004. Development of Cu-based oxygen carriers for chemical-looping combustion. *Fuel* 83 (13), 49–57.
- Eyring, E., Konya, G., Lighty, J., Sahir, A., Sarofim, A., Whitty, K., 2011. Chemical looping with copper oxide as carrier and coal as fuel. *Oil and Gas Science and Technology—Revue IFP Nouvelles Technologies* 2, 209–221.
- Gayán, P., Adánez-Rubio, I., Abad, A., de Diego, L.F., García-Labiano, F., Adánez, J., 2012. Development of CuO-based oxygen-carrier materials suitable for chemical-looping with oxygen uncoupling (CLOU) process. *Fuel* 96, 226–238.
- IPCC, 2005. In: Metz, B., Davidson, O., de Coninck, H.C., Loos, M., Meyer, L.A. (Eds.), *IPCC Special Report on Carbon dioxide Capture and Storage*. Working Group III of the Intergovernmental Panel on Climate Change, Cambridge University.
- Kerr, H.R., 2005. In: Thomas, D.C., Benson, S.M. (Eds.), *Capture and Separation Technology Gaps and Priority Research Needs*. Carbon dioxide Capture for Storage in Deep Geologic Formations. Elsevier Science, Amsterdam, pp. 655–660.
- Kolbitsch, P., Bolhär-Nordenkamp, J., Pröll, T., Hofbauer, H., 2009. Comparison of two Ni-based oxygen carriers for chemical looping combustion of natural gas in 140 kW continuous looping operation. *Industrial and Engineering Chemistry Research* 48 (11), 42–47.
- Kvamsdal, H.M., Jordal, K., Bolland, O., 2007. A quantitative comparison of gas turbine cycles with CO<sub>2</sub> capture. *Energy* 32 (1), 10–24.
- Leion, H., Mattisson, T., Lyngfelt, A., 2007. The use of petroleum coke as fuel in chemical-looping combustion. *Fuel* 86, 1947–1958.
- Leion, H., Larring, Y., Bakken, E., Bredesen, R., Mattisson, T., Lyngfelt, A., 2009a. Use of CaMn<sub>0.875</sub>Ti<sub>0.125</sub>O<sub>3</sub> as oxygen carrier in chemical looping with oxygen uncoupling. *Energy and Fuels* 23, 5276–5283.
- Leion, H., Mattisson, T., Lyngfelt, A., 2009b. Using chemical-looping with oxygen uncoupling (CLOU) for combustion of six different solid fuels. *Energy Procedia* 1, 447–453.
- Lewis, W.K., Gilliland, E.R., 1954. Production of pure carbon dioxide. Patent 2665972.
- Linderholm, C., Mattisson, T., Lyngfelt, A., 2009. Long-term integrity testing of spray-dried particles in a 10 kW chemical-looping combustor using natural gas as fuel. *Fuel* 88, 2083–2096.
- Mattisson, T., Lyngfelt, A., Leion, H., 2009a. Chemical-looping oxygen uncoupling for combustion of solid fuels. *International Journal of Greenhouse Gas Control* 3, 11–19.
- Mattisson, T., Leion, H., Lyngfelt, A., 2009b. Chemical-looping with oxygen uncoupling using CuO/ZrO<sub>2</sub> with petroleum coke. *Fuel* 88, 683–690.
- Pröll, T., Mayer, K., Bolhär-Nordenkamp, J., Kolbitsch, P., Mattisson, T., Lyngfelt, A., Hofbauer, H., 2009. Natural minerals as oxygen carriers for chemical looping combustion in a dual circulating fluidized bed system. *Energy Procedia* 1, 27–34.
- Rydén, M., Lyngfelt, A., Mattisson, T., 2011a. CaMn<sub>0.875</sub>Ti<sub>0.125</sub>O<sub>3</sub> as oxygen carrier for chemical oxygen combustion with oxygen uncoupling (CLOU)—experiments in a continuously operating fluidized-bed reactor system. *International Journal of Greenhouse Gas Control* 5, 356–366.
- Rydén, M., Lyngfelt, A., Mattisson, T., 2011b. Combined manganese/iron oxides as oxygen carrier for chemical looping combustion with oxygen uncoupling (CLOU) in a circulating fluidized bed reactor system. *Energy Procedia* 4, 341–348.
- Ryu, H.-J., Jo, S.-H., Park, Y.Ch., Bae, D.-H., Kim, S.D., 2010. Long-term operation experience in a 50 kW<sub>th</sub> chemical looping combustor using natural gas and syngas as fuels. In: *Proceedings from the 1st International Conference on Chemical Looping*, 17–19 March 2010, Lyon, France.
- Scott, S.A., Dennis, J.S., Hayhurst, A.N., Brown, T., 2006. In situ gasification of a solid fuel and CO<sub>2</sub> separation using chemical looping. *AIChE Journal* 52, 3325–3328.
- Shen, L., Wu, J., Xiao, J., Song, Q., Xiao, R., 2009. Chemical-looping combustion of biomass in a 10 kW<sub>th</sub> reactor with iron oxide as an oxygen carrier. *Energy and Fuels* 23, 2498–2505.
- Shulman, A., Cleverstam, E., Mattisson, T., Lyngfelt, A., 2009. Manganese/iron, manganese/nickel, and manganese/silicon oxides used in chemical looping with oxygen uncoupling (CLOU) for combustion of methane. *Energy and Fuels* 23, 5269–5275.
- Shulman, A., Cleverstam, E., Mattisson, T., Lyngfelt, A., 2011. Chemical-looping with oxygen uncoupling using Mn/Mg-based oxygen carriers—oxygen release and reactivity with methane. *Fuel* 90, 941–950.
- Simell, P., Stahlberg, P., Kurkela, E., Albretch, J., Deutch, S., Sjöström, K., 2000. Provisional protocol for the sampling and analysis of tar and particulates in the gas from large-scale biomass gasifiers. Version 1998. *Biomass and Bioenergy* 18, 19–38.
- Walker Jr., P.L., Shelef, M., Anderson, R.A., 1968. *Chemistry and Physics of Carbon 4*. Marcel Dekker, NY, pp. 287–380.





## **Paper VII**





# Biomass combustion with CO<sub>2</sub> capture by chemical looping with oxygen uncoupling (CLOU)



I. Adánez-Rubio, A. Abad\*, P. Gayán, L.F. de Diego, F. García-Labiano, J. Adánez

*Instituto de Carboquímica (ICB-CSIC), Miguel Luesma Castán 4, 50018 Zaragoza, Spain*

## ARTICLE INFO

### Article history:

Received 17 June 2013

Received in revised form 21 February 2014

Accepted 21 February 2014

Available online xxxx

### Keywords:

Carbon capture

Combustion

Biomass

CLOU

Copper

Chemical looping

## ABSTRACT

Economic benefits can be expected in the future if CO<sub>2</sub> capture and storage are implemented in energy generation from biomass combustion. The aim of this work is to investigate the combustion of biomass in a chemical looping with oxygen uncoupling (CLOU) process with inherent CO<sub>2</sub> separation. The performance of biomass combustion in a continuously operated 1.5 kW<sub>th</sub> CLOU unit is presented. Particles prepared by spray drying containing 60 wt.% CuO were used as an oxygen carrier. Milled pine wood chips were used as fuel. The work focused on the effect of fuel reactor temperature on the CO<sub>2</sub> capture and the combustion efficiency of the CLOU process with biomass. Under CLOU operation, biomass combustion was complete to CO<sub>2</sub> and H<sub>2</sub>O without the presence of any unburnt material, including tars. Moreover, high carbon capture efficiencies were achieved using very low oxygen carrier inventories and without a carbon separation unit. This is the first time that the CLOU concept has been demonstrated in a continuous CLC unit using biomass as fuel.

© 2014 Elsevier B.V. All rights reserved.

## 1. Introduction

According to the IPCC report on the mitigation of climate change [1], in order to stabilize CO<sub>2</sub> concentration in the atmosphere, CO<sub>2</sub> capture and storage (CCS) would contribute 15–55% to the cumulative mitigation effort worldwide until 2100. CCS is a process involving the separation of the CO<sub>2</sub> emitted by industry and energy-related sources and its storage for long term isolation from the atmosphere. Chemical looping combustion (CLC) has been suggested as being among the best alternatives to reduce the economic cost of CO<sub>2</sub> capture [2] and to reduce the energy penalty in comparison with other CO<sub>2</sub> capture processes [3]. In this process, CO<sub>2</sub> is inherently separated from other combustion products, N<sub>2</sub> and unused O<sub>2</sub>, through the use of a solid oxygen carrier; thus no energy is expended for CO<sub>2</sub> separation. The CLC process has been demonstrated for the combustion of gaseous fuels such as natural gas or syngas in 10 to 140 kW<sub>th</sub> units using oxygen carrier materials based on nickel, copper and iron. Results obtained for CLC with gaseous fuel with different oxygen carriers have been reviewed by Adánez et al. [4] and Lyngfelt [5].

The direct use of solid fuels in the CLC concept for energy generation is highly relevant because solid fuels are considerably more abundant and less expensive than natural gas. CLC with solid fuels involves the fuel being physically mixed with the oxygen carrier in the fuel reactor. The in-situ gasification of the solid fuel, e.g. coal, biomass or solid

wastes, using steam or CO<sub>2</sub> as a gasification agent [6,7] has been proposed as an intermediate step for fuel conversion. This process has been demonstrated in units of 10 to 100 kW<sub>th</sub> with coal [8–10]. The main limitation found in solid fuel conversion in in-situ gasification chemical looping combustion process (iG-CLC) [4] is the slow gasification process [8,11], as well as the incomplete combustion of gases evolved in the fuel reactor [12].

To overcome the low reactivity of the char gasification step in the iG-CLC, an alternative process, chemical looping with oxygen uncoupling (CLOU), was proposed by Mattisson et al. [13]. They made use of the idea first proposed by Lewis and Gilliland [14] to produce CO<sub>2</sub> from solid carbonaceous fuels by using the gaseous oxygen produced by the decomposition of CuO. The CLOU process is based on the strategy of using oxygen carrier materials which release gaseous oxygen and thereby allows the solid fuel to burn with the gas phase oxygen. These materials can be also regenerated at high temperatures.

Fig. 1 shows a schematic diagram of a CLOU system. The fuel conversion in the fuel reactor is produced by different reactions. First the oxygen carrier releases oxygen according to:



and the solid fuel begins to devolatilize, producing a carbonaceous solid residue (char, mainly composed of carbon and ash) and volatile matter as gaseous product:



\* Corresponding author. Tel.: +34 976 733977; fax: +34 976 733318.  
E-mail address: [abad@icb.csic.es](mailto:abad@icb.csic.es) (A. Abad).

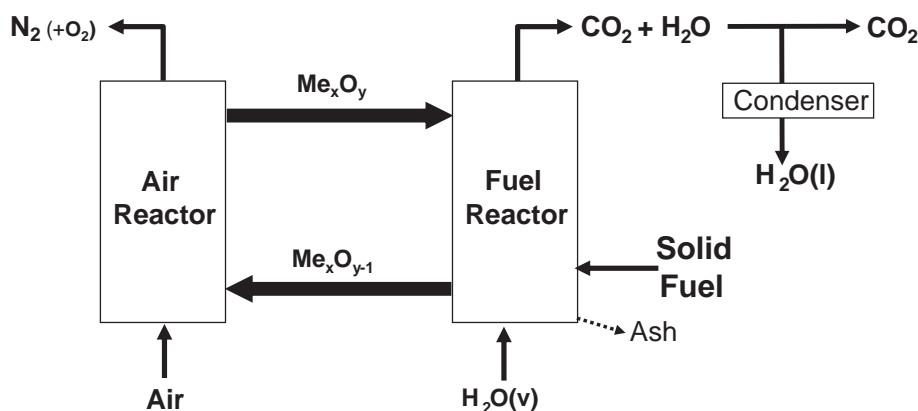


Fig. 1. Schematic layout of the CLOU system.

The volatiles and char are then burnt in a similar way than in the usual combustion process with the gaseous oxygen according to reactions (3) and (4):



After steam condensation, a pure  $\text{CO}_2$  stream is obtained from the fuel reactor. The reduced oxygen carrier is transported to the air reactor, where the oxygen carrier is regenerated to the initial oxidation stage with the oxygen in air in readiness for use in a new cycle. Ideally, the exit stream of the air reactor will contain only  $\text{N}_2$  and unreacted  $\text{O}_2$ . The heat release over the fuel and air reactors is the same as for conventional combustion. Therefore, the CLOU process has a low energy penalty for  $\text{CO}_2$  separation and low  $\text{CO}_2$  capture costs are expected.

The slow gasification step for the direct solid fuel experienced in *iG-CLC* is avoided in the CLOU process, which achieves a much faster solid conversion [15]. It was found that the conversion rate for the solid fuel was increased by a factor of 45 for a petroleum coke [13] and by 60 for a bituminous coal [15] in comparison with those measured using an oxygen carrier without the oxygen uncoupling property. Moreover, the combustion of the fuel consumes the oxygen generated by the oxygen carrier and improves the decomposition reaction of the metal oxide particles [16]. As a consequence, solid inventory as low as  $50 \text{ kg/MW}_{\text{th}}$  was estimated by Adánez-Rubio et al. [16]. This solid inventory is much lower than the ones required in the *iG-CLC* system with solid fuels, which is in the range of  $1000\text{--}2000 \text{ kg/MW}_{\text{th}}$  for Fe-based oxygen carriers [17–20].

Thus, a special requisite applies to the oxygen carrier to be used in the CLOU process in comparison with oxygen carriers for normal CLC, where the fuel reacts directly with the solid oxygen carrier without any release of gas phase oxygen. Only those metal oxides that have a suitable equilibrium partial pressure of oxygen at temperatures of interest for combustion ( $800\text{--}1200 \text{ }^\circ\text{C}$ ) can be used as oxygen carrier materials in the CLOU process. Moreover, this  $\text{O}_2$  release must be reversible in order to oxidize the oxygen carrier in the air reactor and regenerate the material.  $\text{CuO/Cu}_2\text{O}$ ,  $\text{Mn}_2\text{O}_3/\text{Mn}_3\text{O}_4$  and  $\text{Co}_3\text{O}_4/\text{CoO}$  have been identified as redox pairs with the capacity to evolve oxygen at high temperature [13]. To date, there are only a small number of developed materials that are suitable for the CLOU process [4,21–24].

The ICB-CSIC research group performed a screening study that considered 25 different Cu-based oxygen carriers in order to select appropriate materials for the CLOU process [21]. Two promising Cu-based oxygen carriers prepared by pelletizing under pressure ( $60 \text{ wt.}\% \text{ CuO}$  supported on  $\text{MgAl}_2\text{O}_4$ , and  $40 \text{ wt.}\% \text{ CuO}$  supported on  $\text{ZrO}_2$ ) were

selected owing to their high reactivity, low attrition rate and lack of agglomeration. After the screening tests, a batch of  $60 \text{ wt.}\% \text{ CuO}$  supported on  $\text{MgAl}_2\text{O}_4$  was prepared by spray drying and evaluated in a CLOU unit [25]. The validity of the concept of the CLOU process with coal was demonstrated using this material as the oxygen carrier [15] in a  $1.5 \text{ kW}_{\text{th}}$  continuously operated unit consisting of two interconnected fluidized-bed reactors. The effect of the coal rank was also analyzed [26] in this unit using a lignite, two bituminous coals and an anthracite. Complete combustion was achieved using a solid inventory in the fuel reactor of  $235 \text{ kg/MW}_{\text{th}}$ . In conjunction, values close to  $100\%$  in carbon capture efficiency were obtained at  $960 \text{ }^\circ\text{C}$  with reactive coals. However, for low reactivity coals such as anthracite, a carbon separation system would be needed in the system to prevent carbon intrusion into the air reactor. Recently, the fate of sulphur in the CLOU process using a Cu-based oxygen carrier was studied in this plant [27] using a high sulphur content fuel. Most of the sulphur introduced with the fuel exited as  $\text{SO}_2$  at the fuel reactor outlet and the oxygen carrier particles showed good behavior as reactivity was unaffected and agglomeration problems did not occur.

If a  $\text{CO}_2$  capture system is implemented in a biomass combustion process, the global carbon balance in the atmosphere will be negative, because the carbon dioxide generated was previously removed from the atmosphere by the biomass. Consequently, biomass is an interesting fuel for testing in CLC or CLOU processes, because it would be possible to obtain negative  $\text{CO}_2$  emissions. Only a few studies using biomass as fuel in continuous CLC units [28–30] can be found in the literature. In these studies, the biomass was converted through in-situ gasification in the fuel reactor of a CLC system (*iG-CLC*). Iron oxide was used as the oxygen carrier in the units of  $10 \text{ kW}_{\text{th}}$  [30] and  $1 \text{ kW}_{\text{th}}$  with a spouted-bed reactor as fuel reactor [28]. A high char conversion in the fuel reactor owing to the high reactivity of the biomass char was found. At the same time, the outlet gases from the fuel reactor had a relevant fraction of unburnt compounds resulting from the large amount of volatiles. Finally, our research group at ICB-CSIC [29] studied the effect of the fuel reactor temperature, solid circulation rate and gasifying agent on the combustion efficiency of milled pine wood chips using iron ore as the oxygen carrier in a continuous  $500 \text{ W}_{\text{th}}$  CLC plant. Carbon capture efficiencies higher than  $95\%$  in a temperature range of  $880\text{--}915 \text{ }^\circ\text{C}$  were obtained in this study, although combustion efficiency was in the  $85\text{--}95\%$  range.

Although, the benefits of the CLOU process have been shown in comparison with the *iG-CLC* process [15], to date there have been no studies on the combustion of biomass by the CLOU process in the literature. The aim of this work was therefore to investigate the validity of the concept of the CLOU process in a continuously operated CLOU plant using biomass as fuel. In this work, particles prepared by spray drying containing  $60 \text{ wt.}\% \text{ CuO}$  and using  $\text{MgAl}_2\text{O}_4$  as supporting material were used as the oxygen carrier for the CLOU process. Biomass has higher volatile matter

content than coal and different behaviors could be expected during combustion. The effect of fuel reactor temperature on combustion and CO<sub>2</sub> capture efficiencies was investigated.

## 2. Experimental section

### 2.1. The Cu-based oxygen carrier

The oxygen carrier used in this work was a Cu-based material prepared by spray drying. The oxygen carrier particles were manufactured by VITO (Flemish Institute for Technological Research, Belgium) using CuO (Panreac, PRS) and MgAl<sub>2</sub>O<sub>4</sub> spinel (Baikowski, S30CR) as raw materials. The particles were calcined for 24 h at 1100 °C. The CuO content was 60 wt.%. The particle size of the oxygen carrier was +0.1–0.25 mm. From this point on, the oxygen carrier is referred to as Cu60MgAl. Table 1 shows the main properties of this material.

Physical and chemical characterization was carried out with these particles, as shown in Table 1. The copper content was determined by complete reduction in TGA using 15 vol.% H<sub>2</sub> at 850 °C [25]. The oxygen transport capacity,  $R_{OC}$ , was calculated in TGA in nitrogen atmosphere at 1000 °C as  $R_{OC} = (m_{ox} - m_{red}) / m_{ox}$ , where  $m_{ox}$  is the mass of fully oxidized particles and  $m_{red}$  the reduced form after oxygen uncoupling, i.e. once all the CuO is reduced to Cu<sub>2</sub>O [25]. Table 1 also shows the different equipment used to characterize this material.

The preliminary results showed that this material had adequate reactivity values and oxygen transport capacity in fluidized-bed conditions [16,25]. High combustion rates with complete combustion to CO<sub>2</sub> and H<sub>2</sub>O were obtained with this material using a low solid inventory in the fuel reactor of a CLOU unit burning different types of coal [15,26].

### 2.2. Biomass

Milled pine wood chips from Spain were used for the CLOU experiments with Cu60AlMg. The main properties of this biomass are shown in Table 2. The biomass particle size used for this study was +0.5–2 mm. This fuel is characterized by its high volatile matter content (81 wt.%) with respect to coal.

### 2.3. ICB-CSIC-s1 unit for the CLOU process

A schematic view of the experimental set-up used is shown in Fig. 2. The set-up was basically composed of two interconnected fluidized-bed reactors – the air and fuel reactors – joined by a loop seal in the lower and a riser for solid transport from the air reactor to the fuel reactor. A cyclone recovered the solids entrained from the riser. A solid valve controlled the solid circulation flow rate in the system. The reactors were operated at slightly higher than atmospheric pressure, taking into consideration the pressure drops in the beds and pipes to the stack. The fuel reactor (1 in Fig. 2) consisted of a bubbling fluidized bed with a 50 mm inner diameter and 200 mm bed height. N<sub>2</sub> was used as fluidizing gas instead of CO<sub>2</sub> in order to improve the accuracy for calculation of the carbon burnt in the fuel reactor. In a previous work, it had been determined that the fluidization agent did not have any influence on the oxygen

**Table 2**  
Properties of biomass used in this work; including ash composition (wt.%).

Proximate analysis (wt.%)		Ultimate analysis (wt.%)	
Moisture	4.2	C	51.4
Volatile matter	81.0	H	6.5
Fixed carbon	14.4	N	0.3
Ash	0.4	S	0.0
		O <sup>a</sup>	37.2
<i>Ash composition</i>			
Al <sub>2</sub> O <sub>3</sub>	2.4	Na <sub>2</sub> O	0.2
CaO	40.7	SiO <sub>2</sub>	6.6
Fe <sub>2</sub> O <sub>3</sub>	1.3	TiO <sub>2</sub>	0.1
K <sub>2</sub> O	8.9	MnO <sub>2</sub>	0.8
MgO	6.6	P <sub>2</sub> O <sub>5</sub>	1.6
LHV (kJ/kg)	19,186		
Ω <sub>sf</sub> (kg O <sub>2</sub> /kg solid fuel)	1.4		

<sup>a</sup> Oxygen to balance.

carrier behavior [21]. The gas flow was 250 L<sub>N</sub>/h, corresponding to a gas velocity of 0.15 m/s at 900 °C. The minimum fluidizing velocities of the oxygen carrier particles were 0.006 m/s for the smallest particle size and 0.023 m/s for the biggest, while the terminal velocities of particles were 0.40 m/s and 1.45 m/s respectively.

Fuel (9 in Fig. 2) was fed in by a screw feeder (10 in Fig. 2) at the bottom of the bed just above the fuel reactor distributor plate in order to maximize the time that the fuel and volatile matter were in contact with the bed material. The screw feeder consisted of two steps: the first with variable speed to control the fuel flow rate; the second was water cooled and it had high rotating velocity to minimize fuel pyrolysis inside the screw. A small N<sub>2</sub> flow (24 L<sub>N</sub>/h) was introduced at the start of the screw feeder to prevent any possible reverse flow of volatiles.

The oxygen carrier was decomposed in the fuel reactor, evolving gaseous oxygen into the surroundings. The oxygen burnt the volatiles and char proceeding from fuel pyrolysis in the fuel reactor. Reduced oxygen carrier particles overflowed into the air reactor through a U-shaped fluidized bed loop seal (2 in Fig. 2) with a 30 mm inner diameter. A N<sub>2</sub> flow of 60 L<sub>N</sub>/h was introduced into the loop seal. Preliminary experiments were carried out to observe the distribution of gas fed into the loop seal. In the experimental conditions used in this work, the gas in the loop-seal was distributed approximately with 50% in each reactor (air and fuel reactor).

The oxidation of the carrier took place in the air reactor (3 in Fig. 2), which was a bubbling fluidized bed with an 80 mm inner diameter and 100 mm bed height, followed by a riser (4 in Fig. 2) with a 30 mm inner diameter. The air flow was 1740 L<sub>N</sub>/h ( $u_g = 0.40$  m/s). In addition, a secondary air flow (240 L<sub>N</sub>/h) was introduced at the top of the bubbling bed to assist particle entrainment through a riser. N<sub>2</sub> and unreacted O<sub>2</sub> left the air reactor passing through a high-efficiency cyclone (5 in Fig. 2) and a filter before reaching the stack. The oxidized solid particles recovered by the cyclone were sent to a solid reservoir (7 in Fig. 2), with the oxygen carrier prepared to start a new cycle. The regenerated oxygen carrier particles returned to the fuel reactor by gravity from the solid reservoir through a solid valve (8 in Fig. 2) that controlled

**Table 1**  
Properties of the fresh and used oxygen carrier Cu60MgAl.

	Techniques	Fresh	Used
CuO content (wt.%)	TGA, CI Electronics	60	60
Oxygen transport capacity, $R_{OC}$ (wt.%)	TGA, CI Electronics	6	6
Crushing strength (N)	Dynamometer, Shimpo FGN-5X	2.4	1.9
Skeletal density (kg/m <sup>3</sup> )	He picnometry, Micromeritics AccuPyc II 1340	4600	4651
Porosity (%)	Hg intrusion, Quantachrome PoreMaster 33	16.1	22.8
Specific surface area, BET (m <sup>2</sup> /g)	BET method, Micromeritics ASAP-2020	<0.5	0.5
XRD main phases	Diffraction, Bruker AXS	CuO, MgAl <sub>2</sub> O <sub>4</sub>	CuO, MgAl <sub>2</sub> O <sub>4</sub>

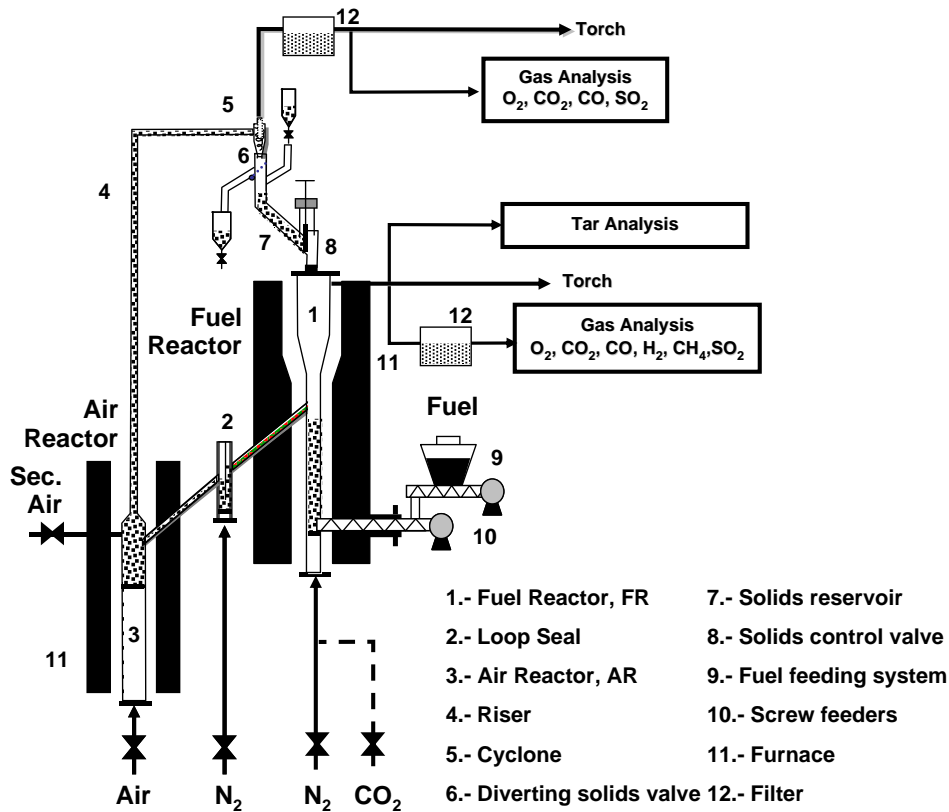


Fig. 2. Schematic view of the ICB-CSIC-s1 unit for the CLOU process (1.5 kW<sub>th</sub>).

the flow rates of solids entering the fuel reactor. A diverting solid valve (6 in Fig. 2) located below the cyclone allowed the measurement of the solid flow rates to be taken at any time. Therefore, this design enabled us to control and measure the solid circulation flow rate between both reactors. The ash particles from char combustion were not recovered by the cyclone and were collected in a filter downstream. Thus, ash particles were not accumulated in the system. Finally, it should be pointed out that leakage of gas between the two reactors was prevented by the presence of the U-shaped loop seal (2 in Fig. 2) and the solid reservoir (7 in Fig. 2). Thus, the presence of oxygen in the fuel reactor was solely the result of oxygen released by reaction (1 in Fig. 2).

The total oxygen carrier inventory in the system was around 2.3 kg, with about 0.7–0.8 kg of this found in the fuel reactor. The amount of solids in the fuel reactor was calculated from pressure drop measurements in the reactor for each test.

CO<sub>2</sub>, CO, H<sub>2</sub>, CH<sub>4</sub>, and O<sub>2</sub> were continuously analyzed at the outlet stream from the fuel reactor, whereas CO<sub>2</sub>, CO and O<sub>2</sub> were analyzed from the flue gases of the air reactor. Non-dispersive infrared (NDIR) analysers (Maihak S710/UNOR) were used for CO, CO<sub>2</sub> and CH<sub>4</sub> concentration determination; a paramagnetic analyzer (Maihak S710/OXOR-P) was used to determine O<sub>2</sub> concentration; and a thermal conductivity detector (Maihak S710/THERMOR) was used for H<sub>2</sub> concentration determination. The amount of tar present in the fuel reactor product gas was determined following the tar protocol [31]. Higher C<sub>2</sub>, C<sub>3</sub> and C<sub>4</sub> hydrocarbons were analyzed off-line by a gas chromatograph (HP5890 Series II).

Because of heat losses, the system was not auto-thermal, and was heated by means of various independent ovens to achieve independent temperature control of the air reactor, fuel reactor and freeboard above the bed in the fuel reactor. During operation, temperatures in the bed and freeboard of the fuel reactor, air reactor bed and riser were monitored, in addition to the pressure drops in important locations of the

system, such as the fuel reactor bed, the air reactor bed and the loop seal. The temperature in the fuel reactor was varied from 860 to 935 °C, whereas the freeboard temperature was 900 °C. The temperature in the air reactor was kept at 900 °C.

The solid circulation rate was maintained at a mean value of 4.1 kg/h, while the biomass feeding rate was 0.22 kg/h, corresponding to a power of 1.2 kW. The oxygen carrier to fuel ratio,  $\phi$ , was around 1.2. The oxygen carrier to fuel ratio was defined as the ratio of the oxygen transported by the oxygen carrier to the oxygen demanded by biomass for complete combustion. A value of  $\phi = 1$  corresponded to the stoichiometric flow of CuO needed to fully convert the fuel to CO<sub>2</sub> and H<sub>2</sub>O, with CuO being reduced to Cu<sub>2</sub>O. Thus,  $\phi$  was calculated with the following equation:

$$\phi = \frac{R_{OC} \dot{m}_{OC}}{\Omega_{SF} \dot{m}_{SF}} \quad (5)$$

where  $\dot{m}_{OC}$  is the solid circulation flow rate in the completely oxidized state and  $\dot{m}_{SF}$  is the mass-based flow of the solid fuel fed into the reactor.  $\Omega_{SF}$  is the stoichiometric kg of oxygen to convert 1 kg of biomass to CO<sub>2</sub> and H<sub>2</sub>O. This value was calculated from the proximate and ultimate analysis of biomass, see Table 2, by using the following equation:

$$\Omega_{SF} = \left( \frac{f_C}{M_C} + 0.25 \frac{f_H}{M_H} - \frac{f_O}{M_{O_2}} \right) \cdot M_{O_2} \quad (6)$$

where  $f_i$  is the mass fraction of the element  $i$  in biomass.

Air flow into the air reactor was maintained constant for all tests and always exceeded the stoichiometric oxygen demanded by the fuel. The

air excess ratio,  $\lambda$ , is defined in Eq. (7), and the values for the experimental work were always above 1.

$$\lambda = \frac{\text{oxygen flow}}{\text{oxygen demanded}} = \frac{0.21 F_{\text{air}} M_{\text{O}_2}}{\Omega_{\text{SF}} \dot{m}_{\text{SF}}} \quad (7)$$

## 2.4. Data evaluation

To analyze the reliability of the results, a mass balance to oxygen and carbon was carried out using the measurements of the gas stream coming from the air and fuel reactors in the continuous CLOU unit. The product gas flow in dry basis in the fuel reactor,  $F_{\text{outFR}}$ , was calculated as:

$$F_{\text{outFR}} = \frac{F_{\text{inFR}}}{1 - (y_{\text{CO}_2, \text{outFR}} + y_{\text{CO}, \text{outFR}} + y_{\text{H}_2, \text{outFR}} + y_{\text{CH}_4, \text{outFR}} + y_{\text{O}_2, \text{outFR}})} \quad (8)$$

where  $F_{\text{inFR}}$  is the inlet flow to the fuel reactor, i.e. the sum of  $\text{N}_2$  for fluidizing,  $\text{N}_2$  from loop seal and  $\text{N}_2$  from the screw-feeder, and  $y_{i, \text{outFR}}$  the  $i$  gas concentration exiting from the fuel reactor on a dry basis.

The outlet gas flow from air reactor,  $F_{\text{outAR}}$ , was calculated by means of the introduced  $\text{N}_2$ .

$$F_{\text{outAR}} = \frac{F_{\text{N}_2, \text{inAR}}}{1 - (y_{\text{O}_2, \text{outAR}} + y_{\text{CO}_2, \text{outAR}})} \quad (9)$$

Thus, the exiting flows of  $\text{O}_2$  and  $\text{CO}_2$  from the air and fuel reactors could be calculated easily using the actual concentration of each gas i:

$$F_{i, \text{out}} = y_{i, \text{out}} F_{\text{out}} \quad (10)$$

Note that nitrogen was used as the fluidizing agent in the fuel reactor during experimental work; thus  $\text{CO}_2$  was produced only by the fuel combustion.

With the gas flows, a mass balance to carbon and oxygen can be performed as:

$$\frac{f_{\text{C}}}{M_{\text{C}}} \cdot \dot{m}_{\text{SF}} = (F_{\text{CO}_2, \text{outFR}} + F_{\text{CO}, \text{outFR}} + F_{\text{CH}_4, \text{outFR}}) + F_{\text{CO}_2, \text{outAR}} + F_{\text{C}, \text{elut}} \quad (11)$$

$$M_{\text{O}_2} (F_{\text{CO}_2, \text{outFR}} + F_{\text{O}_2, \text{outFR}} + 0.5 F_{\text{CO}, \text{outFR}} + 0.5 F_{\text{H}_2\text{O}, \text{outFR}})_{\text{outFR}} - \left( \frac{f_{\text{H}_2\text{O}}}{M_{\text{H}_2\text{O}}} + \frac{f_{\text{O}}}{M_{\text{O}}} \right) \dot{m}_{\text{SF}} = M_{\text{O}_2} [F_{\text{O}_2, \text{inAR}} - (F_{\text{O}_2, \text{outAR}} + F_{\text{CO}_2, \text{outAR}})] \quad (12)$$

where  $F_{\text{C}, \text{elut}}$  is the flow of carbon elutriated from the fuel reactor as unburnt char.

Water concentration was not measured. However, in order to take into account the oxygen exiting with  $\text{H}_2\text{O}$  resulting from the oxidation of hydrogen in the fuel, it was assumed that water came both from the humidity and hydrogen contents in the fuel:

$$F_{\text{H}_2\text{O}, \text{outFR}} = \left( 0.5 \frac{f_{\text{H}}}{M_{\text{H}}} + \frac{f_{\text{H}_2\text{O}}}{M_{\text{H}_2\text{O}}} \right) \dot{m}_{\text{SF}} - F_{\text{H}_2, \text{outFR}} \quad (13)$$

The evaluation of the CLOU performance with solid fuels was carried out by studying the effect of the operational variables on  $\text{CO}_2$  capture efficiency, char conversion and combustion efficiency in the fuel reactor.

$\text{CO}_2$  capture efficiency,  $\eta_{\text{CC}}$ , is defined as the fraction of carbon present in the fuel at the outlet of fuel reactor. This is the real  $\text{CO}_2$

captured in the CLOU system, as the remaining carbon exits as  $\text{CO}_2$  together with nitrogen at the air reactor outlet:

$$\eta_{\text{CC}} = 1 - \frac{F_{\text{CO}_2, \text{outAR}}}{\frac{f_{\text{C}}}{M_{\text{C}}} \cdot \dot{m}_{\text{SF}}} \quad (14)$$

$\text{CO}_2$  capture efficiency depends on the conversion of char in the fuel reactor,  $X_{\text{char}}$ . Its value is calculated by considering that the carbon in gases from the fuel reactor comes from the carbon in volatiles and carbon in converted char. Thus, the carbon from reacting char was the inlet carbon minus the flow of carbon in volatiles,  $F_{\text{C}, \text{vol}}$ , and in elutriated char particles,  $F_{\text{C}, \text{elut}}$ :

$$X_{\text{char}} = \frac{F_{\text{CO}_2, \text{outFR}} + F_{\text{CO}, \text{outFR}} + F_{\text{CH}_4, \text{outFR}} - F_{\text{C}, \text{vol}}}{F_{\text{CO}_2, \text{outFR}} + F_{\text{CO}, \text{outFR}} + F_{\text{CH}_4, \text{outFR}} + F_{\text{CO}_2, \text{outAR}} - F_{\text{C}, \text{vol}}} \quad (15)$$

The molar flow of carbon contained in the volatile matter was calculated as:

$$F_{\text{C}, \text{vol}} = \frac{(f_{\text{C}} - f_{\text{C}, \text{fix}}) \dot{m}_{\text{SF}}}{M_{\text{C}}} \quad (16)$$

where  $f_{\text{C}, \text{fix}}$  is the fixed carbon given by fuel analysis, see Table 2. Eq. (16), assuming that the volatiles evolving in the fuel reactor are the same as those in the proximate analysis measurement.

The conversion of char in the fuel reactor was related to the temperature and the mean residence time of solids in the fuel reactor,  $\tau_{\text{FR}}$ , calculated by the following equation:

$$\tau_{\text{FR}} = \frac{m_{\text{s}, \text{FR}}}{\dot{m}_{\text{OC}}} \quad (17)$$

where  $m_{\text{s}, \text{FR}}$  is the mass of solids in the fuel reactor and  $\dot{m}_{\text{OC}}$  the solid circulation rate between the air and fuel reactors.

The fractional conversion rate of the char ( $-r_{\text{C}}$ ), can be calculated from the values of the char conversion in the fuel reactor and the mean residence time of char particles in this reactor,  $\tau_{\text{char}}$ . The fractional conversion rate of char was calculated as follows:

$$(-r_{\text{C}}) = \frac{X_{\text{char}}}{\tau_{\text{char}}} \quad (18)$$

$\tau_{\text{char}}$  is related to the mean residence time of solids in the fuel reactor with the following equation:

$$\tau_{\text{char}} = \tau_{\text{FR}} \cdot (1 - X_{\text{char}}) \quad (19)$$

Finally, combustion efficiency in the fuel reactor,  $\eta_{\text{comb}, \text{FR}}$ , evaluates the degree of combustion with respect to the fraction of fuel converted in the fuel reactor. The combustion efficiency in the fuel reactor was calculated through the quotient between the oxygen required to fully burn unconverted gases ( $\text{CH}_4$ ,  $\text{CO}$  and  $\text{H}_2$ ) and the oxygen demanded for complete combustion of the biomass converted in the fuel reactor. Therefore, the combustion efficiency in the fuel reactor was calculated as:

$$\eta_{\text{comb}, \text{FR}} = 1 - \frac{4F_{\text{CH}_4, \text{outFR}} + F_{\text{CO}, \text{outFR}} + F_{\text{H}_2, \text{outFR}}}{2\Omega_{\text{SF}} \dot{m}_{\text{SF}} - 2F_{\text{CO}_2, \text{outAR}} - 2F_{\text{C}, \text{elut}}} \quad (20)$$

## 3. Results

### 3.1. Biomass combustion

To investigate the combustion of biomass by a CLOU system, different tests were carried out under continuous operation in the ICB-CSIC-



s1 experimental rig. Cu60MgAl material was used as the oxygen carrier. The effect of the fuel reactor temperature on the combustion efficiency and CO<sub>2</sub> capture efficiency was investigated. Thus, the fuel reactor temperature was varied from 860 °C to 935 °C. A total of 10 h of operation were carried out without agglomeration of the oxygen carrier.

The composition of the exit gases from the fuel and air reactors was determined for every experimental condition. As an example, Fig. 3 shows the concentration of gases (dry basis) measured as a function of the operating time. Several temperatures in the fuel reactor were tested, and each was maintained at steady state for at least 120 min.

When temperature was varied, a transition period appeared and stable combustion was reached usually in less than 10 min. The steady state was reached when the oxygen transferred from the oxygen carrier to the fuel was equal to the oxygen transferred from the air to the oxygen carrier. At steady state, the gas outlet concentration and temperature were maintained uniform throughout the entire combustion time. The mass balances for carbon and oxygen, see Eqs. (11) and (12), were found to be accurate, closing at 95%. Thus, the loss of carbon by elutriation of char particles from the fuel reactor or carbon not recovered by cyclone was negligible with regard to the carbon balance in the system.

For the test carried out at the lower fuel reactor temperature, 860 °C, there was a high concentration of CO in the fuel reactor outlet gas stream, and the oxygen concentration was near 0. The only unburnt gaseous product was CO; neither CH<sub>4</sub> nor H<sub>2</sub> was found at the fuel reactor outlet. These results agreed with those found by Adánez et al. [32] during fluidized bed biomass combustion. They reported CO being the main volatile product during pine wood devolatilization. Moreover, CO was an intermediate product during volatile combustion, with a lower combustion rate than CH<sub>4</sub> and H<sub>2</sub>. All these reasons would justify that the main unburnt product was CO at the lowest temperature in the CLOU experiments.

Besides the large production of volatiles, significant amount of tar compounds can be generated during biomass processing. In order to study the fate of the tar compounds generated during biomass CLOU combustion in the CLC unit, samples were taken at different temperatures according to the tar protocol. Tar compounds were only measured at 860 °C, at a concentration of 0.31 g/Nm<sup>3</sup> (dry basis). The composition of these tars was mainly naphthalene (61.7 wt.%), phenanthrene (13.1 wt.%), acenaphthylene (12.5 wt.%), indene (7.2 wt.%) and styrene (5.5 wt.%). The amount of tar detected in this work during biomass CLOU combustion was four times lower than that found by Mendiara et al. [29] in iG-CLC combustion using the same biomass and similar operating temperature (880 °C). Moreover, the tar composition was different, as it was mainly composed of naphthalene in the biomass iG-CLC

process [29]. The tar content in the fuel reactor exhaust gas may have implications for the further steps of compression, transport and storage, since operational problems may be anticipated if the tar concentration is high. Tar condenses easily, and this property is known to cause fouling in pipes, filter elements and heat exchangers. To prevent these problems, Reed et al. [33] gave an interval of tar concentration between 0.05 and 0.5 g/Nm<sup>3</sup>, for compressing and piping biomass processed gas. According to those limits, the tar content of the FR gas exhaust measured in this work at all temperatures was below those limit values, and thus no additional gas conditioning step should be required.

As was expected given the thermodynamics, the oxygen uncoupling effect at this temperature was low. At the same time, the unburnt char was transferred to the air reactor together with the oxygen carrier particles. There, the char was burnt and the oxygen carrier was regenerated. So, CO<sub>2</sub> appeared as a combustion product from the air reactor.

When the fuel reactor temperature was higher than 900 °C, there was a significant O<sub>2</sub> release due to the CLOU effect and no CH<sub>4</sub>, CO or H<sub>2</sub> were detected in the gases exiting from the fuel reactor. The possible presence of tars or light hydrocarbons was also analyzed. The results showed that there were no tars in the fuel reactor outlet flow, i.e. no hydrocarbons heavier than C<sub>5</sub> at temperatures higher than 900 °C. Furthermore, in these experiments, gas from the outlet stream of fuel reactor was collected in bags and analyzed with a gas chromatograph. The analysis showed that there were no C<sub>2</sub>–C<sub>4</sub> hydrocarbons in the gases. Thus, CO<sub>2</sub>, H<sub>2</sub>O and O<sub>2</sub> were the only gases, together with N<sub>2</sub> introduced as the fluidizing gas at high temperature. Moreover, very low fractions of NO were present in the gases coming from nitrogen present in the biomass. However, nitrogen components were not evaluated in this work. Special experiments should be performed to eliminate any N<sub>2</sub> flow into the fuel reactor to estimate NO<sub>x</sub> formation in a CLC system [34].

Fig. 4(a) shows the combustion and CO<sub>2</sub> capture efficiencies obtained in the plant as a function of the fuel reactor temperature. Complete combustion of biomass to CO<sub>2</sub> and H<sub>2</sub>O was found in the fuel reactor for the experiments at temperatures higher than 900 °C. The solid inventory in the fuel reactor was 565 kg/MW<sub>th</sub> in all tests. Nevertheless, complete combustion can be expected with a lower solid inventory. At temperatures lower than 900 °C, 82% of combustion efficiency was obtained, and there were CO and tars present at the outlet of fuel reactor. Unburnt compounds come mainly from volatile matter, as was shown in previous work in this CLC unit [35]. Biomass contains 81% volatile matter, therefore, the high volatile matter content of the biomass is responsible for the low combustion efficiency showed at the lowest temperature. Note that unburnt compounds are always present at the outlet of the fuel reactor for materials without oxygen uncoupling properties,

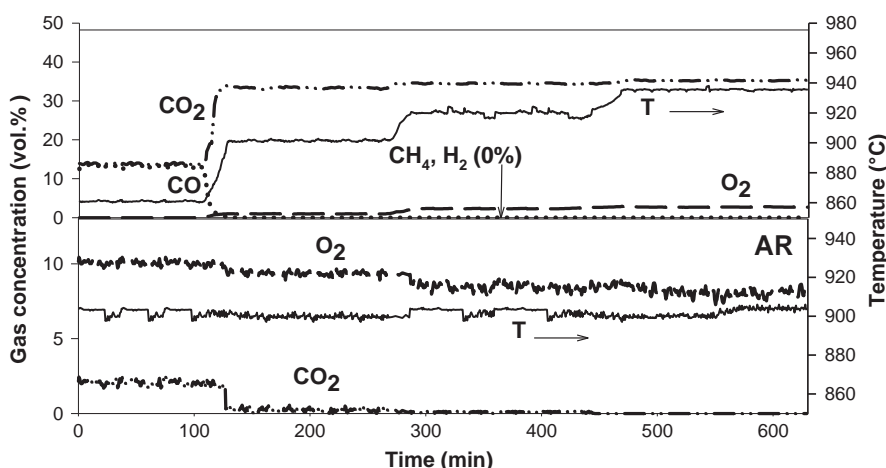


Fig. 3. Evolution of the gas composition in the air and fuel reactors as temperature in the fuel reactor was varied.  $\dot{m}_{SF} = 0.24$  kg/h.

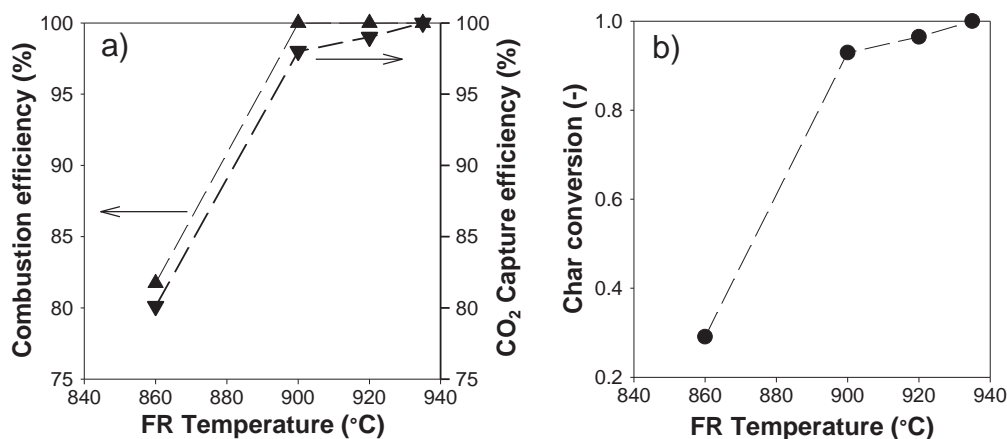


Fig. 4. (a) Combustion efficiency in the fuel reactor and CO<sub>2</sub> capture efficiency and (b) char conversion, as a function of the fuel reactor temperature.

even if highly reactive materials or a high solid inventory was used [12,20]. Similar combustion behavior was obtained in *i*G-CLC made with biomass using an iron based oxygen carrier, i.e.  $\eta_{\text{comb,FR}} = 80\%$  at 880 °C with 1550 kg/MW<sub>th</sub>. With the Cu-based material used in this work,  $\eta_{\text{comb,FR}} = 82\%$  but with much lower amount of solids (565 kg/MW<sub>th</sub>), highlighting the high reactivity of the Cu-based material.

To understand the differences on performance at temperatures lower or higher than 900 °C, it is necessary to take into account that O<sub>2</sub> generated from CuO increases with temperature. This fact is related to the increase in both reaction rate and equilibrium O<sub>2</sub> concentration. At temperatures  $\geq 900$  °C, O<sub>2</sub> released from the oxygen carrier should be of great relevance for the conversion of gaseous compounds proceeding from coal devolatilization. Thus, volatile matter reacts with gaseous O<sub>2</sub> from the oxygen uncoupling mechanism in a homogeneous reaction. On the contrary, at 860 °C, the O<sub>2</sub> generated is extremely low (equilibrium O<sub>2</sub> concentration is 0.5 vol.%). Thus, the gas conversion by a direct gas–solid reaction with the oxygen carrier could be the more relevant mechanism at the lower temperature. At this temperature, oxygen carrier reduction to generate gaseous O<sub>2</sub> is extremely slow [36]. The lack of the oxygen uncoupling is responsible for the relatively low combustion efficiency present in the fuel reactor under these conditions. Nevertheless, it should be noted that the contact between volatile matter and oxygen carrier particles can be poor because they are likely to be generated in a plume. Consequently, gas–solid contact must be seen as a limiting step during combustion of volatile matter instead of the low reactivity of gases with the oxygen carrier material. The presence of a volatile plume and low amounts of solids in the freeboard of this CLC unit [35] is believed to be critical for the low gas conversion at low temperature. Note that when the gas–solid contact is improved, e.g. during combustion of gaseous fuels in previous works [37,38], complete combustion can be achieved at conditions where oxygen uncoupling is not relevant.

In order to obtain complete combustion, an oxygen uncoupling effect is needed. Thus, it was found that volatiles were fully converted into CO<sub>2</sub> and H<sub>2</sub>O in the fuel reactor at temperatures higher than 900 °C by reaction with the oxygen released from CuO decomposition. In addition, the oxygen release rate was high enough to supply an excess of gaseous oxygen (O<sub>2</sub>), which exited together with the combustion gases. The oxygen concentration was at equilibrium conditions for each reactor temperature. At the same time, the O<sub>2</sub> concentration at the air reactor outlet decreased slightly with temperature owing to the oxygen carrier becoming more reduced from the fuel reactor because more oxygen was released there.

CO<sub>2</sub> capture efficiencies are dependent on the carbon transferred in char particles from the fuel to the air reactor. CO<sub>2</sub> capture efficiency increases with the fuel reactor temperature. Thus, high carbon capture

efficiencies were found at fuel reactor temperatures higher than 900 °C, reaching 100% efficiency at 935 °C. As all the carbon in the volatiles was burnt in the fuel reactor, the carbon capture depended only on the unconverted char in the fuel reactor, i.e. on the char conversion, which in a CLOU or a CLC system is dependent on the fuel reactor temperature and the solid circulation flow rate [39]. Nevertheless, the solid flow rate was maintained constant for all the tests. Fig. 4(b) shows the char conversion in the fuel reactor as a function of the fuel reactor temperature. The char conversion increased with the fuel reactor temperature because of the higher char combustion rates. However, low char conversion can be seen at the lowest temperature when only 15% of char conversion is reached in the fuel reactor and there is no gaseous O<sub>2</sub> in the fuel reactor exiting flow. However, the 80% of CO<sub>2</sub> capture efficiency obtained was due to the high amount of volatiles in the biomass composition. This important decrease in the char conversion can be attributed to a change in the mechanism for the combustion of char. At the lower temperature, 860 °C, the oxygen uncoupling effect is low because the O<sub>2</sub> equilibrium concentration is low and the oxygen generation rate by the oxygen carrier particles is low. So the conversion rate of char by combustion reaction should be low. Char conversion is mainly driven at this temperature by the slow gasification reaction with the low H<sub>2</sub>O or CO<sub>2</sub> concentration inside the fuel reactor.

As the temperature increases, the oxygen uncoupling effect increases. Thus, the O<sub>2</sub> equilibrium at 900 °C is 1.5 vol.%. But what is more relevant is the high oxygen generation rate that the oxygen carrier shows at temperatures higher than 900 °C [16]. As a consequence, the rate of char combustion is directly increased.

This work presents the first experimental hours of burning biomass by means of a CLOU process in a continuous unit. Although the total operation time carried out (10 h) was not long enough for application on an industrial scale, it was sufficiently relevant from the research point of view, since no important drawbacks were found for the process. A future experimental campaign involving the burning of different types of biomass, such as almond shells, olive stones and corn stover, is planned in order to extend the evaluation of the CLOU process with other biomasses.

### 3.2. Characterization of used Cu60MgAl oxygen carrier particles

Samples of solids extracted from the fuel and air reactors after 10 h of continuous operation in the CLOU unit were characterized by different techniques. Table 1 shows relevant properties for used particles compared to the fresh ones.

The XRD analysis of used particles revealed the presence of CuO and MgAl<sub>2</sub>O<sub>4</sub> as major components. Thus, no changes were observed in the chemical structure of the material. In addition, XRD results of some

reduced samples taken from the fuel reactor of the CLOU unit at different times showed only  $\text{Cu}_2\text{O}$  and  $\text{MgAl}_2\text{O}_4$  as the main components. In other words, metallic Cu was never detected in the samples, even in those tests where the variation of the solid conversion was close to unity.

The used particles had a stable CuO content of 60 wt.%, similar to the fresh ones. In addition, reactivity data were obtained in TGA tests from the mass variations during the reduction and oxidation cycles as a function of time. The oxygen carrier reduction conversion was calculated as  $X_{\text{red}} = (m_{\text{ox}} - m) / (m_{\text{ox}} - m_{\text{red}})$  and  $X_{\text{ox}} = 1 - X_{\text{red}}$  where  $m$  is the mass of sample at each time,  $m_{\text{ox}}$  is the mass of the fully oxidized sample, and  $m_{\text{red}}$  is the mass of the sample in the reduced form. Fig. 5 shows the conversion vs. time curves obtained for the decomposition and oxidation reactions for the used samples, as well as for fresh oxygen carrier. The maintenance of the initial reactivity can be clearly seen for used particles both in decomposition and oxidation reactions. This fact justifies their unchanged ability to release oxygen at equilibrium conditions and to be re-oxidized by air observed in the CLOU unit after the large number of reduction–oxidation cycles the oxygen carrier particles underwent.

SEM images of fresh and used particles after 10 h of operation in the CLOU unit are shown in Fig. 6. No significant changes were observed in the particles after operation with biomass. EDX analysis showed that internal CuO distribution inside the particles was uniform and was unchanged. Moreover, the rich alkali metal composition of the biomass ashes (see Table 2) had the potential to produce agglomeration problems in the fuel reactor, owing to bed sintering that can block solid circulation between reactors. Fig. 6(c) of the used oxygen carrier particles shows that no agglomerate resulted from the interaction between the ash compounds and the oxygen carrier, which was in line with the avoidance of tendency towards agglomeration during all the operating time. It must be pointed out that the oxygen carrier particles never showed agglomeration problems, even when the oxygen carrier was highly reduced. EDX analysis of the used particles, Fig. 6(d), was conducted on the surface of the particles in order to test for the presence of alkali metals from biomass ashes (Ca, K, P, Na). No evidence was found of ash deposition on the oxygen carrier particles, being the EDX profile similar to that obtained for fresh particles; see Fig. 6(b). However, it is necessary to highlight that the combination of a short operating time (10 h) and the elutriation of the ash particles would result in a low contacting time between ash and oxygen carrier particles, which could be not representative of the behavior in an industrial CLOU unit. Specific test would be requested to assess the interaction of ash component with oxygen carrier particles.

In addition, a reduction was found in the crushing strength of the particles as operation time increased, which agreed with previous results found with this material [25]. The reduction in the crushing

strength of the particles was associated with an increase in porosity as the operation time in the CLOU unit increased, see Table 1. The durability of this material was in line with results shown in a previous work [25], where the crushing strength decreased to 1.5 N after 18 h of operation. However, fines particles ( $<40\ \mu\text{m}$ ) were not found neither in the fuel reactor nor in the air reactor. No differences on the evolution of these properties were observed whatever coal or biomass was used as fuel.

#### 4. Discussion

From results presented in this work, char conversion in the fuel reactor is a relevant issue affecting  $\text{CO}_2$  capture efficiency in the CLOU process, even where a fuel with a high volatile content is used, as it is the case of biomass. In order to analyze the conversion degree of biomass char in the CLC technology, a deep study was carried out that included char conversion rates obtained in the CLOU process when different fuels were used. Thus, carbon capture efficiency was analyzed by means of the fractional conversion rate of char of different solid fuels, including data from Adánez-Rubio et al. [26] for coals ranging from anthracite to lignite. Also the biomass char conversion rate obtained from the *iG*-CLC process by Mendiara et al. [29] was considered for comparison purposes.

The fractional conversion rate of char per unit of carbon mass in char can be used to carry out a comparison between the different fuels, because char conversion in the fuel reactor, and hence carbon capture, depends directly on this rate. Fig. 7 shows the fractional conversion rate of char as a function of temperature calculated using Eq. (18) for the biomass and coal fuels used in the CLOU unit [26]. As expected, the fractional conversion rate of char increased with temperature. It can be observed that the conversion rate for biomass char in the CLOU process was very similar to that obtained for lignite, the most reactive coal tested in the CLOU unit. This high conversion rate for biomass char, together with the large amount of volatile matter content in biomass, allows very high carbon capture efficiencies to be achieved, even higher than those obtained for lignite under the same conditions. In addition, the biomass char conversion rate in CLOU was higher than that obtained in *iG*-CLC. The char conversion rate for biomass in the CLOU process was 3 to 4 times higher than that obtained in the *iG*-CLC process at temperatures equal to or higher than  $900\ ^\circ\text{C}$ . This was due to the different char conversion mechanisms. In CLOU, char was converted by combustion with gaseous oxygen, while *iG*-CLC involved a slow char gasification process with steam or  $\text{CO}_2$ . This higher char conversion rate in the CLOU process explained the lower oxygen carrier inventories needed in CLOU ( $565\ \text{kg}/\text{MW}_{\text{th}}$ ) compared to those required by *iG*-CLC ( $1550\ \text{kg}/\text{MW}_{\text{th}}$ ) [29] to obtain similar carbon capture efficiencies (97.5/99%). However, at the lowest temperature for CLOU

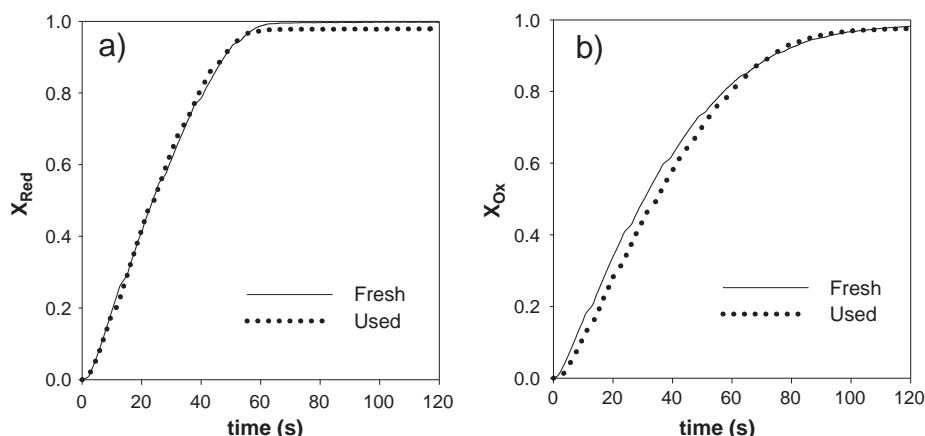


Fig. 5. Conversion vs time curves for (a) reduction and (b) oxidation reactions for fresh and used particles. Reduction in  $\text{N}_2$  and oxidation in air at  $1000\ ^\circ\text{C}$  in TGA.

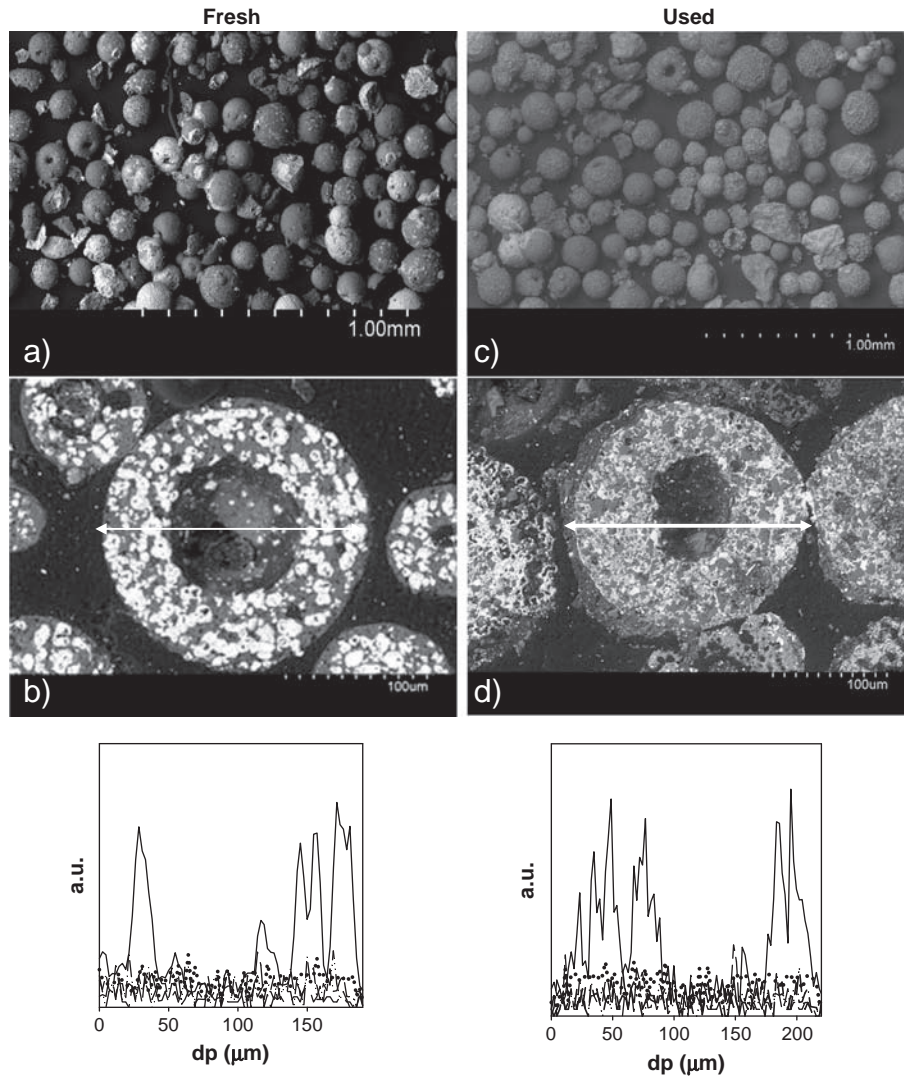


Fig. 6. SEM images of fresh (right) and used (left) particles after 10 h in CLOU unit: (a, c) image of the particles; (b, d) image and EDX line profile of Cu (—), Ca (---), K (---), P (---), and Na (····) in a cross section of a particle.

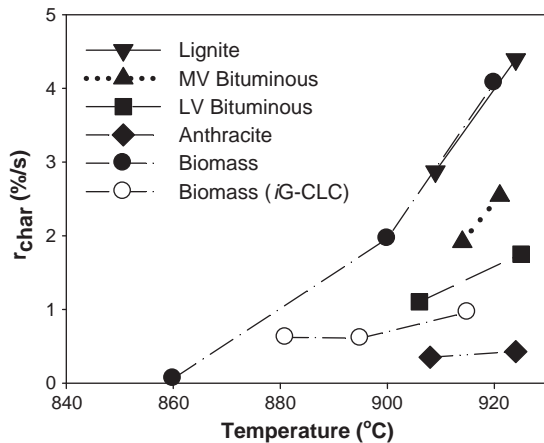


Fig. 7. Experimental fractional conversion rate of char different fuels as a function of fuel reactor temperature: biomass in CLOU process (—●—), biomass in iG-CLC process (---○---) [29], lignite (---▼---) [26], MV bituminous (---▲---) [26], LV bituminous (---■---) [26], and anthracite (---◆---) [26].

process (860 °C) the char conversion rate was lower than the rate for iG-CLC. This may be due to: (a) no gasification agent (steam or CO<sub>2</sub>) is fed into the CLOU fuel reactor, and (b) there was no gaseous oxygen at this temperature to burn the char.

Char conversion in the fuel reactor can be calculated as a function of the solid inventory, solid circulation rate and char conversion rate as follows [26]:

$$X_{\text{char}} = 1 - \frac{\dot{m}_{\text{OC}}(1 - \eta_{\text{CCS}})}{(-r_{\text{C}}) \cdot m_{\text{s,FR}} + \dot{m}_{\text{OC}}(1 - \eta_{\text{CCS}})} \quad (21)$$

In Eq. (21), the incorporation of a carbon separation system, similar to the iG-CLC process, was considered by using the parameter  $\eta_{\text{CCS}}$ , i.e. carbon separation system efficiency. Carbon capture efficiency is related to the char conversion through the following equation:

$$\eta_{\text{CC}} = \frac{f_{\text{C,vol}} + \frac{f_{\text{C,char}}}{f_{\text{C}}} \cdot X_{\text{char}}}{f_{\text{C}}} = \frac{f_{\text{C}} - f_{\text{C,fix}}}{f_{\text{C}}} + \frac{f_{\text{C,fix}}}{f_{\text{C}}} X_{\text{char}} \quad (22)$$

Using Eqs. (21) and (22), it was possible to analyze the effect of the oxygen carrier inventory on char conversion and carbon capture

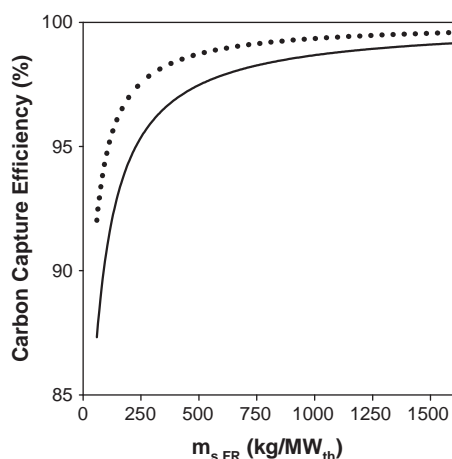


Fig. 8. Carbon capture efficiency as a function of the fuel reactor inventory for biomass at two different temperatures in the fuel reactor: 900 °C (—), 920 °C (---).  $\eta_{\text{CSS}} = 0$ ;  $\phi = 1.1$ .

efficiency in the system, once the value of  $(-r_c)$  was known. In this analysis, the residence time of solids was maximized by operating at a value of the oxygen carrier to fuel ratio,  $\phi = 1.1$ , thus maximizing the  $\text{CO}_2$  capture rate in a CLC unit [18,39]. Therefore, the solid circulation flow rate per  $\text{MW}_{\text{th}}$  of fuel was fixed. With regard to the CLOU process with biomass, Fig. 8 shows carbon capture efficiency as a function of the oxygen carrier inventory in the fuel reactor for two different fuel reactor temperatures without implementing a carbon separation system ( $\eta_{\text{CSS}} = 0$ ). Carbon capture efficiency increased with the fuel reactor solid inventory due to the increase in char conversion. An increase in the fuel reactor temperature also increased the char conversion rate. It is evident that a carbon capture efficiency higher than 95% can be achieved with a very low amount of oxygen carrier inventories (230 and 110  $\text{kg}/\text{MW}_{\text{th}}$  for 900 and 920 °C, respectively). Therefore, the use of a carbon separation system is not necessary for the CLOU process when biomass is used as fuel.

## 5. Conclusions

The performance of CLOU burning a biomass fuel with a Cu-based oxygen carrier was analyzed in a continuous unit. A fuel reactor temperature higher than 900 °C was required to exploit the oxygen uncoupling benefits and resulting in no unburnt compounds at the fuel reactor outlet. Complete combustion and 100%  $\text{CO}_2$  capture efficiency were achieved at a fuel reactor temperature of 935 °C using a low solid fuel reactor inventory. The conversion rate of biomass char was analyzed, and for the CLOU process it was found to be very similar to that obtained with lignite. Moreover, the char conversion rate of biomass in the CLOU process is between 3 and 4 times higher than that corresponding to the iG-CLC process at temperatures above 900 °C.

With the results obtained in the continuous CLOU unit, an optimization of the CLOU process was carried out to maximize  $\text{CO}_2$  capture efficiency with a minimum solid inventory. A carbon capture efficiency higher than 95% can be achieved with a very low amount of oxygen carrier inventories (230 and 110  $\text{kg}/\text{MW}_{\text{th}}$  for 900 and 920 °C respectively) and without the need for a carbon separation system. These encouraging results, first obtained with pine wood biomass in the CLOU process, indicate that a study should be carried out on the use of other types of biomass fuels with CLC technology.

## Notation

### Symbols

$F_i$	molar flow of compound $i$ (mol/s)
$f_c$	mass fraction of carbon in coal (—)
$f_{c,\text{fix}}$	mass fraction of fixed carbon in biomass (—)

$f_{c,\text{vol}}$	mass fraction of carbon in volatiles (—)
$f_i$	mass fraction in fuel of element or compound $i$ (—)
$M_i$	atomic or molecular weight of $i$ elements or compounds (kg/mol)
$\dot{m}_{\text{SF}}$	mass-based flow of solid fuel fed into the fuel reactor (kg/s)
$\dot{m}_{\text{OC}}$	solid circulation rate (kg/s)
$m_{\text{ox}}$	mass of the fully oxidized oxygen carrier sample (kg)
$m_{\text{red}}$	mass of the fully reduced oxygen carrier sample (kg)
$m_{s,\text{FR}}$	mass of solids in the fuel reactor (kg)
$(-r_c)$	fractional conversion rate of the char ( $\text{s}^{-1}$ )
$\tau_{\text{char}}$	mean residence time of char particles in the fuel reactor (s)
$\tau_{\text{FR}}$	mean residence time of solids in the fuel reactor (s)
$R_{\text{OC}}$	oxygen transport capacity (—)
$X_{\text{char}}$	carbon conversion in char particles (—)
$y_i$	molar fraction of the gas $i$ (—)

### Greek letters

$\eta_{\text{CC}}$	$\text{CO}_2$ capture efficiency (—)
$\eta_{\text{comb,FR}}$	combustion efficiency in the fuel reactor (—)
$\eta_{\text{CSS}}$	efficiency of the carbon separation system (—)
$\lambda$	air excess ratio (—)
$\phi$	oxygen carrier to fuel ratio (—)
$\Omega_{\text{SF}}$	stoichiometric mass of $\text{O}_2$ to convert 1 kg of solid fuel (kg/kg)

### Subscripts

AR	air reactor
char	carbon in char particles
elut	elutriated particles from fuel reactor
FR	fuel reactor
inAR	inlet stream to air reactor
inFR	inlet stream to fuel reactor
outAR	outlet stream from air reactor
outFR	outlet stream from fuel reactor
OC	oxygen carrier
SF	solid fuel
vol	volatile matter

### Acronyms

BET	Brunauer–Emmett–Teller
CCS	$\text{CO}_2$ capture and storage
CLC	chemical looping combustion
CLOU	chemical looping with oxygen uncoupling
IPCC	Intergovernmental Panel on Climate Change
LHV	low heating value (kJ/kg)
TGA	thermogravimetric analyzer
XRD	X-ray diffractometer

## Acknowledgments

This work was partially supported by the European Commission, under the RFCS program (ACCLAIM Project, Contract RFCP-CT-2012-00006), and by the Spanish MICINN (ENE2011-26354). I. Adánez-Rubio thanks CSIC for the JAE fellowship co-financed by the European Social Fund.

## References

- [1] IPCC, IPCC special report on carbon dioxide capture and storage, in: B. Metz, O. Davidson, H.C. de Coninck, M. Loos, L.A. Meyer (Eds.), Working Group III of the Intergovernmental Panel on Climate Change, Cambridge University, 2005.
- [2] H.R. Kerr, Carbon dioxide capture for storage in deep geologic formations, in: D.C. Thomas, S.M. Benson (Eds.), Capture and Separation Technology Gaps and Priority Research Needs, Elsevier Science, Amsterdam, 2005, pp. 655–660.
- [3] H.M. Kvamsdal, K. Jordal, O. Bolland, A quantitative comparison of gas turbine cycles with  $\text{CO}_2$  capture, Energy 32 (1) (2007) 10–24.

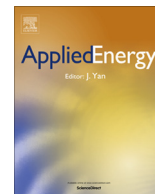
- [4] J. Adáñez, A. Abad, F. García-Labiano, P. Gayán, L.F. de Diego, Progress in chemical-looping combustion and reforming technologies, *Progress in Energy and Combustion Science* 38 (2012) 215–282.
- [5] A. Lyngfelt, Oxygen carriers for chemical looping combustion — 4000 h of operational experience, *Oil & Gas Science and Technology* 66 (2011) 161–172.
- [6] Y. Cao, W.P. Pan, Investigation of chemical looping combustion by solid fuels. 1. Process analysis, *Energy & Fuels* 20 (2006) 57–68.
- [7] S.A. Scott, J.S. Dennis, A.N. Hayhurst, T. Brown, In situ gasification of a solid fuel and CO<sub>2</sub> separation using chemical looping, *AIChE Journal* 52 (2006) 3325–3328.
- [8] N. Berguerand, A. Lyngfelt, Design and operation of a 10 kW<sub>th</sub> chemical-looping combustor for solid fuels — testing with South African coal, *Fuel* 87 (2008) 2713–2726.
- [9] L. Shen, J. Wu, J. Xiao, Experiments on chemical looping combustion of coal with a NiO based oxygen carrier, *Combustion and Flame* 156 (2009) 721–728.
- [10] P. Markström, C. Linderholm, A. Lyngfelt, Chemical-looping combustion of solid fuels — design and operation of a 100 kW<sub>th</sub> unit with bituminous coal, *International Journal of Greenhouse Gas Control* 15 (2013) 150–162.
- [11] A. Cuadrat, A. Abad, F. García-Labiano, P. Gayán, L.F. de Diego, J. Adáñez, Relevance of the coal rank on the performance of the in-situ gasification chemical-looping combustion, *Chemical Engineering Journal* 195–196 (2012) 91–102.
- [12] P. Gayán, A. Abad, L.F. de Diego, F. García-Labiano, J. Adáñez, Assessment of technological solutions for improving chemical looping combustion of solid fuel with CO<sub>2</sub> capture, *Chemical Engineering Journal* 233 (2013) 56–69.
- [13] T. Mattisson, A. Lyngfelt, H. Leion, Chemical-looping oxygen uncoupling for combustion of solid fuels, *International Journal of Greenhouse Gas Control* 3 (2009) 11–19.
- [14] W.K. Lewis, E.R. Gilliland, Production of pure carbon dioxide. Patent 2665972, (1954).
- [15] A. Abad, I. Adáñez-Rubio, P. Gayán, F. García-Labiano, L.F. de Diego, J. Adáñez, Demonstration of chemical-looping with oxygen uncoupling (CLOU) process in a 1.5 kW<sub>th</sub> continuously operating unit using a Cu-based oxygen-carrier, *International Journal of Greenhouse Gas Control* 6 (2012) 189–200.
- [16] I. Adáñez-Rubio, P. Gayán, A. Abad, L.F. de Diego, F. García-Labiano, J. Adáñez, Identification of operational regions in the chemical-looping with oxygen uncoupling (CLOU) process with a Cu-based oxygen-carrier, *Fuel* 102 (2012) 634–645.
- [17] A. Cuadrat, A. Abad, L.F. de Diego, F. García-Labiano, P. Gayán, J. Adáñez, Prompt considerations on the design of chemical-looping combustion of coal from experimental tests, *Fuel* 97 (2012) 219–232.
- [18] A. Cuadrat, A. Abad, P. Gayán, L.F. de Diego, F. García-Labiano, J. Adáñez, Theoretical approach on the CLC performance with solid fuels: optimizing the solids inventory, *Fuel* 97 (2012) 536–551.
- [19] A. Abad, P. Gayán, L.F. de Diego, F. García-Labiano, J. Adáñez, Fuel reactor modelling in chemical-looping combustion of coal: 1. Model formulation, *Chemical Engineering Science* 87 (2013) 277–293.
- [20] F. García-Labiano, L.F. de Diego, P. Gayán, A. Abad, J. Adáñez, Fuel reactor modelling in chemical-looping combustion of coal: 2. Simulation and optimization, *Chemical Engineering Science* 87 (2013) 173–182.
- [21] P. Gayán, I. Adáñez-Rubio, A. Abad, L.F. de Diego, F. García-Labiano, J. Adáñez, Development of CuO-based oxygen-carrier materials suitable for chemical-looping with oxygen uncoupling (CLOU) process, *Fuel* 96 (2012) 226–238.
- [22] I. Adáñez-Rubio, M. Arjmand, H. Leion, P. Gayán, A. Abad, T. Mattisson, A. Lyngfelt, Investigation of combined supports for Cu-based oxygen carriers for chemical-looping with oxygen uncoupling (CLOU), *Energy & Fuels* 27 (2013) 3918–3927.
- [23] T. Mattisson, Materials for chemical-looping with oxygen uncoupling, *ISRN Chemical Engineering* (2013), <http://dx.doi.org/10.1155/2013/526375> (Article ID 526375).
- [24] Q. Imtiaz, D. Hosseini, C.R. Müller, Review of oxygen carriers for chemical looping with oxygen uncoupling (CLOU): thermodynamics, material development, and synthesis, *Energy Technology* 1 (2013) 633–647.
- [25] I. Adáñez-Rubio, P. Gayán, A. Abad, L.F. de Diego, F. García-Labiano, J. Adáñez, Evaluation of a spray-dried CuO/MgAl<sub>2</sub>O<sub>4</sub> oxygen carrier for the chemical looping with oxygen uncoupling process, *Energy & Fuels* 26 (2012) 3069–3081.
- [26] I. Adáñez-Rubio, A. Abad, P. Gayán, L.F. de Diego, F. García-Labiano, J. Adáñez, Performance of CLOU process in the combustion of different types of coal with CO<sub>2</sub> capture, *International Journal of Greenhouse Gas Control* 12 (2013) 430–440.
- [27] I. Adáñez-Rubio, A. Abad, P. Gayán, F. García-Labiano, L.F. de Diego, J. Adáñez, The fate of sulphur in the Cu-based chemical looping with oxygen uncoupling (CLOU) process, *Applied Energy* 113 (2014) 1855–1862.
- [28] H. Gu, L. Sheng, J. Xiao, S. Zhang, T. Song, Chemical looping combustion of biomass/coal with natural iron ore as oxygen carrier in a continuous reactor, *Energy & Fuels* 25 (2011) 446–455.
- [29] T. Mendiara, A. Abad, L.F. de Diego, F. García-Labiano, P. Gayán, J. Adáñez, Biomass combustion in a CLC system using an iron ore as oxygen carrier, *International Journal of Greenhouse Gas Control* 19 (2013) 322–330.
- [30] L. Shen, J. Wu, J. Xiao, Q. Song, R. Xiao, Chemical-looping combustion of biomass in a 10 kW<sub>th</sub> reactor with iron oxide as an oxygen carrier, *Energy & Fuels* 23 (2009) 2498–2505.
- [31] P. Simell, P. Stahlberg, E. Kurkela, J. Albrecht, S. Deutch, K. Sjöstrom, Provisional protocol for the sampling and analysis of tar and particulates in the gas from large-scale biomass gasifiers, version 1998, *Biomass and Bioenergy* 18 (2000) 19–38.
- [32] J. Adáñez, P. Gayán, L.F. de Diego, F. García-Labiano, A. Abad, Combustion of wood chips in a CFBC. Modeling and validation, *Industrial and Engineering Chemistry Research* 42 (5) (2003) 987–999.
- [33] T.B. Reed, B. Levie, M.S. Graboski, Tar conversion, Fundamentals, Development and Scaleup of the Air–Oxygen Stratified Downdraft Gasifier, Solar Energy Research Institute, 1987, (SERI/PR-234-2571).
- [34] T. Mendiara, M.T. Izquierdo, A. Abad, L.F. de Diego, F. García-Labiano, P. Gayán, J. Adáñez, Release of pollutant components in CLC of lignite, *Int. J. Greenhouse Gas Control* 22 (2013) 15–24.
- [35] A. Cuadrat, A. Abad, F. García-Labiano, P. Gayán, L.F. de Diego, J. Adáñez, The use of ilmenite as oxygen-carrier in a 500 W<sub>th</sub> chemical-looping coal combustion unit, *International Journal of Greenhouse Gas Control* 5 (2011) 1630–1642.
- [36] I. Adáñez-Rubio, P. Gayán, A. Abad, F. García-Labiano, L.F. de Diego, J. Adáñez, Kinetics of a Cu-based Oxygen Carrier for Chemical Looping With Oxygen Uncoupling (CLOU): Relevance of Temperature and Oxygen Partial Pressure on Reduction and Oxidation, 2014. (submitted for publication).
- [37] J. Adáñez, P. Gayán, J. Celaya, L.F. de Diego, F. García-Labiano, A. Abad, Chemical looping combustion in a 10 kW<sub>th</sub> prototype using a CuO/Al<sub>2</sub>O<sub>3</sub> oxygen carrier: effect of operating conditions on methane combustion, *Industrial and Engineering Chemistry Research* 45 (17) (2006) 75–80.
- [38] C.R. Forero, P. Gayán, L.F. de Diego, A. Abad, F. García-Labiano, J. Adáñez, Syngas combustion in a 500 W<sub>th</sub> chemical-looping combustion system using an impregnated Cu-based oxygen carrier, *Fuel Processing Technology* 90 (2009) 1471–1479.
- [39] A. Cuadrat, A. Abad, F. García-Labiano, P. Gayán, L.F. de Diego, J. Adáñez, Effect of operating conditions in chemical-looping combustion of coal in a 500 W<sub>th</sub> unit, *International Journal of Greenhouse Gas Control* 6 (2012) 153–163.



## **Paper VIII**







# The fate of sulphur in the Cu-based Chemical Looping with Oxygen Uncoupling (CLOU) Process



Iñaki Adánez-Rubio, Alberto Abad, Pilar Gayán\*, Francisco García-Labiano, Luis F. de Diego, Juan Adánez

*Instituto de Carboquímica (ICB-CSIC), Dept. of Energy & Environment, Miguel Luesma Castán 4, Zaragoza 50018, Spain*

## HIGHLIGHTS

- 15 h of CLOU experiments using lignite were carried out in a continuously unit.
- The sulphur split between fuel- and air-reactor streams in the process was analysed.
- Most of the sulphur introduced with the fuel exits as SO<sub>2</sub> at the fuel-reactor.
- The use of a carbon separation system to reduce the S emission was evaluated.
- Coals with high S content can be burnt in a CLOU process with a Cu-based material.

## ARTICLE INFO

### Article history:

Received 17 December 2012  
 Received in revised form 11 June 2013  
 Accepted 12 June 2013  
 Available online 3 July 2013

### Keywords:

CO<sub>2</sub> capture  
 Cu-based oxygen carrier  
 CLOU  
 Coal  
 Sulphur

## ABSTRACT

The Chemical Looping with Oxygen Uncoupling (CLOU) process is a type of Chemical Looping Combustion (CLC) technology that allows the combustion of solid fuels with air, as with conventional combustion, through the use of oxygen carriers that release gaseous oxygen inside the fuel reactor. The aim of this work was to study the behaviour of the sulphur present in fuel during CLOU combustion. Experiments using lignite as fuel were carried out in a continuously operated 1.5 kW<sub>th</sub> CLOU unit during more than 15 h. Particles containing 60 wt.% CuO on MgAl<sub>2</sub>O<sub>4</sub>, prepared by spray drying, were used as the oxygen carrier in the CLOU process. The temperature in the fuel reactor varied between 900 and 935 °C. CO<sub>2</sub> capture, combustion efficiency and the sulphur split between fuel and air reactor streams in the process were analysed. Complete combustion of the fuel to CO<sub>2</sub> and H<sub>2</sub>O was found in all experiments. Most of the sulphur introduced with the fuel exited as SO<sub>2</sub> at the fuel reactor outlet, although a small amount of SO<sub>2</sub> was measured at the air reactor outlet. The SO<sub>2</sub> concentration in the air reactor exit flow decreased as the temperature in the fuel reactor increased. A carbon capture efficiency of 97.6% was achieved at 935 °C, with 87.9 wt.% of the total sulphur exiting as SO<sub>2</sub> in the fuel reactor. Both the reactivity and oxygen transport capacity of the oxygen carrier were unaffected during operation with a high sulphur content fuel, and agglomeration problems did not occur. Predictions were calculated regarding the use of a carbon separation system in the CLOU process in order to reduce sulphur emissions. Coals with high sulphur content, such as lignite and anthracite, would require a carbon separation system in order to comply with legislation governing sulphur-limits. In conclusion, coals with a high sulphur content can be burnt in a CLOU process using Cu-based material to obtain high carbon capture efficiencies.

© 2013 Elsevier Ltd. All rights reserved.

## 1. Introduction

The Chemical-Looping with Oxygen Uncoupling (CLOU) process is a type of Chemical-Looping Combustion (CLC) technology that allows the combustion of solid fuels with inherent CO<sub>2</sub> separation using oxygen-carriers. CLOU technology may be particularly suitable for solid fuels, such as coal, petroleum coke and biomass. CLOU technology takes advantage of the property of a number of metal oxides for generating gaseous oxygen at high temperatures.

The oxygen generated by the oxygen carrier reacts directly with the solid fuel, which is mixed with the oxygen-carrier in the fuel reactor. The oxygen carriers for CLOU must first have the ability to react with oxygen inside the air reactor, and then to release this oxygen through decomposition inside the fuel reactor. Three metal oxide systems were found to have suitable properties for use as oxygen carriers in the CLOU process: CuO/Cu<sub>2</sub>O, Mn<sub>2</sub>O<sub>3</sub>/Mn<sub>3</sub>O<sub>4</sub>, and Co<sub>3</sub>O<sub>4</sub>/CoO [1].

An analysis of the suitability of different Cu-based materials was previously performed at ICB-CSIC [2,3]. Particles prepared by several methods with different supporting materials and different metal oxide contents were tested. Particles of 60 wt.% CuO were

\* Corresponding author. Tel.: +34 976 733977; fax: +34 976 733318.  
 E-mail address: [pgayan@icb.csic.es](mailto:pgayan@icb.csic.es) (P. Gayán).



**Table 2**  
Properties of lignite coal and its char, as received basis.

	Lignite	Char
C	45.4%	55.8%
H	2.5%	0.4%
N	0.6%	0.5%
S	5.2%	5.03%
O <sup>a</sup>	8.5%	–
Moisture	12.6%	0.52%
Volatile matter	28.6%	1.17%
Fixed carbon	33.6%	54.8%
Ash	25.2%	43.5%
LHV (kJ/kg)	16,250	

<sup>a</sup> Oxygen to balance.

gas, and the gas flow was 186 L<sub>N</sub>/h, corresponding to a gas velocity of 0.11 m/s at 900 °C. The minimum fluidizing velocities of the oxygen carrier particles were 0.006 m/s for the smallest particle size and 0.023 m/s for the largest. Coal was fed by a screw feeder at the bottom of the bed, right above the fuel reactor distributor plate, in order to maximise the time that the fuel and volatile matter were in contact with the bed material.

The oxidation of the carrier took place in the air reactor, consisting of a bubbling fluidized bed with an 8 cm inner diameter and 10 cm bed height, followed by a riser. The air flow was 1740 L<sub>N</sub>/h ( $u_g = 0.40$  m/s). In addition, a secondary air flow (240 L<sub>N</sub>/h) was introduced at the top of the bubbling bed to help particle entrainment through a riser. The total oxygen carrier inventory in the system was around 2.0 kg, with about 0.5–0.6 kg of this in the fuel reactor. The amount of solids in the fuel reactor was calculated from pressure drop measurements in the reactor for each test. Detailed information about the plant and the experimental conditions can be found in [4,5].

CO, CO<sub>2</sub>, H<sub>2</sub>, CH<sub>4</sub>, SO<sub>2</sub>, and O<sub>2</sub> were continuously analysed in the fuel reactor outlet stream, whereas CO<sub>2</sub>, CO, SO<sub>2</sub> and O<sub>2</sub> were continuously analysed in the air reactor flue gases by means of infrared, paramagnetic and conductivity analysers. H<sub>2</sub>S was analysed by GC.

To determine the effect of S on the behaviour of the oxygen carrier, several tests were performed under continuous operation. The fuel reactor temperature was varied between 900 °C and 935 °C. The temperature in the air reactor was kept at around 900 °C in all experiments. The solids circulation rate was kept at a mean value of 3 kg/h, whereas the coal feeding rate was 0.12 kg/h, which corresponded to an oxygen carrier to fuel ratio,  $\phi$ , of 1.2.

To analyse the performance of the CLOU process, the combustion efficiency in the fuel reactor and the carbon capture efficiency were also calculated. Calculations were based on the molar flow of every gas analysed,  $F_i$ , which was determined from the measured concentration. Mass balances were checked and a closing of about 98% was found for the C balance in all cases.

The combustion efficiency in the fuel reactor was calculated through the ratio between the oxygen required to fully burn unconverted gases (CH<sub>4</sub>, CO and H<sub>2</sub>) at the fuel reactor exit and the oxygen required by coal converted in the fuel reactor. Thus, the oxygen required by the C bypassed to the air reactor,  $F_{CO_2,AR}$ , was subtracted from the oxygen required by coal in the denominator. Therefore, the combustion efficiency in the fuel reactor was calculated as:

$$\eta_{\text{comb,FR}} = 1 - \frac{4F_{\text{CH}_4,\text{outFR}} + F_{\text{CO},\text{outFR}} + F_{\text{H}_2,\text{outFR}}}{\frac{1}{M_O} \Omega_{\text{coal}} \dot{m}_{\text{coal}} - 2F_{\text{CO}_2,\text{outAR}}} \quad (1)$$

The carbon capture efficiency,  $\eta_{CC}$ , was defined as the fraction of C initially present in the coal fed into the system which was actually at the outlet of fuel reactor. This was the actual CO<sub>2</sub> captured in the CLOU system; the rest exited together with nitrogen through the air reactor outlet.

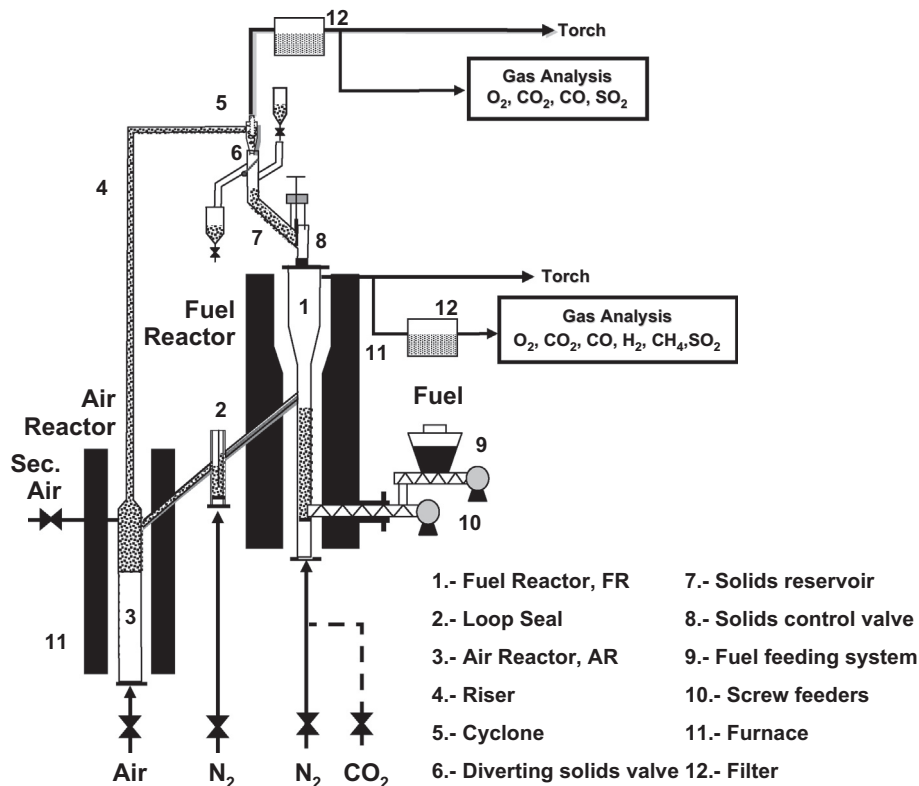


**Fig. 1.** Schematic view of the ICB-CSIC-s1 unit for coal-fuelled CLOU (1.5 kW<sub>th</sub>).

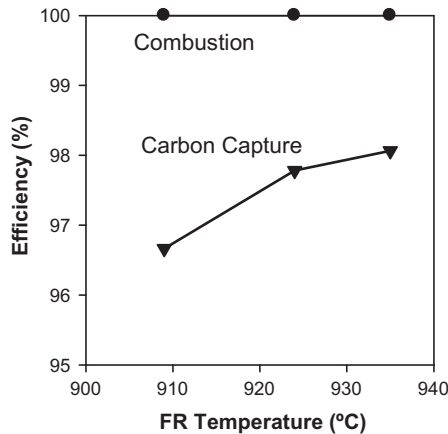


Fig. 2. Effect of the fuel reactor temperature on the combustion efficiency in the fuel reactor (●) and carbon capture efficiency (▼).

$$\eta_{CC} = 1 - \frac{F_{CO_2, outAR}}{F_{CO_2, outFR} + F_{CO, outFR} + F_{CH_4, outFR} + F_{CO_2, outAR}} \quad (2)$$

The mass balance of S was calculated as:

$$f_S \cdot \dot{m}_{coal} = M_S(F_{SO_2, outFR} + F_{SO_2, outAR}) + S_{ash} \quad (3)$$

With the molar flow of  $SO_2$  exiting from the air reactor and the total volume gas flow, the concentration of  $SO_2$  as  $mg/N\ m^3$  was calculated and normalised. EU legislation [11] requires the  $SO_2$  concentration to be normalised using 6%  $O_2$  in the exit stream for power plants, which contains 15%  $CO_2$ .

### 2.3. Batch fluidized-bed reactor

A batch fluidized bed reactor is used to provide a deep analysis of the evolution of S over time during coal combustion. The experimental work was carried out in a set-up consisting of a fluidized-bed reactor, a gas feed system, a solid fuel feed system and a gas analysis system. The reactor – 55 mm inner diameter and 700 mm height – was electrically heated by a furnace, and had a preheating zone just under the distributor plate [12].

A 20 g batch of fuel was burnt in the batch fluidized-bed reactor using a sand bed with a particle size of +200–300  $\mu m$ . The total fluidizing flow was 200  $L_N/h$ , corresponding to a gas velocity of 0.1 m/s at the reactor temperature, which is three times the minimum

fluidization velocity of largest sand particles. The bed was heated in  $N_2$  until 925 °C. The volatile products were burnt in an afterburner reactor using a 7%  $O_2$  concentration. Char combustion was carried out at 925 °C using 2.5%  $O_2$ . A relatively low  $O_2$  concentration was used to simulate fuel reactor conditions in the CLOU unit, where there was a much lower  $O_2$  concentration than that found in a typical air-fired combustor.  $SO_2$ ,  $CO_2$  and  $CO$  gas concentrations were continuously measured.

## 3. Results

### 3.1. Combustion behaviour

During 15 h of combustion operation, no  $CH_4$ ,  $CO$ ,  $H_2S$  or  $H_2$  were detected in the gases exiting from the fuel reactor. The possible presence of tars or light hydrocarbons was also analysed. For one experiment with conditions kept constant for more than two hours, tar measurements in the fuel reactor were taken using a tar protocol [13,14]. The results showed that there were no tars, i.e. no hydrocarbons heavier than  $C_5$ , in the fuel reactor outlet flow. Thus,  $CO_2$ ,  $H_2O$ ,  $SO_2$  and  $O_2$  were the main gases, together the  $N_2$  introduced as fluidizing gas, exiting the fuel reactor. Therefore, volatiles were fully converted into  $CO_2$  and  $H_2O$  in the fuel reactor by reaction with the oxygen released from  $CuO$  decomposition. In addition, the oxygen release rate was high enough to supply an excess of gaseous oxygen ( $O_2$ ) exiting together with the combustion gases at equilibrium concentration at each temperature, with the oxygen concentration at equilibrium conditions being 1.7% at 910 °C, 2.4% at 925 °C, 3.0% at 935 °C.

Fig. 2 shows the effect of the fuel reactor temperature on combustion and carbon capture efficiencies. It can be seen that complete combustion to  $CO_2$  and  $H_2O$  was always achieved. The carbon capture efficiency increased when the fuel reactor temperature increased because of an increase in the char combustion rate. Thus, less char was transferred to the air reactor.

### 3.2. Sulphur emissions

Fig. 3 shows the distribution of S between both reactor exits as a function of the fuel reactor temperature. It can be seen that the S mainly exited as  $SO_2$  in the fuel reactor stream and that the amount increased with increasing temperature, with a corresponding decrease in the amount of  $SO_2$  exiting from the air reactor. This effect was due to increases in char conversion and therefore more S

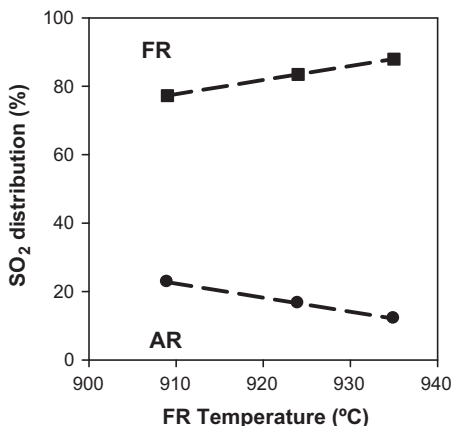


Fig. 3. S distribution in the continuous CLOU plant at the fuel reactor (■) and air reactor (●) outlets.

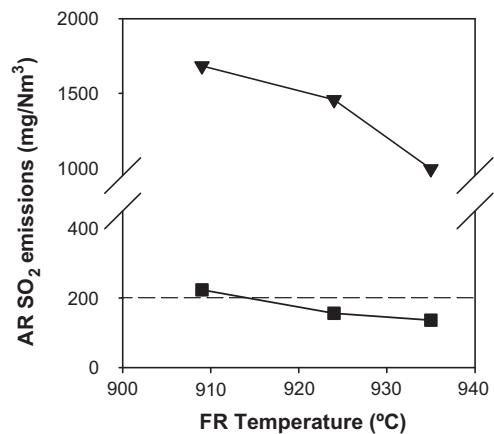


Fig. 4. Effect of the fuel reactor temperature on  $SO_2$  emissions normalised at 6%  $O_2$  in the air reactor: (▼) measures in CLOU unit and (■) calculated using a uniform S release during char conversion; EU legal  $SO_2$  emission limit (---).

being released in the fuel reactor and less S being transferred with the char to the air reactor. SO<sub>2</sub> concentration in the fuel reactor (dry basis) varied between 2400 ppmv at 910 °C and 3000 ppmv at 935 °C.

Fig. 4 shows SO<sub>2</sub> emissions in the air reactor in normalised mg/N m<sup>3</sup> as a function of the fuel reactor temperature. The EU SO<sub>2</sub> emission limits for new coal power plants (>300 MW<sub>th</sub>) are also depicted [11]. It can be seen that SO<sub>2</sub> emissions in the air reactor decreased with increasing temperature. This effect was due to more char being converted in the fuel reactor as the temperature increased. Although, the SO<sub>2</sub> concentration exiting the air reactor stream was lower than 10% of the total S fed at 935 °C, the value of the SO<sub>2</sub> emission was still too high and exceeded the EU legal limit of 200 mg/N m<sup>3</sup>. Note that direct combustion of this coal with air would have produced SO<sub>2</sub> emissions of >20,000 mg/N m<sup>3</sup>.

The amount of char transferred to the air reactor could be determined from the char conversion values measured in the fuel reactor. Therefore, the S emitted as SO<sub>2</sub> in the air reactor could be calculated, assuming a S/C ratio that was constant and equal to the analysis of the nascent char, Fig. 4 shows the corresponding SO<sub>2</sub> emissions assuming a constant S/C ratio in char throughout the combustion time of the char in the fuel reactor. As can be seen, these calculated SO<sub>2</sub> emissions are much lower than the measured ones. This fact could be due to two different effects: S was transferred to the air reactor in the oxygen carrier particles by S reaction with Cu, or S was concentrated in the unburnt char transferred to the air reactor.

To analyse whether the S was concentrated in the char, a detailed study of the S release during char combustion was carried out in the batch fluidized-bed reactor installation. Fig. 5 shows the profiles of C and SO<sub>2</sub> gas concentration at the outlet of the batch reactor during pyrolysis and followed by combustion of the generated char. The mass balance of the exiting gases indicates that 43.1 wt.% of the S exited from the devolatilization and that 56.9 wt.% exited during the char combustion. On the one hand, it can be seen that the S and C in the volatiles evolved at the same rate during devolatilization. However, the S and C profiles were different during char combustion. During char combustion, the SO<sub>2</sub> generation rate was at its peak when almost all the C in the char had been burnt. At this time, the S/C ratio in the char increased by a factor of 10 with respect to the S/C ratio measured in the char analysis. This behaviour could be explained as a result of the high pyritic S (2 wt.%) present in this lignite. At a low O<sub>2</sub> concentration environment, as was the case in the CLOU process, there is competition for oxygen between the C and the pyritic S. As a consequence, C combustion is favoured over pyrite oxidation [15].

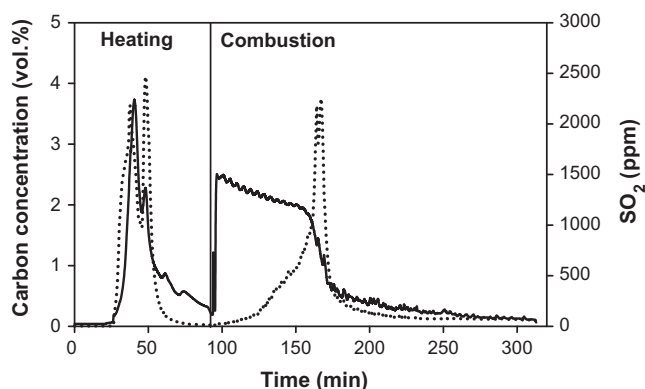


Fig. 5. Gas outlet concentrations of C(–) and SO<sub>2</sub> (···) from the batch fluidized-bed reactor. Heating: N<sub>2</sub>. Combustion: 2.5% O<sub>2</sub> in N<sub>2</sub>.

These results show that the pyritic S present in fuel can affect S emissions from the air reactor of a CLOU system. Thus the S/C in the char passing to the air reactor was higher than that found in the nascent char, and the S emissions from the air reactor were higher than expected. The analysis performed on the collected fines recovered in the different filters of the plant shows that the S/C ratio changed from 0.09 (nascent char) to 1 in the unburnt char exiting the fuel-reactor, owing to the presence of pyritic S.

Fig. 6 shows the splitting of the total S in the continuous plant between gas and solids streams. A major S emission came from the fuel reactor stream in the form of SO<sub>2</sub>. The S balance in the fuel and air reactor gas outlet closed at ~50–55 wt.%. Fines recovered from the filters of the fuel and air reactors showed high S concentrations that has been taken into account in the global S balance. Fig. 6 also shows the amount of S detected in the ashes in the form of pyritic S in both solid reactor streams. Between 8 and 11 wt.% of the total fed S was in the form of unburnt pyritic S. Moreover, it is known that the presence of CaO in the lignite ashes enables the self-retention of S during combustion through the formation of CaSO<sub>4</sub> [16]. In this way, Fig. 6 also shows the amount of S in the ashes produced by self-retention; between 10 and 15 wt.% of the total S fed into the system was retained in this way. Taking the S in both gas and solid phases into account, the S balance closure was approximately 80 wt.%. A possible fate for the rest of S could be accumulation in the oxygen carrier particles. If so, a S content of 0.3 wt.% would be present in oxygen carrier particles, which is below the detection level for XRD or SEM-EDX measurements.

### 3.3. Oxygen carrier behaviour

After 15 h of continuous operation at high temperatures and with a high S content fuel, the oxygen carrier did not show any agglomeration problems.

Samples of oxygen carrier exposed to 15 h of continuous operation were taken from the fuel reactor and analysed by TGA and XRD to determine if there was S retention in the oxygen carrier. Fig. 7 shows the reactivity of the fresh and used samples. It can be seen that both samples exhibited the same reactivity for reduction and oxidation. Also the oxygen transport capacity of the oxygen carrier was not affected. The high S concentration during 15 h did not affect the reactivity of the oxygen carrier. Also, XRD analysis did not show any S compounds in the oxygen carrier, although they could have been below the detection level.

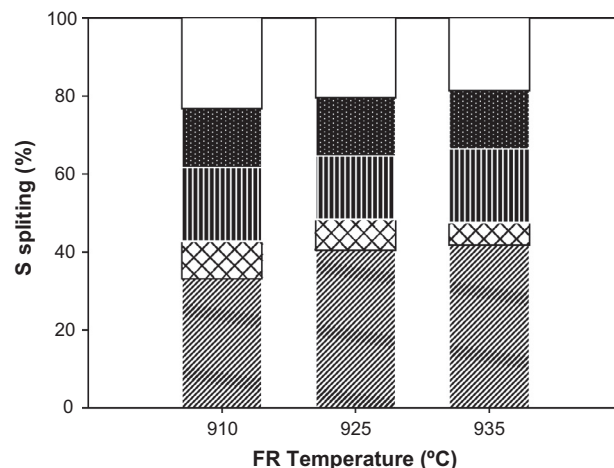


Fig. 6. S splitting in the continuous CLOU plant. ▨: fuel reactor gas outlet; ▩: air reactor gas outlet; ▮: pyritic S in ashes; ▭: self-retention by ashes.

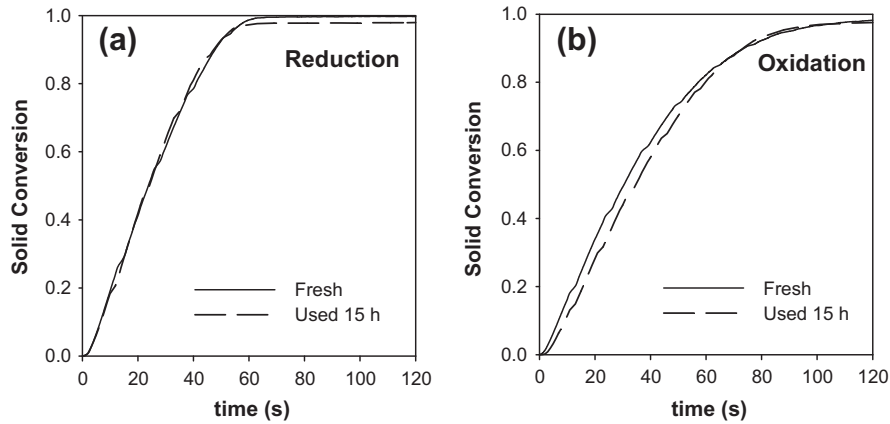


Fig. 7. Conversion vs time curves for (a) reduction and (b) oxidation reactions for fresh and used 15 h CLOU unit particles. Reduction in  $N_2$  and oxidation in air at  $1000^\circ C$  in TGA.

#### 4. Discussion

A number of considerations can be drawn from the results of this work. To comply with the EU legal limits with regard to the  $SO_2$  emission from the air reactor using high S content fuels, different modifications can be made to the system: (1) reducing the pyritic S content in the fuel to reduce the amount of S transferred with the char to the air reactor; (2) increasing the fuel reactor temperature; (3) increasing the solids inventory so as to increase the char conversion in the fuel reactor; or (4) the use of a carbon separation system to decrease the amount of char transferred to the air reactor. Reducing the pyritic S may not be achievable at an industrial scale. Increasing the solids inventory would increase the cost of the process. Increasing the fuel reactor temperature can increase char conversion and oxidation of the pyritic S; however, temperature restrictions up to  $950^\circ C$  are assumed in the fuel reactor in order to prevent high  $O_2$  concentrations at the fuel reactor outlet.

In a previous work [5], optimisation of the CLOU process was carried out by means of a carbon separation system to maximise the  $CO_2$  capture efficiency using the minimum solid inventory. A similar analysis can now be made in order to evaluate the effect of the use of a carbon separation system in the CLOU process in relation to  $SO_2$  emissions in the air reactor.

S emissions in the air reactor directly depend on the transfer of S content in char particles to the air reactor. A carbon separation system can be used to improve char conversion in the fuel reactor.

This system allows the separation of char and oxygen carrier particles by entrainment. In this way, the char is transported back to the fuel-reactor to improve char conversion, whereas oxygen carrier particles are sent to the air reactor. So, as the C flow to the air reactor is reduced, so too are the  $SO_2$  emissions in the air reactor.

When considering a carbon separation system, char conversion can be calculated as a function of carbon separation system efficiency as follows [17]:

$$X_{char} = 1 - \frac{\dot{m}_{OC}(1 - \eta_{CSS})}{(-r_C) \cdot m_{OC,FR} + \dot{m}_{OC}(1 - \eta_{CSS})} \quad (4)$$

where  $\dot{m}_{OC}$  is the oxygen carrier flow rate,  $\eta_{CSS}$  is the carbon separation system efficiency,  $(-r_C)$  the fractional conversion rate of char and  $m_{OC,FR}$  the mass of oxygen carrier in the fuel reactor. The  $SO_2$  emission from the air reactor is related to the char conversion in the fuel reactor. Note that in the CLOU process, gas coming from the air reactor is the only stream emitted into the atmosphere. Thus  $SO_2$  emission was calculated with the following equation:

$$SO_{2,em} = \frac{\dot{m}_{coal} \cdot f_{char} \cdot f_{S,char} \cdot (1 - X_{char})}{V_{air}} 10^6 \quad (5)$$

In this equation,  $\dot{m}_{coal}$  is the kg/s needed to feed  $1 MW_{th}$  of coal into the fuel reactor,  $f_{S,char}$  is the amount of S present in the fixed C and  $V_{air}$  the volume of air needed to burn  $1 MW_{th}$  of coal. For our

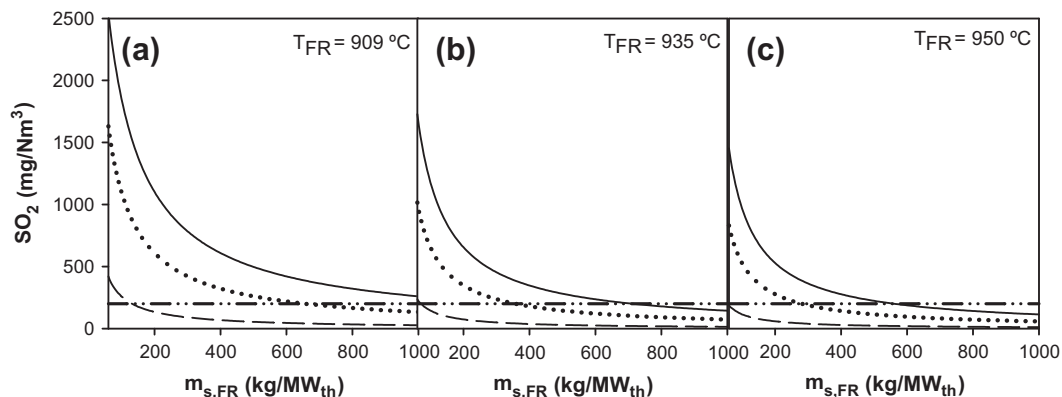
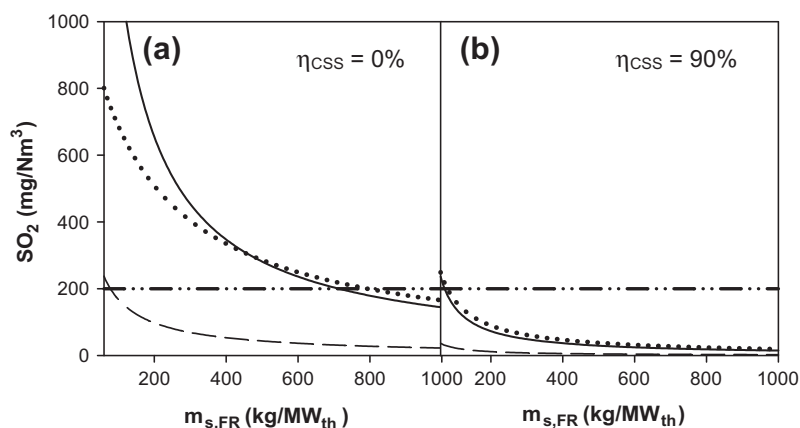


Fig. 8.  $SO_2$  emissions as a function of the fuel reactor inventory for lignite at three different efficiencies of the carbon separation system and three temperatures in the fuel reactor: (a)  $909^\circ C$ , (b)  $935^\circ C$  and (c)  $950^\circ C$ .  $\eta_{CSS}$ : 0% (—), 50% (···), 90% (---).  $\phi = 1.1$ .  $\dot{m}_{OC}$ : 1.35 (kg/s per  $MW_{th}$ ). EU legal  $SO_2$  emission limit (---).



**Fig. 9.** SO<sub>2</sub> emissions as a function of the fuel reactor inventory for three different fuels and two carbon separation system efficiencies: (a)  $\eta_{\text{CCS}} = 0\%$ , (b)  $\eta_{\text{CCS}} = 90\%$ . Fuels: lignite (—), anthracite (···), medium volatile bituminous (---).  $\phi = 1.1$ .  $\dot{m}_{\text{OC}} = 1.35$  (kg/s per MW<sub>th</sub>). EU legal SO<sub>2</sub> emission limit (-·-·-).

preliminary estimation, a uniform S release was assumed during char combustion, i.e. a S/C ratio that was constant and equal to that of the nascent char.

Using Eqs. (4) and (5), it was possible to analyse the effect of the oxygen carrier inventory and the efficiency of carbon separation system on SO<sub>2</sub> emissions in air reactor, once the value of  $(-r_C)$  was known. The char conversion rate at 925 °C was 4.4%/s for lignite. This value was obtained by Adánez et al. in a study for the combustion of different types of coals in a CLOU process [5].

Fig. 8a–c shows the estimated SO<sub>2</sub> emissions as a function of the fuel reactor inventory using this lignite when a carbon separation system with different carbon separation efficiencies ( $\eta_{\text{CCS}} = 0\%$ , 50% and 90%) was considered at 909 (a), 935 (b) and 950 °C (c). As can be seen in Fig. 8a, where the carbon separation system efficiency ( $\eta_{\text{CCS}}$ ) is given, the SO<sub>2</sub> emission decreased when the oxygen carrier inventory increased due to the increase in the residence time of solids in the fuel reactor. For the same reason, where  $\eta_{\text{CCS}}$  increased, more char returned to the fuel reactor, increasing its residence time. As a consequence, SO<sub>2</sub> emission decreased with  $\eta_{\text{CCS}}$ . The effect of the carbon separation system was very great, particularly at the lowest temperatures and lowest oxygen carrier inventories in the fuel reactor.

Predictions have been made in a similar way considering different fuels. A medium volatile bituminous coal (MVB) with 0.9 wt.% S and an anthracite with 1.3 wt.% S were evaluated. In a previous work [5], the rates of char combustion of these coals were determined in the CLOU unit. The char conversion rate at 925 °C was 3.3%/s for MVB and 0.4%/s for the anthracite.

Fig. 9a and b shows the SO<sub>2</sub> emission as a function of the fuel reactor inventory for these coals (lignite, anthracite and MVB) at 930 °C when a carbon separation system is considered (90%) or not (0%). In Fig. 9a shows that coals with high reactivity and low S content, e.g. MVB, would comply with the legislation without a carbon separation system using low solid inventories. On the other hand, a carbon separation system is necessary for coals with a very high S content (lignite) or low reactivity (anthracite) in order to comply with the EU legal limit, with low inventories in the fuel reactor.

These results were obtained assuming that the ratio S/C ratio in the char was constant throughout the entire combustion period. As shown in this work, the presence of pyritic S in the char affected the SO<sub>2</sub> emissions in the air reactor. Therefore, coals with high pyritic S contents require an increase in oxygen carrier inventories in the fuel reactor, in relation to those shown in Figs. 8 and 9, to increase the residence time in the fuel reactor in order to fully burn the pyritic S.

## 5. Conclusions

In this work, 15 h of continuous operation in a CLOU unit was carried out with a high S lignite (5.2 wt.% S) using a Cu-based oxygen carrier. Complete combustion of CO<sub>2</sub> and H<sub>2</sub>O was obtained and high carbon capture efficiency (96% at 935 °C) was achieved. Most of the S present in the coal was released as SO<sub>2</sub> in the fuel reactor. Only a small fraction was transferred to the air reactor and emitted, although emissions higher than 200 mg/N m<sup>3</sup> were found. The emissions may have been due to a non-uniform S release during char combustion resulting from the presence of pyritic S in this coal (2 wt.%).

The oxygen carrier particles never showed agglomeration problems. In addition, the oxygen carrier reactivity remained constant.

The use of a carbon separation system to comply with EU legal SO<sub>2</sub> emission limits was evaluated with different coals. It was found that the carbon separation system was not necessary with coals with high reactivity and low S contents. The use of a high efficiency carbon separation system ( $\eta_{\text{eff}} = 90\%$ ) would enable compliance with the SO<sub>2</sub> emission requirements even for coals with high S contents (lignite) or low reactivity (anthracite).

## Acknowledgements

This work was carried out with financial support from the European Commission, under the RFCS programme (ECLAIR Project, Contract RFCP-CT-2008-0008), ALSTOM Power Boilers (France), the Spanish Ministry of Science and Innovation (PN, ENE2010-19550), and Government of Aragón and La Caixa (Project 2012-GA-LC-076). I. Adánez-Rubio thanks CSIC for the JAE fellowship co-financed by the European Social Fund.

## References

- [1] Mattisson T, Lyngfelt A, Leion H. Chemical-looping with oxygen uncoupling for combustion of solid fuels. *Int J Greenhouse Gas Control* 2009;3:9–11.
- [2] Gayán P, Adánez-Rubio I, Abad A, de Diego LF, García-Labiano F, Adánez J. Development of CuO-based oxygen-carrier materials suitable for Chemical-Looping with Oxygen Uncoupling (CLOU) process. *Fuel* 2012;96:226–38.
- [3] Adánez-Rubio I, Gayán P, García-Labiano F, de Diego LF, Adánez J, Abad A. Development of CuO-based oxygen carrier materials suitable for Chemical-Looping with Oxygen Uncoupling (CLOU). *Energy Procedia* 2011;4:417–24.
- [4] Abad A, Adánez-Rubio I, Gayán P, García-Labiano F, de Diego LF, Adánez J. Demonstration of Chemical-Looping with Oxygen Uncoupling (CLOU) process in a 1.5 kW<sub>th</sub> continuously operating unit using a Cu-based oxygen-carrier. *Int J Greenhouse Gas Control* 2012;6:189–200.
- [5] Adánez-Rubio I, Abad A, Gayán P, de Diego LF, García-Labiano F, Adánez J. Performance of CLOU process in the combustion of different types of coal with CO<sub>2</sub> capture. *Int J Greenhouse Gas Control* 2012;12:430–40.



- [6] Sass B, Monzyk B, Ricci S, Gupta A, Hindin B, Gupta N. Impact of  $\text{SO}_x$  and  $\text{NO}_x$  in flue gas on  $\text{CO}_2$  separation, compression, and pipeline transmission. In: Thomas DC, Benson SM, editors. Carbon dioxide capture for storage in deep geologic formations results from the  $\text{CO}_2$  capture project, vol. 2. Oxford, UK: Elsevier; 2005 [chapter 17].
- [7] Bryant S, Lake LW. Effect of impurities on subsurface  $\text{CO}_2$  storage processes. In: Thomas DC, Benson SM, editors. Carbon dioxide capture for storage in deep geologic formations e results from the  $\text{CO}_2$  capture project, vol. 2. Oxford, UK: Elsevier; 2005 [chapter 18].
- [8] Pipitone G, Bolland O. Power generation with  $\text{CO}_2$  capture: technology for  $\text{CO}_2$  purification. *Int J Greenhouse Gas Control* 2009;3:528–34.
- [9] Forero CR, Gayán P, García-Labiano F, de Diego LF, Abad A, Adáñez J. Effect of gas composition in chemical-looping combustion with copper-based oxygen carriers: fate of sulphur. *Int J Greenhouse Gas Control* 2010;4:762–70.
- [10] Adáñez-Rubio I, Gayán P, Abad A, de Diego LF, García-Labiano F, Adáñez J. Evaluation of a spray-dried  $\text{CuO/MgAl}_2\text{O}_4$  oxygen carrier for the chemical looping with oxygen uncoupling process. *Energy Fuels* 2012;26:3069–81.
- [11] On the limitation of emissions of certain pollutants into the air from large combustion plants. European Council Directive 2001/80/EC. *Off J Eur Commun* 2001;L309:1–21.
- [12] Adáñez-Rubio I, Gayán P, Abad A, de Diego LF, García-Labiano F, Adáñez J. Identification of operational regions in the Chemical-Looping with Oxygen Uncoupling (CLOU) process with a Cu-based oxygen-carrier. *Fuel* 2012;102:634–45.
- [13] Simell P, Stahlberg P, Kurkela E, Albretch J, Deutch S, Sjoström K. Provisional protocol for the sampling and analysis of tar and particulates in the gas from large-scale biomass gasifiers. *Biomass Bioenergy* 2000;18:19–38.
- [14] Virginie M, Adáñez J, Courson C, de Diego LF, García-Labiano F, Niznansky D, et al. Effect of Fe-olivine on the tar content during biomass gasification in a dual fluidized bed. *Appl Catal B: Environ* 2012;121–122:214–22.
- [15] Benito RG, Dung NV. Emissions of  $\text{SO}_2$  during batch fluidized bed combustion of Rundle retorted shale. *Fuel* 1993;72:869–72.
- [16] De Diego LF, Rufas A, García-Labiano F, de las Obras-Loscertales M, Abad A, Gayán P, et al. Optimum temperature for sulphur retention in fluidised beds working under oxy-fuel combustion conditions. *Fuel* 2012. <<http://dx.doi.org/10.1016/j.fuel.2012.02.064>>.
- [17] Cuadrat A, Abad A, de Diego LF, García-Labiano F, Gayán P, Adáñez J. Prompt considerations on the design of chemical-looping combustion of coal from experimental tests. *Fuel* 2012;97:219–32.

## **Paper IX**



GHGT-11

## Use of Chemical-Looping processes for coal combustion with CO<sub>2</sub> capture

J. Adánez\*, P. Gayán, I. Adánez-Rubio, A. Cuadrat, T. Mendiara, A. Abad  
F. García-Labiano, L. F. de Diego

*Dept. Energy and Environment, Instituto de Carboquímica (ICB-CSIC), Miguel Luesma Castán 4, E-50018-Zaragoza, Spain*

### Abstract

Chemical-Looping Combustion, CLC, is one of the most promising processes to capture CO<sub>2</sub> at a low cost. It is based on the transfer of the oxygen from air to the fuel by using a solid oxygen carrier that circulates between two interconnected fluidized-bed reactors: fuel and air reactors. The CO<sub>2</sub> capture is inherent to this process, as the air does not get mixed with the fuel. In this work two options are evaluated in a 1 kW<sub>th</sub> continuously operated unit for coal fueled Chemical-Looping. The first one is the gasification of coal in the fuel reactor –*in-situ* Gasification Chemical-Looping Combustion (*i*G-CLC)–. Ilmenite or a bauxite waste material is used as oxygen carrier. The second one is the combustion of coal in the fuel reactor by using oxygen carriers which release gaseous oxygen –Chemical-Looping with Oxygen Uncoupling (CLOU)–. A Cu-based material is used in this mode. Coals ranging from anthracite to lignite were used. Complete combustion was always reached in CLOU mode, whereas unburnt compounds were present in *i*G-CLC. Both in *i*G-CLC and CLOU processes the CO<sub>2</sub> capture increased with temperature and decreased with the coal rank. The highest CO<sub>2</sub> capture rate was obtained for lignite, being 93% for *i*G-CLC and 99% for CLOU, even without a carbon separation system. The key aspects for the good performance of *i*G-CLC and CLOU processes are analyzed through the performance results obtained with different coals.

© 2013 The Authors. Published by Elsevier Ltd.

Selection and/or peer-review under responsibility of GHGT

*Keywords:* CLC; CLOU; coal; combustion; CO<sub>2</sub> capture; ilmenite; iron; copper

### 1. Introduction

Chemical-Looping Combustion (CLC) is one of the most promising technologies to carry out CO<sub>2</sub> capture at low cost. A CLC system is based on the use of an oxygen carrier which transfers the oxygen necessary for the fuel combustion from the air to the fuel. Frequently, a CLC system is composed by two interconnected fluidized bed reactors, the air reactor and the fuel reactor, and the oxygen carrier circulating between them. In CLC, the fuel is introduced to the fuel reactor where it is converted by the

\* Corresponding author. Tel.: +34-976-733977; fax: +34-976-733318

E-mail address: [jadanez@icb.csic.es](mailto:jadanez@icb.csic.es)

oxygen carrier to produce CO<sub>2</sub> and H<sub>2</sub>O. The spent oxygen carrier must be transported to the air reactor to be oxidized by air and then start a new cycle. The CO<sub>2</sub> capture is inherent to this process, as the air does not get mixed with the fuel. A review of CLC processes has been recently done by Adanez et al. [1].

The use of coal in CLC is very attractive in future sceneries with restriction in CO<sub>2</sub> emissions, since coal will keep on being a main energy source in the medium-term. In the so-called solid fuelled-CLC the solid fuel is physically mixed with the oxygen carrier in the fuel reactor. Two options have been proposed, depending on how the solid fuel is converted. The *in-situ* Gasification Chemical-Looping Combustion (*iG-CLC*) involves the *in-situ* gasification of the fuel in the fuel reactor by H<sub>2</sub>O and/or CO<sub>2</sub> [2]. The gasification step is the limiting step in the coal conversion in the fuel reactor. To overcome the slow gasification stage in the *iG-CLC*, the Chemical-Looping with Oxygen Uncoupling (CLOU) process was proposed by Mattisson and coworkers [3]. In CLOU an oxygen carriers that dissociated to produce gaseous oxygen is used, so the solid fuel conversion goes via fast combustion. Moreover, in CLOU the fluidization gas can be recycled CO<sub>2</sub>, reducing in this way the steam duty of the plant and energy penalty.

The main reactions involved in each process are depicted in Fig. 1. The most relevant chemical processes during coal conversion in the *iG-CLC* process are showed in reactions (1-4), and the corresponding processes for the CLOU mode includes reaction (1), followed by (5-6). Both in *iG-CLC* and CLOU the char must be highly converted in the fuel reactor to avoid leaking of char particles to the air reactor where they would be burnt with air. This fact would reduce the CO<sub>2</sub> capture efficiency because CO<sub>2</sub> emitted from the air reactor is not captured. As a consequence of the ashes present in the solid fuel it is necessary the draining of ashes from the system to avoid its accumulation in the reactors. However, the drain stream will also contain some amount of oxygen carrier. Thus, a partial loss together with the fuel ashes is expected and low cost materials or materials readily separable from the ashes are desirable.

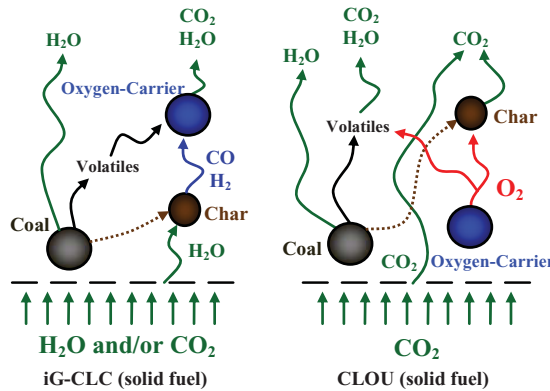
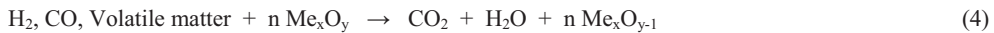
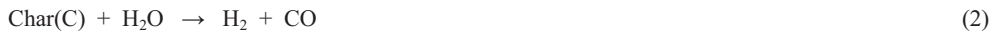


Fig. 1. Main processes involved in fuel reactor for the *iG-CLC* and CLOU modes.

Mainly low cost materials have been analyzed for the *i*G-CLC process by several authors [1]. The most used material was ilmenite, which is a mineral mainly composed of  $\text{FeTiO}_3$ . There are an interesting number of recent studies showing an acceptable performance of ilmenite as oxygen carrier in CLC. Leion et al. [4] analyzed the reactivity of ilmenite in a batch fluidized bed, obtaining high conversion of CO and  $\text{H}_2$  but moderate conversion of  $\text{CH}_4$ . Adánez et al. [5] found that ilmenite gains reactivity with the redox cycles, and eventually the reactivity was maintained constant. Good performance of ilmenite has been proven for *i*G-CLC with coal in continuously operated units ranging from 500  $\text{W}_{\text{th}}$  [6] to 10  $\text{kW}_{\text{th}}$  [7]. The effect of the operating variables on the *i*G-CLC was investigated by Cuadrat et al. [8,9] working with coals of different rank from lignite to anthracite. Temperatures above 1000 °C [7] and values of the oxygen carrier to fuel ratios slightly above the stoichiometric value are beneficial to maximize the carbon capture in the *i*G-CLC process [8]. Recently it has started the use of ilmenite in a 100 $\text{kW}_{\text{th}}$  unit at Chalmers University of Technology [10] and 1  $\text{MW}_{\text{th}}$  unit at TU Darmstadt [11].

In the CLOU process, the material used as oxygen carrier must have suitable thermodynamic properties for oxygen uncoupling. Three metal oxide systems have been so far identified:  $\text{CuO/Cu}_2\text{O}$ ,  $\text{Mn}_2\text{O}_3/\text{Mn}_3\text{O}_4$ , and  $\text{Co}_3\text{O}_4/\text{CoO}$  [3]. In general, Cu-based materials have faster release of oxygen than Mn-based particles [12]. From a screening study, a Cu-based oxygen carrier 60 wt.% CuO supported on  $\text{MgAl}_2\text{O}_4$  was selected according to its high reactivity, low attrition rate and avoidance of agglomeration during successive redox cycles [13]. This material was used to demonstrate the proof of CLOU concept with coal in a 1.5  $\text{kW}_{\text{th}}$  unit located at ICB-CSIC (Spain) [14]. The temperature (900-960°C), coal feeding rate and solids circulation flow rate was varied to analyze the effect of the kinetics of the processes, the solids inventory per  $\text{MW}_{\text{th}}$  and the residence time of particles in the fuel reactor, respectively, on the CLOU performance. In all cases, unburnt volatile matter was not present in the fuel reactor outlet, which was composed by  $\text{CO}_2$  and  $\text{H}_2\text{O}$  with the equilibrium  $\text{O}_2$  concentration at the operating temperature. Coal conversion in the fuel reactor was limited by the char combustion, which was mainly affected by the temperature and the mean residence time. In spite of the lack of carbon stripper in the CLOU unit, the carbon capture was always higher than 97% even when the solids inventory was as low as 235  $\text{kg/MW}_{\text{th}}$ .

The objective of this work is to do a comprehensive comparison of the *i*G-CLC and CLOU processes based on the experimental results obtained with different coals in the CLC-CLOU unit existing in ICB-CSIC. Results obtained at several fuel reactor temperatures and with different type of coals are used, and a discussion based on the carbon capture and combustion efficiency is done.

## 2. Experimental

### 2.1. Materials

Two materials are used as oxygen carriers for *i*G-CLC: ilmenite and a Fe-enriched *sand fraction* (71 wt.%  $\text{Fe}_2\text{O}_3$ ) from bauxite digestion (Fe-ESF). Ilmenite was initially activated during 3 hours of continuous operation [6]. The Fe-ESF was supplied by Alcoa Europe-Alumina Española S.A. Prior to its use, the sample was calcined at 1200°C for stabilization purposes. The material used for CLOU mode was a Cu-based oxygen carrier prepared by spray drying (Cu60MgAl). Oxygen carrier particles were manufactured by VITO (Flemish Institute for Technological Research, Belgium). The CuO content was 60 wt.%. Details about composition and physical properties of these materials are shown in Table 1 and references [6,14,15].

Three different coals were used for *i*G-CLC and CLOU experiments. A Lignite from Teruel basin (Spain), a Bituminous coal from South Africa, and an Anthracite from El Bierzo (Spain) were used with the aim to cover a wide range of coals. Main properties of selected coals are showed in Table 2. The coal particle size used for this study was +0.2–0.3 mm with all fuels.

Table 1. Characterization of oxygen carrier particles.

	Ilmenite	Fe-ESF	Cu60MgAl
XRD main phases	Fe <sub>2</sub> TiO <sub>5</sub> , Fe <sub>2</sub> O <sub>3</sub> , TiO <sub>2</sub>	Fe <sub>2</sub> O <sub>3</sub> , β-Al <sub>2</sub> O <sub>3</sub>	CuO, MgAl <sub>2</sub> O <sub>4</sub>
Particle diameter (μm)	+150-300	+150-300	+100-200
Crushing strength (N)	2.0	2.8	2.4
Oxygen transport capacity, R <sub>OC</sub> , (%)	3.9	2.4	6.0
Porosity (%)	18.0	3.7	16.1
Skeletal density (kg/m <sup>3</sup> )	4200	4500	4600
Specific surface area, BET (m <sup>2</sup> /g)	0.4	0.1	0.5

Table 2. Properties of coals used in this work.

	Anthracite	Bituminous	Lignite
Proximate Analysis (wt.%)			
Moisture	1.0	4.2	12.6
Volatile matter	7.5	25.5	28.6
Fixed carbon	59.9	55.9	33.6
Ash	31.6	14.4	25.2
Ultimate Analysis (wt.%)			
C	60.7	69.3	45.4
H	2.1	3.9	2.5
N	0.9	1.9	0.6
S	1.3	0.9	5.2
LHV (kJ/kg)	21900	25500	16250

## 2.2. Experimental set-up

A schematic view of the experimental set-up is shown in Fig. 2. The set-up was basically composed of two interconnected fluidized-bed reactors joined by a loop seal, a riser for solids transport from the air reactor to the fuel reactor, a cyclone and a solids valve to control the solids circulation flow rate between both reactors. A diverting solids valve located below the cyclone allowed the measurement of the solids flow rates at any time. Thus, this design allowed us to control and measure the solids circulation flow rate. The gas velocity at 900°C in the fuel-reactor was 11 cm/s and 60 cm/s for the air-reactor. Coal is fed in by a two-step screw feeder at the bottom of the bed right above the fuel reactor distribution plate in order to maximize the time that the fuel and volatile matter is in contact with the bed material. The ash particles remaining after char combustion were not retained by the cyclone and were collected in a reservoir downstream. Thus, ashes were not accumulated in the system. The absence of a carbon stripper facilitates the interpretation of the effect of these operational conditions on the results obtained, specially the effect of the mean residence time. CO, CO<sub>2</sub>, H<sub>2</sub>, CH<sub>4</sub>, and O<sub>2</sub> were analyzed in the exiting streams from the air and fuel reactors. Higher hydrocarbons (C2-C5) were analyzed by chromatography and the amount of tar was analyzed following a tar protocol. More information is given in [6,14].

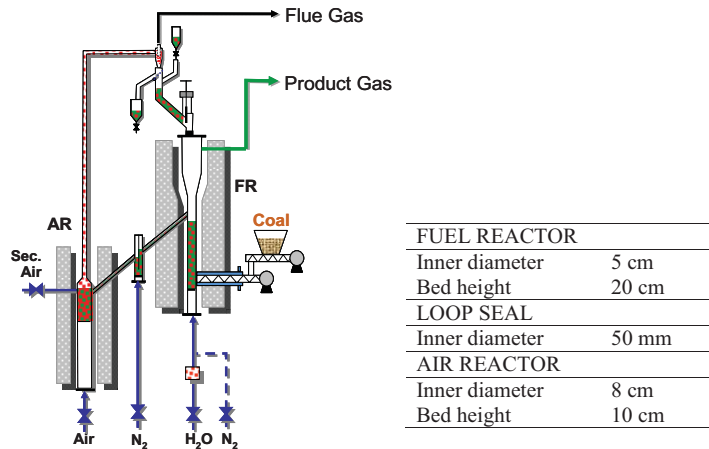


Fig. 2. Schematic diagram of the ICB-CSIC-s1 facility for coal-fuelled *i*G-CLC and CLOU.

The performance of the *i*G-CLC and CLOU processes is assessed by evaluating two parameters: the carbon capture efficiency and the combustion efficiency in the fuel reactor. The carbon capture efficiency,  $\eta_{CC}$ , is defined as the fraction of carbon exiting in the fuel reactor outlet gas stream. The combustion efficiency in the fuel reactor is defined as the percentage of the oxygen demanded by the effective coal that is supplied by the oxygen carrier in the fuel reactor.

$$\eta_{CC} = \frac{(F_{CH_4} + F_{CO} + F_{CO_2})_{outFR}}{(F_{CH_4} + F_{CO} + F_{CO_2})_{outFR} + (F_{CO_2})_{outAR}} \quad (7)$$

$$\eta_{comb,FR} = 1 - \frac{(4F_{CH_4} + F_{CO} + F_{H_2})_{outFR}}{2\Omega_{coal}\dot{m}_{coal} - 2(F_{CO_2})_{outAR}} \quad (8)$$

$\Omega_{coal}$  being the stoichiometric mol of  $O_2$  to convert 1 kg of coal to  $CO_2$  and  $H_2O$ .

### 3. Results

In the *i*G-CLC mode, ilmenite was mainly used as oxygen carrier, whereas Cu60MgAl material was used for CLOU. To consider specific characteristics of both processes, different residence times in the fuel reactor were used, around 16 min in *i*G-CLC ( $\sim 1500$  kg/MW<sub>th</sub>) while 7 min were used for CLOU ( $\sim 900$  kg/MW<sub>th</sub>). Additional experiments were carried out in *i*G-CLC mode using Fe-ESF with anthracite as fuel. In this case, mean residence time of solids in the fuel reactor was 11 min (2000 kg/MW<sub>th</sub>).

Differences between *i*G-CLC and CLOU are evident when results are compared. Fig. 3 shows the comparison on the carbon capture efficiency obtained for different coals as a function of the fuel reactor temperature. As much for *i*G-CLC as for CLOU the carbon capture was higher when the temperature was increased because the gasification or combustion rate was enhanced. Carbon capture is much higher in CLOU because the char is converted faster when it is burnt with gaseous  $O_2$  than when it is gasified by  $H_2O$ . In both *i*G-CLC and CLOU, the type of coal affected to the carbon capture efficiency.



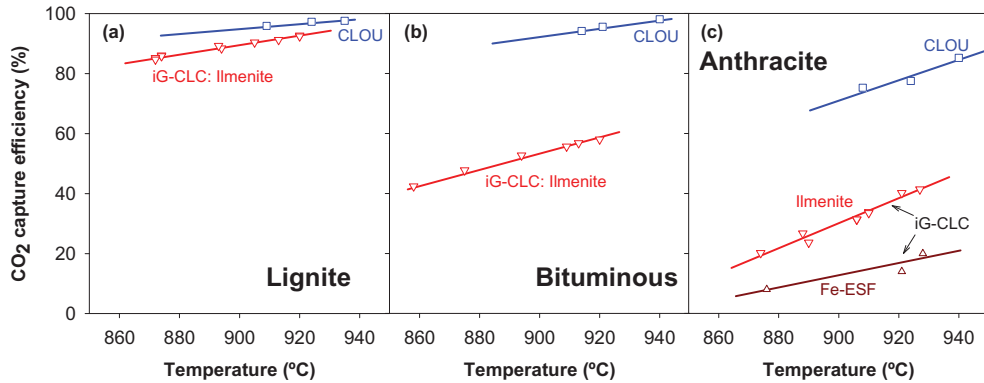


Fig. 3. Carbon capture efficiency in *iG-CLC* or CLOU as a function of the fuel reactor temperature.

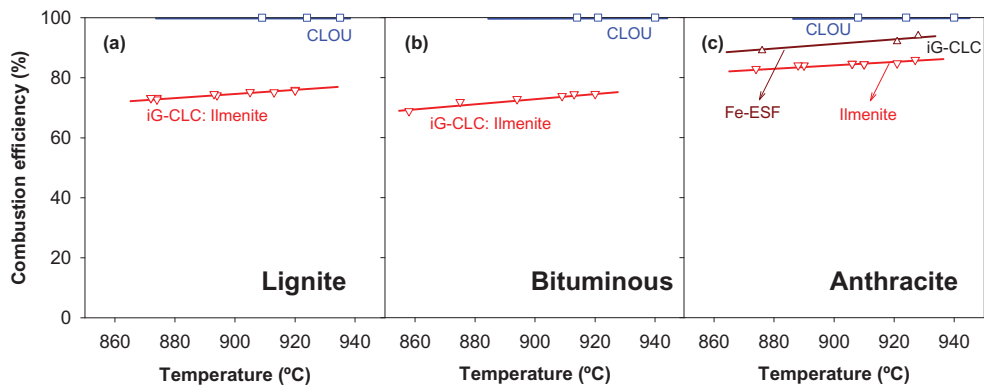


Fig. 4. Combustion efficiency in *iG-CLC* or CLOU as a function of the fuel reactor temperature.

In general, the carbon capture followed the order Lignite > Bituminous > Anthracite. Since the carbon from the volatiles exits with the fuel reactor outlet stream, that fraction of carbon is always captured. Thus, the carbon capture efficiency depends on the fraction of carbon in the volatile matter and on the char conversion rate. So, less reactive coals gave lower carbon capture. More in detail, the type of coal showed a high effect on the carbon capture in *iG-CLC* with ilmenite. So, at 920°C the carbon capture was as high as 93% with Lignite and it was reduced to 58% and 40% with the Bituminous coal and Anthracite, respectively. In the CLOU mode high carbon capture efficiency was obtained for Lignite and Bituminous coal ( $\eta_{CC} = 97\%$  at 935°C with both coals). Nevertheless, lower values were obtained for Anthracite ( $\eta_{CC} = 84\%$  at 940°C).

Experiments in *iG-CLC* mode were carried out with anthracite using a more reactive material: Fe-ESF. In this case, the carbon capture was lower than with ilmenite. The main factor affecting the carbon capture was the lower residence time of solids in the fuel reactor with Fe-ESF. This fact was because the higher

solids circulation rate with Fe-ESF due to its lower oxygen transport capacity compared to ilmenite, see Table 1. The oxygen carrier reactivity would have little influence on the carbon capture efficiency [16].

The Lignite showed the highest carbon capture efficiency, being the difference obtained between *i*G-CLC and CLOU of low relevance at high temperatures. On the contrary, Bituminous coal and Anthracite showed higher differences when *i*G-CLC and CLOU performance was compared.

Fig. 4 shows the combustion efficiency in the fuel reactor for all fuels tested at the different temperatures in *i*G-CLC and CLOU modes. Results on CLOU with the Cu-based oxygen carrier showed that full combustion of coal to CO<sub>2</sub> and H<sub>2</sub>O was reached for all coals tested. On the contrary, unburnt gases exit from the fuel reactor in *i*G-CLC with ilmenite; CH<sub>4</sub>, CO and H<sub>2</sub> were the only unburnt compounds found. Any tarry material or higher hydrocarbons were fully converted by the oxygen carrier. Correspondingly the combustion efficiency was lower than 100%. The combustion efficiency in *i*G-CLC mode was higher for solid fuels with lower volatile content, but it was slightly affected by the reactor temperature. Also, the use of a more reactive oxygen carrier in *i*G-CLC mode, as Fe-ESF is, increased the combustion efficiency in 9%, see Fig. 4(c). Note that a higher solids inventory was used per MW<sub>th</sub> with Fe-ESF, which can contribute to an increase in the range 3-6% in the combustion efficiency [16,17], the rest being attributable to the higher reactivity of Fe-ESF. But the low values of combustion efficiency in *i*G-CLC are not fully justified by the reactivity of the oxygen carrier. Ilmenite has enough high reactivity to fully convert gasification products to CO<sub>2</sub> and H<sub>2</sub>O [5]. However, unburnt compounds in CLC with coal mainly proceed from volatiles generated during coal devolatilization [6]. This fact explains the higher value of combustion efficiency found for anthracite, which was due to the lower volatile content of this fuel. So, the way that gases are converted in *i*G-CLC or CLOU has influence on combustion. In *i*G-CLC volatiles must diffuse until solids to react, whereas in CLOU oxygen from oxygen carrier reacts in gas phase with gases. This is a more effective way for gas conversion.

#### 4. Discussion

The carbon capture efficiency, the combustion efficiency in the fuel reactor and the separation of ash from the oxygen carrier are the key factors that must be maximized for the development of an optimized *i*G-CLC or CLOU process. From results above showed, the combustion efficiency was complete for the CLOU mode, whereas unburnt compounds were always present in *i*G-CLC both with ilmenite or Fe-ESF as oxygen carrier. In CLOU mode, complete combustion would be still possible even lowering the solids inventory to 60 kg/MW<sub>th</sub> [18]. On the contrary, in *i*G-CLC it is not worth to increase the solids inventory above 2000 kg/MW<sub>th</sub> to improve the combustion efficiency [16]. Different possibilities have been proposed to process the unburnt compounds. The use of a more reactive oxygen carrier has a residual effect on this improvement, unless the gain in reactivity is important [17]. A second fuel reactor downstream where exhaust gases are fed can be used. From a preliminary study, a solids inventory of 45 kg/MW<sub>th</sub> should be necessary in the second reactor [16] to reach complete combustion of gases. Improve the gas-solid contact in the fuel reactor or the separation and recirculation of unburnt compounds can be also other options. Finally, if any of the above solution becomes valid, an oxygen polishing step could be added to the fuel reactor down-stream. Thus, unburnt components are fully burnt to CO<sub>2</sub> and H<sub>2</sub>O with pure oxygen, being necessary an air separation unit (ASU) of small size. In conditions in the ICB-CSICs1 unit, the oxygen demand was 5-9% of the oxygen required by coal combustion with ilmenite; some lower (3-7%) with Fe-ESP as oxygen carrier. In CLOU process, oxygen polishing would not be required but fuel reactor gases contains some oxygen which has to be taken into account.

The carbon capture efficiency was higher for CLOU process than for *i*G-CLC. No further actions would be needed to reach values of  $\eta_{CC} \approx 98\%$  when high reactive coals are used in CLOU. However, the residence time of char should be increased when low reactive coals are used in CLOU, but in any case for

the *i*G-CLC mode. The carbon capture efficiency was limited by the char conversion rate in the fuel reactor. Table 3 shows the char conversion rate in the fuel reactor for different coals and processes. Model simulations indicated the relevance of a carbon separation system (e.g. a carbon stripper) on the carbon capture efficiencies [19]. The carbon stripper separates char particles away from oxygen carrier particles which are returned to the fuel reactor, whereas oxygen carrier particles are left to pass to the air reactor with minor amounts of char.

Table 3. Carbon capture efficiency, combustion efficiency in the fuel reactor and char conversion rate obtained using ilmenite or Fe-ESF in *i*G-CLC or Cu60MgAl in CLOU with several coals. T = 930°C.

	Anthracite			Bituminous		Lignite	
	Ilmenite	Fe-ESF	Cu60MgAl	Ilmenite	Cu60MgAl	Ilmenite	Cu60MgAl
Solids inventory (kg/MW <sub>th</sub> )	1400	2000	900	1380	1000	1770	850
Mean residence time (min)	16	11	7	16	7	16	7
Carbon Capture (%)	42	20	80	60	98	93	98
Combustion efficiency FR (%)	85	94	100	75	100	76	100
Char conversion rate (%/min)	3.7	3.6	40	5.0	360	55	400

Considering a carbon separation system, the carbon capture efficiency can be calculated as a function of the carbon separation system efficiency ( $\eta_{CSS}$ ), the solids inventory in the fuel reactor ( $m_{s,FR}$ ), the solids circulation flow rate ( $\dot{m}_{OC}$ ), the carbon content ( $f_C$ ) and fixed carbon ( $f_{C,fix}$ ) in coal [20].

$$\eta_{CC} = \frac{f_C - f_{C,fix}}{f_C} + \frac{f_{C,fix}}{f_C} \left[ 1 - \frac{\dot{m}_{OC}(1-\eta_{CSS})}{(-r_C)m_{s,FR} + \dot{m}_{OC}(1-\eta_{CSS})} \right] \tag{9}$$

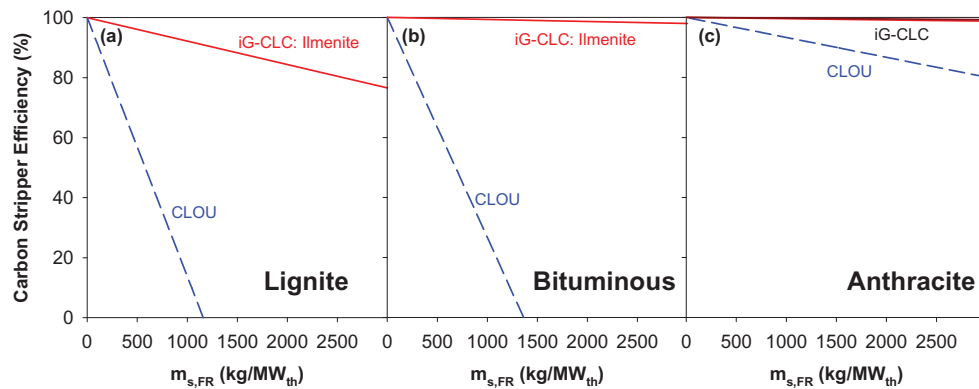


Fig. 5. Efficiency of the carbon stripper required for a carbon capture of 98% as a function of the solids inventory in the fuel reactor for *i*G-CLC and CLOU processes. T<sub>FR</sub> = 930°C. Oxygen carrier to fuel ratio:  $\phi = 1.5$ .

Thus, the solids inventory and the efficiency of the carbon separation system can be calculated to obtain a certain value of the carbon capture efficiency for every oxygen carrier-coal pair. Fig. 5 shows the efficiency of the carbon stripper ( $\eta_{\text{CSS}}$ ) required to reach a carbon capture of  $\eta_{\text{CC}} = 98\%$  for different coals. The  $\eta_{\text{CSS}}$  value required decreases as the solids inventory in the fuel reactor increases. Nevertheless, it is necessary a highly efficient carbon stripper ( $\eta_{\text{CSS}} > 98\%$ ) in the *i*G-CLC mode with low reactive coals (bituminous and anthracite) if the solids inventory was limited to 2000 kg/MW<sub>th</sub> at maximum. Lower is the requirement for the carbon stripper using lignite in *i*G-CLC or in the CLOU mode. It is worthy to note that 60 kg/MW<sub>th</sub> of Cu60MgAl material in CLOU mode should be enough to avoid unburnt compounds from the fuel reactor. However, a higher solids inventory is required depending on the efficiency of the carbon separation system. Thus, if a carbon stripper is not present, 1000-1500 kg/MW<sub>th</sub> should be necessary to reach a carbon capture efficiency of 98% in CLOU with lignite or bituminous coal.

The use of CLOU process for solid fuel combustion using oxygen carriers that can release oxygen at high temperature is a promising alternative to *i*G-CLC which does not need an oxygen polishing step and reach very high carbon capture efficiencies specially with reactive coals. A cornerstone in the successful development of CLOU process is the oxygen carrier material. It is necessary the development of resistant and cheap materials with CLOU properties that can be easily separated from coal ashes.

## 5. Conclusions

The performance regarding the carbon capture and combustion efficiency for CLOU was better than for *i*G-CLC. Whereas complete combustion was reached in CLOU mode, the incomplete combustion in *i*G-CLC process requires the use of additional actions, e.g. an oxygen polishing step. The characteristics of coal have an important effect on combustion and gasification processes and it is expected that also affect to *i*G-CLC and CLOU processes. The use of coals with high volatile content or highly reactive during the gasification or combustion reaction enhances the carbon capture efficiency of the process. In order to reach high carbon capture efficiency, the existence of the carbon separation system is imperative in the *i*G-CLC mode for all type of coals and in CLOU mode with low reactive coals, e.g. anthracite. Nevertheless, the use of a carbon separation system is also recommended in CLOU mode with lignite or bituminous coal.

## Acknowledgements

This work was partially supported by the European Commission, under the RFCS program (ECLAIR Project, Contract RFCP-CT-2008-0008), ALSTOM Power Boilers (France) and the Spanish Ministry of Science and Innovation (PN, ENE2010-19550).

## References

- [1] Adanez J, Abad A, Garcia-Labiano F, Gayan P, de Diego LF. Progress in Chemical-Looping Combustion and Reforming technologies. *Prog Energy Comb Sci* 2012;**38**:215–82.
- [2] Cao Y, Pan WP. Investigation of Chemical Looping Combustion by Solid Fuels. 1. Process Analysis. *Energy Fuel* 2006;**20**:1836–44.
- [3] Mattisson T, Lyngfelt A, Leion H. Chemical-looping with oxygen uncoupling for combustion of solid fuels. *Int J Greenhouse Gas Control* 2009;**3**:11–9.

- [4] Leion H, Lyngfelt A, Johansson M, Jerndal E, Mattisson T. The use of ilmenite as an oxygen carrier in chemical-looping combustion. *Chem Eng Res Des* 2008;**86**:1017–26.
- [5] Adánez J, Cuadrat A, Abad A, Gayán P, de Diego LF, García-Labiano F. Ilmenite Activation during Consecutive Redox Cycles in Chemical-Looping Combustion. *Energy Fuels* 2012;**24**:1402–13.
- [6] Cuadrat A, Abad A, García-Labiano F, Gayán P, de Diego LF, Adánez J. The use of ilmenite as oxygen-carrier in a 500 W<sub>th</sub> Chemical-Looping Coal Combustion unit. *Int J Greenhouse Gas Control* 2011;**5**:1630–42.
- [7] Berguerand N, Lyngfelt A. Chemical-Looping Combustion of Petroleum Coke Using Ilmenite in a 10 kW<sub>th</sub> Unit-High-Temperature Operation. *Energy Fuels* 2009;**23**:5257–68.
- [8] Cuadrat A, Abad A, García-Labiano F, Gayán P, de Diego LF, Adánez J. Effect of operating conditions in Chemical-Looping Combustion of coal in a 500 W<sub>th</sub> unit. *Int J Greenhouse Gas Control* 2012;**6**:153–63.
- [9] Cuadrat A, Abad A, García-Labiano F, Gayán P, de Diego LF, Adánez J. Relevance of the coal rank on the performance of the in situ gasification chemical-looping combustion. *Chem Eng J* 2012;**195-196**:91–102.
- [10] Markström P, Linderholm C, Lyngfelt A. Operation of a 100 kW chemical-looping combustor with Mexican petroleum coke and Cerrejón coal. Proceedings from the 2<sup>nd</sup> International Conference on Chemical Looping, 26-28 September 2012, Darmstadt, Germany.
- [11] Orth M, Ströhle J, Epple B. Design and Operation of a 1 MW<sub>th</sub> Chemical Looping Plant. Proceedings from the 2<sup>nd</sup> International Conference on Chemical Looping, 26-28 September 2012, Darmstadt, Germany.
- [12] Leion H, Larring Y, Bakken E, Bredesen R, Mattisson T, Lyngfelt A. Use of CaMn<sub>0.875</sub>Ti<sub>0.125</sub>O<sub>3</sub> as Oxygen Carrier in Chemical-Looping with Oxygen Uncoupling. *Energy Fuels* 2009;**23**:5276–83.
- [13] Gayán P, Adánez-Rubio I, Abad A, de Diego LF, García-Labiano F, Adánez J. Development of Cu-based oxygen carriers for Chemical-Looping with Oxygen Uncoupling (CLOU) process. *Fuel* 2012;**96**:226–38.
- [14] Abad A, Adánez-Rubio I, Gayán P, García-Labiano F, de Diego LF, Adánez J. Demonstration of chemical-looping with oxygen uncoupling (CLOU) process in a 1.5 kW<sub>th</sub> continuously operating unit using a Cu-based oxygen-carrier. *Int J Greenhouse Gas Control* 2012;**6**:189–200.
- [15] Mendiara T, Abad A, de Diego LF, García-Labiano F, Gayán P, Adánez J. Use of an Fe-Based Residue from Alumina Production as an Oxygen Carrier in Chemical-Looping Combustion. *Energy Fuels* 2012;**26**:1420–31.
- [16] Cuadrat A, Abad A, Gayán P, de Diego LF, García-Labiano F, Adánez J. Theoretical approach on the CLC performance with solid fuels: Optimizing the solids inventory. *Fuel* 2012;**97**:536–51.
- [17] García-Labiano F, de Diego L, Gayán P, Abad A, Adánez J. Fuel reactor modelling in chemical-looping combustion of coal: 2. Simulation and optimization. *Chem Eng Sci* 2012;accepted for publication.
- [18] Adánez-Rubio I, Abad A, Gayán P, de Diego LF, García-Labiano F, Adánez J. Identification of operational regions in the Chemical-Looping with Oxygen Uncoupling (CLOU) process with a Cu-based oxygen carrier. *Fuel* 2012;**102**:634–45.
- [19] Abad A, Gayán P, de Diego LF, García-Labiano F, Adánez J. Fuel reactor modelling in Chemical-Looping Combustion of coal: 1. Model formulation. *Chem Eng Sci* 2012;accepted for publication.
- [20] Adánez-Rubio I, Abad A, Gayán P, de Diego LF, García-Labiano F, Adánez J. Performance of CLOU process in the combustion of different types of coal with CO<sub>2</sub> capture. *Int J Greenhouse Gas Control* 2012;submitted for publication.

**Paper X**





# Kinetic analysis of a Cu-based oxygen carrier: Relevance of temperature and oxygen partial pressure on reduction and oxidation reactions rates in Chemical Looping with Oxygen Uncoupling (CLOU)



I. Adánez-Rubio, P. Gayán\*, A. Abad, F. García-Labiano, L.F. de Diego, J. Adánez

*Instituto de Carboquímica (ICB-CSIC), Miguel Luesma Castán 4, 50018 Zaragoza, Spain*

## HIGHLIGHTS

- Kinetic of reduction and oxidation of Cu-based oxygen carrier for CLOU was determined.
- Nucleation and nuclei growth model described solids conversion evolution with time.
- Langmuir–Hishelwood model was able to describe the effect of oxygen concentration.
- Activation energies were 270 and 30 kJ mol<sup>-1</sup> for reduction and oxidation respectively.
- A tool for design and optimization of CLOU process was developed using kinetic data.

## ARTICLE INFO

### Article history:

Received 6 May 2014

Received in revised form 23 June 2014

Accepted 24 June 2014

Available online 3 July 2014

### Keyword:

CO<sub>2</sub> capture  
Chemical looping  
CLOU  
Copper  
Kinetic

## ABSTRACT

The kinetic of reduction of CuO to Cu<sub>2</sub>O with N<sub>2</sub> + O<sub>2</sub> mixtures and the oxidation of Cu<sub>2</sub>O to CuO with O<sub>2</sub> of a Cu-based oxygen carrier for the CLOU process has been determined in a TGA. For kinetic determination, the O<sub>2</sub> concentrations were varied between 0 and 9 vol.% for reduction, and between 21 and 1.5 vol.% for oxidation reactions; temperature was varied between 1148 and 1273 K for the reduction and between 1123 and 1273 K for the oxidation. The oxygen carrier showed high reactivity both in oxidation and reduction reactions. The nucleation and nuclei growth model with chemical reaction control properly described the evolution of solids conversion with time. The Langmuir–Hinshelwood model was able to describe the effect of oxygen concentration on reduction and oxidation rates. The reaction order was 0.5 for reduction and 1.2 for the oxidation. The kinetic constant activation energies were 270 kJ mol<sup>-1</sup> for the reduction and 32 kJ mol<sup>-1</sup> for the oxidation. The kinetic model was used to calculate the solids inventory needed in the fuel reactor for complete combustion of three different rank coals. It was possible to use a low oxygen carrier inventory in the fuel reactor (160 kg/MW<sub>th</sub>) to supply the oxygen required to full lignite combustion. However, to reach high CO<sub>2</sub> capture efficiencies (>95%), oxygen carrier inventories in fuel reactor higher than 600 kg/MW<sub>th</sub> were needed with the lignite.

© 2014 Elsevier B.V. All rights reserved.

## 1. Introduction

Chemical Looping with Oxygen Uncoupling (CLOU) was proposed by Mattisson et al. [1] as an efficient way to burn solid fuels with CO<sub>2</sub> capture avoiding the slow gasification step happening in the fuel reactor of a Chemical Looping Combustion (CLC) unit, which was usually required for converting carbon in char into gaseous compounds. CLOU process is based on CLC technology where the oxygen is transferred to the fuel by an oxygen carrier that circulates between two reactors; fuel and air reactors. CLOU process is based on the use of oxygen carrier materials which

release gaseous oxygen and thereby allowing the solid fuel to burn with gas phase oxygen. These materials can be also regenerated at high temperatures in the air reactor. CuO, Mn<sub>2</sub>O<sub>3</sub> and Co<sub>3</sub>O<sub>4</sub> have been identified as possible metal oxides with the property of release oxygen [1].

Fig. 1 shows a schematic diagram of a CLOU system. The fuel is physically mixed with the oxygen carrier in the fuel reactor. In the fuel reactor the fuel conversion is produced by different reactions. First the oxygen carrier releases oxygen according to:



and the solid fuel begins to devolatilize producing a carbonaceous solid residue (char, mainly composed by carbon and ash) and volatile matter as gas product:

\* Corresponding author. Tel.: +34 976 733977; fax: +34 976 733318.

E-mail address: [pgayan@icb.csic.es](mailto:pgayan@icb.csic.es) (P. Gayán).





FR	fuel reactor	Red	reduction reaction
OC	oxygen carrier		
Ox	oxidation reaction		

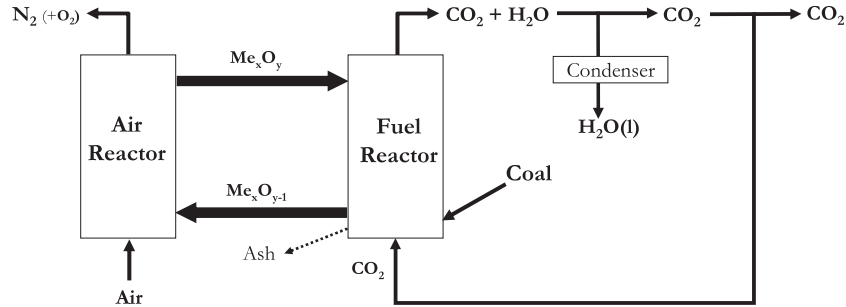
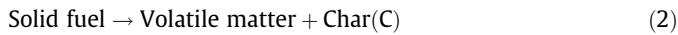
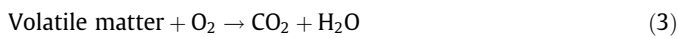


Fig. 1. Schematic layout of the CLOU system.



Then, volatiles and char are burnt as in usual combustion with gaseous oxygen according to reactions (3) and (4):



After steam condensation, a pure CO<sub>2</sub> stream is obtained from the fuel reactor. The reduced oxygen carrier is transported to the air reactor, where the oxygen carrier is regenerated to the initial oxidation stage with the oxygen of the air to be ready for a new cycle. Ideally, the exit stream of the air reactor contains only N<sub>2</sub> and unreacted O<sub>2</sub>. The heat release over the fuel and air reactors is the same as for conventional combustion. Therefore CLOU process has a low energy penalty for CO<sub>2</sub> separation and low CO<sub>2</sub> capture costs are expected.

Up to date, several materials have been proposed to be used as oxygen carriers in the CLOU process. Cu-based [2–4] and Mn-based materials mixed with Ca, Mg, Cu, Ni, Fe or Si [5] have focused great attention. Adánez et al. [6] and Mattisson [7] summarize the oxygen carrier developed for CLOU and the facilities where have been tested. However, the proof of the concept of CLOU process burning coal in a continuous unit has been only demonstrated with a Cu-based oxygen carrier [8]. This oxygen carrier, consists of 60 wt.% of CuO and 40 wt.% MgAl<sub>2</sub>O<sub>4</sub> prepared by spray drying [8,9], and it was named as Cu60MgAl. The effect of the coal rank was also analysed [10] in the CLOU unit using one anthracite, two bituminous coals, a lignite with high sulphur content [11] and biomass [12]. Complete combustion using a solids inventory in the fuel reactor of 235 kg/MW<sub>th</sub> was reached. In conjunction, values close to 100% of carbon capture efficiency were obtained at 1233 K with reactive coals and biomass. In all cases, the oxygen carrier particles showed good behaviour, as reactivity was unchanged and agglomeration problems did not occur.

For the design of the air and fuel reactors of a CLOU unit it is necessary to know the kinetic of oxidation and reduction rates of the oxygen carrier together with the kinetic of coal combustion reactions in the operation window for CLOU process. Previous kinetic studies of Cu-based oxygen carriers were mainly carried out in the window of CLC conditions, in a range of temperature between 723 and 1073 K [13]. This temperature interval is lower than that needed in CLOU process. The main difference between

the CLC and the CLOU process is that in CLOU process the oxygen carrier reduction is from CuO to Cu<sub>2</sub>O. This reaction is favoured at high temperatures as can be seen with the equilibrium diagram in Fig. 2, being the oxygen concentration at equilibrium a function of the temperature as:

$$\begin{aligned} C_{\text{O}_2, \text{eq}} &= \frac{101325}{R_g T} K_{\text{eq}} \\ &= \frac{101325}{R_g T} \exp(22 - 2.993 \cdot 10^4 T^{-1} - 1.048 \cdot 10^6 T^{-2}) \quad (5) \end{aligned}$$

Thermodynamic equilibrium set the temperatures and oxygen concentrations suitable for the CLOU process. So, the oxygen concentration at equilibrium conditions must be high enough to allow the O<sub>2</sub> release in the fuel reactor and also the combustion of the fuel at the fuel reactor temperature. Moreover, the oxygen carrier must be able to oxidize by oxygen in the air reactor, but the oxygen concentration should be as low as possible in order to maximize the oxygen utilization. For example, with Cu-based materials the temperatures should be between 1173 and 1223 K in both reactors [8,10] corresponding to oxygen concentration values at equilibrium conditions of 1.4 and 4.2 vol.%, respectively.

At high temperature and in an atmosphere with oxygen concentration lower than the equilibrium, the CuO is reduced to Cu<sub>2</sub>O

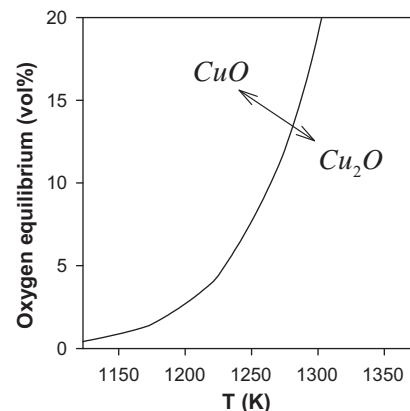


Fig. 2. Equilibrium oxygen concentration over the CuO/Cu<sub>2</sub>O system as a function of temperature.

generating gaseous oxygen. This fact makes that the oxygen concentration at equilibrium a thermodynamic restriction in the reduction reaction affecting to the reduction rate. Thus, the oxygen concentration must be in a range from 0 to the oxygen equilibrium concentration in the fuel reactor. Furthermore, in the CLOU process the reduction stops at  $\text{Cu}_2\text{O}$  instead of at Cu, allowing to work at higher temperatures in CLOU than in CLC without the risk of oxygen carrier agglomeration by melting ( $T_{\text{fusion}} = 1508 \text{ K}$  for  $\text{Cu}_2\text{O}$  and  $1357 \text{ K}$  for Cu). Oxidation would be carried out at the air reactor in an oxygen concentration range between 21 vol.%  $\text{O}_2$  and the oxygen equilibrium concentration.

There are some studies on the reduction, or oxygen uncoupling, and oxidation kinetic for Cu-based materials. Table 1 shows a resume of the main kinetic parameters studied in the literature for CLOU or similar processes for the reduction and oxidation reactions; also the oxygen carrier (CuO content, support and preparation method) and the model used were shown. Most of the works were focused on the evaluation of the effect of temperature on reaction rate, thus calculating the activation energy of the process. Two types of reaction rate equations have been used to represent the CuO oxygen uncoupling and  $\text{Cu}_2\text{O}$  oxidation reaction for the CLOU process [14,15]:

$$(-r_{\text{Red}})_{\text{OC}} = k_1 \cdot f(X) \quad (6)$$

$$(-r_{\text{Red}})_{\text{OC}} = k_2 \cdot (C_{\text{O}_2, \text{eq}} - C_{\text{O}_2})^m \cdot f(X) \quad (7)$$

It can be seen that in Eq. (6) the reduction rate only depends on temperature (included in the kinetic constant) and on oxygen carrier conversion,  $f(X)$ . On the other hand, reaction rate also depends on the oxygen concentration in Eq. (7). Different values for the activation energy were obtained either Eq. (6) or (7) was considered.

Thus, a global activation energy ( $E_1$ ) for  $k_1$  in Eq. (6) was calculated when the effect of temperature on both the chemical reaction barrier and the thermodynamic barrier was considered. But the kinetic activation energy was calculated for  $k_2$  in Eq. (7), which separates the thermodynamic barrier ( $E_{\text{th}}$ ) from the chemical reaction barrier ( $E_2$ ).

Eqs. (6) and (7) are also valid for the oxidation reaction considering the oxidation reaction rate,  $(r_{\text{Ox}})_{\text{OC}}$ , can be calculated by  $(r_{\text{Ox}})_{\text{OC}} = (-1)^m (-r_{\text{Red}})_{\text{OC}}$ . If the reaction order is  $n' \approx 1$ , the global activation energy for  $k_1$  can be calculated approximately as  $E_1 \approx E_2 + E_{\text{th}}$ , being  $E_{\text{th}} = 255 \cdot 10^3 \text{ J/mol}$  in Eq. (5). It can be seen that different values for the activation energy were obtained either Eq. (6) or (7) was considered. Thus, a global activation energy ( $E_1$ ) for  $k_1$  in Eq. (6) was calculated when the effect of temperature on both the chemical reaction barrier and the thermodynamic barrier was considered jointly. But kinetic activation energy due to chemical reaction barrier ( $E_2$ ) calculated for  $k_2$  in Eq. (7) was decoupled from the thermodynamic barrier ( $E_{\text{th}}$ ) considered by the oxygen concentration at equilibrium condition.

Respect to the reduction, Chadda et al. [16] did an analysis of the copper oxide capacity of storage chemical energy for a process similar to CLOU. They studied the same reaction of decomposition of CuO in a range of temperatures from 1033 to 1183 K. In this work, a global activation energy of 313 kJ/mol for the decomposition reaction was found. Eyring et al. [17] studied the reduction kinetic for a pure CuO oxygen carrier in a TGA. They obtained a value of the activation energy for the reduction of 327 kJ/mol using an empirical first order reaction, developed for their purposes of modelling.

Similar results were found by Clayton and Whitty [15]. They determined in a TGA the reduction kinetic rate for two different

**Table 1**  
Relevant kinetic studies for CLOU conditions on CuO reduction and  $\text{Cu}_2\text{O}$  oxidation.

Oxygen carrier (wt.% CuO)	Support	Preparation method <sup>a</sup>	$dp$ ( $\mu\text{m}$ )	Facility <sup>b</sup>	$T$ (K)	$E_A$ (kJ/mol)		Model	Ref.
						Global	Kinetic		
<i>Reduction</i>									
Pure	–	–	10	TGA	1033–1183	313	–	First order	[14]
Pure	–	–	104–152	TGA	1123–1233	327	–	First order	[17]
40	$\text{MgAl}_2\text{O}_4$	FG	125–180	bFBR	1123–1173	139	–	Avrami–Erofeev ( $N = 2$ )	[22]
42	SiC	I	105–150	TGA	1123–1223	220	–	First order	[20]
60	$\text{SiO}_2$	MM	200–315	TGA	1073–1223	145	–	Avrami–Erofeev ( $N = 3$ )	[21]
20	$\text{SiO}_2$	IW	<45	TGA	1173–1273	170	–	First order	[19]
			75–125	bFBR					
18	$\text{SiO}_2$	I	125–210	FxBR					
			106–150	TGA	1073–1173	315	–	Avrami–Erofeev ( $N = 2$ )	[18]
60	$\text{TiO}_2$	MM	1173–1248		176				
			200–315	TGA	1073–1223	155	–	Avrami–Erofeev ( $N = 3$ )	[21]
50	$\text{TiO}_2$	MM	<45	TGA	1173–1273	180	–	First order	[19]
			75–125	bFBR					
50	$\text{TiO}_2$	MM	125–210	FxBR					
			<45	TGA	1073–1173	284	58	First order	[15]
60	$\text{ZrO}_2$	MM	200–315	TGA	1073–1223	153	–	Avrami–Erofeev ( $N = 3$ )	[21]
55	$\text{ZrO}_2$	FG	<45	TGA	1073–1273	147	–	First order	[19]
			75–125	bFBR					
45	$\text{ZrO}_2$	FG	125–210	FxBR					
			<45	TGA	1048–1198	264	67	First order	[15]
40	$\text{ZrO}_2$	FG	125–180	bFBR	1173–1258	281	20	First order	[14]
<i>Oxidation</i>									
Pure	–	–	Disc (5 mm i.d. <sup>c</sup> )	TGA	>1173	173–98	–	First order	[23]
Pure	–	–	10	TGA	673–773	76.5	–	First order	[14]
18	$\text{SiO}_2$	I	106–150	TGA	1073–1173	3	–	Phase boundary reaction ( $N = 2$ )	[18]
					1173–1248	–43			
55	$\text{ZrO}_2$	FG	<45	TGA	1123–1273	–	202	First order	[19]
			75–125	bFBR					
			125–210	FxBR					

<sup>a</sup> Key for preparation method: I = impregnation; IW = incipient wetness; MM = mechanical mixing; FG = freeze granulation.

<sup>b</sup> Key for facility: bFBR = batch fluidized bed reactor; FxBR = fixed bed reactor; TGA = thermogravimetric analyzer.

<sup>c</sup> i.d = Inner diameter.

Cu-based oxygen carriers: 50 wt.% CuO/TiO<sub>2</sub> and 45 wt.% CuO/ZrO<sub>2</sub>, prepared by mechanical mixing and freeze granulation respectively. The global activation energies determined were 284 kJ/mol (CuO/TiO<sub>2</sub>) and 264 kJ/mol (CuO/ZrO<sub>2</sub>). These values were slightly lower than the values obtained by Chadda et al. [16,17] or Eyring et al. [16,17], but they were still high when compared to results from others.

Song et al. [18] studied in a TGA the kinetic of a Cu-based oxygen carrier with 18 wt.% of CuO supported on SiO<sub>2</sub>, prepared by impregnation for the Chemical Looping Air Separation (CLAS) process, which uses the same oxygen uncoupling property of some metal oxides to separate oxygen from air. They considered the best model to be the Avrami–Erofeev nucleation model ( $N = 2$ ) with two different zones as a function of the temperature range, for temperatures between 1073 and 1173 K the global activation energy was 315 kJ/mol and in the range 1173–1248 K they obtained a value of 176 kJ/mol. This suggests that the temperature could affect to the calculated activation energy. This behaviour was also found for a CuO (50 wt.%) oxygen carrier with TiO<sub>2</sub> as supporting material [19]. Thus, an activation energy of 284 kJ/mol was found in the 1073–1173 K temperature interval [15], but it was lower (180 kJ/mol) if the range of temperature was increased to 1173–1273 K [19]. The same authors reported average activation energy for a Cu-based material supported on ZrO<sub>2</sub> of 147 kJ/mol in the temperature interval of 1073–1273 K [19], but also a decrease in the activation energy with temperature could be seen from the Arrhenius plot they showed. Similarly, Peterson et al. [20] prepared Cu-based oxygen carrier materials by impregnation on SiC. They obtained a value of global activation energy for an oxygen carrier with 42 wt.% of CuO in the middle interval (220 kJ/mol) when the temperature was varied from 1123 to 1223 K.

However, other authors have determined activation energy values in the lower range at the low temperature interval, and even high activation energy values in the upper temperature interval; see Table 1. The reasons for obtaining high or low activation energy values are not clear. Thus, comparing results obtained with similar materials, e.g. Cu-based oxygen carriers with copper content in the range 40–60 wt.% and using ZrO<sub>2</sub> as inert material, activation energy values ranged from 147 to 281 kJ/mol [14,15,19,21]. Nevertheless, the global activation energy was calculated to be in the lower range in most of the works. Arjmand et al. [22] studied the kinetic in a batch fluidized bed reactor of a Cu-based oxygen carrier (40 wt.% of CuO and 60 wt.% MgAl<sub>2</sub>O<sub>4</sub>) prepared by freeze granulation. They obtained a value of the global activation energy of 139 kJ/mol using the Avrami–Erofeev model ( $N = 2$ ). Wang et al. [21] studied the reduction reaction kinetic using three Cu-based oxygen carrier with 60 wt.% of CuO and 40 wt.% of three different supports (ZrO<sub>2</sub>, TiO<sub>2</sub> and SiO<sub>2</sub>) for CLAS process. The oxygen carriers were prepared by mechanical mixing and tested in a TGA. They obtained a value of the global activation energy of 153 kJ/mol (CuO/ZrO<sub>2</sub>), 155 kJ/mol (CuO/TiO<sub>2</sub>) and 145 kJ/mol (CuO/SiO<sub>2</sub>) and they proposed to use the Avrami–Erofeev model ( $N = 3$ ). Similar global activation energy value of 170 kJ/mol was found for a CuO/SiO<sub>2</sub> material by Whitty and Clayton [19].

Also, the equipment used for reactivity investigation seems to be of low relevance. For example, Whitty and Clayton [19] studied the effect of the temperature in the reduction of three Cu-based oxygen carriers: 20 wt.% CuO/SiO<sub>2</sub>, 50 wt.% CuO/TiO<sub>2</sub> and 55 wt.% CuO/ZrO<sub>2</sub>, prepared by incipient wetness, mechanical mixing and freeze granulation, respectively. They tested the oxygen carriers in 3 different reactor types (TGA, fluidized bed reactor and fixed bed reactor) obtaining similar results with the three facilities.

If the kinetic and the thermodynamically barriers were separated, lower values of the kinetic activation energies were determined, as result of including the temperature effect on the

thermodynamic barrier; see Eq. (7). Thus, the following values for the kinetic activation energy has been reported: 58 kJ/mol [15] for CuO/TiO<sub>2</sub>, and 67 kJ/mol [15] or 20 kJ/mol [14] for CuO/ZrO<sub>2</sub>.

Moreover, Clayton and Whitty [15] studied the reaction order with respect to the oxygen partial pressure; they observed that the reaction rate decreased as the driving force decreased, and with an unexpected great decrease when the oxygen partial pressure was near the equilibrium pressure. However, only experiments far from the O<sub>2</sub> equilibrium were considered to obtain a reaction order of 1. Sahir et al. [14] calculated the reaction order with respect to CuO and obtained a value of 0.

Respect to the oxidation rate, Chadda et al. [16] did an analysis of the capacity of chemical energy storage with copper materials during the oxidation of Cu<sub>2</sub>O in a range of temperatures from 673 to 773 K. In this work, an activation energy value of 76.5 kJ/mol for oxidation was found. Zhu et al. [23] reviewed the oxidation rate of a Cu plate of very high purity in a high range of temperatures from 623 to 1323 K, for metallurgical purposes. They conclude that at high temperatures (>1173 K, typical for CLOU operation) lattice diffusion controlled the copper oxidation, and the activation energy were between 173 and 98 kJ/mol as a function of the formation of a double- or single-layer respectively.

Also, some works have studied the kinetic behaviour during oxidation of Cu<sub>2</sub>O for CLC. Peterson et al. [20] observed that the oxidation rate decreased somewhat when the temperature increases, due to the decrease of the driving force, i.e. the difference ( $C_{O_2} - C_{O_2,eq}$ ). Whitty and Clayton [19] obtained an activation energy of 202 kJ/mol in the temperature interval of 1123–1273 K when the driving force was maintained constant, which suggests that the activation energy of the thermodynamic barrier is some higher than the kinetic activation energy. The activation energy calculated by Whitty and Clayton [19] was higher than the values obtained by Zhu et al. [23]. They blame this higher apparent activation energy due to the presence of defects in the material that inhibits the lateral grown of the CuO grains [23]. Finally, Song et al. [18] studied the oxidation of different Cu-based oxygen carriers prepared by dry impregnation for CLAS (18, 29 and 48 wt.% of CuO). They evaluated the effect of the temperature in the oxidation rate, obtaining two different zones respect to the activation energy: in the range of 1073–1173 K the activation energy is positive with a value of 3 kJ/mol, but at temperatures in the 1173–1248 K interval the value of the activation energy is –43 kJ/mol. They considered that the negative value is due to both the thermodynamic barriers of the Cu<sub>2</sub>O oxidation and the high diffusional barrier caused by the sintering effects at high temperatures [18,23]. Also, they considered that the best model to describe the oxidation rate is a Boundary reaction model. Using this model they analysed the effect of the oxygen partial pressure during the oxidation and they obtained a reaction order for the oxygen partial pressure of 0.5. However, they use O<sub>2</sub> partial pressures far from the equilibrium partial pressure. Whitty and Clayton, [19] observed the oxidation rate decreased when the O<sub>2</sub> concentration decreased, but lower than they expected when the O<sub>2</sub> concentration approached to equilibrium. Chuang et al. [24] studied the oxidation kinetic with a CuO/Al<sub>2</sub>O<sub>3</sub> oxygen carrier prepared by co-precipitation in a fluidized bed reactor. They studied the reaction order for the oxygen concentration and they observed that the order varied with the O<sub>2</sub> concentration. They explain that this behaviour is typical when the reaction rate is controlled by a Langmuir–Hinshelwood mechanism.

As a conclusion, very disperse values for the kinetic data of Cu-based materials for CLOU were found. These data were found from studies analyzing only temperature dependency or oxygen concentration but far away from equilibrium conditions. For these reasons, it is necessary to analyze the effect of temperature and

oxygen concentration on oxidation and reduction reactions in a broad range of operation values.

The aim of this work was to determine the kinetic of reduction in  $N_2$ – $O_2$  mixtures and oxidation reactions with  $O_2$  of a Cu-based oxygen carrier (Cu60MgAl) prepared by spray drying in the range of operation of the CLOU process. This material has been previously used to successfully prove the CLOU concept with several solid fuels. The effect of  $O_2$  concentration and temperature was investigated both for oxygen uncoupling and oxidation processes in TGA. The kinetic parameters obtained were used to determine the solids inventories needed in a CLOU system working with this Cu-based oxygen carrier. Kinetic parameters obtained in this work can be implemented in a design and optimization tool for CLOU process.

## 2. Experimental

### 2.1. The Cu-based oxygen carrier

The oxygen carrier used in this work was a Cu-based material prepared by spray drying. Oxygen carrier particles were manufactured by VITO (Flemish Institute for Technological Research, Belgium) using CuO (Panreac, PRS) and  $MgAl_2O_4$  spinel (Baikowski, S30CR) as raw materials. The particles were calcined 24 h at 1373 K. The CuO content was 60 wt.%. The particle size of the oxygen carrier was +0.1 to 0.3 mm. From now on, the oxygen carrier is named as Cu60MgAl. Table 2 shows the main properties of this material, which were presented in previous works [2,8–11,25].

The oxygen transport capacity,  $R_{OC}$ , is an important characteristic of the oxygen carrier.  $R_{OC}$  has relevance on the solids circulation rate and solids inventory in a CLC unit [26].  $R_{OC}$  was calculated in TGA in nitrogen atmosphere as  $R_{OC} = (m_{Ox} - m_{Red})/m_{Ox}$ , being  $m_{Ox}$  the mass of fully oxidized particles and  $m_{Red}$  in the reduced form after oxygen uncoupling, i.e. when all CuO has been reduced to  $Cu_2O$ .

Preliminary results showed that this material has adequate values of reactivity and oxygen transport capacity in fluidized-bed conditions [9,25]. High combustion rates with complete combustion to  $CO_2$  and  $H_2O$  were obtained with this material using a low solids inventory in the fuel reactor of a CLOU unit burning different types of coal and biomass [8,10].

### 2.2. Experimental set-up

Multicycle tests to analyze the reactivity of the oxygen carrier during successive reduction–oxidation cycles were carried out in a TGA CI Electronics type described elsewhere [2]. The desired mass of oxygen carrier was loaded in a platinum wired mesh basket (14 mm diameter and 8 mm height). Initially, to establish whether thermodynamic limitations, external film mass transfer and/or inter-particle diffusion were affecting the reaction rate, the sample weight and the gas flow rate were varied in the range of 40–100 mg and from 10 to 40 NL/h. The composition of the gas flow were pure  $N_2$  for the reduction and air for the oxidation.

**Table 2**  
Properties of the oxygen carrier Cu60MgAl.

CuO content (wt.%)	60
Oxygen transport capacity, $R_{OC}$ (wt.%)	6
Crushing strength (N)	2.4
Skeletal density ( $kg/m^3$ )	4600
Porosity (%)	16.1
Specific surface area, BET ( $m^2/g$ )	<0.5
XRD main phases	CuO, $MgAl_2O_4$

\* Reduction from CuO to  $Cu_2O$ .

It was found that using a sample mass lower than 70 mg, the control of gas diffusion inside the particles was avoided. On the other hand, it was found that the reaction rate was not controlled by interparticle diffusion or diffusion through the gas film around the particle when  $N_2$  flow was higher than 20 NL/h. Therefore, gas flow rate of 25 NL/h and 50 mg of solids were used to reduce mass transfer resistance around the solid sample. As it was shown by Gayán et al., [2], the use of these conditions ensured the minimization of external film mass transfer and/or inter-particle diffusion effects in the TGA. Moreover, the temperature in the reaction zone can greatly affect to the reaction rate and it was carefully checked. Deviations lower than 2 K were found in all cases during the reaction period. Moreover, previous studies showed that oxygen carrier particles can be considered isothermal during reduction or oxidation [27].

The sample was heated to the set operating temperature in air atmosphere. After stabilization, the experiment started by exposing the oxygen carrier to alternating reducing and oxidizing conditions. The experiments were carried out at temperatures between 1123 and 1273 K for the reduction and oxidation reactions. These temperatures were selected as a function of the thermodynamic equilibrium of the CuO/ $Cu_2O$  system, as shown in Fig. 2, being this temperature interval of interest for fuel and air reactors in CLOU process [8,10].

The reaction gas mixture was composed by  $O_2$  and  $N_2$  in different relations for the reduction and oxidation. Table 3 summarizes both temperature and oxygen concentrations used for reduction and oxidation tests. For the reduction, the amount of  $O_2$  varied from 0 to 9 vol.%. In the case of the oxidation, the oxidation reaction was carried out after reducing the oxygen carrier in  $N_2$  at 1273 K and the concentration of  $O_2$  was varied between 21 and 2.5 vol.%. These conditions allowed studying the effect of the oxygen concentration far away and near the equilibrium conditions. Three cycles of reduction and oxidation were carried out for each experiment. In all cases, reaction rate was stable during cycles. Conversion vs. time curves showed in this work corresponded to the third cycle of each experimental condition.

### 2.3. Data evaluation

The release of  $O_2$  (reduction of CuO) and the oxidation of  $Cu_2O$  is given by the following equilibrium:



The oxygen carrier conversion was calculated for the reduction and oxidation as:

$$X_{Red} = \frac{m_{Ox} - m}{m_{Ox} - m_{Red}} \quad (9)$$

$$X_{Ox} = 1 - \frac{m_{Ox} - m}{m_{Ox} - m_{Red}} \quad (10)$$

**Table 3**  
Experimental conditions for TGA tests.  $O_2$  concentrations at thermodynamic equilibrium also shown.

Reduction			Oxidation		
T (K)	$y_{O_2}$ (%) <sup>*</sup>	$y_{O_2,eq}$ (%)	T (K)	$y_{O_2}$ (%) <sup>*</sup>	$y_{O_2,eq}$ (%)
1148	0	0.8	1148	21	0.4
1173	0	1.4	1173	21, 11, 9, 4, 2.5	0.8
1198	0	2.4	1198	21	1.4
1223	0, 1.5, 2.5	4.2	1223	21	2.4
1248	0, 1.5, 4	7.0	1248	21	4.2
1273	0, 1.5, 4, 6, 8, 9	11.6	1248	21	7.0
			1273	21	11.6

\*  $N_2$  to balance.

being  $m$  the mass of sample at each time,  $m_{\text{Ox}}$  is the mass of the sample fully oxidized and  $m_{\text{Red}}$  is the mass of the sample in the reduced form, i.e. when copper was in the  $\text{Cu}_2\text{O}$  form.

The reaction rate for both, reduction and oxidation, are calculated from TGA conversion data using the following expressions:

$$(-r_{\text{Red}})_{\text{OC}} = R_{\text{OC}} \frac{dX_{\text{Red}}}{dt} \quad (11)$$

$$(r_{\text{Ox}})_{\text{OC}} = R_{\text{OC}} \frac{dX_{\text{Ox}}}{dt} \quad (12)$$

### 3. Results

To obtain the reduction and oxidation kinetic, TGA tests were carried out varying the temperature and the oxygen concentration in a wide range of values, from faraway of the equilibrium to values near the equilibrium.

#### 3.1. TGA results for oxygen uncoupling ( $\text{CuO}$ to $\text{Cu}_2\text{O}$ )

Fig. 3(a) shows conversion versus time curves for the Cu60MgAl oxygen carrier for different temperatures between 1148 and 1273 K, using pure  $\text{N}_2$  in the reacting environment during the reduction, and a  $\text{O}_2$  concentration equal to 0 vol.%. It can be seen that when the temperature increases, the reduction rate increases. Considering reduction rate given by Eq. (7), reaction rate increased with temperature because the increase of the kinetic constant and the oxygen driving force. Often, this effect is expressed by means of the difference between the oxygen concentration at equilibrium and the oxygen concentration in the system surrounding of the particles, i.e.  $(C_{\text{O}_2,\text{eq}} - C_{\text{O}_2})$ . Thus, the reduction rate depends on the  $\text{O}_2$  concentration at the external surface of the particles and the  $\text{O}_2$  concentration at equilibrium conditions, which also increases with temperature following Eq. (5).

Fig. 3(b) shows the conversion versus time curves obtained for the Cu60MgAl oxygen carrier for three different temperatures during the reduction, using a concentration of 1.5 vol.% of  $\text{O}_2$  in  $\text{N}_2$ . It can be observed that these curves were slower than the curves at the same temperature without oxygen. This figure confirms that the reaction rate decreases when the driving force decreases due to the approaching of the  $\text{O}_2$  concentration to the equilibrium concentration.

To analyse the effect of the oxygen concentration on the reduction rate, Fig. 4 shows conversion vs. time curves for oxygen

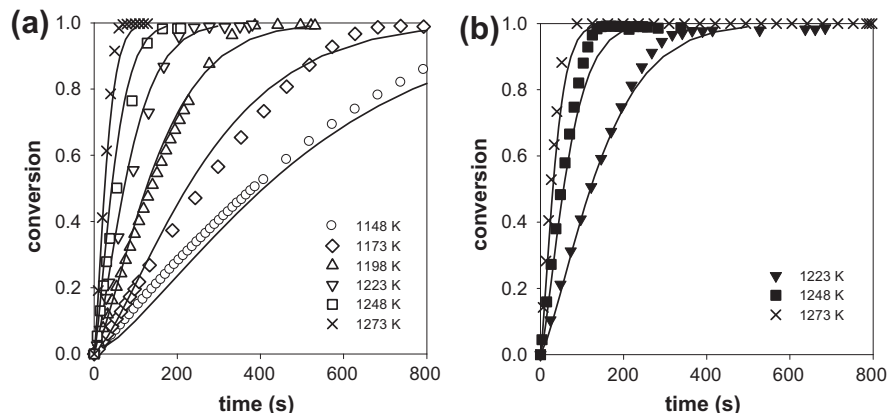


Fig. 3. Effect of temperature (a)  $y_{\text{O}_2} = 0$  vol.%, and (b)  $y_{\text{O}_2} = 1.5$  vol.%, on the oxygen carrier reduction rate using  $\text{N}_2$ . Symbols, experimental data; continuous line, model predictions.

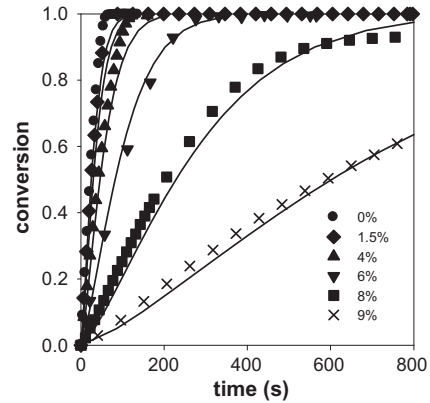


Fig. 4. Effect of oxygen concentration (vol.%) at 1273 K on the oxygen carrier reduction, using  $\text{N}_2 + \text{O}_2$  mixtures. Symbols, experimental data; continuous line, model predictions.

reduction reaction of Cu60MgAl obtained for  $\text{O}_2$  concentration values from 0 to 9 vol.% at 1273 K. This interval of  $\text{O}_2$  concentration has been chosen due to the maximum  $\text{O}_2$  concentration is limited by the  $\text{O}_2$  concentration at equilibrium condition, e.g. 12 vol.% at 1273 K; so  $\text{O}_2$  concentration during TGA test was lower than equilibrium concentration. The oxygen uncoupling rate decreases when the  $\text{O}_2$  concentration increases due to the decrease in the driving force of the reaction. This decrease was more pronounced when the  $\text{O}_2$  partial pressure was close to the equilibrium concentration. Moreover, it was not possible to detect a change in the mass of the sample in the TGA when the  $\text{O}_2$  concentration was very close to the equilibrium ( $y_{\text{O}_2} > 9$  vol.%), because the reaction rate was very slow. This behaviour was also described by Clayton and Whitty [15], during the reduction when the driving force was close to zero.

#### 3.2. TGA results for oxidation ( $\text{Cu}_2\text{O}$ to $\text{CuO}$ )

Fig. 5(a) shows conversion vs. time curves obtained for oxidation of  $\text{Cu}_2\text{O}$  in reduced oxygen carrier samples at oxygen concentration values from 21 to 2.5 vol.% at 1173 K. The oxidation rate was fast when the oxygen concentration was much higher than the oxygen concentration at equilibrium conditions, but quickly decreases as the oxygen concentration approach to the equilibrium concentration. This effect also was observed by Whitty and Clayton [19] when the driving force of the oxidation reaction decreased. Fig. 5(b) shows conversion vs. times curves for the Cu60MgAl oxy-

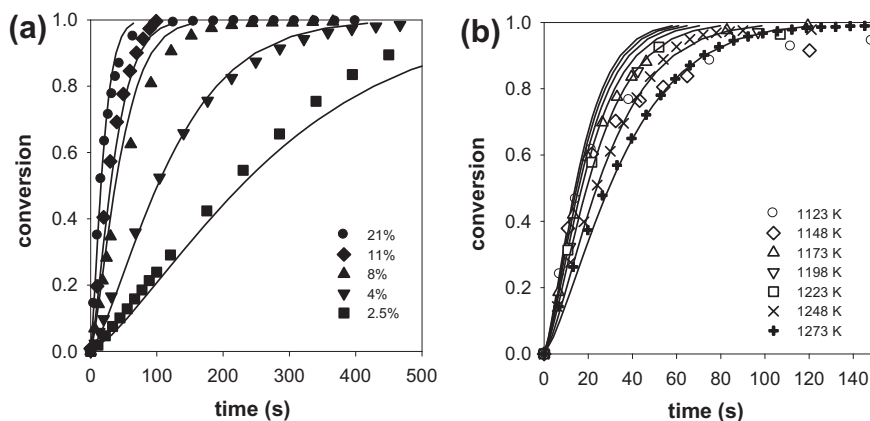


Fig. 5. Effect of (a)  $O_2$  concentration (vol.%) at 1173 K and (b) temperature with a  $y_{O_2} = 21$  vol.%, on the oxygen carrier oxidation. Symbols, experimental data; continuous line, model predictions.

gen carrier for different temperatures between 1123 and 1273 K, using air as reactant gas. It can be seen that reaction rate decreased when the temperature increased, being the slowest the reaction at 1273 K, due to the decrease in the driving force of the reaction, which in this case is  $(C_{O_2} - C_{O_2,eq})$ . So, the oxygen driving force decreases as temperature increases due to  $C_{O_2,eq}$  increases with temperature. This behaviour was observed by Zhu et al. [23] for the oxidation of pure copper, but with an additional reason to justify their results. They considered that the decrease in the oxidation rate with the temperature was due to the high diffusional barrier caused by the sintering effects at high temperatures, additionally to the thermodynamic barriers of the  $Cu_2O$  oxidation.

### 3.3. Kinetic information from conversion curves

With the different conversion vs. time curves obtained for the reduction and oxidation as a function of the temperature, it was possible to obtain the evolution of the reaction rate with solids conversion. The maximum values calculated for every curve was used to obtain the global activation energy for the reduction and oxidation rates from the Arrhenius plot; see Fig. 6. The calculated value of the global activation energy for the reduction reaction was 245 kJ/mol, which is in the same order than the values obtained by Sahir et al. [14] with a oxygen carrier 40 wt.% of CuO supported by  $ZrO_2$  (281 kJ/mol), Peterson et al. [20] for a material with 42 wt.% CuO being SiC the support (220 kJ/mol), and Clayton

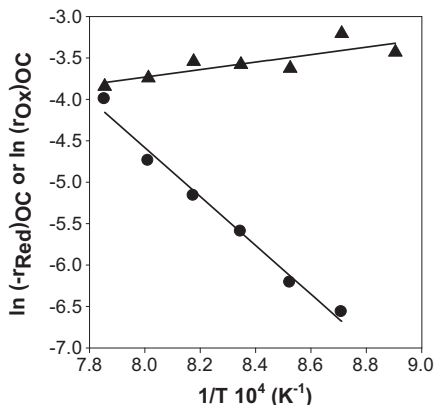


Fig. 6. Arrhenius plots to calculate global activation energy in Eq. (6): ●, reduction; ▲, oxidation; for the Cu60MgAl.

and Whitty [15] for two Cu-based oxygen carriers with a 50 wt.% and 45 wt.% of CuO supported on  $TiO_2$  (284 kJ/mol) and  $ZrO_2$  (264 kJ/mol), respectively.

Following the same procedure, a value for the apparent activation energy of  $-37$  kJ/mol was calculated for the oxidation reaction; see Fig. 6. This value is similar to the value obtained by Song et al. [18], who calculated a negative apparent activation energy of  $-43$  kJ/mol in the range of temperature 1173–1248 K.

Moreover, from the conversion vs. time curves obtained at different oxygen concentrations, some information can be extracted about the reaction order with respect to the oxygen concentration considering Eq. (7). Fig. 7(a) shows the curve of the  $\ln(-r_{Red})_{OC}$  as a function of the  $\ln(C_{O_2,eq} - C_{O_2})$ . Considering Eq. (7), the reaction order corresponded to the slope in Fig. 7(a). However, a constant slope cannot be calculated, which means that the reaction order changed with the oxygen concentration. Considering results showed in Fig. 7(a), an expression for the effect of oxygen concentration such Eq. (7), i.e.  $f(C_g) = (C_{O_2,eq} - C_{O_2})^{n'}$ , seemed to be not valid when a wide range of values of oxygen concentration was considered.

Similarly to the analysis of the reduction period, Fig. 7(b) shows the reaction rate as a function of the oxygen concentration. In this case a constant slope can be calculated. Therefore, the reaction order does not depend on the oxygen concentration, and it was found a  $n'$  value of 1. However, Chuang et al. [24] observed a change in the reaction order with the oxygen concentration for the oxidation of a Cu-based oxygen carrier, similarly to what we found for the reduction in this work. Chuang et al. [24] suggested that this behaviour can be explained by using a Langmuir–Hinshelwood mechanism for the  $Cu_2O$  oxidation.

Subsequently, the Langmuir–Hinshelwood mechanism was considered in this work to determine the kinetic for the reduction reaction. To be consequent with the reduction, also a Langmuir–Hinshelwood mechanistic model was used to describe the oxidation in the CLOU process. In this way, results obtained here and found by Chuang et al. [24] could be adequately predicted for the oxidation reaction.

### 3.4. Kinetic model

#### 3.4.1. Reduction from CuO to $Cu_2O$

A surface reaction model using a Langmuir–Hinshelwood mechanism is here proposed to describe the CuO reduction reaction to  $Cu_2O$  with  $O_2$  generation. The CuO in the surface decomposes into  $Cu_2O$  by reaction with  $a$  active sites giving oxygen adsorbed in the

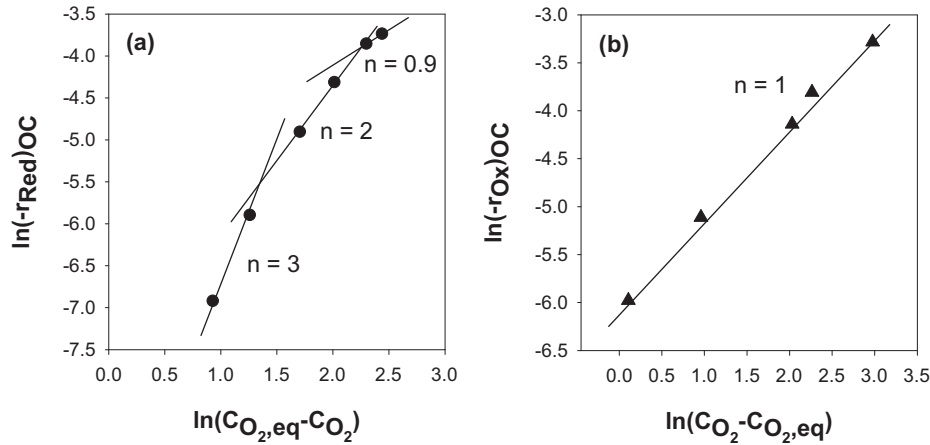
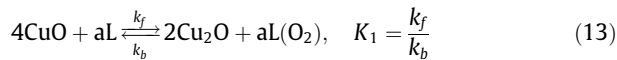


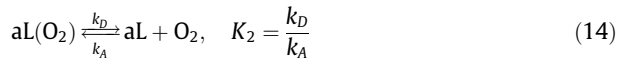
Fig. 7. Effect of the oxygen concentration in the reaction order of Eq. (7) for: (a) reduction; (b) oxidation.

surface. Then oxygen is desorbed to  $O_2$ , regenerating the  $a$  active sites in the surface [28]. Applying this model to the decomposition of CuO, following equations are obtained:

- (1) Chemical decomposition of CuO into  $Cu_2O$  and adsorbed  $O_2$ , which is a dynamic equilibrium between forward and backward reaction:



- (2) Desorption of adsorbed  $O_2$ :



$aL(O_2)$  is one molecule of  $O_2$  chemisorbed on  $a$  active sites  $L$ .

When the reaction is controlled by chemical decomposition, Eq. (13), the reaction rate is given by:

$$\frac{dX_{Red}}{dt} = k_{Red} S_{CuO} (1 - \theta) \left(1 - \frac{C_{O_2}}{C_{O_2,eq}}\right) \cdot f(X_{Red}) \quad (15)$$

where  $\theta$  is the fraction of active sites occupied by  $O_2$ . At these conditions, it is possible to use different adsorption isotherms to obtain the value of  $\theta$ . García-Labiano et al. [29] selected the Freundlich isotherm to properly describe the  $CaCO_3$  calcination [29]. In this case, the use of the Freundlich isotherm successfully described the effect of  $CO_2$  concentration on the  $CaCO_3$  calcination rate, which showed an effect of the  $CO_2$  concentration on the reaction rate similar to the  $O_2$  effect observed for the reduction reaction in this work. Thus, the Freundlich isotherm was selected in this work to describe the fraction of occupied active sites, i.e.  $\theta$  parameter, which was calculated by the following equation:

$$\theta = c C_{O_2}^{1/n} \quad (16)$$

$$c = c_0 e^{-E_c/R_g T} \quad (17)$$

Combining Eqs. (15) and (16), the reaction rate expression is as follow:

$$\frac{dX_{Red}}{dt} = k_{Red} f(X_{Red}) S_{CuO} \left(1 - c C_{O_2}^{1/n}\right) \left(1 - \frac{C_{O_2}}{C_{O_2,eq}}\right) \quad (18)$$

Different models have been used for the  $f(X_{Red})$  function in Eq. (18), including nucleation mechanism [18,21,22] or first order chemical reaction [14,16]. The Langmuir–Hinshelwood mechanism is a surface reaction model widely used for gas–solid catalytic

reactions. Due to this surface reaction, in this work it was proposed using the nucleation model to describe the conversion dependency in the reaction at the grain surface of the oxygen carrier particles.

The Avrami–Erofeev [30] equation corresponding to the nucleation mechanism is the following:

$$f(X_{Red}) = N^{-1} (1 - X_{Red}) [-\ln(1 - X_{Red})]^{1-N} \quad (19)$$

The final expression for the reduction reaction rate, including Eq. (19) for the conversion function, is the following:

$$\frac{dX_{Red}}{dt} = k_{Red} S_{CuO} \left(1 - c C_{O_2}^{1/n}\right) \left(1 - \frac{C_{O_2}}{C_{O_2,eq}}\right) \cdot \left(N^{-1} (1 - X_{Red}) [-\ln(1 - X_{Red})]^{1-N}\right) \quad (20)$$

By integration of Eq. (20), the following equation was obtained to calculate the conversion evolution with time:

$$[-\ln(1 - X_{Red})]^N = k_{Red} S_{CuO} \left(1 - c C_{O_2}^{1/n}\right) \left(1 - \frac{C_{O_2}}{C_{O_2,eq}}\right) t \quad (21)$$

An effective kinetic constant was defined as:

$$k'_{Red} = k_{Red} S_{CuO} = k'_{Red,0} e^{-E_{Red}/R_g T} \quad (22)$$

The kinetic model has four parameters at each temperature ( $N$ ,  $n$ ,  $k'_{Red}$  and  $c$ ), which must be calculated as a function of temperature. The value of  $N$  represent the type of nucleation and the nuclei growth in the model, which value is usually fixed between 1/4 and 3. To calculate the best value of  $N$ , Fig. 8(a) shows a plot of  $(-\ln(1 - X_{Red}))^N$  vs. time for different values of  $N$  using conversion vs. time data of Fig. 3. Linear regression of each data shows the fit to a linear plot. Table 4 shows the values of the correlation coefficients for the different values of  $N$ . Best fitting to a linear curve correspond to  $N$  equal to 3/4. This procedure has been done for the conversion data at each temperature and oxygen concentration analysed in this work, obtaining the same result of  $N$  for all of them.

To determine the values of the chemical rate constant,  $k'_{Red}$ , and its variation with temperature, experiments carried out at different temperatures between 1148 and 1273 K with an atmosphere of 100 vol.%  $N_2$  were considered. In this case, Eq. (21) is simplified to  $[-\ln(1 - X_{Red})]^N = k'_{Red} t$ . Considering an Arrhenius dependence of  $k'_{Red}$ , Fig. 9 shows the Arrhenius plot for the reduction reaction, and Table 5 shows the kinetic parameters for pre-exponential factor and activation energies obtained. The value of the activation energy was 270 kJ mol<sup>-1</sup>. This value cannot be compared with activation energy data from the literature because the kinetic model here proposed has not been previously used. The activation energy



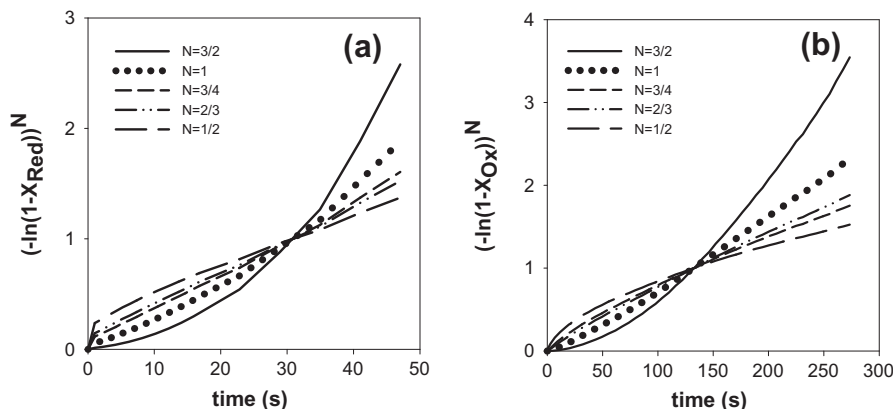


**Fig. 8.** Determination of  $N$  parameter using conversion data to calculate  $(-\ln(1-X))^N$  vs time (Eq. (21)) at (a) 1273 K, 4 vol.%  $O_2$  for reduction; and (b) 1173 K, 6 vol.%  $O_2$  for oxidation.

**Table 4**

Correlation coefficients of the linear dependence of  $(-\ln(1-X_{Red}))^N$  vs time plots for various values of  $N$  for Cu60MgAl oxygen carrier.  $T_{Red} = 1273$  K;  $y_{O_2,Red} = 4$  vol.%;  $T_{Ox} = 1173$  K;  $y_{O_2,Ox} = 6$  vol.%;

$N$	Reduction	Oxidation
3/2	0.9017	0.9570
1	0.9769	0.9970
3/4	0.9961	0.9977
2/3	0.9951	0.9926
1/2	0.9838	0.9703

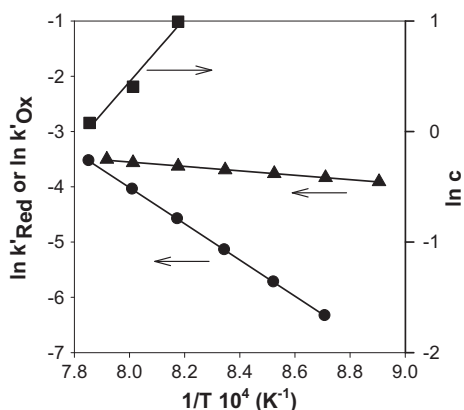


**Fig. 9.** Temperature dependence of kinetic parameters for Cu60MgAl: kinetic constant for oxygen uncoupling (●); kinetic constant for oxidation (▲); and adsorption parameter  $c$  for reduction (■).

**Table 5**

Kinetic parameters determined in this work for Cu60MgAl.

<b>Reduction</b>	
$k'_{Red,0}$ ( $s^{-1}$ )	$3.6 \cdot 10^9$
$E_{Red}$ ( $kJ mol^{-1}$ )	$2.7 \cdot 10^2$
$c_0$ ( $(m^3 mol^{-1})^{1/n}$ )	$1.8 \cdot 10^{-10}$
$E_c$ ( $kJ mol^{-1}$ )	$-2.4 \cdot 10^2$
$n$	0.5
<b>Oxidation</b>	
$k'_{Ox,0}$ ( $(m^3 mol^{-1})^{1/n} s^{-1}$ )	$6.2 \cdot 10^{-1}$
$E_{Ox}$ ( $kJ mol^{-1}$ )	$3.2 \cdot 10^1$
$n$	1.2

determined depends on the number of temperature dependent parameters considered in the kinetic model. Thus, the global activation energy was calculated with only  $k_1$  as function of tempera-

ture, see Eq. (6). Kinetic activation energy was calculated with two temperature dependent parameters, i.e.  $k_2$  and  $C_{O_2,eq}$ , see Eq. (7); in this work the activation energy had an additional parameter,  $c$ , affected by temperature in the kinetic model proposed.

Parameters  $n$  and  $c$  in Eq. (21) were calculated considering the effect of the partial pressure of oxygen in the oxygen carrier reduction rate. After integration and some algebra with Eq. (20), the following expression was obtained:

$$Y_R = \ln \left\{ 1 - \frac{1}{k'_{Red} \left(1 - \frac{C_{O_2}}{C_{O_2,eq}}\right) (N-1) (1-X_{Red}) [-\ln(1-X_{Red})]^{1-N}} \left[ \frac{dX_{Red}}{dt} \right]_{X_{Red}=0.2} \right\}$$

$$= \ln(c) + \frac{1}{n} \ln(C_{O_2}) \quad (23)$$

Reaction rate was calculated for  $X_{Red} = 0.2$  due to a maximum conversion rate at this  $X_{Red}$  value is reached using this model with  $N = 3/4$ .

Plotting the left handside of Eq. (23),  $Y_R$ , parameters  $c$  and  $n$  can be calculated from the origin and slope of the plot  $Y_R$  vs.  $\ln(C_{O_2})$ ; see Fig. 10(a). From this, a value of 0.5 for  $n$  (see Table 5) for all temperatures was found. Different values of  $c$  were obtained at each temperature. Considering an Arrhenius dependence of  $c$ , Fig. 9 shows the Arrhenius plot for the reduction reaction, and Table 5 shows the parameters for pre-exponential factor and activation energies obtained for  $c$  from Eq. (17). It can be seen that the value of the activation energy for the parameter  $c$  is negative ( $-240$   $kJ mol^{-1}$ ), as it corresponds to an adsorption process.

The Freundlich isotherm and the nucleation model were used to fit experimental conversion vs. time data for different  $O_2$  concentrations and temperatures. Fig. 3 (a) shows experimental and theoretical conversion vs. time curves at different temperatures and 0 vol.% of  $O_2$ . Fig. 3(b) shows experimental and theoretical lines of conversion vs time for three different temperatures (1223, 1248 and 1273 K) during reduction period using an  $O_2$  concentration of 1.5%. Fig. 4 shows a comparison between experimental data and model predictions for different  $O_2$  concentrations at constant temperature. It can be seen a very good fit between experimental and theoretical curves with the proposed kinetic model for all the temperature and oxygen concentration intervals, including reaction conditions with  $O_2$  concentration far away and close to the equilibrium. This result indicates that the Freundlich isotherm with a nucleation model with  $N = 3/4$  was valid to describe the decomposition of the CuO in a broad range of  $O_2$  concentrations. Thus, the kinetic model here proposed properly predicted the reaction rates when the  $O_2$  concentrations was close to the equilibrium, where previous literature models had failed

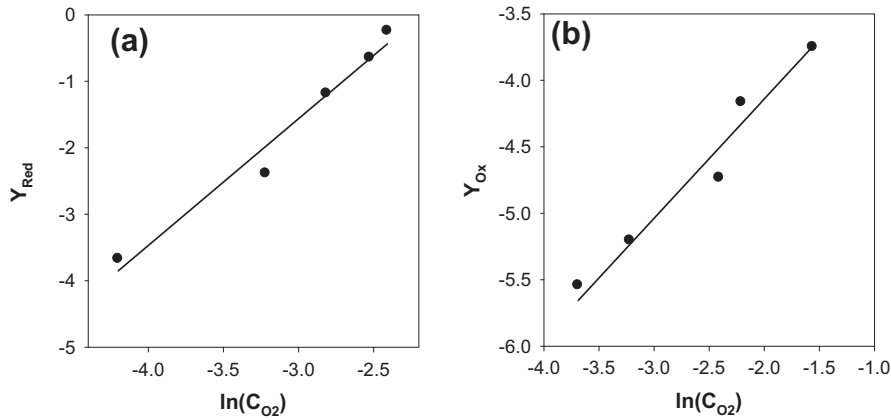


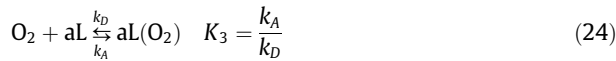
Fig. 10. Determination of (a)  $n$  and  $c$  parameters using Eq. (23) for reduction; and (b)  $n$  parameter using Eq. (30) for oxidation reactions.

[15]. This condition is required in the fuel reactor of a CLOU unit to avoid unconverted compounds exiting the fuel reactor [8,25].

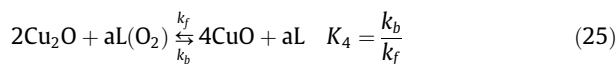
### 3.4.2. Oxidation from $\text{Cu}_2\text{O}$ to $\text{CuO}$

Also, a Langmuir–Hinshelwood mechanistic model has been used to describe the chemical reaction of  $\text{Cu}_2\text{O}$  oxidation in the CLOU process.

- (1) Adsorption of  $\text{O}_2$  over the surface of  $\text{Cu}_2\text{O}$ :



- (2) Chemical reaction of  $\text{Cu}_2\text{O}$  oxidation to give  $\text{CuO}$ :



When the reaction is controlled by the surface chemical reaction, Eq. (25), the reaction rate is given by:

$$\frac{dX_{\text{Ox}}}{dt} = k_{\text{Ox}} S_{\text{Cu}_2\text{O}} c_{\text{O}_2}^{1/n} \left(1 - \frac{C_{\text{O}_2, \text{eq}}}{C_{\text{O}_2}}\right) f(X_{\text{Ox}}) \quad (26)$$

Similar to the reduction analysis, value of  $\theta$  was calculated with Freundlich isotherm, i.e. Eq. (16). The nucleation model was also considered for the oxidation reaction. The expression for the oxidation reaction rate, including the conversion evolution function, is the following:

$$\frac{dX_{\text{Ox}}}{dt} = k_{\text{Ox}} S_{\text{Cu}_2\text{O}} \cdot c_{\text{O}_2}^{1/n} \left(1 - \frac{C_{\text{O}_2, \text{eq}}}{C_{\text{O}_2}}\right) \cdot \left(N^{-1}(1 - X_{\text{Ox}})[- \ln(1 - X_{\text{Ox}})]^{1-N}\right) \quad (27)$$

Integrating Eq. (27) the following expression was obtained to calculate the conversion evolution with time:

$$[- \ln(1 - X_{\text{Ox}})]^N = k_{\text{Ox}} S_{\text{Cu}_2\text{O}} c_{\text{O}_2}^{1/n} \left(1 - \frac{C_{\text{O}_2, \text{eq}}}{C_{\text{O}_2}}\right) t \quad (28)$$

Parameters  $k_{\text{Ox}}$  and  $c$  could not be calculated separately for oxidation reaction. In this case, an effective kinetic constant for oxidation reaction was defined as:

$$k'_{\text{Ox}} = k_{\text{Ox}} S_{\text{Cu}_2\text{O}} c = k'_{\text{Ox},0} e^{-E_{\text{Ox}}/R_g T} \quad (29)$$

Thus, it is necessary to determine three parameters for each temperature:  $N$ ,  $n$  and  $k'_{\text{Ox}}$ . To know the best value of  $N$ , Fig. 8(b) shows a plot of  $(- \ln(1 - X_{\text{Ox}}))^N$  vs. time for different values of  $N$ .

Linear regression of each data show the fit to a linear plot. Table 4 shows the values of the correlation coefficients for the different values of  $N$ . Best fitting correspond to  $N$  equal to 3/4. This procedure has been done for the conversion data obtained at each temperature analyzed in this work, obtaining the same result of  $N$  for all of them.

Parameters  $n$  and  $k'_0$  for the oxidation reaction were obtained from a plot of  $Y_{\text{Ox}}$  vs.  $\ln(C_{\text{O}_2})$  at 1173 K, as it was described by the following equation derived from Eqs. (27) and (29), for  $X_{\text{Ox}} = 0.2$ .

$$Y_{\text{Ox}} = \ln \left\{ \frac{1}{\left(1 - \frac{C_{\text{O}_2, \text{eq}}}{C_{\text{O}_2}}\right) \left(N^{-1}(1 - X_{\text{Ox}})[- \ln(1 - X_{\text{Ox}})]^{1-N}\right)} \left[ \frac{dX_{\text{Ox}}}{dt} \right]_{X_{\text{Ox}}=0.2} \right\} = \ln(k'_{\text{Ox}}) + \frac{1}{n} \ln(C_{\text{O}_2}) \quad (30)$$

Fig. 10(b) shows the plot and the linear regression of  $Y_{\text{Ox}}$  vs.  $\ln(C_{\text{O}_2})$ . A value of  $n$  equal to 1.2 was obtained. Experiments at different temperatures between 1123 and 1273 K and 21 vol.%  $\text{O}_2$  were considered to calculate the temperature dependence of the kinetic constant. Considering an Arrhenius dependence of  $k'_{\text{Ox}}$ , pre-exponential factor and activation energy can be obtained. Fig. 9 shows the Arrhenius plot for the oxidation reaction, and Table 5 shows the kinetic parameters for pre-exponential factor and activation energy obtained. An activation energy of 32 kJ mol<sup>-1</sup> was obtained in this work for the oxidation kinetic constant.

Finally, Fig. 5(a) shows experimental and theoretical conversion vs. time curves obtained for different  $\text{O}_2$  concentrations. It can be seen that there was a good agreement between the experimental and predicted data by the kinetic model with the Freundlich isotherm. The predictions were good in all the range of  $\text{O}_2$  concentrations used. This result indicates that the kinetic model with Freundlich isotherm was valid to describe the oxidation of the  $\text{Cu}_2\text{O}$  in a broad range of  $\text{O}_2$  concentrations, even at concentrations very close to the equilibrium conditions. On the other hand, Fig. 5(b) shows experimental and theoretical conversion vs. time curves at different temperatures. It can be seen that a very good fitting was obtained with the nucleation model.

We can conclude that with the kinetic model developed in this work, it is possible to predict the reduction and oxidation reaction rates at different oxygen concentrations and different temperatures in a broad range of operation conditions suitable for the CLOU operation process.

#### 4. Simulation of the CLOU process with kinetic data

In order to design a CLOU system, the most important parameters are the solids inventory in the system and the oxygen carrier circulation rate. Both parameters are highly influenced by the material reactivity and its oxygen transport capacity. With the kinetic data determined in this work, the CLOU process was simulated by determining the carbon capture efficiency for different coals as a function of solids inventory and solids circulation rate.

##### 4.1. Solids inventory and solids circulation rate to transfer oxygen from air to fuel

The solids circulation rate was calculated by an oxygen mass balance in the system. A simplified model was developed by the authors [26] and later modified for the iG-CLC process [31] for the use of solid fuels. The circulation rate of solids per MW<sub>th</sub>,  $\dot{m}_{OC}$ , that depends on the composition and heat value of the solid fuel, can be calculated as:

$$\dot{m}_{OC} = \frac{10^3 m_o}{LHV \cdot R_{OC} \cdot \Delta X_{OC}} \quad (31)$$

$m_o$  being the mass of oxygen required per kg of solid fuel to full combustion, as for the case of the conventional combustion with air, LHV the lower heating value of the solid fuel and  $\Delta X_{OC}$  the variation of the oxygen carrier conversion in every reactor.

The circulation rate of solids between both reactors was calculated as a function of the variation of the oxygen carrier conversion and it was shown in Fig. 11 when a lignite is used, with a corresponding  $m_o = 1.2$  kg oxygen per kg of coal and a LHV of 16250 kJ/mol. The circulation rate is higher at low values of  $\Delta X_{OC}$ , and decreases quickly when the conversion variation of the oxygen carrier at the fuel reactor increases, reaching low values when the conversion is near to 1. Abad et al. [26] estimated the maximum circulation rate feasible in a CLC plant without increased costs and with commercial experience to be 16 kg s<sup>-1</sup> per MW<sub>th</sub>. This means that the minimum value of  $\Delta X_{OC}$  must be 0.1 and it is necessary to operate at higher values.

The minimum mass of solids in the fuel and air reactors per MW<sub>th</sub> of fuel,  $m_{OC}$ , for the combustion of solid fuels was calculated by doing a mass balance to the fuel reactor [31]:

$$m_{OC} = \frac{10^3 m_o}{LHV \cdot R_{OC} \left( \frac{dX_i}{dt} \right)} \quad (32)$$

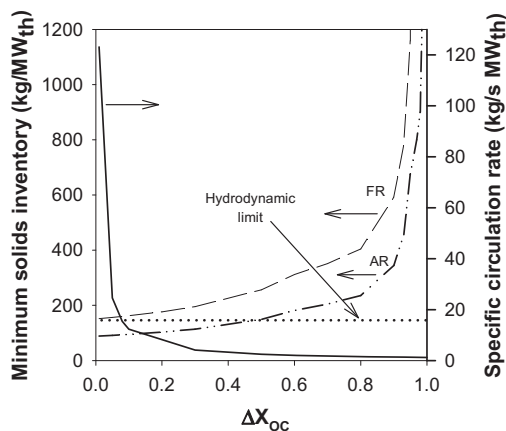


Fig. 11. Minimum solids inventories per MW<sub>th</sub>: fuel reactor (---), air reactor (- · - ·); and specific circulation rate of solids (—) using a lignite as a function of the variation of the oxygen carrier conversion between the fuel and air reactors.  $T = 1223$  K. Solids flux hydrodynamic limit (.....) also shown.

The average reactivity for each reactor was obtained considering the average gas concentration in the reactor and the solids residence time distribution in the reactor as perfect mixing.

Different average oxygen concentration was assumed either in fuel or air reactor. In a CLOU process, the minimum solids inventory in the fuel reactor to transfer the required oxygen for fuel combustion corresponds to the condition where the oxygen uncoupling reaction rate is maximized. This condition is reached when the oxygen concentration in Eq. (20) is considered to be zero, corresponding to the asymptotic limit in which all the O<sub>2</sub> released is consumed by the fuel and there is not an excess of O<sub>2</sub> in gases [25].

On the other hand, the solids inventory in the air reactor was calculated considering an air excess of 20%. The average oxygen concentration in the air reactor was those that fulfil Eq. (33), in this case 11 vol.%; see reference [26] for more information.

$$\left[ \frac{dX_g}{dt} \right]_{O_2} = \int_{X_{g,in}}^{X_{g,out}} \frac{dX_g}{\left[ \frac{dX_i}{dt} \right]} \quad (33)$$

The residence time distribution of particles in the reactor was also considered to calculate the average reaction rate. Assuming perfect mixing of solids in the reactors, the average reaction rate was calculated as [26]:

$$\left( \overline{\frac{dX_i}{dt}} \right) = \int_0^{t_c} \left[ \frac{dX_i}{dt} \right] \frac{e^{-t/t_m}}{t_m} dt \quad (34)$$

This equation considers particles enter to the reactor partially converted. The reaction time necessary to reach complete conversion will be  $t_c$ , being this value the upper limit of the integration of Eq. (34). Following the method presented in [26],  $t_c$  is defined here for the nucleation model as:

$$t_c = \frac{1}{k} \left( -\ln \bar{X}_{Red,inFR} \right)^{3/4} \quad (35)$$

Thus, initial reaction rate was calculated for conversion  $X_{Red} = 0$ , and  $t_c$  corresponded to the time reaching complete reduction, in this case for  $X_{Red} = 1 - \bar{X}_{Red,inFR}$ .

The expression that describe the reactivity using a nucleation model is the following

$$\left[ \frac{dX_{Red}}{dt} \right] = \frac{4}{3} k \cdot t^{1/3} \cdot e^{-(k \cdot t)^{4/3}} \quad (36)$$

Parameter  $k$  includes the kinetic constant and the function of the oxygen concentration.

$$k = k'_{Red} \left( 1 - c C_{O_2}^{1/n} \right) \left( 1 - \frac{C_{O_2}}{C_{eq}} \right) \quad (37)$$

$t_m$  is the mean residence time of the oxygen carrier particles in the fuel reactor, which is dependent on the solid recirculation rate and on the reactor size.

$$t_m = \frac{m_{OC,FR}}{\dot{m}_{OC}} = \frac{\Delta X_{Red}}{\left[ \frac{dX_{Red}}{dt} \right]} \quad (38)$$

The average reactivity has been expressed to consider that the oxygen carrier can be introduced to the fuel reactor with a mean solid conversion reduction,  $\bar{X}_{Red,inFR}$ , higher than 0. Following nucleation model, it was assumed that the unconverted solid was in the surface of the particle. It is worth noting that the minimum oxygen inventory calculated in this section is a function of the oxygen carrier reactivity, and corresponds to the amount of solids to supply oxygen at the required rate determined by the coal feeding rate. Later on, the oxygen consumption by the coal will be further analysed, which will depend on the coal reactivity.

The minimum oxygen carrier inventory in the fuel or air reactor was calculated considering complete conversion in each reactor. Fig. 11 shows the minimum oxygen carrier inventories for both fuel and air reactor as a function of the variation in the oxygen carrier conversion at 1223 K. It can be seen that low values of variation of oxygen carrier conversion gives high values of oxygen carrier circulation rate and low amount of solid inventories in both reactors. If a value of  $\Delta X_{OC} = 0.1$  was assumed, the minimum values of oxygen carrier inventories are 160 kg/MW<sub>th</sub> and 95 kg/MW<sub>th</sub> for the fuel and air reactor, respectively. A high solid inventory in the fuel reactor (235 kg/MW<sub>th</sub>) was experimentally used in combustion tests in a 1.5 kW<sub>th</sub> CLOU unit with this oxygen carrier [8]. However, there was an O<sub>2</sub> excess at the fuel reactor exit, therefore lower inventories would be possible in that unit with complete combustion of the fuel.

#### 4.2. Carbon capture efficiency for different fuels

In addition to the solids inventory needed to transfer the required oxygen to full combustion determined by the coal feeding rate, it is necessary to reach high combustion efficiency in the fuel reactor. So, the solids residence time in the fuel reactor must allow the char conversion, which is related to the CO<sub>2</sub> capture efficiency. It is worth noting that unconverted char in the fuel reactor reaches the air reactor, where it will be burnt to CO<sub>2</sub> which is not captured. Thus, the CO<sub>2</sub> capture efficiency would depend on the solid inventory in the fuel reactor.

The performance of the fuel reactor in a CLOU system is influenced by the pseudo-equilibrium reached between the oxygen released by the oxygen carrier and the oxygen consumed by fuel. Therefore, the oxygen balance in the fuel reactor must consider the oxygen release from the oxygen carrier and the different uses of this oxygen, for conversion of char, volatiles and O<sub>2</sub> concentration in gas stream:

$$(-r_{O_2})_{OC} = (r_{O_2})_C + (r_{O_2})_{vol} + (r_{O_2})_{gas} \quad (39)$$

The oxygen release rate depends on the oxygen carrier reactivity and the oxygen concentration in the reactor

$$(-r_{O_2})_{OC} = R_{OC} m_{OC,FR} \left[ \frac{dX_{Red}}{dt} \right] \quad (40)$$

The oxygen released from the oxygen carrier is used to:

- (1) To burn carbon in char particles. During TGA tests of char combustion with gaseous O<sub>2</sub>, constant reaction rate with time was observed [10,32]. Thus, the char reaction rate can be calculated by

$$(r_{O_2})_C = \frac{M_{O_2}}{M_C} \frac{m_{C,FR}}{1 - X_C} \left[ \frac{dX_C}{dt} \right] \quad (41)$$

- (2) To burn volatile matter. It is assumed complete combustion of volatile matter. The oxygen reacted with volatile matter is the difference between the oxygen demand of the solid fuel fed and the oxygen demand of the fixed carbon.

$$(r_{O_2})_{vol} = \dot{m}_{coal} \left\{ m_O - \frac{M_{O_2}}{M_C} [C_{fix}] \right\} \quad (42)$$

- (3) To accumulate in the exit gas stream. Oxygen can be present in the gaseous stream from the fuel reactor, but always at concentrations below the equilibrium concentration at the reactor temperature. The rate of oxygen release in the gaseous stream depends on the gas at the fuel reactor exit, which in turn depends on the gas inlet to the fuel reactor inlet.

$$(r_{O_2})_{gas} = M_{O_2} [F_{gas} y_{O_2}]_{outFR} \quad (43)$$

$(r_{O_2})_{gas}$  only depends on oxygen concentration and  $(r_{O_2})_C$  also depends on char concentration in the fuel reactor. To determine the char concentration, a carbon balance was done considering the different streams where carbon is: carbon in fuel, carbon in volatiles, carbon in converted char in the fuel reactor, and carbon in the solids stream from the fuel reactor.

$$F_{C,SF} = F_{C,vol} + X_C F_{C,char} + (1 - X_C) F_{C,char} \quad (44)$$

Each carbon flow is calculated as:

$$F_{C,coal} = \frac{1}{M_C} \dot{m}_{coal} [C_{coal}] \quad (45)$$

$$F_{C,vol} = \frac{1}{M_C} \dot{m}_{coal} [C_{coal} - C_{fix}] \quad (46)$$

$$F_{C,char} = \frac{1}{M_C} \dot{m}_{coal} [C_{fix}] \quad (47)$$

$$(1 - X_C) F_{C,char} = \frac{1}{M_C} \dot{m}_{OC} \frac{f_{C,FR}}{1 - f_{C,FR}} (1 - \eta_{CSS}) \quad (48)$$

$f_C$  being the mass fraction of carbon in solids in the fuel reactor:

$$f_C = \frac{m_{C,FR}}{m_{OC,FR} - m_{C,FR}} \quad (49)$$

The char fraction  $f_C$  affects to the solids transfer to the air reactor and the oxygen consumed in the fuel reactor. The effect of a carbon stripper efficiency,  $\eta_{CSS}$ , on char conversion is also considered in Eq. (48). A carbon stripper makes a selective recirculation of unconverted char particles to the fuel reactor from the solids stream exiting the fuel reactor in order to minimize the flow of unconverted carbon in the air reactor [32], thus obtaining high CO<sub>2</sub> capture efficiencies [10,32].

By fixing the mass of oxygen carrier in the fuel reactor, an iterative process can be done modifying the oxygen concentration and the mass fraction of carbon in the fuel reactor to obtain the oxygen generation rate and the consumption rate in Eqs. (40) and (41). The objective of the iterative process was to fulfil simultaneously the oxygen and carbon balances showed in Eqs. (39) and (44). Once each carbon flow is known, the CO<sub>2</sub> capture efficiency,  $\eta_{CC}$ , can be obtained for the assumed solids inventory.

$$\eta_{CC} = \frac{F_{C,vol} + X_C F_{C,char}}{F_{C,coal}} \quad (50)$$

It is worth noting that the CO<sub>2</sub> capture efficiency also depends on the solids circulation flow rate because: (1) the circulation of solids affects to the solids residence time, and therefore to the reactivity of oxygen carrier; and (2) affects to the carbon flow exiting the fuel reactor.

In this work, three fuels have been considered for the analysis: a high reactive bituminous coal (HRB), a low volatile bituminous coal (LVB) and a lignite. These coals were tested before at the continuous CLOU 1.5 kW<sub>th</sub> unit [8,10], showing different behaviour during the combustion tests. The char reactivity kinetic parameters needed for this study have been taken from Hurt and Mitchell [33]. Proximate and ultimate analysis and the corresponding kinetic parameters are shown in Table 6 for each coal.

Fig. 12(a) shows the O<sub>2</sub> concentration at the fuel reactor outlet as a function of the oxygen carrier conversion using the lignite fuel and different fuel reactor solid inventories (150, 250, 500 and 1500 kg/MW<sub>th</sub>). Fuel reactor temperature was 1223 K and the use of a carbon separation system ( $\eta_{CSS} = 0$ ) was not considered. The O<sub>2</sub> concentration at equilibrium conditions is also included for

**Table 6**  
Properties and kinetic parameters for the different coals considered taken from [33].

	Lignite	Low Volatile Bituminous	High Volatile Bituminous
<i>Proximate analysis (wt.%)</i>			
Moisture	12.6	2.0	2.3
Volatile matter	28.6	17.1	33.0
Fixed carbon	33.6	68.8	55.9
Ash	25.2	12.1	8.8
<i>Ultimate analysis (wt.%)</i>			
C	45.4	75.8	65.8
H	2.5	3.7	3.3
N	0.6	1.9	1.6
S	5.2	0.4	0.6
O <sup>a</sup>	8.5	4.1	17.6
<i>Kinetic parameters</i>			
$k_0$ (m <sup>3</sup> mol <sup>-1</sup> s <sup>-1</sup> )	2.7·10 <sup>7</sup>	1.8·10 <sup>7</sup>	1.5·10 <sup>5</sup>
$E_0$ (kJ mol <sup>-1</sup> )	91.5	94.1	64.0
$p$	0.5	0.5	0.5
LHV (kJ kg <sup>-1</sup> )	16250	28,950	25,000
$m_o$ (kg O <sub>2</sub> /kg coal)	1.2	2.2	2.0

<sup>a</sup> Oxygen to balance.

comparison purposes. It can be observed that the oxygen concentration decreases when the variation of the conversion increases. This is due to the fact that more coal is converted in the fuel reactor and the average oxygen carrier reactivity decreases as  $\Delta X_{OC}$  increases, see Eq. (39). It can be also seen that the oxygen

concentration increases when the solids inventory in the fuel reactor increases, because there is more oxygen in solids available for oxygen uncoupling. Underline that when the CO<sub>2</sub> capture efficiency is low there are O<sub>2</sub> at the fuel reactor outlet. This means, that this oxygen carrier is highly reactive and can release O<sub>2</sub> although the residence time in the fuel reactor is not enough to convert completely the char.

Fig. 12(b) shows the CO<sub>2</sub> capture efficiency as a function of the variation of the oxygen carrier conversion for same conditions. CO<sub>2</sub> capture efficiency increases when the solid inventory and the oxygen carrier conversion increase due to the associated increase in the solids residence time. Note that all lines converge to a CO<sub>2</sub> capture value of 24% at  $\Delta X_{OC} = 0$  which corresponds to the combustion of the volatile matter of this coal. At high values of the solids conversion, the increase in the CO<sub>2</sub> capture efficiency is smoother. This behaviour is due to two additive reasons: (1) the residence time in the fuel reactor is inversely proportional to the conversion variation, producing that the char conversion is not proportional to the variation of oxygen carrier conversion; (2) a less O<sub>2</sub> concentration in the fuel reactor decrease the char conversion rate in the fuel reactor. In fact, the CO<sub>2</sub> capture efficiency can decrease slightly at high values of  $\Delta X_{OC}$ . Therefore, a maximum in the CO<sub>2</sub> capture efficiency for each solids inventory in the fuel reactor was observed by changing the solids conversion variation. This maximum is due to the oxygen concentration decrease toward 0, and the effect of low oxygen concentration on the decrease of the char combustion rate is higher than the beneficial effect of the residence time increase.

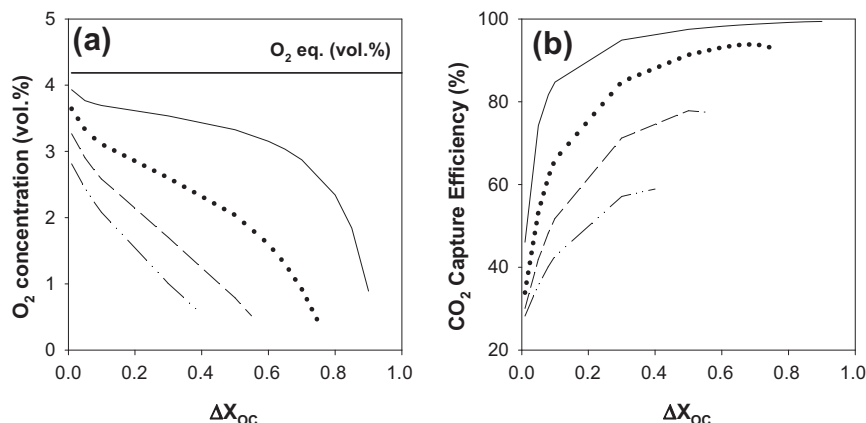


**Fig. 12.** (a) O<sub>2</sub> concentration at the fuel reactor outlet and (b) CO<sub>2</sub> capture efficiency as a function of the variation of oxygen carrier conversion in the fuel reactor using lignite as fuel and different solids inventories in the fuel reactor: 1500 (—), 500 (····), 250 (---) and 150 (-·-·) kg/MW<sub>th</sub>.  $T_{FR} = 1223$  K,  $\eta_{CSS} = 0$ .

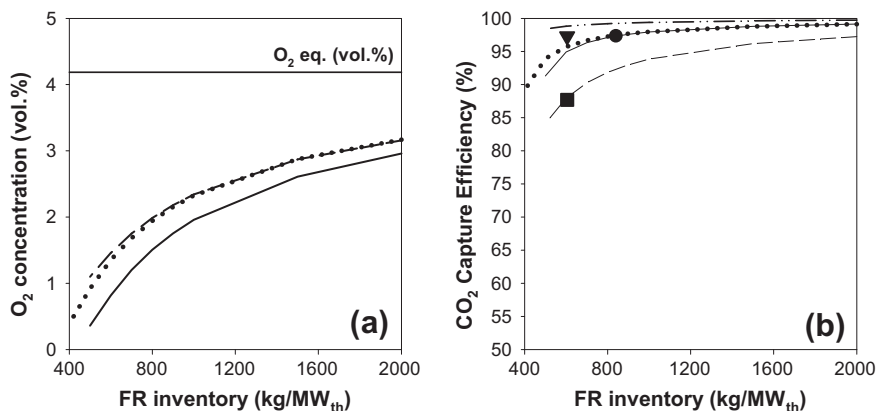


**Fig. 13.** (a) O<sub>2</sub> concentration at the fuel reactor outlet and (b) CO<sub>2</sub> capture efficiency, as a function of the fuel reactor inventory for three different coals: HRB (—), lignite (····), LVB (-·-·),  $T_{FR} = 1223$  K,  $\eta_{CSS} = 0\%$ ,  $\Delta X_{OC} = 0.7$ . LVB with a  $\eta_{CSS} = 90\%$  also shown (---). Experimental points obtained in the 1.5 kW<sub>th</sub> continuous unit for CLOU process: HRB (▼) [8], lignite (●), LVB (▲) [10].

CO<sub>2</sub> capture efficiencies higher than 90% can be only reached with oxygen carrier inventories higher than 500 kg/MW<sub>th</sub> and  $\Delta X_{OC} > 0.5$ , without the use of a carbon separation system ( $\eta_{CSS} = 0$ ). Therefore, it is recommended to work with high values of  $\Delta X_{OC}$ , i.e. low solids circulation rate to obtain high CO<sub>2</sub> capture efficiencies.

Fig. 13(a) shows the O<sub>2</sub> concentration at the outlet of the fuel reactor as a function of the fuel reactor solids inventory for the three different coals (HRB, lignite and LVB). Fuel reactor temperature was 1223 K and the use of a carbon separation system ( $\eta_{CSS} = 0$ ) was not considered. It can be observed that the O<sub>2</sub> concentration increases with the inventory in the fuel reactor due to the increase of solids generating oxygen. The O<sub>2</sub> concentration is very similar for the lignite and LVB, but it is lower for the HRB, due to the high amount of volatiles that the HRB contains, which consume more O<sub>2</sub>. As an example, for fuel reactor solids inventories <600 kg/MW<sub>th</sub>, oxygen concentrations at fuel reactor outlet are of the order of 1 vol.% which are lower than that found in oxy-combustion process for coal.

The effect of fuel reactor solids inventory on the CO<sub>2</sub> capture efficiency was also evaluated for the different coals: HRB, lignite and LVB. Fig. 13(b) shows the variation of the CO<sub>2</sub> capture efficiency as a function of the solid inventory in the fuel reactor for these coals at the same conditions, but considering a solid conversion variation of  $\Delta X_{OC} = 0.7$ . In all cases the CO<sub>2</sub> capture efficiency increases with the solids inventory because of a higher solid residence time and higher oxygen availability. It can be seen that for the high reactive coals, i.e. HRB and lignite, it is possible to reach high CO<sub>2</sub> capture efficiencies ( $\geq 95\%$ ) with around 600 kg/MW<sub>th</sub> in the fuel reactor. However, for low reactive coals, i.e. LVB, it is necessary higher values of solids inventory to achieve high CO<sub>2</sub> capture efficiency, with values near 1500 kg/MW<sub>th</sub>. Moreover, Fig. 13(b) shows experimental results obtained in the 1.5 kW<sub>th</sub> continuous unit for CLOU process with different coals: HVB, lignite and LVB [8,10]. It can be seen that experimental results match with data obtained from the model for each coal simulated. Fig. 13(b) also shows the CO<sub>2</sub> capture efficiency for a LVB when a carbon stripper with a 90% of efficiency was included in the simulation. It can be seen the important effect of this separation unit allowing high CO<sub>2</sub> capture efficiencies even with low values of solids inventories, 99% with 700 kg/MW<sub>th</sub>. Therefore, for low reactive coals it is necessary to use a carbon stripper to reach high CO<sub>2</sub> capture rates. But even for reactive coals, the use of an efficient carbon tripper reduces also the oxygen carrier inventories in the fuel reactor and the SO<sub>2</sub> emissions in the air reactor [11,34].

It is worth noting that the fuel reactor solids inventory needed to supply the stoichiometric oxygen flow rate to burn a lignite (about 300 kg/MW<sub>th</sub>, with  $\Delta X_{OC} = 0.7$ ; see Fig. 11) is lower than the solids inventory needed to reach a CO<sub>2</sub> capture higher than 95% without a carbon stripper ( $\approx 600$  kg/MW<sub>th</sub>). This fact agree with previous results obtained from the analysis of the oxygen carrier reactivity [25] and results obtained in a CLOU unit [8,10]. It can be concluded that the kinetic parameters determined together with the simulation tool developed in this work, configure a useful instrument for the design and optimization of CLOU process.

## 5. Conclusions

Reaction rates of reduction and oxidation of a Cu-based oxygen carrier (60 wt.% of CuO and 40 wt.% of MgAl<sub>2</sub>O<sub>4</sub>) for CLOU process has been measured by TGA to determine the redox kinetic. Relevant reactions were decomposition of CuO to Cu<sub>2</sub>O and oxidation of Cu<sub>2</sub>O to CuO. A nucleation model for the variation of the solid conversion with time and a Langmuir–Hinshelwood surface kinetic control together with Freundlich's isotherm was valid to predict

the experimental data in a broad range of O<sub>2</sub> concentration and temperatures. In fact good predictions were obtained even at O<sub>2</sub> concentrations very close to the equilibrium conditions.

The kinetic model was further used to analyze the design and operation conditions of CLOU process using this oxygen carrier. Minimum solids inventory of 160 kg/MW<sub>th</sub> in the fuel reactor and 95 kg/MW<sub>th</sub> in air reactor were determined to transfer the oxygen flow demanded for full combustion of the coal. The CO<sub>2</sub> capture efficiency as a function of the oxygen carrier circulation rate and the fuel reactor solids inventory for three different coals have been also estimated. For high reactive coals, i.e. HRB and lignite, it would be possible to reach high CO<sub>2</sub> capture rates ( $\geq 95\%$ ) with 600 kg/MW<sub>th</sub>. However, for low reactive coals, i.e. LVB, 1500 kg/MW<sub>th</sub> would be needed to achieve high CO<sub>2</sub> capture efficiencies. These results highlight the need of using an efficient carbon stripper which allows CO<sub>2</sub> capture efficiencies higher than 95% with low solids inventories.

## Acknowledgement

This work was supported by the European Commission, under the RFCS program (ACCLAIM Project, Contract RFCP-CT-2012-00006), the Spanish Ministry of Science and Innovation (MICINN Project: ENE2011-26354) and the European Union FEDER Funds. I. Adánez-Rubio thanks CSIC for the JAE fellowship co-financed by the European Social Fund.

## References

- [1] T. Mattisson, A. Lyngfelt, H. Leion, Chemical-looping with oxygen uncoupling for combustion of solid fuels, *Int. J. Greenhouse Gas Control* 3 (2009) 11–19.
- [2] P. Gayán, I. Adánez-Rubio, A. Abad, L. de Diego, F. García Labiano, J. Adánez, Development of Cu-based oxygen carriers for Chemical-Looping with Oxygen Uncoupling (CLOU) process, *Fuel* 96 (2012) 226–238.
- [3] I. Adánez-Rubio, P. Gayán, F. García-Labiano, L. de Diego, J. Adánez, A. Abad, Development of CuO-based oxygen-carrier materials suitable for Chemical-Looping with Oxygen Uncoupling (CLOU) process, *Energy Procedia* 4 (2011) 417–424.
- [4] I. Adánez-Rubio, M. Arjmand, H. Leion, P. Gayán, A. Abad, T. Mattisson, A. Lyngfelt, Investigation of combined supports for Cu-based oxygen carriers for Chemical-Looping with Oxygen Uncoupling (CLOU), *Energy Fuels* 27 (2013) 3918–3927.
- [5] M. Rydén, H. Leion, T. Mattisson, A. Lyngfelt, Combined oxides as oxygen-carrier material for Chemical-Looping with Oxygen Uncoupling, *Appl. Energy* 113 (2014) 1924–1932.
- [6] J. Adánez, A. Abad, F. García Labiano, P. Gayán, L. de Diego, Progress in chemical-looping combustion and reforming technologies, *Progr. Energy Combust. Sci.* 38 (2012) 215–282.
- [7] T. Mattisson, *Materials for Chemical-Looping with Oxygen Uncoupling*, ISRN Chem. Eng. 2013 (2013) 19.
- [8] A. Abad, I. Adánez-Rubio, P. Gayán, F. García Labiano, L. de Diego, J. Adánez, Demonstration of chemical-looping with oxygen uncoupling (CLOU) process in a 1.5kW<sub>th</sub> continuously operating unit using a Cu-based oxygen-carrier, *Int. J. Greenhouse Gas Control* 6 (2012) 189–200.
- [9] I. Adánez-Rubio, P. Gayán, A. Abad, L. de Diego, F. García Labiano, J. Adánez, Evaluation of a spray-dried CuO/MgAl<sub>2</sub>O<sub>4</sub> oxygen carrier for the Chemical Looping with Oxygen Uncoupling process, *Energy Fuels* 26 (2012) 3069–3081.
- [10] I. Adánez-Rubio, A. Abad, P. Gayán, L.F. de Diego, F. García Labiano, J. Adánez, Performance of CLOU process in the combustion of different types of coal with CO<sub>2</sub> capture, *Int. J. Greenhouse Gas Control* 12 (2013) 430–440.
- [11] I. Adánez-Rubio, A. Abad, P. Gayán, F. García Labiano, L. de Diego, J. Adánez, The fate of sulphur in the Cu-based Chemical Looping with Oxygen Uncoupling (CLOU) Process, *Appl. Energy* 113 (2014) 1855–1862.
- [12] I. Adánez-Rubio, A. Abad, P. Gayán, L.F. de Diego, F. García-Labiano, J. Adánez, Biomass combustion with CO<sub>2</sub> capture by chemical looping with oxygen uncoupling (CLOU), *Fuel Process. Technol.* 124 (2014) 104–114.
- [13] F. García-Labiano, L.F. de Diego, J. Adánez, A. Abad, P. Gayán, Reduction and oxidation kinetics of a copper-based oxygen carrier prepared by impregnation for chemical-looping combustion, *Ind. Eng. Chem. Res.* 43 (2004) 8168–8177.
- [14] A. Sahir, H. Sohn, H. Leion, J. Lighty, Rate analysis of Chemical-Looping with Oxygen Uncoupling (CLOU) for solid fuels, *Energy Fuels* 26 (2012) 4395–4404.
- [15] C. Clayton, K. Whitty, Measurement and modeling of decomposition kinetics for copper oxide-based chemical looping with oxygen uncoupling, *Appl. Energy* (2013).
- [16] D. Chadda, J.D. Ford, M.A. Fahim, Chemical energy storage by the reaction cycle CuO/Cu<sub>2</sub>O, *Int. J. Energy Res.* 13 (1989) 63–73.

- [17] E.M. Eyring, G. Konya, J.S. Lighty, A.H. Sahir, A.F. Sarofim, K. Whitty, Chemical looping with copper oxide as carrier and coal as fuel, *Oil Gas Sci. Technol.* 66 (2011) 209–221.
- [18] H. Song, K. Song, E. Shah, T. Doroodchi, B. Wall Moghtaderi, Analysis on chemical reaction kinetics of CuO/SiO<sub>2</sub> oxygen carriers for chemical looping air separation, *Energy Fuels* 28 (2014) 173–182.
- [19] K. Whitty, C. Clayton, Measurement and Modeling of Kinetics for Copper-Based Chemical Looping with Oxygen Uncoupling, 2nd International Conference on Chemical Looping 26–28 September 2012, Darmstadt, Germany, (2012).
- [20] S. Peterson, G. Konya, C. Clayton, R. Lewis, B. Wilde, E. Eyring, K. Whitty, Characteristics and CLOU performance of a novel SiO<sub>2</sub>-supported oxygen carrier prepared from CuO and β-SiC, *Energy Fuels* 27 (2013) 6040–6047.
- [21] K. Wang, Q. Yu, Q. Qin, Reduction kinetics of Cu-based oxygen carriers for chemical looping air separation, *Energy Fuels* 27 (2013) 5466–5474.
- [22] M. Arjmand, M. Keller, H. Leion, T. Mattisson, A. Lyngfelt, Oxygen release and oxidation rates of MgAl<sub>2</sub>O<sub>4</sub>-supported CuO oxygen carrier for Chemical-Looping Combustion with Oxygen Uncoupling (CLOU), *Energy Fuels* 26 (2012) 6528–6539.
- [23] Y. Zhu, K. Mimura, J.W. Lim, M. Isshiki, Q. Jiang, Brief review of oxidation kinetics of copper at 350 °C to 1050 °C, *Metall. Mater. Trans. A* 37 (2006) 1231–1237.
- [24] S.Y. Chuang, J.S. Dennis, A.N. Hayhurst, S.A. Scott, Kinetics of the oxidation of a co-precipitated mixture of Cu and Al<sub>2</sub>O<sub>3</sub> by O<sub>2</sub> for Chemical-Looping Combustion, *Energy Fuels* 24 (2010) 3917–3927.
- [25] I. Adáñez-Rubio, A. Abad, P. Gayán, L. de Diego, F. García Labiano, J. Adáñez, Identification of operational regions in the Chemical-Looping with Oxygen Uncoupling (CLOU) process with a Cu-based oxygen carrier, *Fuel* 102 (2012) 634–645.
- [26] A. Abad, J. Adáñez, F. García Labiano, L. de Diego, P. Gayán, J. Celaya, Mapping of the range of operational conditions for Cu-, Fe-, and Ni-based oxygen carriers in chemical-looping combustion, *Chem. Eng. Sci.* 62 (2007) 533–549.
- [27] F. García Labiano, L. de Diego, J. Adáñez, A. Abad, P. Gayán, Temperature variations in the oxygen carrier particles during their reduction and oxidation in a chemical-looping combustion system, *Chem. Eng. Sci.* 60 (2005) 851–862.
- [28] C.N. Hinshelwood, The kinetics of heterogeneous reactions, in: *Kinetics of Chemical Change*, Clarendon Press, Oxford, 1940, pp. 178–234.
- [29] F. García-Labiano, A. Abad, L.F. de Diego, P. Gayán, J. Adáñez, Calcination of calcium-based sorbents at pressure in a broad range of CO<sub>2</sub> concentrations, *Chem. Eng. Sci.* 57 (2002) 2381–2393.
- [30] B.V. Erofe'Ev, *Comptes Rendus de l'Académie des Sciences de l'Urss*, (1946) 511.
- [31] A. Abad, J. Adáñez, A. Cuadrat, F. García Labiano, P. Gayán, L. de Diego, Kinetics of redox reactions of ilmenite for chemical-looping combustion, *Chem. Eng. Sci.* 66 (2011) 689–702.
- [32] Y. Cao, W.P. Pan, Investigation of chemical looping combustion by solid fuels. 1. Process analysis, *Energy Fuels* 20 (2006) 1836–1844.
- [33] R. Hurt, R. Mitchell, Unified high-temperature char combustion kinetics for a suite of coals of various rank, *Symp. Int. Comb.* 24 (1992) 1243–1250.
- [34] J. Adáñez, P. Gayán, I. Adáñez-Rubio, A. Cuadrat, T. Mendiara, A. Abad, F. García-Labiano, L.F. de Diego, Use of Chemical-Looping processes for coal combustion with CO<sub>2</sub> capture, *Energy Procedia* 37 (2013) 540–549.

